INTERNATIONAL DOCTORAL
SCHOOL OF THE USC

Silvia
Cobelo Gómez

PhD Thesis

Unravelling the Pathogenesis of Celia's Encephalopathy (PELD): The Role of Seipin in Neurodegeneration, Lipodystrophy, and other Tissue Damage in a Humanized Murine Model

Santiago de Compostela, 2024

Doctoral Programme in Endocrinology

ESCOLA DE DOUTORAMENTO
INTERNACIONAL DA USC

DOCTORAL THESIS

UNRAVELLING THE PATHOGENESIS OF CELIA'S ENCEPHALOPATHY (PELD): THE ROLE OF SEIPIN IN NEURODEGENERATION, LIPODYSTROPHY, AND OTHER TISSUE DAMAGE IN A HUMANIZED MURINE MODEL

Silvia Cobelo Gómez

Supervisors: David Araújo Vilar and Sofía Sánchez Iglesias

Tutor: David Araújo Vilar

DOCTORAL PROGRAMME IN ENDOCRINOLOGY

SANTIAGO DE COMPOSTELA 2024

DECLARACIÓN DE CONFLICTO DE INTERESES Y FINANCIACIÓN

The doctoral candidate, **Silvia Cobelo Gómez**, declares that she has no conflict of interest to her doctoral thesis entitled "**Unravelling the Pathogenesis of Celia's Encephalopathy (PELD): The Role of Seipin in Neurodegeneration, Lipodystrophy, and other Tissue Damage in a Humanized Murine Model**".

This doctoral thesis received support from the Instituto de Salud Carlos III, ISCIII (grant numbers PI18/01890 and PI22/00514), as well as from the Fundación Mutua Madrileña (call 2015), with co-funding from the European Union. Additionally, it received an intramural grant from the Xunta de Galicia (grant numbers ED341b2017/19 and ED431B 2020/37). Furthermore, support was provided by the Asociación Española de Familiares y Afectados de Lipodistrofias (AELIP).

A mis padres y a Gerard

AGRADECIMIENTOS

Quisiera expresar mi más sincero agradecimiento a todas las personas que han contribuido, de manera directa o indirecta, al desarrollo de esta tesis doctoral.

En primer lugar, deseo reconocer el valioso apoyo brindado por todas las instituciones y organizaciones que facilitaron financiamiento, recursos y acceso a instalaciones para llevar a cabo esta investigación. En particular, agradezco profundamente a la AELIP, a Juan y a Naca, por su gran compromiso.

Quiero agradecer especialmente a mi director de la tesis, David Araújo Vilar, por su guía experta, su apoyo constante y su compromiso a lo largo de este viaje académico. Su dedicación y consejos han sido fundamentales para el desarrollo de este proyecto.

También quiero expresar mi gratitud a mi codirectora de tesis, Sofía Sánchez Iglesias, quien se ha convertido en mentora, referente y amiga durante estos años. Gracias por todo lo que me has enseñado y por tu infinita paciencia con cada pregunta, momento difícil o calendario mal organizado.

Gracias a Laura, por enseñarme a disfrutar del trabajo y por ser una fuente constante de inspiración. De ti he aprendido que con algo de humor todo puede ser positivo.

Por supuesto, a mis amigos. Por esos vinos entre semana para hablar de todo y de nada. A mis amigas de Viveiro, gracias por ser mi refugio de desconexión. A Meri, mi alter ego en Cataluña, gracias por ser tú. Y a ti, Laura, por estar siempre presente, por creer en mí y por recordarme que, a veces, me exijo demasiado.

También quiero agradecer a todos aquellos que hicieron que mi estancia en Cambridge fuera una experiencia inolvidable, tanto en el ámbito laboral como personal.

No puedo dejar de expresar mi profunda gratitud a mi familia, en especial a mis padres. Gracias por vuestra infinita paciencia para soportar mis malos momentos y mis constantes llamadas. Por vuestro cariño y aliento incondicionales. Nunca sabré cómo agradecéroslo. Sin vosotros, no sería quién soy hoy.

Y, por último, a Gerard. Por apoyarme en todas las decisiones de mi vida, por más arriesgadas que sean. Gracias por estar siempre ahí de manera incondicional y aportarme la calma que tanto necesito.

SUMMARY

The human *BSCL2* gene is located on chromosome 11q12.3. This gene encodes for seipin, an endoplasmic reticulum resident protein with two transmembrane domains, an intraluminal loop, and two amino- and carboxy-terminal tails in the cytoplasm. In humans, seipin forms 11-unit homooligomers that constitute a toroid. The main function of seipin, a highly evolutionarily conserved protein, is to modulate the formation of lipid droplets. Seipin operates at the interface of lipid droplets and the endoplasmic reticulum, playing a critical role in the early formation of normal lipid droplets and in the maintenance of mature lipid droplets. Additionally, it is involved in the regulation of triglyceride and phospholipid synthesis, as well as in the participation of nerve impulse transmission in neurons. This latter aspect highlights its importance not only in metabolic processes but also in the proper functioning of the nervous system. Three isoforms of seipin are primarily encoded by this gene, consisting of 462 (*BSCL2*-203/227/217), 398 (*BSCL2*-205/207/210), and 287 (*BSCL2*-201) amino acids in length, respectively. In humans, this gene exhibits its highest expression not in adipose tissue as might be expected, but in the central nervous system, the pituitary gland, and the testes. *BSCL2*-203/227/217 is predominantly expressed in the brain (80%), while in other tissues, the expression of *BSCL2*-203/227/217 and *BSCL2*-205/207/210 transcripts is similar, and the expression of *BSCL2*-201 is negligible in all tissues (<1%).

Congenital generalized lipodystrophy type 2 is a very rare autosomal recessive disorder caused by pathogenic variants in the *BSCL2* gene. Patients typically present with a generalized absence of adipose tissue that is evident from birth or during the first year of life. This lack of adipose tissue results in well-defined muscles, giving them a robust and Herculean appearance as they age. Additionally, these patients exhibit hyperinsulinemia at an early age, hypoleptinemia, hypoadiponectinemia, and hypertriglyceridemia, and develop non-ketotic diabetes mellitus in the second decade of life. The ectopic deposition of fat in the liver leads to hepatic steatosis, explaining the significant hepatomegaly that can progress to cirrhosis. Due to severe insulin resistance, these children develop acanthosis nigricans as early as the first few years of life, indicating severe dysfunction in glucose and lipid metabolism. Furthermore, cardiac complications and renal impairment are commonly observed in these patients. Unlike other subtypes of congenital generalized lipodystrophy, these patients tend to have a degree of intellectual disability ranging from mild to moderate. At the molecular level, most cases of congenital generalized lipodystrophy type 2 arise from homozygous or compound heterozygous variants. These variants often result in premature stop codons or frameshift variants, leading to a loss of seipin function.

On the other hand, specific heterozygous missense variants in *BSCL2* can give rise to a wide spectrum of upper and/or lower motor neuron diseases. These variants cause the formation of abnormal seipin structures, contributing to various neurological disorders, such as Silver syndrome (also known as spastic paraplegia type 17) and autosomal dominant distal hereditary motor neuropathy-13.

In 2013, our group described a new childhood neurodegenerative disease, Celia's encephalopathy, or progressive encephalopathy with or without lipodystrophy. This disease could be considered a particular variant of congenital generalized lipodystrophy type 2 with a devastating neurological presentation. This extremely rare disease is due to different variants in the *BSCL2* gene. The most common and first described was the c.985C>T variant in exon 7, in homozygous or compound heterozygous form. Homozygous patients may not show typical characteristics of generalized lipodystrophy but may have hypertriglyceridemia and hepatomegaly. However, some homozygous cases have exhibited lipodystrophy. In contrast, compound heterozygotes often show signs of congenital generalized lipodystrophy type 2 early in childhood. Neurologically, these patients experience psychomotor delay with significant language deterioration from the age of two. Neurological regression begins at ages 3-4 and is characterized by a gradual loss of previously acquired skills. Over time, the neurodegenerative profile becomes more pronounced with a sudden onset of severe myoclonic epilepsy, spastic tetraparesis, and severe encephalopathy. This rapid evolution of neurodegenerative symptoms is a key feature of the disease. Celia's encephalopathy currently lacks a cure, and the typical cause of death is usually the overall deterioration of the patient's health before the age of nine.

The c.985C>T variant located in exon 7 of the *BSCL2*-203/227/217 transcript induces changes in splicing that lead to skipping of exon 7, resulting in a seipin variant lacking the second transmembrane domain. This structural loss compromises the protein's function, giving rise to a new aberrant form of seipin, termed Celia seipin, which includes 64 additional amino acids. The expression of this Celia *BSCL2* transcript is elevated in both neural and non-neural tissues of affected individuals, potentially influencing disease progression. Thus, the overexpression of aberrant forms of seipin suggests a toxic gain-of-function process. Celia seipin triggers oxidative stress and endoplasmic reticulum stress, leading to endoplasmic reticulum dilation and the formation of nuclear inclusions containing seipin. This suggests that the neuronal damage triggered by endoplasmic reticulum stress in Celia encephalopathy may promote the translocation of seipin molecules to the nucleoplasm. This translocation could lead to defective oligomerization and aggregation of Celia seipin, thereby contributing to the pathogenesis of Celia encephalopathy, similar to the mechanisms observed in Huntington's disease. Interestingly, simple heterozygous carriers remain asymptomatic, possibly due to the interaction between wild type seipin and Celia seipin. Wild type seipin could potentially sequester Celia seipin in mixed oligomers, thereby mitigating toxic effects. This phenomenon of rescue by wild type seipin is a new concept in neurodegenerative diseases caused by improper protein folding. Furthermore, the dysfunction of peroxisomes,

abundant in neurons and playing a vital role in defence against oxidative stress, may contribute to the neurodegenerative phenotype observed in this disease.

The understanding of the pathogenic mechanisms of Celia's encephalopathy, of which our group has already elucidated part, involves the development of biological models of the disease, given its low prevalence, severity, and the brain as the primarily affected organ, which makes its study in humans difficult. In this context, the overall objective of this thesis is to improve the understanding of the molecular mechanisms underlying neurodegeneration, lipodystrophy, and non-alcoholic steatohepatitis in Celia's encephalopathy using two mouse models. Therefore, this study generated the first global mouse model of the aberrant human *BSCL2* transcript using a Cre/loxP recombination-based strategy. Simultaneously, a global mouse model deficient in seipin was created by replacing the ATG start codon for the first time with an inverted *cassette* that induces ubiquitous interruption of the seipin protein.

This allowed for a detailed comparative analysis between generalized congenital lipodystrophy type 2 and progressive encephalopathy with or without lipodystrophy, facilitating an exhaustive study of the differences and similarities between both conditions. For the assessment of motor and cognitive functions, various well-established behavioural tests were employed. Motor functions were analysed through studies such as the open field, which allowed for the evaluation of the general locomotor activity level and the spontaneous exploration of the animals. This test is fundamental for detecting possible alterations in physical activity or movement due to neurological changes. The elevated zero maze, on the other hand, helped study the anxiety and spatial navigation ability of the animals, allowing for an understanding of how they respond to stressful situations. The rotarod test measured the motor coordination and balance of the animals, while the walking on the beam walking test assessed dexterity and the ability for precise movement. Additionally, the wire suspension test was used to analyse muscle strength and endurance, providing an overall view of the motor functions under study. Regarding the assessment of cognitive functions, the Morris water maze was employed as the main tool. This test is widely used to measure spatial memory and learning, as it requires the animals to orient themselves and find a hidden platform in a pool. The ability to remember the location of the platform in subsequent sessions reveals information about their memory state and the integrity of cognitive functions. To complement these behavioural studies, a deeper neurological characterization was performed through histological studies, as well as positron emission tomography, which allowed visualization of brain metabolism and detection of abnormalities in brain function. This technology is particularly useful for identifying areas of the brain affected by metabolic alterations or neurodegeneration. Furthermore, a detailed analysis of the expression of the Celia *BSCL2* transcript and other mitochondrial and peroxisomal genes (*Pparγ*, *Pex16*, *Cat*, *Gpx1*, *Pex11g*, *Sod1*, *Sod2*), as well as the expression of Celia seipin in six brain areas, was conducted, allowing for a clearer understanding of the genetic mechanisms underlying Celia's encephalopathy. Along with the neurological studies, a complete biochemical and hematological profile of both models was performed. Additionally, levels of triglycerides, insulin, and glucose were evaluated, which are fundamental indicators for understanding the

metabolic alterations present in both disorders. The liver, kidney, heart, and adipose tissues were evaluated from a histological perspective. In particular, an analysis of the expression of the *Fgf21* gene, a key marker in energy metabolism, was conducted in the liver. These analyses provided a comprehensive understanding of the possible multisystemic consequences of the pathologies.

Thus, both mouse models were extensively monitored to identify any neurodegenerative symptoms. As expected, only the knock-in mice harbouring the variant of the human *BSCL2* transgene exhibited symptoms resembling those present in humans with Celia encephalopathy. The symptoms included weight stagnation, abnormal limb crossing, kyphosis, tremors, myoclonus, tail spasticity, and paraparesis or paraplegia. Consistent with the human condition, these symptoms appeared early in life and progressively worsened until the animals succumbed to severe encephalopathic conditions, resulting in dramatically reduced life expectancy. However, despite the notable similarities with Celia encephalopathy in humans, only 11.9% of the homozygous knock-in mice exhibited evident neurodegeneration. Additionally, 5.4% of the heterozygous knock-in animals also developed this neurological phenotype, suggesting that the protective mechanism of wild type seipin, proposed in humans, may not be the same in the mouse brain. This may be due to differences in the seipin protein between mice and humans, as well as interspecies differences in the expression patterns of the *Bscl2*/*BSCL2* genes across different brain regions.

Additional studies were conducted to delve into the foundations of neurodegeneration, considering the possible variations among severely affected animals, heterozygotes, and homozygotes. It is important to note that both severely affected animals exhibited increased proliferation of glial cells in the thoracic marrow, consistent with the observed phenotype of kyphosis, paraparesis, or paraplegia. Furthermore, brain examinations revealed a patchy loss of Purkinje cells and distinctive alterations of glial cells in the cerebellum of these severely affected animals. Interestingly, it was expected that regions with higher expression of the Celia *BSCL2* transgene would exhibit greater brain damage. However, in severely affected mice, elevated transgene expression was only evident in the cortex of homozygous animals. In contrast, positron emission tomography results indicated reduced glucose uptake in the cortex of heterozygous animals, but not in homozygous ones. In humans, areas with the highest expression of Celia *BSCL2* include the pituitary gland and cerebellum, and the occipital lobes showed the most significant reduction in glucose uptake. The discrepancies between the mouse model and human patients may be attributed to several factors. On one hand, the mouse brain is much smaller compared to that of humans, making regional analysis challenging in mouse samples. Additionally, possible differences in the expression patterns of *Bscl2*/*BSCL2* genes in tissues and brain regions between mice and humans could contribute to the observed discrepancies.

Additionally, several studies have proposed an association between seipin and various organelles of the endoplasmic reticulum, including mitochondria and peroxisomes. Our previous research suggested a relationship between the expression of *BSCL2* in human brains

and genes that encode protective enzymes against oxidative stress. Although our findings in the present study did not perfectly align with those found in human brains, severely affected animals exhibited a notable reduction in the expression of *Sod1* and *Sod2* in the cortex. This implies a possible role of seipin in peroxisome biogenesis and suggests that its deficiency could affect genes associated with mitochondrial and peroxisomal function in the brain, thereby contributing to the pathogenesis of Celia's encephalopathy.

Understanding the spectrum of behaviour is crucial for assessing the impact of brain disorders, such as neurodegenerative diseases. To this end, various behavioural tests were conducted to evaluate both motor and cognitive functions. Severely affected animals, whether heterozygous or homozygous, showed decreased locomotor activity and increased anxiety. Similarly, non-severely affected homozygous animals exhibited reduced locomotor activity, increased anxiety, and impaired coordination. However, no discernible alterations in cognitive or memory functions were observed. Interestingly, these discrepancies in behavioural and psychomotor studies were not evident when comparing homozygous animals from both murine models, knock-in and knock-out. This suggests that the differences observed with wild type animals may be due to the absence of the murine *Bscl2* gene rather than the presence of the aberrant human transgene.

Moreover, it could be assumed that the promoter is functioning correctly, although the lack of a specific antibody for Celia seipin complicates the execution of more detailed studies to reveal the underlying pathogenic mechanism of these findings. However, the possible ubiquitination observed in the deep layers of the cerebellum in severely affected homozygous mice suggests the presence of nuclear inclusions reactive to ubiquitin positive for seipin. This strongly suggests a pathogenic mechanism similar to that observed in humans. Thus, these findings underscore the idea that the abnormal aggregation and accumulation of the Celia seipin variant may serve as a focal point in the pathogenesis of Celia's encephalopathy, potentially operating through a toxic gain-of-function mechanism.

In addition to the neurological characteristics observed in these severely affected animals, the severely affected homozygous animals exhibited severe generalized lipodystrophy along with mild hepatic steatosis. The levels of triglycerides in serum and in the liver, as well as glucose metabolism, remained within normal ranges, with no insulin resistance, but with severe hypoleptinemia. In contrast, the non-severely affected homozygous mice, both knock-in and knock-out, exhibited a marked decrease in adipose tissue and severe hypoleptinemia similar to that of the neurologically affected mice. However, despite this, they showed hyperinsulinemia, insulin resistance, and a progressive increase in serum triglyceride concentration over time. These metabolic characteristics reflect those observed in both generalized congenital lipodystrophy type 2 and progressive encephalopathy with or without lipodystrophy in humans, although without the presence of diabetes mellitus or hypertriglyceridemia.

In both models of homozygous knock-out and knock-in mice, regardless of whether they were severely affected or not, the absence of white fat (inguinal and gonadal) was almost complete,

with areas of fibrosis and smaller adipocytes. However, the amount of brown fat (interscapular) was lower than reported in most other studies, with adipocytes presenting larger lipid vacuoles and areas of necrosis. On the other hand, ectopic fat deposition in the liver of non-severely affected homozygous mice led to pronounced hepatomegaly, accompanied by mixed hepatic steatosis predominantly of the macrovesicular type. This condition progressed to steatohepatitis and fibrosis over time, but despite the long follow-up of liver evolution in both mouse models, no evidence of cirrhosis was observed. Surprisingly, severely affected homozygous mice presented moderate steatosis. These findings contrast with the natural history of the disease in humans, where the development of steatohepatitis associated with metabolic dysfunction and fibrosis is a frequent and early event. Additionally, both non-severely affected knock-in and knock-out homozygous animals exhibited significant accumulation of triglycerides in the liver. The precise mechanisms driving these observations are still unclear, indicating a possible disparity between the hepatic physiology of mice and humans regarding the lipotoxicity of hepatocytes. Furthermore, homozygous animals, regardless of being knock-in or knock-out, showed enlargement of the spleen, heart, and kidneys. Also, along with the severely affected ones, they displayed renal damage characterized by diffuse mesangial expansion and arteriolar hyalinosis.

Clinical evidence suggests that there are often significant gender differences in the genetic forms of lipodystrophy, indicating that female patients frequently exhibit a more severe physical and metabolic phenotype compared to male patients. This phenomenon is not limited to the clinical expression of lipodystrophy, but it may also influence associated complications and treatment responses. However, sexual dimorphism has not been clearly evident in the current murine models. Consequently, the diversification of adipose metabolic control and neurological outcomes between women and men, as well as between humans and mice, or among different variants in generalized congenital lipodystrophy type 2, is not yet fully defined and requires further research to elucidate the underlying mechanisms.

In summary, the results presented in this thesis provide a global murine model of Celia's encephalopathy, which partially reflects the severe neurodegenerative profile suffered by these patients. Furthermore, this study presented a global murine model with seipin depletion, effectively replicating the typical phenotype of generalized congenital lipodystrophy, thereby serving as a valuable tool for studying this disease. Although these models may not perfectly mimic human conditions, they represent significant advancements in developing preclinical tools for investigating pathogenesis and exploring potential therapeutic interventions for seipinopathies, including Celia's encephalopathy and generalized congenital lipodystrophy type 2. Continuous improvement and further characterization of these animal models will be imperative to bridge the gap between the murine and human manifestations of these rare genetic disorders. A detailed understanding of signalling pathways and cellular responses in different generic contexts could provide critical insights to more effectively address the clinical challenges associated with these diseases.

RESUMEN

El gen humano *BSCL2* se encuentra ubicado en el cromosoma 11q12.3. Este gen codifica para la seipina, una proteína residente del retículo endoplasmático que presenta dos dominios transmembrana, un bucle intraluminal y dos colas amino y carboxilo-terminales en el citoplasma. En los seres humanos, la seipina forma homooligómeros de 11 unidades que constituyen un toroide. La función principal de la seipina, una proteína altamente conservada evolutivamente, es modular la formación de gotitas lipídicas. La seipina actúa en la interfaz entre las gotas lipídicas y el retículo endoplasmático, desempeñando un papel crítico en la formación temprana de gotas lipídicas normales y en el mantenimiento de las gotas lipídicas maduras. Además, está implicada en la regulación de la síntesis de triglicéridos y fosfolípidos, así como en la participación en la transmisión del impulso nervioso en neuronas. Este último aspecto destaca su importancia no solo en procesos metabólicos, sino también en el correcto funcionamiento del sistema nervioso. Tres isoformas de seipina son principalmente codificadas por este gen, de 462 (*BSCL2*-203/227/217), 398 (*BSCL2*-205/207/210) y 287 (*BSCL2*-201) aminoácidos de longitud, respectivamente. En los seres humanos, este gen tiene su mayor expresión no en el tejido adiposo, como se esperaría, sino en el sistema nervioso central, la hipófisis y los testículos. *BSCL2*-203/227/217 se expresa principalmente en el cerebro (80%), mientras que en otros tejidos la expresión de los transcritos *BSCL2*-203/227/217 y *BSCL2*-205/207/210 es similar, y la expresión de *BSCL2*-201 es insignificante en todos los tejidos (<1%).

La lipodistrofia congénita generalizada tipo 2 es un trastorno autosómico recesivo muy raro debido a variantes patogénicas en el gen *BSCL2*. Los pacientes suelen presentar una ausencia generalizada de tejido adiposo que es evidente desde el nacimiento o durante el primer año de vida. Esta falta de tejido adiposo resulta en músculos bien definidos, dándoles una apariencia robusta y hercúlea a medida que envejecen. Además, estos pacientes presentan hiperinsulinemia a una edad temprana, hipoleptinemia, hipoadiponectinemia e hipertrigliceridemia, y desarrollan diabetes mellitus no cetogénica en la segunda década de vida. La deposición ectópica de grasa en el hígado conduce a esteatosis hepática, lo que explica la hepatomegalia importante, que puede progresar a cirrosis. Debido a su grave resistencia a la insulina, estos niños desarrollan acantosis nigricans ya en los primeros años de vida, indicando una disfunción grave en el metabolismo de la glucosa y los lípidos. Además, las complicaciones cardíacas y la lesión renal son habitualmente observadas en estos pacientes. A diferencia de otros subtipos de lipodistrofia congénita generalizada, estos pacientes suelen tener un grado de discapacidad intelectual de leve a moderada. A nivel molecular, la mayoría de los casos de lipodistrofia congénita generalizada tipo 2 surgen de

variantes homocigotas o heterocigotas compuestas. Estas variantes a menudo dan lugar a codones de parada prematuros o variantes de cambio de marco, causando una pérdida de función de la seipina.

Por otro lado, variantes específicas de sentido erróneo heterocigotas en *BSCL2* pueden dar lugar a un amplio espectro de enfermedades de las neuronas motoras superiores y/o inferiores. Estas variantes provocan la formación de estructuras anormales de la seipina, contribuyendo a trastornos neurológicos diversos, como el síndrome de Silver (también conocido como paraplejía espástica tipo 17) y la neuropatía motora distal hereditaria autosómica dominante-13.

En 2013, nuestro grupo describió una nueva enfermedad neurodegenerativa infantil, la encefalopatía de Celia, o encefalopatía progresiva con o sin lipodistrofia. Esta enfermedad podría considerarse como una variante particular de la lipodistrofia congénita generalizada tipo 2 con un cuadro neurológico devastador. Esta enfermedad extremadamente rara se debe a diferentes variantes en el gen *BSCL2*. La más común y la primera descrita fue la variante c.985C>T, en el exón 7, en homocigosis o en heterocigosis compuesta. Los pacientes homocigotos pueden no mostrar características típicas de la lipodistrofia generalizada, pero podrían tener hipertrigliceridemia y hepatomegalia. Sin embargo, algunos casos homocigotos exhibieron lipodistrofia. Por el contrario, los heterocigotos compuestos suelen mostrar signos de lipodistrofia generalizada congénita tipo 2 de forma temprana en la infancia. Neurológicamente, estos pacientes experimentan retraso psicomotor con deterioro significativo del lenguaje desde los dos años de edad. La regresión neurológica comienza a los 3-4 años de edad y se caracteriza por una pérdida gradual de las habilidades previamente adquiridas. Con el paso del tiempo, el perfil neurodegenerativo se hace más pronunciado con un inicio repentino de epilepsia mioclónica severa, tetraparesia espástica y encefalopatía grave. Esta evolución rápida de los síntomas neurodegenerativos es una característica clave de la enfermedad. La encefalopatía de Celia carece actualmente de cura, y la causa típica de muerte suele ser el deterioro general de la salud del paciente antes de los nueve años de edad.

La variante c.985C>T situada en el exón 7 del transcrito *BSCL2*-203/227/217 induce cambios en el empalme que llevan al salto del exón 7, lo que resulta en una variante de seipina que carece del segundo dominio transmembrana. Esta pérdida estructural compromete la función de la proteína, dando lugar a una nueva forma aberrante de seipina, denominada seipina de Celia, que incluye 64 aminoácidos adicionales. La expresión de este transcrito Celia *BSCL2* está elevada tanto en tejidos neurales como no neurales de individuos afectados, lo que potencialmente influye en la progresión de la enfermedad. De este modo, la sobreexpresión de formas aberrantes de seipina sugiere un proceso de ganancia de función tóxica. La seipina de Celia desencadena estrés oxidativo y de retículo endoplásmico, lo que lleva a la dilatación del retículo endoplásmico y a la formación de inclusiones nucleares que contienen seipina. Esto sugiere que el daño neuronal desencadenado por el estrés del retículo endoplásmico en la encefalopatía de Celia puede promover la translocación de moléculas de seipina al nucleoplasma. Esta translocación podría llevar a una oligomerización y agregación defectuosa

de la seipina de Celia, contribuyendo de este modo a la patogénesis de la encefalopatía de Celia, similar a los mecanismos observados en la enfermedad de Huntington. Es interesante destacar que los portadores heterocigotos simples permanecen asintomáticos, posiblemente debido a la interacción entre la seipina tipo salvaje y la seipina de Celia. La seipina de tipo salvaje podría potencialmente secuestrar a la seipina de Celia en oligómeros mixtos, mitigando así los efectos tóxicos. Este fenómeno de rescate por parte de la seipina tipo salvaje es un concepto nuevo en enfermedades neurodegenerativas causadas por el mal plegamiento de proteínas. Además, la disfunción de los peroxisomas, abundantes en las neuronas y que desempeñan un papel vital en la defensa contra el estrés oxidativo, puede contribuir al fenotipo neurodegenerativo observado en esta enfermedad.

El conocimiento de los mecanismos patogénicos de la encefalopatía de Celia, de los cuales nuestro grupo ya ha elucidado parte, implica el desarrollo de modelos biológicos de la enfermedad, dada su baja prevalencia, gravedad y el cerebro como el órgano principalmente afectado, lo que dificulta su estudio en humanos. En este contexto, el objetivo general de esta tesis radica en mejorar la comprensión de los mecanismos moleculares subyacentes a la neurodegeneración, la lipodistrofia y la esteatohepatitis no alcohólica de la encefalopatía de Celia mediante el uso de dos modelos murinos. Por ello, este estudio generó el primer modelo murino global del transcrito humano *BSCL2* aberrante utilizando una estrategia basada en recombinación Cre/loxP. Simultáneamente, se creó un modelo murino global deficiente en seipina al sustituir por primera vez el codón de inicio ATG por un *cassette* invertido que induce la interrupción ubicua de la proteína seipina.

Esto permitió un análisis comparativo detallado entre la lipodistrofia congénita generalizada tipo 2 y la encefalopatía progresiva con o sin lipodistrofia, facilitando un estudio exhaustivo de las diferencias y similitudes entre ambas condiciones. Para la evaluación de las funciones motoras y cognitivas, se emplearon diferentes pruebas de comportamiento bien establecidas. Las funciones motoras fueron analizadas a través de estudios como el campo abierto, que permitió evaluar el nivel de actividad locomotora general y la exploración espontánea de los animales. Esta prueba es fundamental para detectar posibles alteraciones en la actividad física o en el movimiento debido a cambios neurológicos. El laberinto elevado en cero, por otra parte, ayudó a estudiar la ansiedad y la capacidad de navegación espacial de los animales, permitiendo comprender cómo responden a situaciones de estrés. La prueba del *rotarod*, por su parte, midió la coordinación motora y el equilibrio de los animales, mientras que la prueba de caminar sobre la barra permitió evaluar la destreza y la capacidad de movimiento preciso. Además, la prueba de suspensión por alambre fue utilizada para analizar la fuerza muscular y la resistencia, ofreciendo una visión global de las funciones motoras en estudio. En lo que respecta a la evaluación de las funciones cognitivas, el laberinto de agua de Morris fue empleado como la herramienta principal. Esta prueba es ampliamente utilizada para medir la memoria espacial y el aprendizaje, dado que requiere que los animales se orienten y encuentren una plataforma oculta en una piscina. La capacidad de recordar la localización de la plataforma en sesiones posteriores revela información sobre el estado de su memoria y la integridad de las funciones cognitivas. Para complementar estos estudios de comportamiento,

se realizó una caracterización neurológica más profunda a través de estudios histológicos, así como de la tomografía por emisión de positrones, que permitió visualizar el metabolismo cerebral y detectar anomalías en el funcionamiento del cerebro. Esta tecnología es especialmente útil para identificar áreas del cerebro afectadas por alteraciones metabólicas o neurodegeneración. Además, se llevó a cabo un análisis detallado de la expresión del transcrito *BSCL2* de Celia y de otros genes mitocondriales y peroxisomales (*Pparγ*, *Pex16*, *Cat*, *Gpx1*, *Pex11g*, *Sod1*, *Sod2*), así como la expresión de la seipina de Celia en seis áreas cerebrales, lo que permitió una comprensión más clara de los mecanismos genéticos subyacentes a la encefalopatía de Celia. Junto con los estudios neurológicos, se realizó un perfil bioquímico y hematológico completo de ambos modelos. Además, se evaluaron los niveles de triglicéridos, insulina y glucosa, indicadores fundamentales para entender las alteraciones metabólicas presentes en ambos trastornos. Los tejidos hepático, renal, cardíaco y adiposo fueron evaluados desde una perspectiva histológica. En particular, en el hígado se llevó a cabo un análisis de la expresión del gen *Fgf21*, un marcador clave en el metabolismo energético. Estos análisis permitieron una comprensión integral de las posibles consecuencias multisistémicas de las patologías.

Así, ambos modelos murinos fueron monitorizados exhaustivamente para identificar cualquier síntoma neurodegenerativo. Como era de esperar, solo los ratones *knock-in* que albergaban la variante del transgén humano *BSCL2* exhibieron síntomas que se asemejaban a los presentes en humanos con la encefalopatía de Celia. Los síntomas incluyeron estancamiento ponderal, cruces anómalos de miembros, cifosis, temblores, mioclonías, espasticidad de la cola y paraparesia o paraplejía. Coherentes con la condición humana, estos síntomas aparecieron pronto en la vida y empeoraron progresivamente hasta que los animales sucumbieron a la condición encefalopática grave, lo que resultó en una esperanza de vida dramáticamente reducida. Sin embargo, a pesar de las notables similitudes con la encefalopatía de Celia en humanos, solo el 11,9% de los ratones *knock-in* homocigotos exhibieron neurodegeneración evidente. Además, el 5,4% de los animales *knock-in* heterocigotos también desarrollaron este fenotipo neurológico, lo que sugiere que el mecanismo de protección de la seipina tipo salvaje, propuesto en humanos, puede no ser el mismo en el cerebro del ratón. Esto puede deberse a que la proteína seipina en los ratones difiere de la de los humanos, pero también a que existen diferencias interespecíficas en los patrones de expresión de los genes *Bscl2*/*BSCL2* en las distintas regiones del cerebro.

Se realizaron estudios adicionales para profundizar en los fundamentos de la neurodegeneración, considerando las posibles variaciones entre animales gravemente afectados, heterocigotos y homocigotos. Es importante destacar que ambos animales gravemente afectados mostraron una proliferación aumentada de células gliales en la médula espinal torácica, coherente con el fenotipo observado de cifosis, paraparesia o paraplejía. Además, los exámenes cerebrales revelaron una pérdida parcheada de células de Purkinje y alteraciones distintivas de células gliales en el cerebelo de estos animales gravemente afectados. Curiosamente, se esperaba que las regiones con una mayor expresión del transgén Celia *BSCL2* manifestaran un mayor daño cerebral. Sin embargo, en los ratones gravemente

afectados, la expresión elevada del transgén solo fue evidente en el córtex de los animales homocigotos. En contraposición, los resultados de la tomografía por emisión de positrones indicaron una captación reducida de glucosa en el córtex de los heterocigotos, pero no en los homocigotos. En humanos, las áreas con mayor expresión de Celia *BSCL2* incluyen la hipófisis y el cerebelo, y los lóbulos occipitales mostraron la reducción más significativa en la captación de glucosa. Las discrepancias entre el modelo murino y los pacientes humanos pueden atribuirse a varios factores. Por un lado, el cerebro del ratón es mucho más pequeño en comparación con el humano, lo que hace que el análisis por regiones sea un desafío en las muestras murinas. Pero también las posibles diferencias en los patrones de expresión de los genes *Bscl2*/*BSCL2* en los tejidos y regiones cerebrales entre ratones y humanos podrían contribuir a las discrepancias observadas.

Además, varios estudios propusieron una asociación entre la seipina y diversos orgánulos del retículo endoplasmático, incluidas las mitocondrias y los peroxisomas. Nuestra investigación anterior sugirió una relación entre la expresión de *BSCL2* en cerebros humanos y genes que codifican enzimas protectoras contra el estrés oxidativo. Aunque nuestros hallazgos en el presente estudio no se alinearon perfectamente con los encontrados en cerebros humanos, los animales gravemente afectados exhibieron una notable reducción en la expresión de *Sod1* y *Sod2* en la corteza. Esto implica un posible papel de la seipina en la biogénesis de peroxisomas y sugiere que su deficiencia podría afectar genes asociados con la función mitocondrial y de peroxisomas en el cerebro, contribuyendo de esta manera a la patogénesis de la encefalopatía de Celia.

La comprensión del espectro de comportamiento es crucial para evaluar el impacto de los trastornos cerebrales, como las enfermedades neurodegenerativas. Con este fin, se realizaron diversas pruebas de comportamiento para evaluar tanto las funciones motoras como las cognitivas. Los animales gravemente afectados, ya sean heterocigotos o homocigotos, mostraron actividades locomotoras disminuidas y ansiedad aumentada. De igual manera, los animales homocigotos no gravemente afectados exhibieron actividades locomotoras reducidas, ansiedad aumentada y coordinación deteriorada. Sin embargo, no se observaron alteraciones discernibles en las funciones cognitivas o de memoria. Curiosamente, estas discrepancias en los estudios de comportamiento y psicomotricidad no se evidenciaron al comparar animales homocigotos de ambos modelos murinos, *knock-in* y *knock-out*. Esto sugiere que las diferencias observadas con los animales tipo salvaje pueden deberse a la ausencia del gen *Bscl2* murino en lugar de la presencia del transgén humano aberrante.

Además, se podría asumir que el promotor está funcionando correctamente, aunque la falta de un anticuerpo específico para Celia-seipina dificulta la realización de estudios más detallados para revelar el mecanismo patogénico subyacente a estos hallazgos. Sin embargo, la posible ubiquitinación observada en las capas profundas del cerebelo en ratones homocigotos gravemente afectados sugiere la presencia de inclusiones nucleares reactivas a la ubiquitina positiva para la seipina. Esto sugiere fuertemente un mecanismo patogénico similar al observado en humanos. Así pues, estos hallazgos subrayan la idea de que la agregación y

acumulación anormales de la variante de Celia-seipina pueden servir como un punto focal en la patogénesis de la encefalopatía de Celia, operando potencialmente a través de un mecanismo de ganancia tóxica de función.

Unidos a las características neurológicas observadas en estos animales gravemente afectados, los animales homocigotos severamente afectados mostraron una lipodistrofia generalizada grave junto con esteatosis hepática leve. Los niveles de triglicéridos en suero y en el hígado, así como el metabolismo de la glucosa, permanecieron dentro de rangos normales, sin resistencia a la insulina, pero con hipoleptinemia grave. Por el contrario, los ratones homocigotos no gravemente afectados, tanto *knock-in* como *knock-out*, exhibieron una pronunciada disminución del tejido adiposo y una hipoleptinemia grave similar a la de los ratones afectados neurológicamente. Sin embargo, a pesar de esto, mostraron hiperinsulinemia, resistencia a la insulina y un aumento progresivo en la concentración de triglicéridos en suero con el tiempo. Estas características metabólicas reflejan las observadas tanto en la lipodistrofia congénita generalizada tipo 2 como en la encefalopatía progresiva con o sin lipodistrofia en humanos, aunque sin la presencia de diabetes mellitus o hipertrigliceridemia.

En ambos modelos de ratos homocigotos *knock-out* y *knock-in*, independientemente de si estaban gravemente afectados o no, la ausencia de grasa blanca (inguinal y gonadal) fue casi completa, con áreas de fibrosis y adipocitos más pequeños. Sin embargo, la cantidad de grasa parda (interescapular) fue menor que la reportada en la mayoría de los otros estudios, con adipocitos que presentaban vacuolas lipídicas más grandes y áreas de necrosis. Por otra parte, la deposición ectópica de grasa en el hígado de los ratos homocigotos no gravemente afectados condujo a una hepatomegalia pronunciada, acompañada de una esteatosis hepática mixta predominantemente del tipo macrovesicular. Esta condición progresó a esteatohepatitis y fibrosis con el tiempo, pero, a pesar del largo seguimiento de la evolución hepática en ambos modelos murinos, no se observó evidencia de cirrosis. Sorprendentemente, los ratos homocigotos gravemente afectados presentaron una esteatosis moderada. Estos hallazgos contrastan con la historia natural de la enfermedad en humanos, donde el desarrollo de esteatohepatitis asociada a disfunción metabólica y fibrosis es un evento frecuente y temprano. Además, tanto los animales homocigotos *knock-in* como *knock-out* no gravemente afectados exhibieron una acumulación significativa de triglicéridos en el hígado. Los mecanismos precisos que impulsan estas observaciones aún no están claros, lo que indica una posible disparidad entre la fisiología hepática de los ratones y los humanos respecto a la lipotoxicidad de los hepatocitos. Además, los animales homocigotos, independientemente de ser *knock-in* o *knock-out*, mostraron agrandamiento del bazo, el corazón y los riñones. También, junto con los gravemente afectados, mostraron daño renal caracterizado por una expansión mesangial difusa y una hialinización arteriolar.

La evidencia clínica sugiere que a menudo existen diferencias significativas de género en las formas genéticas de lipodistrofia, evidenciando que, a menudo, las pacientes femeninas muestran un fenotipo físico y metabólico más grave en comparación con los pacientes

masculinos. Este fenómeno no se limita solo a la expresión clínica de la lipodistrofia, sino que también puede influir en las complicaciones asociadas y en la respuesta al tratamiento. Sin embargo, el dimorfismo sexual no ha sido claramente evidente en los modelos murinos actuales. En consecuencia, la diversificación del control metabólico adiposo y los resultados neurológicos entre mujeres y hombres, así como entre humanos y ratones, o entre diferentes variantes en la lipodistrofia congénita generalizada tipo 2, aún no está completamente definida y requiere más investigaciones para elucidar los mecanismos subyacentes.

En definitiva, los resultados mostrados en esta tesis presentan un modelo murino global de la encefalopatía de Celia, que refleja parcialmente el cuadro neurodegenerativo grave sufrido por estos pacientes. Además, este estudio presentó un modelo murino global con depleción de seipina, que replica efectivamente el fenotipo típico de la lipodistrofia congénita generalizada, sirviendo así como una herramienta valiosa para estudiar esta enfermedad. Aunque estos modelos pueden no imitar perfectamente las condiciones humanas, representan avances significativos en el desarrollo de herramientas preclínicas para la investigación de la patogénesis y para la exploración de intervenciones terapéuticas potenciales para las seipinopatías, incluida la encefalopatía de Celia y la lipodistrofia congénita generalizada tipo 2. La mejora continua y la caracterización adicional de estos modelos animales serán imperativas para cerrar la brecha entre las manifestaciones murinas y humanas de estos trastornos genéticos raros. La comprensión detallada de las vías de señalización y las respuestas celulares en diferentes contextos genéricos podría proporcionar información crítica para abordar de manera más efectiva los desafíos clínicos asociados con estas enfermedades.

RESUMO

O xene humano *BSCL2*, atópase situado no cromosoma 11q12.3. Este xene codifica para a seipina, unha proteína residente do retículo endoplasmático con dous dominios transmembrana, un bucle intraluminal e dúas colas amino e carboxilo-terminais no citoplasma. Nos seres humanos, a seipina forma homooligómeros de 11 unidades que constitúen un toroide. A función principal da seipina, unha proteína altamente conservada evolutivamente, é modular a formación de pingas lipídicas. A seipina opera na interfaz das pingas lipídicas e do retículo endoplasmático, desempeñando un papel crítico na formación temperá de pingas lipídicas normais e no mantemento das pingas lipídicas maduras. Ademais, está implicada na regulación da síntese de triglicéridos e fosfolípidos, así como na participación na transmisión do impulso nervioso en neuronas. Este último aspecto resalta a súa importancia non só en procesos metabólicos, senón tamén no correcto funcionamento do sistema nervioso. Tres isoformas de seipina son principalmente codificadas por este xene, de 462 (*BSCL2*-203/227/217), 398 (*BSCL2*-205/207/210) e 287 (*BSCL2*-201) aminoácidos de lonxitude, respectivamente. Nos seres humanos, este xene ten a súa maior expresión, non no tecido adiposo como se esperaría, senón no sistema nervioso central, a hipófise e os testículos. *BSCL2*-203/227/217 exprésase principalmente no cerebro (80%), mentres que noutros tecidos a expresión dos transcritos *BSCL2*-203/227/217 e *BSCL2*-205/207/210 é similar, e a expresión de *BSCL2*-201 é insignificante en todos os tecidos (<1%).

A lipodistrofia conxénita xeneralizada tipo 2 é un trastorno autosómico recesivo moi raro debido a variantes patoxénicas no xene *BSCL2*. Os pacientes adoitan presentar unha ausencia xeneralizada de tecido adiposo que é evidente dende o nacemento ou durante o primeiro ano de vida. Esta falta de tecido adiposo resulta en músculos ben definidos, dándolles unha aparencia robusta e hercúlea a medida que envellecen. Ademais, estes pacientes presentan hiperinsulinemia a unha idade temperá, hipoleptinemia, hipoadiponectinemia e hipertrigliceridemia, e desenvolven diabetes mellitus non cetoxénica na segunda década de vida. A deposición ectópica de graxa no fígado conduce a esteatose hepática, o que explica a hepatomegalia importante, que pode progresar a cirrose. Debido a súa resistencia á insulina grave, estes nenos desenvolven acantose nigricans xa nos primeiros anos de vida, indicando unha disfunción grave no metabolismo da glicosa e lípidos. Ademais, as complicacións cardíacas e a lesión renal son habitualmente observadas nestes pacientes. A diferenza de outros subtipos de lipodistrofia conxénita xeneralizada, estes pacientes adoitan ter un grado de discapacidade intelectual de leve a moderada. A nivel molecular, a maioría dos casos de lipodistrofía conxénita xeneralizada tipo 2 xorden de variantes homocigotas ou heterocigotas

compostas. Estas variantes a miúdo dan lugar a codóns de parada prematuros ou variantes de cambio de marco, causando unha perda da función de seipina.

Por outra banda, variantes específicas de sentido erróneo heterocigotas en *BSCL2* poden dar lugar a un amplo espectro de enfermidades das neuronas motoras superiores e/ou inferiores. Estas variantes provocan a formación de estruturas anormais da seipina, contribuíndo a trastornos neurolóxicos diversos, como o síndrome de Silver (tamén coñecido como paraplexía espástica tipo 17) e a neuropatía motora distal hereditaria autosómica dominante-13.

En 2013, o noso grupo describiu unha nova enfermidade neurodexenerativa infantil, a encefalopatía de Celia, ou encefalopatía progresiva con ou sen lipodistrofia. Esta enfermidade podería considerarse como unha variante particular da lipodistrofia conxénita xeneralizada tipo 2 cun cadro neurolóxico devastador. Esta enfermidade extremadamente rara débese a diferentes variantes no xene *BSCL2*. A máis común e a primeira descrita foi a variante c.985C>T, no exón 7, en homocigosis ou en heterocigosis composta. Os pacientes homocigotos poden non amosar características típicas da lipodistrofia xeneralizada, pero poderían ter hipertrigliceridemia e hepatomegalia. Sen embargo, algúns casos homocigotos exhibiron lipodistrofia. Pola contra, os heterocigotos compostos adoitan amosar signos de lipodistrofia xeneralizada conxénita tipo 2 de forma temperá na infancia. Neurolóxicamente, estes pacientes experimentan retraso psicomotor con deterioro significativo da linguaxe dende os dous anos de idade. A regresión neurolóxica comeza aos 3-4 anos de idade, e caracterízase por unha perda gradual das habilidades previamente adquiridas. Co paso do tempo, o perfil neurodexenerativo faise máis pronunciado cun inicio repentino de epilepsia mioclónica severa, tetraparesia espástica e encefalopatía grave. Esta evolución rápida dos síntomas neurodexenerativos é unha característica clave da enfermidade. A encefalopatía de Celia carece actualmente de cura, e a causa típica de morte adoita ser o deterioro xeral da saúde do paciente antes dos nove anos de idade.

A variante c.985C>T situada no exón 7 do tránscrito *BSCL2*-203/227/217 induce cambios no empalme que levan ao salto do exón 7, o que resulta nunha variante de seipina que carece do segundo dominio transmembrana. Esta perda estrutural compromete a función da proteína, dando lugar a unha nova forma aberrante de seipina, denominada seipina de Celia, que inclúe 64 aminoácidos adicionais. A expresión deste tránscrito Celia *BSCL2* está elevada tanto en tecidos neurais como non neurais de individuos afectados, o que potencialmente inflúe na progresión da enfermidade. Deste xeito, a sobreexpresión de formas aberrantes de seipina suxire un proceso de ganancia de función tóxica. A seipina de Celia desencadea estrés oxidativo e de retículo endoplasmático, o que leva á dilatación do retículo endoplasmático e a formación de inclusións nucleares que conteñen seipina. Isto suxire que o dano neuronal desencadeado polo estrés do retículo endoplasmático na encefalopatía de Celia pode promover a translocación de moléculas de seipina ao nucleoplasma. Esta translocación podería levar a unha oligomerización e agregación defectuosa da seipina de Celia, contribuíndo desta maneira a patoxénese da encefalopatía de Celia, similar aos mecanismos

observados na enfermidade de Huntington. É interesante destacar que os portadores heterocigotos simples permanecen asintomáticos, posiblemente debido á interacción entre a seipina tipo silvestre e a seipina de Celia. A seipina de tipo silvestre podería potencialmente secuestrar a seipina de Celia en oligómeros mixtos, mitigando así os efectos tóxicos. Este fenómeno de rescate por parte da seipina tipo silvestre é un concepto novo en enfermidades neurodexenerativas causadas polo dobramento incorrecto de proteínas. Ademais, a disfunción dos peroxisomas, abundantes nas neuronas e que desempeñan un papel vital na defensa contra o estrés oxidativo, pode contribuír ao fenotipo neurodexenerativo observado nesta enfermidade.

O coñecemento dos mecanismos patoxénicos da encefalopatía de Celia, do cal o noso grupo xa elucidou parte, implica o desenvolvemento de modelos biolóxicos da enfermidade, dada a súa baixa prevalencia, gravidade e o cerebro como o órgano principalmente afectado, o que dificulta o seu estudo en humanos. Neste contexto, o obxectivo xeral desta tese radica en mellorar a comprensión dos mecanismos moleculares subxacentes á neurodexeneración, a lipodistrofia e a esteatohepatite non alcólica da encefalopatía de Celia mediante o emprego de dous modelos murinos. Por iso, este estudo xerou o primeiro modelo murino global do tránscrito humano *BSCL2* aberrante utilizando unha estratexia baseada en recombinación Cre/loxP. Simultaneamente, creouse un modelo murino global deficiente en seipina ao substituír por primeira vez o codón de inicio ATG cun *cassette* invertido que induce a interrupción ubicua da proteína seipina.

Isto permitiu unha análise comparativa detallada entre a lipodistrofia conxénita xeneralizada tipo 2 e a encefalopatía progresiva con ou sen lipodistrofia, facilitando un estudo exhaustivo das diferenzas e semellanzas entre ambas as dúas condicións. Para a avaliación das funcións motoras e cognitivas, empregáronse diferentes probas de comportamento ben establecidas. As funcións motoras foron analizadas a través de estudos como o campo aberto, que permitiu avaliar o nivel de actividade locomotora xeral e a exploración espontánea dos animais. Esta proba é fundamental para detectar posibles alteracións na actividade física ou no movemento debido a cambios neurolóxicos. O labirinto elevado en cero por outra parte axudou a estudar a ansiedade e a capacidade de navegación espacial dos animais, permitindo comprender como responden a situacións de estrés. A proba do *rotarod*, pola súa parte, mediu a coordinación motora e o equilibrio dos animais, mentres que a proba de camiñar sobre a barra permitiu avaliar a destreza e a capacidade de movemento preciso. Ademais, a proba de suspensión por arame foi utilizada para analizar a forza muscular e a resistencia, ofrecendo unha visión global das funcións motoras en estudo. No que respecta á avaliación das funcións cognitivas, o labirinto de auga de Morris foi empregado como a ferramenta principal. Esta proba é amplamente empregada para medir a memoria espacial e a aprendizaxe, dado que require que os animais se orienten e atopen unha plataforma oculta nunha piscina. A capacidade de recordar a localización da plataforma en sesións posteriores revela información sobre o estado da súa memoria e a integridade das funcións cognitivas. Para complementar estes estudos de comportamento, realizouse unha caracterización neurolóxica máis profunda a través de estudos histolóxico, así como da tomografía por emisión de positróns, que permitiu visualizar

o metabolismo cerebral e detectar anomalías no funcionamento do cerebro. Esta tecnoloxía é especialmente útil para identificar áreas do cerebro afectadas por alteracións metabólicas ou neurodexeneración. Ademais, levouse a cabo unha análise detallada da expresión do transcrito *BSCL2* de Celia e doutros xenes mitocondriais e peroxisomais (*Pparγ*, *Pex16*, *Cat*, *Gpx1*, *Pex11g*, *Sod1*, *Sod2*), así como a expresión da seipina de Celia en seis áreas cerebrais, o que permitiu unha comprensión máis clara dos mecanismos xenéticos subxacentes á encefalopatía de Celia. Xunto cos estudos neurolóxicos, realizouse un perfil bioquímico e hematolóxico completo de ambos modelos. Ademais, avaliáronse os niveis de triglicéridos, insulina e glucosa, indicadores fundamentais para entender as alteracións metabólicas presentes en ambos os dous trastornos. Os tecidos hepático, renal, cardíaco e adiposo foron avaliados desde unha perspectiva histolóxica. En particular, no fígado levouse a cabo unha análise da expresión do xene *Fgf21*, un marcador clave no metabolismo enerxético. Estas análises permitiron unha comprensión integral das posibles consecuencias multisistémicas das patoloxías.

Deste modo, ambos modelos murinos foron monitorizados exhaustivamente para identificar calquera síntoma neurodexenerativo. Como era de agardar, só os ratos *knock-in* que albergaban a variante do transxene humano *BSCL2* exhibiron síntomas que se asemellaban aos presentes en humanos coa encefalopatía de Celia. Os síntomas incluíron estancamento ponderal, cruces anómalos de membros, cifose, tremores, mioclonías, espasticidade da cola e paraparesia ou paraplexia. Coherentes coa condición humana, estes síntomas apareceron axiña na vida e empeoraron progresivamente ata que os animais sucumbiron á condición encefalopática grave, o que resultou nunha esperanza de vida dramaticamente reducida. Sen embargo, pese ás similitudes notables coa encefalopatía de Celia en humanos, só o 11,9% dos ratos *knock-in* homocigotos exhibiron neurodexeneración evidente. Ademais, o 5,4% dos animais *knock-in* heterocigotos tamén desenvolveron este fenotipo neurolóxico, o que suxire que o mecanismo de protección da seipina tipo silvestre, proposto en humanos, pode non ser o mesmo no cerebro do rato. Isto pode deberse a que a proteína seipina nos ratos difire da dos humanos, pero tamén a que existen diferenzas interespecíficas nos patróns de expresión dos xenes *Bscl2*/*BSCL2* nas distintas rexións do cerebro.

Realizáronse estudos adicionais para afondar nos fundamentos da neurodexeneración, considerando as posibles variacións entre animais gravemente afectados, heterocigotos e homocigotos. É importante destacar que ambos animais gravemente afectados amosaron unha proliferación aumentada de células gliais na medula espinal torácica, coherente co fenotipo observado de cifose, paraparesia ou paraplexia. Ademais, os exames cerebrais revelaron unha perda parcheada de células de Purkinje e alteracións distintivas de células gliais no cerebelo destes animais gravemente afectados. Curiosamente, esperábase que as rexións cunha maior expresión do transxene Celia *BSCL2* manifestaran un maior dano cerebral. Sen embargo, en ratos gravemente afectados, a expresión elevada do transxene só foi evidente no cortex dos animais homocigotos. En contraposición, os resultados da tomografía por emisión de positróns indicaron unha captación reducida de glicosa no cortex dos heterocigotos, pero non nos homocigotos. En humanos, as áreas coa maior expresión de Celia *BSCL2* inclúen a

hipófise e o cerebelo, e os lóbulos occipitais amosaron a redución máis significativa na captación de glicosa. As discrepancias entre o modelo murino e os pacientes humanos poden atribuírse a varios factores. Por un lado, o cerebro do rato ten un tamaño moito menor en comparación co do humano, o que fai que a análise por rexións sexa desafiante nas mostras murinas. Pero tamén as posibles diferenzas nos patróns de expresión de xenes *Bscl2*/*BSCL2* nos tecidos e rexións cerebrais entre ratos e humanos podería contribuír as discrepancias observadas.

Ademais, varios estudos propuxeron unha asociación entre a seipina e diversos orgánulos do retículo endoplasmático, incluídas as mitocondrias e os peroxisomas. A nosa investigación anterior suxeriu unha relación entre a expresión de *BSCL2* en cerebros humanos e xenes que codifican enzimas protectoras contra o estrés oxidativo. Aínda que os nosos achados no presente estudo non se alinearon perfectamente cos atopados en cerebros humanos, os animais gravemente afectados exhibiron unha notable redución na expresión de *Sod1* e *Sod2* no cortex. Isto implica un posible papel da seipina na bioxénesis de peroxisomas e suxire que a súa deficiencia podería afectar xenes asociados coa función mitocondrial e de peroxisomas no cerebro, contribuíndo deste maneira a patoxénesis da encefalopatía de Celia.

A comprensión do espectro de comportamento é crucial para avaliar o impacto dos trastornos cerebrais, como as enfermidades neurodexenerativas. Con este fin, realizáronse diversas probas de comportamento, para avaliar tanto as funcións motoras como cognitivas. Os animais gravemente afectados, xa sexan heterocigotos ou homocigotos, amosaron actividades locomotoras diminuídas e ansiedade aumentada. Do mesmo xeito, os animais homocigotos non gravemente afectados exhibiron actividades locomotoras reducidas, ansiedade aumentada e coordinación deteriorada. Sen embargo, non se observaron alteracións discernibles nas funcións cognitivas ou de memoria. Curiosamente, estas discrepancias nos estudos de comportamento e psicomotricidade non se evidenciaron ao comparar animais homocigotos de ambos modelos murinos, *knock-in* e *knock-out*. Isto suxire que as diferenzas observadas cos animais tipo silvestre poden deberse á ausencia do xene *Bscl2* murino en lugar da presenza do transxene humano aberrante.

Ademais, poderíase asumir que o promotor está funcionando correctamente, aínda que a falta dun anticorpo específico para Celia-seipina dificulta a realización de estudos máis detallados para revelar o mecanismo patoxénico subxacente a estes achados. Sen embargo, a posible ubiquitinación observada nas capas profundas do cerebelo en ratos homocigotos gravemente afectados suxire a presenza de inclusións nucleares reactivas á ubiquitina positiva para a seipina. Isto suxire fortemente un mecanismo patoxénico similar ao observado en humanos. Así pois, estes achados subliñan a idea de que a agregación e acumulación anormais da variante de Celia-seipina poden servir como un punto focal na patoxénese da encefalopatía de Celia, potencialmente operando a través dun mecanismo de ganancia tóxica de función.

Unido ás características neurolóxicas observadas nestes animais gravemente afectados, os animais homocigotos severamente afectados amosaron unha lipodistrofia xeneralizada grave xunto con esteatose hepática leve. Os niveis de triglicéridos en soro e no fígado, así como o

metabolismo da glicosa, permaneceron dentro de rangos normais, sen resistencia á insulina, pero con hipoleptinemia grave. Pola contra, os ratos homocigotos non gravemente afectados, tanto *knock-in* como *knock-out*, exhibiron unha pronunciada diminución do tecido adiposo e unha hipoleptinemia grave similar á dos ratos afectados neurolóxicamente. Sen embargo, a pesar disto, amosaron hiperinsulinemia, resistencia á insulina e un aumento progresivo na concentración de triglicéridos en soro co tempo. Estas características metabólicas reflicten as observadas tanto na lipodistrofia conxénita xeneralizada tipo 2 como na encefalopatía progresiva con ou sen lipodistrofia en humanos, aínda que sen a presenza de diabetes mellitus ou hipertrigliceridemia.

En ambos modelos de ratos homocigotos *knock-out* e *knock-in*, independentemente de si estaban gravemente afectados ou non, a ausencia de graxa branca (inguinal e gonadal) foi case completa, con áreas de fibrose e adipocitos máis pequenos. Sen embargo, a cantidade de graxa parda (interescapular) foi menor ca reportada na maioría dos outros estudos, con adipocitos que presentaban vacuolas lipídicas máis grandes e áreas de necrose. Por outra banda, a deposición ectópica de graxa no fígado dos ratos homocigotos non gravemente afectados conduciu a unha hepatomegalia pronunciada, acompañada dunha esteatose hepática mixta predominantemente do tipo macrovesicular. Esta condición progresou a esteatohepatite e fibrose co tempo, pero, a pesar do longo seguimento da evolución hepática en ambos modelos murinos, non se observou evidencia de cirrose. Sorprendentemente os ratos homocigotos gravemente afectados presentaron unha esteatose moderada. Estes achados contrastan coa historia natural da enfermidade en humanos, onde o desenvolvemento de esteatohepatite asociada a disfunción metabólica e fibrose é un acontecemento frecuente e temperán. Ademais, tanto os animais homocigotos *knock-in* como *knock-out* non gravemente afectados exhibiron unha acumulación significativa de triglicéridos no fígado. Os mecanismos precisos que impulsan estas observacións aínda non están claros, o que indica unha posible disparidade entre a fisioloxía hepática de ratos e humanos respecto á lipotoxicidade dos hepatocitos. Ademais, os animais homocigotos, independentemente de ser *knock-in* ou *knock-out*, amosaron agrandamento do bazo, o corazón e os riles. Tamén, xunto cos gravemente afectados, amosaron dano renal caracterizado por unha expansión mesanxial difusa e unha hialinización arteriolar.

A evidencia clínica suxire que a miúdo existen diferenzas significativas de xénero nas formas xenéticas de lipodistrofia, evidenciando que, a miúdo, as pacientes femininas amosan un fenotipo físico e metabólico máis grave en comparación cos pacientes masculinos. Este fenómeno non se limita só á expresión clínica da lipodistrofia, senón que tamén pode influír nas complicacións asociadas e na resposta ao tratamento. Sen embargo, o dimorfismo sexual non foi claramente evidente nos modelos murinos actuais. En consecuencia, a diversificación do control metabólico adiposo e os resultados neurolóxicos entre mulleres e homes, así como entre humanos e ratos, ou entre diferentes variantes na lipodistrofia conxénita xeneralizada tipo 2, aínda non está completamente definida e require máis investigacións para elucidar os mecanismos subxacentes.

En definitiva, os resultados amosados nesta tese presentan un modelo murino global da encefalopatía de Celia, que reflicte parcialmente o cadro neurodexenerativo grave sufrido por estes pacientes. Ademais, este estudo presentou un modelo murino global con depleción de seipina, que replicando efectivamente o fenotipo típico da lipodistrofia conxénita xeneralizada, servindo así como unha ferramenta valiosa para estudar esta enfermidade. Aínda que estes modelos poden non imitar perfectamente as condicións humanas, representan avances significativos no desenvolvemento de ferramentas preclínicas para a investigación da patoxénese e para a exploración de intervencións terapéuticas potenciais para as seipinopatías, incluída a encefalopatía de Celia e a lipodistrofia conxénita xeneralizada tipo 2. A mellora continua e a caracterización adicional destes modelos animais serán imperativas para pechar a fenda entre as manifestacións murinas e humanas destes trastornos xenéticos raros. A comprensión detallada das vías de sinalización e as respostas celulares en diferentes contextos xenéricos podería proporcionar información crítica para abordar de forma máis efectiva os desafíos clínicos asociados con estas enfermidades.

ABBREVIATIONS AND ACRONYMS

[^{18}F]-FDG: [^{18}F]-2-fluoro-2-deoxy-D-glucose

Ad-B2$^{(-/-)}$: adipose tissue-specific *Bscl2* knock-out

AGPAT2: 1-acylglycerol-3-phosphate O-acyltransferase 2

ANCOVA: analysis of covariance

ApoE: apolipoprotein E

ATGL: adipocyte triglyceride lipase

BAC: bacterial artificial chromosome

BiP: binding immunoglobulin protein

BSCL2/Bscl2: *BSCL2* lipid droplet biogenesis associated, seipin

cAMP: cyclic adenosine monophosphate

CAT/Cat: catalase

CAV1: caveolin 1

CAVIN1: caveolae associated protein 1

cDNA: complementary deoxyribonucleic acid

CDS: coding sequence

Celia *BSCL2*-TG: Celia Berardinelli-Seip congenital lipodystrophy transgene

CGL: congenital generalized lipodystrophy

CGL1: congenital generalized lipodystrophy type 1

CGL2: congenital generalized lipodystrophy type 2

CGL3: congenital generalized lipodystrophy type 3

CGL4: congenital generalized lipodystrophy type 4

CHOP: C/EBP homologous protein

cm: centimetres

CNS: central nervous system

CREB: cAMP responsive element binding protein

CT: computed tomography

DAB: 3.3’-diaminobenzindine

DAG: diacylglycerol

DEN: diethylnitrosamine

DGAT: diacylglycerol O-acyltransferases

DNA: deoxyribonucleic acid

DTA: Diphtheria toxin A

EDTA: ethylenediaminetetraacetic acid

ENU: N-ethyl-N-nitrosourea

EPSC: excitatory postsynaptic current

ER: endoplasmic reticulum

ERK: extracellular signal-regulated kinase

ESC: embryonic stem cells

FGF21/*Fgf21*: Fibroblast growth factor 21

F-IRKO: fat-specific insulin receptor knock-out mice

FSGS: focal segmental glomerulosclerosis

G: gauges

g: relative centrifugal force

GCL: ganglion cell layer

GFAP: glial Fibrillary acid protein

Gng3: guanine nucleotide binding protein (G protein), gamma 3

gonWAT: gonadal white adipose tissue

GPAT3: glycerol-3-phosphate acyltransferase 3

Gpx1: glutathione peroxidase 1

GSK3β: glycogen synthase kinase-3β

GTT: glucose tolerance test

H&E: hematoxylin and eosin

HA: homology arm

HFD: high fat diet

HIV: human immunodeficiency virus

HMND13: distal hereditary motor neuropathy-13

HSL: hormone-sensitive lipase

HTF: human tubal fluid

iBAT: interscapular brown adipose tissue

IHBs intracytoplasmic hyaline bodies

IL-6: interleukin-6

ingWAT: inguinal white adipose tissue

INL: inner nuclear layer

INM inner nuclear membrane

IP3R: inositol 3 phosphate receptor

IPL: inner plexiform layer

IPSC: inhibitory postsynaptic current

IU: international units

Kg: kilograms

KI: knock-in

KO: knock-out

LD: lipid droplet

LDAF1: lipid droplet assembly factor 1

LPIN1: Lipin 1

LTP: long-term potentiation

LVH: left ventricular hypertrophy

m/v: mass per volume

MAM: mitochondria-associated membrane

MASL: metabolic-dysfunction associated steatotic liver

MASLD: metabolic dysfunction-associated steatotic liver disease

MASH: metabolic dysfunction-associated steatohepatitis

MBq: Megabecquerel

MEK: mitogen-activated protein kinase

mL: millilitres

MLEM: maximum likelihood expectation maximization

mm: millimetres

mRNA: messenger ribonucleic acid

NAFL: non-alcoholic fatty liver

NAFLD: non-alcoholic fatty liver disease

NAS: NAFLD activity score

NASH CRN: non-alcoholic steatohepatitis clinical research network

NASH: non-alcoholic steatohepatitis

NEFA: non-esterified fatty acids

Neurod1: neurogenic differentiation 1

Neurog1: neurogenin 1

NL: neutral lipid

NMDA: N-methyl-D-aspartate

NPC2: Niemann Pick type C2

ONL: outer nuclear layer

OLs: oligodendrocytes

OPCs: oligodendrocyte precursor cells

OPL: outer plexiform layer

ORP5: oxysterol binding related protein 5

ORP8: oxysterol binding related protein 8

OS: outer segment

PA: phosphatidic acid

PAS: periodic acid schiff

PELD: progressive encephalopathy with or without lipodystrophy

PET: positron emission tomography

PEX1: peroxisomal biogenesis factor 1

PEX11G/Pex11g: peroxisomal biogenesis factor 11 gamma

PEX16/Pex16: peroxisomal biogenesis factor 16

PI3K/AKT/mTOR: phosphoinositide-3 kinase/protein kinase-B/mammalian target of rapamycin

PKA: protein kinase A

PLIN1: Perilipin 1

PPARγ/*Pparγ*: peroxisome proliferator-activated receptor gamma

qPCR: quantitative real-time polymerase chain reaction

Rn18s: 18S ribosomal RNA

ROS: reactive oxygen species

RPE: retinal pigment epithelium

rpm: revolutions per minute

S.A.: severely affected

SD: standard deviation

Seipin$^{-/-}$apoE$^{-/-}$: seipin-deficient and apolipoprotein E null

Seipin-nKO: neuronal-specific seipin knock-out

SEM: standard error of mean

SERCA: sarco/endoplasmic reticulum Ca^{2+}-ATPase

SKO: seipin knock-out

SOD1/Sod1: superoxide dismutase 1

SOD2:Sod2: superoxide dismutase 2

SPG17: spastic paraplegia type 17

STZ: streptozotocin

SUV_{mean}: standardized uptake value

TAG: triacylglycerol

TMD: transmembrane domain

TRL: triacylglycerol-rich lipoproteins

UPR: unfolded protein response

v/v: volume per volume

VDAC: voltage-dependent anion channel

VLDL: very low-density lipoproteins

VOI: volumes of interest

WAT: white adipose tissue

WNT3: proto-oncogene Wnt-3

LIST OF PUBLICATIONS

Title
Celia's Encephalopathy (*BSCL2*-Gene-Related): Current Understanding
Authors and affiliation
Sofía Sánchez-Iglesias[1], Antía Fernández-Pombo[1,2], Silvia Cobelo-Gómez[1], Álvaro Hermida-Ameijeiras[1,3], Helena Alarcón-Martínez[4], Rosario Domingo-Jiménez[4], Alejandro Iván Ruíz Riquelme[5], Jesús R. Requena[6] and David Araújo-Vilar[1,2] *[1] UETeM-Molecular Pathology Group, Department of Psychiatry, Radiology, Public Health, Nursing and Medicine, IDIS-CIMUS, University of Santiago de Compostela, 15782 Santiago de Compostela, Spain* *[2] Division of Endocrinology and Nutrition, University Clinical Hospital of Santiago de Compostela, 15706 Santiago de Compostela, Spain* *[3] Division of Internal Medicine, University Clinical Hospital of Santiago de Compostela, 15706 Santiago de Compostela, Spain* *[4] Department of Pediatric Neurology, Hospital Virgen de la Arrixaca and IMIB-Arrixaca, CIBERER-ISCIII, 28029 Madrid, Spain* *[5] German Center for Neurodegenerative Diseases (DZNE), 72076 Tübingen, Germany* *[6] Prion Laboratory, CIMUS Biomedical Research Institute, University of Santiago de Compostela-IDIS, Santiago de Compostela, 15782 Santiago de Compostela, Spain*
Date of publication
April 2021

Journal	**Publisher**	**ISSN**	***Volume* (number), pages**
Journal of Clinical Medicine	MDPI	2077-0383	*10* (7),1435

Impact factor	**Journal citation indicator Rank**	**Journal citation indicator Quartile**
4.964	48/329	Q1

Specific contribution of the PhD candidate to the article
Silvia Cobelo Gómez was responsible for the writing-review and editing.
Content included in
Introduction.
DOI
https://doi.org/10.3390/jcm10071435
Link to the article
https://www.mdpi.com/2077-0383/10/7/1435
Journal authorisation
This thesis has the authorisation of the journal for the reproduction of this Article because is in Open Access under a Creative Commons license (https://creativecommons.org/licenses/by/4.0/).

Title
A murine model of *BSCL2*-associated Celia's encephalopathy

Authors and affiliation
Silvia Cobelo-Gómez[a], Sofía Sánchez-Iglesias[a], Alberto Rábano[b], Ana Senra[c], Pablo Aguiar[d,e], Noemí Gómez-Lado[d,e], Lara García-Varela[d,e], Iván Burgueño-García[b], Laura Lampón-Fernández[a], Antía Fernández-Pombo[a,f], Everardo Josué Díaz-López[a,f], Teresa Prado-Moraña[a,f], Beatriz San Millán[g,h], David Araújo-Vilar[a,f] [a] *UETeM-Molecular Pathology Group. Department of Psychiatry, Radiology, Public Health, Nursing and Medicine, IDIS-CIMUS, University of Santiago de Compostela, Spain* [b] *Alzheimer's Disease Research Unit, CIEN Foundation, Queen Sofia Foundation Alzheimer Center, Madrid, Spain* [c] *Department of Physiology, CIMUS, University of Santiago de Compostela, Spain* [d] *Molecular Imaging and Medical Physics, University of Santiago de Compostela-IDIS, Spain* [e] *Nuclear Medicine and Molecular Imaging Group, IDIS, University Clinical Hospital of Santiago de Compostela, Spain* [f] *Division of Endocrinology and Nutrition, University Clinical Hospital of Santiago de Compostela, Spain* [g] *Grupo de Enfermedades Raras y Medicina Pedi´atrica, Instituto de Investigaci´on Sanitaria Galicia Sur (IISGS), Vigo, Spain* [h] *Pathology Department, Alvaro Cunqueiro Hospital, Vigo, Spain*

Date of publication
September 2023

Journal	Publisher	ISSN	*Volume*
Neurobiology of Disease	ELSEVIER	1095-953X	***187***

Impact factor	Journal citation indicator Rank	Journal citation indicator Quartile
6.1	47/306	Q1

Specific contribution of the PhD candidate to the article
Silvia Cobelo Gómez was responsible for the conceptualization, formal analysis, investigation, methodology, visualization, writing-original draft and writing-review and editing.
Content included in
Material and methods and results.
DOI
https://doi.org/10.1016/j.nbd.2023.106300
Link to the article
https://www.sciencedirect.com/science/article/pii/S0969996123003157?via%3Dihub
Journal authorisation
This thesis has the authorisation of the journal for the reproduction of this Article because is in Open Access under a Creative Commons license (https://creativecommons.org/licenses/by-nc-nd/4.0/).

INDEX

LIST OF TABLES

LIST OF FIGURES

LIST OF ANNEXES

1 INTRODUCTION

1.1 *BSCL2* GENE

The human *BSCL2* gene, also known as seipin (OMIM #606158; HGNC:15832), is situated on chromosome 11q12.3 and has up to 27 reported transcripts. This gene primarily codes for three seipin isoforms under natural conditions as outlined in **Table 1**. Specifically, three transcripts encode isoform 1 (*BSCL2*-203/227/217), three code for isoform 2 (*BSCL2*-205/207/210), and one encodes isoform 3 (*BSCL2*-201). The initial transcript described was *BSCL2*-205/207/210, identified by Magre et al. (1), which comprises 11 exons with protein coding commencing on exon 2 and concluding in exon 11. This results in a 398 amino acid protein featuring two strongly predicted transmembrane domains (TMDs) coded in exons 2 and 7. In contrast, *BSCL2*-203/227/217 is a longer transcript generated with an alternative first exon (exon 1 and part of exon 2). This transcript, similar to *BSCL2*-205/207/210, includes an N-terminal extension of 64 amino acids, resulting in a 462 amino acid protein (2, 3). Furthermore, *BSCL2*-201 differs from the other transcripts by skipping exon 7, leading to a shortened and altered carboxy terminus in exon 10 and producing a protein of 287 amino acids (2, 3). Additionally, there is one transcript encoding a 464 amino acid protein with a unique 6-base insertion in exon 9 (3).

The expression pattern of the human *BSCL2* gene reveals significant localization in the testes and in the central nervous system (CNS) and pituitary. Notably, *BSCL2* mRNA expression is moderate in adipose tissue, pancreas, kidney, skeletal muscle, liver, ovary, and prostate, while being weak in other tissues (1). Variations exist in the expression levels of different *BSCL2* transcripts. The *BSCL2*-203/227/217 transcript exhibits predominant expression in the CNS (80%), whereas in other tissues, the expression of *BSCL2*-203/227/217 and *BSCL2*-205/207/210 transcripts is comparable (50:50). Conversely, the transcript encoding the shorter seipin demonstrates minimal expression (<1%) not only in the CNS but also in non-nervous tissues. This distinct expression profile implies specific tissue-related functions for the various *BSCL2* transcripts (4).

Sequence alignment of human and mouse *BSCL2/Bscl2* orthologues demonstrates a substantial sequence identity of 83.55 %. The mouse *Bscl2* gene (MGI:1298392) is situated on chromosome 19 and gives rise to four coding transcripts, resulting in two seipin isoforms: a 383 amino acid protein (*Bscl2*-206/203-201) and a 443 amino acid protein (*Bscl2*-210) as detailed in **Table 1**. In terms of expression, *Bscl2* mRNA levels are moderate in skeletal muscle and adrenal gland. Notably, unlike in humans, *Bscl2* expression is higher in adipose

tissue in mice, while being detectable but lower in the brain (5). This indicates inter-species differences in *BSCL2/Bscl2* expression across various brain regions. In mice, strong expression is observed in the basal forebrain, hippocampus, hypothalamus, dorsal and ventral brainstems, with lower expression in the cortex, moderate expression in the midbrain, and no detectable expression in the caudate putamen (6, 7). Conversely, humans exhibit higher *BSCL2* gene expression in the caudate, putamen, cerebellum, and protuberance, particularly in the forebrain and hindbrain (4).

Table 1. Transcript table for the *BSCL2* lipid droplet biogenesis associated, seipin gene (*BSCL2*/*Bscl2*). Transcript name, identification (ID) and length in base pairs (bp) and protein length in amino acids (aa), consensus coding sequences (CCDS) and isoform from Ensembl.

Transcript name	Transcript ID	Transcript length (bp)	Protein length (aa)	CCDS	Isoform	Specie
BSCL2-203	ENST00000360796.10	1710				
BSCL2-227	ENST00000679883.1	2001	462	CCDS44627	1	
BSCL2-217	ENST00000524862.6	1863				
BSCL2-205	ENST00000403550.5	1693				Human (*Homo sapiens*)
BSCL2-207	ENST00000407022.7	1516	398	CCDS8031	2	
BSCL2-210	ENST00000421906.5	1440				
BSCL2-201	ENST00000278893.11	1364	287	CCDS55769	3	
BSCL2-206	ENST00000405837.5	1984	464	CCDS91493	-	
Bscl2-206	ENSMUST00000160556.8	1795				
Bscl2-203	ENSMUST00000159634.8	1684	383	CCDS70931	-	Mouse (*Mus musculus*)
Bscl2-201	ENSMUST00000086058.13	1388				
Bscl2-210	ENSMUST00000171649.8	1962	443	CCDS29551	-	

1.2 SEIPIN PROTEIN

1.2.1 Structure and Localization

Seipin, a protein localized in the endoplasmic reticulum (ER), comprises two TMDs (depicted in **Figure 1A** in blue and purple), a conserved core region (luminal loop) shown in grey in **Figure 1A**, featuring an N-glycosylation site, and two cytoplasmic domains, the amino- and carboxi- terminal regions (1, 8). While the protein sequences diverge outside the central region, there is a high conservation between mouse and human within the region spanning amino acids 1 to 280 (88 %) as illustrated in **Figure 1B**. Furthermore, a CAAX box motif (CSSS) at the C-terminus remains completely conserved across mammals, with its biological significance yet to be fully elucidated (3, 9). The longest isoform (isoform 1) differs from the intermediate isoform (isoform 2) by possessing an additional 64 amino acids in the N-terminal cytoplasmic domain highlighted in red in **Figure 1A**. On the other hand, the short isoform (isoform 3) lacks the second TMD (**Figure 1C**), resulting in all protein content being located within the ER lumen from amino acid 111 onwards (10).

A.

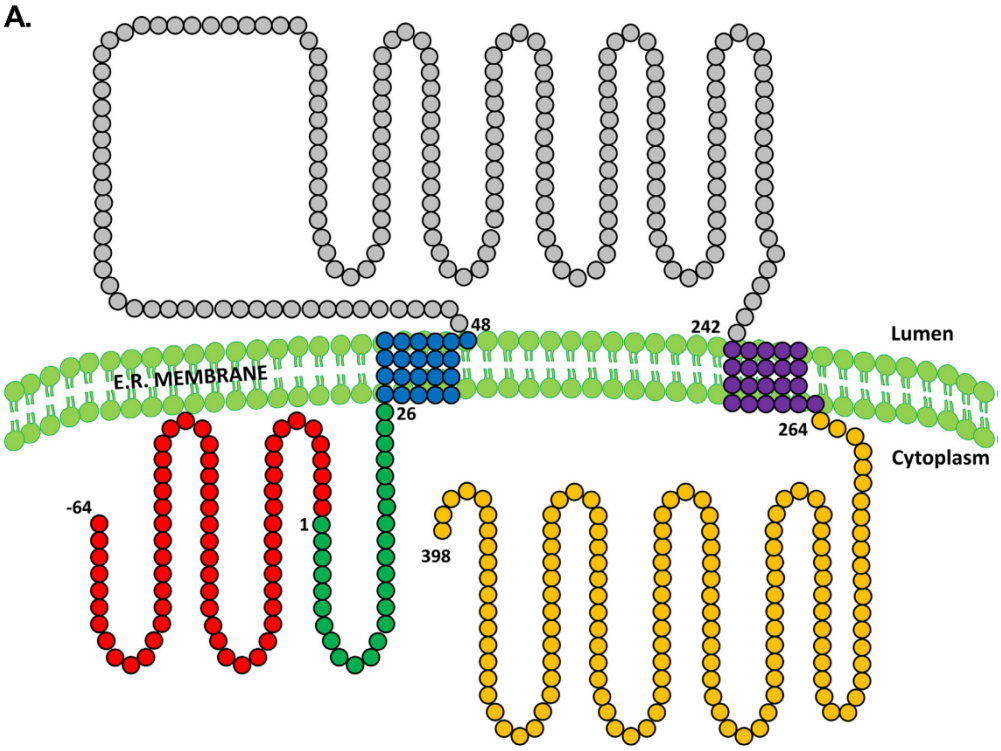

B.

	64 aa N-ext.	Cytoplasmic 1-26 aa	Transmembrane 27-47 aa	Lumenal 48-242 aa	Transmembrane 243-263 aa	Cytoplasmic 264-398 aa	Total 462 aa
Homo sapiens	100 %	100 %	100 %	100 %	100 %	100 %	100 %
Mus musculus	59.4 %	96.2 %	95.2 %	94.4 %	90.5 %	74.8 %	83.8 %

C.

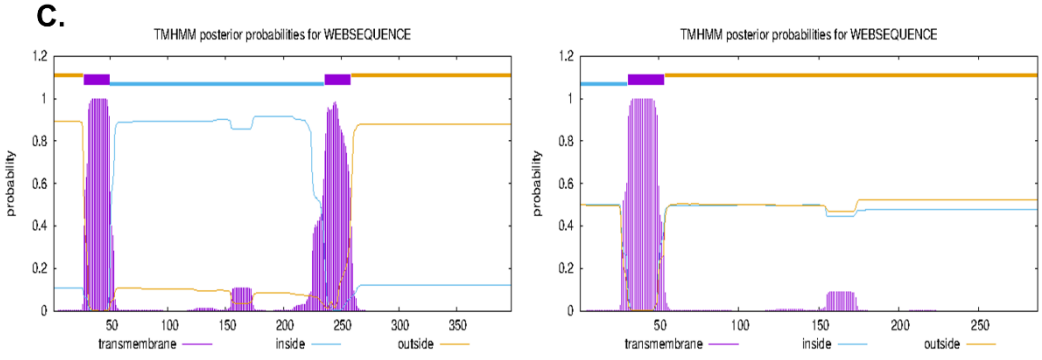

Isoform 1 (*BSCL2-203*) **Isoform 3** (*BSCL2-201*)

Figure 1. Seipin topology and homology. A. Schematic illustration of human 462-residue-long form of seipin protein. Seipin protein contains a central domain loop at the lumen of the endoplasmic reticulum (E.R.) that is highly conserved, two hydrophobic domains (blue and purple) and a N- and C-termini in the cytoplasm that appear to be variable among species. **B.** Seipin homology of the different seipin regions between humans (*Homo sapiens*) and mice (*Mus musculus*). Values are expressed in percentage of homology (%). aa: amino acids. **C.** Prediction of transmembrane helices for isoform 1 and isoform 3. Estimated using the hidden Markov model for predicting transmembrane helices in protein sequences (TMHMM 2.0 - DTU Health Tech - Bioinformatic Services) https://services.healthtech.dtu.dk/services/TMHMM-2.0/. Own elaboration (Power Point) modified from Sánchez-Iglesias et al. (4) under a Creative Commons license.

The seipin protein forms oligomers with a specific stoichiometry unique to each species (11). In yeast, this protein forms ring-shaped homooligomers consisting of 10 subunits with a central cavity (12) (**Figure 2A**). Contrasting this, human seipin assembles undecameric rings (13), while fly seipin forms dodecameric rings (14) (**Figure 2A**). Despite variations in subunit numbers, a common feature across eukaryotic seipin is the ring-like arrangement characterized by β-sandwich motifs, reminiscent of the lipid-binding protein Niemann Pick type C2 (NPC2) (12-14). This structural similarity is illustrated in **Figure 2B** and **Figure 2E**. In yeast, the luminal helical region within the seipin ring exhibits notable differences in size, position, and characteristics compared to the corresponding regions in human and fly seipin (12). In human and fly seipin, the helix is substantial, rich in hydrophobic amino acids (**Figure 2C**), particularly on the lower surface, encompassing α2 and α3 helices in humans (13) and α3 and α4 in flies (14) (**Figure 2B**). This feature allows the hydrophobic helix of human and fly seipin to embed into the luminal leaflet of the bilayer due to its size and amino acid composition (**Figure 2D**) (13, 14). Conversely, the luminal domain of yeast presents a distinct configuration with two small orthogonal hydrophilic helices (α1 and α2) that do not penetrate into the membrane (12). These structural variations are depicted in **Figure 2B-D**.

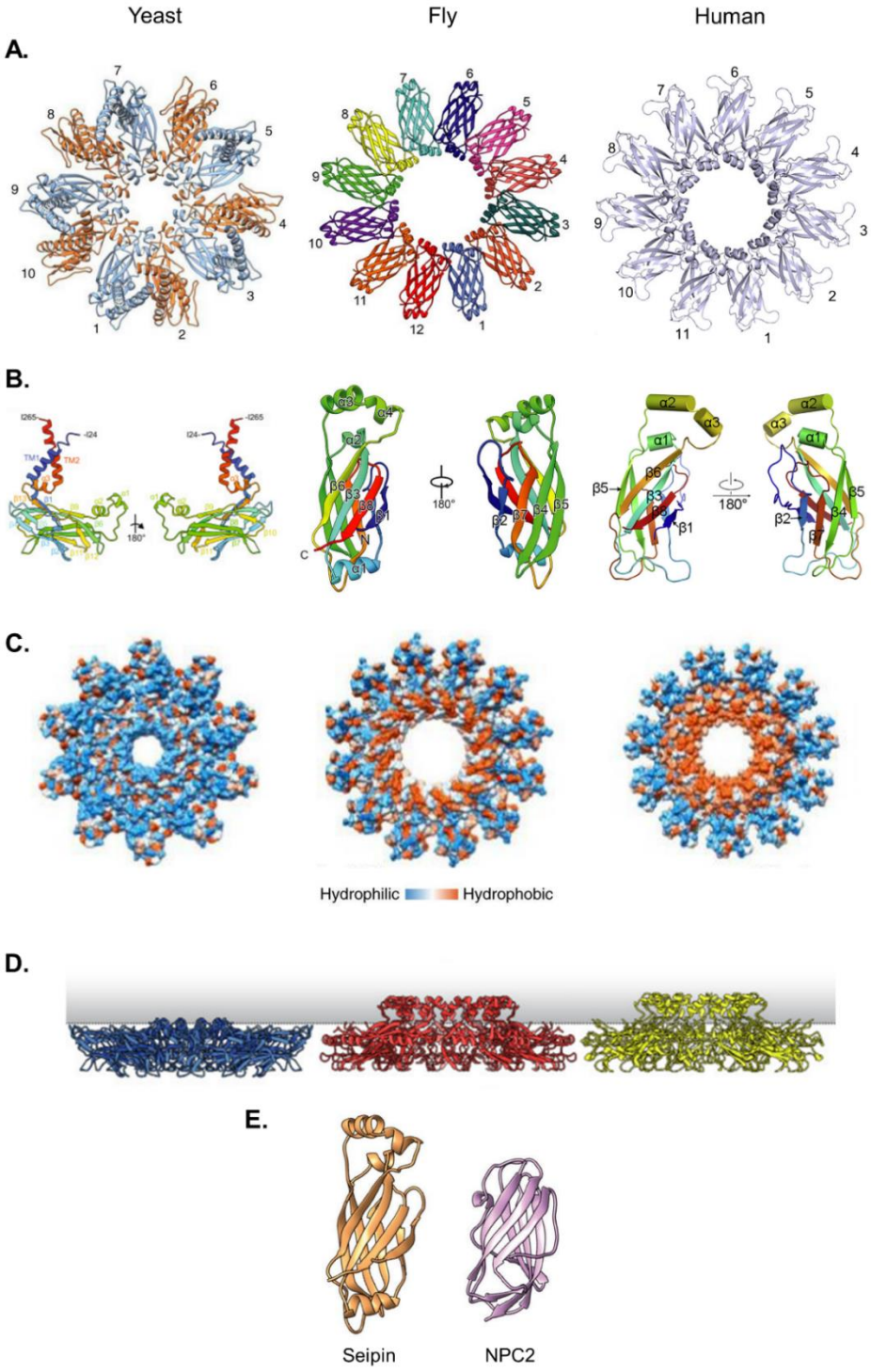

Figure 2. Structural determination of yeast, fly and human seipin protein. A. Top-view ribbon diagrams depicting the luminal domains of yeast, fly, and human seipin proteins with 10, 12, and 11 protomers, respectively. **B.** Monomeric structure of yeast, fly, and human seipin proteins coloured in rainbow gradient from N-terminus (blue) to C-terminus (red). **C.** Representation of the hydrophobic surfaces of yeast, fly, and human seipin luminal domains. Blue denotes the least hydrophobic regions, while orange indicates the most hydrophobic residues. **D.** Side view illustrations of the luminal domains of yeast, fly, and human seipin proteins in relation to the plane of the endoplasmic reticulum (ER) membrane, delineated by a dotted line. **E.** Comparative structural analysis between seipin (orange) and the cholesterol-binding protein NPC2 (pink). This visualization is a modified representation based on data from various sources (12-15). These publications are either under Creative Common license or their permission authorization is provided in **Annex 17**.

1.2.2 Functions

Numerous functions of seipin have been elucidated to date, yet its complete role remains incompletely understood. Seipin operates at the interface of the lipid droplets (LDs) and the ER, playing a critical role in the early formation of normal LDs and the maintenance of mature LDs (11). Additionally, it is implicated in regulating triglyceride and phospholipid synthesis (16-18), as well as participating in nerve impulse transmission in neurons (19). The multifaceted functions of seipin likely vary across different tissue. Consequently, seipin contributes to lipid homoeostasis by inhibiting lipogenesis and LD accumulation in non-adipocytes while facilitating adipogenesis to store excess energy efficiently in adipocytes (10, 20).

Role in Adipogenesis

Seipin is implicated in adipogenesis, although its precise role remains to be fully elucidated. Studies indicated that the absence of seipin results in impaired adipogenesis (5, 21), possibly linked to alterations in peroxisome proliferator-activated receptor gamma (PPARγ) signalling due to changes in phospholipid metabolism. Seipin interacts with glycerol-3-phosphate acyltransferase 3 (GPAT3), leading to reduced enzymatic activity and decreased phosphatidic acid (PA) production. This reduction in PA levels allows for the fully activation of PPARγ during the initial stages of adipocyte differentiation, facilitating normal adipogenesis progression (see **Figure 3A**). Consequently, the loss of functional seipin could elevate PA levels, potentially inhibiting PPARγ activity or other signalling pathways in preadipocytes, there by impeding adipogenesis (17) (see **Figure 3B**). Seipin is capable of biding to two key lipid metabolism enzymes essential for PPARγ activation during adipogenesis: 1-acylglycerol-3-phosphate O-acyltransferase 2 (AGPAT2) and Lipin 1 (LPIN1) (22, 23). The concurrent binding of seipin to AGPAT2 and LPIN1 likely facilitates the transfer of PA from AGPAT2 to LPIN1, with seipin exhibiting a specific interaction with PA through its NPC2-like domain (13) (refer to **Figure 3A**). Therefore, a deficiency in seipin may result in aberrant PA accumulation, potentially inhibiting PPARγ activity and impeding adipogenesis (16, 24) (**Figure 3B**).

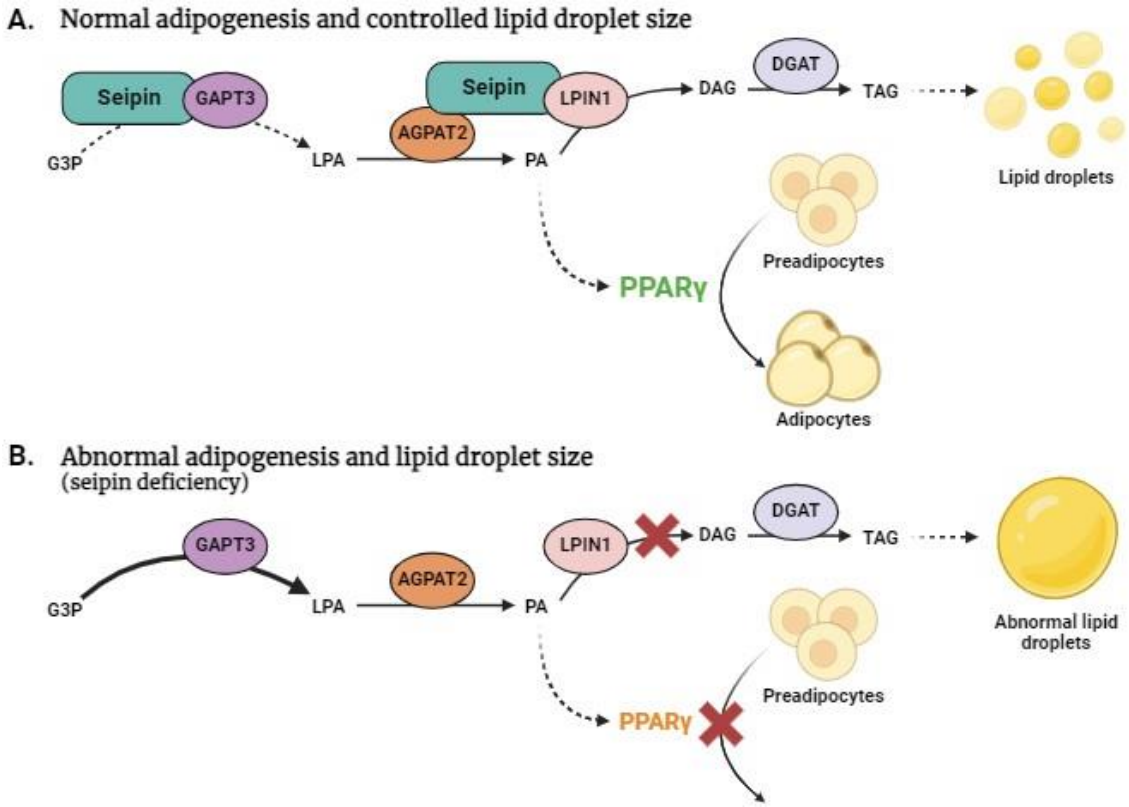

Figure 3. Model of seipin function in adipogenesis and lipid droplet morphology. A. Normal adipogenesis and controlled lipid droplet size. **B.** Seipin deficiency leads to abnormal adipogenesis and lipid droplet size. Seipin interacts with the GPAT3 that catalyses the synthesis of LPA that is transformed into PA by the AGPAT2 then, Lipin1 allows the synthesis of DAG which then serves as substrate for TAG synthesis by DGAT enzymes. Seipin diminishes the over-production PA, which would otherwise block PPARγ-mediated adipogenesis, and controls lipid droplets expansion. G3P: glycerol-3-phosphate; GAPT3: glycerol-3-phosphate acyltransferase 3; LPA: lysophosphatidic acid; AGPAT2: 1-acylglycerol-3-phosphate O-acyltransferase 2; PA: phosphatidic acid; PPARγ: peroxisome proliferator-activated receptor gamma; LPIN1: Lipin 1; DAG: diacylglycerol; DGAT: diacylglycerol O-acyltransferases; TAG: triacylglycerol. Own elaboration (BioRender) modified from Pagat et al. and Craveiro Sarmento et al. (17, 25) under Creative Common license.

Seipin plays a crucial role in regulating adipogenesis by orchestrating actin cytoskeleton remodelling, a vital process for adipocyte differentiation. During adipogenesis, the influx of excess nutrients triggers lipid uptake by preadipocytes, leading to lipid accumulation in the ER, which is sensed by seipin. Seipin then utilizes the 14-3-3β protein to transmit a lipid storage signal to the cytoplasm, initiating cofilin-1-mediated cytoskeleton reorganization. This process facilitates the necessary remodelling for preadipocytes to transition into mature adipocytes (26). Furthermore, seipin is also linked to adipogenesis through its involvement in regulating mitochondrial calcium influx at ER-mitochondria contact sites (MAMs). Seipin promotes proximity to sarco/endoplasmic reticulum Ca^{2+}-ATPase (SERCA), inositol 3 phosphate receptor (IP3R), and the voltage-dependent anion channel (VDAC) in a nutrition-dependent manner. By doing so, seipin controls mitochondrial calcium influx and energy supply in adipocytes, contributing to the regulation of adipogenesis (27, 28).

Role in Lipid Droplet Biogenesis

The precise mechanisms through which seipin influences LD formation remain incompletely understood. LDs serve as intracellular compartments dedicated to storing neutral lipids (NLs), predominantly triacylglycerol (TAG) and sterol esters. These structures consist of a hydrophobic core of NLs shielded by a phospholipid monolayer, housing LD-specific proteins such as lipases, acyltransferases, and scaffolding proteins (29). LDs play a pivotal role in cellular metabolism and nutrient regulation. They store lipids during times of nutrients abundance, which can be mobilized for energy production during starvation or utilized for phospholipids synthesis crucial for membrane formation. Increasing evidence suggests LD involvement in various cellular processes, including ER stress response, protein degradation, membrane trafficking, signal transduction, virus assembly, and transient protein storage (30). Moreover, LDs act as buffers against potentially harmful lipids, playing a key role in preventing lipotoxicity and oxidative stress (10, 29). The biogenesis of LDs occurs at the ER membrane, where enzymes responsible for NL formation are situated. Reach in yeast and animal cells indicates that the establishment of the ER-LD sites, LD formation, and their release into the cytoplasm involve a complex interplay among localized LD biogenesis factors, lipid biosynthetic enzymes and regulators, specific lipids, and distinct biophysical properties of the membrane like lipid composition, curvature, and surface tension (31-33).

Apparently, the seipin toroid is hypothesized to move swiftly within the ER membrane, capable of sensing minor accumulations of NLs that manifest as small lenses within the ER phospholipid bilayer (34). Seipin is believed to utilize its hydrophobic helix to tether the emerging LD at the interface between the ER and LD structures (14, 35). The establishment of these ER sites necessitates the co-localization of seipin with the Lipin complex to facilitate localized diacylglycerol (DAG) production. Subsequent recruitment of diacylglycerol O-acyltransferases (DGAT) drives the targeted synthesis of TAG in a specific region (**Figure 4A**) (17). LD biogenesis factors, including seipin, engage with TAG to facilitate lipid influx into the developing LD (**Figure 4A**), thereby fostering the expansion of the NL lens until detachment from the ER into cytoplasm occurs (see **Figure 4B**) (34, 36, 37). Seipin is proposed to regulate the quantity, size, and structure of LDs (**Figure 3**). Additionally, the budding of secretory vesicles from the ER towards the cytosol, rather than towards the ER lumen, appears to be influenced by the phospholipid composition and surface tension of the ER membrane (38-42). Maintaining minimal contact between NLs area and the aqueous cytosol is crucial, with surface tension playing a key role in shaping LDs. The rounded morphology of LDs is influenced by surface tension regulation, while phospholipid composition primarily impacts budding efficiency through geometric considerations. Specifically, molecules with conical geometry like DAG or phosphatidylethanolamine hinder budding, whereas those with opposing geometry such as lysophospholipids promote this process (42, 43). Moreover, membrane tension appears to dictate budding directionality (44). Phospholipids or proteins that mask the oil–water interface create tension imbalances between membrane monolayers that determine budding orientation (29).

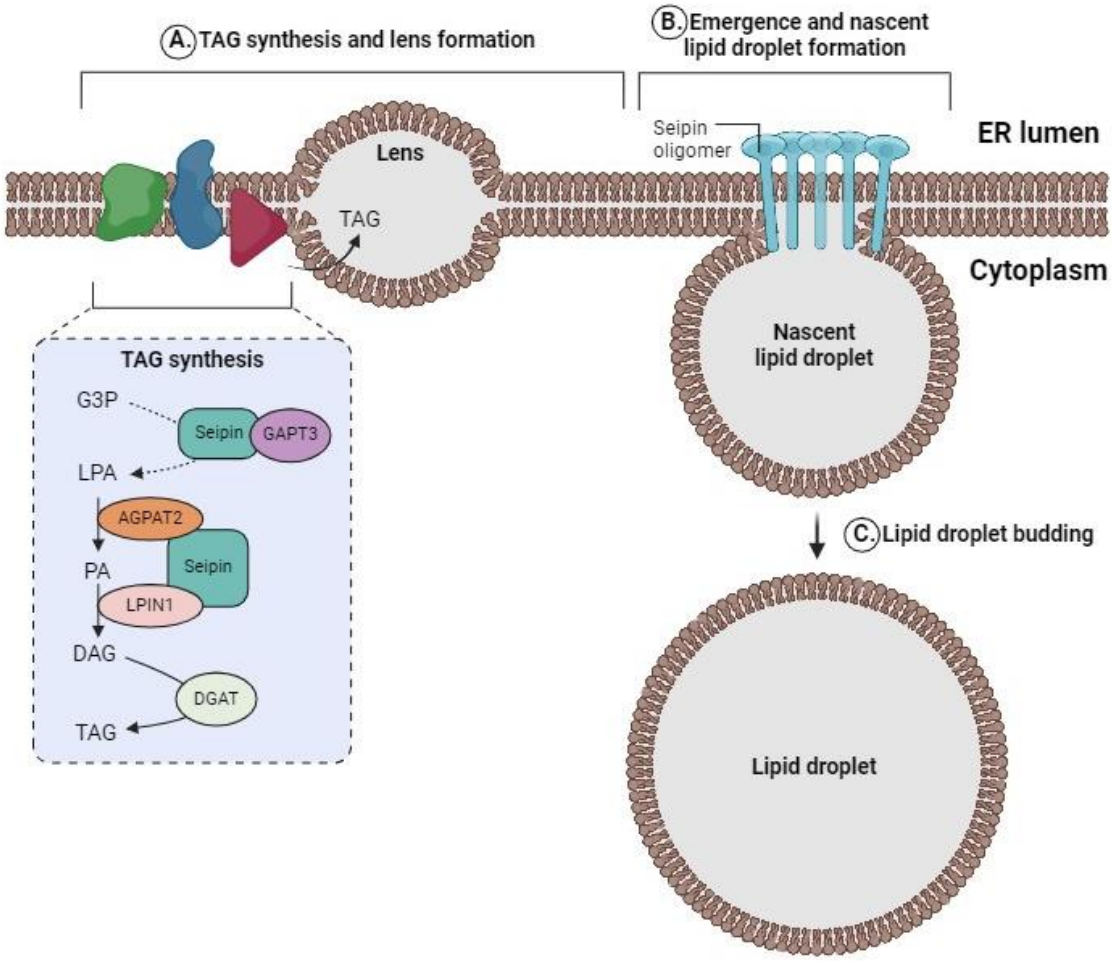

Figure 4. Steps in lipid droplet biogenesis. A. Triacylglycerol (TAG) synthesis (see box) enzymes and seipin protein deposit neutral lipids in between the leaflets of the endoplasmic reticulum (ER) bilayer. Beyond a certain concentration, the neutral lipids demix and coalesce into a lens. **B.** Seipin and other lipid droplet biogenesis factors are recruited to the lens structure and facilitate the growth of the nascent lipid droplet. **C.** The emergence of the lipid droplet into the cytosol is affected by differences in surface tension of the luminal and cytosolic leaflets of the ER bilayer. G3P: glycerol-3-phosphate; GAPT3: glycerol-3-phosphate acyltransferase 3; LPA: lysophosphatidic acid; AGPAT2: 1-acylglycerol-3-phosphate O-acyltransferase 2; PA: phosphatidic acid; LPIN1: Lipin 1; DAG: diacylglycerol; DGAT: diacylglycerol O-acyltransferases. Own elaboration (BioRender) modified from Olzmann et al. (29). The authorization for publication is provided in **Annex 17**.

The collaboration between seipin and the Peroxisomal membrane protein PEX30 in the formation of LDs is a significant aspect of cellular biology (45). PEX30, known as an ER resident protein, traditionally associated with peroxisome formation (46), has been found to also contribute to LD formation in conjunction with seipin (45). This partnership between PEX30 and seipin is particularly notable in ER domains where LDs and pre-peroxisomal vesicles originate. When seipin and PEX30 are simultaneous deleted, LD budding is impeded, leading to the accumulation of NLs within the ER membrane, resulting in an abnormal composition (29). The association between seipin and PEX30 appears to be crucial in structuring ER subdomains conducive to TAG synthesis and droplet assembly (33). Local alterations in membrane geometry and lipid composition facilitated by Pex30 at LD formation sites are believed to be essential for accommodating DAG and promoting TAG nucleation within the ER bilayer (45, 47, 48). This intricate interplay between seipin and PEX30 underscores their pivotal roles in cellular lipid metabolism and organelle biogenesis.

Recently, additional proteins have been identified that play essential roles in LD formation when associated with seipin. One such protein is Promethin, also known as lipid droplet assembly factor 1 (LDAF1) (49). It has been observed that seipin and Promethin/LDAF1 interact to functionally support LD growth (50). Recent investigations (51) have proposed a model where Promethin/LDAF1 is positioned at the centre of the seipin toroid, with its hydrophobic helical domain adopting a double hairpin structure that enables anchoring to the ER membrane or the LD surface. The hypothetical seipin-LDAF1 complex is suggested to contain multiple hydrophobic domains at its core, potentially aiding in catalysing lipid lens nucleation by creating a phospholipid-free space conducive to triglycerides nucleation. Alternatively, it is theorized that LDAF1 may form a channel within the seipin toroid, facilitating lipid transfer to growing LDs in conjunction with seipin's putative NPC2-like lipid-binding domain (51). Seipin, through its luminal hydrophobic helices, could potentially capture TAGs, acting as a catalyst to aggregate TAGs from monomers within the seipin ring and stablishing a binding interface favourable for LDAF1 (52). These intricate interactions between seipin and Promethin/LDAF1 shed light on their collaborative roles in LD biogenesis and highlight the sophisticated mechanisms underlying lipid metabolism within cells.

In addition to the ER, LDs interact with various cellular organelles, including mitochondria and peroxisomes. The lipid transfer proteins ORP5 and ORP8 (oxysterol binding related proteins 5 and 8) play a crucial role in LD biogenesis at the MAM subdomains, which are rich in PA. Notably, ORP5/8 are essential for regulating seipin recruitment to these MAM–LD contacts, and their depletion hinders LD formation (27). On the other hand, peroxisomes are vital metabolic organelles involved in cellular lipid metabolism, such as the β-oxidation of very long-chain fatty acids, synthesis of myelin sheath lipids, and modulation of reactive oxygen species (ROS), particularly hydrogen peroxide. Recent research has highlighted additional non-metabolic roles of peroxisomes, including responses to cellular stress, immune defence against pathogens and virus, functioning as cell signalling hubs, and contributing to healthy aging. These discoveries underscore the

protective nature of peroxisomes beyond their metabolic functions, indicating broader implications for human health and potential relevance to various significant diseases like neurodegenerative disorders, obesity, cancer, and age-related conditions (10, 53, 54). The multifaceted roles of peroxisomes suggest their involvement in diverse cellular processes with far-reaching implications for human health and disease pathogenesis.

LDs have been identified within the nucleus, although their formation and functions remain less elucidated. It has been suggested that nuclear LD synthesis could play a significant role in cellular stress resilience (55). In yeast, seipin localizes to the inner nuclear membrane (INM) and is crucial for establishing the membrane bridge linking the INM with nuclear LDs (56). Conversely, in mammalian cells, seipin is not typically found in this position (57); instead, it is detected near the outer nuclear membrane, which is contiguous with the ER. This suggests that LD formation within the INM occurs independently of the seipin. Nevertheless, seipin appears to indirectly impact nuclear LD biogenesis in mammalian cells by influencing the expression of LPIN1 (57, 58). The discrepancy in seipin's localization and function between yeast and mammalian cells remains a topic for further investigation (10). Understanding these variations may provide insights into the distinct mechanisms governing LD formation in different cell types and species.

Role in Lipolysis

Adipocyte differentiation involves a rise in triglyceride synthesis alongside controlled lipolysis. The interplay of cyclic adenosine monophosphate (cAMP) levels and adipocyte triglyceride lipase (ATGL) governs the regulation of lipolysis. Increased cAMP levels tigger the activation of cAMP-dependent protein kinase A (PKA), initiating the phosphorylation of Perilipin 1 (PLIN1) and hormone-sensitive lipase (HSL). This phosphorylation event is crucial for HSL activation and its recruitment to LDs (59), where it collaborates with ATGL to break down stored lipids effectively (**Figure 5**) (60). Maintaining a precise equilibrium between triglyceride synthesis and lipolysis is vital for normal adipose tissue function, as disruption in these processes can lead to conditions like lipodystrophy or obesity (61). Seipin plays a role in regulating adipogenesis by influencing cAMP/PKA-mediated lipolysis. Seipin deficiency can chronically activate ATGL, resulting in heightened HSL and PLIN1 phosphorylation, accelerating lipolysis and halting adipogenesis (61-64). Despite these insights, the specific mechanism by which seipin modulates cAMP/PKA-driven lipolysis remains to be fully elucidated, presenting an intriguing area for further research into the intricate regulatory pathways governing adipocyte metabolism.

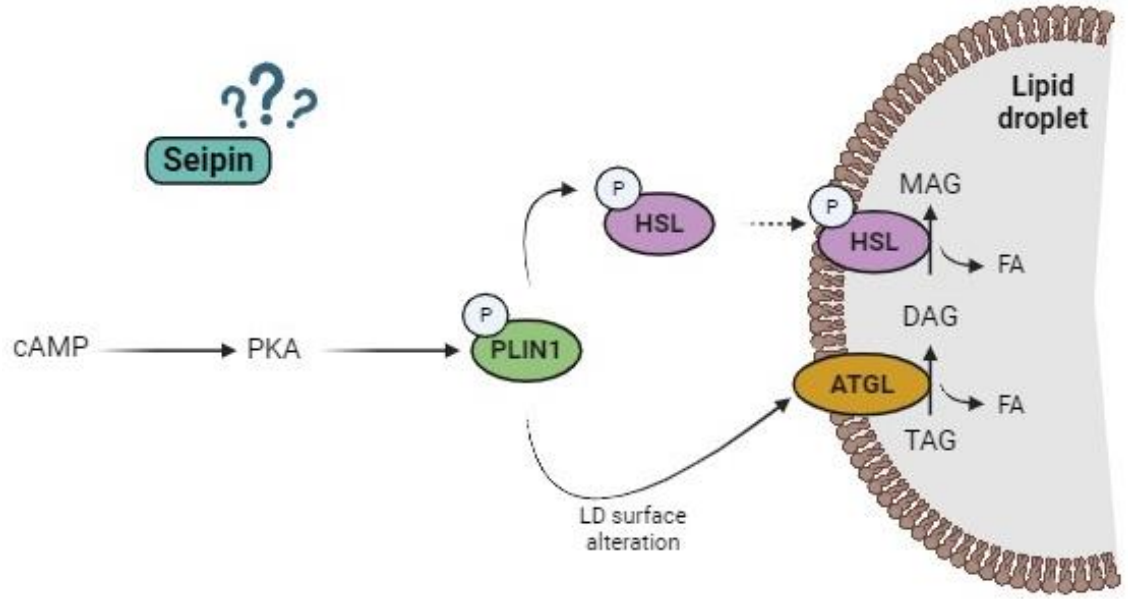

Figure 5. Molecular mechanism of human lipolysis via cAMP/PKA pathway. PKA is involved in PLIN1 phosphorylation which induces an important physical alteration of the lipid droplet surface that facilitates the activation of ATGL and HSL and the initiation of TAG hydrolysis. HSL phosphorylation promotes its translocation from the cytosol to the surface of the lipid droplet (LD). cAMP: cyclic adenosine monophosphate; PKA: protein kinase A; PLIN1: Perilipin 1; ATGL: adipose triglyceride lipase; HSL: hormone-sensitive lipase; TAG: triacylglycerol; DAG: diacylglycerol; MAG: monoacylglycerol; FA: fatty acid. Own elaboration (BioRender).

Role in Central Nervous System

The CNS, being the second most lipid-rich organ, harbours approximately 20% of the body's total cholesterol (65, 66). Perturbations in the lipid composition of CNS cells can disrupt normal neuronal function and cellular processes (67, 68). Maintaining lipid homeostasis is paramount for optimal neuronal activity and synaptic plasticity (69), as dysregulation of lipids has been associated with neurodegenerative conditions such as Alzheimer's and Parkinson's disease (70-72). While LDs are predominantly observed in microglia (73), emerging evidence suggests their presence across all brain cell types (72). The subventricular zone stands out as a well-studied region for LD formation (74), yet structures like the frontal cortex, hippocampus, olfactory bulbs, and hypothalamus have also been identified to accumulate LDs (72). Notably, research has linked LD formation in the brain to neurodegenerative diseases. Studies have demonstrated an increase in both number and size of LDs in aging rats (75), a correlation between LD content in flies' brains and accelerated neurodegeneration (76), transfer of toxic fatty acids from neurons to astrocyte LDs via ApoE-positive lipid particles (77), and alterations in the function of aging-related lipid-accumulating microglia (73). The interplay among aging, inflammation, and oxidative stress, factor implicated in neurodegenerative disease pathogenesis, has been associated with LD formation (10, 73, 75, 78, 79). These intricate relationships underscore the potential significance of LDs in the context of brain health and disease progression, highlighting a promising avenue for further exploration into the role of LDs in neurodegenerative disorders.

Seipin plays a crucial role in the formation of synaptic vesicles and the machinery essential for neurotransmitter release. Depletion of seipin neuronal cells of mice disrupts PPARγ function, resulting in neural impairment (**Figure 6**) (80, 81). In hippocampal regions, inhibition of PPARγ can specifically downregulate α-amino-3-hydroxy-5-methyl-4-isoxazole propionic acid receptor (AMPAR) expression by reducing extracellular signal-regulated kinase (ERK) and cAMP responsive element binding protein (CREB) activity, thereby affecting N-methyl-D-aspartate (NMDA) receptor-mediated long-term potentiation (LTP) and spatial memory (81). Moreover, seipin deficiency interferes with excitatory synaptic transmission through a postsynaptic mechanism involving AMPAR modulation. This leads to impaired excitatory postsynaptic currents (EPSCs), while inhibitory postsynaptic currents (IPSCs) remain unaffected (19). These findings highlight the intricate role of seipin in synaptic function and neurotransmission, shedding light on its significance in maintaining proper neuronal communication and synaptic plasticity. Moreover, a presynaptic role of N-glycosylated seipin may modulate synaptic vesicle exocytosis by directly influencing synaptic vesicle docking (82). In the hippocampus, inhibition of PPARγ not only restricts stem cell proliferation by supressing ERK phosphorylation but also impedes progenitor cell differentiation. This effect is attributed to decreased expression of neurogenin 1 (*Neurog1*) and neurogenic differentiation 1 (*Neurod1*) due to WNT3 (Proto-oncogene Wnt-3) signal inhibition (83). Furthermore, PPARγ inhibition tiggers hyperphosphorylation and aggregation of tau (tubulin associated unit) protein at Thr^{212}/Ser^{214} and Ser^{202}/Thr^{205} by upregulating phosphoinositide-3 kinase/protein kinase-B/mammalian target of rapamycin (PI3K/AKT/mTOR) pathway signalling. This cascade suppresses autophagy, enhances glycogen synthase kinase-3β (GSK3β) activity, ultimately leading to axonal atrophy (84, 85). In dopaminergic neurons, inhibition of PPARγ exacerbates activated GSK3β-induced α-synuclein phosphorylation and neuroinflammation mediated by interleukin-6 (IL-6). Reduced PPARγ levels contribute to α-synuclein aggregation, resulting dopaminergic cells loss (24, 86). These intricate molecular mechanisms underscore the diverse impacts of PPARγ modulation on neuronal function and neurodegenerative processes.

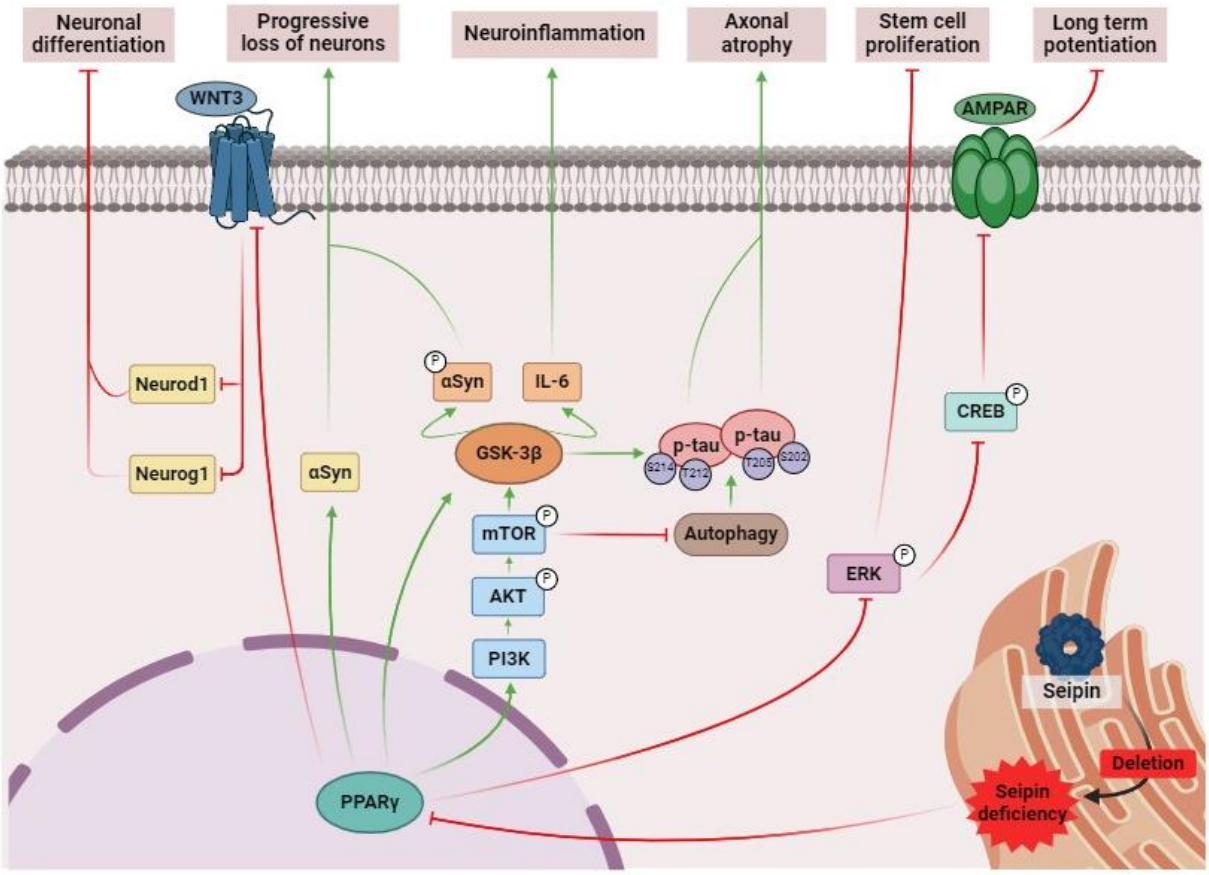

Figure 6. Summary of the possible mechanisms in neurons leading to neurodegenerative phenotypes. Seipin deficiency suppresses PPARγ expression, leading to a cascade of effects. Reduced PPARγ inhibits neuronal differentiation via the WNT3 pathway, promotes the phosphorylation and aggregation of α-Syn and p-tau, and triggers neuroinflammation by activating both the PI3K/AKT/mTOR pathway and the GSK-3β pathway. Additionally, it impairs stem cell proliferation and the current of AMPAR, as well as long-term potentiation, by inhibiting the ERK pathways. WNT3: Proto-oncogene Wnt-3; Neurod1: neurogenic differentiation 1; Neurog1: neurogenin 1; α-Syn: α-synuclein; IL-6: interleukin-6; GSK-3β: glycogen synthase kinase-3β;mTOR: mammalian target of rapamycin; AKT: protein kinase-B; PI3K: phosphoinositide-3 kinase; p-tau: phosphorylated tau protein; ERK: extracellular signal-regulated kinase; CREB: cAMP responsive element binding protein and AMPAR: α-amino-3-hydroxy-5-methyl-4-isoxazole propionic acid receptor. Own elaboration (BioRender) modified from Li et al. (24) under Creative Common license.

However, recent studies suggest that the impairment of cognitive functions caused by seipin deficiency may be due to compromised myelin plasticity. Mechanistically, seipin deficiency suppresses sphingolipid metabolism-related genes in oligodendrocyte precursor cells (OPCs) and causes morphological abnormalities in LDs, significantly impeding OPC differentiation. This results in decreased numbers of oligodendrocytes (OLs), myelin proteins, the proportion of myelinated fibres, and the thickness of myelin (87). Additionally, it has been reported that OLs regulate glutamate vesicle release and LTP production at presynaptic terminals, and myelination can facilitate synaptogenesis, ultimately promoting synaptic integration and the remodelling of neuronal networks (87-89). These findings indicate that seipin plays important roles in brain plasticity from both myelin and synaptic aspects.

Seipin is implicated in pre-peroxisomal vesicle formation, a process crucial for safeguarding neurons against aberrant neuronal migration, differentiation, demyelination, inflammation, oxidative stress, and other detrimental factors (24, 54, 90). The expression of *BSCL2* is linked to various peroxisome-related genes such as *CAT* (catalase), *PEX1* (peroxisomal biogenesis factor 1), *PEX11G* (peroxisomal biogenesis factor 11 gamma), *PEX16* (peroxisomal biogenesis factor 16), *SOD1* (superoxide dismutase 1), as well as *PPARγ* in human brain specimens and SH-SY5Y cells induced to differentiate into neurons with upregulated *BSCL2* (4). These associations highlight the intricate network of molecular interactions involving seipin and peroxisome-related genes in neuronal function and neuroprotection.

1.3 SEIPINOPATHIES

1.3.1 Congenital Generalized Lipodystrophy Type 2

Congenital generalized lipodystrophy (CGL), also known as Berardinelli-Seip syndrome, is a rare autosomal recessive disorder characterized by almost total absence of adipose tissue. Initially documented in 1954 by Berardinelli and subsequently by Seip in 1959 (91, 92), CGL manifests through variants in *AGPAT2*, *BSCL2*, *CAV1* (caveolin 1) and *CAVIN1* (caveolae associated protein 1) genes, linked to the distinct subtypes CGL1 (OMIM #608594), CGL2 (OMIM #269700), CGL3 (OMIM #612526) and CGL4 (OMIM # 613327) correspondingly (93). Among these subtypes, CGL2 represents the most prevalent form, accounting for 50.3% of all CGL cases and exhibiting the most severe clinical outcomes (93, 94). Notably, current literature does not report significant phenotypic variations among different variant forms in CGL2 patients (93). However, emerging evidence suggests a potential association between the severity of CGL2 and gender, with females displaying a more pronounced disease presentation. Studies by Huang-Doran et al. (95), Raygada et al. (96), and Li et al. (24) have hinted at this sex-related disparity in the clinical manifestation of CGL2.

In comparison to other forms of CGL, individuals with CGL2 experience a more pronounced and severe loss of adipose tissue that is noticeable either at birth or within the first year of life (97, 98). These patients exhibit a distinctive triangular facial shape, without the typical Bichat (buccal) fat pad. The lack of adipose tissue results in well-defined muscles, giving then a robust, Herculean appearance as they age. The deficiency in subcutaneous fat accounts for the significant phlebomegaly observed in both the upper and lower extremities (**Figure 7**) (10, 99).

Figure 7. Patient with Congenital generalized lipodystrophy type 2. Recovery from Araújo-Vilar et al. (100).

Apart from the lack of metabolically active adipose tissue, individuals with CGL2 exhibit early onset hyperinsulinemia, hypoleptinemia, hypoadiponectinemia, and hypertriglyceridemia. With time, likely influenced by hyperinsulinemia, patients manifest acromegaloid characteristics (99). Due to their profound insulin resistance, these children can develop acanthosis nigricans in the initial years of life, a condition that progress with age. Furthermore, as a consequence of insulin resistance, these individuals frequently develop non-ketotic diabetes mellitus, typically emerging during their second decade of life (10, 93).

Cardiac complications and renal injury are usually observed in CGL2 patients. The cardiac issues observed in these patients are primarily marked by concentric left ventricular hypertrophy. This condition is linked to diastolic dysfunction while maintaining systolic function, ultimately culminating in ventricular dysfunction and heart failure (26, 101). CGL is frequently associated with kidney complications, including proteinuria and various renal pathologies (102, 103). These renal issues can progress to chronic renal failure, end-stage renal disease, and other complications such as hematuria, kidney stones, and renal hypoplasia (104-106). Microscopic examination frequently reveals focal segmental glomerulosclerosis, membranoproliferative glomerulonephritis, arteriolar hyalinization, and severe diabetic glomerulosclerosis in these patients (102, 107).

Conversely, the abnormal accumulation of fat in the liver leads to hepatic steatosis, contributing to significant hepatomegaly and potentially progressing to cirrhosis. Alongside hepatomegaly, splenomegaly is frequently observed (24, 108, 109). Additionally, individuals with CGL2 often face reproductive system impairments affecting both genders, with more pronounced effects seen in males, including enlarged external genitalia and infertility (110). Unlike other CGL subtypes, a substantial proportion (80%) of these patients exhibit mild to moderate intellectual disability (111). The most common causes of death are liver cirrhosis, infections, and complications of diabetes (104, 112).

At the molecular level, the majority of CGL2 cases stem from homozygous or compound heterozygous variants. These variants often result in premature stop codons or frameshift variants, causing a loss of seipin function. The pathogenic mechanisms underlying how various variants lead to lipodystrophy may involve a decreased protein stability, resulting in a lack of functional protein, impaired oligomerization, and reduced ability to bind LPIN1 and target it to the ER. Nevertheless, the precise molecular mechanism through which seipin loss contributes to CGL2 remains uncertain (113, 114).

1.3.2 *BSCL2*-associated Motor Neuron Diseases

Specific single heterozygous missense variants in *BSCL2* can result in a broad spectrum of upper and/or lower motor neuron diseases. Variants like c.263A>G (p.N88S), c.269C>T (p.S90L), and c.269C>G (p.S90W) affect amino acids located within the N-glycosylation site in the luminal loop of the seipin protein (115-117), in addition to the c.287G>A (p.R96H) variant (118). These variants lead to the formation of abnormal seipin structures, contributing to a range of clinically diverse neurological disorders, including Silver syndrome (also known as spastic paraplegia type 17 (SPG17; OMIM #270685)), and autosomal dominant distal hereditary motor neuropathy-13 (HMND13, OMIM #619112). Silver syndrome is characterized by amyotrophy, weakness in small hand muscles, and varying degrees of spasticity in the lower extremities, indicating involvement of upper motor neurons. This spectrum of disorders encompasses individuals who may be clinically asymptomatic but exhibit electromyographic abnormalities (10, 115). The clinical presentation of HMND13 typically involves weakness and muscle wasting, primarily in the hands, starting in the fourth decade of life. This may manifest as symmetric or asymmetric involvement, with muscle loss predominantly affecting the thenar eminence and the interosseous hand muscles. While sensory loss is rare, generally vibratory, foot deformities are common. There is a decrease in motor nerve conduction velocities, with the sensory conduction being normal. There may be gait disturbances, which suggests the involvement of the pyramidal pathway (10, 119). At the molecular level, these variants in *BSCL2* prompt the formation of abnormal seipin structures that disrupt proper glycation, resulting in misfolding and accumulation in the ER. This misfolding triggers the unfolded protein response (UPR), leading to increased expression of UPR markers such as C/EBP homologous protein (CHOP) and binding immunoglobulin protein (BiP), causing ER stress and ultimately cell death. Seipin is expressed in spinal cord

motor neurons, the primary cells affected in these conditions, contributing to motor neuron neurodegeneration (120, 121). Furthermore, variants such as p.N88T or p.S141A (122) also result in one patient with motor neuron diseases, although further study is needed to fully understand the phenotypes caused by these variants (24).

1.3.3 Celia's Encephalopathy or Progressive Encephalopathy with or without Lipodystrophy

Clinical Course

Celia's encephalopathy or progressive encephalopathy with or without lipodystrophy (PELD; OMIM #615924) is a fatal pediatric neurodegenerative recessive condition due to different variants in *BSCL2* gene. This disorder was first described by our group in 2013 (2), identifying the variant c.985C>T, in exon 7, in homozygosis or compound heterozygosis. Subsequently, other variants have been identified as causative of PELD: c.974dupG, c.1048C>T, c.1076dupC and, c.566T>A (111, 123-125).

As of now, nine cases of the c.985C>T variant have been identified, with four being homozygous, while the remaining five are compound heterozygous. The compound heterozygous individuals carry the c.985C>T variant along with a lipodystrophic *in trans* variant (c.507_511del, c.538G>T or c.1004A>C) (**Table 2**, case #1-9) (10).

Table 2. Cohort of patients suffering from *BSCL2* progressive encephalopathy with or without lipodystrophy. Own elaboration modified from Sánchez-Iglesias et al. (10) under Creative Common license.

Case	*BSCL2* variant	Genotype	Sex	Country	Generalized lipodystrophy	Encephalopathy	Seizures	Neurological symptoms	Other symptoms	Reported or deceased age	Ref.
1	c.985C>T	Homozygote	Female	Spain	No	Yes	Generalized tonic-clonic	Poor motor coordination, ataxic gait, generalized fine tremor, dystonia, sleep disturbances, severe spasticity, tetraparesis, pyramidal and extrapyramidal signs, loss of motor skills, social, language and cognitive development	Hypertriglyceridemia, hepatic steatosis	Deceased (8 years)	(2)
2	c.985C>T and c.507_511del	Compound heterozygote	Female	Spain	Yes	Yes	Progressive myoclonic epilepsy	Gait ataxia, intellectual disability, dystonia, difficulty swallowing, loss of language	Hypertriglyceridemia, hepatic steatosis	Reported (11 years)	(2)
3	c.985C >T and c.538G>T	Compound heterozygote	Male	Spain	Yes	Yes	Progressive myoclonic epilepsy	Cognitive impairment, pyramidal signs, language loss, dystonia, difficulty swallowing	No reported	Deceased (8 years)	(2)
4	c.985C>T and c.507_511del	Compound heterozygote	Male	Spain	Yes	Yes	Progressive myoclonic epilepsy	Cognitive impairment, ataxic gait	No reported	Deceased (7 years)	(2)
5	c.985C>T and c.507_511del	Compound heterozygote	Male	Spain	Yes	Yes	Progressive myoclonic epilepsy	Cognitive impairment, ataxic gait	Hypertriglyceridemia, hepatic steatosis	Deceased (7 years)	(2)
6	c.985C>T	Homozygote	Female	Spain	No	Yes	Progressive myoclonic epilepsy	Cognitive impairment, irritability, dysphagia, sleep disorder and pyramidal signs, ataxic gait	No reported	Deceased (6 years)	(2)
7	c.985C>T	Homozygote	Male	Iran	Yes	Yes	Myoclonic	Autism, repetitive and stereotypic hand movements, repetitive upward staring, ataxia, generalized hypertonia, severe global developmental delay	Inguinal hernia, generalized hypertrichosis	Deceased (8 years)	(126)

8	c.985C>T	Homozygote	Male	Brazil	Yes	Yes	Myoclonic	Gait ataxia, intellectual disability	Hypertriglyceridemia, hepatic steatosis	Reported (5 years)	Not published
9	c.985C>T and c.1004A>C	Compound heterozygote	Female	France	No	Yes	No	Regressive autism spectrum disorder, atypical Parkinsonism, loss of communication and language skills, dystonic hypertonia, and extrapyramidal and pyramidal features, camptocormia, dysphagia marked frontal lobe syndrome	No reported	Deceased (28 years)	(127)
10	c.974dupG	Homozygote	Female	Spain	Yes	Yes	Myoclonic	Language delay, myoclonus, dystonia, seizures, gait ataxia, abnormal behaviour	Hypertriglyceridemia, hepatic steatosis	Deceased (9 years)	(128)
11	c.974dupG and c.1015C>T	Compound heterozygote	Female	Spain	Yes	No	No	Language delay	Hypertriglyceridemia, hepatic steatosis, hyperinsulinemia	Reported (2 years)	(128)
12	c.974dupG and c.1020_1021delAA	Compound heterozygote	Male	Italy	Yes	Yes	Absence seizures, eyelid myoclonus	Pyramidal signs, loss of language, dystonic tetraplegia	Hypertriglyceridemia, hypertransaminasemia, hepatic steatosis, hypertrophic cardiomyopathy	Deceased (9 years)	(129)
13	c.974dupG	Homozygote	Female	Italy	Yes	Yes	Absence seizures, slight eyelid myoclonus, myoclonicatonic seizures	Cognitive decline, pyramidal signs, tetraparesis, intellectual disability	Hypertriglyceridemia, muscle hypertrophy, hepatic steatosis, cardiomegaly, acanthosis nigricans	Deceased (7 years)	(129)
14	c.974dupG	Homozygote	Female	Italy	Yes	Yes	Absence seizures, slight eyelid myoclonus, myoclonicatonic seizures	Cognitive decline, pyramidal signs, tetraparesis, intellectual disability	Hypertriglyceridemia	Deceased (11 years)	(129)
15	c.974dupG	Homozygote	Male	Chine	Yes	Yes	Progressive myoclonic epilepsy	Generalized hypertonia	None	Reported (17 years)	(130)
16	c.974dupG and c.157G>T	Compound heterozygote	Male	Taiwan	Yes	No	No	Gait disturbance, torticollis, abnormal posturing of the fingers, axial dystonia abnormal thigh abduction and foot dystonia, mild intellectual disability	Muscular hypertrophy, acromegaloid features, acanthosis nigricans, hypertriglyceridemia, hepatic steatosis	Reported (28 years)	(131)

17	c.974dupG	Homozygote	Male	Taiwan	Yes	No	No	None	Prominent musculature, eruptive xanthomas, hepatic steatosis, hypertriglyceridemia, hyperinsulinemia	Reported (1.8 years)	(132)
18	c.974dupG	Heterozygote	Female	China	Yes	No reported	No reported	Intellectual disability	Diabetes mellitus	No reported	(111)
19-28	c.974dupG	No reported	No reported	Taiwan	No reported	No reported	No reported	No reported	No reported	No reported	Not published (personal communication)
29	c.1048C>T	Homozygote	Female	Italy	Yes	Yes	Progressive myoclonic epilepsy	Dyskinetic, distonic, and choreoathetotic movements, psychomotor regression, languagimpairment, bulbar signs, loss of gait	Coarse facial features, synophrys, bulbous nasal tip, large ear pinnae, wide mouth, long fingers and toes, hypertrichosis	Reported (15 years)	(123)
30	c.1048C>T	Homozygote	Female	Italy	Yes	Yes	Progressive myoclonic epilepsy	Dyskinetic, distonic, and choreoathetotic movements, psychomotor regression, language impairment, bulbar signs, loss of gait, aphasia	Coarse facial features, synophrys, bulbous nasal tip, large ear pinnae, wide mouth, long fingers and toes, hypertrichosis, abnormal glucose tolerance	Deceased (18 years)	(123)
31	c.1076dupC	Homozygote	Male	Macedonia	Yes	Yes	Progressive myoclonic epilepsy	Language impairment, severe hyperactivity, drop attacks, ataxic gate, psychomotor delay, ataxic gait	Hypertriglyceridemia, hypertransaminasemia, hepatic steatosis	Reported (6 years)	(124)
32	c.566T>A	Heterozygote	Male	Spain	No	Yes	Generalized tonic-clonic	Delays in social skills, eyelid myoclonus, absence, atonic seizures, moderate intellectual disability, autism spectrum disorder, ataxic gait	None	Reported (10 years)	(125)
33	c.566T>A	Heterozygote	Female	Spain	No	yes	Asymmetric tonic seizures	Mild psychomotor delay	None	Deceased (0.9 years)	(125)

The patients are typically born seemingly healthy (**Figure 8A**), but often experience difficulties with sucking and weight loss within the first month. Homozygous patients generally do not exhibit the characteristic features of generalized lipodystrophy, although they may present with hypertriglyceridemia and hepatomegaly. Notably, two patients homozygous for c.985C>T have been reported to have generalized lipodystrophy (**Table 2**; case #7 and #8) (10, 126). Conversely, in compound heterozygotes, characteristics of CGL2 are typically noticeable from early infancy. Acanthosis nigricans or impairments in carbohydrate metabolism have not been observed in any of the cases reported to date (2, 10).

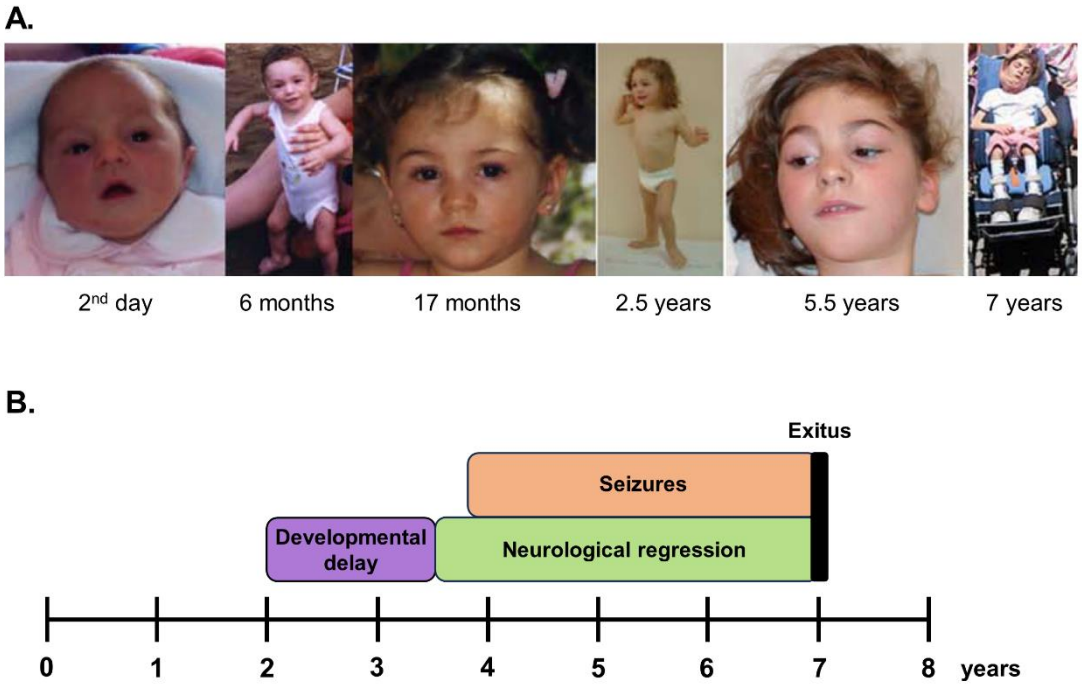

Figure 8. The common natural history of Celia's encephalopathy. A. Images from a c.985C>T homozygous case deceased at 8 years of age (**Table 2**, case #1). This patient had a lipoatrophic appearance at 6 months of age, which regressed subsequently. Note full cheeks at 17 months, 2.5 and 5.5 years of age. **B.** The disease time-course of six patients (**Table 2**, case #1 and case #3-7). Developmental delays started at 2 years of age and extended until age 3.5 years (purple). Neurological regression was subsequently apparent (green), and seizures (orange) began before age 4 years. The patients died at an average age of 7 years (black). Own elaboration (Power Point) modified from Guillen-Navarro et al. (2) and Araújo-Vilar et al. (133), respectively. The authorization for publication is provided in **Annex 17**.

From a neurological perspective, these patients exhibit a delay in reaching developmental milestones post-birth, particularly affecting speech development. Most children struggle to acquire basic phrases initially, with gradual progress observed up to approximately three years of age. However, their psychomotor skills tend to develop at a slower rate compared to their peers. While they may achieve fundamental tasks like walking, running, object manipulation, and understanding simple commands, sphincter control remains challenging. Around age three, a neurodevelopment regression occurs, characterized by a gradual loss of previous acquired skills. As time progresses, the neurodegenerative profile becomes more pronounced, leading to gait disturbances, frequent falls, diminished speech and comprehension abilities, the onset of spasticity, and the emergence of epileptic signs in the form of subtle myoclonic

seizures (e.g. blinking or drooling). As the disease advances, patients commonly develop tonic-clonic seizures and various forms of epilepsy, accompanied by the loss of head support and spastic paraparesis. Ultimately, individuals undergo a significant disconnection from their environment, facing challenges with swallowing that can result in frequent choking episodes and a subsequent deterioration in their nutritional status (**Figure 8**).

Celia's encephalopathy currently lacks a cure, and the typical cause of death often seems from the patient's overall health decline. This deterioration may be attributed to respiratory sepsis resulting from malnutrition compounded by bronchial aspiration, or from status epilepticus that remains unresponsive to anticonvulsant medications or other therapeutic interventions (2, 10). The age at which death occurs varies among reported cases, with six cases (**Table 2**; case #1 and #3-7) passing away before the age of nine years (between six and eight years) (133), while only one case died at the age of 28 years (**Table 2**; case #9) (134). A comprehensive therapeutic approach involving the management of metabolic complications in cases of generalized lipodystrophy, as well as the treatment of epileptic seizures and early psychomotor care, is crucial (10). Post-mortem examinations conducted on two patients (**Table 2**; case #1 and #3) revealed a severe deficiency in subcutaneous and visceral adipose tissue. Additionally, significant atrophy of the caudate nuclei, and moderate cortical atrophy in the frontal, parietal and occipital lobes were observed. Both cases exhibited profound neuronal loss and astrogliosis in the caudate-putamen nuclei, particularly pronounced in the dorsal and medial regions (2, 10).

Case #9 (**Table 2**) (127), a young woman with compound heterozygosity for the variants c.985C>T and c.1004A>C in the *BSCL2* gene, presented a remarkable neurological profile. Initially diagnosed with regressive autism spectrum disorder, she later developed atypical Parkinsonism in adulthood. Neurological signs and symptoms first appeared at three years old with mild behavioural disturbances, evolving into more pronounced rituals, social withdrawal, attention deficits, and sleep disturbance over time. Within months, the patient exhibited a decline in communication and language skills, followed by the emergence of motor stereotypies, limited language abilities, trichotillomania, and lower limb hypertonia by age six. By 16 years of age, neurological deterioration was evident, characterized by bilateral dystonic hypertonia and extrapyramidal and pyramidal signs. Camptocormia manifested at 21, progressing to falls and dysphagia at 23, ultimately leading to a diagnosis of significant frontal lobe syndrome. Imaging revealed atrophy of the caudate nuclei. The patient passed away at 28 years of age. This case notably diverges from the typical clinical course associated with the c.985C>T variant in compound heterozygosity, both in its neurological presentation (late onset of neurodegeneration, lack of evident epileptic seizures, Parkinsonism) and the absence of lipodystrophy, a consistent feature in compound heterozygotes. The second variant, c.1004A>C, also triggers exon 7 skipping, although the extent of abnormal transcript expression remains uncertain. It is conceivable that this case resembles classic homozygous forms of PELD, albeit with a slower neurological decline possibly linked to a reduced accumulation rate of the short isoform of seipin (10).

The c.974dupG variant in *BSCL2* has been reported in nine patients (**Table 2**; case #10-18) (10), with an additional ten unreported patients (five alive) from Taiwan (Dr. Ni-Chung Lee, Department of Pediatrics and Medical Genetics, National Taiwan University Hospital, personal communication) (**Table 2**; case #19-28). This variant was first documented by Agarwal et al. (111) in a 9-year-old girl with compound heterozygosity for the variant c.1126insG (**Table 2**; case #18). This girl exhibited CGL2 and intellectual disability. Years later, Wu et al. (131) reported the case of a 28-year-old male, compound heterozygote, c.[974dupG];[757G>T] (**Table 2**; case #16). This patient had CGL2, with symptoms including muscular hypertrophy, acromegaloid features, acanthosis nigricans, diabetes, hypertriglyceridemia, and hepatic steatosis. Additionally, he presented neurological symptoms such as mild intellectual disability, gait disorders, axial dystonia, and behavioural disturbances, but no seizures or encephalopathy. Additionally, Huang et al. (132) reported the case of a 1.8-year-old boy who was homozygous for the c.974dupG variant (**Table 2**; case #17). He exhibited CGL2, characterized by well-defined musculature, severe hypertriglyceridemia, and hepatic steatosis. However, no neurological involvement was observed, although there was no evidence of subsequent follow-up. In 2016, Opri et al. (129) reported three cases of CGL2 associated with progressive epileptic encephalopathy (**Table 2**; case #12-14). These cases included two girls who were homozygous for the c.974dupG variant, and a compound heterozygous boy for the variants c.[974dupG];[1020_1021delAA]. All three patients exhibited CGL2, characterized by well-defined musculature, hypertriglyceridemia, acanthosis nigricans, hepatic steatosis, and hypertrophic cardiomyopathy, with at least two cases showing these symptoms. Furthermore, these patients displayed a neurological profile comparable to Celia's encephalopathy. The onset of neurological symptoms occurred around 4-5 years of age and included absence seizure, myoclonus, and ataxic gait. Neurological decline progressed rapid, manifesting as pyramidal signs, language loss, severe intellectual impairment with dystonic tetraplegia, and continuous myoclonus. Epilepsy in these cases varied from absence seizure to myoclonic-atonic seizures. Neuroimaging revealed significant involvement of the head of the caudate and lenticular nuclei, along with hypertensive signals in brain MRI in these structures and the periventricular white matter. Moreover, our group documented two additional cases of CGL2 associated with the c.974dupG variant (**Table 2**; case #10 and #11), one in homozygosity and the other in compound heterozygosity (c.[974dupG];[1015C>T]). The first case involved a girl exhibiting generalized lipodystrophy, hypertriglyceridemia, and hepatomegaly. However, she did not display acanthosis nigricans, phlebomegaly, or muscle hypertrophy. Language acquisition delays became apparent at the age of two, although other nervous system functions remained relatively normal. Despite initially acquiring relatively complex language skills, she experienced language and psychomotor regression starting at age 5, leading to severe impairments by age 6, including altered gait with frequent falls and stereotypical orolingual dystonia. Over subsequent months, her neurological condition deteriorated progressively, marked by dysphagia, loss of the ability to walk, pyramidal signs, spasticity, hyperreflexia, and severe cognitive decline. By the age of nine, she developed prolonged tonic-clonic epileptic seizures and passed away at 9 years. Neuroimaging revealed significant

involvement of the caudate nuclei and a pronounced hypometabolism in the parietal and occipital lobes, akin to observations in a patient with the classic form of PELD (**Table 2**; case #2) (2, 128). Conversely, the second patient, a 2-year-old with compound heterozygosity, presented with typical CGL2 symptoms, including hypertriglyceridemia, hepatomegaly, and mild language impairment. In 2019, Zhang et al. (130) documented the case of a 17-year-old man diagnosed with CGL2 resulting from the homozygous c.974dupG variant (**Table 2**; case #15). This patient exhibited intellectual disability and severe epileptic manifestations starting at the age of three.

The c.1048C>T variant (123) and the c.1076dupC variant (124) have also been observed in individuals with CGL2, movement disorders, and progressive epileptic encephalopathy. In 2019, Serino et al. (124) published the case of a child with CGL2, myoclonic epilepsy, and progressive neurological deterioration due to the variant c.1076dupC (exon 9) in the *BSCL2* gene (**Table 2**; case #31). However, Ferranti et al. (123) documented two sisters, aged 11 and 18, who carried the c.1048C>T biallelic variant in the *BSCL2* gene, inherited from asymptomatic carrier parents (**Table 2**; case #29 and #30). However, the characterization of the lipodystrophic phenotype in these cases was limited. They experienced early language developmental delays, with generalized epileptic seizures emerging at the age of 5. Neurological deterioration ensued, marked by myoclonic seizures, and dyskinetic, dystonic, and choreoathetotic movements. Despite treatment attempts with various anticonvulsant combinations, their epileptic conditions remained resistant. By late childhood, psychomotor agitation, progressive language decline, and signs of bulbar involvement were evident. At 10 years old, both sisters lost their gait, and by 15, the elder became aphasic, succumbing at 18 due to deteriorating general health. MRI scans revealed supra and infratentorial atrophy, along with shrinkage of the caudate and putamen nuclei. These presentations closely resembled Celia's encephalopathy, albeit with slightly prolonged life (10).

The first documented case report of siblings carrying a heterozygous c.566T>A *BSCL2* variant (exon 4) (**Table 2**; case #32 and #33) (125) established a connection between early-onset epileptic encephalopathy, neurodevelopmental issues, and a heterozygous *BSCL2* variant. Neurological manifestations appeared early, with developmental delays and frequent febrile seizures. The older sibling exhibited myoclonus and absence episodes from the age of two, along with atonic seizures. By the age of 4, generalized tonic seizures became very frequent. Presently, at 11 years old, the child experiences intellectual deficit, autism spectrum disorder, ataxic gait, and significant language impairment. The younger sister began showing neurological symptoms at three months of age, with asymmetric tonic seizures emerging at 8 months. She succumbed at 10 months old due to refractory status epilepticus (10). More recently, the c.445C>G variant in heterozygosity has also been linked to epileptic encephalopathy (135).

Mutation and Molecular Mechanisms

The c.985C>T variant, situated in exon 7 of the *BSCL2*-203/227/217 transcript, was initially expected to introduce a premature stop codon, p.(Arg329*). However, Guillen-Navarro et al. (2) studies indicate that the cytosine to thymine transition at this position induces a change in the branch site consensus sequence (CCC**C**GAC > CCC**T**GAC), promoting splicing from a donor site at the start of intron 6–7 (CTGGGCTCAG**gt**gaggggcc) to an acceptor site at the end of intron 7–8 (tcctccac**ag**GTTAACATCC). This alteration leads to complete intronization of exon 7 (**Figure 8**). The skipping of exon 7 results in the transcription of a seipin variant lacking the second TMD. Consequently, starting from the first TMD, the remaining portion of the protein is confined within the ER lumen. This particular seipin variant may correspond to the short isoform, comprising 287 amino acids, or to a novel aberrant seipin form (referred to as Celia seipin) consisting of 287 amino acids plus an additional 64 amino acids (arising from the inclusion of exon 1 during transcription) (**Figure 9**) (2, 10).

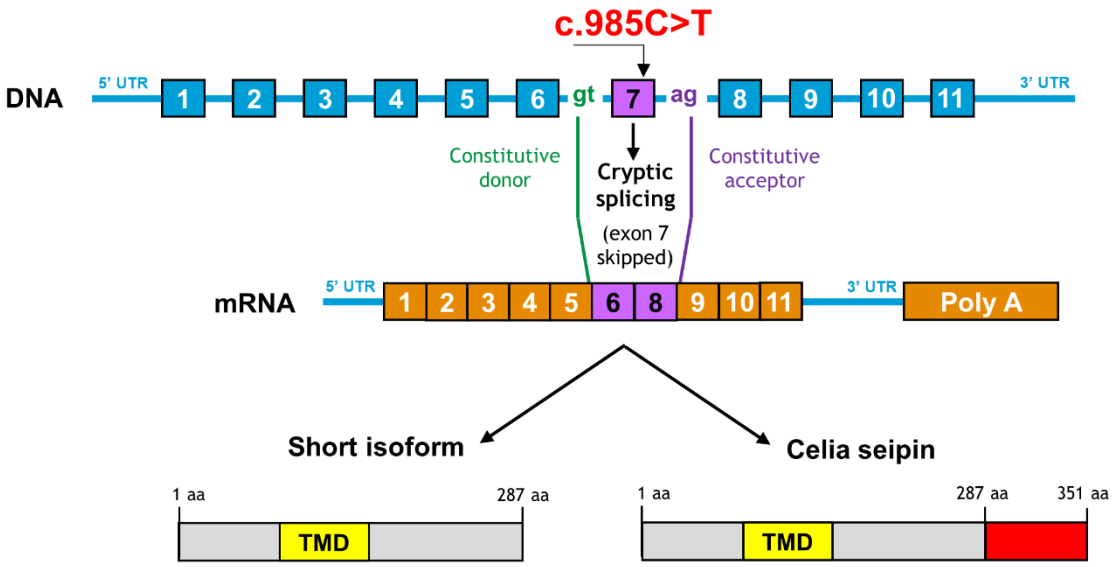

Figure 9. Splicing and protein model representation of the *BSCL2* c.985C>T mutation. The *BSCL2* c.985C>T mutation within exon 7 triggers cryptic splicing between the two constitutive splicing sites (donor to acceptor), leading to the omission of exon 7. Consequently, this transcription will give rise to two possible variants of seipin (both with only one transmembrane domain (TMD)). On the one hand, the short isoform of seipin (287 amino acids (aa)), and on the other hand, an aberrant seipin called Celia seipin (351 aa). Own elaboration (Power Point).

The analysis of *BSCL2* transcript expression in the brain of case #1 (**Table 2**) revealed that the transcript lacking exon 7 was expressed at a level of up to 21%, compared to only 0.3% in the brains of healthy individuals. Notably, the expression of this transcript was also significantly elevated in non-neural tissues of case #1 (**Table 2**) (2, 10). The potential implications of this heightened expression in the PELD patient, particularly in relation to any protective effects against lipodystrophy, remains to be fully elucidated.

Conversely, it has been demonstrated that this novel variant of seipin triggers oxidative and ER stress, consistent with the pronounced dilation of the ER cisterns filled with proteinaceous material observed in the primary preadipocytes of case #1 (**Table 2**) (2, 136). Furthermore, brain samples from this case initially displayed ubiquitin-positive intranuclear inclusions within neurons (2). However, these inclusions were found to actually be positive for seipin, likely a result of impaired oligomerization and aggregation of Celia seipin, predominantly presenting as singular and round-shaped structures, although occasional multiple inclusions are also noted (136). While the presence of seipin, an ER protein, within the nucleus may initially appear unexpected, it is worth noting that as discussed in **section 1.2.2**, seipin can also localize to the outer nuclear membrane in mammalian cells (57). Both wild type and Celia seipin have been observed to be situated around the nucleus, with a more pronounced distribution in cells that overexpress Celia seipin (2, 136). Given the increased formation of nuclear LD under stressful conditions (55), it is plausible to be hypothesize that neuronal damage triggered by ER stress in PELD may promote the translocation of seipin molecules to the nucleoplasm. This translocation could lead to the formation of aggregates that potentially contribute to the pathogenesis of PELD (**Figure 10A**), akin to mechanisms observed in Huntington's disease (137).

The severe neurodegenerative phenotype, coupled with the presence of inclusions containing Celia seipin and the disrupted oligomerization induced by the c.985C>T variant, implies a gain of toxic function in Celia's encephalopathy (136). Consequently, it might be anticipated that individuals who are simple heterozygous carriers would manifest some degree of pathology due to the expression of a small quantity of Celia seipin. However, they remain entirely asymptomatic (2). This observation could be elucidated by the interplay between wild type and Celia seipin. Wild type seipin could potentially sequester Celia seipin into mixed oligomers, thereby averting ER stress and the subsequent response to misfolded proteins (**Figure 10B**). In compound heterozygous patients lacking wild type seipin, this proposed rescue of phenotype would not be feasible (136). It could be postulated that the wild type seipin functions as an "anti-prionoid" in this context (10, 138).

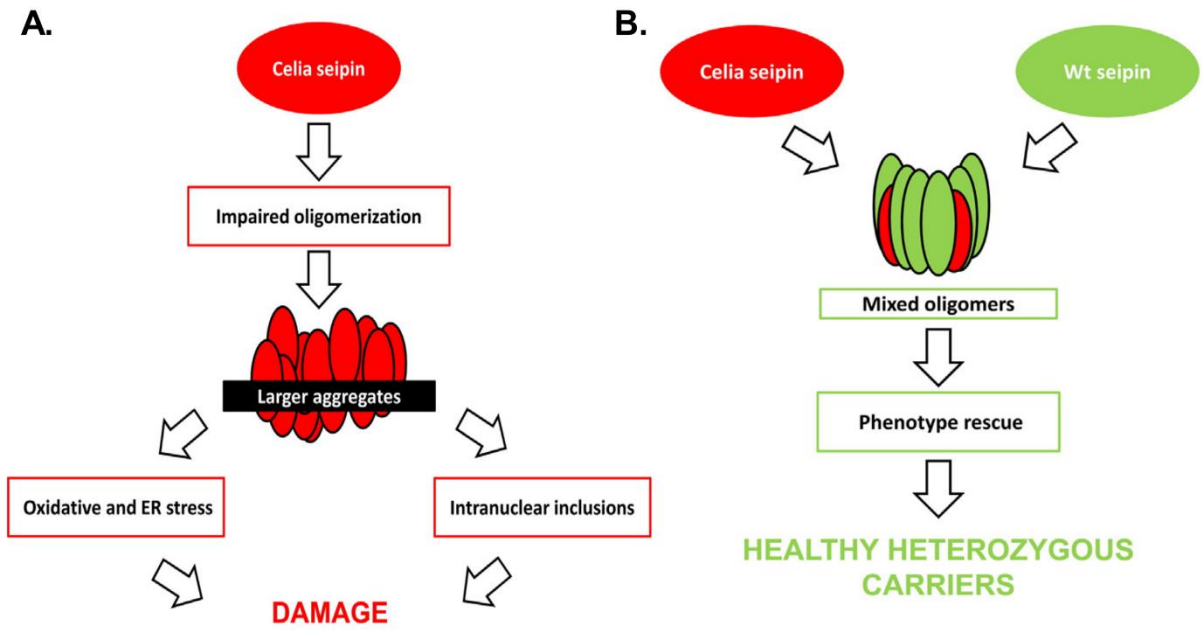

Figure 10. Proposed model for the mechanism of Celia seipin. A. Pathogenic model in homozygote carriers. **B.** Phenotype rescue model in healthy heterozygous carriers. Recovery from Ruiz-Riquelme et al. (136). The authorization for publication is provided in **Annex 17**.

This mechanism, considered responsible for the neurodegenerative presentation in the classic variant, may also be applicable to the c.974dupG variant. Thus, the c.974dupG variant, situated in exon 7 of the *BSCL2* gene, similarly induces exon skipping, mirroring the process seen in the classic form of PELD (2, 128). This variant disrupts specific splicing regulatory sequences known as exonic splicing enhancers (ESE), resulting in the creation of a novel ESE (10).

However, the mechanisms observed in the remaining variants may differ (10). The c.1048C>T variant can introduce a premature stop codon (p.(Arg350*), R[CGA] > *[TGA]) in the long seipin isoform (462 aa), as well as in the *BSCL2*-207 transcript, encoding the 398 amino acid seipin, (c.856C>T, p.(Arg286*), R[CGA] > *[TGA]). However, this event does not occur in the *BSCL2*-201 transcript, which encodes the short seipin isoform (287 amino acids) directly associated with Celia's encephalopathy pathogenesis. In this transcript, the c.714C>T variant would not lead to a premature stop codon (p.(Asn238=), N[AAC] > N[AAT]) (139). The stop codon present in both *BSCL2*-203 (encoding the 462 amino acid seipin) and *BSCL2*-207 (encoding the 398 amino acid seipin) transcripts satisfies the 50–55 nucleotide rule (140). Therefore, it could be inferred that these transcripts might undergo degradation via the nonsense-mediated decay (NMD) pathway, suggesting a potential overexpression of an aberrant longer isoform of Celia seipin, consistent with proposed pathogenetic mechanisms, although expression studies supporting this hypothesis are lacking.

Similarly, the c.1076dupC variant would result in a premature stop codon in the *BSCL2*-203 transcript, p.(Glu360*), [CCT (Pro) GAA (Glu) >> CCC (Pro) TGA (*)], as well as in the *BSCL2*-207 transcript, p.(Glu295*), where the variant notation would be c.884dupC.

However, in the *BSCL2*-201 transcript, which encodes the short isoform, the insertion of a cytosine (c.742dupC) does not generate a premature stop codon. Instead, it induces a frameshift leading to an extension of 83 amino acids at the intraluminal carboxy-terminal domain's end. Consequently, a 370-amino acid-long seipin would be translated, deviating from the 287 amino acids of the short canonical isoform of seipin, p.Leu228Glu*fs*TER103. Although the premature stop codons predicted in the long and intermediate transcripts do not adhere to the 50–55 nucleotide rule indicative of NMD mechanism (140), it is conceivable that they undergo degradation via alternative mechanisms unrelated to the exon junction complex (141). In this regard, it has been proposed that mRNA degradation resulting from premature stop codons could influence the increased expression of other transcripts (142).

The case of c.566T>A variant is particularly notable since it neurologically resembles Celia's encephalopathy, despite being heterozygous in the *BSCL2* gene and not affecting short seipin. However, this variant would result in the change p.(Met189Lys) in the luminal loop of the protein, similar what is observed in motor neuron diseases associated with *BSCL2*. The underlying mechanism responsible for this remains to be clarified (10).

In addition to the proposed mechanisms of neuronal death in PELD, dysfunction of peroxisomes may contribute to the neurodegenerative phenotype observed in this disease (4, 53, 54). As outlined in **section 1.2.2**, peroxisomes are abundant in neurons and play a vital role in defending against oxidative stress. The peroxisome biomarker *PEX16* was found in close proximity to seipin in healthy human brains; however, its presence was notably absent in samples from case #1 (**Table 2**). *PEX16*, an essential protein for peroxisomal biogenesis crucial for *de novo* synthesis of peroxisomes (143), is also implicated in adipogenesis (144). This observation further supports the hypothesis concerning the pathogenetic mechanisms underlying Celia's Encephalopathy.

1.4 MURINE MODELS FOR SEIPINOPATHIES

1.4.1 Congenital Generalized Lipodystrophy Type 2 Models

The first model for CGL2 in mice, also referred to as seipin knock-out (SKO) mice, was established by disrupting *Bscl2* through homologous recombination in embryonic stem cells (ESC) (59). Given that the expression pattern of seipin in rat organs more closely resembles that in humans than in mice, a CGL2 rat model was created using ENU (N-ethyl-N-nitrosourea) mutagenesis to induce SKO (145). Several mouse models have been developed to date, successfully replicating most of the metabolic phenotypes observed in human CGL2 patients (24, 62).

The complete deletion of seipin in mice results in a significant reduction in white adipose tissue (WAT), with inguinal (ingWAT) and mesenteric WAT remaining at less than 10%, and gonadal WAT (gonWAT) being entirely absent in nearly all models (59, 61, 146). Similarly, SKO rats exhibit severe lipodystrophy, showing a 95% decrease in adipose tissue (145).

Conversely, the reduction in interscapular brown adipose tissue (iBAT) mass is less pronounced, with a 30 to 55% decrease observed in both mice and rats (59, 61, 145, 146). In all mouse models, leptin levels decreased by 30 to 40%, while plasma adiponectin concentrations experienced a substantial decline, with a 90% reduction noted in mice aged between 8 to 12 weeks (59, 61, 146). This metabolic phenotype is characterized by impaired glucose tolerance, reduced insulin sensitivity, and significant hyperinsulinemia (59, 61, 62, 146). Interestingly, SKO mice exhibit hypotriglyceridemia (59, 61, 146), potentially attributed to enhanced clearance of TAG-rich lipoproteins and increased uptake of fatty acids by the liver, accompanied by decreased basal energy expenditure in mice (24, 59, 146). Conversely, seipin-deficient rats display hypertriglyceridemia, indicating that rats may offer a more suitable model for investigating lipoproteins in the context of lipodystrophy (62, 145). These findings indicate that lipodystrophy may result, at least in part, from a reduction in mature adipocytes (62). Notably, deletion of *Bscl2* under the adipocyte-specific promoter of the *Adipoq* gene using CRE-mediated mechanisms results in early and severe lipodystrophy, characterized by significant loss of gonadal and subcutaneous WAT and an 80% decrease in circulating adiponectin levels (62, 147). Conversely, deletion of seipin under the *aP2* promoter (148) leads to a less severe and more gradual loss of adipose tissue (62). In both models, leptin levels remained unchanged while adiponectin levels decreased, indicating that the remaining adipose tissue was adequate for critical production of this satiety hormone (62, 147, 148). Furthermore, seipin deletion driven by the *aP2* promoter results in insulin resistance and glucose intolerance (62, 148). In contrast, seipin deletion under the constitutive *Adipoq* promoter does not lead to glucose intolerance initially; however, exposure to a high fat diet (HFD) for 48 hours triggers glucose intolerance, suggesting heightened susceptibility to metabolic complications in these mice (62, 147). Overall, the lack of adipose tissue plays a pivotal role in the metabolic complications associated with BSCL, with adipocyte seipin playing a significant role in the development of carbohydrate metabolism abnormalities (62). Nonetheless, the onset of metabolic issues later on or their reliance on an HFD trigger raises questions about the function of seipin in metabolic tissues (62).

Associated with the absence of adipose tissue and metabolic complications, both SKO mice and rats exhibit significant hepatomegaly characterized by extensive liver steatosis (59, 61, 145, 146). Analysis of liver lipids revealed a 3 to 4-fold increase in TAG content (59, 62, 146, 149). Notably, adipose-specific SKO mice demonstrate hepatic steatosis (148), while liver-specific knock-out mice do not develop hepatic steatosis or associated metabolic issues (149, 150). These findings suggest that the normal TAG storage function of adipose tissue serves as a protective mechanism against liver steatosis (24), indicating no apparent cell-autonomous role for seipin in the hepatocytes (62). Cardiomyopathy is a common occurrence in *BSCL2* patients; however, the phenotype in mice varies significantly, and its cause remains unclear (62). Hearts from SKO mice exhibit increased weight and display concentric left ventricular hypertrophy (LVH) (62, 63, 151, 152). The potential causes of LVH range from a potential association with hypertriglyceridemia (151) to excessive lipid catabolism (63) or neutrophil infiltration and severe fibrosis (152), both exacerbated by seipin deficiency.

Interestingly, heart-specific seipin deletion does not result in cardiac dysfunction, supporting the notion that cardiomyopathy is a consequence of lipodystrophy (62, 153). Furthermore, lipodystrophic SKO mice exhibit polyuria along with increased excretion of albumin, creatinine, and ions. These changes are associated with an increase in glomerular and mesangial surface area, lipid deposition, and signs of oxidative stress in the kidneys, indicating renal abnormalities (62, 154). Regarding reproductive system changes in SKO mice, males have both teratozoospermia and complete infertility (110, 155), while all females have accelerated mammary gland ductal growth but delayed vaginal opening (156), insufficient milk production (157), and defective parturition (24, 158).

In line with CGL2 patients, SKO mice exhibit CNS abnormalities, including anxiety (80), depression (80, 83), spatial cognitive deficits (81), and impaired motor coordination (24, 86). These impairments have been noted in SKO mice and in neuronal-specific seipin knock-out (seipin-nKO) mice but not in adipose-specific SKO mice. This suggests that these deficits are not a result of lipodystrophy and highlights the intrinsic role of seipin in the CNS (62, 81, 86).

1.4.2 *Bscl2*-associated Motor Neuron Disease Models

BSCL2-associated motor neuron diseases manifest distinct effects on upper motor neurons, lower motor neurons, and peripheral motor axons (159). Currently, there are three animal models for these conditions: N88S mutant seipin transgenic (N88S seipin Tg) mice (160), N88S seipin Tg zebrafish (161), and N88S/S90L mutant seipin transgenic (N88S/S90L seipin Tg) mice (162). Both the N88S seipin Tg mice and N88S/S90L seipin Tg mice replicate the most severe phenotype observed in patients with *BSCL2*-associated motor neuron diseases, displaying progressive spastic motor deficits, reactive gliosis in the spinal cord, and neurogenic muscular atrophy (24, 160, 162). The primary phenotype observed in N88S seipin Tg zebrafish is a decrease in spontaneous free-swimming activity (161).

At the molecular level, variants such as N88S and S90L in *Bscl2* inhibit seipin glycosylation, leading to protein misfolding and aggregation, excessive accumulation of misfolded proteins, and subsequent induction of ER stress in neurons (115, 120, 121). Expression of the N88S seipin mutant in mice has been found elevate specific ER stress markers, underscoring the intimate connection between the pathological mechanisms of these diseases and ER stress (160). Conversely, there is no apparent ER stress in both N88S/S90L seipin Tg mice and N88S seipin Tg zebrafish (161, 162). However, in N88S/S90L seipin Tg mice, a notable activation of the autophagic response in the CNS has been demonstrated to specifically contribute to motor neuron degeneration, rather than an increase in ER stress or inflammatory reactions (162). In line with previous *in vitro* investigations demonstrating the formation of protein inclusions by N88S and S90L seipin mutants (120, 121), both N88S seipin Tg mice and N88S/S90L seipin Tg mice display the presence of inclusion bodies in neuronal cytoplasm (160, 162). These inclusion bodies may serve as an adaptive response to counteract the accumulation of N88S and/or S90L mutant seipin in the ER and the associated ER stress (160). However, only aggresomes, not inclusion bodies, have been documented in

patients (115). Furthermore, the expression of seipin N88S alters LD morphology and reduces TAG storage in both motor neuron cells and zebrafish (161, 163), although this aspect has not been explored at the murine level (24).

1.4.3 Treatment Strategies

Currently, treatments for diseases stemming from *BSCL2* variants predominantly address symptoms, lacking precise and targeted therapeutic interventions. And research on targeted therapy for PELD and *BSCL2*-associated motor neuron diseases remains limited (10, 24, 93).

The restoration of adipose tissue function, which involves enhancing TAG storage capacity and restoring adipokine levels, plays a crucial role in managing metabolic disorders and complications in CGL2 (164). In SKO mice, metabolic disruptions, and associated complications such as insulin resistance, severe hypoleptinemia, pronounced hepatic steatosis, and renal injury are ameliorated by adipose tissue transplantation (24, 154, 165). This metabolic improvement is further supported by the restoration of seipin expression in adipose tissue (166). Treatment with PPARγ agonists like pioglitazone, not only enhances insulin sensitivity but also improves liver steatosis (146) and hypertrophic cardiomyopathy (151). Rosiglitazone treatment not only corrects metabolic disorders in SKO mice (148, 167) but also mitigates hyperlipidaemia and atherosclerosis (24, 168). However, in SKO rats, both pioglitazone and rosiglitazone do not effectively address fatty liver issues, prompting inquiries into species-specific responses or the methodology of SKO animal generation (24, 169). Conversely, leptin-replacement therapy not only restores impaired vascular function (170, 171) but also alleviates kidney injury stemming from metabolic disturbance (24, 154). Fibroblast growth factor 21 (Fgf21), another adipokine, has been utilized to enhance insulin sensitivity and elevate plasma adiponectin levels in SKO mice (24, 172). Moreover, the deletion of GPAT3 markedly enhances insulin sensitivity and diminishes liver steatosis in SKO mice by augmenting adipocyte tissue mass (24, 173). Likewise, adipose tissue mass correlates closely with ATGL expression in SKO mice, and the partial deletion of ATGL significantly ameliorates metabolic disorders and cardiac hypertrophy. Complete ablation of ATGL even completely reverses the lipodystrophy induced by seipin deficiency (24, 63).

Gene therapy has also been proposed as a novel, safe, and effective treatment to reverse severe metabolic complications that develop in patients with lipodystrophy. Authors such as Sommer et al. (174) revealed that systemic delivery of human *BSCL2* using adeno-associated virus (AAV) vectors can target adipose progenitor cells *in vivo* and substantially restore white adipose tissue development in adult SKO mice. Although this approach only achieved partial adipose tissue depot development, it resulted in both rapid and prolonged beneficial effects on metabolic health, such as normalizing hyperglycemia, decreasing serum triglycerides, reducing hepatomegaly, and restoring insulin sensitivity.

In organs where seipin functions autonomously within cells, targeting seipin-related PPARγ pathways is essential for mitigating disorders in these organs in CGL2. Rosiglitazone treatment has demonstrated efficacy in improving anxiety, depression (80, 83), spatial

cognitive impairment (81), motor deficits (86), and $A\beta_{25\text{-}35/1\text{-}42}$-induced Alzheimer's disease (24, 85) in SKO mice. In seipin-nKO male mice, both rosiglitazone or oestradiol have shown effectiveness in alleviating anxiety and depression by restoring PPARγ function (24, 80). Moreover, rosiglitazone or oestradiol has exhibited potential in restoring pancreatic function in male mice with heterozygous seipin deletion (24, 167). The downstream targets of PPARγ present significant therapeutic promise: a mitogen-activated protein kinase (MEK) inhibitor blocks the rosiglitazone-rescued depression and spatial memory impairments in seipin-nKO mice (81, 83); a GSK3 inhibitor ameliorates α-synuclein phosphorylation, neuroinflammation and the hyperphosphorylation and aggregation of tau protein in seipin-nKO mice (84, 86); and a PI3K or mTOR inhibitor accelerates p-tau and tau protein clearance, thereby alleviating axonal atrophy in the hippocampal neurons of seipin-nKO mice (24, 84).

2 OBJETIVES

Lipodystrophies are rare disorders, with Celia's encephalopathy, identified by our research group in 2013, being exceptionally rare with only 33 cases to date (10). Over the years, our group has elucidated some of this disease's pathogenic mechanisms (2, 128, 136, 175, 176). However, due to its low prevalence, severity, and predominant brain involvement, studying it in humans is challenging Therefore, this study proposed developing a biological model of the disease using a knock-in mouse model that expresses the aberrant human *BSCL2* transcript. Additionally, and due to the strategy employed for the generation of the knock-in mouse, a *Bscl2* knock-out mouse model was generated, allowing for the comparison of the effects of *Bscl2* deficiency versus the overexpression of the aberrant human *BSCL2* transcript.

The primary objective of this research was to enhance understanding of the molecular mechanisms underlying neurodegeneration, lipodystrophy, and non-alcoholic steatohepatitis of Celia's encephalopathy by employing two murine models. This effort aimed to contribute to the comprehension of this syndrome.

Detailed objectives

- Generate a global knock-in murine model for the Celia human transcript (*Bscl2*$^{Celia/Celia}$) and a seipin knock-out model (*Bscl2*$^{-/-}$).
- Analyse the expected neurodegenerative process in knock-in mice, their clinical manifestations, pathocronia, prevalence, life expectancy, and causes of death.
- Evaluate the neurological phenotype through free locomotion, memory, motor strength, and coordination.
- Evaluate the histological, cellular, subcellular, and molecular alterations in the different brain regions of these mice.
- Determine the hematological, biochemical and glucose metabolism.
- Evaluate the impact that both the ablation of murine *Bscl2* and the insertion of the human transgene have on adipose tissue, liver, kidneys, heart, and spleen in these mice, considering morphological, histopathological, and functional aspects.

3 ANIMALS AND METHODS

3.1 MICE

Murine models were established through collaboration with Cyagen Bioscience (Santa Clara, CA, US). As a result, certain data pertaining to the methods outlined in **sections 3.1.1** and **3.1.2** are considered proprietary to the industry and are not publicly available.

Ethical approval

All animal work and procedures were conducted in accordance with the ethical standards outlined by the institutional Ethics Committee of the Xunta de Galicia (approval numbers 15010/17/004 and 15012/2021/014, see **Annex 15**) and the University of Santiago de Compostela. The research was carried out at the Biomedical Experimental Centre (CEBEGA) of the University of Santiago de Compostela, under the REGA number ES150780292901. These procedures adhered to the principles of laboratory animal care as mandated by European Union Law (2010/63/UE) and the Spanish Government (RD 53/2013) concerning the protection of animals used for scientific purposes.

3.1.1 Vector Construction

The *Bscl2* gene (MGI:1298392) is located on mouse chromosome 19. Eleven exons have been identified, with the second ATG start codon in exon 2 and the TGA stop codon in exon 11 (Transcript: *Bscl2*-201 ENSMUST00000086058.13) (**Figure 11A**). For both murine models, knock-out (*Bscl2*$^{-/-}$) and knock-in (*Bscl2*$^{Celia/Celia}$), the ATG start codon in exon 2 of *Bscl2* gene was replaced with a reversely positioned cassette (LoxP-Lox2272-reverse His tag-Human *BSCL2* CDS without exon7-reverse LoxP-Neo cassette-reverse Lox2272) (**Figure 11B-C**) in such a way that in the targeted allele the human transgene (3'-5') was not transcribed before Cre mediated recombination, thus obtaining the knock-out (KO) murine model for seipin (*Bscl2*$^{-/-}$). Upon the introduction of Cre recombinase, the inversion of the cassette facilitated the expression of His-tagged, aberrant human seipin (**Figure 11E**), leading to the development of the knock-in (KI) murine model (*Bscl2*$^{Celia/Celia}$).

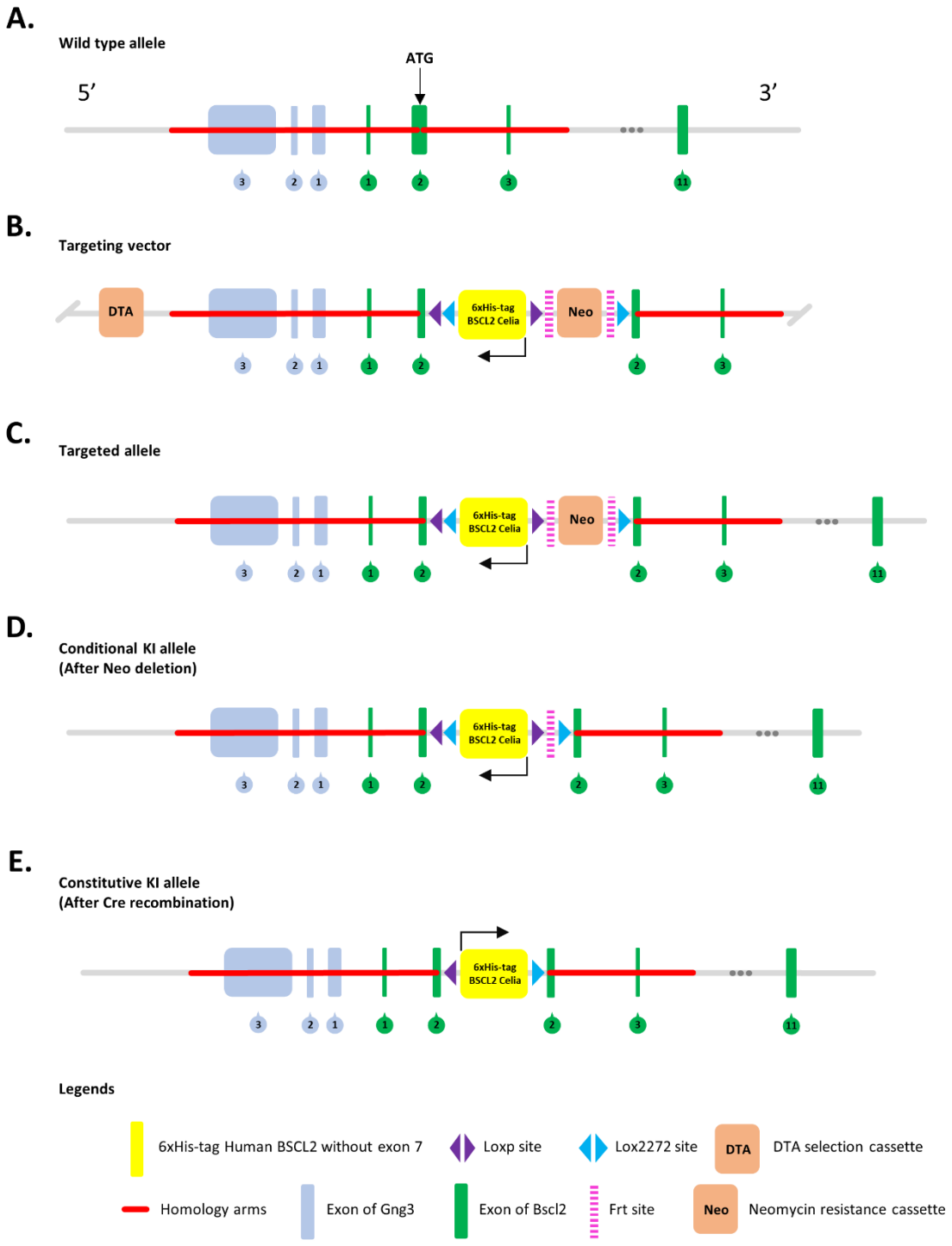

Figure 11. Targeting strategy for the *BSCL2* knock-in murine model. A. Wild type allele (Transcript: *Bscl2*-201). **B.** Targeting vector. **C.** Targeting allele. **D.** Conditional knock-in (KI) allele after Neo deletion. **E.** Constitutive knock-in (KI) allele after Cre recombination. Recovery from Cobelo-Gomez et al. (177) under Creative Common license.

The homology arms (HAs) region for constructing the targeting vector was generated via PCR using high-fidelity Taq polymerase, utilizing bacterial artificial chromosome (BAC) clones RP23-83P21 and RP23-125I21 from the C57BL/6J library as templates. Subsequently, mouse genomic fragments containing these HAs were sequentially integrated into the targeting vector along with recombination sites and selection markers, as illustrated in **Figure 11B**. The Neo cassette was flanked by Frt sites, and Diphtheria toxin A (DTA) was employed for negative selection. The targeting vector underwent restriction enzymes digestion for validation purposes, with the sequence provided in **Annex 1**.

3.1.2 Generation of Transgenic Mice

The linearized vector was delivered to C57BL/6 ESC through electroporation, followed by drug selection, PCR screening, and Southern Blot confirmation. The specific regions chosen for PCR screening and Southern Blot analysis, along with their respective conditions and expected fragments sizes, are detailed in **Figure 12**.

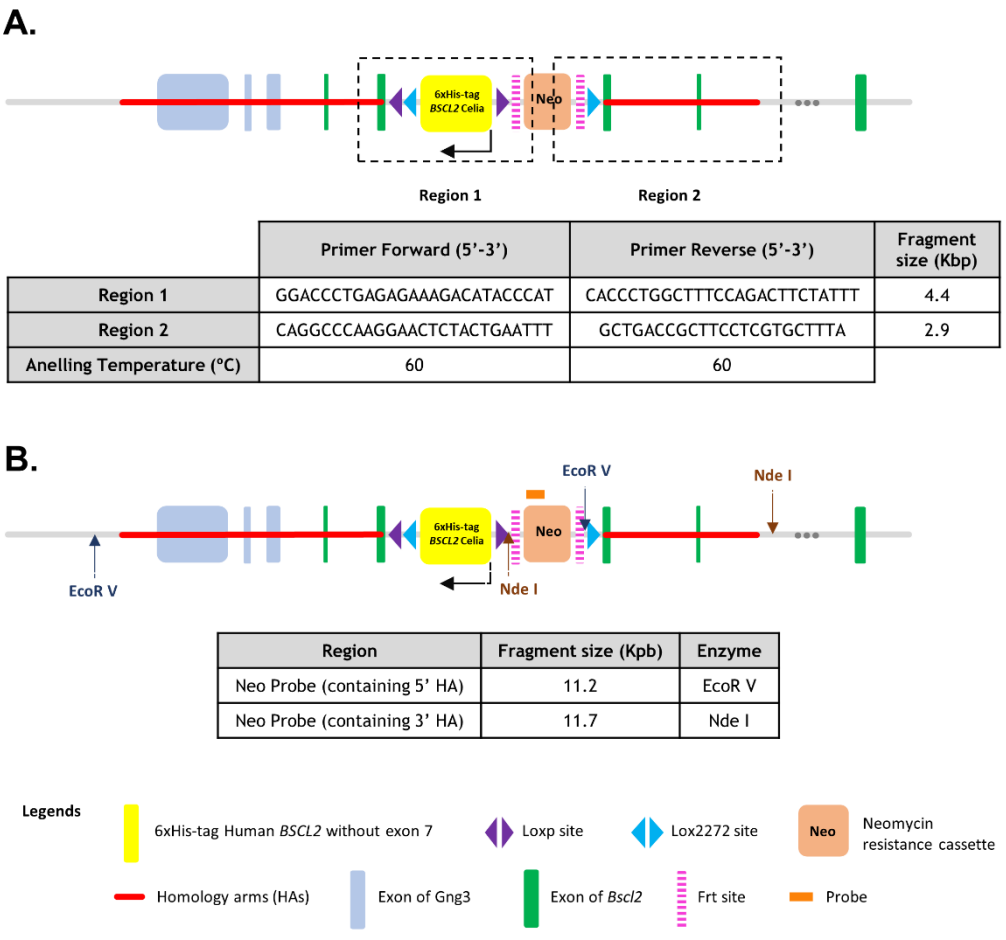

	Primer Forward (5'-3')	Primer Reverse (5'-3')	Fragment size (Kbp)
Region 1	GGACCCTGAGAGAAAGACATACCCAT	CACCCTGGCTTTCCAGACTTCTATTT	4.4
Region 2	CAGGCCCAAGGAACTCTACTGAATTT	GCTGACCGCTTCCTCGTGCTTTA	2.9
Anelling Temperature (°C)	60	60	

Region	Fragment size (Kpb)	Enzyme
Neo Probe (containing 5' HA)	11.2	EcoR V
Neo Probe (containing 3' HA)	11.7	Nde I

Figure 12. Conditions for the targeted ESC clones confirmation by PCR screening and Southern Blot. A. Regions and primers selected for the PCR screening. **B.** Regions and enzymes for Southern Blotting. Expected fragment size in kilo-base pairs (Kpb) for both experiments. Own elaboration (Power Point).

After confirming correctly targeted ESC clones, some clones were selected for blastocyst microinjection, followed by chimera production. Founders (F0) were confirmed as germline-transmitted via crossbreeding with Flp-deleter mouse. The resulting heterozygous mutant mice (*Bscl2*$^{+/-}$) were confirmed by PCR (**Figure 13A**). One of this male heterozygous seipin knock-out mouse (*Bscl2*$^{+/-}$) was bred with Cre-global female mouse (E2a-Cre, 2.B6.FVB-Tg(EIIa-cre)C5379Lmgd/J, ref. J003724, The Jackson Laboratory, Bar Harbor, ME, US, http://jaxmice.jax.org/strain/003724.html) to obtain the heterozygous constitutive knock-in mice (*Bscl2*$^{+/Celia}$), confirming them by PCR (**Figure 13B**).

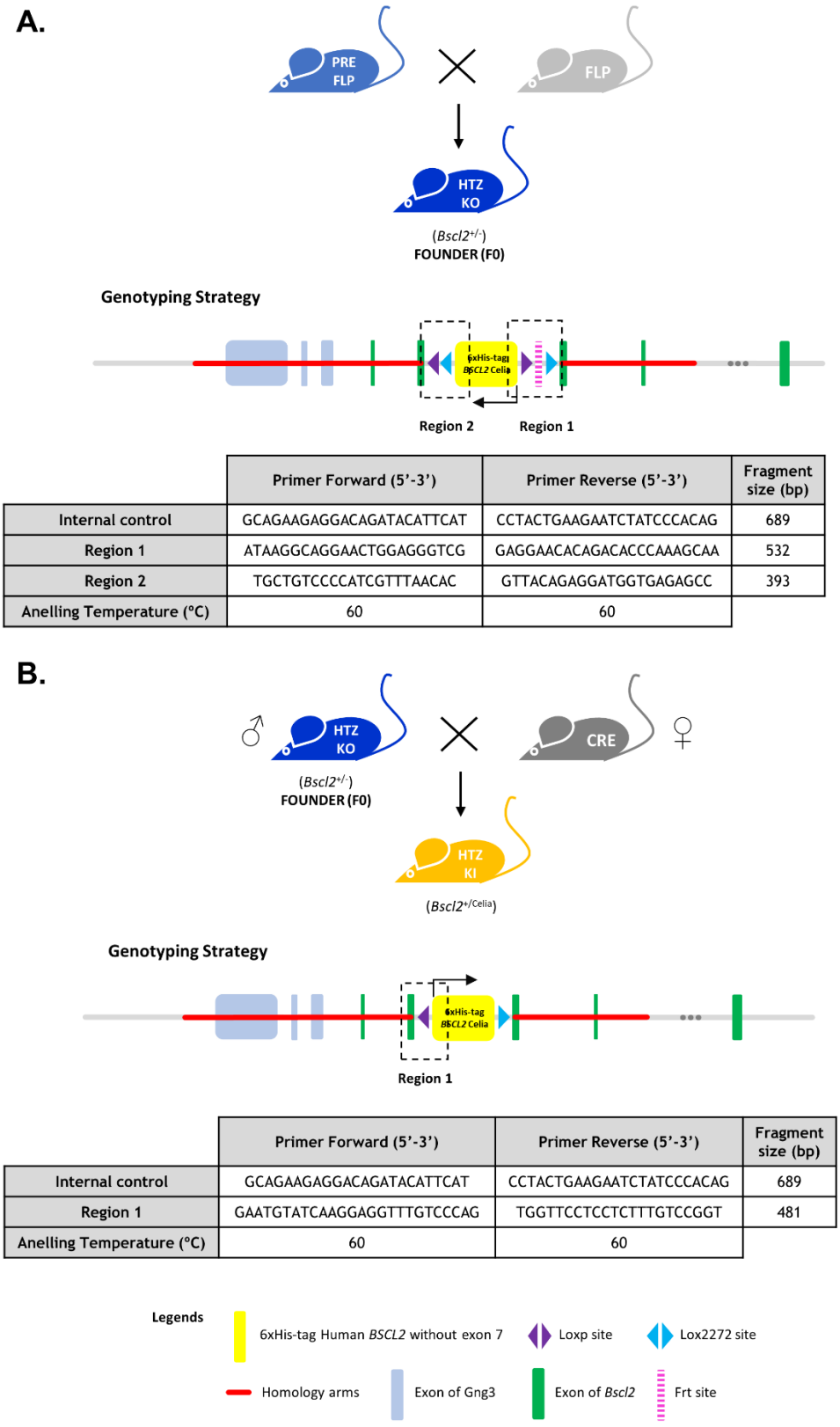

	Primer Forward (5'-3')	Primer Reverse (5'-3')	Fragment size (bp)
Internal control	GCAGAAGAGGACAGATACATTCAT	CCTACTGAAGAATCTATCCCACAG	689
Region 1	ATAAGGCAGGAACTGGAGGGTCG	GAGGAACACAGACACCCAAAGCAA	532
Region 2	TGCTGTCCCCATCGTTTAACAC	GTTACAGAGGATGGTGAGAGCC	393
Anelling Temperature (°C)	60	60	

	Primer Forward (5'-3')	Primer Reverse (5'-3')	Fragment size (bp)
Internal control	GCAGAAGAGGACAGATACATTCAT	CCTACTGAAGAATCTATCCCACAG	689
Region 1	GAATGTATCAAGGAGGTTTGTCCCAG	TGGTTCCTCCTCTTTGTCCGGT	481
Anelling Temperature (°C)	60	60	

Figure 13. Chimera production and PCR confirmation strategy. A. Strategy for founder obtention (heterozygous knock-out (KO) for seipin) and PCR confirmation. **B.** Crossbreeding strategy for the obtention of heterozygous knock-in (KI) for human truncated *BSCL2* protein and the necessary conditions for the PCR confirmation. Own elaboration (Power Point).

A round of intercrossing was required to obtain homozygous mice (*Bscl2*$^{Celia/Celia}$) (**Figure 14**).

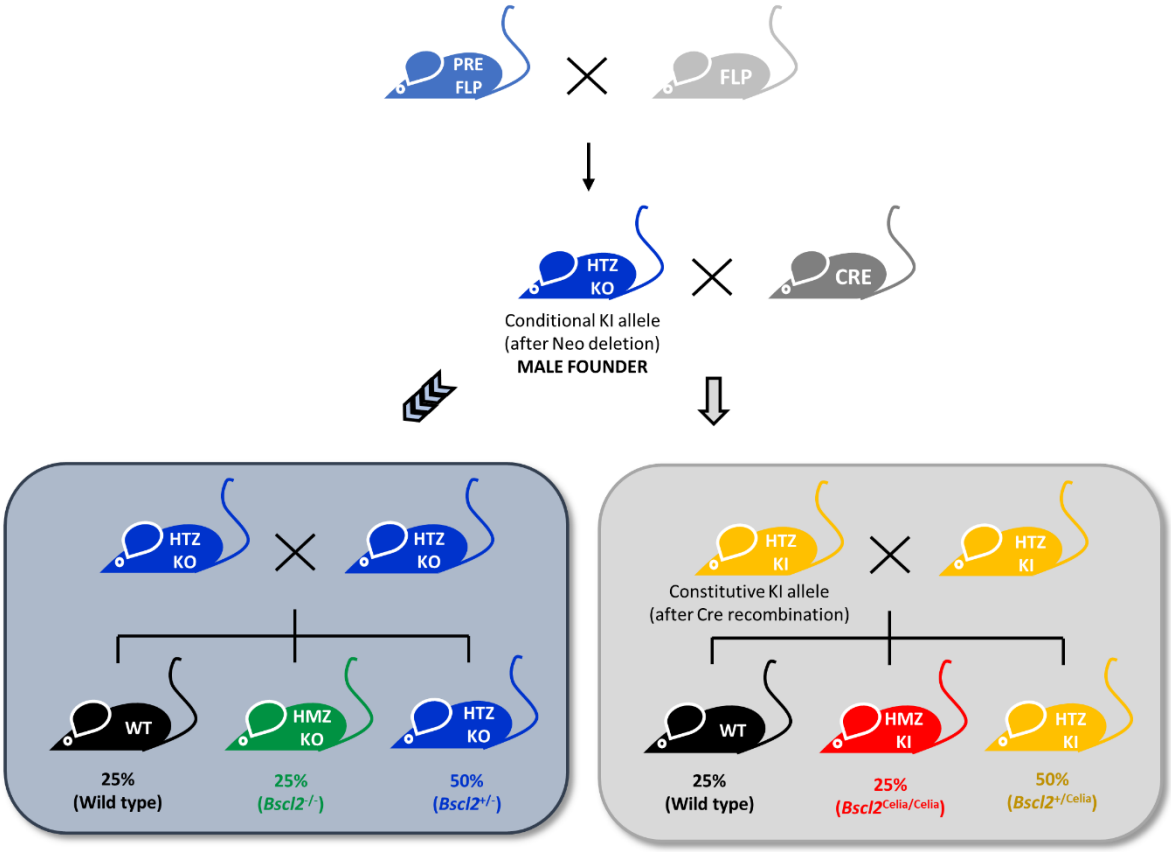

Figure 14. Crossbreeding strategy for the obtention of both murine models, knock-out for seipin (*Bscl2*$^{-/-}$) and knock-in for the truncated human seipin (*Bscl2*$^{Celia/Celia}$). Own elaboration (Power Point) modified from Cobelo-Gómez et al. (177) under Creative Common license.

3.1.3 Sequencing

One knock-out (*Bscl2*$^{-/-}$) and one knock-in (*Bscl2*$^{Celia/Celia}$) mouse, were sequenced in order to verify the correct generation of each murine model.

Isolation of genomic DNA was carried out from the tail tissue using E.Z.N.A Tissue DNA Kit (#cat D3396-02, Omega Bio-Tek, Norcross, GA, US) following the manufacturer's recommendations. The samples were then quantified on the NanoDrop2000 spectrophotometer (Thermo Fisher Scientific, Waltham, MA, US).

For the sequencing procedure DNA concentration was adjusted to 100 µg/mL. Specific primers were designed with the Primer3Plus software (http://www.bioinformatics.nl/cgi-bin/primer3plus/primer3plus.cgi) (**Table 3**). Prime's hybridization sites are shown in **Annex 2.**

Table 3. Primers used for the sequence verification of knock-out (KO) and knock-in (KI) murine models. Sequences, fragment size in base pairs (bp) and primer names (Forward 1, 1b, 2, 3, 4, 5 (F1, F1b, F2, F3, F4, F5), Reverse 1, 1b, 3, 5 (R1, R1b, R3, R5)).

	Forward primers		Reverse primers		Fragment size (bp)
	Sequence (5'-3')		Sequence (5'-3')		
KO sequencing	F1	AATAAGGCAGGAACTGGAGGGTCG	R1	GAGGAACACAGACACCCAAAGCAA	532
	F1b	TGCTGTCCCCATCGTTTAACAC	R1b	GTTACAGAGGATGGTGAGAGCC	394
	F2	GTCTCCAGCTACCCTGGAAAAGAAA	R1	GAGGAACACAGACACCCAAAGCAA	1813
	F3	GAATGTATCAAGGAGGTTTGTCCCAG	R1	GAGGAACACAGACACCCAAAGCAA	1982
	F5	GCGCATGTGAAGCAATGACT	R5	ACCCTCGGTCAATACTGGGA	2055
KI sequencing	F2	GTCTCCAGCTACCCTGGAAAAGAAA	R1	GAGGAACACAGACACCCAAAGCAA	1642
	F2	GTCTCCAGCTACCCTGGAAAAGAAA	R3	TGGTTCCTCCTCTTTGTCCGGT	313
	F3	GAATGTATCAAGGAGGTTTGTCCCAG	R1	GAGGAACACAGACACCCAAAGCAA	1811
	F3	GAATGTATCAAGGAGGTTTGTCCCAG	R3	TGGTTCCTCCTCTTTGTCCGGT	482
	F4	CCGGAAGGAAGTCCAACGAA	R1	GAGGAACACAGACACCCAAAGCAA	533
	F5	GCGCATGTGAAGCAATGACT	R5	ACCCTCGGTCAATACTGGGA	1884

A final volume of 13 µL per sample was used for PCR, using 0.5 µL of each primer (forward and reverse), 2.5 µL of 5x buffer and 0.1 µL of MyTaq HS enzyme, both included in the MyTaq™ HS DNA Polymerase kit (cat# BIO-2111, Bioline, London, GB). The amplification process was carried out in the thermocycler (FlexCycler, Analytik Jena, Jena, DE) following the conditions below (**Table 4**).

Table 4. Programming conditions for the amplification process. Stage or step, temperature (ºC), time (min) and cycles.

Stage/step	Temperature	Time	Cycles
Incubate	95 ºC	3 min	-
Denature	95 ºC	15 s	x 35
Anneal	60 ºC	30 s	x 35
Extend	72 ºC	30 s	x 35
Final extend	72 ºC	10 min	-
Hold	4 ºC	∞	-

Samples were analysed by electrophoresis on a 1 % agarose gel (#cat BP160 Low-EEO/Multi-Purpose/Molecular Biology Grade, Fisher Scientific, Pittsburgh, PA, US) in presence RedSafe (20,000x, #cat 21141, iNtRON Biotechnology, Seongnam-si, KR) and visualized with QUANTUM ST4-1000/26MX (Vilber Lourmat, Collégien, FR).

Enzymatic cleanup of PCR reaction was performed with ExoSAP-IT PCR Product Cleanup (#cat. 78205.10.ML, Applied Biosystems, Thermo Fisher Scientific, Waltham, MA, US). 5 µL of each PCR product was treated with 2 µL of ExoSAP-IT reagent. Treatment was carried out at 37°C for 15 minutes followed by an incubation period at 80°C for 15 minutes to inactivate both enzymes.

For Sanger sequencing reaction the BigDye™ Terminator v3.1 Cycle Sequencing Kit (#cat. 4337455, Applied Biosystems, Thermo Fisher Scientific, Waltham, MA, US) was used. For each "PCR + ExoSAP-IT" sample, two reactions (forward and reverse) of 9 µL total were prepared (**Table 5**) and 1 µL of sample was added to each of the reactions.

Table 5. Reaction mixes for Sanger's sequencing. Forward and reverse reaction volumes (µL).

	Forward reaction mix	Reverse reaction mix
Deionized water (RNase/DNase free)	5.5 µL	5.5 µL
5X Sequencing Buffer	2 µL	2 µL
M13 (-21) forward primer	1 µL	-
M13 (-21) reverse primer	-	1 µL
BigDye Terminator v3.1 Ready Reaction Mix	0.5 µL	0.5 µL

The sequencing reaction was carried out in the thermocycler following the conditions below (**Table 6**).

Table 6. Programming conditions for the Sanger's sequencing. Stage or step, temperature (ºC), time (min) and cycles.

Stage/step	Temperature	Time	Cycles
Incubate	96 ºC	5 min	-
Denature	96 ºC	10 s	x 35
Anneal	50 ºC	5 s	x 35
Extend	60 ºC	4 min	x 35
Hold	4 ºC	∞	-

To prevent signal interference in the sequencing process, the ethanol/EDTA purification method was employed. Each sequencing reaction sample was treated with 30 µL of 100% ethanol and 2.5 µL of 125mM EDTA (#cat E5513**,** Sigma-Aldrich, Burlington, MA, US), followed by a 15-minute incubation at room temperature. Subsequently, centrifugation was carried out at 4ºC, 20,817 g for 20 minutes. The supernatant was carefully removed, and 30 µL of 70% ethanol was added to each sample. After another round of centrifugation for 10 minutes, the supernatant was aspirated, and any residual ethanol traces were allowed to evaporate at room temperature in the absence of light.

The purified samples were resuspended in 10 µL of Hi-Di™ Formamide (#cat 4311320, Applied Biosystems, Thermo Fisher Scientific, Waltham, MA, US) and transferred to a MicroAmp™ Optical 96-Well Reaction Plate (#cat 8010560, Applied Biosystems, Thermo Fisher Scientific, Waltham, MA, US), then covered with MicroAmp™ Clear Adhesive Film (#cat 4306311, Applied Biosystems, Thermo Fisher Scientific, Waltham, MA, US).

For capillary electrophoresis, the ABI Prism 3100 Genetic Analyzer (Applied Biosystems, Thermo Fisher Scientific, Waltham, MA, US) with the polymer type POP-6^{TM} was used. The electropherograms obtained were analysed with the DNA Baser sequence assembler software (release 5.20, Heracle BioSoft, Arges, RO).

3.1.4 Maintenance and Care of Colonies

After establishing the two murine lines (KO and KI) as detailed in **section 3.1.2** (**Figure 14**), the colonies were maintained. Three pairs of heterozygous mice from each line were bred, resulting in the production of wild type, homozygous and heterozygous KO mice for seipin or KI mice for Celia seipin. This breeding strategy also helped avoid heterozygous crosses between siblings.

The animals were housed in ventilated racks and cages under specific pathogen-free conditions. Room temperature (22º C ± 1º C), humidity (55% ± 2%) and light/dark rhythm (12:12) was under control. All mice had *ad libitum* access to water and standard chow (Teklad Global 18% Protein Rodent Diet, Envigo, Inotiv, Indianapolis, IN, US). Phenotypic, weight and behaviour monitoring were carried out throughout the animal's entire life. For the weight monitoring a FisherBrand portable balance (cat# FCS221, Fisher Scientific, Pittsburgh, PA, US) was used.

3.1.5 Identification and Genotyping Protocol

The animals were identified during the 14 days of age using a numbered ear-tag (Stoelting, Dublin, Ireland) and a small tissue fragment from the tail was collected using sterilized material.

Isolation of genomic DNA was carried out from the tail tissue as in **section 3.1.3**.

For the genotyping strategy DNA concentration was adjusted to 100 µg/mL. Specific primers were designed with the Primer3Plus software (http://www.bioinformatics.nl/cgi-bin/primer3plus/primer3plus.cgi). For KO genotyping strategy three primers were combined allowed us to distinguish between wild type, heterozygous and homozygous animals in one design, while for KI genotyping strategy the combination of four different designs was necessary (**Table 7**). Prime's hybridization sites are shown in **Annex 2.**

Table 7. Primer designs for the genotyping strategy of knock-out (KO) and knock-in (KI) murine models. Sequences, annealing temperature (AT), fragment size in base pairs (bp) where NA is No Annealing and genotype interpretation of the fragments. In parentheses the abbreviated names of the primers: Forward 1, 2, 3, 4, 5 (F1, F2, F3, F4, F5), Reverse 1, 3, 5 (R1, R3, R5).

	Forward primer		Reverse primer		Fragment size (bp)	Genotype interpretation
	Sequence (5'-3')	AT (°C)	Sequence (5'-3')	AT (°C)		
KO Strategy	AATAAGGCAGGAACTGGAGGGTCG (F1)	59	GAGGAACACAGACACCCAAAGCAA (R1)	60	532	Heterozygous or homozygous
					NA	Wild type
	GTCTCCAGCTACCCTGGAAAAGAAA (F2)	59			301	Wild type or heterozygous
					1813	Homozygous
KI Strategy	GAATGTATCAAGGAGGTTTGTCCCAG (F3)	60	TGGTTCCTCCTCTTTGTCCGGT (R3)	62	482	Heterozygous or homozygous
					NA	Wild type
	GCGCATGTGAAGCAATGACT (F5)	59	ACCCTCGGTCAATACTGGGA (R5)	59	543	Wild type or heterozygous
					1884	Homozygous
	GTCTCCAGCTACCCTGGAAAAGAAA (F2)	59	GAGGAACACAGACACCCAAAGCAA (R1)	60	301	Wild type or heterozygous
					1642	Homozygous
	CCGGAAGGAAGTCCAACGAA (F4)	57	GAGGAACACAGACACCCAAAGCAA (R1)	60	534	Heterozygous or homozygous
					NA	Wild type

In both cases, a final volume of 13 µL per sample was used for the PCR, using 2.5 µL of 5x buffer and 0.1 µL of MyTaq HS enzyme, both included in the MyTaq™ HS DNA Polymerase kit (cat# BIO-2111, Bioline, London, GB). Regarding the primers, 0.5 µL of each one (forward and reverse) was added for each design, considering that the KO design presents two forward primers, 0.25 µL was added for each one.

The amplification process and the sample analysis were carried out following the same steps as in **section 3.1.3** (**Table 4**).

After confirming the genotype, the animals were weaned from the mother at 28 days of age.

3.2 BEHAVIOURAL TESTS

On the day of testing, the mice were weighed using a Fisher Scientific portable balance (cat# FCS221, Pittsburgh, PA, US) and then placed in their home cages to acclimatize to the red light-controlled testing room (4 lux) for at least 60 minutes. The testing sequence was structured such that tasks with lower stress levels preceded those with higher stress levels, as follow: open field test, elevated zero maze, rotarod test, beam walking test, wire hang test, and Morris water maze. Each test was separated by a minimum of two weeks. The behavioural experiments that required video capture were recorded by an overhead camera linked to a computer with AnyMaze Video Tracking software (release v. 7.16, Stoelting, Addison Township, IL, US) to track the position of the animals.

3.2.1 Nest Building and Gnawing Tests

For the assessment of nest building behaviour, the animals were placed in a clean box containing a standardized amount of enrichment (three cotton balls). After a seven-day period, the presence or absence of a constructed nest was evaluated.

Additionally, the level of enrichment interaction was quantified by assessing the amount of material bitten. For this evaluation, mice were placed in a clean box with a paper roll, pre-weighed using a scale (cat# FCS221, Fisher Scientific, Pittsburgh, PA, US). After seven days, the remaining paper roll was weighted to determine the amount consume by each animal.

3.2.2 Welfare State and NeuroScore

The mice were scored from 0 (normal) to 4 (severely impaired) for all the tests.

The welfare state of the mice was evaluated taking into account the following characteristics throughout the life of the animals: tremor, kyphosis, fur and motion.

For NeuroScore evaluation the following test were conducted:

Hindlimb and Forelimb Flexion Tests

To assess hindlimb function, the mouse was grasped at the base of the tail, with the forepaws remaining on a flat surface, and the position of the hindpaws was observed for 10 seconds. For the forelimb assessment, the mouse was held by the base of the tail and lifted, with the head slowly lowered towards a flat surface, and the behaviour of the forepaws was observed for 10 seconds.

Lateral Pulsion Task Test

The coordination of all four limbs was measured using the lateral pulsion task test. The mouse was placed with its back facing the observer, and a gentle lateral pressure was applied to the middle section using a pen previously sterilized with 70% ethanol. The resistance to the applied pressure was then recorded.

Vibrissae-evoked Forelimb Placing Test

This test was used to assess asymmetry in the sensorimotor cortex and striatum. The animal was held such that all four limbs were free, and vibrissae were stimulated by brushing each side against the corner of a table. The response of the forelimb on the same side was observed. Three trials were allowed on each side (178-181).

3.2.3 Open Field Test

The mice were assessed in a cuboid plexiglass box measuring 45 cm x 45 cm x 40 cm (Cibertec, Madrid, ES), with the floor divided into nine equal squares. The central zone was designated as the central square (15 cm x 15 cm). Each mouse was introduced into the central zone of the arena and allowed to explore freely for six minutes. The mice underwent daily testing for four consecutive days, consisting of one habituation trial and three replicates (182, 183). The evaluation included the following parameters: total distance travelled, mean speed, duration of movement, time spent in the central region of the area, and the number of times of crossing from top to bottom and left to right by each mouse.

3.2.4 Elevated Zero Maze

The elevated zero maze is elevated to a height of 64 cm above the floor and is divided into four equal quadrants, with two opposite quadrants darkened and enclosed, while the other two are open and exposed. The maze has a diameter of 70 cm and a runway width of 5 cm. The mice underwent daily testing for four consecutive days, including one habituation trial and three replicates. To initiate the test, the animal was positioned at a randomly selected boundary between an open and a closed zone, facing the interior of the closed zone. Each test lasted five minutes (184, 185). The analysis included parameters such as total distance travelled, mean speed, duration of movement, duration of stillness, rotations, and time spent in the open and/or closed zones of the maze.

3.2.5 Rotarod Test

The RotaRod apparatus (Ugo Basile, Varese, IT) was used to perform the experiment. All mice were trained for four consecutive days and given three trials per day, separated by 30-minutes inter-trial intervals. The rotarod was set at a starting speed of 5 rpm with continuous acceleration for 90 seconds, up to a speed of 44 rpm (186, 187). The mean latency to fall off

from the rotarod, the revolutions, speed and distance were recorded. In the case of a full passive rotation, the timer was stopped, and the previous data also recorded.

3.2.6 Beam Walking Test

The objective of this test is to assess the mouse's ability to traverse an elevated narrow beam to reach a safe platform. The test is conducted over a single day, with each mouse given three trials. During the first trial, some animals may require encouragement, such as an occasional nudge with a finger, to traverse the full length of the beam. The following parameters were measured: time taken by the mouse to cross the beam, percentage of immobility, backward motion and drag walk, and the number of paw slips and falls. The apparatus consisted of a 1-meter smooth, square-shaped wooden beam (9 mm wide), elevated 50 cm above the tabletop and supported by two narrow stands to hold up the start section. A goal box containing nesting material from the home cages was placed at the end of the beam to attract the mouse to the finish point. A white LED lamp (590 lumens) was used as an aversive stimulus (bright light) shining above the start point (187, 188). The apparatus was custom-built.

3.2.7 Wire Hang Test

The mice underwent three trials in a single day. The apparatus was constructed manually using a 40-cm-long metal wire with a diameter of 2 mm, suspended at a height of 50 cm by two metal bars. Each animal was positioned in the middle of the wire and allowed to hang. The duration it maintained its grip before releasing the wire was recorded (189). Animals that fell within less than five seconds were repositioned for another attempt. If a full passive hold occurred, the timer was stopped, and the previous data was also documented.

3.2.8 Morris Water Maze

The Morris water maze comprised a circular pool (90 cm in diameter and 60 cm in height) constructed from light grey-coloured plastic (Cibertec, Madrid, ES). The pool was filled with water maintained at a temperature of 28 ºC ± 2 ºC to a depth of 40 cm. Non-toxic tempera paint was added to the water obscure visibility. The pool was divided into four equally-sized quadrants, with designated positions at the North, South, East and West points. The testing protocol spanned four consecutive days, which each day consisting of four trials from each of the cardinal starting positions. Following this initial phase, the mice had a three-day rest period before being retested on day eight. During the first four days of training, a cylindrical transparent platform (80 mm in diameter) was placed discreetly in the North-East quadrant just below the water surface as a hidden target. The escape latency to reach this platform was recorded. If a mouse failed to locate the platform within 60 seconds, it was gently guided to it and allowed to remain there for 10 seconds. The mouse was then dried and returned to its cage for a rest period of at least 30 minutes before the next trial. On day eight, the platform was removed, and the mice underwent four trials released from each cardinal

starting position to observe their search patterns over a 60-seconds period. Various parameters including swimming distance and speed, time spent moving, stillness or floating time, as well as time spent in the platform zone in terms of distance covered and duration were measured for the analysis (190-192).

3.3 GLUCOSE METABOLISM

A small incision was made in the tail tissue using a sterile scalpel (Nº 11, Nahita International LTD, Dubai). Blood samples were then collected via capillarity and analyse using an Accu-Chek Performa glucometer (Roche, Basel, CH) in duplicate for glucose levels.

3.3.1 Basal Glucose

The mice were fasted for four hours, after which blood measurements were taken. The animals were weighed before and after the fasting period using a portable balance (cat# FCS221, Fisher Scientific, Pittsburgh, PA, US).

3.3.2 Glucose and Insulin Tolerance Tests

For the glucose tolerance test (GTT), the mice were fasted for 16 hours. In contrast, for the insulin tolerance test (ITT), the animals were fasted 4 hours. During the GTT procedure, mice received an intraperitoneal injection of 2 g/kg glucose (cat# G8270, D-(+)-Glucose, Sigma-Aldrich, Burlington, MA, US). For the ITT procedure, mice were injected intraperitoneally with 1 IU/kg of insulin (Actrapid 100 IU/ml, Novo Nordisk Pharma, Madrid, ES). A 25 G Sterican needle (B. Braun, Melsungen, DE) was used for the injections. Blood samples were collected at the following timepoints: before injection (time 0), and 15, 30, 60, 90 and 120 minutes post-injection (193).

3.4 [^{18}F]-2-FLUORO-2-DEOXY-D-GLUCOSE BY POSITRON EMISSION TOMOGRAPHY WITH COMPUTED TOMOGRAPHY

Prior to image acquisition, the animals were acclimatized to the local animal facility for a minimum of two days. One day before the experiments, the mice were fasted overnight for approximately 16 hours. After the fasting period, the mice were anesthetized with 3% isoflurane (Baxter International, Deerfield, IL, US) for induction and 2.5% for maintenance. An intravenous administration of 5.86 ± 0.54 MBq of [^{18}F]-2-fluoro-2-deoxy-D-glucose ([^{18}F]-FDG) (Galaria, Galicia, ES) in a volume of 0.07-0.08 mL was then performed via the tail vein using a 30 G needle (B. Braun, Melsungen, DE). The animals were then allowed to recover and were placed back in their cages for 20 minutes before being anesthetized again and positioned in prone orientation on the bed of the microPET scanner (Albira PET/CT Preclinical scanner, Bruker, Billerica, MA, US). Positron emission tomography (PET) and computed tomography (CT, Standard Quality, 200 µA y 35 kV) imaging were acquired 30

minutes after the radiotracer injection. The PET scan consisted of a single-bed position acquisition (149 mm along the axial direction) with a duration of 10 minutes, followed by a single-bed position CT scan (64 mm along the axial direction) also lasting 10 minutes.

The PET data acquisitions were reconstructed using the maximum likelihood expectation maximization (MLEM) algorithm with 12 iterations, resulting in a pixel size of 0.25 x 0.25 x 0.25 mm^3. This reconstruction was performed using Bruker Albira Suite Software (release version 5.0, Bruker, Billerica, MA, US). For imaging analysis, the PET images were manually fused with the CT images. The PET/CT images were then spatially normalized to a specific mouse T2 MRI Template (Ma-Benveniste-Mirrione mouse brain) using rigid transformation in the PMOD software (release v4.2, PMOD Technologies, Zürich, CH) (194, 195). Mean radioactivity concentrations were estimated within predefined volumes of interest (VOIs) based on the of the Ma-Benveniste-Mirrione mouse brain VOI template. Subsequently, mean standardized uptake values (SUV_{mean}) were calculated by normalizing the radioactivity concentration by the injected dose (MBq) and the body weight (Kg) of each mouse using the following formula:

$$SUVmean = \frac{Radioactivity\ concentration\ in\ voxel\ (KBq/mL)}{Injected\ dose\ (MBq)/Body\ weight\ (Kg)}$$

Equation 1

3.5 SPERM QUALITY ANALYSIS

In a 35 mm culture plate (Corning, Corning, NY, US), 60 µL of EmbryoMax Human Tubal Fluid (HTF) (cat# MR-070-D, Sigma-Aldrich, Burlington, MA, US) were dispensed into the centre of the plate. The solution was then overlaid with mineral oil (cat# M8410, Sigma-Aldrich, Burlington, MA, US), followed by an additional 60 µL of HTF. The plate was then incubated 30 minutes at 37ºC with 5% CO_2 in a designated incubator (Galaxy 170S, New Brunswick Scientific, Edison, NJ, US).

The epididymis was aseptically excised and promptly transferred to the prepared HTF drop. Subsequently, the plate containing the sample was positioned on a heated water bath set at 37°C (cat# 462-0557, Avantor, Radnor, PA, US). Using Vanna's scissor under a stereomicroscope (cat# SMZ-140, Motic, Fujian, CN), five to six incisions were mad in de epididymis. After one-minute settling period, gentle circular agitation was applied for three minutes. Following this preparation, 10 µL of sperm sample were retrieved and assessed for quality using a DMi1 microscope (Leica Microsystems, Wetzlar, DE) equipped with a 16-quadrant Neubauer chamber (Paul Marienfeld, Lauda-Königshofen, DE). Sperm motility was graded on a scale from 0 (motionless) to 5 (rapid and linear progressive motility), while sperm concentration was determined using the following formula:

$$\text{Concentration (nº spermatozoons}/10^6\text{mL)} = \text{Dilution Factor} * \text{nº spermatozoons in 5 quadrants} * 7812{,}5$$

Equation 2

3.6 TISSUE COLLECTION AND PROCESSING

The animals were primarily sacrificed at an average age of 9.5 months, with this age specification provided for each experiment. Additionally, for animals deemed severely affected, the timing of sacrifice was adjusted based on the severity of their condition. A CO_2 chamber was used and followed by cardiac puncture with a 25 G Sterican needle (B. Braun, Melsungen, DE) to collected blood samples in a BD Vacutainer® SST™ II Advance tubes (Fisher Scientific, Pittsburgh, PA, US).

The CNS tissues, including cerebellum, midbrain, hypothalamus, cortex, hippocampus, and striatum were dissected, with the right and left hemisphere separated. Samples from the right hemisphere were used for RNA extraction, while those from the left hemisphere were designated for histological analysis. The liver, heart, kidneys, and spleen were weighed using a scale. Liver tissue was collected for both RNA extraction and histological analyses, while the heart and kidney were used solely for histology, as were the thoracic marrow and the eyeballs. Adipose tissue, including iBAT, ingWAT and gonWAT, was also collected when possible.

The collected samples were processed according to their intended use. For RNA extraction, the samples were stored in liquid nitrogen and subsequently maintained at -80ºC until further analysis. The samples designated for histological examination were placed in a cassette (Labolan, Navarra, ES) submerged in 4% m/v neutral buffered formalin for 24 hours, and then transferred to 70% ethanol for storage until subsequent analysis.

3.7 SERUM EXTRACTION

Blood was collected by submandibular or cardiac puncture using a 25 G Sterican needle (B. Braun, Melsungen, DE) in BD Vacutainer® SST™ II Advance tubes (Fisher Scientific, Pittsburgh, PA, US). Serum was obtained after a centrifugation of 2,000 g, 4 ºC, 10 min (196-198).

3.8 HEMATOLOGY AND BIOCHEMICAL PROFILE

For hematology assessment, whole blood samples were collected via cardiac puncture using a 25 G Sterican needle (B. Braun, Melsungen, DE) and transferred to BD Vacutainer® K2EDTA or K3EDTA blood collection tubes (Fisher Scientific, Pittsburgh, PA, US).

The hematological analyses were performed by mixing 20 µL of whole blood mixed with 480 µL of V-52D diluent (Mindray, Shenzhen, CN) and analysing the samples in triplicate using a

BC5000-Vet analyser (Mindray, Shenzhen, CN). A total of 23 hematological parameters were measured.

For biochemical analyses, a volume of 120 µL of serum was required. The quantitative determinations were conducted using the VetScan Comprehensive Diagnostic Profile reagent rotor in a VetScan VS2 Chemistry Analyzer (Zoetis, Parsippany, NJ, US).

3.9 Insulin and Leptin Analysis

Insulin levels were determined using the Mercodia Ultrasensitive Mouse Insulin ELISA (cat# 10-1249-01, Mercodia, Uppsala, SE). Serum samples were diluted based on the genotype: wild type and heterozygous (both KI and KO) animals were either undiluted or diluted 1:2, homozygous (both KI and KO) animals were diluted 1:10, 1:20, or 1:40.

Leptin was measured using the Mouse Leptin ELISA Kit (cat# KMC2281, Invitrogen, Carlsbad, CA, US), within all serum samples diluted 1:5.

Both the insulin and leptin analysis were performed in duplicate, following the manufacturer's recommendations. Measurements were obtained using a Multiskan™ GO Microplate Spectrophotometer (Thermo Fisher Scientific, Waltham, MA, US), and the results were analysed using a 4PL (Four Parameter Logistic) method as specified by the manufacturers.

3.10 Triglycerides Analysis

Triglyceride levels were determined using an enzymatic-colorimetric assay with the Spinreact GPO-POD kit (cat# 1001314, Spinreact, Girona, Spain). Measurements were obtained using a Multiskan™ GO Microplate Spectrophotometer (Thermo Fisher Scientific, Waltham, MA, US), and the results were analysed based on a calibration curve.

3.10.1 In Serum

A standard curve was generated using eight concentration points ranging from 0 to 50 mg/dL. This was prepared by diluting the Cal Triglycerides (200 mg/dL) reagent from the kit with 0.9% NaCl. The serum samples were diluted 1:10 using 0.9% NaCl prior analysis. The quantification was performed in triplicate by adding 100 µL of Work Reagent WR provided in the kit and 25 µL of the diluted sample. The standard curve was also prepared in duplicate using the same reagent volumes.

3.10.2 In Liver

Approximately 100 mg of liver tissue (wet weight) was homogenized for 5 minutes at 26 rpm using a TissueLyser II (Qiagen, Tegelen, NL) in 1 mL of 2:1 (v/v) chloroform/methanol solution at 4ºC. Each liver sample was processed in duplicate. The homogenates were agitated overnight (12 rpm, 4ºC) using a Multi-Purpose Tube Rotator (Fisher Scientific, Pittsburgh,

PA, US). Subsequently, 300 µL of milliQ water were added, and the samples were centrifuged at 8,600 g for 20 minutes at room temperature. The upper aqueous layer was discarded, and the lower organic layer was collected by passing it through the intermediate solid remains. The organic extracts were then allowed to evaporate overnight at room temperature. The lipid pellets were resuspended in 900 µL (for wild type and heterozygous samples) or 1400 µL (for homozygous samples, diluted 1:2) of chloroform (199). Aliquots of 30 µL from each sample were evaporated in a thermoblock at 37ºC for 30-40 minutes, and the resulting pellets were resuspended in 350 µL of the Work Reagent provided in the kit. For the triglyceride quantification, 150 µL of each resuspended sample were added to wells in duplicate. Additionally, a standard curve was prepared in duplicate using eight concentration points (0-50 mg/dL) made from the Cal Triglycerides (200 mg/dL) reagent and 0.9% NaCl, with 140 µL of the Work Reagent and 10 µL of standard added to each well.

3.11 HISTOLOGY

3.11.1 Tissue Processing

The tissues were fixed in 10% m/v neutral buffered formalin (cat# 05-K01022, Bio-Optica, Milano, IT) for 24 hours at room temperature and subsequently paraffin-embedded using a standard procedure (200) in an Automatic Benchtop Tissue Processor (Leica TP1020, Leica Biosystems, Nußloch, DE). Samples were sectioned at a thickness of 4 µm using a microtome (Epredia HM 355S, Epredia, Kalamazoo, MI, US). The sections underwent a series of steps including deparaffinization (1 hour at 60ºC and 10 minutes immersion in xylene), hydration in decreasing concentrations of ethanol (absolute, 96%, 70%, and 50% ethanol for 5 minutes each), and final washing in distilled water.

For hematoxylin and eosin (H&E) staining, tissues (refer to **Table 8**) were first stained with hematoxylin (cat# 05-06004/L, Bio-Optica, Milano, IT) for 10 minutes, followed by a for 10-minutes water wash, and then stained with eosin (cat# 05-10003/L, Bio-Optica, Milano, IT) for 5 minutes. On the other hand, for Periodic Acid Schiff (PAS) staining (cat# 395B, Sigma-Aldrich, Burlington, MA, US), tissues were oxidized in a 0.5% periodic acid solution for 5 minutes, followed by a water wash. Then samples were placed in Schiff's reagent for 15 minutes, washed in lukewarm tap water for 5 minutes, and counterstained in Mayer's hematoxylin for 1 minute. In contrast, Masson's trichrome staining was utilized for fibrosis analysis in liver. The samples were initially stained with Weigert's hematoxylin (cat# 05-10003/A/B, Bio-Optica, Milano, IT) for 10 minutes, followed by a water wash. Subsequently, the samples were stained with fuchsine Ponceau (cat# 05-B10005, Bio-Optica, Milano, Italy) for 10 minutes, phosphomolybdic acid (cat# 05-M05003, Bio-Optica, Milano, IT) for 10 minutes, and finally with aniline blue (cat# 05-B10006, Bio-Optica, Milano, IT) for three minutes.

Immunodetection was conducted for the cerebellum, striatum, thoracic marrow, and eyeball (refer to **Table 8**). An antigen retrieval protocol was implemented by treating the

samples with PT-link (Dako, California, USA) for 20 minutes at 97 ºC in Tris/EDTA buffer, pH 9.0 (cat# ab93684, Abcam, Cambridge, UK) for GFAP or in Citrate buffer (cat# ab93678, Abcam, Cambridge, UK) for CD68 and Ubi-1. Following two washes with PBS, the slides were blocked with hydrogen peroxide at room temperature for 10 minutes, washed again with PBS, and then incubated for 1 hour at room temperature with the ready-to-use (RTU) anti-Glial Fibrillary acid protein antibody (GFAP, cat# IR524, Agilent Dako, Madrid, Spain). For CD68 and Ubi-1 antibodies, incubation was carried out overnight at 4ºC using a 1:1,000 dilution of anti-CD68 antibody (CD68, cat# ab125212, Abcam, Cambridge, UK) or 1:1,000 dilution of anti-Ubiquitin antibody (Ubi-1, cat# ab7254, Abcam, Cambridge, UK). Subsequently, the slides were washed twice with PBS and incubated with the RTU EnVision FLEX-HRP detection reagent (cat# SM802, Agilent, Dako, Santa Clara, CA, US) for 30 minutes. After washing again, the samples were revealed using 3.3'-diaminobenzindine (DAB) (cat# K3468, Agilent, Dako, Santa Clara, CA, US), followed by another wash and counterstaining for 10 minutes with Mayer's hematoxylin (cat# 05-M06002, Bio-Optica, Milano, IT).

Following the completion of the respective staining or immunodetection procedures, a dehydration step was carried out using a series of ethanol solutions (50%, 70%, 96%, and absolute ethanol, 5 min each). Subsequently, the samples were mounted in DePeX mounting medium (cat# 361254D, Avantor, Radnor, PA, US).

However, for the eyeball samples, once hydrated, they were mounted using an aqueous medium containing DAPI (cat# 17985-10, Fluoro-Gel (with Tris Buffer), Electron Microscopy Science, Hatfield, PA, US).

For lipid deposition analysis in liver using *Oil red O* staining, frozen liver tissue samples were cryosectioned at a thickness of 10 µm using a cryostat (Epredia Microm HM525 NX, Epredia, Kalamazoo, MI, US). The sections were then fixed with 10% m/v neutral buffered formalin (cat# 05-K01022, Bio-Optica, Milano, IT) for 2 hours. Next, the sections were stained with *Oil red O* colour solution (cat# 102419, Merck-Millipore, Burlington, MA, US) for 20 minutes. After staining, the sections were washed with water. They were then counterstained with Harris' hematoxylin (cat# 05-06004/L, Bio-Optica, Milano, IT) for 5 minutes, followed by another water wash. Finally, the stained sections were mounted in an aqueous mounting medium (cat# 05-1740, Bio-Optica, Milano, IT).

Table 8. Staining and immunodetection type for each tissue or organ. Hematoxylin and eosin (H&E), Periodic acid-Schiff (PAS), *Oil red O*, Masson's trichrome and/or 4',6-diamidino-2-phenylindole (DAPI) staining and Glial Fibrillary acidic protein (GFAP), cluster of differentiation 68 (CD68) and/or ubiquitin (Ubi-1) immunodetection for liver, heart, thoracic marrow, eyeball, adipose and central nervous system (CNS) tissues.

Tissue/Organ		Staining				Immunodetection			
		H&E	PAS	*Oil red O*	Masson's trichrome	DAPI	GFAP	CD68	Ubi-1
Liver		✓	-	✓	✓	-	-	-	-
Heart		✓	-	-	-	-	-	-	-
Thoracic marrow		✓	-	-	-	-	✓	✓	-
Kidneys		✓	✓	-	✓	-	-	-	-
Eyeball		-	-	-	-	✓	-	-	-
Adipose tissue	iBAT	✓	-	-	-	-	-	-	-
	ingWAT	✓	-	-	-	-	-	-	-
	gonWAT	✓	-	-	-	-	-	-	-
CNS	Cerebellum	✓	-	-	-	-	✓	✓	✓
	Midbrain	✓	-	-	-	-	-	-	-
	Hypothalamus	✓	-	-	-	-	-	-	-
	Cortex	✓	-	-	-	-	-	-	-
	Hippocampus	✓	-	-	-	-	-	-	-
	Striatum	✓	-	-	-	-	-	-	✓

3.11.2 Imaging

The samples were observed using an Olympus BX51 microscope (Olympus, Tokyo, JP) and captured with an Olympus DP72 digital camera. The images were acquired using the cellSens software from Olympus (Tokyo, JP, https://www.olympus-lifescience.com/en/software/cellsens/#!cms[focus]=cmsContent6016).

3.11.3 Tissue Analysis

The liver sections were scored blindly by two experienced pathologists using the Non-alcoholic Steatohepatitis Clinical Research Network (NASH CRN) scoring system (201). The non-alcoholic fatty liver disease (NAFLD) activity score (NAS) ranged from 0 to 8, which was calculated as the sum of individual scores for steatosis (0–3), lobular inflammation (0–3), and hepatocyte ballooning degeneration (0–2). Moreover, the presence or absence of non-alcoholic steatohepatitis (NASH), currently known as metabolic dysfunction-associated steatohepatitis (MASH) (202), was assessed using a NAS value of ≥ 4 as a criterion. Non-alcoholic fatty liver (NAFL), now renamed as metabolic-dysfunction associated steatotic liver (MASL) (202), was identified if a value of ≥ 1 was present. Fibrosis evaluation was conducted following NASH CRN criteria, with 0 indicating the absence of fibrosis and 4 representing cirrhosis.

CNS and thoracic marrow were semiquantitatively evaluated according by two expert pathologists (203). The percentage of astrogliosis in the cerebellum was assessed in triplicate using CellProfiler software (version 4.2.6, Broad Institute, Cambridge, MA, US), calculated as the percentage of positivity (positive pixels/total pixels).

For kidney lesions, renal evaluations were blindly assessed by two expert pathologists following the recommendations of Haas et al. 2020 (204).

Myocardium assessment was performed blindly by an expert pathologist according to the recommendations of the Committee of Translational Research of the Heart Failure Association of the European Society of Cardiology (205). Ventricular thickness measurements were performed using NIS-Elements Imaging software (Nikon Instruments Inc., Melville, NY, US).

Finally, the evaluation of the eyes was performed according to the recommendations of the Organisation for Economic Co-operation and Development (OECD) (206).

3.12 RNA ISOLATION

Total RNA was extracted from liver and various CNS tissues (cerebellum, midbrain, hypothalamus, cortex, hippocampus, striatum) collectively using a single-step method of RNA isolation involving acid guanidinium thiocyanate–phenol–chloroform extraction and the ReliaPrep™ RNA Tissue Miniprep System kit (cat# Z6112, Promega, Fitchburg, WI, US).

The extraction followed the protocol provided with the ReliaPrep™ RNA Tissue Miniprep System. After homogenization with a TissueRuptor II (Qiagen, Tegelen, NL), 750 µL of TRI Reagent® (4ºC) (cat# TR 118, Molecular Research Center (MRC), Cincinnati, OH, US) and 200 µL of chloroform (cat# C/4960/15, Fisher Scientific, Pittsburgh, PA, US) were added and centrifuged for 15 minutes at 4°C and 12,000 g. Subsequently, the manufacture's recommended protocol for the commercial kit was followed. The RNA samples were quantified using a NanoDrop2000 spectrophotometer (Thermo Fisher Scientific, Waltham, MA, US).

3.13 REVERSE TRANSCRIPTION

For reverse transcription, the RNA concentration was adjusted to 1 µg. The first step involved adding 1uL of random hexamer primer pd(N)6 (0.2 mg/mL) (cat# 11034731001, Roche, Basel, CH) and 2 µL of dTTP solution (20 mM) (cat# 10219012, Invitrogen, Carlsbad, CA, US). Subsequently, 4 µL of 5x First-Strand Buffer and 2 µL of 0.1 M DTT from the M-MLV Reverse transcriptase kit (cat# 10338842, Invitrogen, Carlsbad, CA, US) were added. As the final step, 1 µL of M-MLV transcriptase enzyme (cat# 10338842, Invitrogen, Carlsbad, CA, US) was added to the reaction mixture (207). The reverse transcription reaction was carried out in a FlexCycler thermocycler (Analytik Jena, Jena, DE) following the conditions outlined in **Table 9**.

Table 9. Programming conditions for the 3 steps of the reverse transcription process.

	Temperature	Time
Step 1	65 ºC	5 min
	4ºC	∞
Step 2	37 ºC	2 min
	4 ºC	∞
Step 3	25 ºC	10 min
	37 ºC	1 h
	70 ºC	15 min
	4 ºC	∞

3.14 QUANTITATIVE REAL-TIME PCR

The expression of the following genes was determined by quantitative real-time PCR (qPCR): *Gng3*, *Fgf21*, *Bscl2*, Celia *BSCL2*-TG, *Pparγ*, *Pex16*, *Sod1*, *Sod2*, *Cat*, *Pex11g*, and *Gpx1*. Specific primers and probes were designed using different approaches.

For the *BSCL2* spliced transcript, *Bslc2, Gng3*, and *Fgf21*, genes, primers were designed using the Universal ProbeLibrary (Roche Diagnostics, Basel, CH).

For the remaining genes, primers and probes were designed using the TaqMan Assay Search Wizard guide (Applied Biosystems, Thermo Fisher Scientific, Waltham, MA, US).

The details of the primer and probe sequences are provided in **Table 10**.

Table 10. Primer and probe designs for the quantitative real-time PCR. Gene name and symbol, primer sequences (forward and reverse) and probe sequences with double dye type (reporter and quencher).

Gene			Primer sequence (5'-3')		Probe		
Name	Symbol	Amplicon length (bp)	Forward	Reverse	Sequence (5'-3')	Reporter (5')	Quencher (3')
18S ribosomal RNA	*Rn18s*	108	AAACGGCTACCACATCCAAG	TACAGGGCCTCGAAAGAGTC	CGCAAATTACCCACTCCCGACCCG	6FAM	BHQ1
Guanine nucleotide binding protein (G protein), gamma 3	*Gng3*	76	TCCATCCGTTCAGGCAAT	TCTTCAAATGCCTTTACCTTTCA	CCTGGAGC	FAM	Dark quencher dye
Fibroblast growth factor 21	*Fgf21*	64	AGCATACCCCATCCCTGACT	GTACCTCTGCCGGACTTGAC	CTCCTCCA	FAM	Dark quencher dye
BSCL2 lipid droplet biogenesis associated, seipin	*Bscl2*	102	CCAAGGGTATCGTCCCTGT	GGGACTGGTGGGTCATTG	TTCCTGGC	FAM	Dark quencher dye
Celia Berardinelli-Seip congenital lipodystrophy transgene	Celia *BSCL2*-TG	144	GTATCGTCCCTGTGGAAGAC	TAGAGTGATGGTGATGGTGATG	AGCCAGGAACTCAAAGCCTGAGG	6FAM	BHQ1
Peroxisome proliferator activated receptor gamma	*Ppary*	150	CTTGACAGGAAAGACAACGG	TGGCACCCTTGAAAAATTCG	GCAGGAGCAGAGCAAAGAGGTGGCC	6FAM	OQA
Peroxisomal biogenesis factor 16	*Pex16*	115	TATGTGACTCGTCATCCAGC	AGTACACCAGTTCAGACAGC	ACGGCTGTGCGGGGCCTCAGTT	6FAM	OQA
Superoxide dismutase 1	*Sod1*	124	TGGGGACAATACACAAGGC	CTTTCCAGCAGTCACATTGC	TGGCCCGGCGGATGAAGAGAGGCA	6FAM	OQA
Superoxide dismutase 2	*Sod2*	118	GCACTGAAGTTCAATGGTGG	CAAAGTCACGCTTGATAGCC	ACCTGAGCCCTAAGGGTGGTGGAGA	6FAM	OQA
Catalase	*Cat*	148	GTCTCTCCATCAGGTTTC	CTGGTCGGTCTTGTAATG	CAATAGACTGCCTCTCCATCTGC	6FAM	BHQ1
Peroxisomal biogenesis factor 11 gamma	*Pex11g*	146	GTGACTGACCAACTGTACTA	CACAGGGCCTTGACAG	CCTTGTGAGCATATCGCCTGG	6FAM	BHQ1
Glutathione peroxidase 1	*Gpx1*	95	GATGAACGATCTGCAGAAGC	CATTCTTGCCATTCTCCTGG	ACCTCGTGGACTGGTGGTGCTCGGT	6FAM	OQA

For the *Gng3* and *Fgf21* genes, the qPCR amplifications were carried out in 20 µL reaction mixtures. Each reaction contained 4 µL of LightCycler® TaqMan® Master (cat# 04535286001, Roche, Basel, CH), 2 µL of each forward and reverse primer (5 µM), and 0.2 µL of probe (10 µM). Each sample was tested in duplicated using 1 µg of cDNA, and the reactions were performed in LightCycler Capillaries (cat# 04929292001, Roche, Basel, CH).

The amplifications for the other target genes were processed in 384-well reaction plates (MicroAmp™ EnduraPlate™ Optical, cat# 4483285, Applied Biosystems, Thermo Fisher Scientific, Waltham, MA, US) in 10 µL reaction mixtures. Each reaction contained 5 µL of TaqMan Gene expression Master mix (cat# 4370048, Applied Biosystems, Thermo Fisher Scientific, Waltham, MA, US), 1 µL of each forward and reverse primer (5 µM), and 0.1 µL of probe (10 µM). In this case, each sample was tested in triplicate using 1 µg of cDNA.

The qPCR analysis for the *Gng3* and *Fgf21* genes were performed using a Light Cycler 2.0 instrument (Roche Diagnostics, Basel, CH), while the analyses for the other genes were carried out on a QuantStudio™ 5 Real-Time PCR System (Applied Biosystems, Thermo Fisher Scientific, Waltham, MA, US).

The gene expression levels were normalized to the *Rn18s* reference gene using the $2^{-\Delta\Delta}$ CT method (208).

The specific real-time PCR cycling conditions are provided in **Table 11**.

Table 11. Programming conditions for the qPCR. Different steps, temperature (ºC), time (s; min) and number of cycles for all the murine genes tested I both QuantStudio™ 5 Real-Time PCR System and Light Cycler 2.0.

QuantStudio™ 5 Real-Time PCR System					
Stage	**Temperature**	**Time**	**Cycles**		
			Rn18s	**Celia *BSLC2*-TG**	**Other genes**
Hold	50 ºC	2 min	-	-	-
	95 ºC	10 min	-	-	-
PCR	95 ºC	15 s	x 30	x 50	x 40
	60 ºC	1 min	x 30	x 50	x 40
Light Cycler 2.0					
Stage	**Temperature**	**Time**	**Cycles**		
Denature	95 ºC	15 min	-		
PCR	95 ºC	20 s	x 50		
	60 ºC	1 min	x 50		
Hold	4 ºC	∞	-		

3.15 TISSUE PROTEIN EXTRACTION

The phenol-ethanol supernatant obtained after DNA precipitation with ethanol during the RNA extraction procedure (**section 3.12**) using TRI Reagent® (4ºC) (cat# TR 118, Molecular Research Center (MRC), Cincinnati, OH, US) was stored at -80ºC. Following the addition of 300 µL of 100% ethanol (Sigma-Aldrich, Burlington, MA, US) for each millilitre of TRI Reagent used in the RNA extraction procedure (**section 3.12**), the tube was gently inverted for 15 seconds, incubated for 3 minutes at room temperature, and then centrifuged for 5 minutes at 2,000 g at 4 ºC.

Subsequently, 1 mL of isopropanol (Sigma-Aldrich, Burlington, MA, US) was added to a 0.5 mL aliquot of supernatant. The tube was inverted for 15 seconds, incubated for 10 minutes at room temperature, and centrifuged for 10 minutes at 12,000 g at 4 ºC. After discarding the supernatant, 1 mL guanidine-HCl solution (0.3M in 95% ethanol) from Sigma-Aldrich was added. The pellet was resuspended by vortexing and incubated for 20 minutes at room temperature before being centrifuged for 5 minutes at 7,500 g at 4 ºC; the supernatant was then discarded. This washing step was repeated twice. The tubes were inverted to dry the pellet before adding 200 µL of 0.05% SDS (#cat L4509-500G, Sigma-Aldrich, Burlington, MA, US) and 200 µL of 10M urea (#cat U5378-100G, Sigma-Aldrich, Burlington, MA, US) per each 10-20 mg of tissue.

The tubes were sonicated 3 seconds at 30% amplitude with an ultrasonic homogenizer sonicator (Branson digital sonifier, Emerson, MO, US), incubated for 10 minutes at 55 ºC, and then centrifuged for 10 minutes at 10,000 g at room temperature. Any insoluble material was removed, and the resulting supernatant was transferred to a new sterile tube for protein quantification using the Bradford protein assay method (209).

3.16 WESTERN BLOTTING

Protein samples were transferred to a PVDF transfer membrane (Amersham Hybond PVDF 0.45 µm, Cytiva, Marlborough, MA, US). Blots were blocked for 25 minutes at room temperature in 2% or 5% fat-free milk powder (TBS, Tween-20 0.1%). Incubation with primary antibodies was performed overnight at 4ºC. The blots were probed with anti-6xhis-tag dilution 1:1,000 (#cat MA1-21315, Thermo Fisher Scientific, Waltham, MA, US). Anti-GAPDH dilution 1:25,000 (#cat G9545, Sigma-Aldrich, Burlington, MA, US) was used as loading control. Conjugated peroxidase anti-mouse (#cat ab6789, Abcam, Cambridge, UK) or conjugated peroxidase anti-rabbit IgG (#cat A16104, Thermo Fisher Scientific, Waltham, MA, US) were the secondary antibodies, dilution 1:5,000 and 1:10,000 respectively. Bands were revealed by chemiluminescence with the Immobilon Forte Western HRP Substrate (#cat WBLUF0100, Merc Millipore, Burlington, MA, US). Images were processed using ImageJ software (release 1.53k; National Institutes of Health, Bethesda, MD, USA).

3.17 STATISTICAL ANALYSIS

The data are presented as mean ± standard deviation (SD), mean ± standard error of mean (SEM), n (%) values ± standard deviation (SD), or as n (%) values.

The distribution of the quantitative data was assessed using the Kolmogorov-Smirnov test or the Shapiro-Wilk test, depending on the sample size: the Kolmogorov-Smirnov test was applied to larger samples ($n > 50$), while Shapiro-Wilk test was used in smaller samples ($n \leq 50$).

When a non-normal distribution was observed, statistical significance was assessed using the non-parametric Kruskal-Wallis test, followed by a Mann-Whitney U post-hoc analysis for pairwise comparisons. Conversely, if a normal distribution was identified, an ANOVA was conducted, followed by appropriate post hoc tests. The Bonferroni post hoc test was employed when no significant differences were initially detected, while T3 Dunnet test was utilized when significant differences among groups were found, effectively controlling for Type I error in both cases.

Additionally, an analysis of covariance (ANCOVA) was conducted to eliminate the potential confounding effects of covariates such as body weight and liver weight.

The qualitative data statistical significance was determined with Fisher's exact test.

The level of statistical significance was set at $p < 0.05$ for all analyses.

All statistical analyses were performed using IBM SPSS Statistics (release 25.0; SPSS, Chicago, IL, USA).

4 RESULTS

4.1 GENERATION OF *BSCL2*$^{-/-}$ AND *BSCL2*$^{CELIA/CELIA}$ MURINE MODELS

4.1.1 Targeting Vector

The final targeting vector, which contained HAs, recombination sites, and selection markers (as shown in **Figure 11B**), was linearized using the restriction enzyme NotI.

The result of this linearization process is depicted in **Figure 15**.

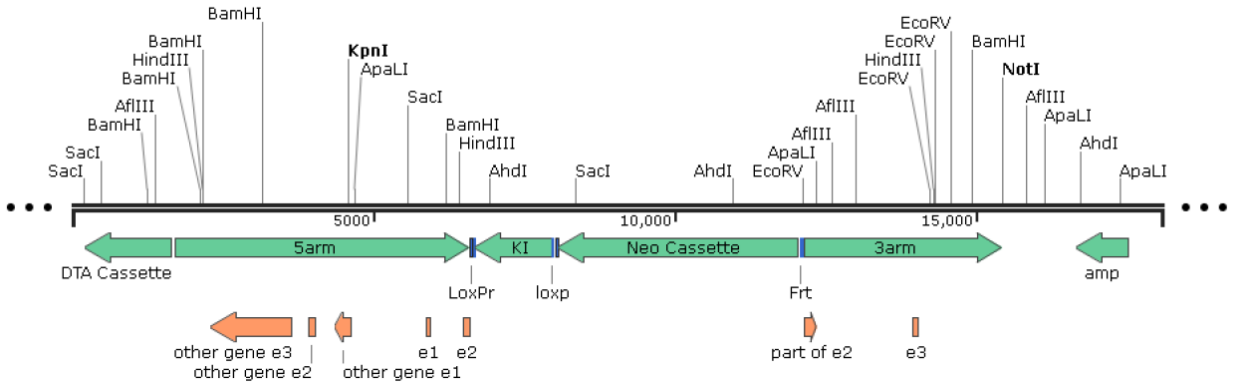

Figure 15. Diagram of the linearized targeting vector after using NotI enzyme. In the figure restriction enzymes are shown, as well as, the homology arms (5arm and 3arm), selection markers (DTA Cassette and Neo Cassette) and recombination sites (LoxP and Ftr). Figure recovery from SnapGene software (www.snapgene.com).

To confirm the assembly of all the parts which constitute the final targeting vector, the vector was digested by different restriction enzymes. The restriction enzymes used, and the expected fragment lengths are shown in **Table 12**.

Table 12. Restriction enzymes used for confirmation purposes. Name and size of the different fragments generated in kilo-base pair units (Kpb).

Enzymes	Size (Kbp)
AhdI	8.3 + 5.8 + 4.0
ApaLI	7.7 + 5.4 + 3.8 + 1.2
BamHI	8.7 + 4.4 + 3.1 + 1.0 + 0.9 + 0.1
HindIII	7.9 + 6.0 + 4.3
SacI	9.9 + 5.1 + 2.8 + 0.3
NotI	18.1

To visualize the lengths of the DNA fragments generated by the restriction enzyme digestion, an agarose gel electrophoresis was performed (**Figure 16**). This allowed for the confirmation that the assembly of the targeting vector had been carried out correctly.

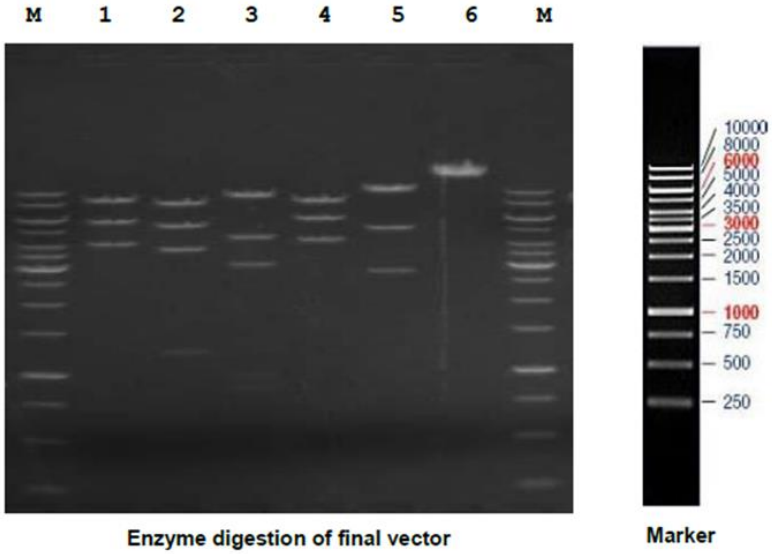

Figure 16. Visualization of the fragments in the agarose gel after the digestions of the targeting vector. On the left the two markers (M) and the six samples (1, 2, 3, 4, 5 and 6) loaded on the gel are shown. Reference marker with the lengths of each band in base pairs (bp) on the right of the image. Own elaboration (Powe Point) modified from the one provided by Cyagen (Santa Clara, US).

4.1.2 Vector Transfection into ES Cells

The confirmed linearized vector was introduced into ES cells (C57BL/6). Following the selection process, 95 drug-resistant clones were obtained, and a PCR screening was conducted. Two specific regions of the targeted allele were analysed, as illustrated in **Figure 12A**. For region 1, no amplification was anticipated in wild type animals, while a 4.4 Kbp fragment was expected in mutant-type animals (**Figure 17AI**). Similarly, for region 2, amplification was not expected in wild type animals, while a predicted 2.9 Kbp fragment in mutant-type mice (**Figure 17AII**).

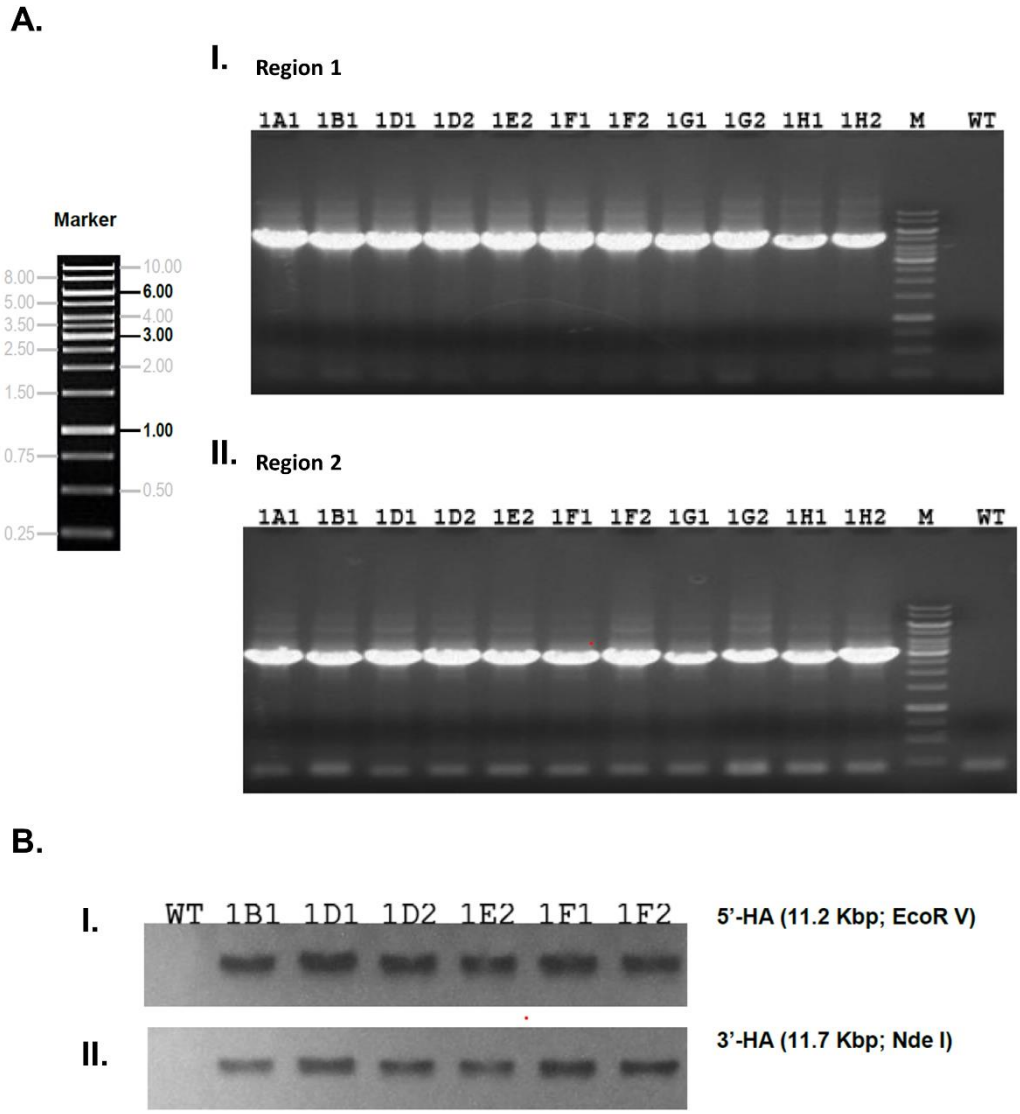

Figure 17. Confirmation of targeted vector transfection into ES cells. A. Visualization of the ES cells' PCR screening in an agarose gel. I. Results for Region 1. II. Results for Region 2. Reference marker with the lengths of each band in kilo-base pairs (Kbp) on the left. Mutant-type mice (1A1, 1B1, 1D1, 1D2, 1E2, 1F1, 1F2, 1G1, 1G2, 1H1, 1H2), marker (M) and one wild type (WT) mouse as control. **B. Southern Blot confirming analysis for ES clones.** Analysis of the mutant-type mice (1B1, 1D1, 1D2, 1E2, 1F1, 1F2) and a wild type (WT) mouse for two regions: **I. region containing the 5' homology arm** (5'-HA) (EcoR Enzyme V) and **II. region containing the 3' homology arm** (3'-HA) (Enzyme Nde I). Both fragments in kilo-base pairs (Kbp). Own elaboration (Power Point) modified from the one provided by Cyagen (Santa Clara, US).

A total of 11 clones were identified as potentially targeted clones (1A1, 1B1, 1D1, 1D2, 1E2, 1F1, 1F2, 1G1, 1G2, 1H1, 1H2), with 6 of them selected for expansion and subsequent Southern Blot analysis (clones 1B1, 1D1, 1D2, 1E2, 1F1, and 1F2). The results of the Southern Blot analysis, including the enzymes used and the expected fragments sizes, are presented in **Figure 17B**.

4.1.3 Crossbreeding Strategy

Selected ES clones were utilized to generate chimeras. The chimera was then crossed with a Flp-deleter mouse in the initial breeding step to establish the seipin KO murine model. To validate the resulting heterozygous mice (*Bscl2*$^{+/-}$), a PCR screening was conducted (**Figure 13A**).

Initially, a PCR assay was performed with an internal control (689 bp fragment) to detect any false negatives (**Figure 18A**). Subsequently, a PCR screening for region 1 was carried out, where a 532 bp band was expected for the mutant-type animals and no amplification for wild type animals (**Figure 18B**). Four *Bscl2*$^{+/-}$ mice (43, 44, 46, 47) were identified and confirmed through PCR screening of region 2. In this instance, a combined PCR targeting the internal control (389 bp) and region 2 (wild type: no amplification; mutant-type: 393 bp) was executed (**Figure 18C**).

Ultimately, two male and two female heterozygous knock-out mice (*Bscl2*$^{+/-}$) were successfully confirmed.

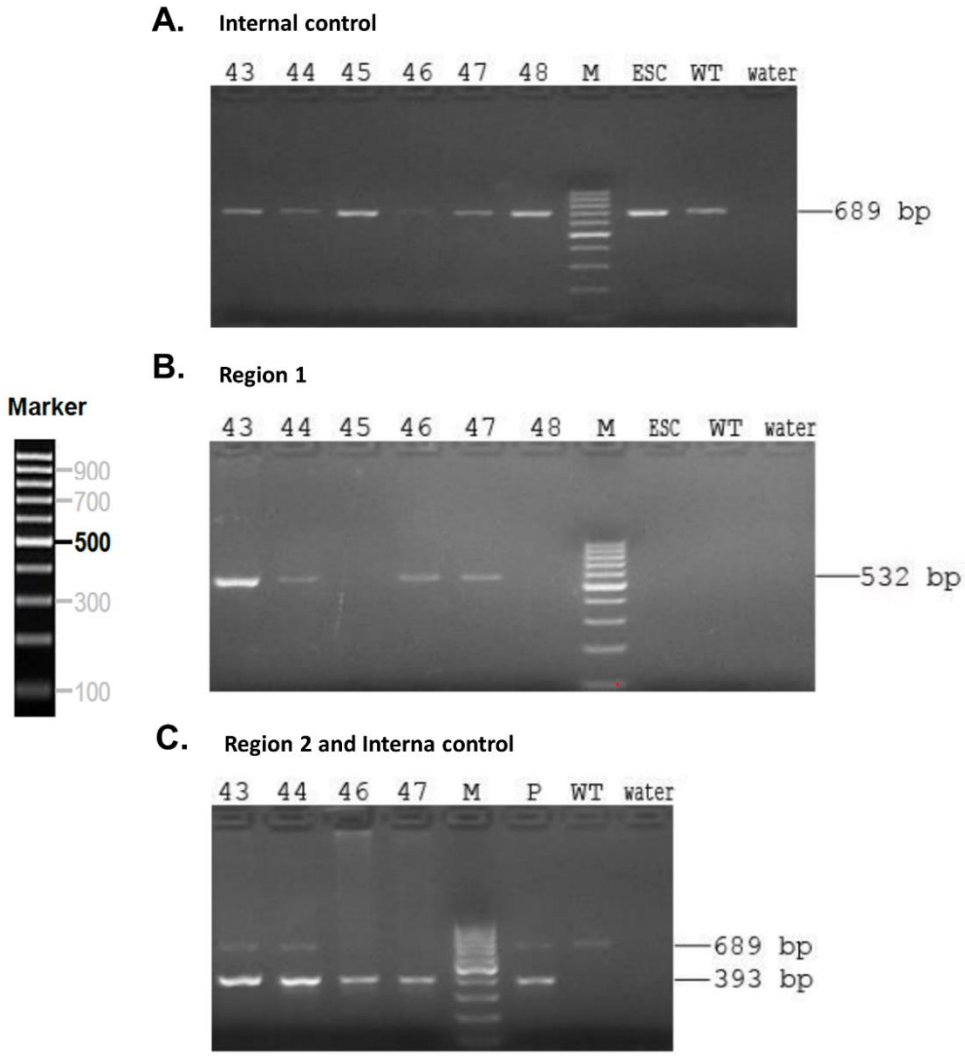

Figure 18. Agarose gel for the *Bscl2*$^{+/-}$ mice PCR confirmation. A. Results for the internal control. Possible mutant-type mice (43, 44, 45, 46, 47, 48), marker (M) and one wild type (WT), water, and super competent embryonic stem cell line (ESC) as controls. **B. Results for Region 1.** Possible mutant-type mice (43, 44, 45, 46, 47, 48), marker (M) and one wild type (WT), water, and super competent embryonic stem cell line (ESC) as controls. **C. Results for Region 2** (with internal control). Mutant-type mice (43, 44, 46, 47), marker (M) and one wild type (WT), water, and P (confidential) as controls. Reference marker with the lengths of each band in base pairs (bp) on the left. Own elaboration (Power Point) modified from the one provided by Cyagen (Santa Clara, US).

One of the heterozygous seipin knock-out (*Bscl2*$^{+/-}$) male mice obtained was used as the founder to obtain the Celia seipin knock-in murine model. For this, the male *Bscl2*$^{+/-}$ mouse was breed with a commercially available Cre-global female mouse.

Confirmation of the resulting mouse model was carried out through PCR screening of region 1 (**Figure 13B**). A 481 bp band was expected for the mutant-type animals, while no amplification was anticipated for the wild type animals (**Figure 19A**). The results confirmed the identification of three male and two female mice that were heterozygous for the Celia seipin (*Bscl2*$^{+/Celia)}$, which were further reconfirmed by an additional PCR screening of region 1 (**Figure 19B**).

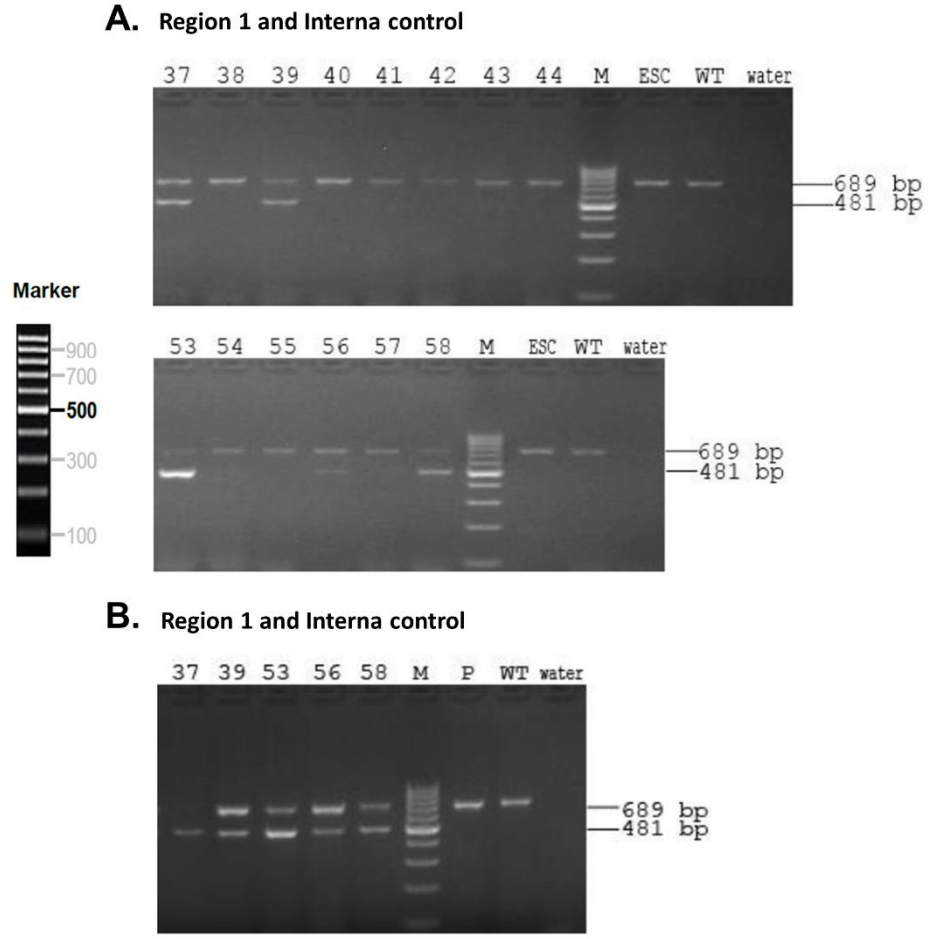

Figure 19. Agarose gel for the *Bscl2*$^{+/Celia}$ mice PCR confirmation. A. Results for the Region 1 and internal control. Possible mutant-type mice (37, 38, 39, 40, 41, 42, 43, 44, 53, 54, 55, 56, 57, 58), marker (M) and one wild type (WT), water, and super competent embryonic stem cell line (ESC) as controls. **B. Results for Region 1 and internal control reconfirmation.** Mutant-type mice (37, 39, 53, 56, 58), marker (M) and one wild type (WT), water, and P (confidential) as controls. Reference marker with the lengths of each band in base pairs (bp) on the left. Own elaboration (Power Point) modified from the one provided by Cyagen (Santa Clara, US).

4.1.4 Transgene Sequence Verification

The transgene sequence was validated by Sanger sequencing of one SKO and one Celia seipin KI mouse (see **Annex 2**).

Additionally, the normal expression of *Gng3*, a gene adjacent to *Bscl2* (as shown in **Figure 11**), was detected in various brain regions (cerebellum, midbrain, hypothalamus, cortex, hippocampus, striatum). This confirming that transgene insertion did not affect the expression of the *Gng3* gene (**Figure 20**, see **Annex 6**).

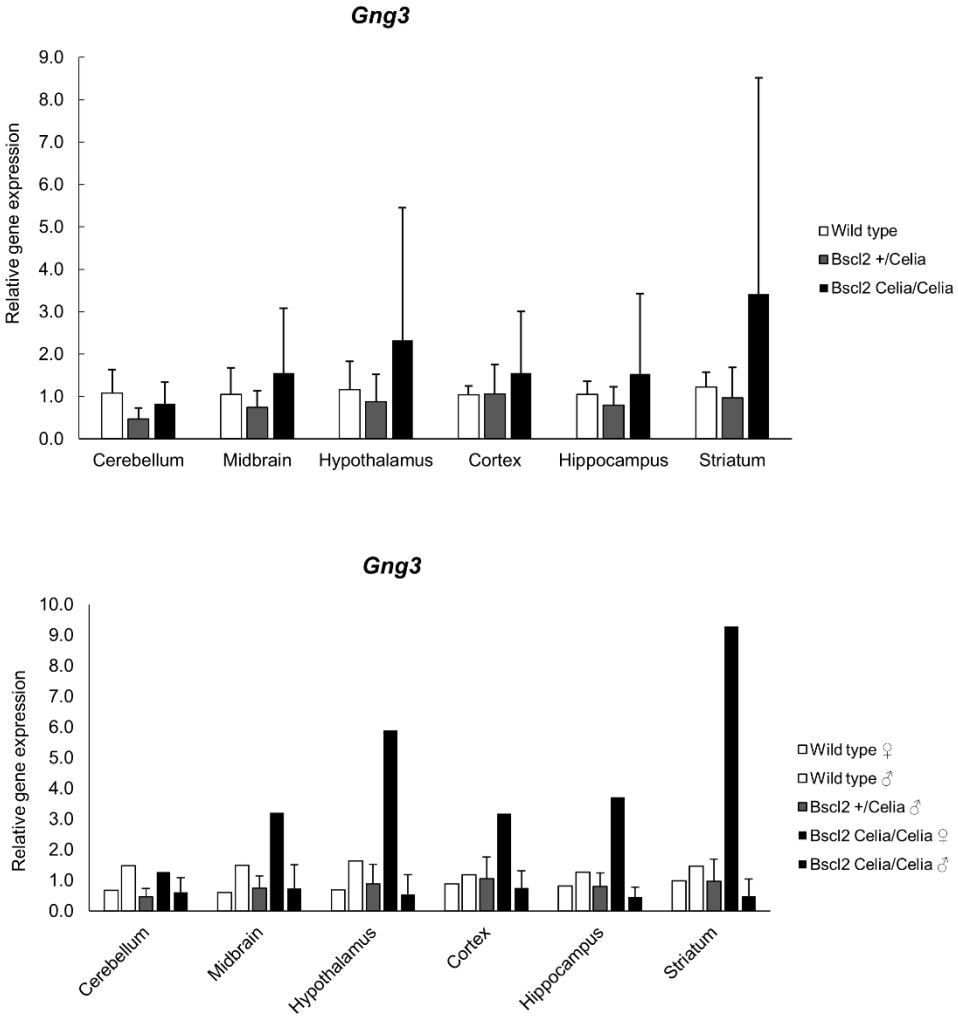

Figure 20. Relative expression of *Gng3* gene in brain tissues. Wild type, n= 1 ♀ and 1 ♂ (6-months-old); *Bscl2*$^{+/Celia}$, n= 2 ♂ (7.5-months-old) and *Bscl2*$^{Celia/Celia}$, n= 1 ♀ (9-months-old) and 2 ♂ (5-months-old). Data is presented as mean ± SD.

4.2 Characterization of Seipin Murine Models

4.2.1 Genotyping of the Lines

For the genotypic characterization of all the mice born from both the seipin knock-ou (*Bscl2*$^{+/-}$) and Celia seipin knock-in (*Bscl2*$^{+/Celia}$) murine lines, a genotyping strategy different from the one used for the initial line generation was employed (**Table 7**).

The genotyping for the KO model was performed using a single PCR with three primers (two forward, one reverse), while for the KI model required four different combinations. An example of the genotyping results for both murine lines and genotypes is shown in **Figure 21**. For the KO genotyping, sample 1 corresponds to a heterozygous mouse, sample 2 to a homozygous mouse, and sample 3 to a wild type mouse. For the KI genotyping, sample 4

corresponds to a heterozygous mouse, sample 5 to a homozygous mouse, and sample 6 to a wild type mouse.

This genotyping strategy was consistently applied to all mice included in the study.

	Primer combination	Gel bands	Genotype interpretation	Gel results
KO murine model	F1/R1 + F2/R1	532 bp	Homozygous	2
		301 bp	Wild type	3
		532 bp + 301 bp	Heterozygous	1
KI murine model	F3/R3	482 bp	Heterozygous or Homozygous	4, 5
		NA	Wild type	6
	F5/R5	543 bp	Wild type or Heterozygous	6, 4
		1884 bp or NA	Homozygous	5
	F2/R1	301 bp	Wild type or Heterozygous	6, 4
		1642 bp	Homozygous	5
	F4/R1	534 bp	Heterozygous or Homozygous	4, 5
		NA	Wild type	6

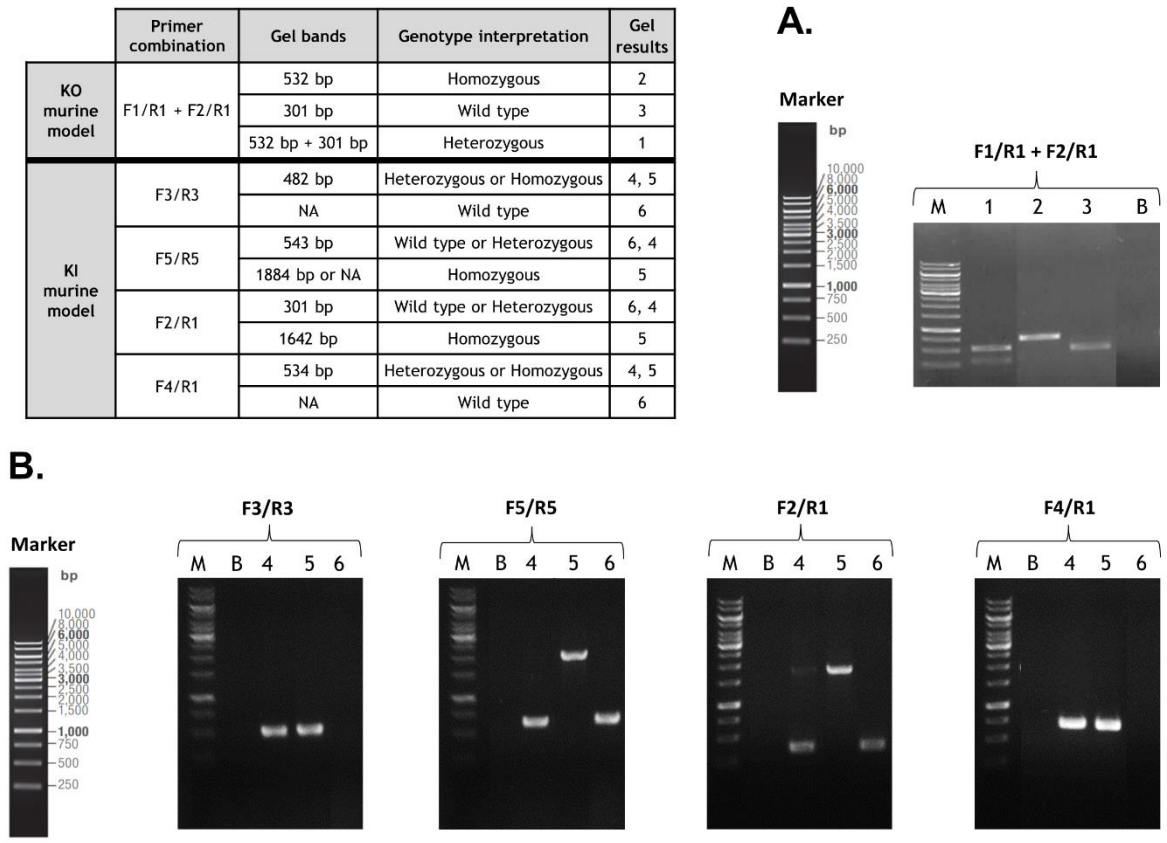

Figure 21. Genotyping example for knock-out (KO) and knock-in (KI) murine models. A table with the primer combinations, the length of the fragments in base pairs (bp) and the results for the gels of both strategies is shown on the upper left. **A. Agarose gel results for PCR genotyping of the KO model (*Bscl2*$^{+/-}$).** Animals for genotyping (1, 2, 3), marker (M) and blank (B). **B. Agarose gel results for PCR genotyping of the KI model (*Bscl2*$^{+/Celia}$).** Animals to genotype (4, 5, 6), marker (M) and blank (B). GeneRuler 1 kb DNA Ladder (cat# SM0311, Thermo Scientific, Madrid, Spain) as reference marker with the lengths of each band in base pairs (bp).

4.2.2 Colony Maintenance

By breeding homozygous *Bscl2*$^{Celia/Celia}$ and *Bscl2*$^{-/-}$ animals, it was observed that both females and males were either sterile or unable to carry their offspring to term. Consequently, the colony was sustained through the breeding of heterozygous *Bscl2*$^{+/Celia}$ or *Bscl2*$^{+/-}$ mice.

Additionally, it was confirmed that heterozygous mice exhibited sperm quality comparable to that of wild type mice. However, neurologically affected heterozygous mice were found to be sterile (**Table 13**).

Table 13. Sperm quality analysis. Motility and concentration for wild type, *Bscl2*$^{+/Celia}$ and severely affected (S.A.) *Bscl2*$^{+/Celia}$ mice. Data is presented as mean ± SD. Statistical analysis was not carried out because the less animals in the study.

	Male		
	Wild type	***Bscl2*$^{+/Celia}$**	**S.A. *Bscl2*$^{+/Celia}$**
Sperm quality			
N (Age (months))	3 (7.6)	5 (7.4)	1 (5.4)
Motility (0-5)	4.33 ± 0.29	4.00 ± 1.22	0
Concentration (nº spz/10^6 mL)	43.70 ± 22.70	39.11 ± 16.66	16.48

The observed genotypes followed a Mendelian inheritance pattern. For the Celia seipin KI model, the genotype frequencies were: 24.3% wild type (n=132), 24.7% homozygous *Bscl2*$^{Celia/Celia}$ (n=134), and 51.0% heterozygous *Bscl2*$^{+/Celia}$ (n=277). Similarly, for the SKO model, the genotype frequencies were: 24.9% wild type (n=86), 24.6% homozygous *Bscl2*$^{-/-}$ (n=85), and 50.6% heterozygous *Bscl2*$^{+/-}$ (n=175) (**Figure 14**).

Furthermore, the male-to-female ratio was approximately 50:50 % across all genotypes.

4.3 Neurological Clinical Phenotype

A total of 31 mice exhibited severe neurological alterations. Of these, 16 were *Bscl2*$^{Celia/Celia}$ mice (11.9% of the total *Bscl2*$^{Celia/Celia}$), and 15 were *Bscl2*$^{+/Celia}$ mice (5.4% of the total *Bscl2*$^{+/Celia}$). Within the *Bscl2*$^{Celia/Celia}$ group, 50% were female and 50% were male. In the *Bscl2*$^{+/Celia}$ group, 40% were female and 60% were male.

The neurological signs began to manifest at approximately 4.8 months of age and progressively worsened over the lifespan of the affected animals, which was severely reduced (average lifespan of 8.4 months).

4.3.1 Observation and Phenotypic Monitoring

The key neurological manifestations observed in the severely affected (S.A.) mice included: ponderal stagnation, abnormal limb crossing, kyphosis, tremor or myoclonus, tail spasticity and paraparesis or paraplegia (**Figure 22A**). This neurological phenotype was corroborated by the NeuroScore and Welfare tests performed at 7.5 months of age (**Figure 22B,** see **Annex 3 Table S1**). The S.A. mice exhibited up to 20-fold greater impairment in neurological functions compared to mice that did not develop neurodegenerative symptoms. Furthermore, the analysis by sex of the non-severely affected animals (wild type, KI, and KO) revealed greater neurological severity in *Bscl2*$^{-/-}$ males compared to the other genotypes (**Figure 22B**).

The assessment of welfare in these neurologically affected animals revealed a quality-of-life impairment up to 30-fold greater than wild type and non-S.A. heterozygous animals (*Bscl2*$^{+/Celia}$ and *Bscl2*$^{+/-}$). The non-S.A. homozygous animals (*Bscl2*$^{Celia/Celia}$ and *Bscl2*$^{-/-}$) also exhibited poorer welfare compared to wild type and heterozygous mice, though not as severe

as the neurologically affected cohort. Further analysis by sex showed a greater decline in quality of life for wild type and heterozygous male mice compared to females. This sex-based difference was not as pronounced in the homozygous genotypes. However, it was observed that the *Bscl2*$^{Celia/Celia}$ males presented a worse welfare condition than the *Bscl2*$^{-/-}$ females (**Figure 22B**).

It should be noted that the S.A *Bscl2*$^{+/Celia}$ mice did not exhibit statistically significant differences, likely due to the limited sample size of a single animal in this group. However, based on the available data, it can be considered that there were no substantial differences in the severity of neurological and welfare impairments between S.A. heterozygous (S.A. *Bscl2*$^{+/Celia}$) and homozygous (S.A. *Bscl2*$^{Celia/Celia}$) animals (**Figure 22B**).

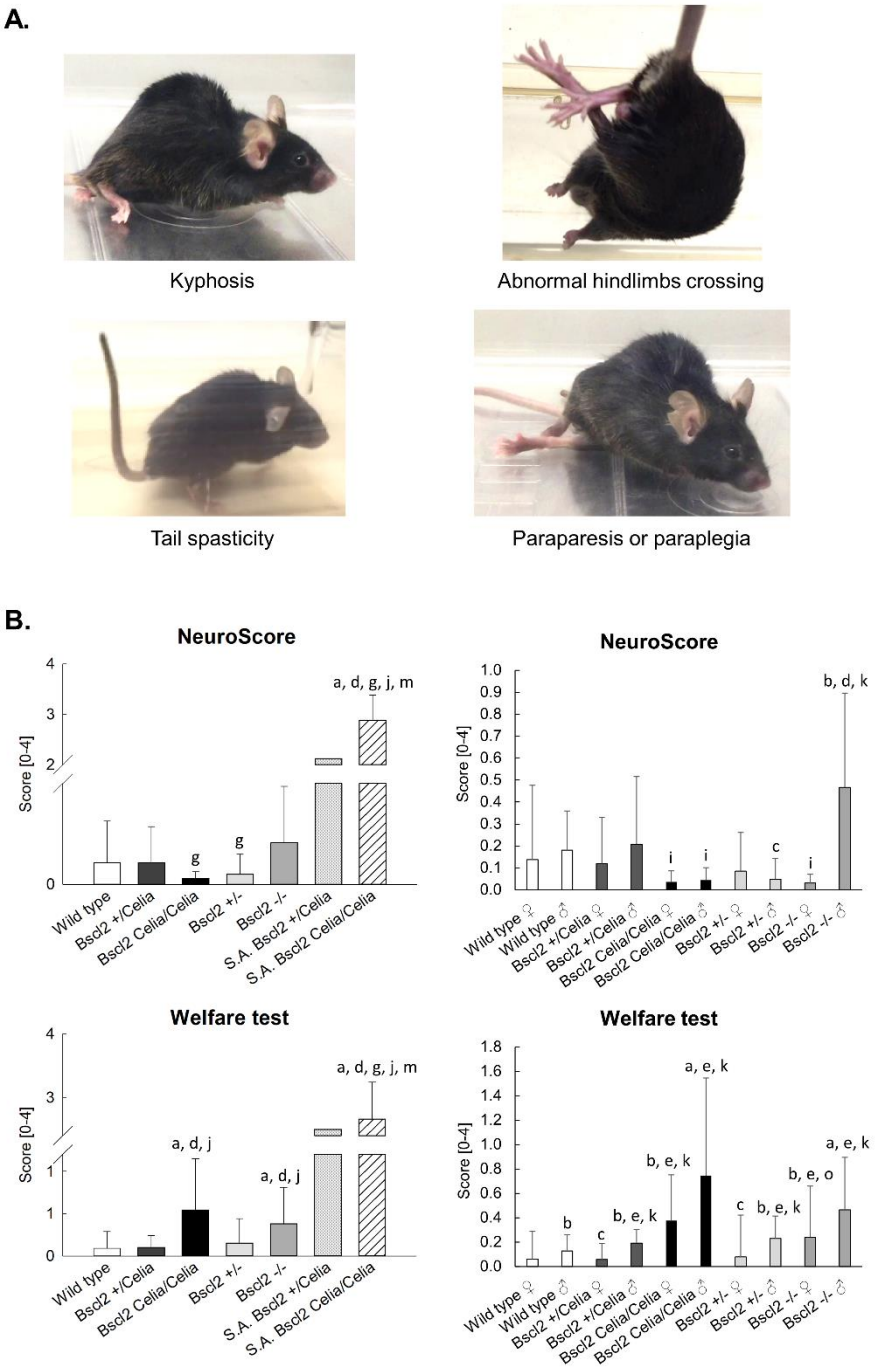

Figure 22. Neurological signs and NeusoScore and welfare test. A. Images of common neurological signs of a severely affected animal. Kyphosis, abnormal hindlimbs crossing, tail spasticity and paraparesis or paraplegia. **B. NeuroScore and welfare test.** Wild type, n= 32 (20 ♀ and 12 ♂); *Bscl2*$^{+/Celia}$, n= 37 (25 ♀ and 12 ♂); *Bscl2*$^{Celia/Celia}$, n= 25 (14 ♀ and 11 ♂); *Bscl2*$^{+/-}$, n= 36 (19 ♀ and 17 ♂); *Bscl2*$^{-/-}$, n= 25 (10 ♀ and 15 ♂) and 4 severely affected (S.A.), n= 1 *Bscl2*$^{+/Celia}$ and n= 3 *Bscl2*$^{Celia/Celia}$, animals. Mean age 7.5-months-old. Data is presented as mean ± SD. Data were analysed using a Kolmogorov-Smirnov test for normality, followed by a Kruskal-Wallis test with Mann-Whitney post hoc comparisons. [a] $p < 0.05$ vs wild type ♀/♂; [b] $p < 0.05$ vs wild type ♀; [c] $p < 0.05$ vs wild type ♂; [d] $p < 0.05$ vs *Bscl2*$^{+/-}$ ♀/♂; [e] $p < 0.05$ vs *Bscl2*$^{+/-}$ ♀; [g] $p < 0.05$ vs *Bscl2*$^{-/-}$ ♀/♂; [i] $p < 0.05$ vs *Bscl2*$^{-/-}$ ♂; [j] $p < 0.05$ vs *Bscl2*$^{+/Celia}$ ♀/♂; [k] $p < 0.05$ vs *Bscl2*$^{+/Celia}$ ♀; [m] $p < 0.05$ vs *Bscl2*$^{Celia/Celia}$ ♀/♂ and [o] $p < 0.05$ *Bscl2*$^{Celia/Celia}$ ♂.

In addition to the neurological and welfare assessments, a detailed observation of the animal's behaviour within their cages was conducted. This included a gnawing test, which measured the amount of enrichment material consumed by each animal. The results showed that the mice exhibited increased gnawing behaviour during the fertile period, between 2 and 7.5 months of age. However, from the 8 months onward, the gnawing tendency decreased to below 0.1 grams per day across nearly all groups. Notably, the homozygous mice displayed a lower amount of gnawing behaviour, with the *Bscl2*$^{-/-}$ genotype showing the least amount of enrichment consumption (**Figure 23**). This suggests a distinct behavioural phenotype in the homozygous animals compared to the wild type and heterozygous counterparts. It should be noted that the *Bscl2*$^{+/-}$ group did not show statistically significant differences, potentially due to the small sample size. However, a trend similar to the wild type and *Bscl2*$^{+/Celia}$ mice was observed.

Furthermore, despite not having tested both sexes separately across all genotypes, a reduction in gnawing behaviour was observed in male mice compared to females (**Figure 23**).

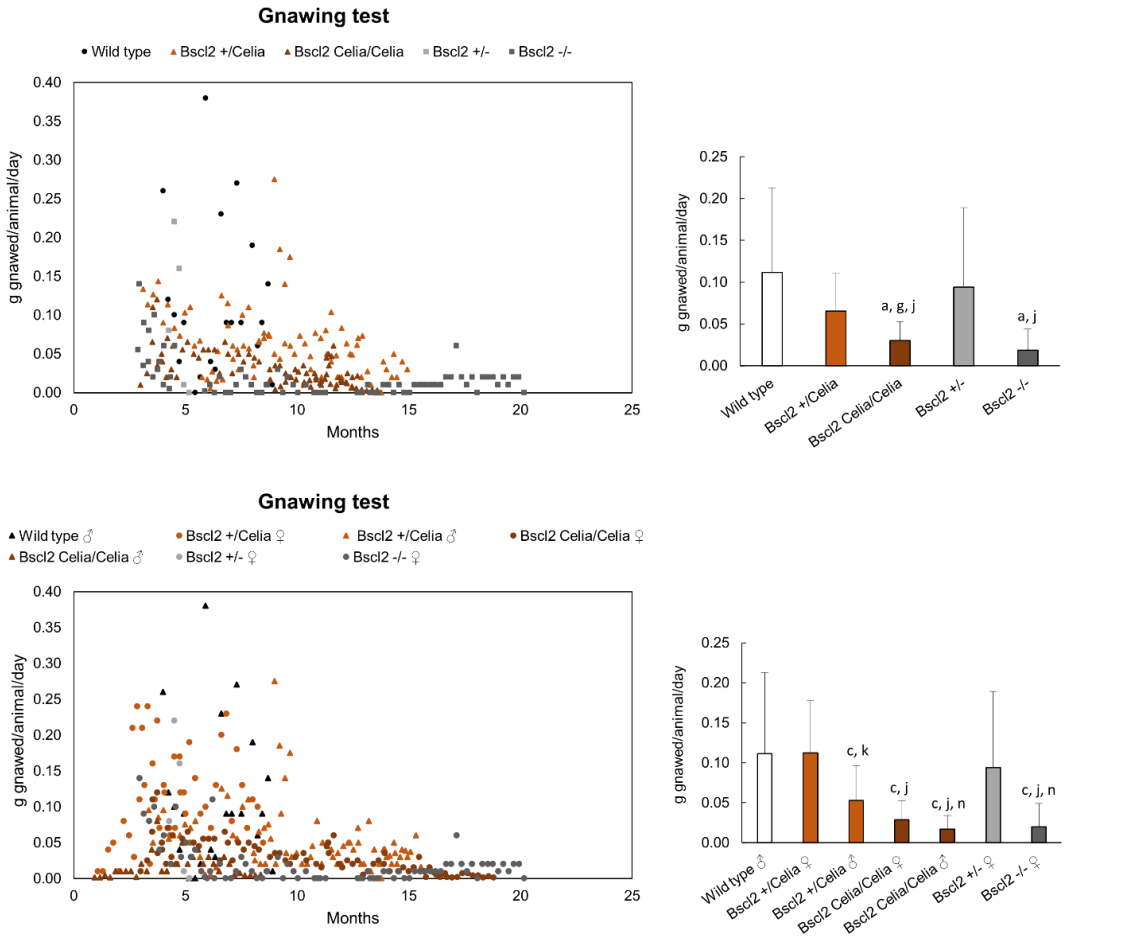

Figure 23. Gnawing test for wild type, *Bscl2*$^{+/Celia}$, *Bscl2*$^{Celia/Celia}$, *Bscl2*$^{+/-}$ and *Bscl2*$^{-/-}$ animals. For mean age and number of animals per genotype see **Annex 3, Table S2**. The grams gnawed per and animal and per day were measure as evolution over time and mean ± SD. Data were analysed using a Kolmogorov-Smirnov test for normality, followed by a Kruskal-Wallis test with Mann-Whitney post hoc comparisons. [a] $p < 0.05$ vs wild type ♀/♂; [c] $p < 0.05$ vs wild type ♂; [g] $p < 0.05$ vs *Bscl2*$^{-/-}$ ♀/♂; [j] $p < 0.05$ vs *Bscl2*$^{+/Celia}$ ♀/♂; [k] $p < 0.05$ vs *Bscl2*$^{+/Celia}$ ♀; [n] $p < 0.05$ vs *Bscl2*$^{Celia/Celia}$ ♀.

In addition to the gnawing behaviour, the animals' nesting behaviour was also observed to evaluate their levels of distress. The results showed that the non-S.A. homozygous animals (*Bscl2*$^{Celia/Celia}$ and *Bscl2*$^{-/-}$) constructed poorer quality nests, indicating greater distress, compared to the wild type and heterozygous mice (**Figure 24**). No significant difference were found between the KI and KO animals. Unfortunately, it was not possible to evaluate the nesting behaviour of the severely affected mice. This was due to the inability to isolate these animals into individual cages, as doing so would have caused them greater discomfort.

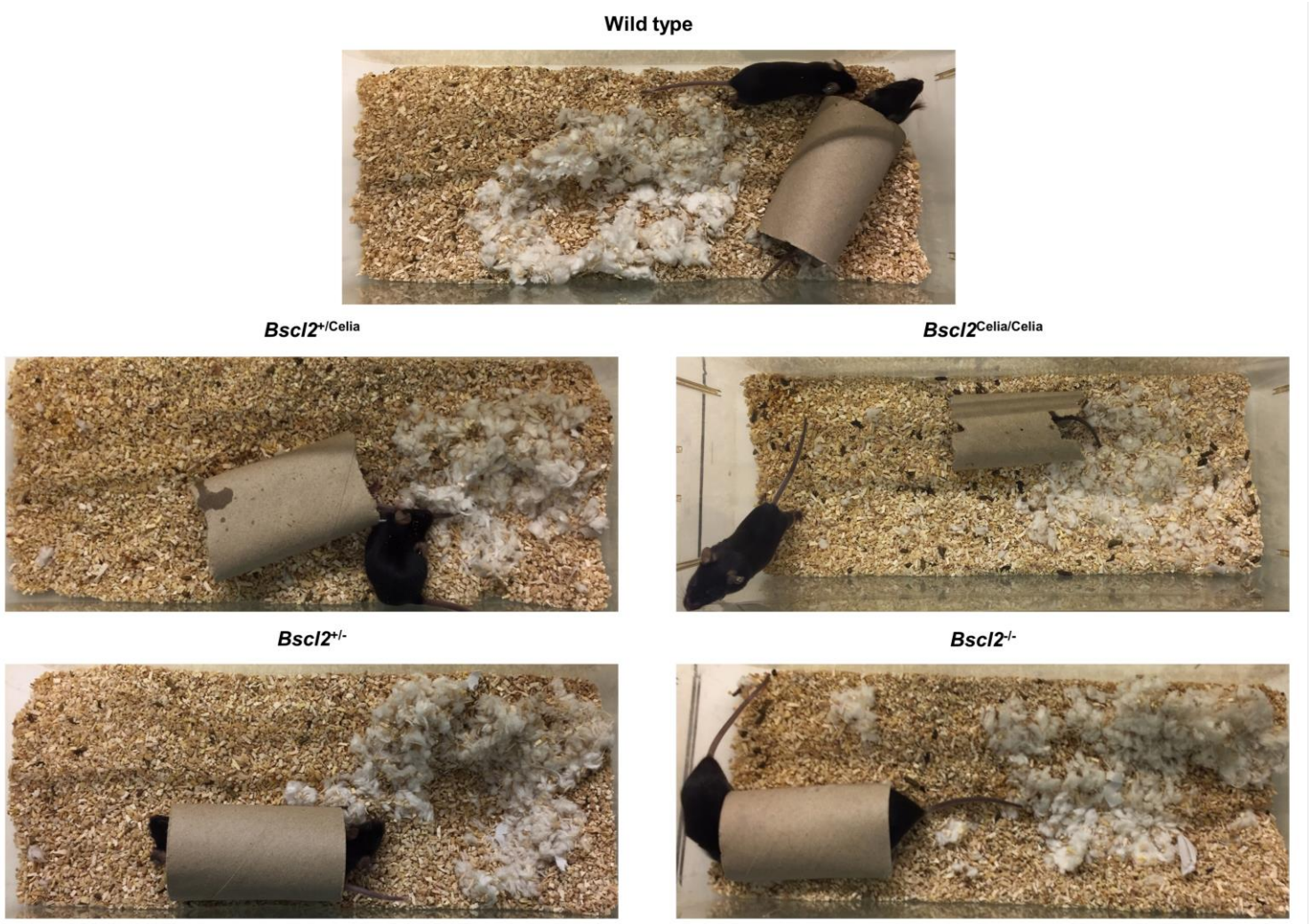

Figure 24. Nest building. Wild type (n= 2♀), *Bscl2*$^{+/Celia}$ (n= 2♀), *Bscl2*$^{Celia/Celia}$ (n= 1♀ + 1♂), *Bscl2*$^{+/-}$ (n= 2♀) and *Bscl2*$^{-/-}$ (n= 2♀ + 1♂) animals. Mean age 2.8-months-old.

4.3.2 Behavioural Study at Neurological and Motor Level

The transgenic murine models and wild type mice control were evaluated for potential sensorimotor impairments using the open field and elevated zero maze tests (see **Annex 4, Table S3**). In the open field and elevated zero maze tests, the homozygous animals exhibited decreased locomotor activity, as evidenced by shorter distance travelled, lower average speed, and less time in motion compared to the wild type and heterozygous mice. Additionally, these homozygous animals displayed greater anxiety-like behaviour, as indicated by their preference to stay closer to the walls of the arena (thigmotaxis) and in the closed areas (**Figure 25** and **Figure 26**). Further analysis by sex revealed that the homozygous male mice showed a more pronounced decrease in motor activity and greater anxiety compared to homozygous females in the open field test (**Figure 25**). In the elevated zero maze test, *Bscl2*$^{-/-}$ males exhibited worse locomotion and greater anxiety-like behaviour in some parameters compared to *Bscl2*$^{Celia/Celia}$ females (**Figure 26**). Additionally, *Bscl2*$^{Celia/Celia}$ displayed greater anxiety-like behaviour, as measured by the "time in centre" parameter, compared to *Bscl2*$^{-/-}$ males in the open field test (**Figure 25**). No other significant differences were found between the murine models in the remaining parameters analysed.

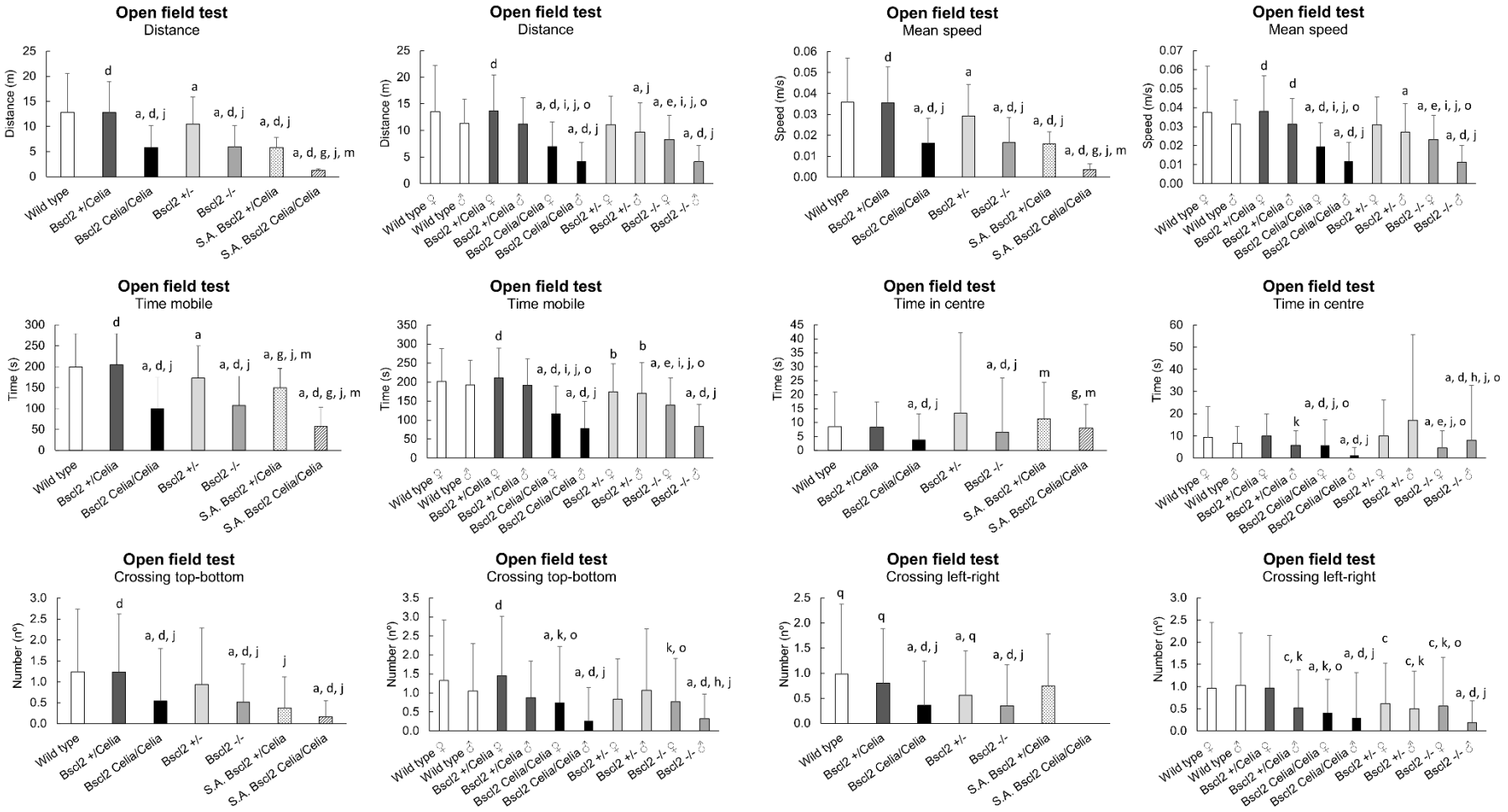

Figure 25. Open field test. Wild type, n= 29 (20 ♀ and 9 ♂); *Bscl2*$^{+/Celia}$, n= 27 (17 ♀ and 10 ♂); *Bscl2*$^{Celia/Celia}$, n= 25 (14 ♀ and 11 ♂); *Bscl2*$^{+/-}$, n= 30 (16 ♀ and 14 ♂); *Bscl2*$^{-/-}$, n= 23 (10 ♀ and 13 ♂) and 5 severe affected (S.A.) animals, 2 S.A. *Bscl2*$^{+/Celia}$ and 3 S.A. *Bscl2*$^{Celia/Celia}$. Mean age 6.5 months. Data is presented as mean ± SD. Data were analysed using a Kolmogorov-Smirnov test for normality, followed by a Kruskal-Wallis test with Mann-Whitney post hoc comparisons. [a] $p < 0.05$ vs wild type ♀/♂; [b] $p < 0.05$ vs wild type ♀; [c] $p < 0.05$ vs wild type ♂; [d] $p < 0.05$ vs *Bscl2*$^{+/-}$ ♀/♂; [e] $p < 0.05$ vs *Bscl2*$^{+/-}$ ♀; [g] $p < 0.05$ vs *Bscl2*$^{-/-}$ ♀/♂; [h] $p < 0.05$ vs *Bscl2*$^{-/-}$ ♀; [i] $p < 0.05$ vs *Bscl2*$^{-/-}$ ♂; [j] $p < 0.05$ vs *Bscl2*$^{+/Celia}$ ♀/♂; [k] $p < 0.05$ vs *Bscl2*$^{+/Celia}$ ♀; [m] $p < 0.05$ vs *Bscl2*$^{Celia/Celia}$ ♀/♂; [o] $p < 0.05$ vs *Bscl2*$^{Celia/Celia}$ ♂ and [q] $p < 0.05$ vs S.A. *Bscl2*$^{Celia/Celia}$ ♀/♂.

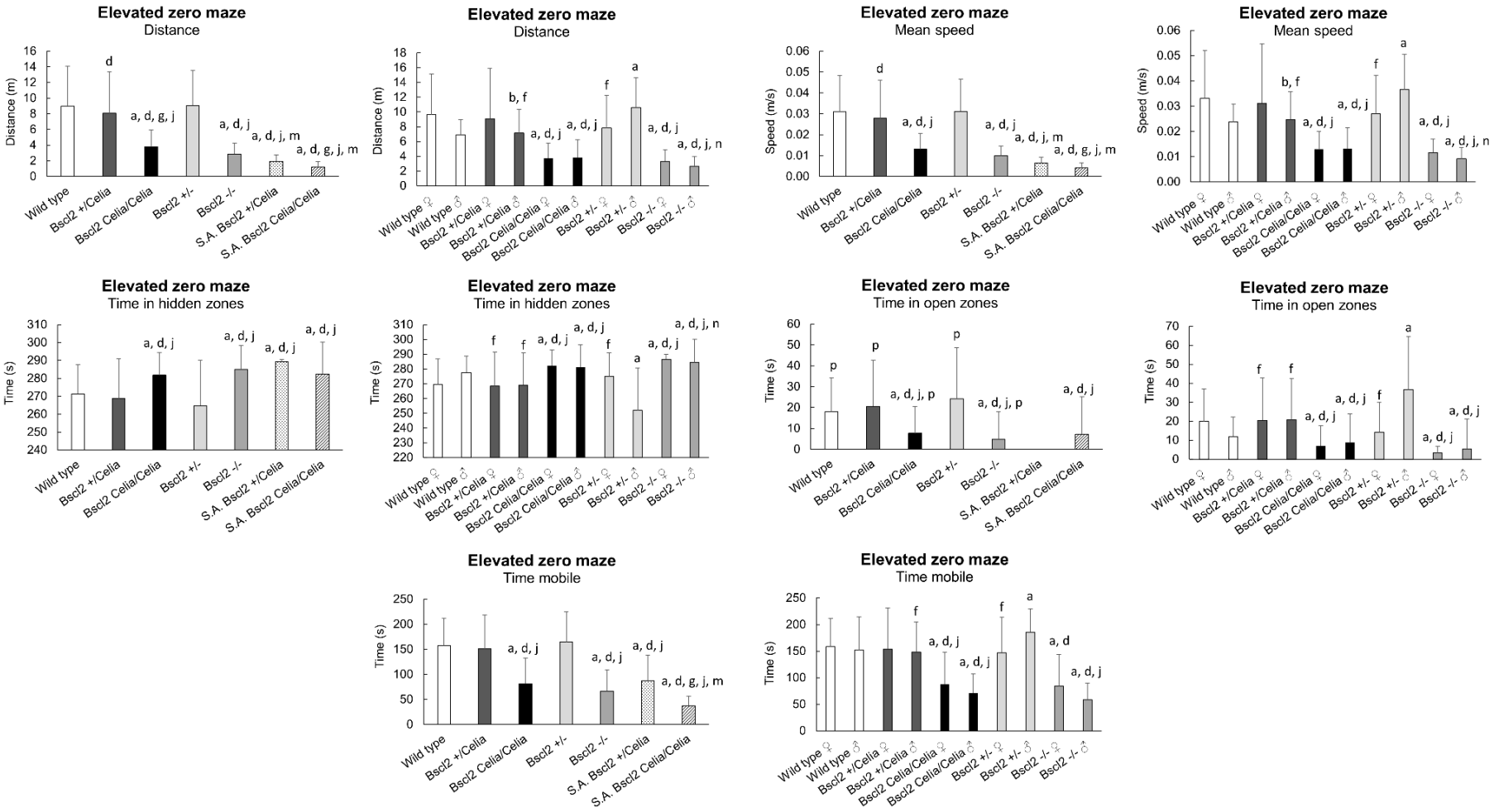

Figure 26. Elevated zero maze. Wild type, n= 20 (15 ♀ and 5 ♂); *Bscl2*$^{+/Celia}$, n= 21 (10 ♀ and 11 ♂); *Bscl2*$^{Celia/Celia}$, n= 19 (11 ♀ and 8 ♂); *Bscl2*$^{+/-}$, n= 25 (14 ♀ and 11 ♂); *Bscl2*$^{-/-}$, n= 10 (3 ♀ and 7 ♂) and 4 severe affected (S.A.) animals, 1 S.A. *Bscl2*$^{+/Celia}$ and 3 S.A. *Bscl2*$^{Celia/Celia}$. Mean age 7.4 months. Data is presented as mean ± SD. Data were analysed using a Kolmogorov-Smirnov test for normality, followed by a Kruskal-Wallis test with Mann-Whitney post hoc comparisons. [a] $p < 0.05$ vs wild type ♀/♂; [b] $p < 0.05$ vs wild type ♀; [d] $p < 0.05$ vs *Bscl2*$^{+/-}$ ♀/♂; [f] $p < 0.05$ vs *Bscl2*$^{+/-}$ ♂; [g] $p < 0.05$ vs *Bscl2*$^{-/-}$ ♀/♂; [j] $p < 0.05$ vs *Bscl2*$^{+/Celia}$ ♀/♂; [m] $p < 0.05$ vs *Bscl2*$^{Celia/Celia}$ ♀/♂; [n] $p < 0.05$ vs *Bscl2*$^{Celia/Celia}$ ♀; and [p] $p < 0.05$ vs S.A. *Bscl2*$^{+/Celia}$ ♀/♂.

The rotarod test further revealed that the *Bscl2*$^{-/-}$ animals exhibited impaired coordination and balance, while this effect was not as clearly observed in the *Bscl2*$^{Celia/Celia}$ mice (**Figure 27A**). Consistent with the findings in the open field test, homozygous males showed a more pronounced decrease in motor activities compared to homozygous females. Additionally, the beam walking test demonstrated that both homozygous murine models (*Bscl2*$^{Celia/Celia}$ and *Bscl2*$^{-/-}$) displayed reduced coordination and balance compared to the wild type and heterozygotes animals (**Figure 27B**). However, the wire hang test did not show significant differences between both murine models (see **Annex 4**).

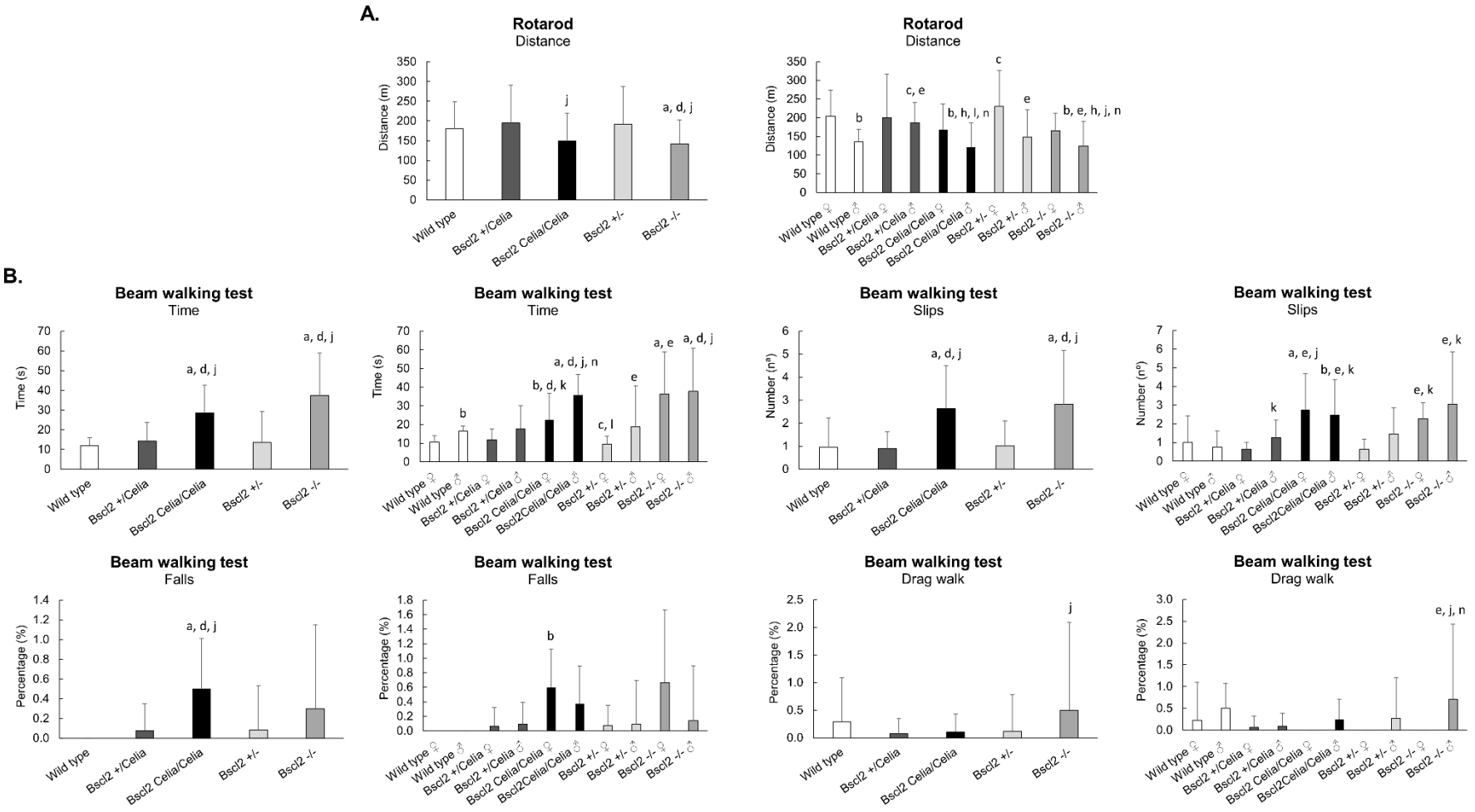

Figure 27. Rotarod and Beam walking test. A. Rotarod test. Wild type, n= 29 (19 ♀ and 10 ♂); *Bscl2*$^{+/Celia}$, n= 28 (17 ♀ and 11 ♂); *Bscl2*$^{Celia/Celia}$, n= 25 (15 ♀ and 10 ♂); *Bscl2*$^{+/-}$, n= 30 (16 ♀ and 14 ♂) and *Bscl2*$^{-/-}$, n= 23 (10 ♀ and 13 ♂) animals. Mean age 7.1 months. **B. Beam walking test.** Wild type, n= 17 (13 ♀ and 4 ♂); *Bscl2*$^{+/Celia}$, n= 26 (15 ♀ and 11 ♂); *Bscl2*$^{Celia/Celia}$, n= 18 (10 ♀ and 8 ♂); *Bscl2*$^{+/-}$, n= 24 (13 ♀ and 11 ♂) and *Bscl2*$^{-/-}$, n= 10 (3 ♀ and 7 ♂) animals. Mean age 9.0 months. Data is presented as mean ± SD. Data were analysed using a Kolmogorov-Smirnov test for normality, followed by a Kruskal-Wallis test with Mann-Whitney post hoc comparisons. [a] $p < 0.05$ vs wild type ♀/♂; [b] $p < 0.05$ vs wild type ♀; [c] $p < 0.05$ vs wild type ♂; [d] $p < 0.05$ vs *Bscl2*$^{+/-}$ ♀/♂; [e] $p < 0.05$ vs *Bscl2*$^{+/-}$ ♀; [h] $p < 0.05$ vs *Bscl2*$^{-/-}$ ♀; [j] $p < 0.05$ vs *Bscl2*$^{+/Celia}$ ♀/♂; [k] $p < 0.05$ vs *Bscl2*$^{+/Celia}$ ♀; [l] $p < 0.05$ vs *Bscl2*$^{+/Celia}$ ♂; [n] $p < 0.05$ vs *Bscl2*$^{Celia/Celia}$ ♀.

The Morris water maze test further revealed that the homozygous animals exhibited slower swimming speeds and reduced distance travelled, specifically in the *Bscl2*$^{Celia/Celia}$ mice, indicative of a decreased motor activity in these genotypes. However, no significant differences were observed in parameters such as moving time, despite the *Bscl2*$^{Celia/Celia}$ mice showing shorter time in motion compared to the *Bscl2*$^{-/-}$ group. Interestingly, in contrast to the findings from the open field and elevated zero maze tests, the homozygous animals displayed lower anxiety levels, as measured by the floating time in the Morris water maze (**Figure 28**). Additionally, the Morris water maze was used to assess memory-related cognitive functions, evaluating the animals' ability to process, consolidate, and retain visual cues to successfully navigate and locate the hidden platform. In this regard, the homozygous animals did not exhibit significant differences compared to the wild type or heterozygous mice (**Figure 28**).

Due to the significant physical discomfort experienced by the severely affected animals, their behavioural assessment at the neurological and motor levels was only feasible for tests involving the lowest levels of stress, namely the open field and elevated zero maze. Despite this limitation, the S.A. mice exhibited high levels of anxiety, similar to the non-S.A. homozygous animals (KI and KO). Additionally, these S.A mice displayed decreased locomotor activities, with an even more pronounced reduction observed in the S.A. *Bscl2*$^{Celia/Celia}$ group (**Figure 25** and **Figure 26**).

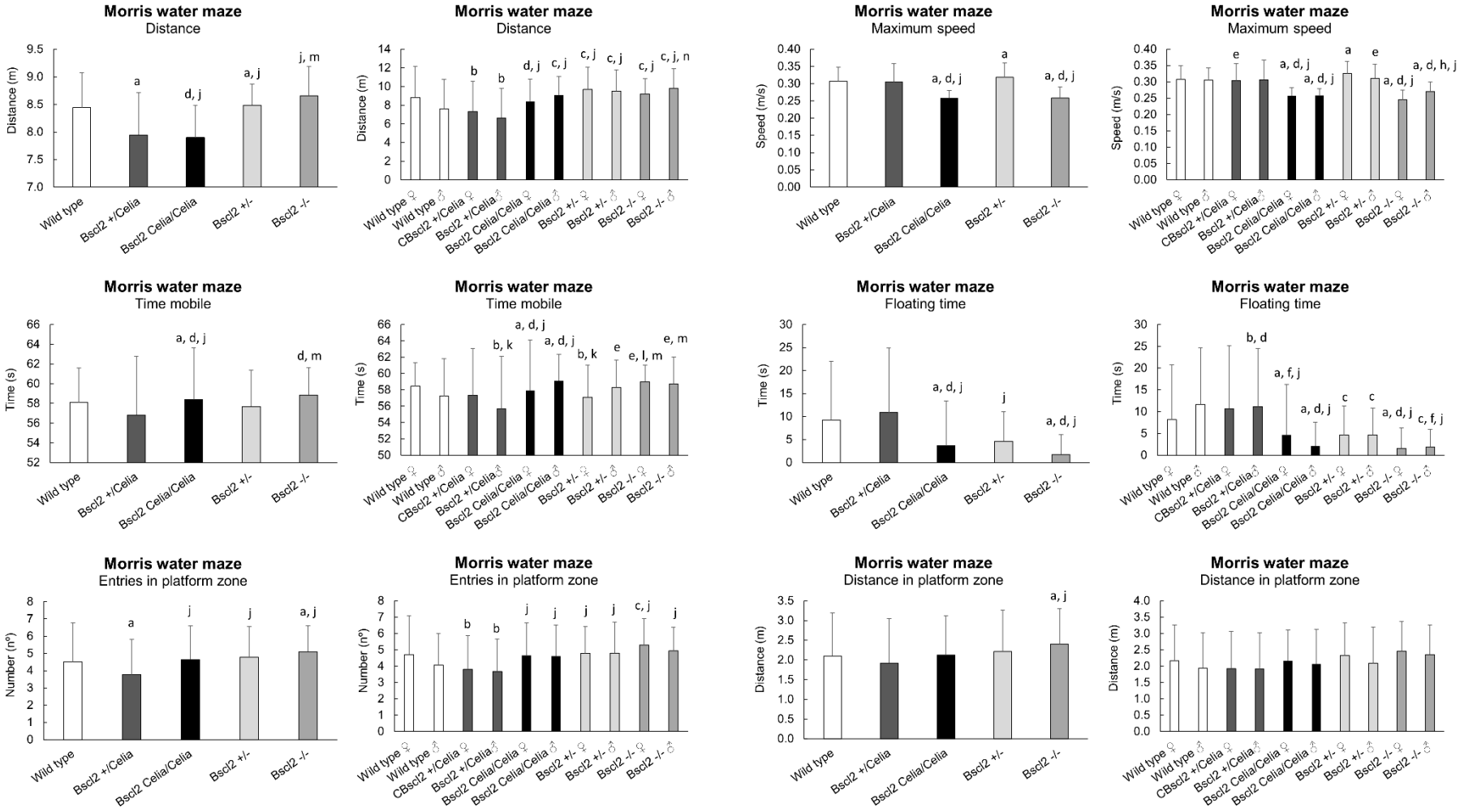

Figure 28. Morris water maze. Wild type, n= 27 (19 ♀ and 8 ♂); *Bscl2*$^{+/Celia}$, n= 29 (20 ♀ and 9 ♂); *Bscl2*$^{Celia/Celia}$, n= 23 (14 ♀ and 9 ♂); *Bscl2*$^{+/-}$, n= 27 (14 ♀ and 13 ♂) and *Bscl2*$^{-/-}$, n= 15 (7 ♀ and 8 ♂) animals. Mean age 8.3 months. Data is presented as mean ± SD. Data were analysed using a Kolmogorov-Smirnov test for normality, followed by a Kruskal-Wallis test with Mann-Whitney post hoc comparisons. [a] $p < 0.05$ vs wild type ♀/♂; [b] $p < 0.05$ vs wild type ♀; [c] $p < 0.05$ vs wild type ♂; [d] $p < 0.05$ vs *Bscl2*$^{+/-}$ ♀/♂; [e] $p < 0.05$ vs *Bscl2*$^{+/-}$ ♀; [f] $p < 0.05$ vs *Bscl2*$^{+/-}$ ♂; [g] $p < 0.05$ vs *Bscl2*$^{-/-}$ ♀/♂; [j] $p < 0.05$ vs *Bscl2*$^{+/Celia}$ ♀/♂; [k] $p < 0.05$ vs *Bscl2*$^{+/Celia}$ ♀; [l] $p < 0.05$ vs *Bscl2*$^{+/Celia}$ ♂; [m] $p < 0.05$ vs *Bscl2*$^{Celia/Celia}$ ♀/♂.

To verify whether the observed results in the homozygous animals were genuine or potentially influenced by their body weight or liver weight (in some cases, the liver represented up to 25% of the total weight), analysis of covariance (ANCOVA) was performed.

Firstly, ANCOVA was conducted on the parameters and tests that showed differences between the wild type and the *Bscl2*$^{Celia/Celia}$ or *Bscl2*$^{-/-}$ genotypes. This analysis aimed to determine whether accounting for the liver or body weight variables would affect the differences observed between the homozygous groups. Secondly, ANCOVA was used to assess whether there were any differences between *Bscl2*$^{Celia/Celia}$ and *Bscl2*$^{-/-}$ homozygous murine models when controlling for liver or body weight. These analyses were performed separately for each sex. It is important to note that a smaller group of animals was used for this ANCOVA analysis due to the inability to obtain liver weight measurements for all individuals.

The ANCOVA analysis revealed that in the open field test, the decreased locomotor activities and increased anxiety observed in *Bscl2*$^{Celia/Celia}$ female mice appeared to be conditioned by the large size of their livers compared to wild type females. However, this confounding effect of liver weight was not observed in the male *Bscl2*$^{Celia/Celia}$ mice, where the decreases in locomotor activities and increases in anxiety were not influenced by the liver size (**Figure 29A**). Conversely, the ANCOVA analysis did not show a significant influence of liver weight on the locomotor activities and coordination impairments observed in the elevated zero maze and rotarod tests for either sex. Interestingly, the high anxiety levels seen in *Bscl2*$^{Celia/Celia}$ females on the elevated zero maze were found to be conditioned by their liver weight (**Figure 29B-C**).

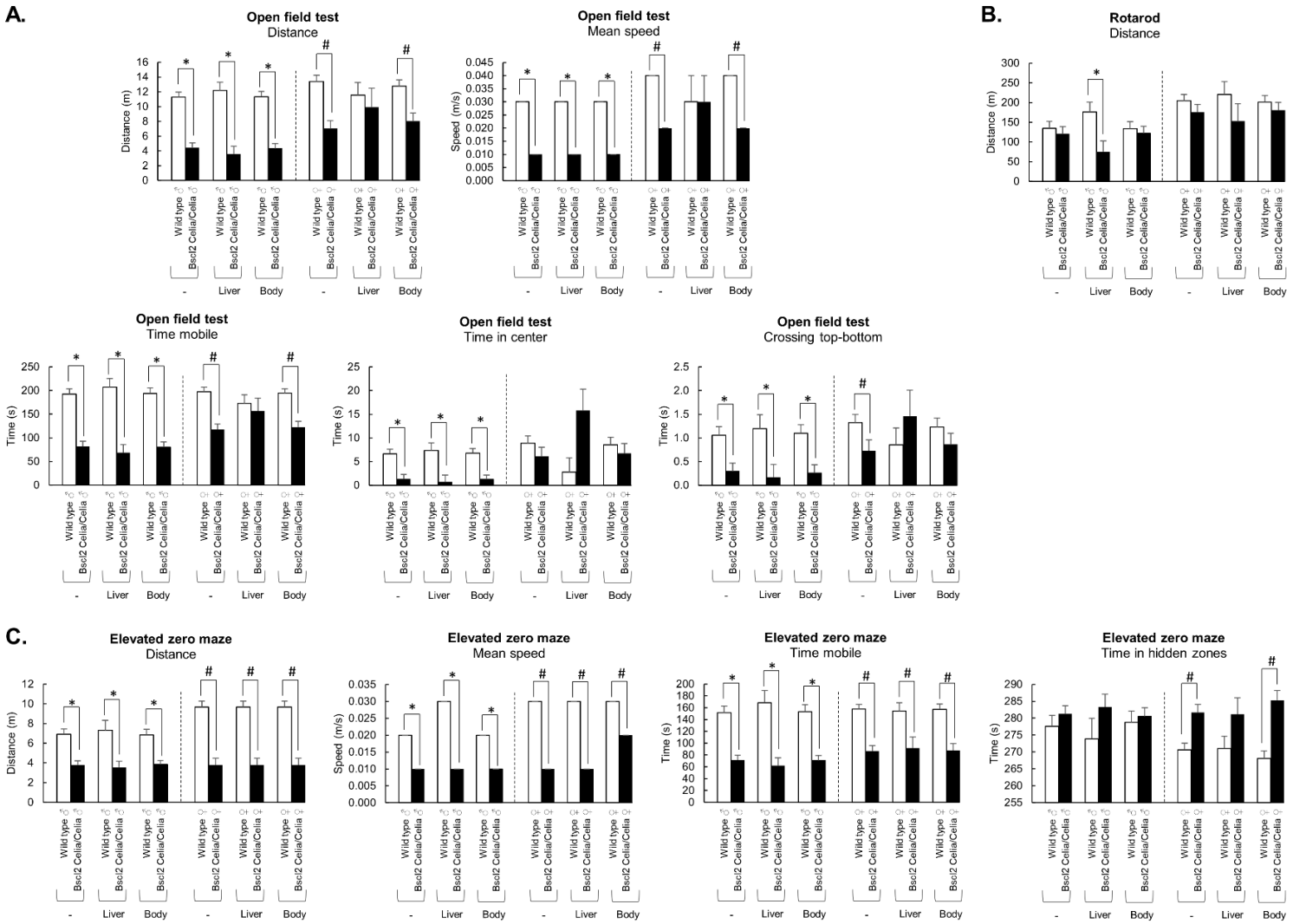

Figure 29. Covariance analysis for open field test (A), rotarod (B) and elevated zero maze (C) considering the covariates liver and body weight between wild type and *Bscl2*$^{Celia/Celia}$ mice separated by sex. For mean age and number of animals per genotype see **Annex 4, Table S4.** Data is presented as mean ± SEM. Data were analysed using Analysis of Covariance (ANCOVA) to control for liver weight and overall body weight. Significant differences between males were as * $p < 0.05$ and between females as $^{\#}$ $p < 0.05$.

In the Morris water maze, the initial analysis had shown that the homozygous mice exhibited decreased motor activities compared to wild type controls. However, when the data was separated by sex, this difference was no longer observed in the case of female mice. In fact, some parameters indicated better locomotion in the homozygous male compared to wild type males (**Figure 28**). The ANCOVA analysis revealed that the motor differences observed in the *Bscl2*$^{Celia/Celia}$ male mice were conditioned by both their body weight and liver weight. Interestingly, the increased anxiety levels in the *Bscl2*$^{Celia/Celia}$ female mice also appeared to contribute to their motor performance in the Morris water maze (**Figure 30**). Regarding cognitive function and memory, the results were less homogeneous. The *Bscl2*$^{Celia/Celia}$ female mice seemed to exhibit normal cognitive functioning. In the male mice, when accounting for liver weight, their cognitive performance also appeared normal. However, when considering body weight as a covariate, the *Bscl2*$^{Celia/Celia}$ males showed indications of memory impairment compared to wild type controls (**Figure 30**).

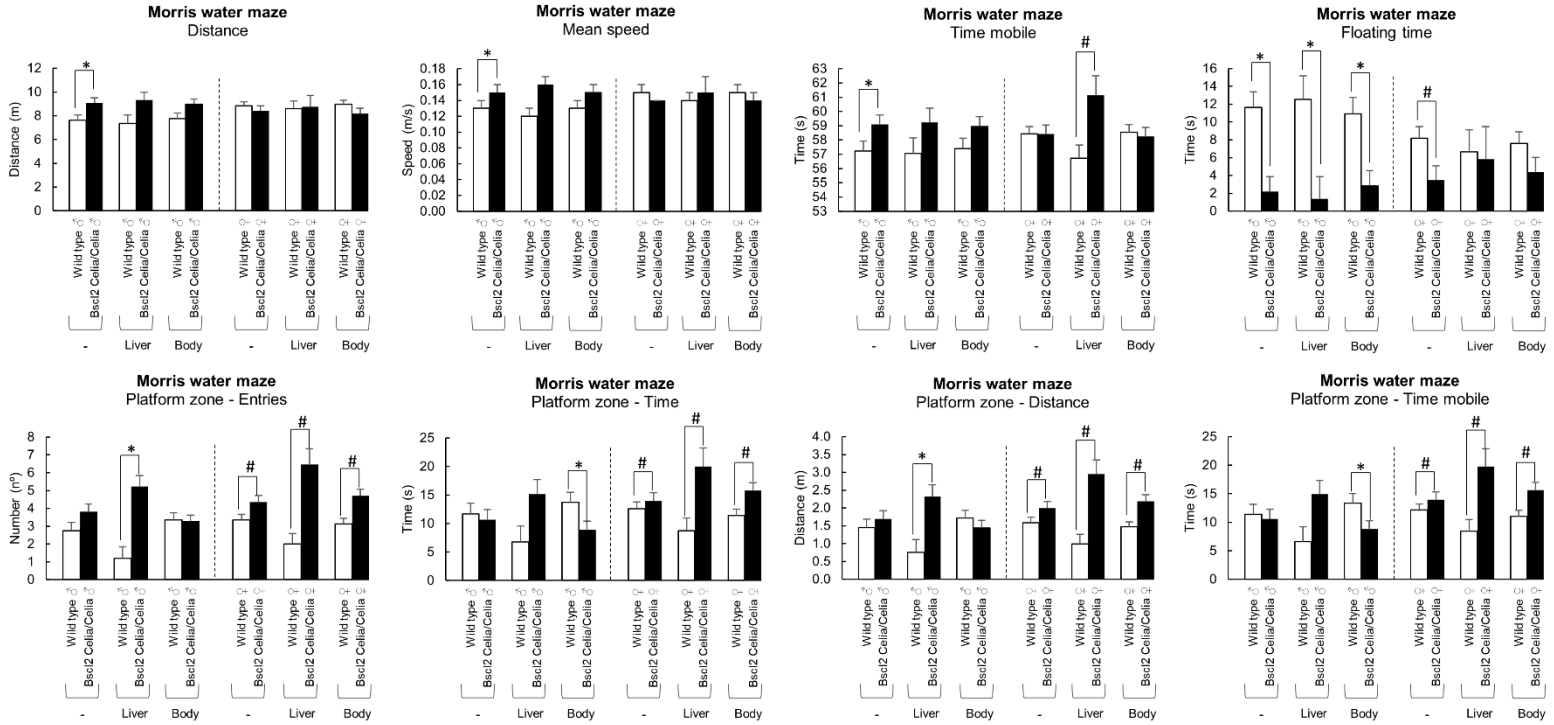

Figure 30. Covariance analysis for Morris water maze considering the covariates liver and body weight between wild type and *Bscl2*$^{Celia/Celia}$ mice separated by sex. For mean age and number of animals per genotype see **Annex 4, Table S4.** Data is presented as mean ± SEM. Data were analysed using Analysis of Covariance (ANCOVA) to control for liver weight and overall body weight. Significant differences between males were as * $p < 0.05$ and between females as $^{\#}$ $p < 0.05$.

The same ANCOVA analyses were conducted to compare the *Bscl2*$^{-/-}$ KO mice with the wild type controls. In the open field test, the decreased locomotor activities observed in *Bscl2*$^{-/-}$ male mice were not influenced by their liver weight, unlike the case with the *Bscl2*$^{Celia/Celia}$ males. Interestingly, the increased anxiety levels in *Bscl2*$^{-/-}$ males were found to be conditioned by their larger liver size (**Figure 31A**). Furthermore, this influence of liver weight on the locomotor and anxiety-like behaviour was also evident in the elevated zero maze, suggesting that *Bscl2*$^{-/-}$ animals exhibited similar levels of locomotion and anxiety as the wild type controls (**Figure 31C**). Regarding coordination, the *Bscl2*$^{-/-}$ mice did not show any differences compared to the wild type animals in the rotarod test, and this finding was not affected by the animals' liver weight or body weight (**Figure 31B**).

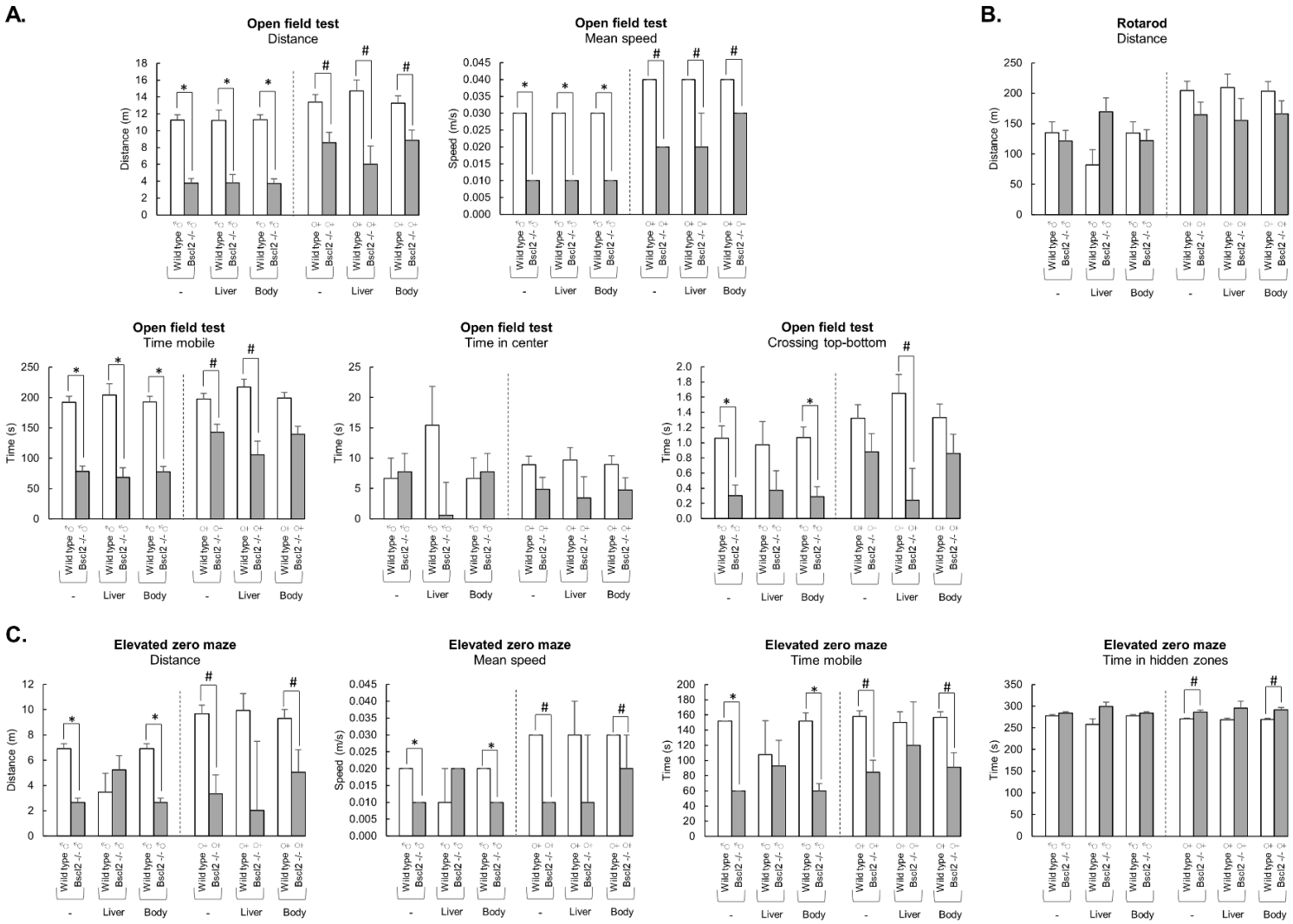

Figure 31. Covariance analysis for open field test (A), rotarod (B) and elevated zero maze (C) considering the covariates liver and body weight between wild type and *Bscl2*$^{-/-}$ mice separated by sex. For mean age and number of animals per genotype see **Annex 4, Table S5.** Data is presented as mean ± SEM. Data were analysed using Analysis of Covariance (ANCOVA) to control for liver weight and overall body weight. Significant differences between males were as * $p < 0.05$ and between females as $^{\#}$ $p < 0.05$.

Similarly, in the Morris water maze, the parameters assessing motor activity did not show any influence of the liver weight or body weight variables in the *Bscl2*$^{-/-}$ mice. This confirmed that, like the *Bscl2*$^{Celia/Celia}$ animals, the *Bscl2*$^{-/-}$ mice did not exhibit differences in locomotion compared to the wild type controls. However, the increased anxiety-like behaviour observed in the *Bscl2*$^{-/-}$ animals on the Morris water maze appeared to be influenced by their liver weight (**Figure 32**).

Regarding memory and cognitive functions, the results were not as homogeneous as those observed in the *Bscl2*$^{Celia/Celia}$ mice. The *Bscl2*$^{-/-}$ female mice, similar to the *Bscl2*$^{Celia/Celia}$ males, seemed to perform worse than the wild type controls (**Figure 28**). But when accounting for the weight variables, these differences were found to be influenced by the animals' body weight or liver weight. In the *Bscl2*$^{-/-}$ male mice, the ANCOVA analysis revealed that their liver weight conditioned certain memory-related parameters, suggesting a worsening of memory compared to wild type males (**Figure 32**).

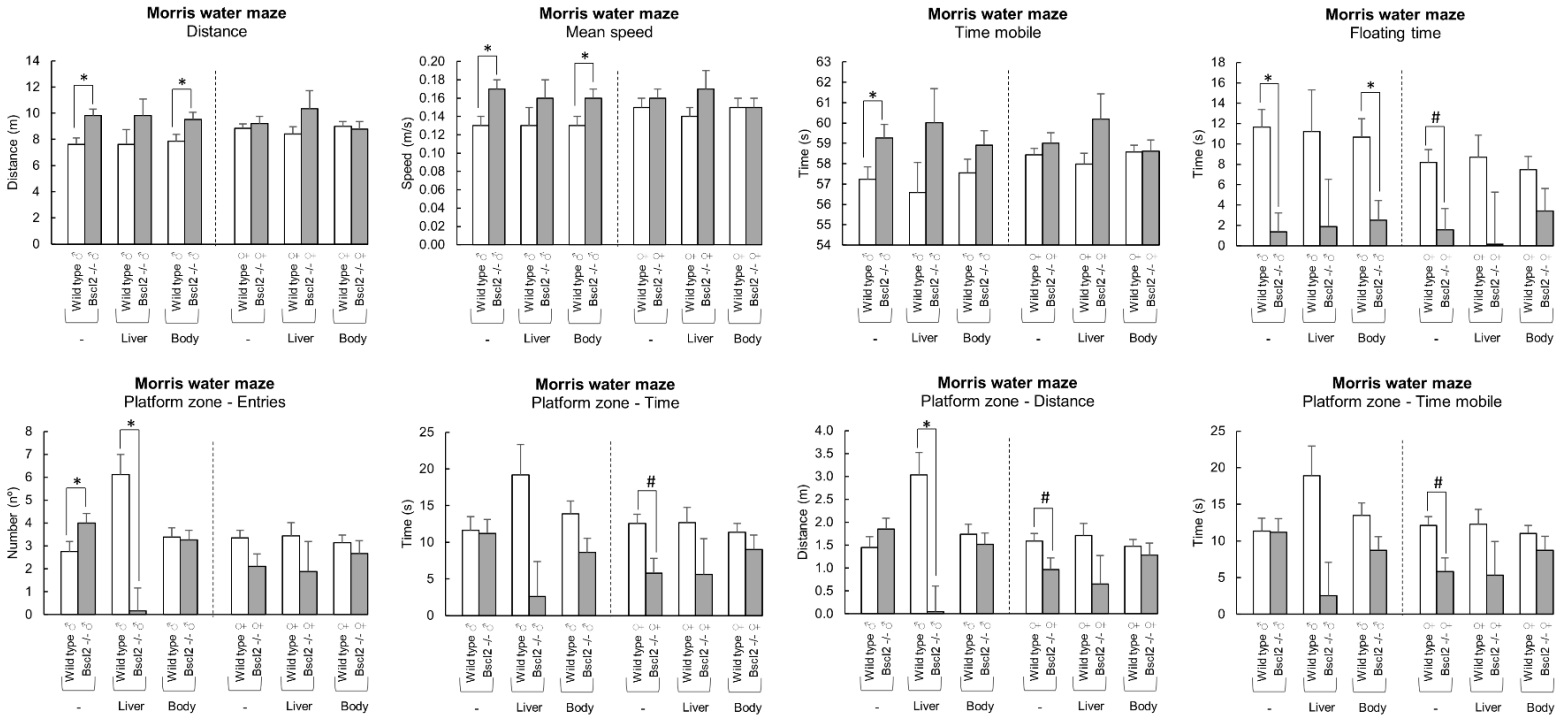

Figure 32. Covariance analysis for Morris water maze considering the covariates liver and body weight between wild type and *Bscl2*$^{-/-}$ mice separated by sex. For mean age and number of animals per genotype see **Annex 4, Table S5.** Data is presented as mean ± SEM. Data were analysed using Analysis of Covariance (ANCOVA) to control for liver weight and overall body weight. Significant differences between females were as $^{\#}$ $p < 0.05$ and between females as $^{\#}$ $p < 0.05$.

After observing that some of the differences between the homozygous (*Bscl2*$^{Celia/Celia}$ or *Bscl2*$^{-/-}$) and wild type mice were influenced by their large liver weight or overall body weight, further analysis were conducted to determine if these variables also impacted the comparisons between the two homozygous models.

In the open field test and rotarod, the ANCOVA analysis did not reveal any influence of the liver weight or body weight variable. Consequently, no significant differences were found between the *Bscl2*$^{Celia/Celia}$ and *Bscl2*$^{-/-}$ homozygous animals in these tests (**Figure 33A-B**). Similarly, on the elevated zero maze, no differences were observed between the homozygous female mice. However, in the male mice, the worsening of performance in the *Bscl2*$^{-/-}$ group compared to the *Bscl2*$^{Celia/Celia}$ group was found to be conditioned by their liver weight (**Figure 33C**).

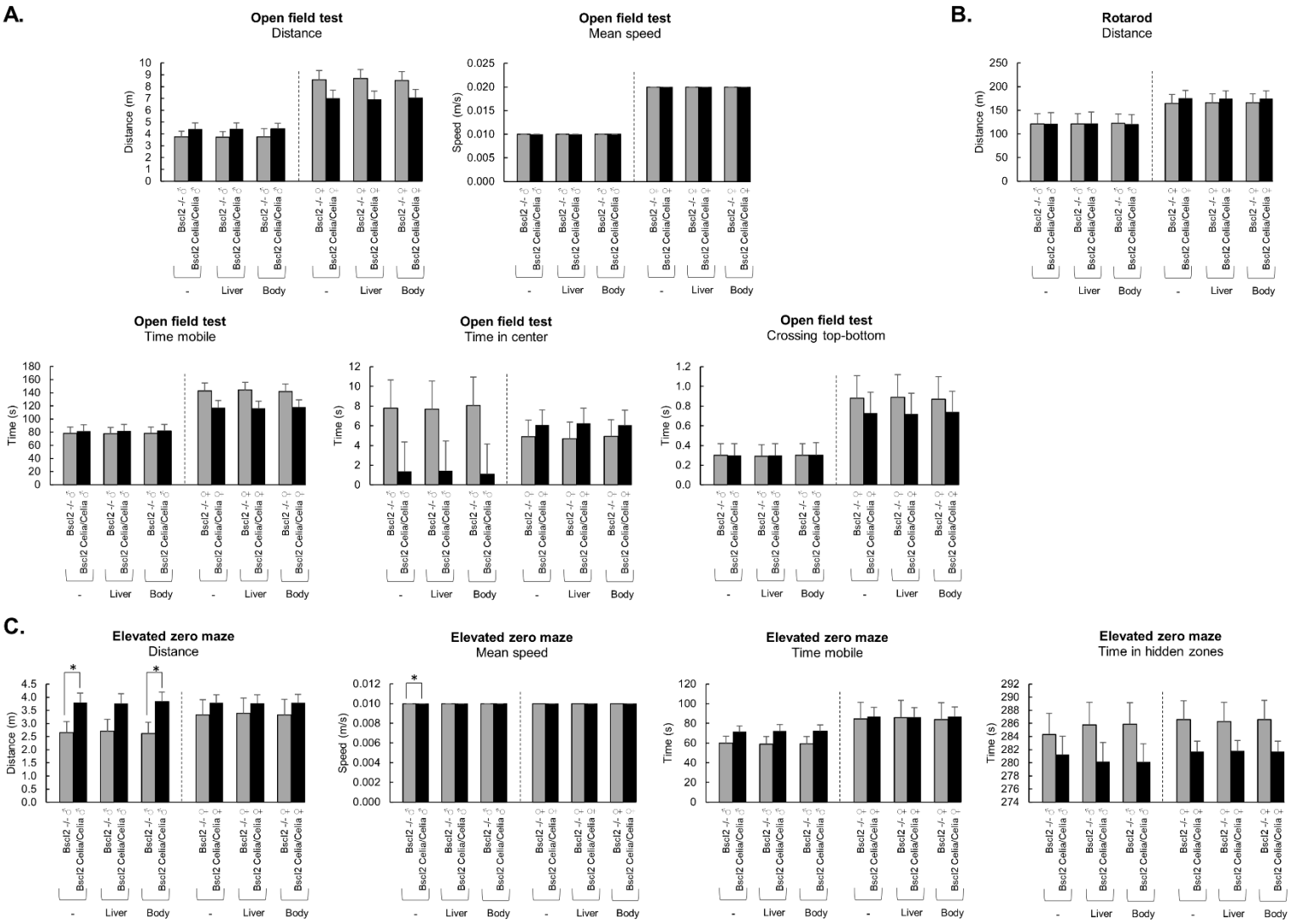

Figure 33. Covariance analysis for open field test (A), rotarod (B) and zero maze (C) considering the covariates liver and body weight between *Bscl2*$^{-/-}$ and *Bscl2*$^{Celia/Celia}$ mice separated by sex. For mean age and number of animals per genotype see **Annex 4, Table S6.** Data is presented as mean ± SEM. Data were analysed using Analysis of Covariance (ANCOVA) to control for liver weight and overall body weight. Significant differences between males were as * $p < 0.05$.

In the Morris water maze, the ANCOVA analysis revealed that both the liver weight and body weight variables influenced the motor functions of the *Bscl2*$^{Celia/Celia}$ female mice, who exhibited greater impairment compared to the *Bscl2*$^{-/-}$ females. However, these weight-related influences were not observed in the male mice. Furthermore, no differences were found between the *Bscl2*$^{Celia/Celia}$ and *Bscl2*$^{-/-}$ homozygous genotypes in terms of cognitive functions or anxiety-like behaviour on the Morris water maze (**Figure 34**).

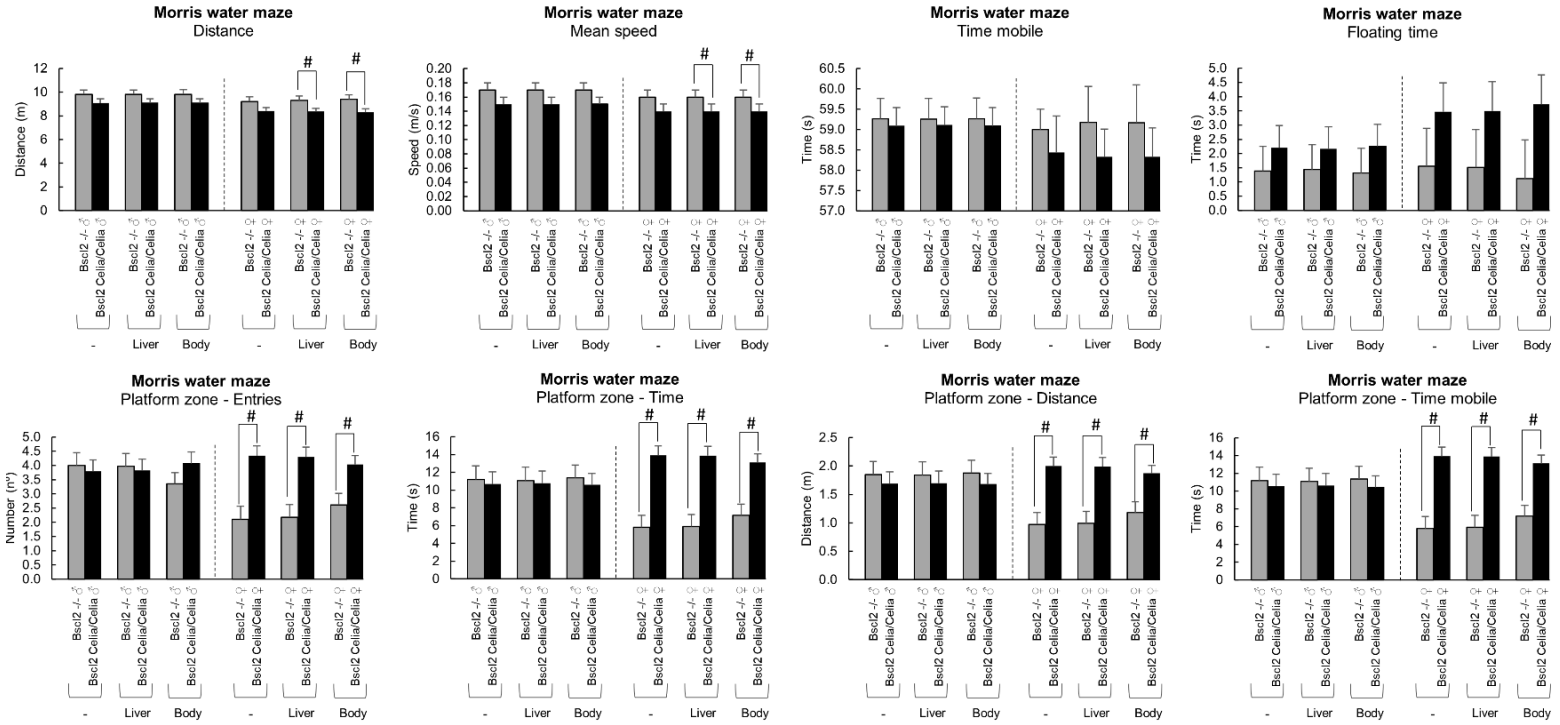

Figure 34. Covariance analysis for Morris water maze considering the covariates liver and body weight between *Bscl2*$^{-/-}$ and *Bscl2*$^{Celia/Celia}$ mice separated by sex. For mean age and number of animals per genotype see **Annex 4, Table S6.** Data is presented as mean ± SEM. Data were analysed using Analysis of Covariance (ANCOVA) to control for liver weight and overall body weight. Significant differences between females were as $^{\#}$ $p < 0.05$.

4.3.3 Brain PET

[^{18}F]-FDG PET/CT imaging was performed on a cohort of animals, including six wild type mice, six *Bscl2*$^{Celia/Celia}$ mice, and two severely affected mice (one *Bscl2*$^{+/Celia}$ and one *Bscl2*$^{Celia/Celia}$). Visual inspection of the PET/CT images revealed a reduction in [^{18}F]-FDG brain uptake in the brains of both the severely affected and non-S.A. *Bscl2*$^{Celia/Celia}$ mice, compared to the wild type controls (**Figure 35**).

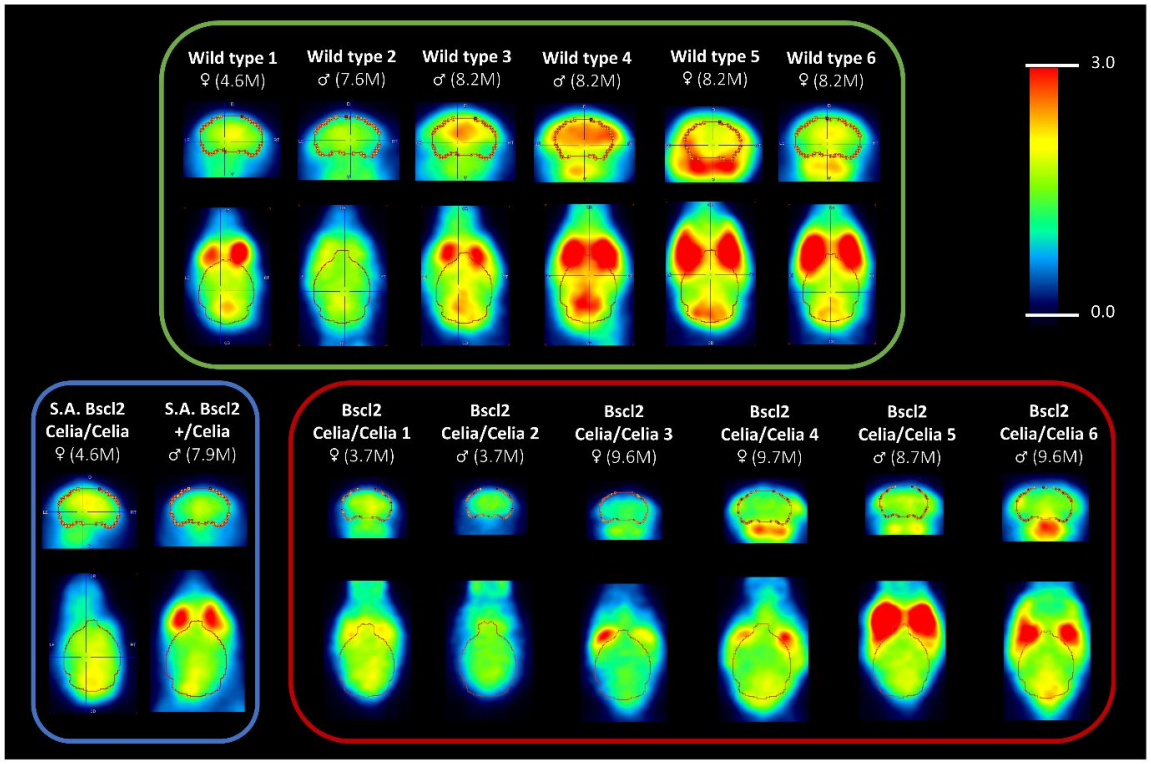

Figure 35. Brain [^{18}F]-2-fluoro-2-deoxy-D-glucose by positron emission tomography with computed tomography images. Wild type, n= 6; *Bscl2*$^{Celia/Celia}$, n= 6 and severely affected (S.A) animals, *Bscl2*$^{Celia/Celia}$, n= 1 and *Bscl2*$^{+/Celia}$, n= 1.

Due to the limited sample size, no statistical analysis could be performed on the [^{18}F]-FDG PET/CT imaging data. However, a global decrease in the Standardized Uptake Value (SUV_{mean}) of glucose was visually observed in the non-S.A. *Bscl2*$^{Celia/Celia}$ mice, as well as the S.A *Bscl2*$^{+/Celia}$ mouse (**Figure 36A**). Interestingly, this global reduction in brain [^{18}F]-FDG uptake was less evident in the S.A. *Bscl2*$^{Celia/Celia}$ mouse (**Figure 36A**). In S.A. *Bscl2*$^{+/Celia}$ mouse, a 21% global reduction in brain [^{18}F]-FDG uptake was quantified compared to wild type controls, and a 2% reduction compared to non-S.A. *Bscl2*$^{Celia/Celia}$ mice. Specifically, some of the brain regions most affected in the S.A. *Bscl2*$^{+/Celia}$ mouse were the olfactory bulb (28% and 14% reduction), cortex (31% and 7% reduction), amygdala (29% and 5% reduction), and left striatum (24% and 5% reduction) compared to wild type and non-S.A. *Bscl2*$^{Celia/Celia}$ animals, respectively. In the S.A. *Bscl2*$^{Celia/Celia}$ mouse, an 8.4% global reduction in brain [^{18}F]-FDG uptake was observed compared to the wild type controls, but no global decrease was found when compared to non-SA. *Bscl2*$^{Celia/Celia}$. However, reductions were

noted in the olfactory bulb (37% and 23% reduction) and amygdala (16% and 9% reduction) compared to wild type and non-S.A. *Bscl2*$^{Celia/Celia}$, respectively (**Figure 36B**).

The analysis by sex showed a 6% more of decrease in glucose metabolism in non-S.A. *Bscl2*$^{Celia/Celia}$ females compared to non-S.A. *Bscl2*$^{Celia/Celia}$ males (**Figure 36**).

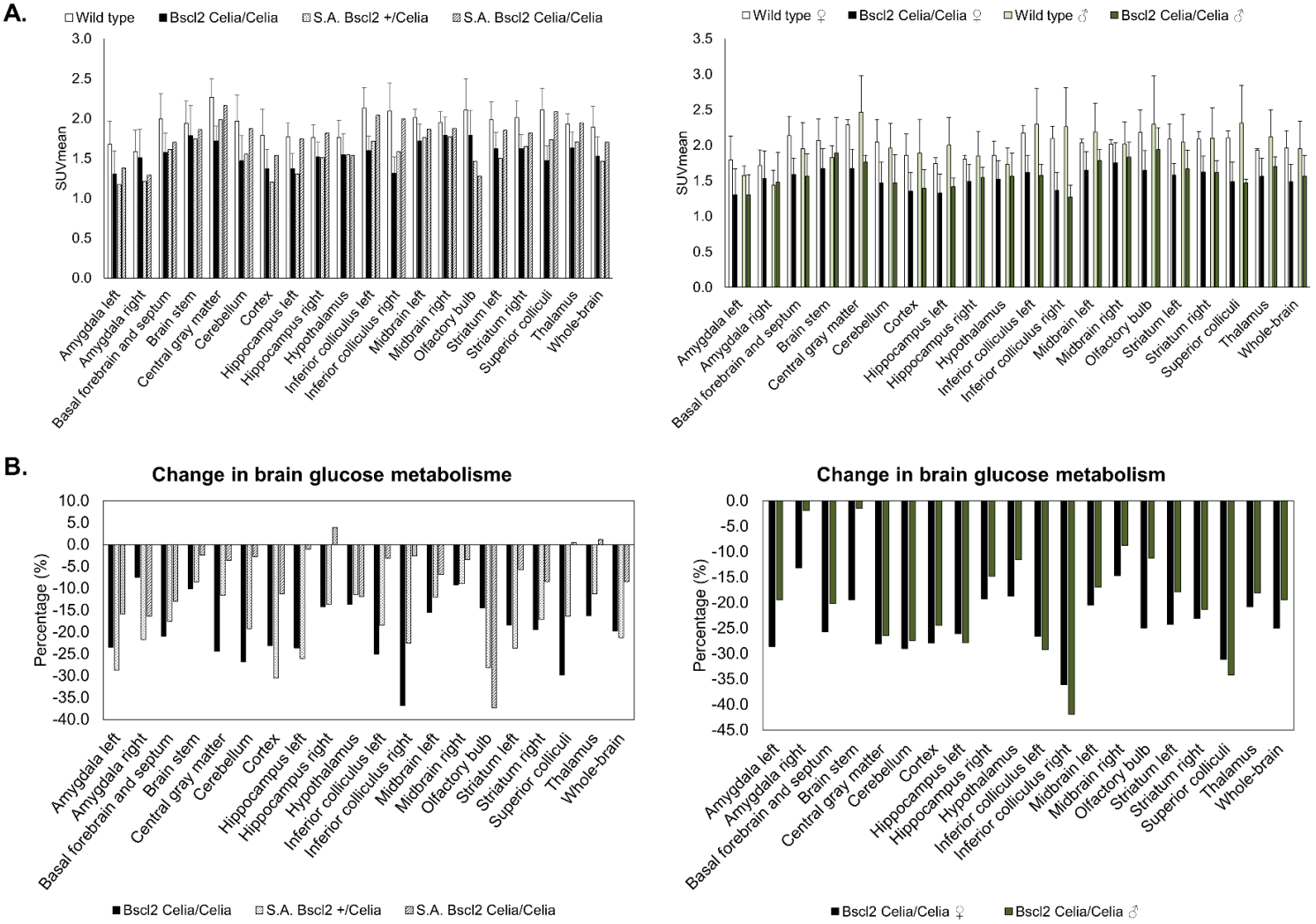

Figure 36. Brain [^{18}F]-2-fluoro-2-deoxy-D-glucose by positron emission tomography with computed tomography comparing severely affected (S.A.) with wild type and *Bscl2*$^{Celia/Celia}$ animals. A. Mean standardized uptake value (SUV_{mean}) without considering sex and separated by sex. **B.** Mean % of change related to wild type animals without considering sex and separated by sex. Wild type, n= 6 (3 ♀ and 3 ♂); *Bscl2*$^{Celia/Celia}$, n= 6 (3 ♀ and 3 ♂) and S.A., n= 2 (1 *Bscl2*$^{+/Celia}$ and 1 *Bscl2*$^{Celia/Celia}$). Data is presented as mean ± SD or mean %. Data were analysed using a Shapiro-Wilk test for normality, followed by an ANOVA test.

Due to the different ages of the two severely affected mice (4.6 months for the *Bscl2*$^{Celia/Celia}$ mouse and 7.9 months for the *Bscl2*$^{+/Celia}$ mouse), the numerical [^{18}F]-FDG PET/CT results were analysed considering two age groups: 4.3 months (one wild type and two *Bscl2*$^{Celia/Celia}$ mice) and 8.4 months (five wild type and four *Bscl2*$^{Celia/Celia}$ mice). Separation by sex was not possible due to the low number of animals per group. The data showed a reduction in brain [^{18}F]-FDG uptake in the *Bscl2*$^{Celia/Celia}$ mice compared to wild type controls at both the 4.3-month and 8.4-month age. Interestingly, the decrease in [^{18}F]-FDG uptake was less pronounced in the younger, 4.3-month-old *Bscl2*$^{Celia/Celia}$ animals compared to the older, 8.4-month-old group (**Figure 37A**). However, this age-related reduction in [^{18}F]-FDG uptake was not clearly evident in the 4.6-months-old S.A. *Bscl2*$^{Celia/Celia}$ mouse (**Figure 37**), in contrast to the previous analysis that did not account for age (**Figure 36**). In the S.A. *Bscl2*$^{+/Celia}$ mouse at the mean age of 8.4 months, a 26% global reduction in brain [^{18}F]-FDG uptake was observed compared to wild type controls, and a 5% reduction compared to non-S.A. *Bscl2*$^{Celia/Celia}$ mice. The most affected brain regions in the S.A. *Bscl2*$^{+/Celia}$ mouse at 8.4 months were the olfactory bulb (34% and 16% reduction), cortex (36% and 13% reduction), amygdala (31% and 15% reduction), and left striatum (27% and 9% reduction), compared to wild type and non-S.A. *Bscl2*$^{Celia/Celia}$ animals, respectively (**Figure 37B**). Importantly, the affected brain areas were consistent across both analyses, with or without considering the age factor. However, the percentage of decrease in glucose metabolism was higher at the older age, suggesting a worsening of the metabolic impairment over time.

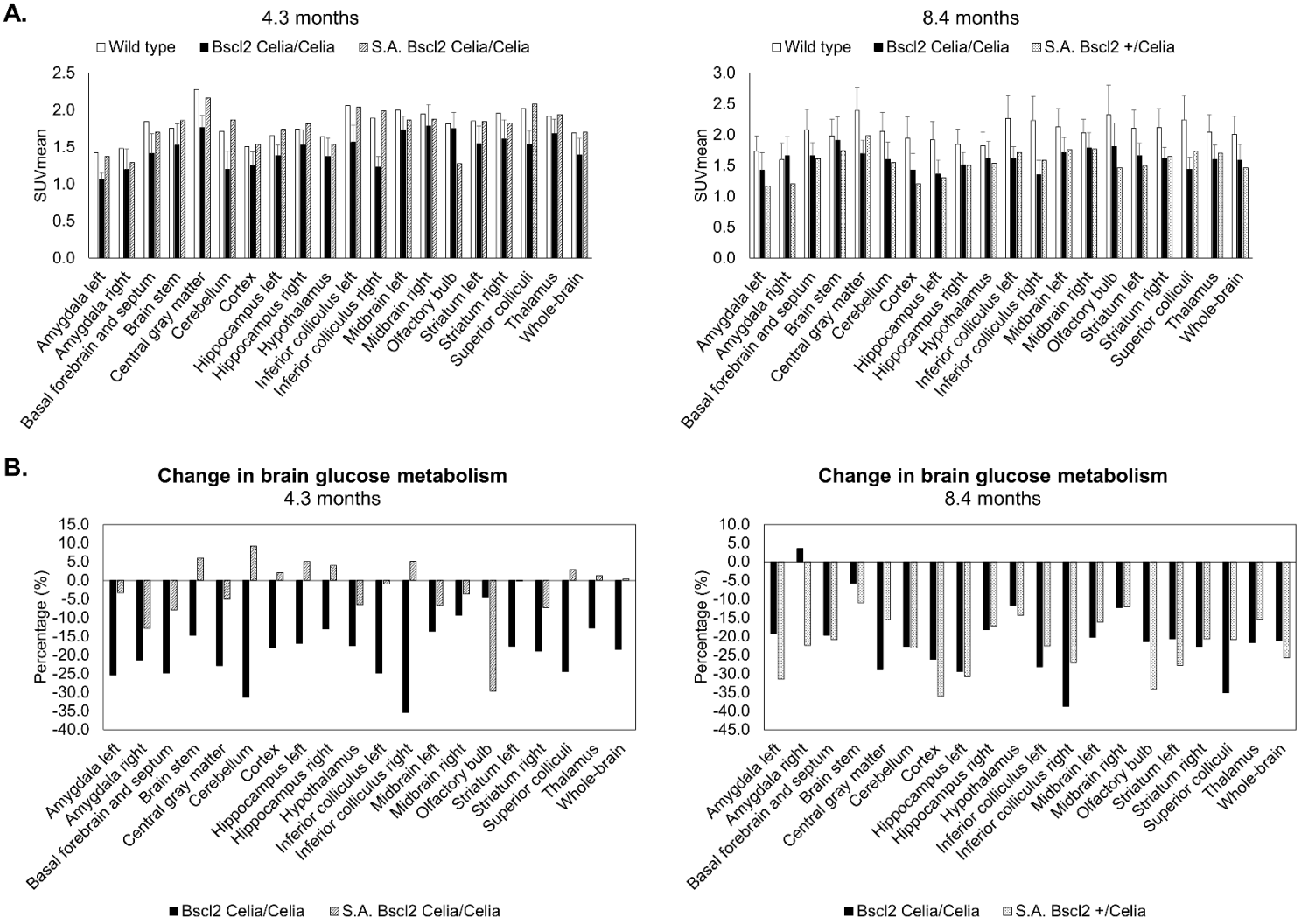

Figure 37. Brain [^{18}F]-2-fluoro-2-deoxy-D-glucose by positron emission tomography with computed tomography comparing severely affected (S.A.) (n=2) **with wild type** (n=6) **and *Bscl2*$^{Celia/Celia}$** (n=6) **animals separated by age. A.** Mean standardized uptake value (SUV_{mean}) for 4.3 and 8.4 months old. **B.** Mean % of change related to wild type animals for 4.3 and 8.4 months. Data is presented as mean ± SD or mean %. Data were analysed using a Shapiro-Wilk test for normality, followed by an ANOVA test.

4.3.4 Brain and Thoracic Marrow Histology

Histological analyses were conducted on six brain regions: cerebellum, midbrain, hypothalamus, cortex, hippocampus, and striatum.

The H&E stained sections did not reveal any differences between the genotypes in the midbrain, hypothalamus, cortex, hippocampus, or striatum (**Figure 38**).

Additionally, a specific assessment of neuropil vacuolization was performed in the striatum, and no differences were observed between the genotypes (**Table 14**).

Table 14. Assessment of vacuolization in the striatum tissue for wild type, *Bscl2*$^{Celia/Celia}$, and severely affected animals (S.A). Vacuolization score: no vacuoles or minimal (1); mild intensity (2) and moderate or intense (3).

	Sex	Age (months)	Vacuolization [0-3]
Wild type	♀	9.5	3
	♀	24.8	3
	♂	9.5	2
Bscl2$^{Celia/Celia}$	♀	13.9	1
	♂	8.6	3
S.A. *Bscl2*$^{+/Celia}$	♀	5.4	1
	♀	5.4	1
	♀	6.8	3
	♀	8	2
	♂	5.8	1
	♂	7.4	1
	♂	8.6	1
S.A. *Bscl2*$^{Celia/Celia}$	♀	3.6	1
	♀	4.2	1
	♀	9.4	3
	♀	13.9	2
	♂	3.9	1
	♂	9.3	1

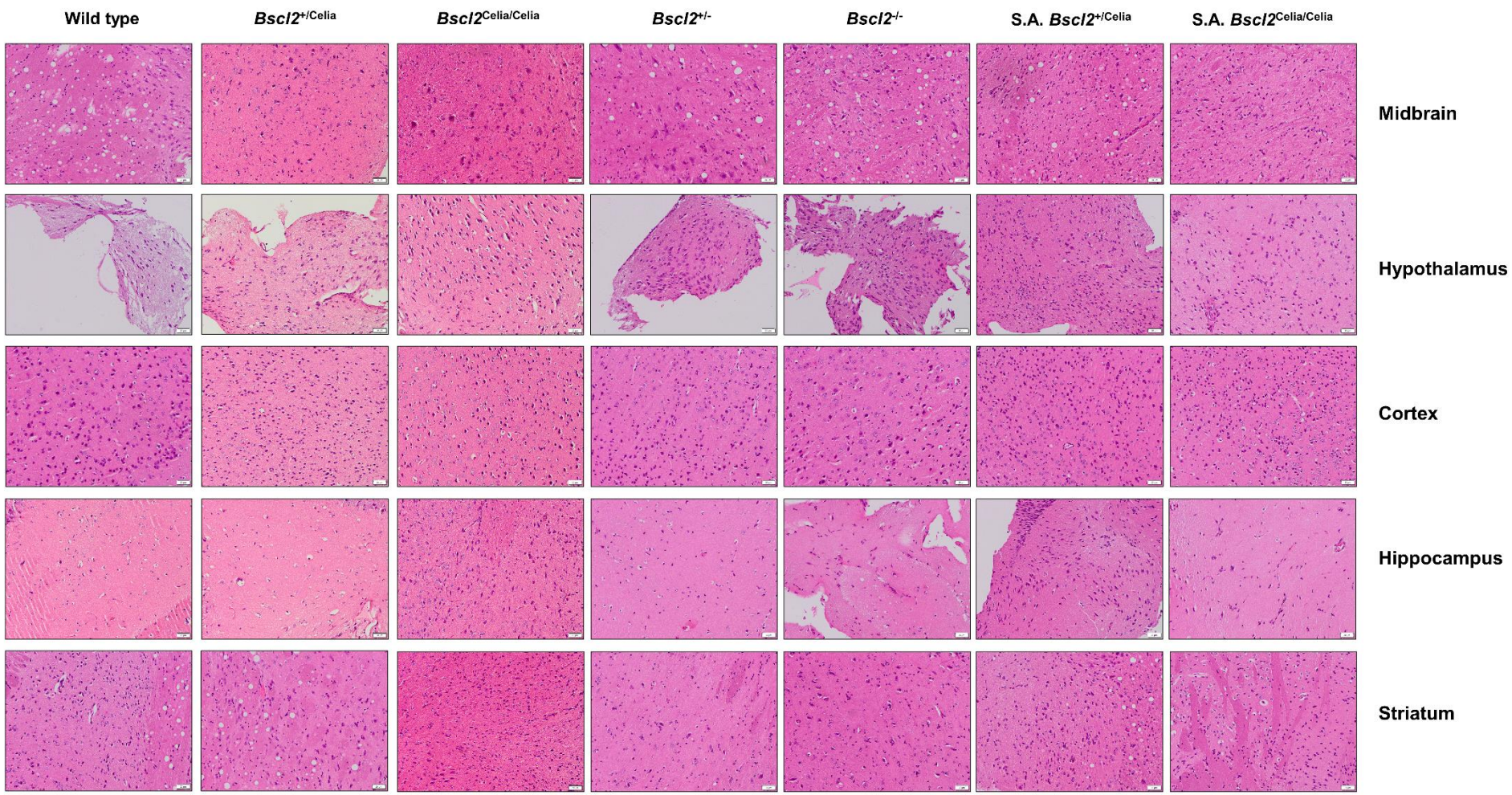

Figure 38. Histology of brain tissue. Midbrain, hypothalamus, cortex, hippocampus, and striatum of 6.1-months-old wild type ♀, *Bscl2*$^{+/Celia}$ ♂, *Bscl2*$^{Celia/Celia}$ ♂, *Bscl2*$^{+/-}$ ♂, *Bscl2*$^{-/-}$ ♂ and severely affected (S.A.) mice: *Bscl2*$^{+/Celia}$ (5.4-months-old ♂), *Bscl2*$^{Celia/Celia}$ (4.6-months-old ♂). H&E, scale bar: 20 µm.

In contrast, the histological analysis of H&E stained sections of the cerebellum revealed a moderate, patchy loss of Purkinje cells (the functional units involved in motor coordination) in 75% of the S.A. *Bscl2*$^{Celia/Celia}$ mice. The Purkinje cell loss was observed in only 17% of the S.A. *Bscl2*$^{+/Celia}$ (**Figure 39A**). Furthermore, in the S.A. *Bscl2*$^{Celia/Celia}$ animals, the ubiquitin immunostaining showed that the remaining Purkinje cells were surrounded by distinct groups of glial cells with a prominent nucleoli. These glia cells, likely corresponding to Bergmann astrocytes, were present in the areas still containing Purkinje cells (**Figure 39A**). No evident ubiquitin-reactive intranuclear inclusions were observed in the Purkinje cells or other cell types examined. However, the deep cerebellar layer did contain occasional granule cell nuclei with prominent nucleoli (**Figure 39A**). Because of this, the presence of ubiquitin-reactive nuclear inclusions in these cell types could not be definitively ruled out (**Figure 39**). The GFAP staining indicated a higher percentage of astrogliosis in the S.A. *Bscl2*$^{Celia/Celia}$ animals, as well as the non-S.A. *Bscl2*$^{Celia/Celia}$ animals, though these differences were not conclusive given the limited sample size (**Figure 39B**). Similarly, non-S.A. *Bscl2*$^{Celia/Celia}$ mice exhibited a potential moderate, patchy loss of Purkinje cells, but no other clear signs of cerebellar damage were observed. No differences were found in the CD68 staining, a marker of microglial activation, between genotypes. In summary, the neurologically affected homozygous animals (S.A. *Bscl2*$^{Celia/Celia}$) exhibited more pronounced histological damage in the cerebellum compared to the other genotypes (**Figure 39**).

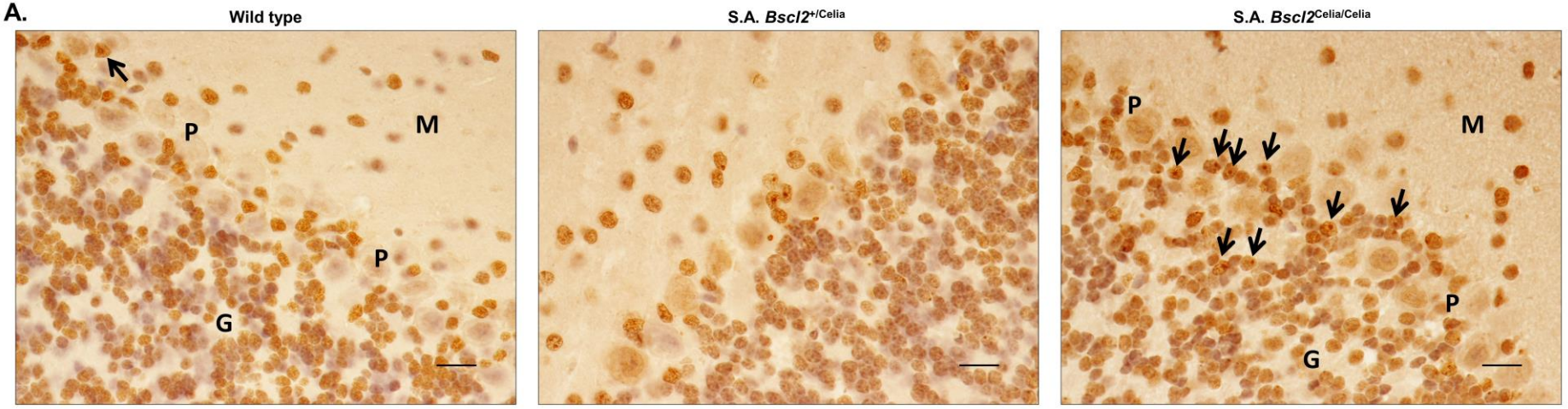

B.

	Sex	N	Age (months)	GFAP Astrogliosis (%)	H&E Vacuolization [0-3]	H&E Purkinje loss [0-1]	CD68 Microglial nodules [0-1]	Ubi-1 Intranuclear inclusions [0-1]
Wild type	♀/♂	4	7.8	1.91 ± 0.45	2.50 ± 0.58	0.25 ± 0.29	0.25 ± 0.50	0.75 ± 0.96
Bscl2 +/Celia	♂	1	7.4	1.40	2.00	0.50	0.00	0.00
Bscl2 Celia/Celia	♀/♂	3	8.7	2.54 ± 0.60	1.67 ± 1.15	0.67 ± 0.29	0.67 ± 0.58	0.33 ± 0.58
S.A. Bscl2 +/Celia	♀/♂	6	6.2	1.85 ± 1.11	1.83 ± 0.75	0.08 ± 0.20	0.17 ± 0.41	0.67 ± 0.82
S.A. Bscl2 Celia/Celia	♀/♂	4	6.6	2.17 ± 0.51	0.75 ± 0.96	0.38 ± 0.25	0.25 ± 0.50	1.25 ± 0.96

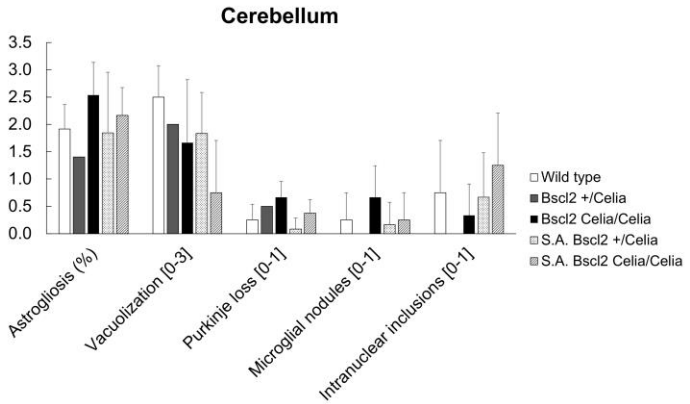

Figure 39. Cerebellar histological analysis. A. High magnification microphotography of the cerebellar cortex Purkinje cell layer of a wild type ♀ and two severely affected (S.A.) animals. *Bscl2*$^{+/Celia}$ ♀ (6.8 months-old), *Bscl2*$^{Celia/Celia}$ ♀ (9.4 months-old) and wild type ♀ (6.9 months-old). M: molecular layer; P: Purkinje cell layer; G: granular layer; arrows: prominent nucleoli. H&E, scale bar: 20 µm. **B. Cerebellar evaluation of astrogliosis, vacuolization, Purkinje cell loss, microglial nodules and intranuclear inclusions.** Data is present as mean ± SD or n (%) ± SD. Data were analysed using a Shapiro-Wilk test for normality, followed by a Kruskal-Wallis test.

To further investigate the histological changes potentially underlying the observed neurological symptoms, such as abnormal limb crossing, kyphosis, and paraparesis/paraplegia in the S.A. animals (**Figure 22A, section 4.3.1**), a thoracic spinal cord analysis was performed.

The CD68 staining, a marker of microglial activation, revealed greater gliosis in the S.A mice compared to the non-S.A. animals. This increased gliosis was specifically observed in the S.A. *Bscl2*$^{+/Celia}$ mice (**Figure 40**). However, these results should be interpreted with caution, as a potential "edge effect" was noted in some sections.

To corroborate these findings, the cellularity of the spinal cord grey matter was analysed. This analysis confirmed the presence of hypercellularity in the S.A. *Bscl2*$^{Celia/Celia}$ mice. Some degree of hypercellularity was also observed in the non-S.A. animals, but it was less pronounced.

No differences were found in the degree of vacuolization, which appeared to affect the grey and white matter equally across the genotypes (**Figure 40**).

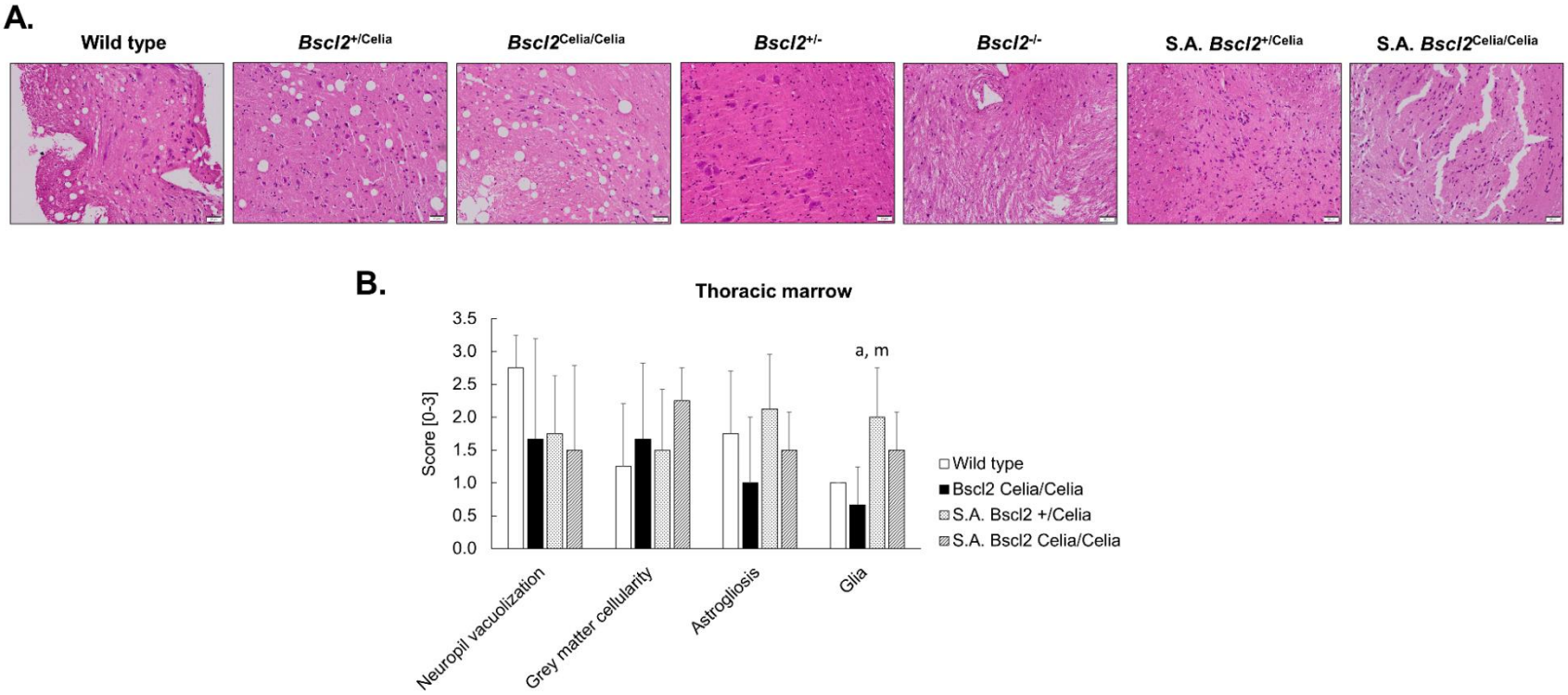

	Sex	N	Age (months)	H&E Neuropil vacuolization [0-3]	H&E Grey matter cellularity [0-3]	GFAP Astrogliosis [0-3]	CD68 Glia [0-3]
Wild type	♀/♂	4	13.3	2.75 ± 0.50	1.25 ± 0.96	1.75 ± 0.96	1.00 ± 0.00
Bscl2 Celia/Celia	♀/♂	3	8.7	1.67 ± 1.53	1.67 ± 1.15	1.00 ± 1.00	0.67 ± 0.58
S.A. Bscl2 +/Celia	♀/♂	8	6.6	1.75 ± 0.89	1.50 ± 0.93	2.13 ± 0.83	2.00 ± 0.76
S.A. Bscl2 Celia/Celia	♀/♂	4	6.6	1.50 ± 1.29	2.25 ± 0.50	1.50 ± 0.58	1.50 ± 0.58

Figure 40. Thoracic marrow analysis. A. Histology of the thoracic marrow. Mean age 6 months (wild type ♀, *Bscl2*$^{+/Celia}$ ♀, *Bscl2*$^{Celia/Celia}$ ♂, *Bscl2*$^{+/-}$ ♀, *Bscl2*$^{-/-}$ ♂ and S.A. *Bscl2*$^{+/Celia}$ ♂) except for S.A. *Bscl2*$^{Celia/Celia}$ ♂ (9.3-months-old) mice. H&E, scale bar: 20 µm. **B. Evaluation of neuropil vacuolization, grey matter cellularity, astrogliosis and glia.** Data is present as mean ± SD. [a] $p < 0.05$ vs wild type ♀/♂; [m] $p < 0.05$ vs *Bscl2*$^{Celia/Celia}$ ♀/♂. Data were analysed using a Shapiro-Wilk test for normality, followed by a Kruskal-Wallis test with Mann-Whitney post hoc comparisons

4.3.5 Gene Expression in Brain Tissues

Real-time PCR studies were conducted to examine the expression of the Celia *BSCL2* transgene, wild type *Bscl2*, and mitochondrial and peroxisome genes (**Table 15**).

Table 15. Main characteristics of the mitochondrial and peroxisome genes analysed in brain tissues. Gene symbol, identifier, genomic location, and main functions.

Gene	IDs		Localization	Function
	MGI	NCBI		
Ppary	97747	19016	6 E3; 6 53.41 cM	This gene encodes a nuclear receptor protein belonging to the peroxisome proliferator-activated receptor (Ppar) family. The encoded protein is a ligand-activated transcription factor that is involved in the regulation of adipocyte differentiation and glucose homeostasis. [provided by RefSeq, Apr 2015]
Pex16	1338829	18633	2 E1; 2 50.98 cM	The protein encoded by this gene is an integral peroxisomal membrane protein. Expression of this gene product morphologically and biochemically restores the formation of new peroxisomes, suggesting that is involved in peroxisome organization and protein to membrane docking. [provided by Alliance of Genome Resources, Apr 2022 and RefSeq, Jul 2008]
Cat	88271	12359	2 E2; 2 54.43 cM	This gene encodes catalase, a key antioxidant enzyme in the bodies defense against oxidative stress. Acts upstream of or within several processes, including hydrogen peroxide catabolic process; positive regulation of phosphatidylinositol 3-kinase signaling; and regulation of DNA-binding transcription factor activity. [provided by Alliance of Genome Resources, Apr 2022 and RefSeq, Oct 2009]
Gpx1	104887	14775	9 F2; 9 59.24 cM	The protein encoded by this gene belongs to the glutathione peroxidase family, members of which catalyze the reduction of organic hydroperoxides and hydrogen peroxide (H2O2), and thereby protect cells against oxidative damage. H2O2 is also essential for growth-factor mediated signal transduction, mitochondrial function, and maintenance of thiol redox-balance. [provided by RefSeq, Jul 2016]
Pex11g	1920905	69129	8 A1.1; 8 1.92 cM	The protein encoded by this gene is predicted to be involved in peroxisome fission and regulation of peroxisome size. [provided by Alliance of Genome Resources, Apr 2022]
Sod1	98351	20655	16 C3.3; 16 51.56 cM	Enables superoxide dismutase activity. Involved in axonal transport; negative regulation of inflammatory response; and positive regulation of phagocytosis. Acts upstream of or within several processes, including hydrogen peroxide biosynthetic process; muscle cell cellular homeostasis; and neurogenesis. [provided by Alliance of Genome Resources, Apr 2022]
Sod2	98352	20656	17 A1; 17 8.75 cM	Enables superoxide dismutase activity. Acts upstream of or within several processes, including animal organ development; apoptotic signaling pathway; and regulation of cellular biosynthetic process. Located in mitochondrion. [provided by Alliance of Genome Resources, Apr 2022]

As expected, the wild type and SKO animals did not show any expression of the human Celia *BSCL2* transgene, while the homozygous KI and KO mice did not express the wild type *Bscl2* gene (**Figure 41** and **Figure 42**). Regarding the expression of the Celia *BSCL2* transgene in KI mice, it was significantly higher in non-S.A. *Bscl2*$^{Celia/Calia}$ mice compared to the non-S.A. *Bscl2*$^{+/Celia}$ and S.A *Bscl2*$^{+/Celia}$ animals in the cerebellum (Δ131%; Δ268%), hypothalamus (Δ242%; Δ242%), cortex (Δ74%), and striatum (Δ197%; Δ316%) (**Figure 42**). It should be noted that in the cortex, the differences were only found when compared to the non-S.A. *Bscl2*$^{+/Celia}$ group.

Further analysis by sex revealed that the *Bscl2*$^{Celia/Celia}$ male mice exhibited the highest transgene expression in the hypothalamus and cerebellum, compared to *Bscl2*$^{+/Celia}$ males and females. In the cerebellum, *Bscl2*$^{Celia/Celia}$ females also showed higher transgene expression than *Bscl2*$^{+/Celia}$ males. In the cortex, the *Bscl2*$^{Celia/Celia}$ females had higher transgene expression compared to the *Bscl2*$^{+/Celia}$ females. The sex-based differences were not observed in the striatum.

In the S.A. *Bscl2*$^{Celia/Celia}$ mice, the Celia *BSCL2* transgene was significantly higher than heterozygous animals in the midbrain (Δ158% vs non-S.A. *Bscl2*$^{+/Celia}$; Δ280% vs S.A. *Bscl2*$^{+/Celia}$), hippocampus (Δ284% vs non-S.A. *Bscl2*$^{+/Celia}$; Δ370% vs S.A. *Bscl2*$^{+/Celia}$), striatum (Δ182% vs non-S.A. *Bscl2*$^{+/Celia}$; Δ295% vs S.A. *Bscl2*$^{+/Celia}$), and cortex (Δ238% vs non-S.A. *Bscl2*$^{+/Celia}$; Δ151% vs S.A. *Bscl2*$^{+/Celia}$), within the latter region also showing a 94% higher expression compared to non-S.A. *Bscl2*$^{Celia/Celia}$ (**Figure 42**).

In contrast, the Celia *BSCL2* transgene expression in the S.A. *Bscl2*$^{+/Celia}$ mice was not different than in non-S.A. *Bscl2*$^{+/Celia}$ animals. However, wild type *Bscl2* expression was lower in the S.A. *Bscl2*$^{+/Celia}$ mice compared to non-S.A. *Bscl2*$^{+/Celia}$, particularly in the cerebellum (**Figure 41**).

Across all genotypes, the expression of both the wild type *Bscl2* and Celia *BSCL2* transgene was lower in the cortex and higher in the cerebellum, although these differences were not statistically significant in all cases (**Figure 43,** see **Annex 6**).

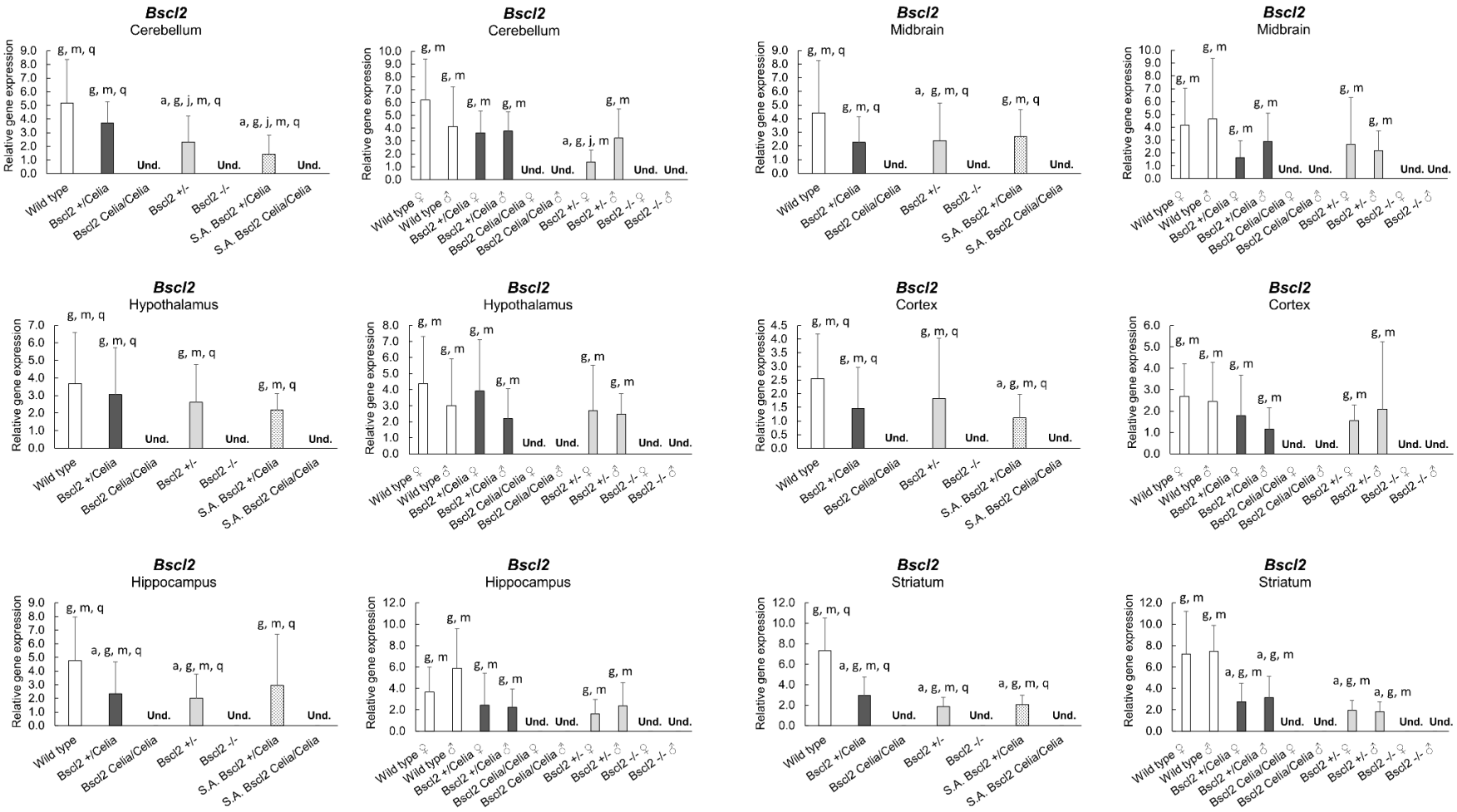

Figure 41. Relative expression of *Bscl2* gene in cerebellum, midbrain, hypothalamus, cortex, hippocampus, and striatum. Wild type, *Bscl2*$^{+/Celia}$, *Bscl2*$^{Celia/Celia}$, *Bscl2*$^{+/-}$ and *Bscl2*$^{-/-}$ mice, n= 14 (7 ♀ and 7 ♂) for each genotype (mean age 9.5 months). Severely affected (S.A) *Bscl2*$^{Celia/Celia}$ and *Bscl2*$^{+/Celia}$ animals, n = 5 and n = 6 respectively, mean age 6.4 months. Data is presented as mean ± SD. Data were analysed using a Kolmogorov-Smirnov test for normality, followed by a Kruskal-Wallis test with Mann-Whitney post hoc comparisons. Undetermined (Und.). Results were normalized for the *Rn18S* gene and referred to Cerebellum of *Bscl2*$^{+/Celia}$ in Celia *BSCL2*-TG gene. ^{a} $p < 0.05$ vs wild type ♀/♂; ^{j} $p < 0.05$ vs *Bscl2*$^{+/Celia}$ ♀/♂; ^{g} $p < 0.05$ vs *Bscl2*$^{-/-}$ ♀/♂; ^{m} $p < 0.05$ vs *Bscl2*$^{Celia/Celia}$ ♀/♂; ^{q} $p < 0.05$ vs S.A. *Bscl2*$^{Celia/Celia}$ ♀/♂.

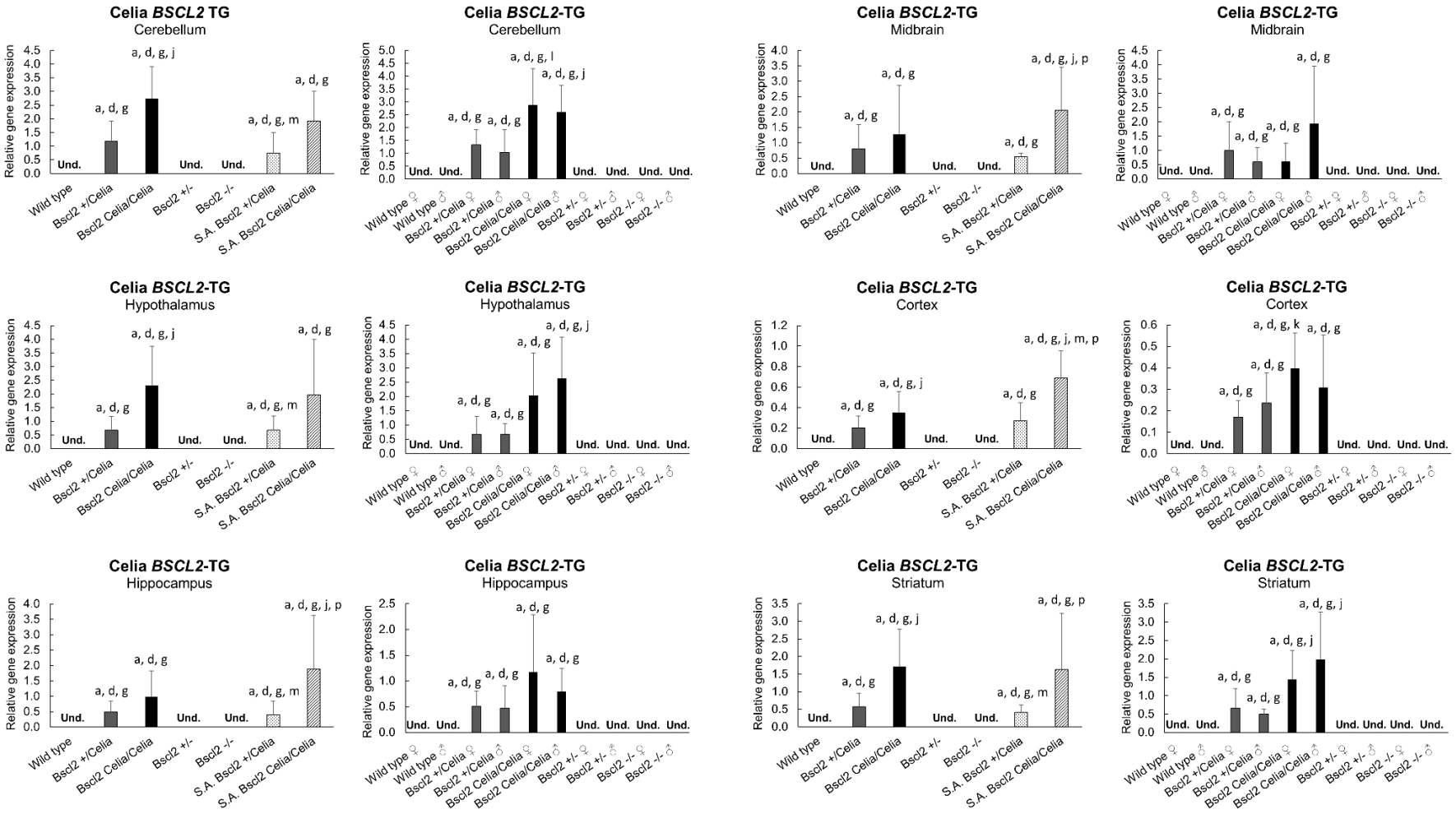

Figure 42. Relative expression of Celia *BSCL2*-TG in cerebellum, midbrain, hypothalamus, cortex, hippocampus, and striatum. Wild type, *Bscl2*$^{+/Celia}$, *Bscl2*$^{Celia/Celia}$, *Bscl2*$^{+/-}$ and *Bscl2*$^{-/-}$ mice, n= 14 (7 ♀ and 7 ♂) for each genotype (mean age 9.5 months). Severely affected (S.A) *Bscl2*$^{Celia/Celia}$ and *Bscl2*$^{+/Celia}$ animals, n = 5 and n = 6 respectively, mean age 6.4 months. Data is presented as mean ± SD. Data were analysed using a Kolmogorov-Smirnov test for normality, followed by a Kruskal-Wallis test with Mann-Whitney post hoc comparisons. Undetermined (Und.). Results were normalized for the *Rn18S* gene and referred to Cerebellum of *Bscl2*$^{+/Celia}$ in Celia *BSCL2*-TG gene. [a] $p < 0.05$ vs wild type ♀/♂; [d] $p < 0.05$ vs *Bscl2*$^{+/-}$ ♀/♂; [g] $p < 0.05$ vs *Bscl2*$^{-/-}$ ♀/♂; [j] $p < 0.05$ vs *Bscl2*$^{+/Celia}$ ♀/♂; [k] $p < 0.05$ vs *Bscl2*$^{+/Celia}$ ♀; [l] $p < 0.05$ vs *Bscl2*$^{+/Celia}$ ♂; [m] $p < 0.05$ vs *Bscl2*$^{Celia/Celia}$ ♀/♂; [p] $p < 0.05$ vs S.A. *Bscl2*$^{+/Celia}$ ♀/♂.

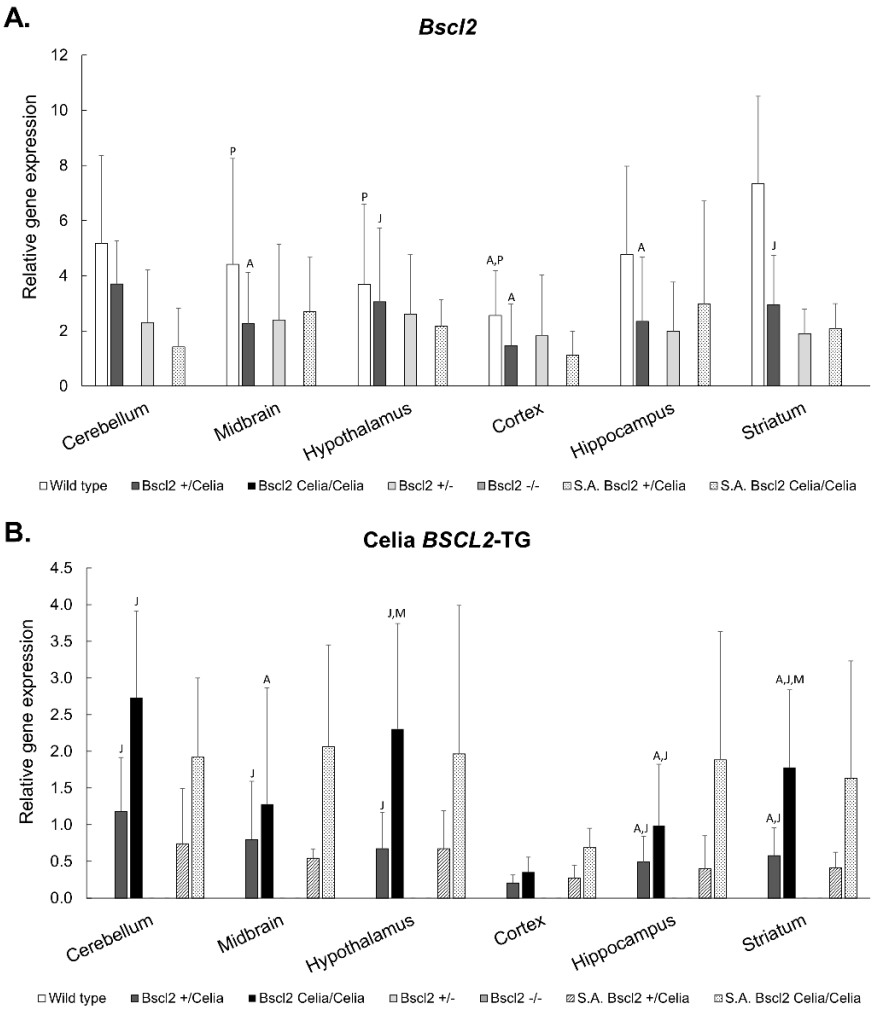

Figure 43. Relative expression of *Bscl2* and Celia *BSCL2*-TG in wild type, *Bscl2*$^{+/Celia}$, *Bscl2*$^{Celia/Celia}$, *Bscl2*$^{+/-}$, *Bscl2*$^{-/-}$ and severely affected (S.A.) animals. Relative expression of *Bscl2* (**A**) and Celia *BSCL2*-TG (**B**) in cerebellum, midbrain, hypothalamus, cortex, hippocampus, and striatum of the different murine models. For mean age and number of animals per genotype see **Annex 6**. Data is presented as mean ± SD. Data were analysed using a Kolmogorov-Smirnov test for normality, followed by a Kruskal-Wallis test with Mann-Whitney post hoc comparisons. Results were normalized for the *Rn18S* gene and referred to Cerebellum of *Bscl2*$^{+/Celia}$ in Celia *BSCL2*-TG gene. ^{A} $p < 0.05$ vs cerebellum ♀/♂; ^{J} $p < 0.05$ vs cortex ♀/♂; ^{M} $p < 0.05$ vs hippocampus ♀/♂; ^{P} $p < 0.05$ vs striatum ♀/♂.

In addition to the Celia *BSCL2* transgene expression, the analysis also examined the expression of several other genes: *Pparγ*, *Pex16*, *Cat* and, *Gpx1*. No significant differences in the expression of these genes were found between the genotypes (see **Annex 6**).

However, the expression of these genes was found to vary depending on the brain region examined (**Figure 44,** see **Annex 6**). *Pparγ* expression was higher in the cerebellum compared to other brain regions, while *Pex16* and *Gpx1* expression was higher in the striatum. Moreover, *Pex16* and *Cat* expression was lower in the cortex and hypothalamus, with also less expression of *Pparγ* in the hypothalamus. These regional differences in gene expression were observed across the various genotypes, regardless of their *Bscl2* genotype.

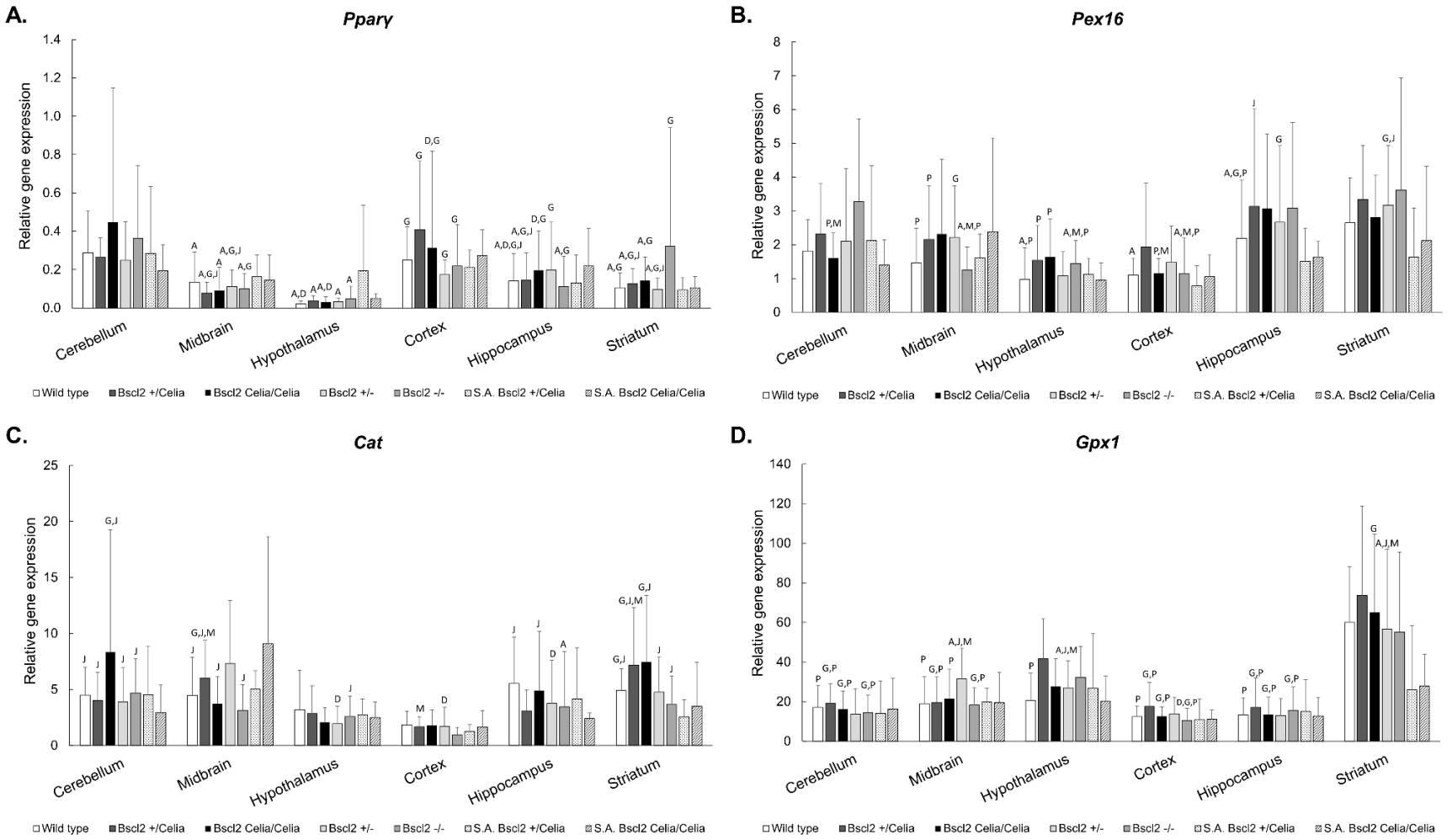

Figure 44. Relative expression of *Ppary*, *Pex16*, *Cat* and *Gpx1* in wild type, *Bscl2*$^{+/Celia}$, *Bscl2*$^{Celia/Celia}$, *Bscl2*$^{+/-}$, *Bscl2*$^{-/-}$ and severely affected (S.A.) animals. Relative expression of *Ppary* (**A**), *Pex16* (**B**), *Cat* (**C**) and *Gpx1* (**D**) in cerebellum, midbrain, hypothalamus, cortex, hippocampus, and striatum of the different murine models. For mean age and number of animals per genotype see **Annex 6**. Data is presented as mean ± SD. Data were analysed using a Kolmogorov-Smirnov test for normality, followed by a Kruskal-Wallis test with Mann-Whitney post hoc comparisons. Results were normalized for the *Rn18S* gene and referred to Cerebellum of *Bscl2*$^{+/Celia}$ in Celia *BSCL2*-TG gene. ^{A} $p < 0.05$ vs cerebellum ♀/♂; ^{D} $p < 0.05$ vs midbrain ♀/♂; ^{G} $p < 0.05$ vs hypothalamus ♀/♂; ^{J} $p < 0.05$ vs cortex ♀/♂; ^{M} $p < 0.05$ vs hippocampus ♀/♂; ^{P} $p < 0.05$ vs striatum ♀/♂.

The expression of the mitochondrial superoxide dismutase gene, *Sod2*, was significantly reduced in striatum of both S.A. homozygous and heterozygous mice, with a 57-48% and 69-62% decrease, respectively, compared to other genotypes (**Figure 45B**). In the cortex, the *Sod2* expression was only reduced in the S.A. homozygous animals, with a 60-21% decrease compared to the other genotypes (**Figure 45B**). It should be noted that the differences observed in the S.A. *Bscl2*$^{Celia/Celia}$ mice did not always reach statistical significance.

The expression of the *Sod1* gene was also reduced in the cortex of both the S.A. *Bscl2*$^{Celia/Celia}$ and S.A. *Bscl2*$^{+/Celia}$ mice, with a 61-46% and 49-30% decrease, respectively, compared to the non-S.A. animals (wild type, KI and, KO). However, these differences were not statistically significant. In contrast, the *Sod1* expression was significantly increased by 288-172% in the midbrain of the S.A. *Bscl2*$^{+/Celia}$ mice compared to the non-S.A. animals, and 130% higher compared to the S.A. *Bscl2*$^{Celia/Celia}$ mice (**Figure 45A**). Additionally, the *Sod1* expression in the hypothalamus appeared to be higher in most genotypes compared to wild type, except for the S.A. *Bscl2*$^{Celia/Celia}$ mice. The *Bscl2*$^{-/-}$ mice also showed higher *Sod1* expression in the hypothalamus than the non-S.A. and S.A. *Bscl2*$^{Celia/Celia}$, independent of sex.

Regarding the *Pex11g* gene, its expression was increased in the hypothalamus of the S.A. animals, as well as in the non-S.A. KI, homozygous, and heterozygous mice, compared to wild type (**Figure 45C**).

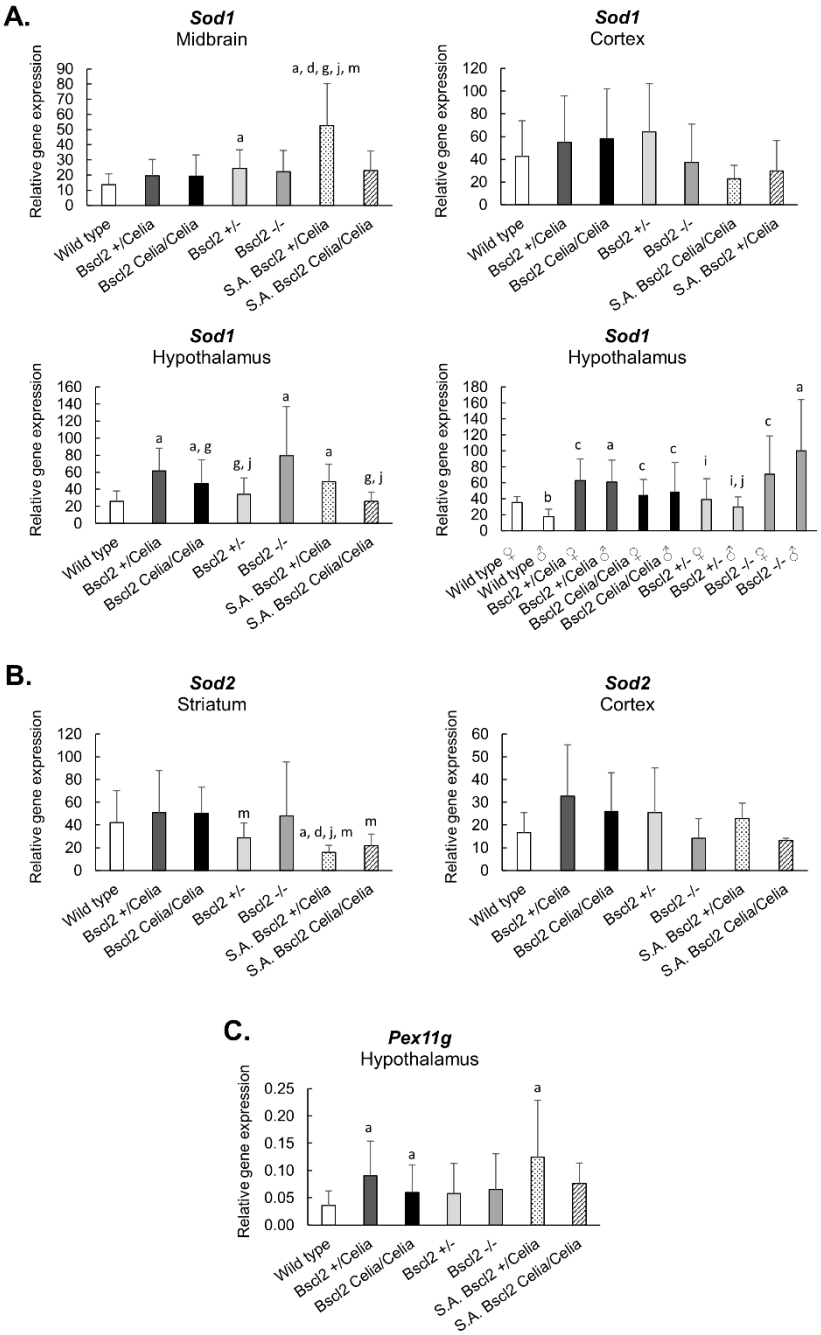

Figure 45. Relative gene expression of *Sod1*, *Sod2* and *Pex11g* in brain tissues. Relative expression of (**A**) *Sod1* in midbrain, cortex, and hypothalamus; (**B**) *Sod2* in striatum and cortex and (**C**) *Pex11g* in hypothalamus. For mean age and number of animals per genotype see **Annex 6**. Data is presented as mean ± SD. Data were analysed using a Kolmogorov-Smirnov test for normality, followed by a Kruskal-Wallis test with Mann-Whitney post hoc comparisons. Results were normalized for the *Rn18S* gene and referred to Cerebellum of *Bscl2*$^{+/Celia}$ in Celia *BSCL2*-TG gene. [a] $p < 0.05$ vs wild type ♀/♂; [b] $p < 0.05$ vs wild type ♀; [c] $p < 0.05$ vs wild type ♂; [d] $p < 0.05$ vs *Bscl2*$^{+/-}$ ♀/♂; [g] $p < 0.05$ vs *Bscl2*$^{-/-}$ ♀/♂; [i] $p < 0.05$ vs *Bscl2*$^{-/-}$ ♂; [j] $p < 0.05$ vs *Bscl2*$^{+/Celia}$ ♀/♂; [m] $p < 0.05$ vs *Bscl2*$^{Celia/Celia}$ ♀/♂.

The analysis of these of the expression pattern of *Sod1, Sod2*, and *Pex11g* across different brain regions revealed that *Sod1* expression was lower in the cerebellum of the KI and KO mice, while the wild type mice showed lower *Sod1* expression in the midbrain (**Figure 46A**). *Sod2* expression was reduced in the hypothalamus across all genotypes. In the S.A. animals, although not statistically significance, there was a trend towards higher *Sod2* expression in the cerebellum and midbrain (**Figure 46B**). Furthermore, *Pex11g* expression was lower in the cortex across all genotypes, and also in the hippocampus of the KI and KO animals (**Figure 46C**).

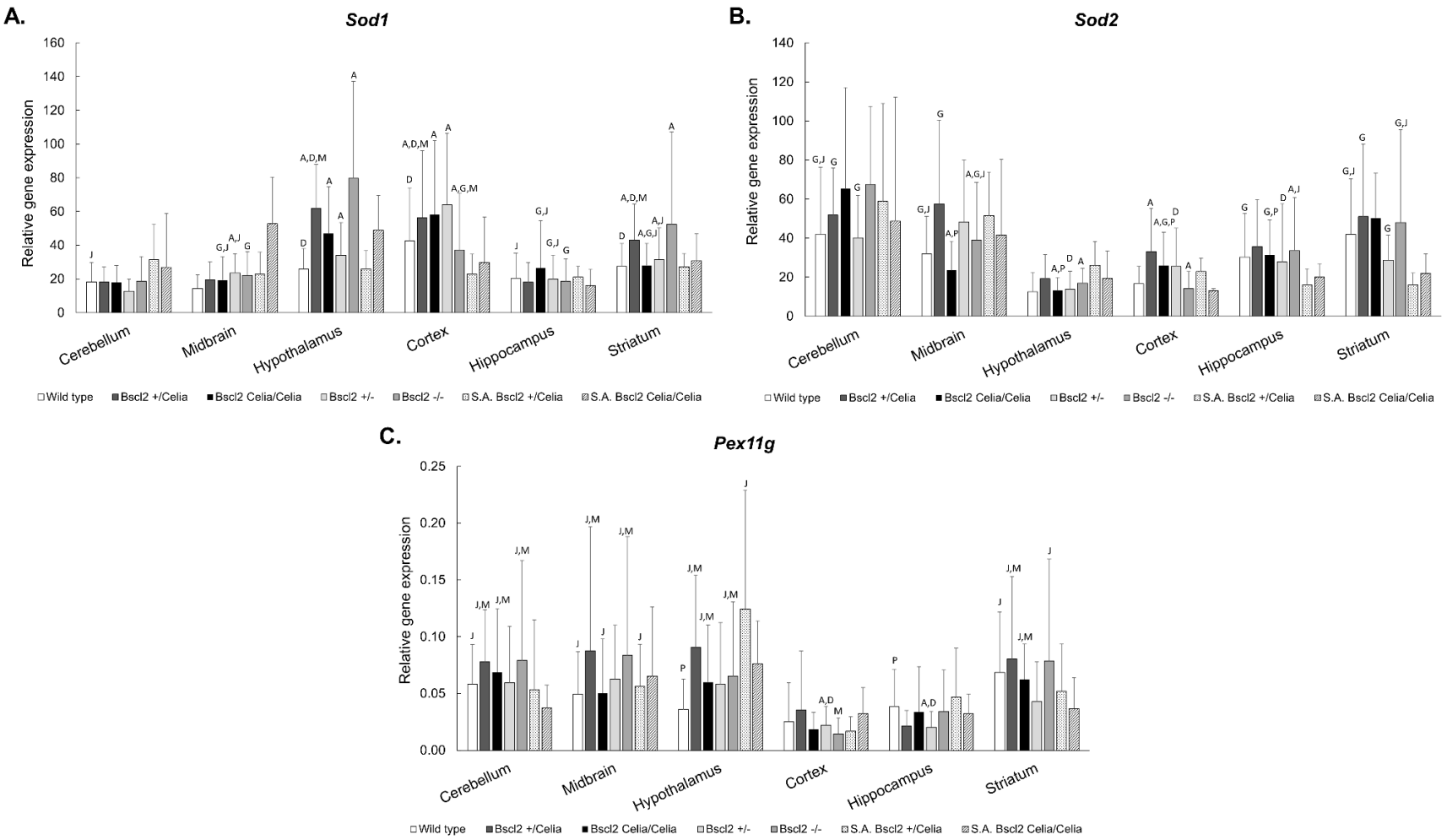

Figure 46. Relative expression of *Sod1*, *Sod2* and *Pex11g* in wild type, *Bscl2*$^{+/Celia}$, *Bscl2*$^{Celia/Celia}$, *Bscl2*$^{+/-}$, *Bscl2*$^{-/-}$ and severely affected (S.A.) animals. Relative expression of *Sod1* (**A**), *Sod2* (**B**) and *Pex11g* (**C**) in cerebellum, midbrain, hypothalamus, cortex, hippocampus, and striatum of the different murine models. For mean age and number of animals per genotype see **Annex 6**. Data is presented as mean ± SD. Data were analysed using a Kolmogorov-Smirnov test for normality, followed by a Kruskal-Wallis test with Mann-Whitney post hoc comparisons. Results were normalized for the *Rn18S* gene and referred to Cerebellum of *Bscl2*$^{+/Celia}$ in Celia *BSCL2*-TG gene. ^{A} $p < 0.05$ vs cerebellum ♀/♂; ^{D} $p < 0.05$ vs midbrain ♀/♂; ^{G} $p < 0.05$ vs hypothalamus ♀/♂; ^{J} $p < 0.05$ vs cortex ♀/♂; ^{M} $p < 0.05$ vs hippocampus ♀/♂; ^{P} $p < 0.05$ vs striatum ♀/♂.

4.3.6 Celia-seipin Protein

Due to the lack of a specific antibody anti-Celia-seipin, the amount of this aberrant human protein was analysed in six non-S.A. KI murine brain areas by Western blot using 6xHis-tagged Celia seipin. The theoretical weight of Celia seipin with 6x His tag was 40.25 kDa (39.43 kDa + 0.84 kDa, respectively). In both genotypes, *Bscl2*$^{+/Celia}$ and *Bscl2*$^{Celia/Celia}$, obvious bands were observed in the cortex, hypothalamus and hippocampus, but the signal detected in the cerebellum, midbrain and striatum was not as evident compared to the hypothalamus of a human without the disease (**Figure 47**). Furthermore, quantification of the relative expression of the 6xHis-tagged Celia seipin protein showed greater expression in these same tissues (cortex, hypothalamus, and hippocampus), with expression in the hypothalamus being clearly predominant in both genotypes (**Figure 47**). However, the comparison of Celia seipin expression between *Bscl2*$^{+/Celia}$ and *Bscl2*$^{Celia/Celia}$ was not possible because the samples were not processed on the same gel.

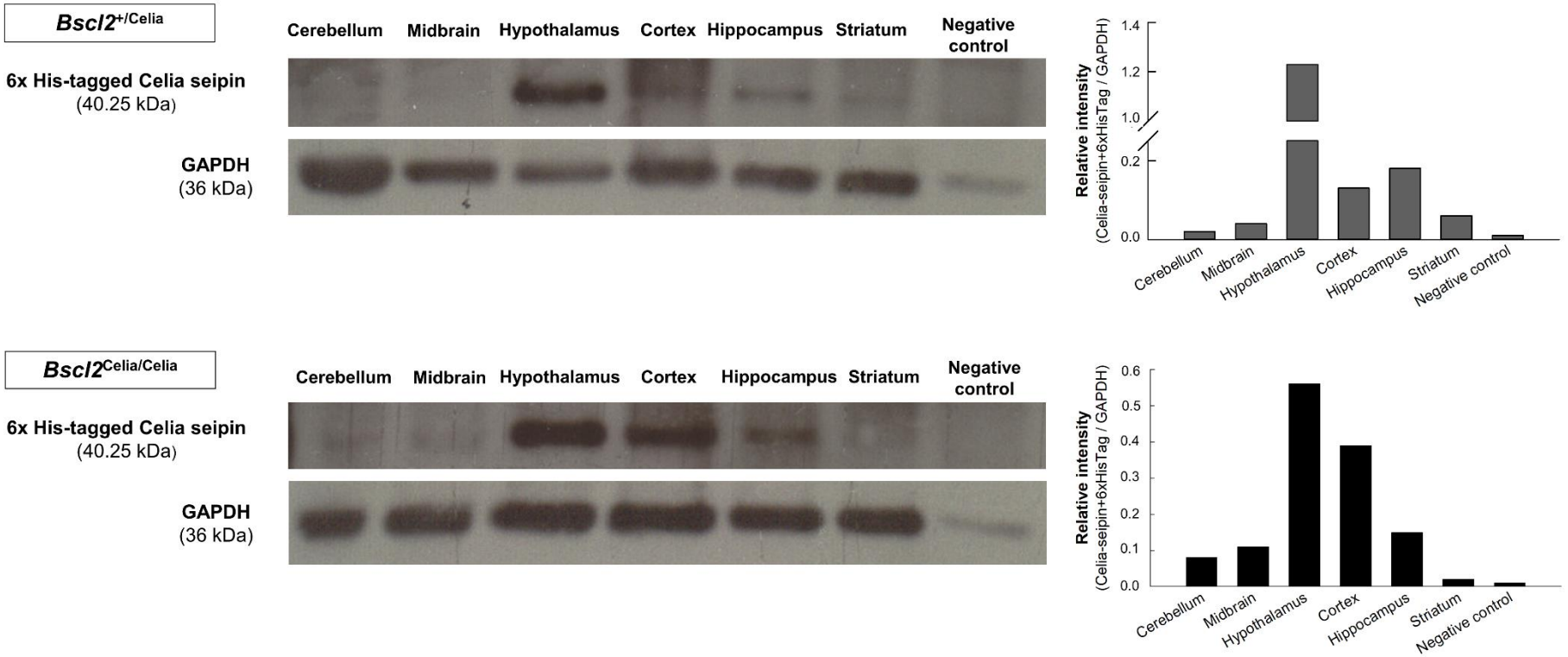

Figure 47. Western blot analysis of 6x His-tagged Celia seipin protein in brain tissues. Western blot and relative protein quantification of (**A**) *Bscl2*$^{+/Celia}$ ♂ (n=1, 6.1 months) and (**B**) *Bscl2*$^{Celia/Celia}$ ♂ (n = 1, 6.1 months) mice. The hypothalamus of a human without the disease was used as negative control. Results were normalized to GADPH. Data is presented in two different gels, one for *Bscl2*$^{+/Celia}$ and one for *Bscl2*$^{Celia/Celia}$, with six brain areas (cerebellum, midbrain, hypothalamus, cortex, hippocampus, striatum) and the negative control each. Full length blot and cropped images are available in **Annex 7**.

4.4 Clinical Signs and Gross Pathological Findings

The animals were dissected, and photographs of the trunk area of each genotype were captured (**Figure 48A**) to conduct a macroscopic analysis of the organs and tissues of interest, including adipose tissue, liver, heart, spleen, kidneys, and eyeball. A detailed analysis of each tissue and organ is provided in the following sections.

The weight of the mice was monitored throughout their lifespan, from 0.5 to 9.5 months. All mice exhibited progressive weight gain until reaching a stable weight in adulthood. Additionally, males across all genotypes displayed higher weights than females. The *Bscl2*$^{Celia/Celia}$ animals exhibited lower weights in their early months compared to other genotypes, but this difference did not persist into adulthood. However, S.A. animals showed a continuous reduction in weight throughout their lifespan compared to non-S.A. mice (wild type, KI, and KO). No significant differences were observed in the severity of weight loss between S.A. *Bscl2*$^{+/Celia}$ and S.A. *Bscl2*$^{Celia/Celia}$ mice (**Figure 48B,** see **Annex 8**).

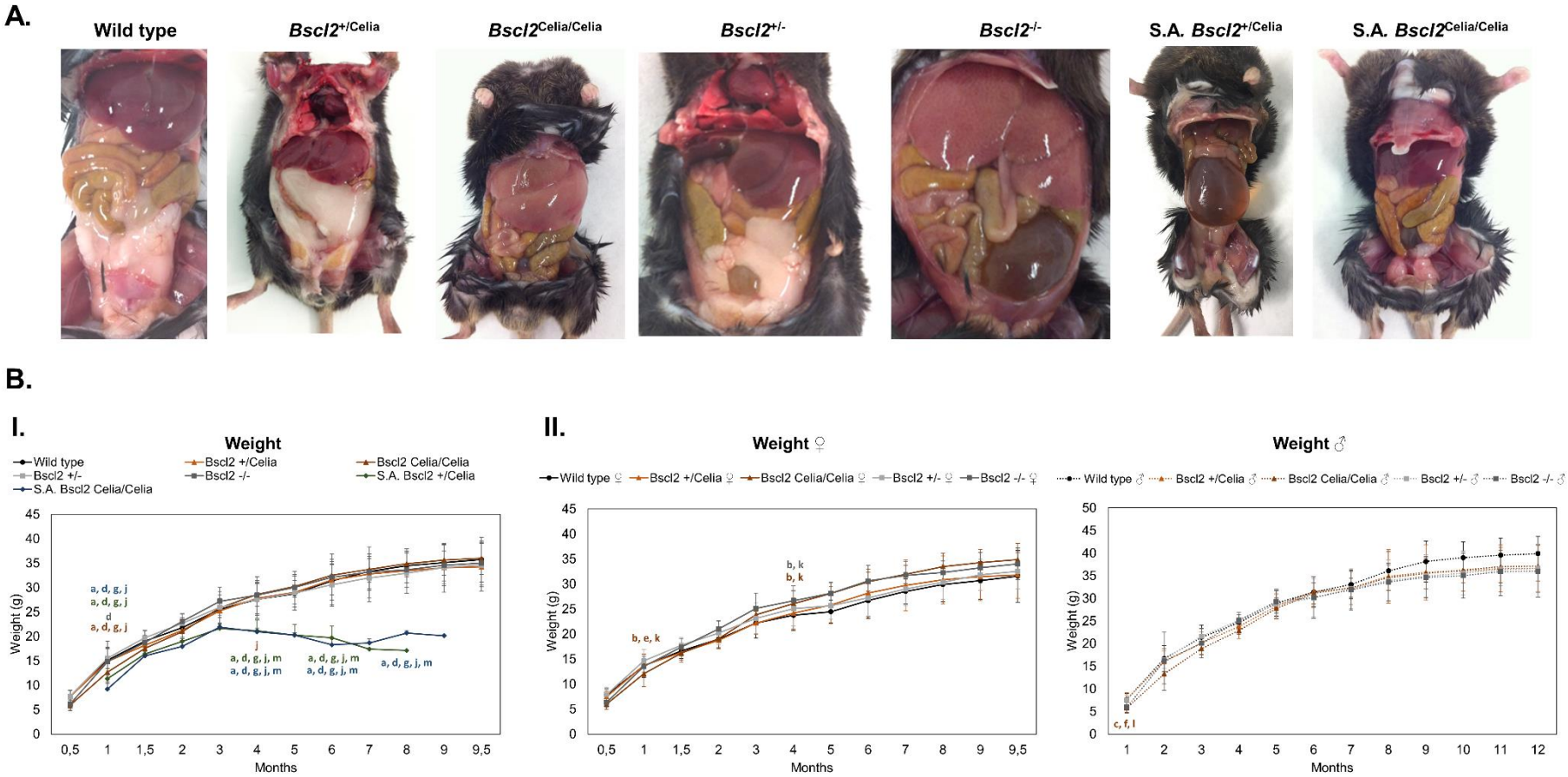

Figure 48. Gross pathology and weight evolution. A. Dissection of the trunk area. Wild type, *Bscl2*$^{+/Celia}$, *Bscl2*$^{Celia/Celia}$, *Bscl2*$^{+/-}$ (9 months old); *Bscl2*$^{-/-}$ (9.5-months-old) and severe affected (S.A.): *Bscl2*$^{+/Celia}$ (8.6 months old) and *Bscl2*$^{Celia/Celia}$ (3.9-months-old) male mice. **B. Weight evolution from 0.5 to 9.5 months-old for wild type, *Bscl2*$^{+/Celia}$, *Bscl2*$^{Celia/Celia}$, *Bscl2*$^{+/-}$, *Bscl2*$^{-/-}$and severely affected (S.A.) animals.** (**I**) Weight evolution for both sexes and (**II**) female weight evolution and male weight evolution. For mean age and number of animals per genotype see **Annex 8**. Data is presented as mean ± SD. Data were analysed using a Kolmogorov-Smirnov test for normality, followed by a Kruskal-Wallis test with Mann-Whitney post hoc comparisons. [a] $p < 0.05$ vs wild type ♀/♂; [b] $p < 0.05$ vs wild type ♀; [c] $p < 0.05$ vs wild type ♂; [d] $p < 0.05$ vs *Bscl2*$^{+/-}$ ♀/♂; [e] $p < 0.05$ vs *Bscl2*$^{+/-}$ ♀; [f] $p < 0.05$ vs *Bscl2*$^{+/-}$ ♂; [g] $p < 0.05$ vs *Bscl2*$^{-/-}$ ♀/♂; [j] $p < 0.05$ vs *Bscl2*$^{+/Celia}$ ♀/♂; [k] $p < 0.05$ vs *Bscl2*$^{+/Celia}$; [l] $p < 0.05$ vs *Bscl2*$^{+/Celia}$ ♂; [m] $p < 0.05$ vs *Bscl2*$^{Celia/Celia}$ ♀/♂.

4.4.1 Adipose Tissue

Upon dissection, *Bscl2*$^{-/-}$ and *Bscl2*$^{Celia/Celia}$ mice exhibited a near-total absence of fat (**Figure 48A**), impacting both white adipose tissue (WAT) and brown adipose tissue (BAT) depots (interscapular BAT, inguinal WAT, gonadal WAT) (**Figure 49A**), indicative of a severe lipoatrophic phenotype. Histological examination of residual brown fat revealed adipocytes with enlarged lipid vacuoles and areas of necrosis, while white fat displayed smaller adipocytes and regions of fibrosis. In both cases, lymphocyte infiltrates were observed (**Figure 49B**).

Conversely, normal fat distribution (**Figure 48A** and **Figure 49A**) and typical fat depots (**Figure 49B**) were noted in wild type and heterozygous mice. No discernible differences were observed between sexes or KI and KO animals. The lipoatrophic phenotype and the fat distribution observed in non-S.A. homozygotes (*Bscl2*$^{Celia/Celia}$ and *Bscl2*$^{-/-}$) persisted in S.A. *Bscl2*$^{Celia/Celia}$ animals (**Figure 48A** and **Figure 49**). Similarly, S.A. heterozygous mice exhibited similar characteristics to non-S.A. heterozygotes (*Bscl2*$^{+/Celia}$ and *Bscl2*$^{+/-}$). However, the fat content observed during dissections was notably lower compared to non-S.A. heterozygous (KI and KO) and wild type mice (**Figure 48A** and **Figure 49**), probably due to their lower weight (**Figure 48B)**.

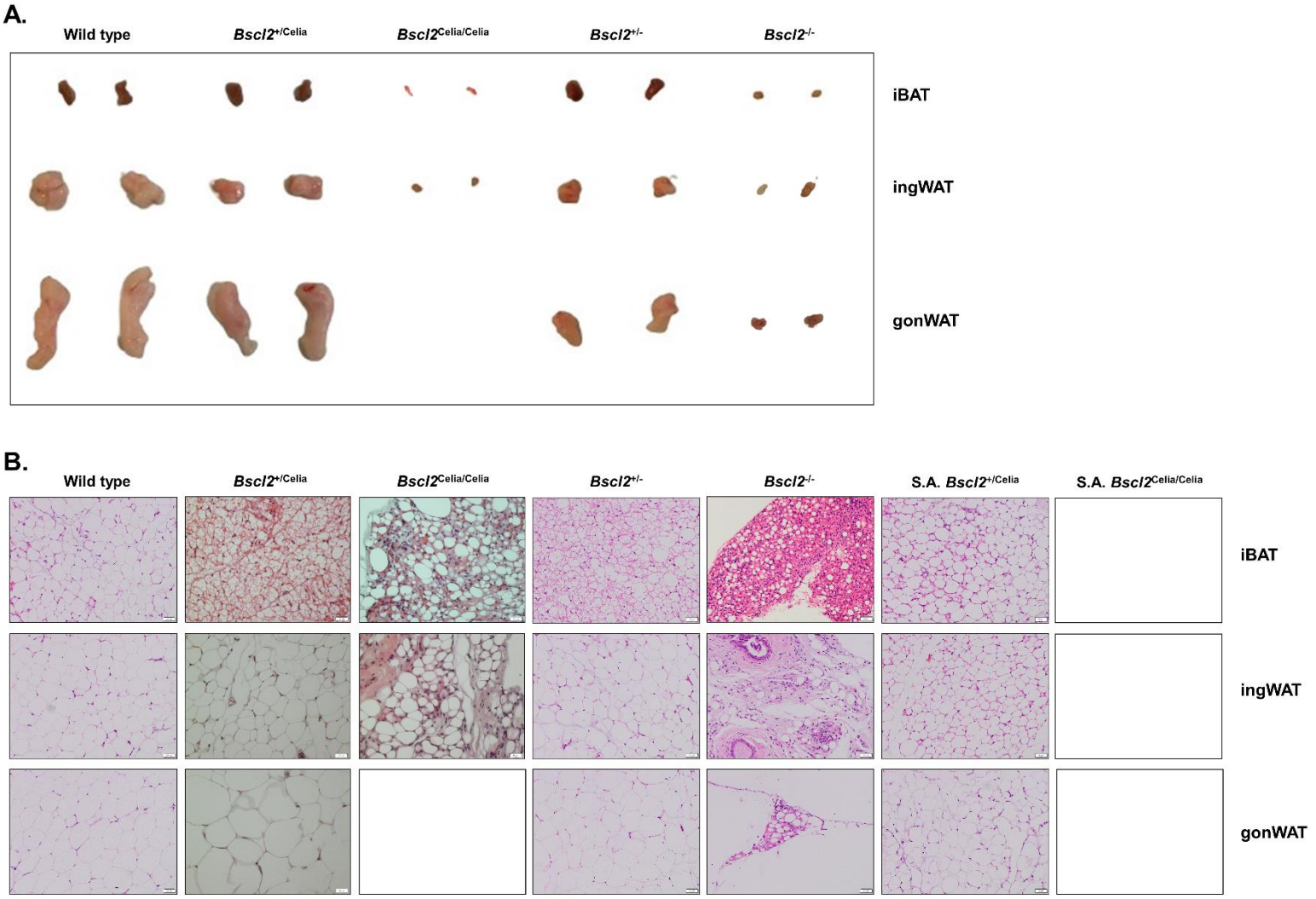

Figure 49. Analysis of the adipose tissue. A. Macroscopic appearances od adipose tissue. Interscapular brown adipose tissue (iBAT), inguinal white adipose tissue (ingWAT) and gonadal white adipose tissue (gonWAT) of 7.2-months-old *Bscl2*$^{+/-}$and *Bscl2*$^{-/-}$; 6.8-months-old wild type and *Bscl2*$^{+/Celia}$ and 5.3-months-old *Bscl2*$^{Celia/Celia}$ ♂ mice. **B. Histology of adipose tissue.** iBAT, ingWAT and gonWAT of 6.1-months-old wild type ♀, *Bscl2*$^{+/Celia}$ ♂, *Bscl2*$^{Celia/Celia}$ ♂ and *Bscl2*$^{+/-}$♂; 7.2-months-old *Bscl2*$^{-/-}$ ♂ (except for iBAT 0.9-months-old ♂) and 5.8-months-old severely affected (S.A.) *Bscl2*$^{+/Celia}$ ♂ mice. H&E; scale bar: 20 µm.

4.4.2 Liver

The livers of wild type and heterozygous mice appeared normal in terms of colour and size. In contrast, homozygous mice presented with an enlarged liver and hepatic pallor (**Figure 50A**), in some cases accounting for up to 25% of the animal's body weight, which was significantly greater compared to wild type, heterozygous, and S.A. animals (**Figure 50B**). The S.A. mice did not exhibit liver pallor, but they did show a greater liver weight compared to wild type and heterozygous animals. However, no significant differences were found between the S.A. *Bscl2*$^{Celia/Celia}$ and *Bscl2*$^{+/Celia}$ animals, although the S.A. *Bscl2*$^{Celia/Celia}$ mice appeared to show a higher liver weight compared to the S.A. *Bscl2*$^{+/Celia}$ mice (**Figure 50B**). Furthermore, these S.A. homozygous mice had much smaller liver sizes compared to the non-S.A. homozygous animals (*Bscl2*$^{Celia/Celia}$ and *Bscl2*$^{-/-}$), more closely resembling the liver characteristics of non-S.A. heterozygous (*Bscl2*$^{+/Celia}$ and *Bscl2*$^{+/-}$) or wild type mice. No differences in liver characteristics were found between sexes or between the KI and KO mouse models.

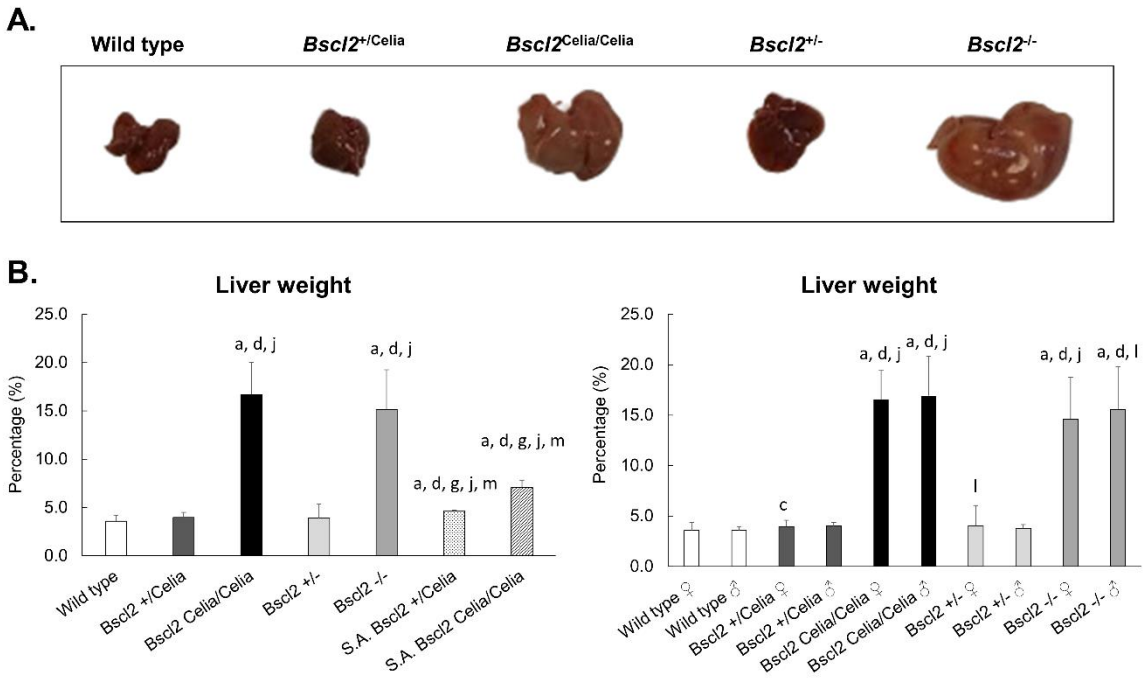

Figure 50. Analysis of the liver tissue. A. Liver macroscopic appearances. 7.2-months-old *Bscl2*$^{+/-}$and *Bscl2*$^{-/-}$; 6.8-months-old wild type and *Bscl2*$^{+/Celia}$ and 5.3-months-old *Bscl2*$^{Celia/Celia}$ ♂ mice. **B. Liver weight comparison in terms of percentage.** For mean age and number of animals per genotype see **Annex 9, Table S16**. Data is presented as n (%) ± SD. Data were analysed using a Kolmogorov-Smirnov test for normality, followed by a Kruskal-Wallis test with Mann-Whitney post hoc comparisons. [a] $p < 0.05$ vs wild type ♀/♂; [c] $p < 0.05$ vs wild type ♂; [d] $p < 0.05$ vs *Bscl2*$^{+/-}$ ♀/♂; [g] $p < 0.05$ vs *Bscl2*$^{-/-}$ ♀/♂; [j] $p < 0.05$ vs *Bscl2*$^{+/Celia}$ ♀/♂; [l] $p < 0.05$ vs *Bscl2*$^{+/Celia}$ ♂; [m] $p < 0.05$ vs *Bscl2*$^{Celia/Celia}$ ♀/♂.

To better understand the underlying anatomopathological alterations responsible for the macroscopic findings, a comprehensive histological study was performed (**Figure 51**).

The liver histology of wild type and heterozygous mice was found to be normal. While the presence of minimal lobular infiltrates was observed in some cases, this was considered a non-specific finding that, in the absence of steatosis and ballooning degeneration, had no diagnostic implications (**Figure 51**).

In contrast, the liver histology of homozygous mice revealed the presence of hepatic steatosis as early as 3 months of age, which persisted as a consistent finding from 6 months onwards (**Figure 51**). This ectopic fat deposition (as shown by *Oil red O* staining in **Figure 51**) exhibited a mixed pathological pattern, comprising both macrovesicular steatosis, characterized by large lipid vacuoles that displaced the nucleus to the periphery, and microvesicular steatosis, characterized by small LDs filling the cytoplasm without nuclear displacement (**Figure 51** and **Figure 52**). However, the steatosis was predominantly macrovesicular, accompanied by the presence of ballooning cells with pale, feathery cytoplasm and small, hyperchromatic nuclei (as shown by H&E 10 µm staining in **Figure 51**).

Foci of lobular inflammation, composed predominantly of mononuclear cells, were also observed with some frequency (**Figure 52**). The histopathological analysis of *Bscl2*$^{Celia/Celia}$ mice further revealed the presence of intracytoplasmic hyaline bodies (IHBs), round or oval structures with a homogeneous, eosinophilic content and a surrounding halo, indicative of cellular damage (**Figure 52**). These IHBs were not detected in the *Bscl2*$^{-/-}$ mice. Additionally, some cases showed a striking chronic perivascular infiltrate.

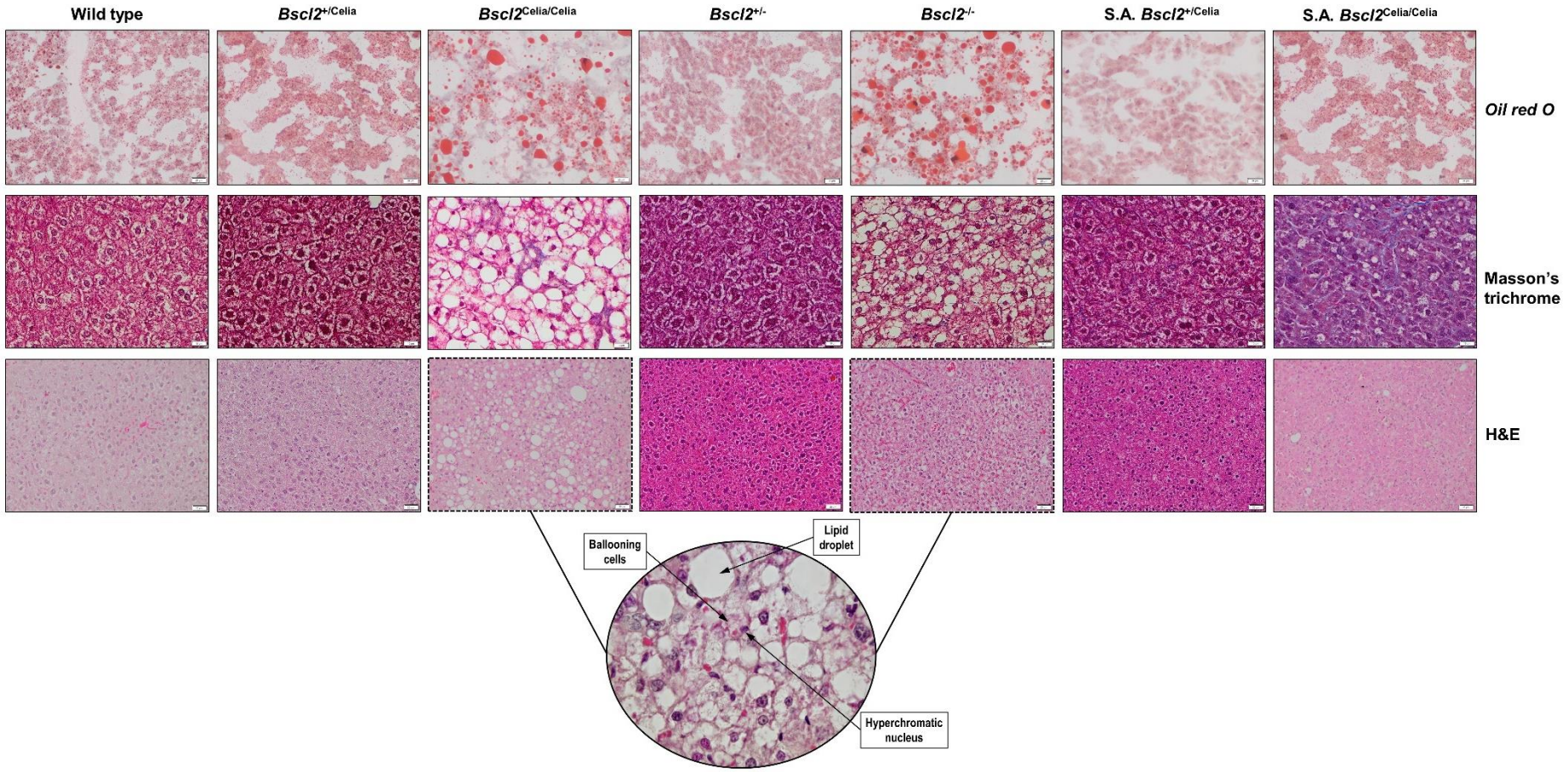

Figure 51. Histology of liver tissue. *Oil red O*, scale bar: 20 μm, mean age 6 months (wild type ♀, *Bscl2*$^{+/Celia}$ ♂, *Bscl2*$^{Celia/Celia}$ ♂, *Bscl2*$^{+/-}$ ♂, *Bscl2*$^{-/-}$ ♂) except for S.A. *Bscl2*$^{+/Celia}$ ♂ (8.6-months-old) and S.A. *Bscl2*$^{Celia/Celia}$ ♂ (4-months-old) mice. Masson's trichrome, scale bar: 10 μm, mean age 9 months (wild type ♂, *Bscl2*$^{+/Celia}$ ♂, *Bscl2*$^{Celia/Celia}$ ♂, *Bscl2*$^{-/-}$ ♂ and S.A. *Bscl2*$^{Celia/Celia}$ ♂) except for *Bscl2*$^{+/-}$ ♂ (6.1-months-old) and S.A. *Bscl2*$^{+/Celia}$ ♂ (5.8-months-old) mice. H&E, scale bar: 20 μm and 10 μm, wild type ♂, *Bscl2*$^{+/Celia}$ ♂ and *Bscl2*$^{-/-}$ ♀ (12-months-old), *Bscl2*$^{Celia/Celia}$ ♀ (14-months-old), *Bscl2*$^{+/-}$ ♂ (6.1-months-old) and severely affected (S.A.) mice: *Bscl2*$^{+/Celia}$ ♂ (5.8-months-old), *Bscl2*$^{Celia/Celia}$ ♂ (19-months-old).

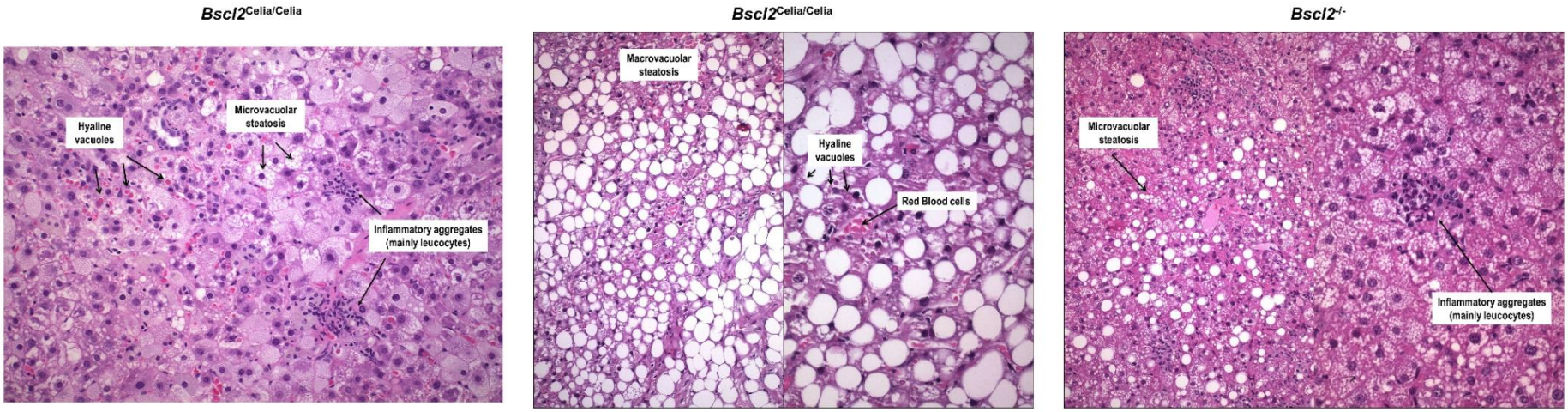

			Steatohepatitits				
			Steatosis		Inflammation		Hyaline vacuoles
	Age (months)	Sex	Score [0-3]	Predominance type	Socre [0-3]	Predominance type	Score [0-3]
Bscl2 Celia/Celia	13.9	♀	2 (moderate)	Microvesicular	1 (mild)	Leucocytes	3 (very numerous)
Bscl2 Celia/Celia	18.3	♀	3 (severe)	Macrovesicular	1 (mild)	Leucocytes	2 (numerous)
Bscl2 -/-	20.3	♀	2 (moderate)	Microvesicular	1 (mild)	Leucocytes	-

Figure 52. Assessment of steatohepatitis in the liver of homozygous mice. Histological assessment of steatosis, inflammation, and hyaline vacuoles. *Bscl2*$^{Celia/Celia}$ (n=2) and *Bscl2*$^{-/-}$ (n=1). H&E.

These histological characteristics were collectively grouped and evaluated using the NAFLD activity score (NAS) system to assess NAFLD. Currently, NAFLD has been renamed metabolic dysfunction-associated steatotic liver disease (MASLD), which allows for moderate alcohol consumption and requires one or more metabolic risk factors as principal differences (202).

Following these criteria, homozygous animals demonstrated a significantly higher total score for MASLD compared to wild type and heterozygous mice (**Figure 53A**). Specifically, the percentage of homozygous animals presenting both MASL (67-76%) and MASH (47-57%) was higher compared to wild type and heterozygous mice (**Figure 53C**). Notably, the *Bscl2*$^{Celia/Celia}$ mice had a higher NAS score, and the percentage of animals with MASL and MASH was also higher compared to S.A. *Bscl2*$^{+/Celia}$ mice, a finding not replicated in *Bscl2*$^{-/-}$ mice. Moreover, fibrosis status analysis indicated that 27-38% of homozygous mice with marked active liver damage also developed mild pericellular fibrosis (as shown by Masson's trichrome staining in **Figure 51** and in **Figure 53B**. No differences were observed between sexes, although in the case of homozygous, *Bscl2*$^{-/-}$ and *Bscl2*$^{Celia/Celia}$ mice, females tended to have slightly higher hepatic involvement than males.

Furthermore, the S.A. *Bscl2*$^{Celia/Celia}$ mice presented with mild hepatic steatosis (**Figure 51**). Similar to the non-S.A. *Bscl2*$^{Celia/Celia}$ mice, the 50% of S.A. *Bscl2*$^{Celia/Celia}$ mice exhibited mild pericellular fibrosis (**Figure 53B**) with a higher total NAS score (**Figure 53A**) compared to wild type, heterozygous and S.A. *Bscl2*$^{+/Celia}$ mice. Additionally, 88% of S.A. *Bscl2*$^{Celia/Celia}$ mice showed MASL, of which 25% developed MASH, whereas only 20% of S.A. *Bscl2*$^{+/Celia}$ mice showed signs of MASL, never progressing to steatohepatitis (**Figure 53C**).

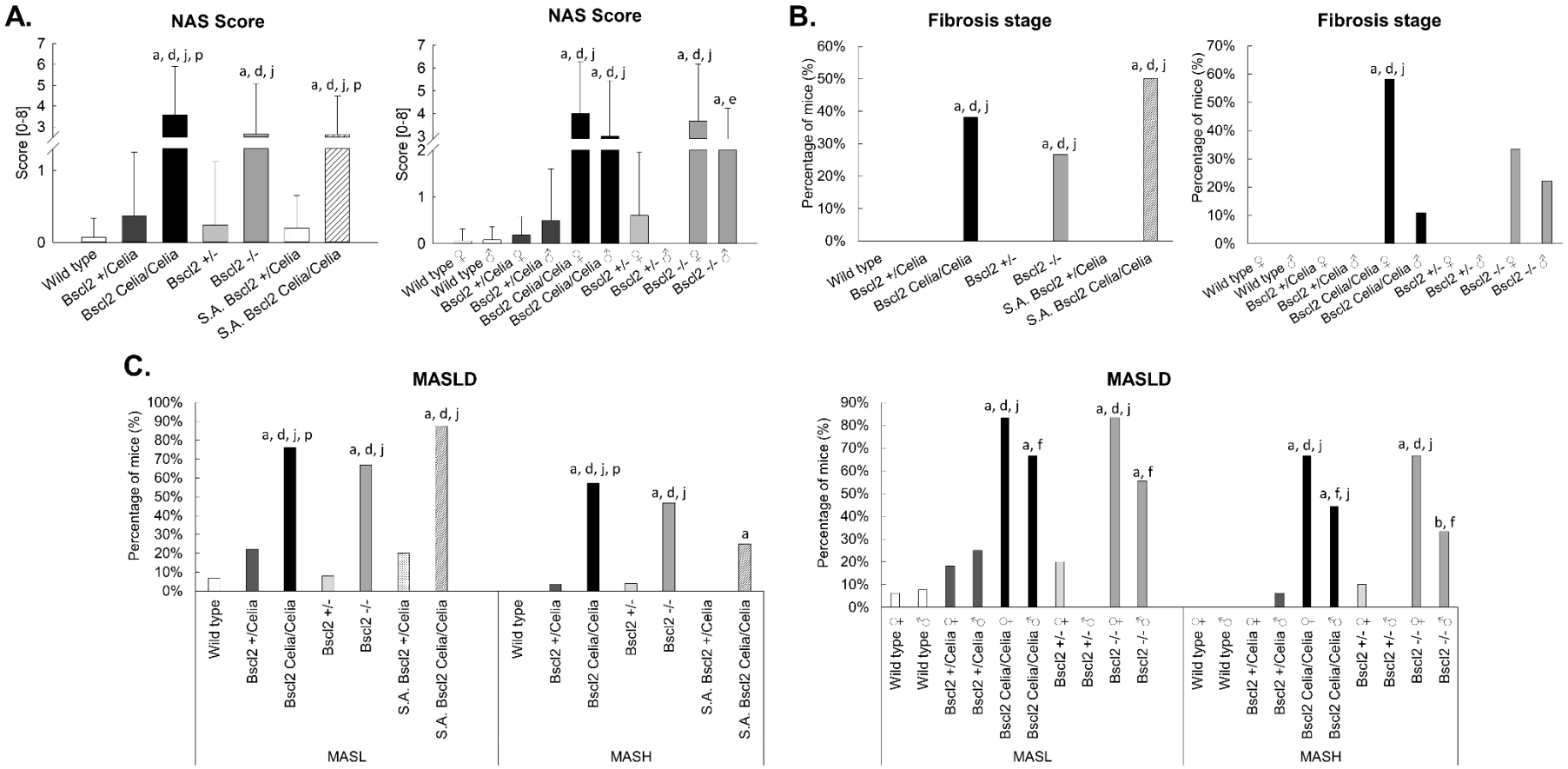

Figure 53. Assessment of liver involvement. A. NAS Score. Degree of activity of metabolic dysfunction-associated steatotic liver disease calculated as the sum of scores for steatosis, ballooning degeneration, and lobular inflammation according to the NAS scoring system of the NASH CRN. Data is presented as mean ± SD. **B. Fibrosis stage.** Assessment of the number of animals with fibrosis stage 1a in the liver according to the NASH CRN System. Data is presented as n (%). **C. Evaluation of subtypes of metabolic dysfunction-associated steatotic liver disease (MASLD).** Assessment of the number of animals with metabolic-dysfunction associated steatotic liver (MASL) and/or with metabolic dysfunction-associated steatohepatitis (MASH). Data is presented as n (%). Statistical significance for categorical data was assessed using Fisher's exact test. For mean age and number of animals per genotype see **Annex 9, Table S17**. [a] $p < 0.05$ vs wild type ♀/♂; [b] $p < 0.05$ vs wild type ♀; [d] $p < 0.05$ vs *Bscl2*$^{+/-}$ ♀/♂; [e] $p < 0.05$ vs *Bscl2*$^{+/-}$ ♀; [f] $p < 0.05$ vs *Bscl2*$^{+/-}$ ♂; [j] $p < 0.05$ vs *Bscl2*$^{+/Celia}$ ♀/♂; [p] $p < 0.05$ vs S.A. *Bscl2*$^{+/Celia}$ ♀/♂.

Additionally, hepatic expression of *Fgf21*, a protective cytokine against glucolipid metabolic disorders, was assessed (**Figure 54**, see **Annex 6**). Non-S.A. heterozygous, KI and KO animals, exhibited a 60-187% increase in the *Fgf21* gene compared to wild type animals. However, the increase in *Fgf21* expression was significantly higher in non-S.A. homozygous animals, both KI and KO (1,376-1,953% compared to wild type animals). Thus, *Bscl2*$^{Celia/Celia}$ mice showed an increase of 820% and 414% compared to *Bscl2*$^{+/Celia}$ and *Bscl2*$^{+/-}$ mice, while this increase in *Bscl2*$^{-/-}$ animals was 1,179% and 614% respectively.

Sex-based analysis revealed that the increase observed in heterozygous animals compared to wild type ones was actually a difference relative to wild type females. Additionally, *Bscl2*$^{-/-}$ male mice exhibited a greater increase compared to *Bscl2*$^{Celia/Celia}$ males.

Furthermore, this increase in *Fgf21* expression compared to wild type and heterozygous, KI and KO animals, was evident in S.A. homozygous animals, at 1,451%, 867%, and 440% respectively. Moreover, S.A. *Bscl2*$^{Celia/Celia}$ animals showed a 3,177% increase compared to S.A. *Bscl2*$^{+/Celia}$ animals. No significant differences were found between S.A. and non-S.A. *Bscl2*$^{Celia/Celia}$ mice. However, differences were observed among *Bscl2*$^{+/Celia}$ mice, with S.A. animals showing a 70% decrease compared to those non-severely affected.

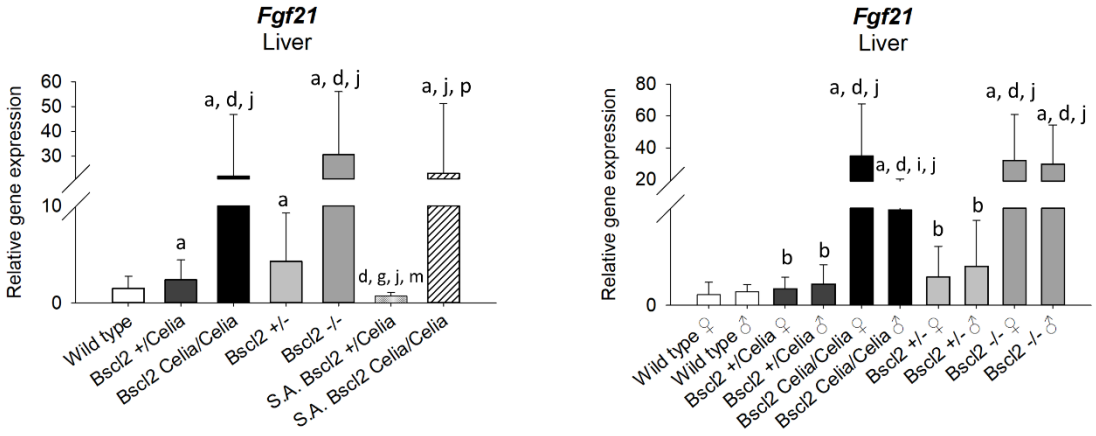

Figure 54. Relative expression of *Fgf21* gene in liver. Wild type, *Bscl2*$^{+/Celia}$, *Bscl2*$^{Celia/Celia}$, *Bscl2*$^{+/-}$, *Bscl2*$^{-/-}$ and severely affected (S.A) *Bscl2*$^{Celia/Celia}$ and *Bscl2*$^{+/Celia}$ animals. For mean age and number of animals per genotype see **Annex 6**. Data is presented as mean ± SD. Data were analysed using a Kolmogorov-Smirnov test for normality, followed by a Kruskal-Wallis test with Mann-Whitney post hoc comparisons. Results were normalized for the *Rn18S* gene and referred to wild type. [a] $p < 0.05$ vs wild type ♀/♂; [b] $p < 0.05$ vs wild type ♀; [d] $p < 0.05$ vs *Bscl2*$^{+/-}$ ♀/♂; [g] $p < 0.05$ vs *Bscl2*$^{-/-}$ ♀/♂; [i] $p < 0.05$ vs *Bscl2*$^{-/-}$ ♂; [j] $p < 0.05$ vs *Bscl2*$^{+/Celia}$ ♀/♂; [m] $p < 0.05$ vs *Bscl2*$^{Celia/Celia}$ ♀/♂; [p] $p < 0.05$ vs S.A. *Bscl2*$^{+/Celia}$ ♀/♂.

4.4.3 Heart

At the macroscopic level, the hearts of homozygous mice were observed to be larger in size and, in some cases, had a darker colour (**Figure 55A**). When analysing the heart weight relative to the animal's body weight, the hearts of the homozygous mice were found to be significantly heavier compared to those of heterozygous and wild type mice.

The S.A. animals, *Bscl2*$^{+/Celia}$ and *Bscl2*$^{Celia/Celia}$ animals, despite not exhibiting significant differences, also showed a greater heart weight, similar to that observed in the homozygous mice (**Figure 55C**).

No differences in heart weight were observed between sexes or between the KI and KO mouse models.

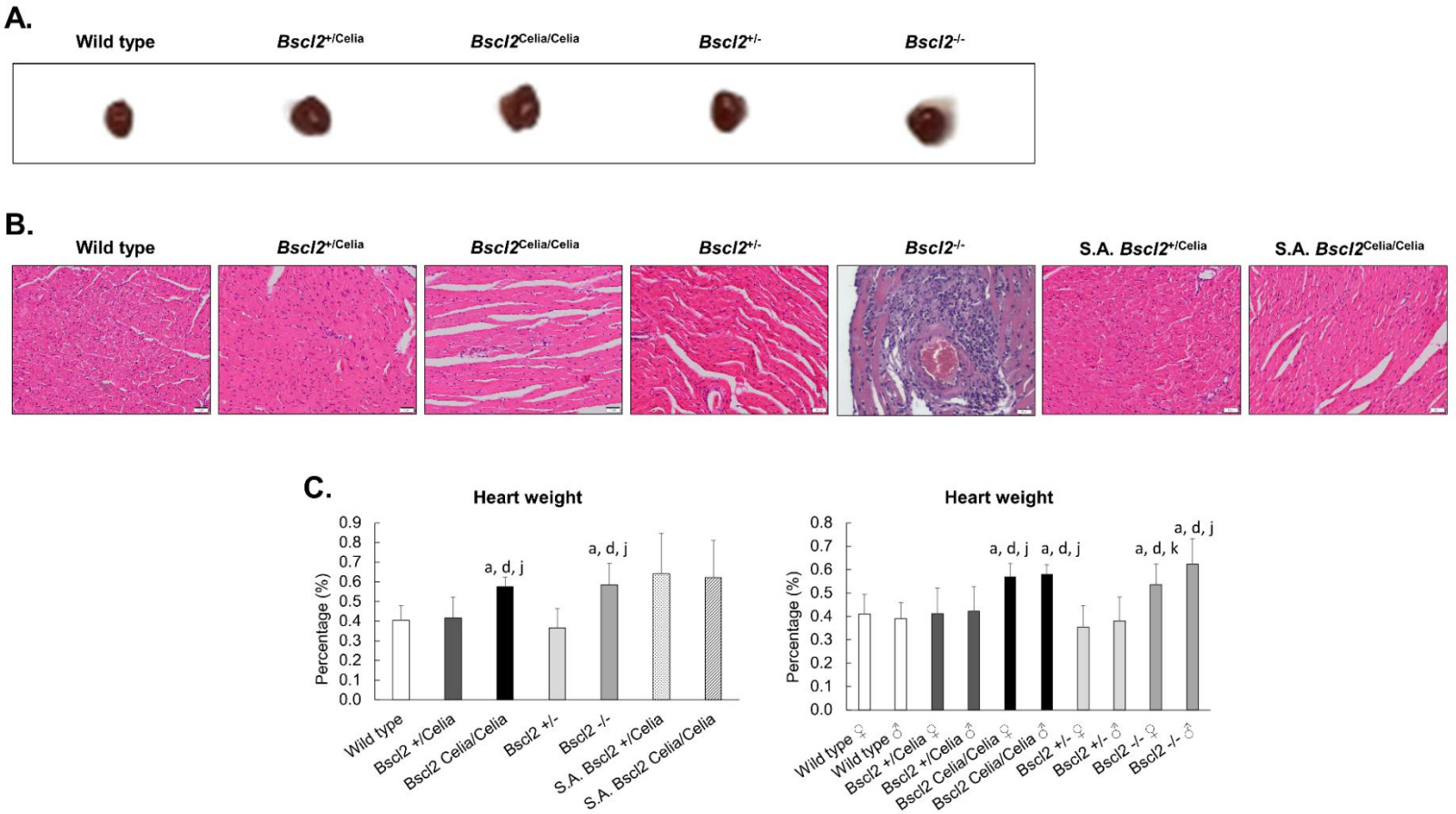

Figure 55. Analysis of the heart tissue. A. Heart macroscopic appearances. 7.2-months-old *Bscl2*$^{+/-}$and *Bscl2*$^{-/-}$; 6.8-months-old wild type and *Bscl2*$^{+/Celia}$ and 5.3-months-old *Bscl2*$^{Celia/Celia}$ ♂ mice. **B. Histology of heart tissue.** Mean age 6 months ♂ (wild type, *Bscl2*$^{+/Celia}$, *Bscl2*$^{Celia/Celia}$, *Bscl2*$^{+/-}$, S.A. *Bscl2*$^{+/Celia}$) except for S.A. *Bscl2*$^{Celia/Celia}$ ♂ (9.3-months-old) mice. *Bscl2*$^{-/-}$♂ animal (7-months-old) with signs of fibrosis and perivascular granulomatous inflammation. H&E; scale bar: 20 µm. **C. Heart weight comparison in terms of percentage.** Wild type, n= 21 ♀ and 12 ♂; *Bscl2*$^{+/Celia}$, n= 26 ♀ and 17 ♂; *Bscl2*$^{Celia/Celia}$, n= 13 ♀ and 10 ♂; *Bscl2*$^{+/-}$, n= 23 ♀ and 23 ♂; *Bscl2*$^{-/-}$, n= 10 ♀ and 14 ♂ and severely affected animals (S.A), n= 2 *Bscl2*$^{+/Celia}$ and n= 2 *Bscl2*$^{Celia/Celia}$. Mean age 9.5-months-old for all genotypes, except 6.1-months-old for those S.A *Bscl2*$^{+/Celia}$. Data is presented as n (%) ± SD. Data were analysed using a Kolmogorov-Smirnov test for normality, followed by an ANOVA test with T3 Dunnett post hoc or Bonferroni post hoc when analysed by sexes. ^{a} $p < 0.05$ vs wild type ♀/♂; ^{d} $p < 0.05$ vs *Bscl2*$^{+/-}$ ♀/♂; ^{j} $p < 0.05$ vs *Bscl2*$^{+/Celia}$ ♀/♂; ^{k} $p < 0.05$ vs *Bscl2*$^{+/Celia}$.

The histological examination of the heart did not reveal any significant differences between genotypes, mouse models, or the S.A. animals (**Figure 55B** and **Table 16**). The potential presence of hypertrophy was assessed through the evolution of inflammation, fibrosis, and nuclear enlargement, but these assessments were challenging in some cases due to the presence of artifacts.

Additionally, the thickness of the right and left ventricles, as well as the interventricular septum, was measured. However, it was not possible to determine these parameters in all cases, as the tissue sections were not consistently in the coronal plane.

Inflammation and focal fibrosis were only observed in one *Bscl2*$^{-/-}$ animal, and it was characterized as granulomatous (with some multinucleated giant cells) and perivascular in nature (**Figure 55B**). This finding was considered an isolated case.

Table 16. Assessment of hypertrophy in the heart tissue. Nuclear enlargement, inflammation, fibrosis and left and right ventricle and septum thickness (μm) of wild type, *Bscl2*$^{+/Celia}$, *Bscl2*$^{Celia/Celia}$, *Bscl2*$^{+/-}$, *Bscl2*$^{-/-}$ and severely affected animals (S.A).

	Sex	Age (months)	Nuclear enlargement	Artifact	Inflammation	Fibrosis	Left ventricle thickness (μm)	Septum thickness (μm)	Right ventricle thickness (μm)
Wild type	♀	-	no	no	No	no	1836.09	1637.25	630.17
		-	no	yes	No	no	1372.68	1211.89	604.81
		9.4	yes	yes	No	no	-	-	-
		9.6	yes (interventricular septum)	yes	No	no	-	-	-
		6.6	yes	yes	No	no	-	-	-
	♂	9.4	no	no	No	no	-	-	-
		9.5	no	yes	No	no	-	-	-
Bscl2$^{+/Celia}$	♀	5.4	no	yes	No	no	-	-	-
		5.4	yes	yes	No	no	-	-	-
		8	no	yes	No	no	-	-	-
		9.6	yes	no	No	no	-	-	-
		9.6	occasional	yes	No	yes	1603.44	-	-
	♂	5.8	yes	yes	No	no	-	-	-
		7.4	no	yes	No	no	-	-	-
		9.6	yes	yes	No	no	-	-	-
		9.6	no	no	No	no	-	-	-
Bscl2$^{Celia/Celia}$	♀	3.6	yes	yes	No	no	1390.47	1227.13	-
		4.2	no	yes	No	no	1319.81	930.97	-
		9.4	yes	yes	no	no	1268.74	-	-
		9.4	yes	yes	no	no	-	-	-
	♂	8.3	yes	yes	no	no	1965.05	1613.42	-
		9.6	occasional	yes	no	no	-	-	-
Bscl2$^{+/-}$	♀	9.3	no	no	no	no	-	-	-
		9.6	occasional	no	no	no	-	-	-
	♂	9.4	no	no	no	no	-	-	-
		9.6	yes	no	no	no	-	-	-
Bscl2$^{-/-}$	♀	9.4	yes	no	no	no	-	-	-
		9.6	yes	no	no	no	-	-	-
		9.4	occasional	no	yes (perivascular granulomatous)	yes	-	-	-
	♂	9.6	yes	no	yes	yes (interventricular septum)	1549.95	892	1209.9
S.A. *Bscl2*$^{+/Celia}$	♀	6.8	no	no	no	no	-	-	-
	♂	8.6	yes	yes	no	no	-	-	-
S.A. *Bscl2*$^{Celia/Celia}$	♀	4.6	yes	no	no	no	2484.49	-	1331.86
		9.4	yes	no	no	no	-	-	-

4.4.4 Spleen

A macroscopic analysis of the spleen was performed (**Figure 56**). The results showed that the spleen weight was significantly greater in homozygous animals compared to wild type, heterozygous, and S.A. *Bscl2*$^{+/Celia}$ mice. The S.A. *Bscl2*$^{Celia/Celia}$ animals exhibited a similar spleen weight pattern to the S.A. *Bscl2*$^{+/Celia}$, wild type, and non-S.A. heterozygotes (*Bscl2*$^{+/Celia}$ and *Bscl2*$^{+/-}$) mice, although the differences were not statistically significant.

Additionally, a difference in spleen weight was observed between *Bscl2*$^{Celia/Celia}$ and *Bscl2*$^{-/-}$ mice, with the *Bscl2*$^{Celia/Celia}$ animals having a higher spleen weight. When the analysis was conducted considering the sex of the animals, it was found that the *Bscl2*$^{-/-}$ males had a lower spleen weight compared to *Bscl2*$^{Celia/Celia}$ males and females. Furthermore, in the case of wild type and KO mice, females exhibited a greater spleen weight compared to males. However, no sex-based differences were observed in the KI mice (**Figure 56B**).

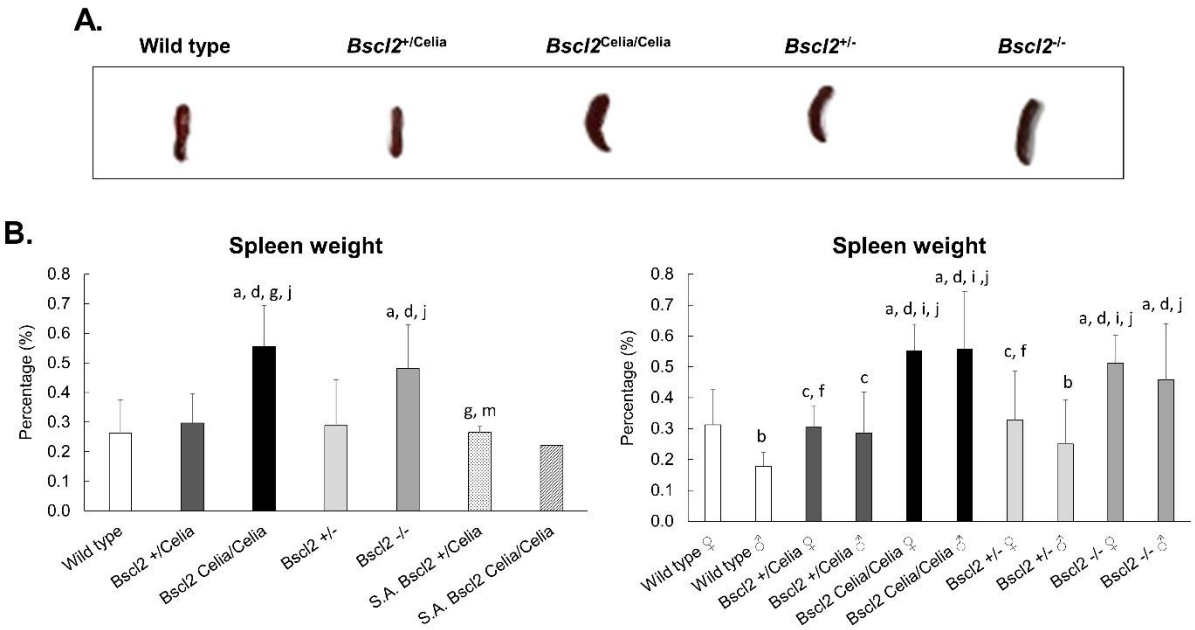

Figure 56. Analysis of the spleen tissue. A. Spleen macroscopic appearances. 7.2-months-old *Bscl2*$^{+/-}$and *Bscl2*$^{-/-}$; 6.8-months-old wild type and *Bscl2*$^{+/Celia}$ and 5.3-months-old *Bscl2*$^{Celia/Celia}$ ♂ mice. **B. Spleen weight comparison in terms of percentage.** Wild type, n= 21 ♀ and 12 ♂; *Bscl2*$^{+/Celia}$, n= 26 ♀ and 17 ♂; *Bscl2*$^{Celia/Celia}$, n= 13 ♀ and 10 ♂; *Bscl2*$^{+/-}$, n= 23 ♀ and 23 ♂; *Bscl2*$^{-/-}$, n= 10 ♀ and 14 ♂ and severely affected animals (S.A), n= 2 *Bscl2*$^{+/Celia}$ and n= 1 *Bscl2*$^{Celia/Celia}$. Mean age 9.5-months-old for all genotypes, except 6.1-months-old for those S.A *Bscl2*$^{+/Celia}$. Data is presented as n (%) ± SD. Data were analysed using a Kolmogorov-Smirnov test for normality, followed by a Kruskal-Wallis test with Mann-Whitney post hoc comparisons. [a] $p < 0.05$ vs wild type ♀/♂; [b] $p < 0.05$ vs wild type ♀; [c] $p < 0.05$ vs wild type ♂; [d] $p < 0.05$ vs *Bscl2*$^{+/-}$ ♀/♂; [f] $p < 0.05$ vs *Bscl2*$^{+/-}$ ♂; [g] $p < 0.05$ vs *Bscl2*$^{-/-}$ ♀/♂; [i] $p < 0.05$ vs *Bscl2*$^{-/-}$ ♂; [j] $p < 0.05$ vs *Bscl2*$^{+/Celia}$ ♀/♂; [m] $p < 0.05$ vs *Bscl2*$^{Celia/Celia}$ ♀/♂.

4.4.5 Kidneys

The macroscopic study of the kidneys showed a larger size (**Figure 57A**) and greater weight (**Figure 57B**) in both KI and KO homozygous mice compared to heterozygous and wild type mice. This weight increase was also observed in the S.A. *Bscl2*$^{+/Celia}$ animals, but in the case of the S.A. *Bscl2*$^{Celia/Celia}$, although there was a trend of increase, statistically significant differences were not shown. When delving into the analysis by sex, it was found that heterozygous male animals, KI and KO, exhibited greater kidney weight compared to heterozygous females. However, this sex difference was not observed in the case of homozygous mice. Instead, a greater weight of *Bscl2*$^{Celia/Celia}$ males compared to *Bscl2*$^{-/-}$ females was observed.

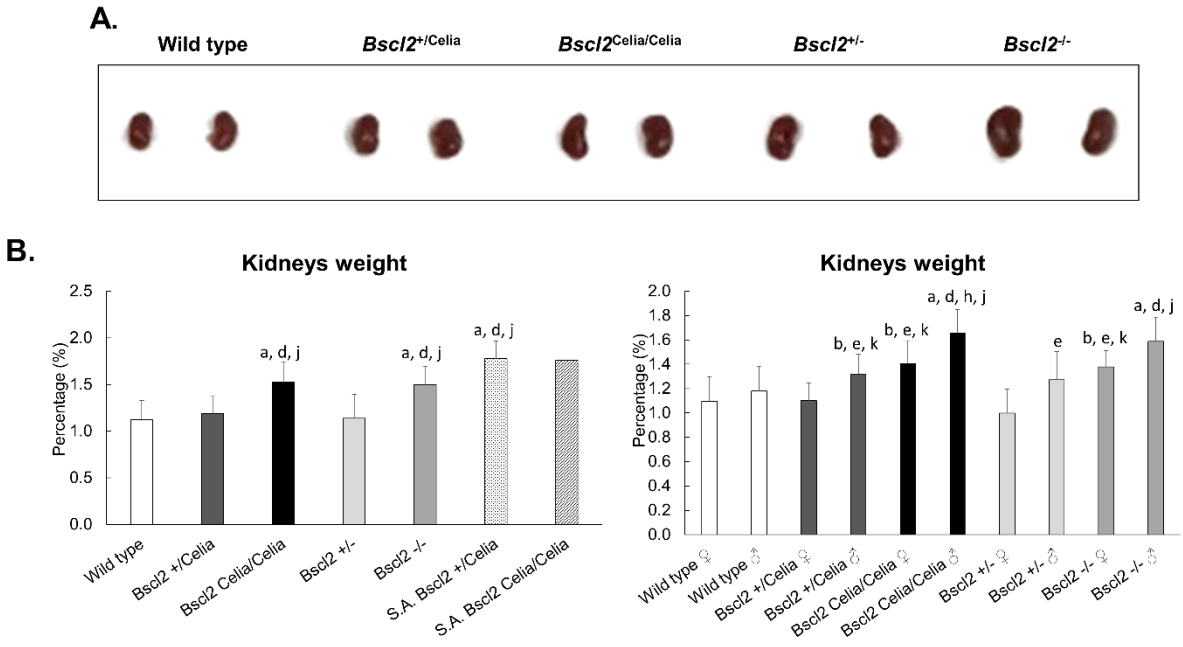

Figure 57. Analysis of the kidneys tissue. A. Kidneys macroscopic appearances. 7.2-months-old *Bscl2*$^{+/-}$and *Bscl2*$^{-/-}$; 6.8-months-old wild type and *Bscl2*$^{+/Celia}$ and 5.3-months-old *Bscl2*$^{Celia/Celia}$ ♂ mice. **B. Kidneys weight comparison in terms of percentage.** Wild type, n= 21 ♀ and 12 ♂; *Bscl2*$^{+/Celia}$, n= 26 ♀ and 17 ♂; *Bscl2*$^{Celia/Celia}$, n= 13 ♀ and 10 ♂; *Bscl2*$^{+/-}$, n= 23 ♀ and 23 ♂; *Bscl2*$^{-/-}$, n= 10 ♀ and 14 ♂ and severely affected animals (S.A), n= 2 *Bscl2*$^{+/Celia}$ ♀/♂ and n= 1 *Bscl2*$^{Celia/Celia}$ ♀/♂. Mean age 9.5-months-old for all genotypes, except 6.1-months-old for those S.A *Bscl2*$^{+/Celia}$. Data is presented as n (%) ± SD. Data were analysed using a Kolmogorov-Smirnov test for normality, followed by an ANOVA with Bonferroni post hoc comparisons. [a] $p < 0.05$ vs wild type ♀/♂; [b] $p < 0.05$ vs wild type ♀; [d] $p < 0.05$ vs *Bscl2*$^{+/-}$ ♀/♂; [e] $p < 0.05$ vs *Bscl2*$^{+/-}$ ♀; [h] $p < 0.05$ vs *Bscl2*$^{-/-}$ ♀; [j] $p < 0.05$ vs *Bscl2*$^{+/Celia}$ ♀/♂; [k] $p < 0.05$ vs *Bscl2*$^{+/Celia}$ ♀.

The renal histopathological study revealed a pattern of diffuse mesangial damage in the glomeruli, as well as arteriolar hyalinization in the blood vessels of those homozygous mice, both KI and KO (**Figure 58,** see **Annex 10**). This pattern of damage, when considering the sex of the animals, seems to only occur in *Bscl2*$^{-/-}$ mice, with no differences found between males and females. Additionally, *Bscl2*$^{Celia/Celia}$ mice, specifically *Bscl2*$^{Celia/Celia}$ males, exhibit inflammation in the renal interstitium, ranging from a mild to severe pattern (see **Annex 10**). On the other hand, *Bscl2*$^{Celia/Celia}$ females show 100% of animals with focal damage in the

glomerulus, as opposed to 17% in *Bscl2*$^{+/-}$ females. However, these focal lesions are highly variable, and the percentage of animals affected, despite appearing higher than in other genotypes, does not show statistical significance (see **Annex 10**). The S.A. animals (*Bscl2*$^{+/Celia}$ and *Bscl2*$^{Celia/Celia}$) displayed a mesangial diffuse pattern similar to that of those homozygous animals, although perhaps less significant in some analyses due to the smaller number of animals used (**Figure 58,** see **Annex 10**).

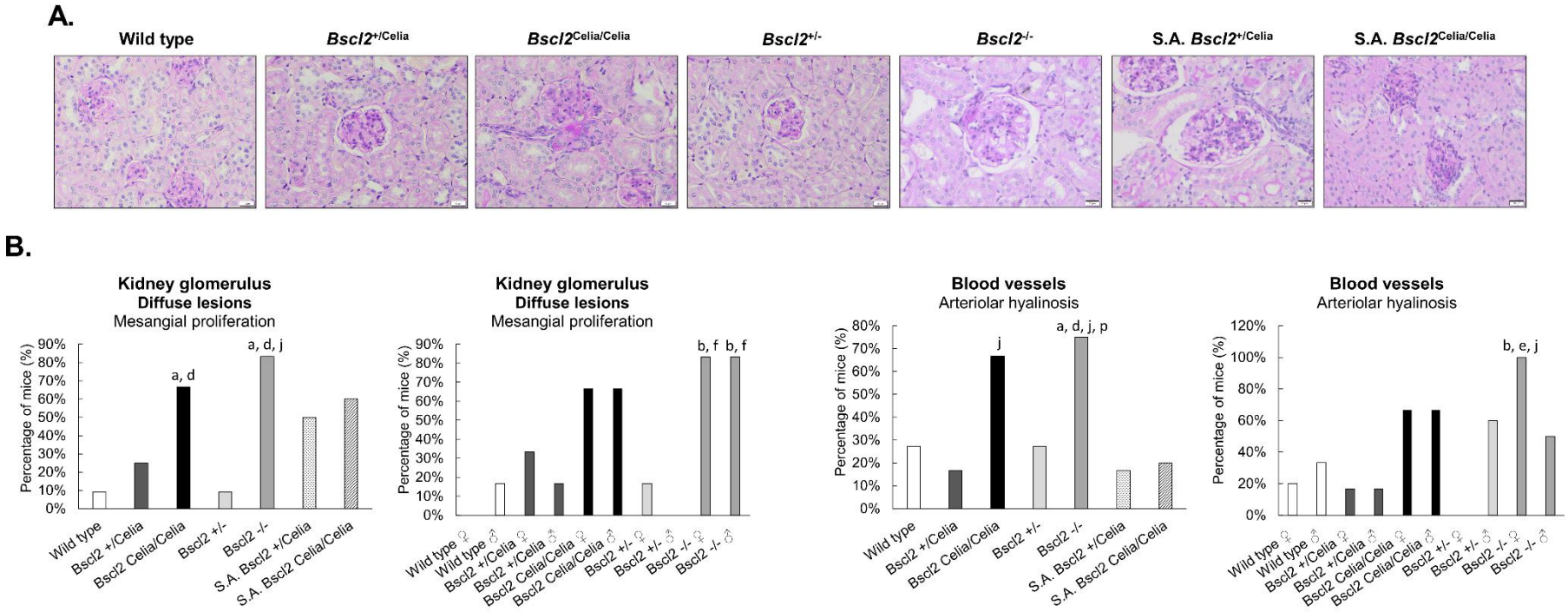

Figure 58. Histological analysis of the kidneys tissue. A. Histology images of kidney tissue. Mean age 9.5 months (wild type ♀, *Bscl2*$^{+/Celia}$ ♀, *Bscl2*$^{Celia/Celia}$ ♂, *Bscl2*$^{+/-}$ ♂, *Bscl2*$^{-/-}$♂) except for S.A. *Bscl2*$^{+/Celia}$ ♀ (3.6-months-old) and S.A. *Bscl2*$^{Celia/Celia}$ ♀ (8-months-old) mice. PAS; scale bar: 10 µm. **B. Renal histopathological evaluation.** Wild type, n= 5 ♀ and 6 ♂; *Bscl2*$^{+/Celia}$, n= 6 ♀ and 6 ♂; *Bscl2*$^{Celia/Celia}$, n= 6 ♀ and 6 ♂; *Bscl2*$^{+/-}$, n= 6 ♀ and 5 ♂; *Bscl2*$^{-/-}$, n= 6 ♀ and 6 ♂ and severely affected animals (S.A), n= 6 *Bscl2*$^{+/Celia}$ ♀/♂ and n= 5 *Bscl2*$^{Celia/Celia}$ ♀/♂. Mean age 9.5-months-old for all genotypes, except 6.1-months-old for those S.A *Bscl2*$^{+/Celia}$. Data is presented as n (%). Statistical significance for categorical data was assessed using Fisher's exact test. [a] $p < 0.05$ vs wild type ♀/♂; [b] $p < 0.05$ vs wild type ♀; [d] $p < 0.05$ vs *Bscl2*$^{+/-}$ ♀/♂; [e] $p < 0.05$ vs *Bscl2*$^{+/-}$ ♀; [f] $p < 0.05$ vs *Bscl2*$^{+/-}$ ♂; [j] $p < 0.05$ vs *Bscl2*$^{+/Celia}$ ♀/♂; [p] $p < 0.05$ vs S.A. *Bscl2*$^{+/Celia}$ ♀/♂.

4.4.6 Eyeball

The presence of cataracts was observed in some mice of both murine models, with a higher incidence in older animals. To assess possible ocular damage, a histological study of the left eyeball was performed (**Figure 59**). The retinal layers showed a normal pattern in all mice analysed (**Figure 59A**), including the ganglion cell layer (GCL, containing ganglion cell nuclei), the inner plexiform layer (IPL, containing dendritic and axonal connections), the inner nuclear layer (INL, containing nuclei of amacrine, bipolar, and horizontal cells), the outer plexiform layer (OPL, containing dendritic and axonal connections), the outer nuclear layer (ONL, containing photoreceptor nuclei), and the outer segment layer of the photoreceptors (OS) (**Figure 59B**). The retinal pigment epithelium (RPE) layer was not visible in some of the sections, likely due to detachment from the retina, which can commonly occur during the processing of the tissue samples.

A.

Genotype	Sex	Age (months)	Retina analysis
Wild type	♀	9.5	Normal
Wild type	♂	9.5	Normal
Bscl2$^{Celia/Celia}$	♀	9.6	Normal
Bscl2$^{Celia/Celia}$	♂	9.4	Normal
Bscl2$^{+/-}$	♂	9.4	Normal
Bscl2$^{-/-}$	♀	9.4	Normal
Bscl2$^{-/-}$	♂	9.5	Normal
S.A. Bscl2$^{+/Celia}$	♀	6.8	Normal

B.

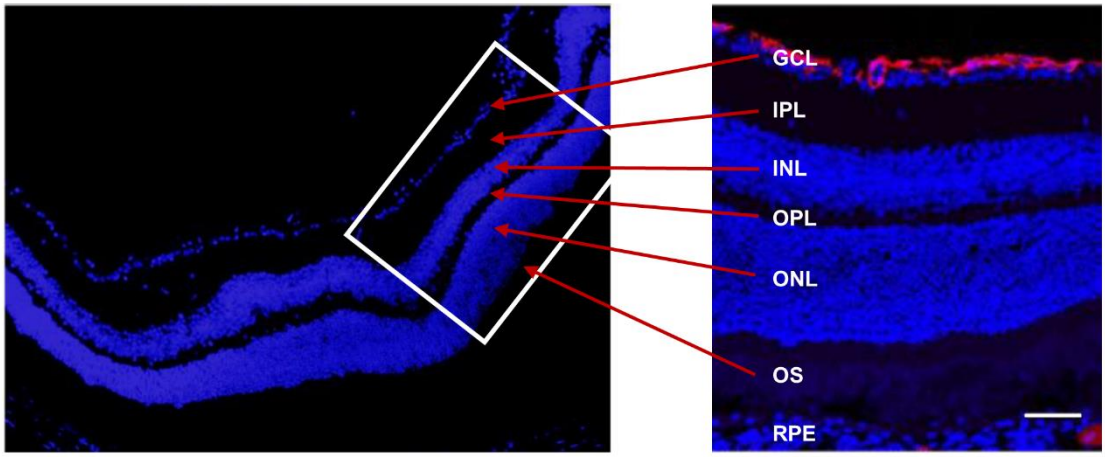

Figure 59. Analysis of the eyeball tissue. A. Animals used in the study. Genotype, sex, age in months, and final assessment of the retina analysis. **B. Histological comparison of the retina of a *Bscl2*$^{Celia/Celia}$ mouse with a wild type mouse.** Ganglion cell layer (GCL); internal plexiform layer (IPL); inner nuclear layer (INL); outer plexiform layer (OPL); outer nuclear layer (ONL); outer segment (OS) and retinal pigment epithelium (RPE). DAPI.

4.5 Glucose Metabolism and Animal Weight Loss

Glucose metabolism was examined in fasting wild type, KO and, KI animals. This fasting state was also used to evaluate the percentage of weight loss, which was greater in all genotypes at an early age until stabilizing in adulthood.

Homozygous mice, *Bscl2*$^{Celia/Celia}$ and *Bscl2*$^{-/-}$, showed more pronounced weight reduction over the different months (12-21%) compared to other genotypes (9-15%) (**Figure 60,** see **Annex 8**). No differences in weight loss were found between sexes or murine models.

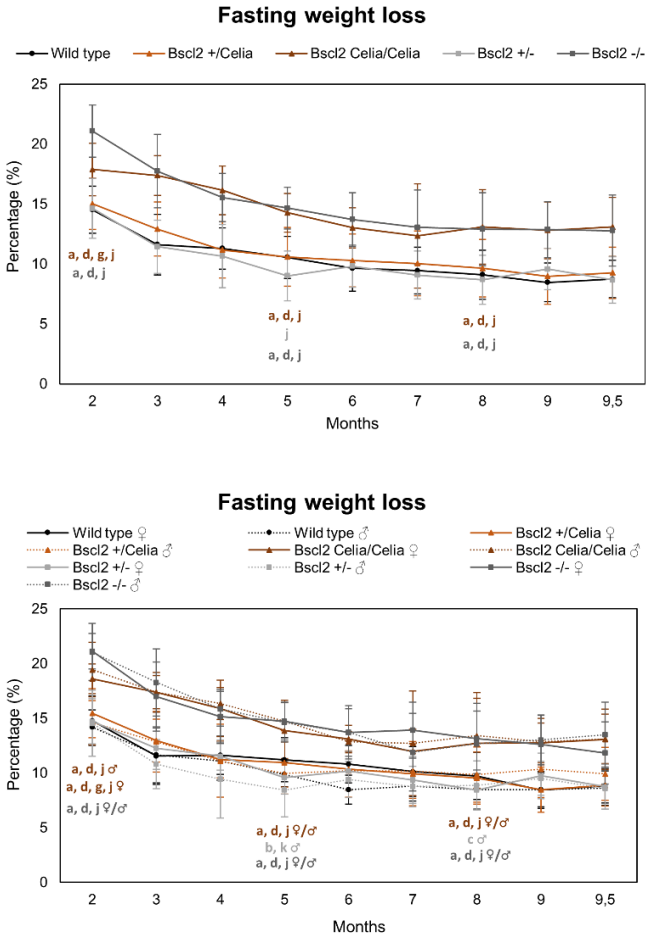

Figure 60. Fasting weight loss for wild type, *Bscl2*$^{+/Celia}$, *Bscl2*$^{Celia/Celia}$, *Bscl2*$^{+/-}$ and *Bscl2*$^{-/-}$ animals. For mean age and number of animals per genotype see **Annex 8**. Data is presented as n (%) ± SD. Data were analysed using a Kolmogorov-Smirnov test for normality, followed by a Kruskal-Wallis test with Mann-Whitney post hoc comparisons. [a] $p < 0.05$ vs wild type ♀/♂; [b] $p < 0.05$ vs wild type ♀; [c] $p < 0.05$ vs wild type ♂; [d] $p < 0.05$ vs *Bscl2*$^{+/-}$ ♀/♂; [g] $p < 0.05$ vs *Bscl2*$^{-/-}$ ♀/♂; [j] $p < 0.05$ vs *Bscl2*$^{+/Celia}$ ♀/♂; [k] $p < 0.05$ vs *Bscl2*$^{+/Celia}$.

To assess glucose metabolism, basal glucose levels were monitored throughout the lifespan of the animals. The wild type and heterozygous animals exhibited relatively linear glucose values over their lifetime. In contrast, the homozygous mice showed a significantly higher glucose values, which decreased and eventually reached the same level as the wild type and heterozygous mice in later adulthood (**Figure 61,** see **Annex 8**). No differences in basal glucose levels were found between the murine models or between sexes.

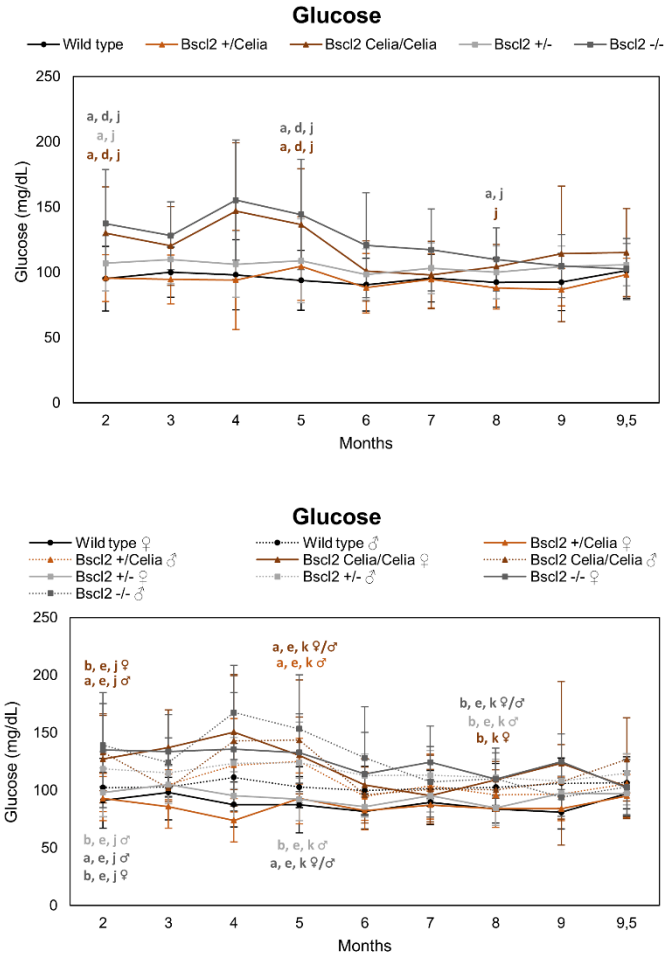

Figure 61. Basal glucose for wild type, *Bscl2*$^{+/Celia}$, *Bscl2*$^{Celia/Celia}$, *Bscl2*$^{+/-}$ and *Bscl2*$^{-/-}$ animals. For mean age and number of animals per genotype see **Annex 8**. Data is presented as mean ± SD. Data were analysed using a Kolmogorov-Smirnov test for normality, followed by a Kruskal-Wallis test with Mann-Whitney post hoc comparisons. [a] $p < 0.05$ vs wild type ♀/♂; [b] $p < 0.05$ vs wild type ♀; [d] $p < 0.05$ vs *Bscl2*$^{+/-}$ ♀/♂; [e] $p < 0.05$ vs *Bscl2*$^{+/-}$ ♀; [j] $p < 0.05$ vs *Bscl2*$^{+/Celia}$ ♀/♂; [k] $p < 0.05$ vs *Bscl2*$^{+/Celia}$.

Glucose tolerance and insulin resistance were evaluated in the animals at 3 and 3.5 months of age. The GTT showed no impairment of glucose metabolism in *Bscl2*$^{Celia/Celia}$ and *Bscl2*$^{-/-}$ animals, displaying a similar pattern across all genotypes. However, the ITT revealed that these homozygous animals had reduced insulin sensitivity compared to both wild type and heterozygous animals (**Figure 62** and **Figure 63,** see **Annex 11**). Specifically, *Bscl2*$^{-/-}$ males presented lower values in the ITT than *Bscl2*$^{Celia/Celia}$ males and females (**Figure 63**). No differences were found between homozygous males and females in both the GTT and ITT. However, in the case of wild type and heterozygous animals, males exhibited greater insulin resistance and an impaired glucose response compared to females (**Figure 62** and **Figure 63**). The S.A. animals could not be tested due to their physical condition.

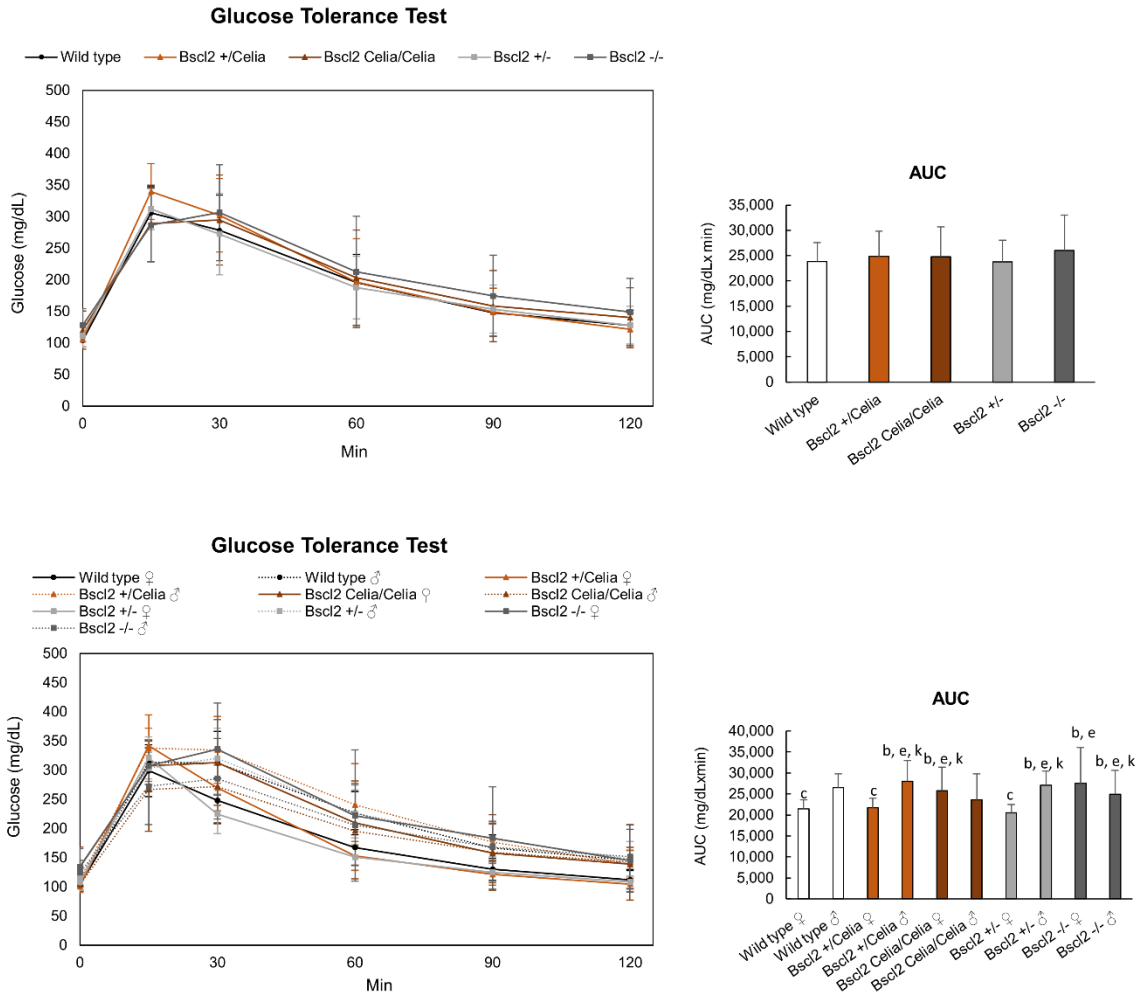

Figure 62. Glucose tolerance (GTT) test for wild type, *Bscl2*$^{+/Celia}$, *Bscl2*$^{Celia/Celia}$, *Bscl2*$^{+/-}$ and *Bscl2*$^{-/-}$ animals. Wild type, n= 23 (12 ♀ and 11 ♂); *Bscl2*$^{+/Celia}$, n= 20 (10 ♀ and 10 ♂); *Bscl2*$^{Celia/Celia}$, n= 29 (16 ♀ and 13 ♂); *Bscl2*$^{+/-}$, n= 24 (12 ♀ and 12 ♂) and *Bscl2*$^{-/-}$, n= 24 (10 ♀ and 14 ♂) animals. Mean age 3.2-months-old. GTT was measure as evolution of glucose concentration over time and area under the curve (AUC). Data is presented as mean ± SD. Data were analysed using a Kolmogorov-Smirnov test for normality, followed by a Kruskal-Wallis test with Mann-Whitney post hoc comparisons. ^{b} $p < 0.05$ vs wild type ♀; ^{c} $p < 0.05$ vs wild type ♂; ^{e} $p < 0.05$ vs *Bscl2*$^{+/-}$ ♀; ^{k} $p < 0.05$ vs *Bscl2*$^{+/Celia}$ ♀.

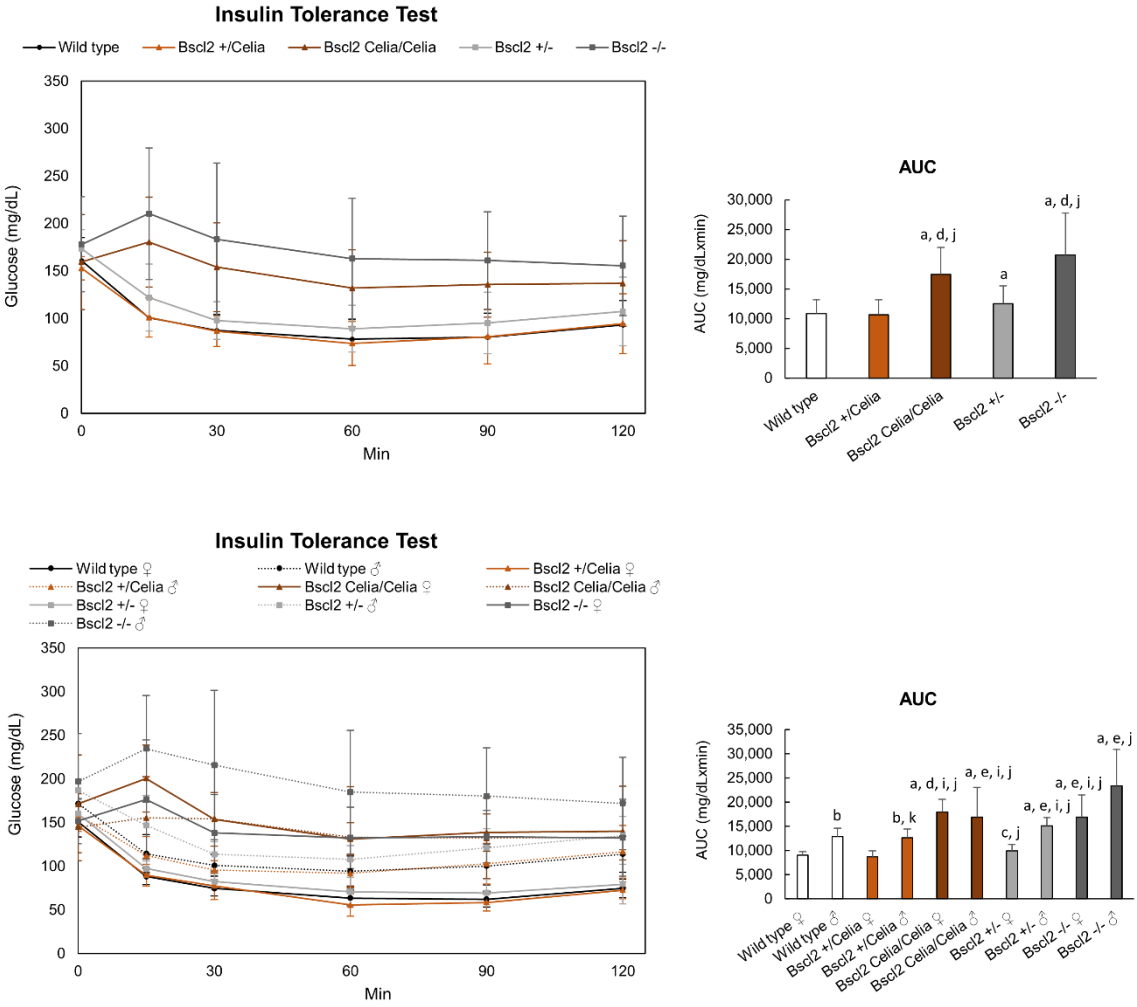

Figure 63. Insulin tolerance test (ITT) for wild type, *Bscl2*$^{+/Celia}$, *Bscl2*$^{Celia/Celia}$, *Bscl2*$^{+/-}$ and *Bscl2*$^{-/-}$ animals. Wild type, n= 23 (12 ♀ and 11 ♂); *Bscl2*$^{+/Celia}$, n= 20 (10 ♀ and 10 ♂); *Bscl2*$^{Celia/Celia}$, n= 29 (16 ♀ and 13 ♂); *Bscl2*$^{+/-}$, n= 24 (12 ♀ and 12 ♂) and *Bscl2*$^{-/-}$, n= 24 (10 ♀ and 14 ♂) animals. Mean age 3.2-months-old. ITT was measure as evolution of glucose concentration over time and area under the curve (AUC). Data is presented as mean ± SD. Data were analysed using a Kolmogorov-Smirnov test for normality, followed by a Kruskal-Wallis test with Mann-Whitney post hoc comparisons. [a] $p < 0.05$ vs wild type ♀/♂; [b] $p < 0.05$ vs wild type ♀; [c] $p < 0.05$ vs wild type ♂; [d] $p < 0.05$ vs *Bscl2*$^{+/-}$ ♀/♂; [e] $p < 0.05$ vs *Bscl2*$^{+/-}$ ♀; [i] $p < 0.05$ vs *Bscl2*$^{-/-}$ ♂; [j] $p < 0.05$ vs *Bscl2*$^{+/Celia}$ ♀/♂; [k] $p < 0.05$ vs *Bscl2*$^{+/Celia}$ ♀.

To further characterized the metabolic profile, the concentrations of insulin and leptin in the serum were evaluated. In this case, it was possible to include a small group of S.A. animals.

The homozygous animals showed severe hyperinsulinemia (**Figure 64B**) and hypoleptinemia (**Figure 64A**). No differences were found between the murine models or between sexes. For the S.A. mice, the metabolic pattern was altered. Despite exhibiting hypoleptinemia (**Figure 64A**), they did not display hyperinsulinemia (**Figure 64B**). However, a trend of increased insulin levels was observed, although it was not statistically significant, potentially due to the small number of animals in this group.

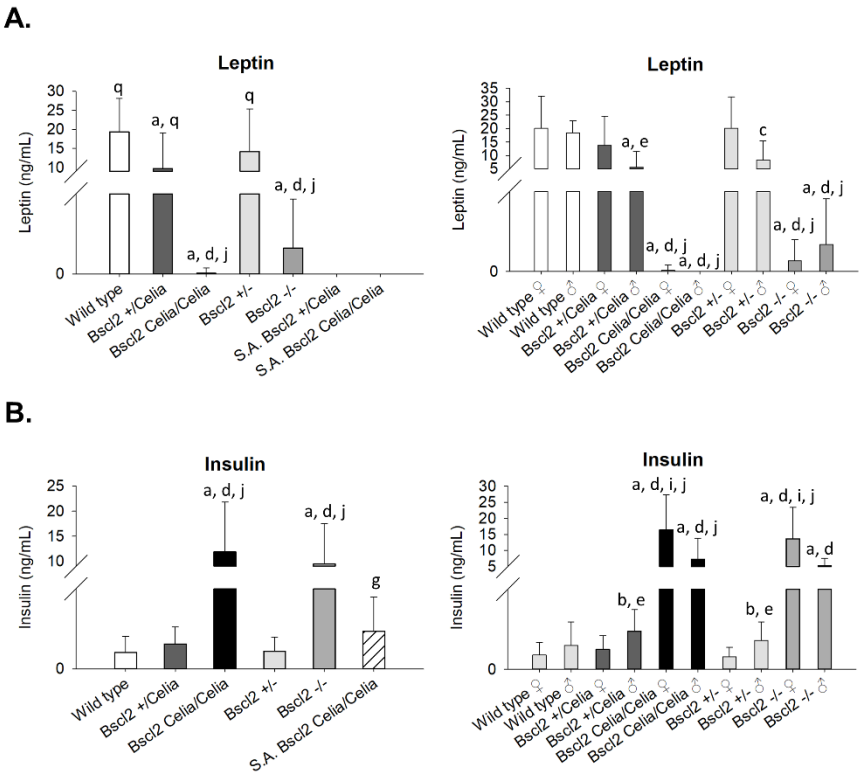

Figure 64. Leptin and insulin concentration for wild type, *Bscl2*$^{+/Celia}$, *Bscl2*$^{Celia/Celia}$, *Bscl2*$^{+/-}$; *Bscl2*$^{-/-}$ and severely affected (S.A.) animals. A. Leptin concentration. Wild type, *Bscl2*$^{+/Celia}$, *Bscl2*$^{Celia/Celia}$ and *Bscl2*$^{+/-}$, n= 16 (8 ♀ and 8 ♂); S.A *Bscl2*$^{+/Celia}$, n= 1 (6.8-months-old) and S.A *Bscl2*$^{Celia/Celia}$, n= 2 animals. Mean age 9.5-months-old. **B. Insulin concentration.** Wild type, *Bscl2*$^{+/Celia}$, *Bscl2*$^{Celia/Celia}$ and *Bscl2*$^{+/-}$, n= 18 (9 ♀ and 9 ♂) and S.A *Bscl2*$^{Celia/Celia}$, n= 2 animals. Mean age 9.5-months-old. Data is presented as mean ± SD. Data were analysed using a Kolmogorov-Smirnov test for normality, followed by a Kruskal-Wallis test with Mann-Whitney post hoc comparisons. [a] $p < 0.05$ vs wild type ♀/♂; [b] $p < 0.05$ vs wild type ♀; [c] $p < 0.05$ vs wild type ♂; [d] $p < 0.05$ vs *Bscl2*$^{+/-}$ ♀/♂; [e] $p < 0.05$ vs *Bscl2*$^{+/-}$ ♀; [g] $p < 0.05$ vs *Bscl2*$^{-/-}$ ♀/♂; [i] $p < 0.05$ vs *Bscl2*$^{-/-}$ ♂; [j] $p < 0.05$ vs *Bscl2*$^{+/Celia}$ ♀/♂.

4.6 TRIGLYCERIDES LEVELS

The homozygous mice used in the present study exhibited significantly lower serum triglycerides levels compared to wild type and heterozygous animals at 4 months of age (**Figure 65A**). However, no differences among genotypes were found at 9.5 months (**Figure 65B**). Interestingly, the homozygous animals showed an increase in triglycerides concentration of up to 3 times from 4 to 9.5 months, whereas this increase was not observed in the other genotypes (**Figure 65C**). No differences were found between sexes or murine models.

In contrast, the S.A. mice did not display an increase in serum triglyceride concentration over time, as was the case with the homozygotes (**Figure 65C**). Instead, the S.A. animals showed similar triglyceride levels to the wild type and heterozygous animals (**Figure 65A-B**).

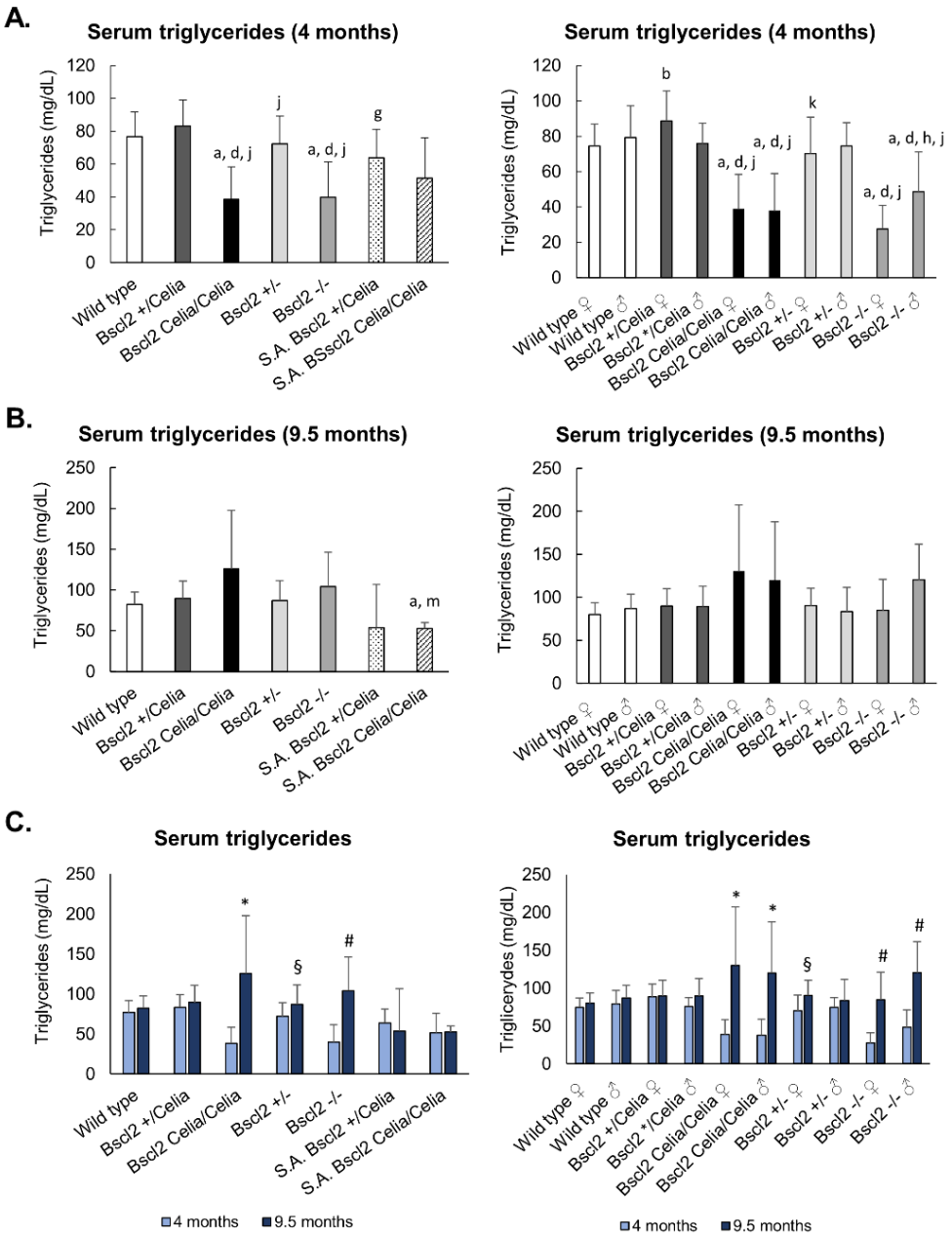

Figure 65. Serum triglycerides concentration for wild type, *Bscl2*$^{+/Celia}$, *Bscl2*$^{Celia/Celia}$, *Bscl2*$^{+/-}$, *Bscl2*$^{-/-}$ and severely affected (S.A.) animals. A. Serum triglycerides concentration at 4 months. Wild type, n= 21 (11 ♀ and 10 ♂); *Bscl2*$^{+/Celia}$, n= 21 (12 ♀ and 9 ♂); *Bscl2*$^{Celia/Celia}$, n= 25 (15 ♀ and 10 ♂); *Bscl2*$^{+/-}$, n= 24 (12 ♀ and 12 ♂); *Bscl2*$^{-/-}$, n= 24 (10 ♀ and 14 ♂); S.A *Bscl2*$^{+/Celia}$, n= 4 and S.A *Bscl2*$^{Celia/Celia}$, n= 3 animals. ^{a} $p < 0.05$ vs wild type ♀/♂; ^{b} $p < 0.05$ vs wild type ♀; ^{d} $p < 0.05$ vs *Bscl2*$^{+/-}$ ♀/♂; ^{g} $p < 0.05$ vs *Bscl2*$^{-/-}$ ♀/♂; ^{h} $p < 0.05$ vs *Bscl2*$^{-/-}$ ♀; ^{j} $p < 0.05$ vs *Bscl2*$^{+/Celia}$ ♀/♂; ^{k} $p < 0.05$ vs *Bscl2*$^{+/Celia}$ ♀. **B. Serum triglycerides concentration at 9.5 months.** Wild type, n= 29 (19 ♀ and 10 ♂); *Bscl2*$^{+/Celia}$, n= 36 (23 ♀ and 13 ♂); *Bscl2*$^{Celia/Celia}$, n= 23 (13 ♀ and 10 ♂); *Bscl2*$^{+/-}$, n= 36 (18 ♀ and 18 ♂); *Bscl2*$^{-/-}$, n= 22 (10 ♀ and 12 ♂); S.A *Bscl2*$^{+/Celia}$, n= 2 and S.A *Bscl2*$^{Celia/Celia}$, n= 2 animals. ^{a} $p < 0.05$ vs wild type; ^{m} $p < 0.05$ vs *Bscl2*$^{Celia/Celia}$ ♀/♂. **C. Comparison between triglyceride concentration at 4 months vs 9.5 months.** * $p < 0.05$ vs *Bscl2*$^{Celia/Celia}$ ♀/♂ 4 months; $^{\$}$ $p < 0.05$ vs *Bscl2*$^{+/-}$ ♀/♂ 4 months; $^{\#}$ $p < 0.05$ vs *Bscl2*$^{-/-}$ ♀/♂ 4 months. Data is presented as mean ± SD. Data were analysed using a Kolmogorov-Smirnov test for normality, followed by a Kruskal-Wallis test with Mann-Whitney post hoc comparisons.

The analysis of triglyceride concentration in the liver of the homozygous animals, *Bscl2*$^{Celia/Celia}$ and *Bscl2*$^{-/-}$, showed a significant accumulation of triglycerides (**Figure 66**). This finding is consistent with the previously described presence of a fatty liver and a marked hepatic steatosis in these animals (see **section 4.4.2**). In contrast, despite the presence of mild steatosis in the S.A. mice (see **section 4.4.2**), the concentration of triglycerides in their liver was similar to that of wild type and heterozygous mice. No differences were found between males and females. However, a higher concentration of triglycerides was observed in the liver of male *Bscl2*$^{-/-}$ mice compared to male *Bscl2*$^{Celia/Celia}$ mice (**Figure 66**).

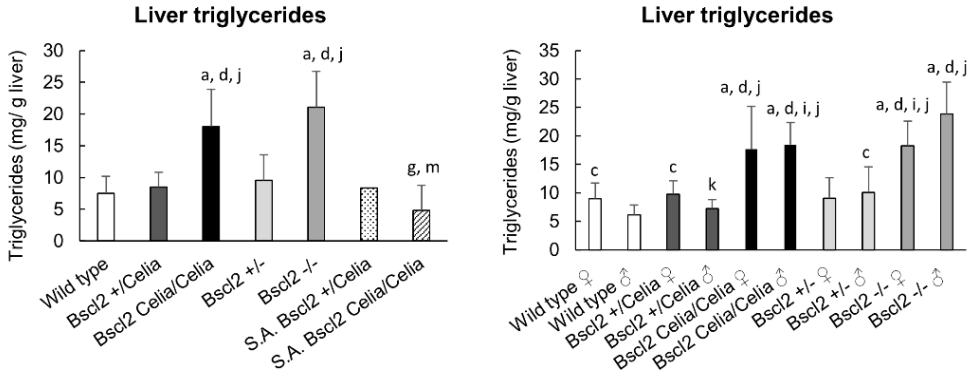

Figure 66. Liver triglycerides concentration for wild type, *Bscl2*$^{+/Celia}$, *Bscl2*$^{Celia/Celia}$, *Bscl2*$^{+/-}$, *Bscl2*$^{-/-}$ and severely affected (S.A.) animals. Wild type, *Bscl2*$^{+/Celia}$, *Bscl2*$^{Celia/Celia}$, *Bscl2*$^{+/-}$, n= 20 (10 ♀ and 10 ♂); S.A *Bscl2*$^{+/Celia}$, n= 1 and S.A *Bscl2*$^{Celia/Celia}$, n= 2 animals. Mean age 9.5-months-old. Data is presented as mean ± SD. Data were analysed using a Kolmogorov-Smirnov test for normality, followed by a Kruskal-Wallis test with Mann-Whitney post hoc comparisons. [a] $p < 0.05$ vs wild type ♀/♂; [c] $p < 0.05$ vs wild type ♂; [d] $p < 0.05$ vs *Bscl2*$^{+/-}$ ♀/♂; [g] $p < 0.05$ vs *Bscl2*$^{-/-}$ ♀/♂; [i] $p < 0.05$ vs *Bscl2*$^{-/-}$ ♂; [j] $p < 0.05$ vs *Bscl2*$^{+/Celia}$ ♀/♂; [k] $p < 0.05$ vs *Bscl2*$^{+/Celia}$ ♀; [m] $p < 0.05$ vs *Bscl2*$^{Celia/Celia}$ ♀/♂.

4.7 HEMATOLOGY AND BIOCHEMICAL PARAMETERS

To further characterize the murine models, both hematological and biochemical analyses were conducted.

The homozygous animals exhibited a higher concentration of white blood cells, specifically lymphocytes, while basophils and eosinophils were reduced in the case of *Bscl2*$^{Celia/Celia}$ mice. Notably, *Bscl2*$^{Celia/Celia}$ females presented lower eosinophil values than *Bscl2*$^{-/-}$ females. Additionally, the decrease in eosinophils was significantly more pronounced in homozygous males compared to homozygous females in both murine models (**Figure 67**). Regarding red blood cell indices, the homozygous mice showed larger cell size and quantity, as well as higher hemoglobin concentration. The latter was higher in *Bscl2*$^{-/-}$ females than in *Bscl2*$^{Celia/Celia}$ females (**Figure 68**). Furthermore, both homozygous murine models exhibited and elevated platelet volume with highly variable platelet size (**Figure 69**).

The S.A. homozygous animals presented similar hematological values to the non-S.A. homozygous mice (*Bscl2*$^{Celia/Celia}$ and *Bscl2*$^{-/-}$) (**Figure 67, Figure 68** and **Figure 69,** see **Annex 13**).

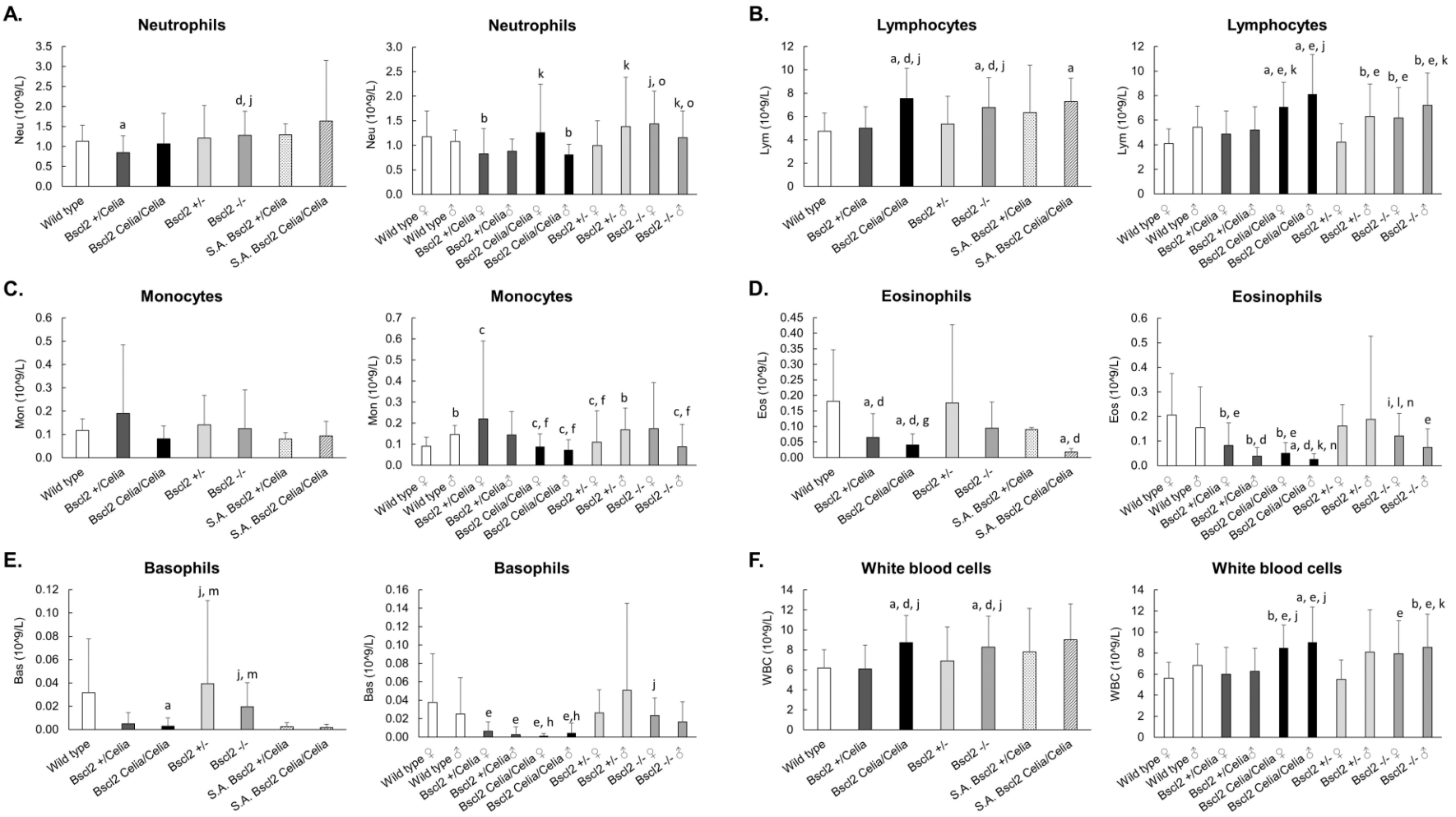

Figure 67. Hematological measurements for wild type, *Bscl2*$^{+/Celia}$, *Bscl2*$^{Celia/Celia}$, *Bscl2*$^{+/-}$, *Bscl2*$^{-/-}$ and severely affected (S.A.) animals. (**A**) Neutrophils, (**B**) lymphocytes, (**C**) monocytes, (**D**) eosinophils, (**E**) basophils and (**F**) white blood cells. For mean age and number of animals per genotype see **Annex 13**. Data is presented as mean ± SD. Data were analysed using a Kolmogorov-Smirnov test for normality, followed by a Kruskal-Wallis test with Mann-Whitney post hoc comparisons. [a] $p < 0.05$ vs wild type ♀/♂; [b] $p < 0.05$ vs wild type ♀; [c] $p < 0.05$ vs wild type ♂; [d] $p < 0.05$ vs *Bscl2*$^{+/-}$ ♀/♂; [e] $p < 0.05$ vs *Bscl2*$^{+/-}$ ♀; [f] $p < 0.05$ vs *Bscl2*$^{+/-}$ ♂; [g] $p < 0.05$ vs *Bscl2*$^{-/-}$ ♀/♂; [h] $p < 0.05$ vs *Bscl2*$^{-/-}$ ♀; [i] $p < 0.05$ vs *Bscl2*$^{-/-}$ ♂; [j] $p < 0.05$ vs *Bscl2*$^{+/Celia}$ ♀/♂; [k] $p < 0.05$ vs *Bscl2*$^{+/Celia}$ ♀; [l] $p < 0.05$ vs *Bscl2*$^{+/Celia}$ ♂; [m] $p < 0.05$ vs *Bscl2*$^{Celia/Celia}$ ♀/♂; [n] $p < 0.05$ vs *Bscl2*$^{Celia/Celia}$ ♀; [o] $p < 0.05$ vs *Bscl2*$^{Celia/Celia}$ ♂.

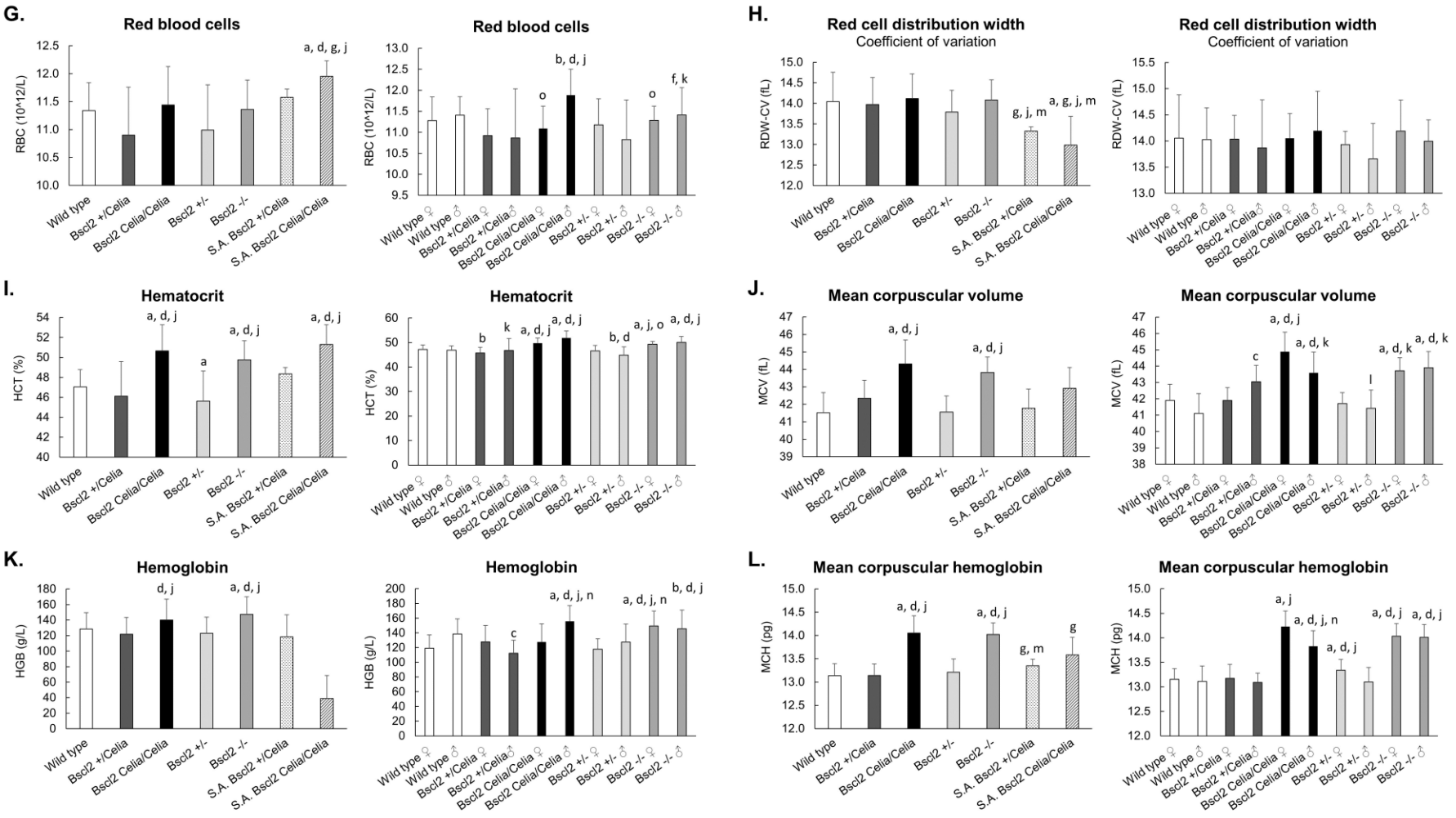

Figure 68. Hematological measurements for wild type, *Bscl2*$^{+/Celia}$, *Bscl2*$^{Celia/Celia}$, *Bscl2*$^{+/-}$, *Bscl2*$^{-/-}$ and severely affected (S.A.) animals. (**G**) Red blood cells, (**H**) red cell distribution width: coefficient variation, (**I**) hematocrit, (**J**) mean corpuscular volume, (**K**) hemoglobin and (**L**) mean corpuscular hemoglobin. For mean age and number of animals per genotype see **Annex 13**. Data is presented as mean ± SD or n (%) ± SD. Data were analysed using a Kolmogorov-Smirnov test for normality, followed by a Kruskal-Wallis test with Mann-Whitney post hoc comparisons. [a] $p < 0.05$ vs wild type ♀/♂; [b] $p < 0.05$ vs wild type ♀; [c] $p < 0.05$ vs wild type ♂; [d] $p < 0.05$ vs *Bscl2*$^{+/-}$ ♀/♂; [f] $p < 0.05$ vs *Bscl2*$^{+/-}$ ♂; [g] $p < 0.05$ vs *Bscl2*$^{-/-}$ ♀/♂; [j] $p < 0.05$ vs *Bscl2*$^{+/Celia}$ ♀/♂; [k] $p < 0.05$ vs *Bscl2*$^{+/Celia}$ ♀; [m] $p < 0.05$ vs *Bscl2*$^{Celia/Celia}$ ♀/♂; [n] $p < 0.05$ vs *Bscl2*$^{Celia/Celia}$ ♀; [o] $p < 0.05$ vs *Bscl2*$^{Celia/Celia}$ ♂.

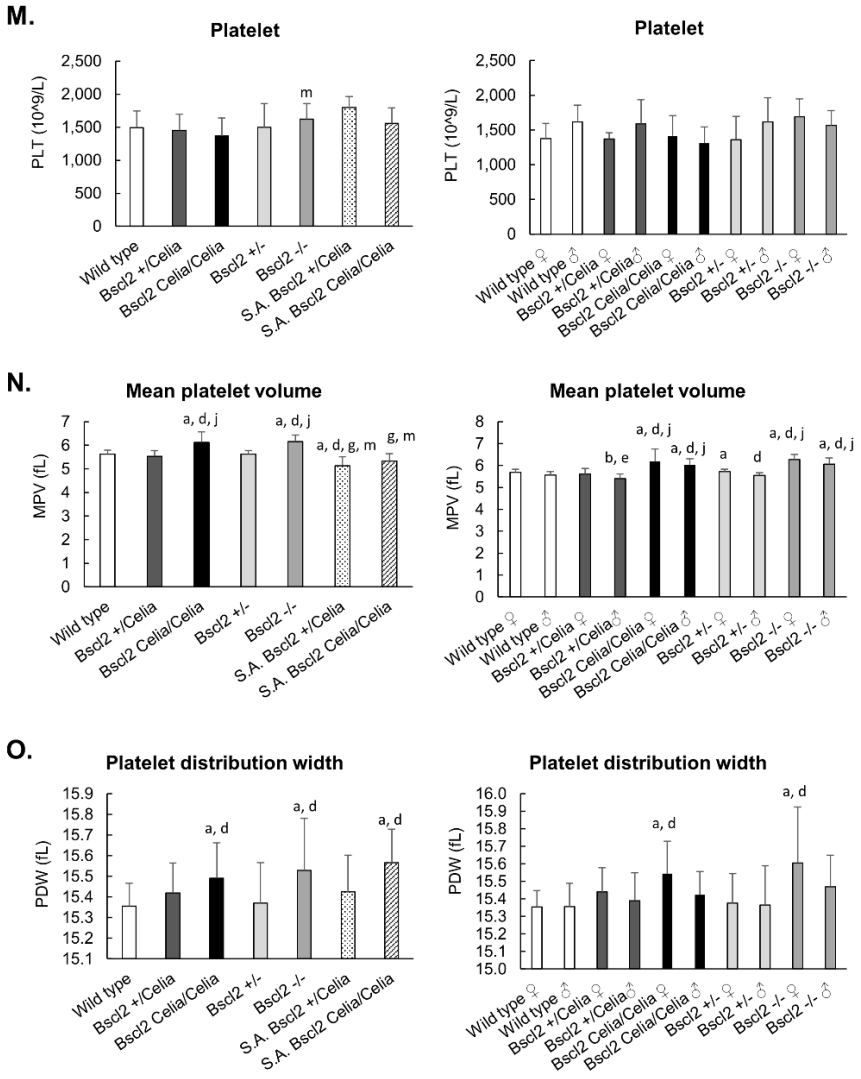

Figure 69. Hematological measurements for wild type, *Bscl2*$^{+/Celia}$, *Bscl2*$^{Celia/Celia}$, *Bscl2*$^{+/-}$, *Bscl2*$^{-/-}$ and severely affected (S.A.) animals. (**M**) Platelet, (**N**) mean platelet volume and (**O**) platelet distribution width. For mean age and number of animals per genotype see **Annex 13**. Data is presented as mean ± SD. Data were analysed using a Kolmogorov-Smirnov test for normality, followed by a Kruskal-Wallis test with Mann-Whitney post hoc comparisons. [a] $p < 0.05$ vs wild type ♀/♂; [b] $p < 0.05$ vs wild type ♀; [d] $p < 0.05$ vs *Bscl2*$^{+/-}$ ♀/♂; [e] $p < 0.05$ vs *Bscl2*$^{+/-}$ ♀; [g] $p < 0.05$ vs *Bscl2*$^{-/-}$ ♀/♂; [j] $p < 0.05$ vs *Bscl2*$^{+/Celia}$ ♀/♂; [m] $p < 0.05$ vs *Bscl2*$^{Celia/Celia}$.

No differences in creatinine values were observed between the genotypes. However, the homozygous mice exhibited significantly higher concentrations of alanine aminotransferase, alkaline phosphatase, and amylase compared to wild type and heterozygotes animals (**Figure 70**). Additionally, the homozygous animals showed elevated levels of urea (**Figure 70E**) and calcium (**Figure 71H**). The total protein analysis revealed increased concentrations of both albumin and globulin, with the latter being higher in *Bscl2*$^{Celia/Celia}$ females than *Bscl2*$^{-/-}$ females (**Figure 71I-K**).

Due to the limited sample volume required, only one S.A. mouse could be analysed in this case. However, the values suggested were similar to those observed in the wild type and heterozygous mice (**Figure 70** and **Figure 71**, see **Annex 12**).

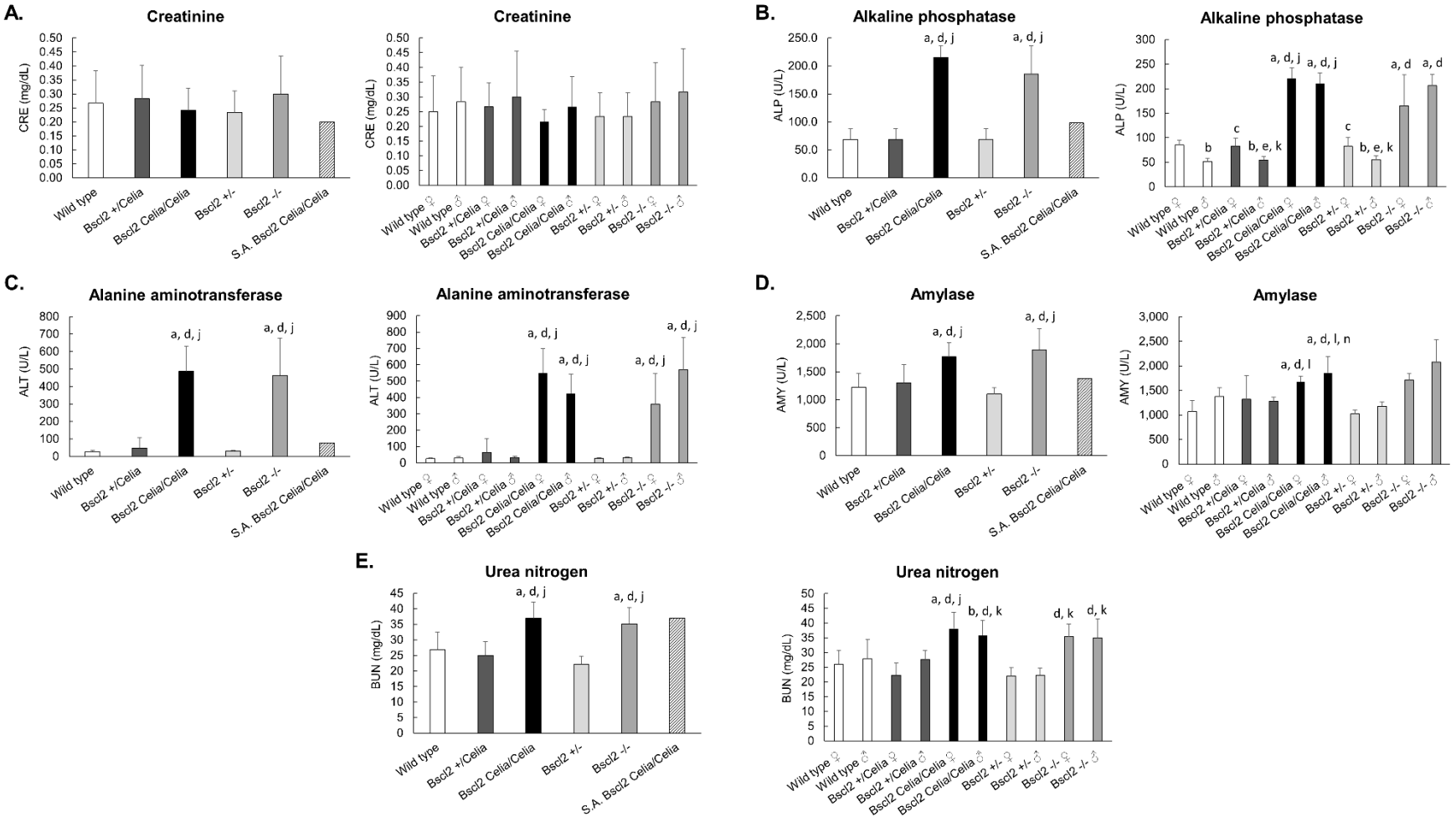

Figure 70. Biochemical measurements for wild type, *Bscl2*$^{+/Celia}$, *Bscl2*$^{Celia/Celia}$, *Bscl2*$^{+/-}$, *Bscl2*$^{-/-}$ and severely affected (S.A.) animals. (**A**) Creatinine, (**B**) alkaline phosphatase, (**C**) alanine aminotransferase, (**D**) amylase and (**E**) urea nitrogen. For mean age and number of animals per genotype see **Annex 12**. Data is presented as mean ± SD. Data were analysed using a Kolmogorov-Smirnov test for normality, followed by a Kruskal-Wallis test with Mann-Whitney post hoc comparisons. [a] $p < 0.05$ vs wild type ♀/♂; [b] $p < 0.05$ vs wild type ♀; [c] $p < 0.05$ vs wild type ♂; [d] $p < 0.05$ vs *Bscl2*$^{+/-}$ ♀/♂; [e] $p < 0.05$ vs *Bscl2*$^{+/-}$ ♀; [j] $p < 0.05$ vs *Bscl2*$^{+/Celia}$ ♀/♂; [k] $p < 0.05$ vs *Bscl2*$^{+/Celia}$ ♀; [l] $p < 0.05$ vs *Bscl2*$^{+/Celia}$ ♂; [n] $p < 0.05$ vs *Bscl2*$^{Celia/Celia}$ ♀.

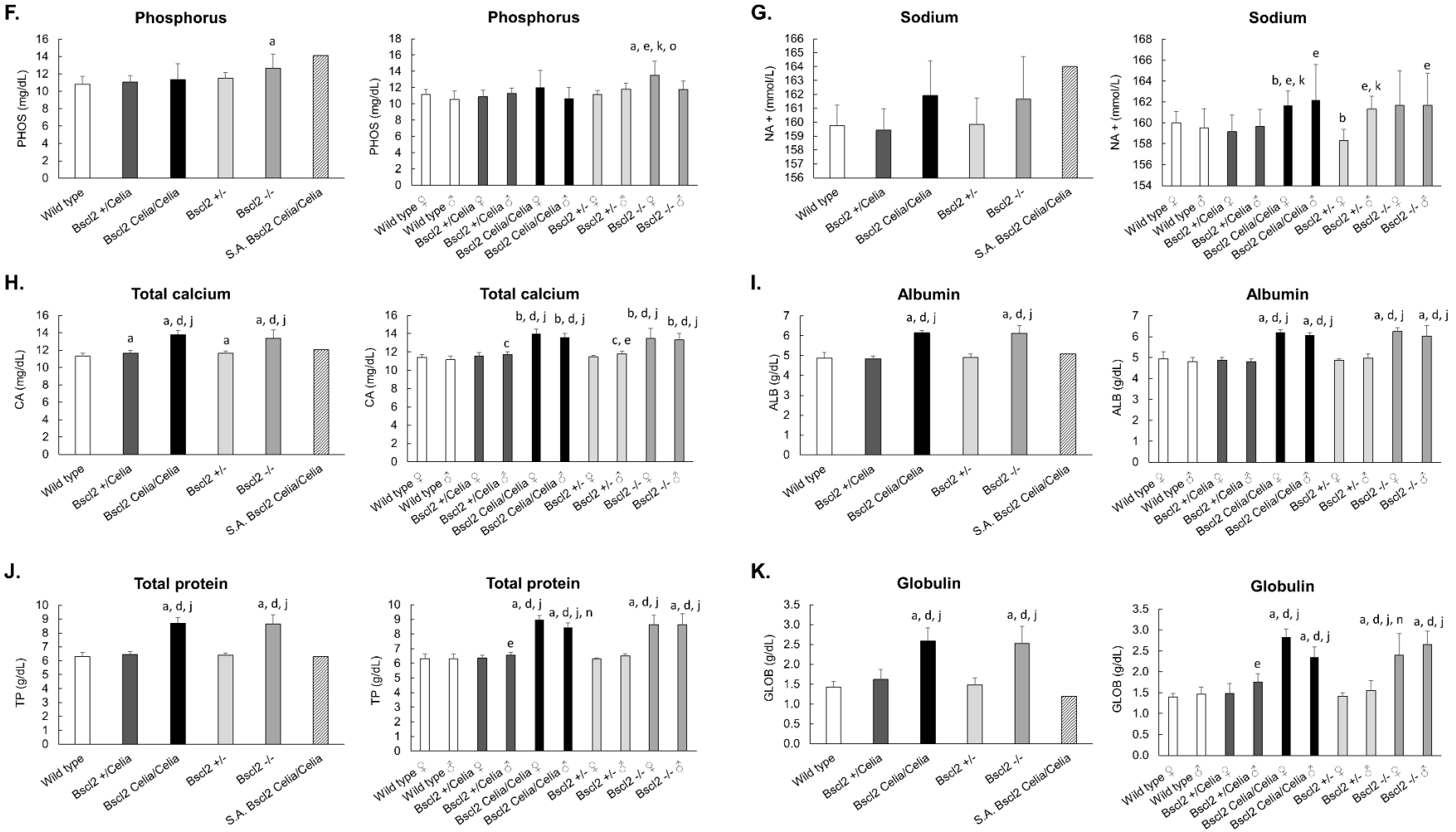

Figure 71. Biochemical measurements for wild type, *Bscl2*$^{+/Celia}$, *Bscl2*$^{Celia/Celia}$, *Bscl2*$^{+/-}$ and *Bscl2*$^{-/-}$ and severely affected (S.A.) animals. (**F**) Phosphorus, (**G**) sodium, (**H**) total calcium, (**I**) albumin, (**J**) total protein and (**K**) globulin. For mean age and number of animals per genotype see **Annex 12**. Data is presented as mean ± SD. Data were analysed using a Kolmogorov-Smirnov test for normality, followed by a Kruskal-Wallis test with Mann-Whitney post hoc comparisons. [a] $p < 0.05$ vs wild type ♀/♂; [b] $p < 0.05$ vs wild type ♀; [d] $p < 0.05$ vs *Bscl2*$^{+/-}$ ♀/♂; [e] $p < 0.05$ vs *Bscl2*$^{+/-}$ ♀; [j] $p < 0.05$ vs *Bscl2*$^{+/Celia}$ ♀/♂; [k] $p < 0.05$ vs *Bscl2*$^{+/Celia}$ ♀; [n] $p < 0.05$ vs *Bscl2*$^{Celia/Celia}$ ♀; [o] $p < 0.05$ vs *Bscl2*$^{Celia/Celia}$ ♂.

5 DISCUSSION

Seipinopathies are a group of diseases associated with variants in the *BSLC2* gene. Different variants in this gene can cause congenital generalized lipodystrophy type 2 (CGL2), upper and/or lower motor neuron diseases, or a progressive encephalopathy. The latter condition, known as progressive encephalopathy with or without lipodystrophy (PELD) or Celia's encephalopathy, is a pediatric neurodegenerative disorder with a fatal prognosis. It is caused by variants in the *BSCL2* genes, such as the c.985C>T variant, which leads to intronization of exon 7 and the production of an aberrant form of seipin protein, called Celia seipin. While some of the pathogenic mechanisms underlying this neurological condition have been previously elucidated, its low prevalence, severity, and the brain as the primarily affected organ make it challenging to study in humans.

In an effort to contribute to the understanding of Celia's encephalopathy, this study has generated the first global murine model for this disease using a Cre/loxP recombination-based strategy. This model partially recapitulates the key features of the human condition. Concurrently, the first global seipin-deficient murine model has been created by replacing the ATG start codon with an inverted *cassette* that induces ubiquitous disruption of the seipin protein. This has allowed for a comparative analysis between CGL2 and PELD.

Both murine models were extensively monitored to identify any neurodegenerative symptoms. As expected, only the knock-in mice harbouring the *BSCL2*-TG variant exhibited symptoms resembling those present in humans with Celia's encephalopathy. The symptoms included ponderal stagnation, abnormal limb crossing, kyphosis, tremor, myoclonus, tail spasticity, and paraparesis or paraplegia. Consistent with the human condition, these symptoms appeared early in life (4.8 months) and progressively worsened until the animals succumbed to the severe encephalopathic condition, resulting in a dramatically reduced lifespan of approximately 8 months (2, 210). In contrast, the seipin-deficient (global knock-out) mice did not display these neurodegenerative phenotypes, allowing for a comparative analysis between the CGL2 and PELD models.

However, only 11.9% of the *Bscl2*$^{Celia/Celia}$ mice exhibited obvious signs of neurodegeneration. In contrast, in human patients, all individuals carrying the classical c.985C>T variant, either in homozygosity or compound heterozygosity, present a severe encephalopathic picture with a fatal outcome (2, 10, 126, 127). It is worth noting that some other cases, due to a different *BSCL2* variant (c.974dupG) that also leads to the skipping of exon 7 (10), only exhibited a mild neurological disorder (128, 131, 132). However, these represent a minority and often involved very young patients. At present, there is no obvious explanation for the discrepancy

between the high penetrance of severe neurodegeneration in human patients and the relatively low incidence in the homozygous *Bscl2*$^{Celia/Celia}$ mice. It is tempting to speculate that the more severe brain damage observed in humans may be attributed to a higher expression of the human transgene in the homozygous severely affected mice, which was only evident in the cortex.

However, this does not fully explain the observation that 5.4% of heterozygous *Bscl2*$^{+/Celia}$ mice also exhibited a severe encephalopathic phenotype, despite the expression of Celia *BSCL2* transgene being similar to that of non-severely affected knock-in heterozygous animals. While it has been reported that a monoallelic *BSCL2* variant (c.566T>A) can be associated with refractory epilepsy and neurological regression (125), this variant does not affect exon 7, and the parents of PELD patients were generally healthy. Given these results, it cannot be ruled out that, at least in the murine brain and in a small number of cases, the Celia *BSCL2* transgene in heterozygosity may still be detrimental to the brain. This is noteworthy, as a loss-of-function mechanism has been assumed for CGL2. When considering the pathogenic mechanism underlying neurodegeneration in PELD, it could be concluded that the damage is caused by a toxic gain-of-function. Previously, our group (136) demonstrated *in vitro* that the presence of wild type human seipin sequester the aberrant Celia-seipin, preventing the formation of large protein macroaggregates in the nucleus, thereby explaining the lack of neurological symptoms in human heterozygous carriers. This fact could be related to the appearance of neurological symptoms in some knock-in heterozygous mice, as these animals may have lower expression of wild type seipin compared to the non-severely knock-in heterozygous mice, particularly in the cerebellum.

Nonetheless, there is currently no evidence that the proposed mechanism, where wild type seipin sequesters the aberrant Celia-seipin, is also occurring in the mouse brain. This is because the seipin protein in mice differs from humans, particularly in the cytoplasmic amino- and carboxyl-terminal ends (4). Furthermore, the expression of the murine *Bscl2* gene is lower in the brain compared to adipose tissue, which is not the case in humans (5). Additionally, there are interspecies differences in the expression patterns of the *Bscl2*/*BSCL2* genes across different brain regions. In mice, the *Bscl2* gene is primarily expressed in the basal forebrain, hippocampus, hypothalamus, and dorsal and ventral brainstem, with lower expression in the cortex and striatum (6, 7). In contrast, in humans, higher *BSCL2* gene expression is found in the caudate and putamen nuclei, cerebellum, and pons, mainly in the forebrain and rhombencephalon (4). This is particularly relevant, as a recurrent finding in human PELD is damage to the caudate nucleus (210). Considering these interspecies differences, and if the proposed protective mechanism is indeed not present in the mouse brain, it would not be surprising to find severely affected heterozygous knock-in mice, rather than the opposite, with just the expected ratio (5.4 vs 11.9%).

Considering the potential differences between severely affected, heterozygous, and homozygous animals, further studies were conducted to better understand the foundations of this neurodegeneration. Both severely affected *Bscl2*$^{+/Celia}$ and *Bscl2*$^{Celia/Celia}$ animals exhibited

gliosis (glial cell proliferation) in the thoracic spinal cord, consistent with the phenotype of kyphosis, paraparesis, or paraplegia observed in these mice. However, despite the pronounced symptoms, the degree of damage to the thoracic marrow may not have been as extensive as one might expect. As reported by Yagi et al. (160) in their N88S murine model, neuronal death may not be a necessary prerequisite for the development of motor phenotypes in seipinopathies. In other words, the motor deficits observed in these animals may not solely depend on overt neuronal loss, but could potentially involve more subtle alterations in neuronal function or connectivity, or other pathological mechanisms involving glial cells. This finding highlights the complex and multifaceted nature of the neurodegeneration associated with Celia's encephalopathy and other seipinopathies, which may not be fully recapitulated by the extent of spinal cord pathology alone.

Brain studies revealed a patchy loss of Purkinje cells and distinctive glial cells in the cerebellum of the severely affected animals. In humans, in variants such as c.566T > A, the architecture of the cerebellum was preserved with normal Purkinje cell density (125). However, in the classic variant, moderate atrophy of the cerebellar vermis was observed (2), a region where Purkinje cells are primarily located (211). Moreover, PET analysis revealed a global reduction in brain glucose uptake in the severely affected *Bscl2*$^{+/Celia}$ animals, with the most affected areas being the cortex, left striatum, olfactory bulb, and amygdala. In the case of the severely affected *Bscl2*$^{Celia/Celia}$ animals, hypometabolism was only observed in the latter two areas, likely due to the younger age of the mouse analysed, as a greater reduction in metabolism over time was confirmed. Interestingly, the non- severely affected *Bscl2*$^{Celia/Celia}$ animals, despite not showing histological damage in any of the brain regions studied, exhibited global brain hypometabolism, suggesting a possible functional impairment. This global reduction in brain glucose uptake, which worsens over time, aligns with the observations in human patients; however, the most affected brain regions differ, with humans showing the basal ganglia, the temporal and occipital lobes and the cerebellum and brainstem as the most severely affected (2, 133).

As mentioned previously, greater brain damage is expected in regions with higher *BSCL2*-TG expression. In humans, the pituitary gland and the cerebellum are the two areas with the highest expression of the Celia *BSCL2* (2), with the occipital lobules showing the higher reduction in glucose uptake (133). However, in severely affected mice, this higher transgene expression was only observed in the cortex of homozygous animals, in contrast to the PET results, which showed a reduction in glucose uptake in the cortex of heterozygotes but not in homozygotes. This discrepancy may be due to the younger age of the homozygous mouse analysed. These differences between the mouse model and human patients can be attributed to several factors. Firstly, the mouse brain has a volume (415 mm^3) (212) compared to the human brain (1200 cm^3) (213), making region-specific analysis more challenging in the smaller murine sample. Additionally, we cannot ignore the fact that there may be differences in the expression patterns of the *Bscl2*/*BSCL2* genes in various tissues and brain regions between mice and humans, which could also contribute to the observed discrepancies.

Several studies suggested an association between seipin and various ER-organelles, such as mitochondria and peroxisomes. In seipin knock-out flies, as well as in mouse and human cell studies, seipin has been shown to influence lipid droplet storage via the mitochondrial calcium flux system (27, 214, 215). Additionally, studies in yeast have demonstrated that the cooperation between seipin and *Pex30* is necessary for the formation of lipid droplets (45, 47). In this regard, our group previously proposed that seipin plays an important role in peroxisome biogenesis in humans (4). Specifically, some genes encoding protective enzymes against oxidative stress (including *SOD1* and *SOD2*) were found to be related to *BSCL2* expression in human brains.

Based on these previous findings, the present study examined the expression of several genes related to mitochondrial and peroxisome function in different brain areas of severely affected and non-severely affected mice. Although the results did not fully mirror those found in human brains, there was a notable decrease in the expression of *Sod2* in the striatum of both the severely affected homozygous and heterozygous animals. In contrast, *Sod1* seemed to be diminished in the cortex of these severely affected animals. Furthermore, *Sod2* also displayed decreased levels within the cortex, but solely in the severely affected *Bscl2*$^{\text{Celia/Celia}}$ animals, coinciding with the highest expression of Celia *BSCL2*-TG. These findings support the hypothesis that aberrant seipin expression in the brain ultimately impairs proteins that protect against neurodegeneration by reducing the production of reactive oxygen species (4, 216, 217). A similar mechanism has also been described in a transgenic mouse model of Alzheimer's disease (218), where the partial deficiency of *Sod2* promotes β-amyloid-induced toxicity, reducing neuronal death and the loss of the neural network, thereby contributing to cognitive decline (4, 219).

Furthermore, recent studies have asserted that the specific suppression of the *Sod2* gene in murine models is associated not only with deficits in cognitive function (220) but also with a motor deficit phenotype (221). Additionally, confocal microscopy studies have shown that both seipin and *PEX16*, a key protein for peroxisomal biogenesis, are closely expressed in the hypothalamus of healthy human brains. In contrast, *PEX16* was absent in the same region of a human PELD case (4). However, the study of *Pex16* expression at the murine level did not show significant differences in its expression in any of the brain areas studied. Taking all these findings into account, it can be suggested that the interplay between seipin, mitochondria, and peroxisomes may be crucial for maintaining cellular homeostasis and that disruptions in these processes could contribute to the pathogenesis of Celia's encephalopathy and other seipinopathies.

A comprehensive characterization of the behavioural spectrum can be useful in assessing the effect of brain disorders, such as neurodegenerative diseases. In this study, various behavioural tests were conducted to evaluate both motor and cognitive functions. The severely affected animals, both heterozygous and homozygous, exhibited reduced locomotor activities and increased anxiety. Similarly, the non-severely affected homozygous animals also showed reduced locomotor activities, increased anxiety, and decreased coordination.

Nevertheless, these differences in behaviour and psychomotor studies were not found when comparing homozygous animals from both murine models, *Bscl2*$^{-/-}$ and *Bscl2*$^{Celia/Celia}$, suggesting that the differences observed with wild type animals may be a consequence of the absence of the murine *Bscl2* gene rather than the presence of the aberrant human transgene.

However, a detailed analysis of the parameters revealed that in the *Bscl2*$^{-/-}$ mice, this impaired behaviour might be influenced by the enlarged liver weight in these animals. Consequently, it was confirmed that only the male non-severely affected *Bscl2*$^{Celia/Celia}$ mice truly exhibited impairment in locomotor activities and higher anxiety, as demonstrated in the open-field and elevated zero maze tests. Similarly, a previous study by Zhou et al. (80) reported that male neuronal-specific seipin knock-out (seipin-nKO) mice, but not females, displayed elevated anxiety levels without obvious locomotion deficits. However, later studies by authors like Wang et al. (86) did find an age-related deficit in motor coordination in seipin-nKO mice. A noteworthy observation in the current behavioural study was the increased floating behaviour in the wild type mice. Several articles have attempted to provide a possible explanation for this phenomenon, with the most convincing being that, rather than a stress response, the floating behaviour may reflect a spatial orientation phase of the animals (222, 223). This suggests that the increased floating behaviour observed in the wild type mice may not necessarily indicate an anxiety-like response, but rather a normal exploratory strategy employed by the animals during the behavioural testing. Careful interpretation of such behavioural parameters is crucial to accurately assess the specific deficits associated with the Celia's encephalopathy phenotype in the mouse models. Overall, these findings highlight the importance of considering sex-specific differences and the potential influence of age-related changes when evaluating the behavioural consequences of seipin deficiency in animal models of seipinopathies.

On the other hand, no conclusive differences were observed in the parameters related to cognitive functions and memory, although a crucial factor was that the severely affected animals could not be assessed due to their physical discomfort. As mentioned earlier, some authors have reported similar findings regarding impaired motor coordination in seipin-nKO mice (86). However, other studies (80, 81, 85) have reported deficits in learning, memory, as well as anxiety- and depression-like behaviours in seipin-nKO mice. Both behavioural and motor deficits observed in these studies were triggered by a reduction in PPARγ activity (81, 84, 85), although the precise mechanism involved in this reduction is not entirely clear. Authors such as Qian et al. (85) have proposed that seipin depletion in mice causes a reduction in PPARγ, similar to what occurs with *Sod2*, leading to β-amyloid neurotoxicity and neuroinflammation. These findings suggest that the cognitive and behavioural impairments associated with seipin deficiency may be mediated, at least in part, through dysregulation of PPARγ signalling and the subsequent induction of neurotoxic and neuroinflammatory processes. Further investigation is needed to fully elucidate the underlying mechanisms. Other studies, like the one by Chan et al. (84), have postulate that seipin deletion causes hyperphosphorylation and aggregation of tau protein, leading to axonal atrophy through reduced PPARγ activity. In the animals examined in the current study, however, the

expression of the *Pparγ* gene was not different among the genotypes in the brain regions analysed. A possible explanation could be that the expression of Celia-seipin variant was somehow influencing PPARγ in a manner similar to that of the wild type seipin, as a positive correlation between *BSCL2* and *PPARγ* has been observed in previous studies (4, 81, 85). However, this would not explain why the *Pparγ* levels were normal in the seipin knock-out (SKO) animals, although protein levels were not analysed in the current study. Further investigation into the specific interactions between seipin, PPARγ, and other downstream signalling pathways would be necessary to fully elucidate the complex mechanisms underlying the neurological deficits observed in the Celia's encephalopathy model and other seipinopathies.

Another important issue is to determine the amount of human Celia-seipin expressed in the different brain regions of these mice. It can be assumed that the promoter is working properly, although this may not necessarily be the case, and differences in Celia *BSCL2*-TG expression could be modulated by unknown epigenetic or non-epigenetic mechanisms (224, 225), which could modify the post-transcriptional regulation of protein expression. The lack of a specific Celia-seipin antibody hinders more detailed studies to reveal the pathogenic mechanism underlying these findings. Although it has been demonstrated using anti-6xHis-tagged seipin antibody that human transgene is translated, these experiments were not carried out on the severely affected animals. The amount of aberrant Celia-seipin is likely a crucial factor in explaining the severity of the neurological symptoms. However, the possible ubiquitination of the deep layers of the cerebellum in the severely affected homozygous mice suggests the presence of ubiquitin-reactive nuclear inclusions, as reported in the hypothalamus of PELD patients (case #1, **Table 2**) (2, 136), strongly suggesting a similar pathogenic mechanism. These inclusions in PELD patients (case #1, **Table 2**), positive for seipin, are likely to form due to the impaired oligomerization and aggregation of Celia-seipin, indicating a gain-of-toxic function in Celia's encephalopathy (136). Neuronal intranuclear inclusions have been identified in various neurodegenerative diseases such as Huntington's disease (226, 227). Similarly, evidence of endoplasmic reticulum stress and inclusion formation was detected in motor neurons in the N88S transgenic mouse, leading to motor neuropathies and linking to the unfolded mutant seipin protein (160). These findings suggest that the aberrant aggregation and accumulation of the Celia-seipin variant may play a central role in the pathogenesis of Celia's encephalopathy, potentially through a toxic gain-of-function mechanism.

In addition to the neurological features observed in PELD patients, it is known that compound heterozygous patients carrying the c.985C>T variant exhibit lipodystrophy, while homozygous patients sometimes do not show a lipodystrophic phenotype. However, in both cases, CGL2 traits, such as hypertriglyceridemia, hypoleptinemia, and abnormal glucose tolerance have been reported (10). The underlying mechanism responsible for this dichotomy is currently unclear. In the current study, the non-severely affected homozygous mice, *Bscl2*$^{Celia/Celia}$ and *Bscl2*$^{-/-}$, exhibited hyperinsulinemia and severe hypoleptinemia. Basal glucose levels were similar among the genotypes and remained so throughout the animals' lifespan. Other authors have reported glucose intolerance in SKO mouse models (59, 146).

This suggests that while the Celia-seipin variant may not directly impact glucose homeostasis, the overall disruption of seipin function can lead to the metabolic abnormalities characteristic of CGL2, such as insulin resistance and impaired glucose tolerance. Further investigation is needed to fully elucidate the complex interplay between the neurological and metabolic manifestations of seipinopathies, and how the specific seipin variants, such as Celia seipin, may differentially impact these pathological processes. However, in the present study, similar to an adipose tissue-specific *Bscl2* knock-out mice [Ad-B2$^{(-/-)}$] (147), no impaired glucose tolerance was found, although there was insulin resistance. These characteristics resemble those found in both CGL2 and PELD in humans (228), albeit without the presence of diabetes mellitus or hypertriglyceridemia.

On the other hand, in the current knock-in murine model in homozygosity, all mice, both severely and non-severely affected, exhibited severe lipoatrophy, suggesting that Celia-seipin variant leads to a loss of function, at least in extra-neural tissues. Similar to the findings in our mice, other authors have reported two patients homozygous for the c.985C>T variant with generalized lipodystrophy. Additionally, this pattern of generalized lipoatrophy has also been reported in other PELD variants, both in homozygosity and compound heterozygosity (10, 126). This severe loss of fat was also observed in the homozygous SKO mice, displaying a clear lipodystrophy phenotype akin to that seen in patients with CGL2 (228). These findings suggest that the Celia-seipin variant, when present in homozygosity, leads to a loss of seipin function in peripheral tissues, resulting in the characteristic lipodystrophic features observed in both the mouse model and human patients. In both homozygous knock-out and knock-in mice, regardless of whether they were severely or non-severely affected, the absence of white fat (inguinal and gonadal) was nearly complete, with areas of fibrosis and smaller adipocytes, similar to other SKO models (59, 61). However, the amount of brown fat (interscapular) was lower than the reported in most other studies, both in SKO mice (59, 61, 146) and in tissue-specific SKO mice (147). This interscapular brown adipose tissue in the current models exhibited adipocytes with larger lipid vacuoles and areas of necrosis, although this histopathology was only previously observed in adipose-specific SKO mice (147, 148). These findings suggest that the complete absence of murine seipin, either through knock-out or the expression of the Celia-seipin variant, leads to a near-total loss of white adipose tissue, accompanied by alterations in the quantity and morphology of the brown adipose tissue. This underscores the critical role of seipin in the proper development and function of both white and brown fat depots.

The ectopic deposition of fat in the liver of the non-severely affected *Bscl2*$^{Celia/Celia}$ and *Bscl2*$^{-/-}$ mice leads to a pronounced hepatomegaly, with a mixed hepatic steatosis predominantly of the macrovesicular type, followed by the development of steatohepatitis and fibrosis. There is no literature on hepatic histopathology in PELD, which is limited in CGL2 and, more broadly, in any form of lipodystrophy. Some studies in CGL2 patients have reported the presence of advanced portal fibrosis (229), while others have described macrovesicular steatosis and advanced fibrosis that could progress to cirrhosis (230). Javor et al. (231) showed a pattern of liver damage similar to that present in the current non-severely affected homozygous animals,

with panacinar macrovesicular steatosis and ballooning degeneration of hepatocytes. To date, the histological analysis of the liver in lipodystrophic mice deficient in seipin has been limited to the study of isolated samples in mice at 8 weeks (232), 3 months (59, 166), and 4 months (146) of age.

According to the authors of the previous studies, the SKO mice developed hepatic steatosis but not steatohepatitis or fibrosis. These findings contrast with the natural history of the disease in humans, where the development of metabolic dysfunction-associated steatohepatitis (MASH) and fibrosis is a frequent and early occurrence. However, it should be noted that metabolic dysfunction-associated steatotic liver disease (MASLD) is a progressively evolving condition. This raises the possibility that the duration of disease progression in these earlier studies may not have been sufficient for the full spectrum of liver pathology to manifest. In support of this, Liu et al. (148) observed in 10-month-old Ad-B2$^{(-/-)}$ mice the presence of steatosis without signs of inflammation. On the other hand, in 2018, Liao et al. (233) described, for the first-time, the presence of steatohepatitis in seipin-deficient and apolipoprotein E null (Seipin$^{-/-}$apoE$^{-/-}$) mice at 9 months of age. This discrepancy with previous studies could be explained in two ways. Firstly, the progression time in the Liao et al. (233) study was sufficient for the development of inflammation and the full spectrum of MASLD to occur. However, both in this study and the study by Liu et al. (148), we must consider whether these mice are comparable to the traditional SKO models. An alternative hypothesis would be to consider that, in Liao et al. (233) study, two factors contribute to the development of steatohepatitis: the deficiency of seipin and, additionally, the deficiency of apoE.

It should also be noted that the non-severely affected homozygous mice in the current study only develop stage 1a fibrosis, which is mild or perisinusoidal, detectable only by Masson's trichrome staining. Therefore, we cannot rule out the possibility that previous studies overlooked this finding, as none of them confirmed the use of this specialized staining technique (59, 61, 146, 232). On the other hand, in the current study, hepatic steatosis was evident from three months of age, but it only became a constant finding from six months in the homozygous animals. This raises the possibility that the progression time in the Chen et al. (61) study may have been insufficient to observe the full spectrum of liver pathology. Furthermore, McIlroy et al. (147) described that Ad-B2$^{(-/-)}$ mice, as well as Ad-B2$^{(-/-)}$ mice with additional ablation of hepatic *Bscl2*, did not develop hepatic steatosis (150). Both the Ad-B2$^{(-/-)}$ mice (studied up to 16 weeks of life) and the Ad-B2$^{(-/-)}$ mice with additional hepatic *Bscl2* ablation (studied up to 32 weeks) showed discreet but significantly higher fat deposition and adipokine secretion capacity compared to SKO models.

According to the findings of McIlroy et al. (147), small amounts of metabolically active adipose tissue would be sufficient to prevent the development of metabolic abnormalities in SKO models. Based on this and in the fact that liver-specific SKO mice did not develop steatosis, the hepatic steatosis observed in the current study may not be directly related to the loss of a liver-specific seipin function, but rather with the reduced amount of metabolically

active adipose tissue (147, 150), which was lower in the homozygous animals, potentially explain the observed histopathological changes in the liver. On the other hand, Tian et al. (234), based on their observations in *Drosophila* deficient in seipin, suggested that in tissues other than adipose, this protein promotes lipid deposition and therefore plays a tissue-specific role. The central region of seipin is proposed to control lipid homeostasis in non-adipocyte cells, being responsible for restricting lipogenesis and lipid accumulation in hepatocytes, as well as promoting adipogenesis in case of excess energy supply (20). Therefore, the loss of seipin at the hepatic level could worsen the metabolic status in the absence or dysfunction of adipose tissue (147). This suggests that seipin may have distinct, tissue-specific functions in regulating lipid metabolism and homeostasis, which could contribute to the complex metabolic phenotypes observed in seipin-deficient animal models and human seipinopathies.

Added to this proposal is the observation of the FGF21 factor. There are multiple functions attributed to this factor, with beneficial effects in the modulation of glucose homeostasis, lipid metabolism and insulin sensitivity (235). Already in 2016, Miehle et al. (236) demonstrated for the first time a significantly higher concentration of circulating FGF21 in patients with non-HIV lipodystrophy. That same year, Dollet et al. (172) observed in *Bscl2*$^{-/-}$ lipodystrophic mice a marked overexpression of *Fgf21* in adipose tissue at four weeks of age, decreasing by twelve weeks. In these mice, treatment with FGF21 appears to promote the maintenance of mature adipocytes by exerting an anti-stress cellular effect, improving metabolic profile. Furthermore, Softic et al. (237) noted that fat-specific insulin receptor knock-out mice (F-IRKO) exhibited increased hepatic expression of *Fgf21*. Since the accumulated fat in the liver of lipodystrophic mice is directed towards ketogenesis, the increase in this metabolic process would result from the higher hepatic expression of *Fgf21* (237). The elevation of *Fgf21* levels observed in our homozygous *Bscl2*$^{Celia/Celia}$ and *Bscl2*$^{-/-}$ mice, as well as in those severely affected homozygous mice, is consistent with previous studies and could be justified in multiple ways, although its pathogenesis remains uncertain for the time being. Upregulation of FGF21 could be considered a compensatory mechanism, yet insufficient to alleviate the metabolic consequences of lipodystrophy. This also applies to the increase in FGF21 in MASLD related to metabolic syndrome. Another possibility, related to circulating microRNAs (miRNAs) derived from adipose tissue, sequences of 21 to 25 nucleotides that inhibit gene expression acting as posttranscriptional regulators. Thomou et al. (238), in 2017, proposed *Fgf21* as a potential target of miRNAs contained in exosomes from brown adipose tissue. They demonstrated that both hepatic expression of *Fgf21* and circulating FGF21 levels are decreased by the action of these microRNAs (primarily miR99a, miR99b, and miR100). According to this, the lower amount of brown adipose tissue (239) and the alteration of its function (64) in seipin-deficient mice would explain the increase in hepatic expression of *Fgf21*.

One surprising finding was that severely affected *Bscl2*$^{Celia/Celia}$ mice had only mild steatosis, with a quite normal liver weight, and did not present hyperinsulinemia. However, these animals exhibited a dramatic lack of fat and severe hypoleptinemia, while being significantly lighter than non-affected *Bscl2*$^{Celia/Celia}$ mice. Although their food uptake was not quantified,

given their severe neurological condition, the most parsimonious explanation would be that their food consumption was severely reduced. This would likely explain their lower liver weight, as well as the improvement in hepatic steatosis and insulin resistance. In this regard, Chen et al. (149) demonstrated that prolonged fasting in SKO mice improved insulin sensitivity and hepatic steatosis. This suggests that the reduced food intake in the severely affected *Bscl2*$^{Celia/Celia}$ mice may have played a protective role against the development of more severe liver pathology. It is also interesting to note that, despite the long follow-up of hepatic evolution in both murine models, up to 24 months (twice as long as in most previous studies), no evidence of cirrhosis was observed. This incomplete picture of MASLD is common to all murine lipodystrophic models studied to date (24). In contrast, some non-lipoatrophic murine models do present cirrhosis (240, 241), but in these cases, the liver damage was chemically induced (by carbon tetrachloride (CCl_4) (242), streptozotocin (STZ) (243), or diethylnitrosamine (DEN) (244)) in combination with appropriate dietary measures. The pathophysiological mechanisms employed in these models do not necessarily match the development of MASLD in humans.

In addition to the other findings, the non-severely affected homozygous animals (both knock-in and knock-out) showed a high accumulation of triglycerides in the liver. However, it was found that their fasting serum triglyceride levels were significantly reduced (by 50%) in the young animals (4 months old), as has been reported by other authors (59, 61, 146). As the animals became older (9.5 months old), the serum triglyceride levels showed a tendency to be higher (by 53%) than their wild type littermates, although this difference did not reach statistical significance. However, the study by Chen et al. 2012, showed a higher plasma triglyceride concentration in *Bscl2*$^{-/-}$ mice compared to wild type, but only in a post-prandial situation (61). In contrast, the severely affected animals presented normal serum and liver triglycerides. Studies like that of Cui et al. (59), based on a decreased expression of hepatic microsomal triglyceride transfer protein (MTP), have suggested that the hypotriglyceridemia in SKO mice may occur due to an alteration of very low-density lipoproteins (VLDL). However, Prieur et al. (146) did not find an impairment of VLDL secretion, proposing instead that the low triglyceride levels might be due to an increased uptake of triacylglycerol-rich lipoproteins (TRL) and non-esterified fatty acids (NEFA) by the liver. The precise mechanisms underlying these findings are not yet well understood, but it is evident that the liver of mice may differ from that of humans in terms of lipotoxicity in hepatocytes. It is possible that the mouse liver has a greater “buffer” capacity when dealing with the spillover of fat that cannot be adequately stored, which may contribute to the differences observed in the triglyceride profiles compared to the human condition.

Homozygous animals, knock-in and knock-out, also exhibited an enlargement in spleen, heart, and kidney size. Examination of the hearts of these homozygous animals revealed a normal phenotypic pattern, differing from reports in other SKO mice which demonstrated left ventricular hypertrophy (LVH) and diastolic dysfunction (151, 152), similar to findings in patients.

However, evidence of renal damage was observed. Consistent with the findings of Liu et al. (154), homozygous knock-out and knock-in mice, as well as severely affected mice, displayed glomerular damage characterized by diffuse mesangial expansion. Additionally, our non-severely affected homozygous animals exhibited arteriolar hyalinization. In contrast, the histological study conducted by Javor et al. (102) in three patients with CGL2 did not show the same pattern observed in mice; instead, these patients presented with clear focal segmental glomerulosclerosis (FSGS) without arteriolar hyalinosis. Numerous clinical studies have indicated that patients with CGL suffer from renal injuries characterized by proteinuria and elevated creatinine levels (245). Although creatinine elevation was not observed in our homozygous mice, a pattern of arteriolar hyalinization similar to that seen in these patients with CGL was noted. Furthermore, serum ion concentration remained unchanged, consistent with findings reported by Liu et al. (154) in plasma. However, ion excretion was not assessed, despite evidence of elevated excretion levels in other studies (154). Additionally, several adipokines, including leptin, play roles in maintaining renal function (246-248). Our homozygous mice, both severely affected and unaffected, exhibited low levels of leptin, potentially contributing to insulin resistance, oxidative stress, and activation of the renin-angiotensin system, leading to kidney damage (247-250). Therefore, renal damage was observed in *Bscl2*$^{Celia/Celia}$ and *Bscl2*$^{-/-}$ animals, as well as in severely affected ones, with no discernible differences between the murine models, suggesting that renal damage, as proposed by Liu et al. (154), is attributed to the global deficiency of murine seipin.

Clinical evidence suggests that gender differences frequently exist in genetic forms of lipodystrophy, such as CGL2 or familial partial lipodystrophy (Dunnigan type), where female patients often exhibit a more severe physical and metabolic phenotype than male patients (95, 96, 251). However, in both the current knock-in and knock-out mouse models, clear sexual dimorphism was not found. Liao et al. (233) suggested that seipin deficiency led to a similar severity of adipose loss in both female and male apoE$^{-/-}$ mice, although females showed greater resistance to developing lipodystrophy-related metabolic consequences. These inconclusive data, inconsistent with the findings in clinical studies, were also reported by Chen. et al. (61) for their SKO murine model, where males were more affected than females. However, McIlroy et al. (252) found no major differences between genders in terms of metabolic dysfunction for the Ad-B2$^{(-/-)}$ mice, which was also the case in the current murine models. Regarding cognitive development, there are fewer studies in humans that mention gender differences, but some, such as Seip and Trygstad, observed that a female patient showed less disability compared to the male patient (96). In line with this, Zhou et al. (80) noticed that female seipin-nKO mice did not show depression-like behaviours and neurogenesis deficits. These findings partly coincide with the observations in the current *Bscl2*$^{Celia/Celia}$ mice, where only males showed impairment in locomotor activities and higher anxiety. However, neither males nor females exhibited a loss of cognitive functions, although the severely affected animals could not be assessed due to the severity of their neurological condition. In summary, how adipose metabolic control and neurological outcomes diversify

between females and males, humans and mice, or across different variants in CGL2, is not yet fully defined and requires further research to elucidate the underlying mechanisms.

Developing a perfect animal model that fully recapitulates a human disease is always a challenging endeavour, and this study has certain limitations. Firstly, the low percentage of severely affected mice in the current model does not correspond to what is observed in human patients with the c.985C>T variant, where all cases present with a severe neurodegenerative condition. Secondly, and perhaps more importantly, there are differences in the pathogenic mechanisms explaining the neurological findings between the mouse model and the human disease. In this regard, it is necessary to further unveil the mechanisms underlying the amount of translated seipin and its lack of correlation with the expression of the human transgene, particularly in heterozygous knock-in mice. Despite these limitations, this study has presented a global murine model of Celia's encephalopathy that partially recapitulates the severe neurodegenerative picture suffered by these patients. Additionally, the study has presented a global murine model with seipin depletion, which recapitulates the typical phenotype of congenital generalized lipodystrophy, thereby becoming a valuable model for this disease as well. While the current models may not fully mirror the human conditions, they represent important steps forward in the development of preclinical tools to study the pathogenesis and potential therapeutic interventions for seipinopathies, including Celia's encephalopathy and congenital generalized lipodystrophy. Continued refinement and further characterization of these animal models will be crucial to bridge the gap between the murine and human manifestations of these rare genetic disorders.

6 CONCLUSIONS

The present research has made it possible to establish the following conclusions:

1. A global murine model for Celia's encephalopathy has been generated for the first time using the Cre/loxP recombination system. This model partially recapitulates the severe neurodegenerative picture suffered by patients with progressive encephalopathy with or without lipodystrophy. Additionally, a global seipin-deficient murine model was generated, allowing comparative monitoring between congenital generalized lipodystrophy type 2 and progressive encephalopathy with or without lipodystrophy.

2. Neurologically affected mice for Celia's encephalopathy exhibit symptoms resembling those seen in humans, including growth retardation, limb abnormalities, tremors, spasticity, and reduced lifespan. These severely affected mice also showed similarities in brain glucose uptake reduction, as well as loss of Purkinje cells and glial cell abnormalities in the cerebellum.

3. At the molecular level, the severely affected animals showed a significant reduction in the expression of *Sod1* and *Sod2* in the cortex, suggesting that seipin may play a role in peroxisome biogenesis, and its deficiency could impact genes related to mitochondrial and peroxisome function in the brain.

4. The homozygous non-severely affected mice, while not exhibiting obvious neurological symptoms, did display reduced locomotor activities, increased anxiety, and impaired coordination. However, no alterations in cognitive functions or memory were detected. These findings regarding behaviour and psychomotor skills were consistent across both knock-in and knock-out mice, suggesting that the behavioural abnormalities are likely due to seipin deficiency and not to the overexpression of *BSCL2* Celia.

5. Regarding the phenotype, severely affected homozygous animals presented severe generalized lipodystrophy and mild hepatic steatosis. Serum and liver triglycerides, as well as glucose metabolism, were normal, without insulin resistance but with a severe hypoleptinemia.

6. In contrast, the homozygous non-severely affected mice showed a severe lack of adipose tissue with a severe hypoleptinemia, similar to the neurologically affected mice. However, these mice non-severely affected exhibited hyperinsulinemia and insulin resistance, as well as increase in serum triglyceride concentration over time and significant accumulation of triglycerides in the liver. Hepatic manifestations,

including steatosis and fibrosis, were observed, although no evidence of cirrhosis was detected, suggesting potential differences in lipotoxicity between mice and humans.

7. Although the current knock-in murine model has remarkable similarities with Celia's encephalopathy in humans, only 11.9% of the homozygous knock-in mice exhibited obvious neurodegeneration, contrasting with the severe neurological symptoms seen in human carriers of the classical c.985C>T variant in homozygosity or compound heterozygosity. Additionally, 5.4% of the heterozygous knock-in animals also developed this neurological phenotype, suggesting that the protective mechanism of wild type seipin, proposed in humans, may not be the same in this mouse model.
8. There are differences in the pathogenic mechanisms explaining neurodegeneration between the mice and humans, but the possible ubiquitination of the deep layers of the cerebellum in the neurologically affected animals suggests the presence of ubiquitin-reactive nuclear inclusions, strongly suggesting a toxic gain-of-function, similar to what occurs in patients with progressive encephalopathy with or without lipodystrophy.
9. Sexual dimorphism was not clearly evident in the current murine models, in contrast to clinical studies suggesting gender-related differences in lipodystrophy phenotypes.

REFERENCES

1. Magre J, Delepine M, Khallouf E, Gedde-Dahl T, Jr., Van Maldergem L, Sobel E, et al. Identification of the gene altered in Berardinelli-Seip congenital lipodystrophy on chromosome 11q13. Nat Genet. 2001;28(4):365-70.

2. Guillen-Navarro E, Sanchez-Iglesias S, Domingo-Jimenez R, Victoria B, Ruiz-Riquelme A, Rabano A, et al. A new seipin-associated neurodegenerative syndrome. J Med Genet. 2013;50(6):401-9.

3. Cartwright BR, Goodman JM. Seipin: from human disease to molecular mechanism. J Lipid Res. 2012;53(6):1042-55.

4. Sanchez-Iglesias S, Fernandez-Liste A, Guillin-Amarelle C, Rabano A, Rodriguez-Canete L, Gonzalez-Mendez B, et al. Does Seipin Play a Role in Oxidative Stress Protection and Peroxisome Biogenesis? New Insights from Human Brain Autopsies. Neuroscience. 2018;396(2019):119-37.

5. Chen W, Yechoor VK, Chang BH, Li MV, March KL, Chan L. The human lipodystrophy gene product Berardinelli-Seip congenital lipodystrophy 2/seipin plays a key role in adipocyte differentiation. Endocrinology. 2009;150(10):4552-61.

6. Garfield AS, Chan WS, Dennis RJ, Ito D, Heisler LK, Rochford JJ. Neuroanatomical characterisation of the expression of the lipodystrophy and motor-neuropathy gene Bscl2 in adult mouse brain. PLoS One. 2012;7(9):e45790.

7. Liu X, Xie B, Qi Y, Du X, Wang S, Zhang Y, et al. The expression of SEIPIN in the mouse central nervous system. Brain Struct Funct. 2016;221(8):4111-27.

8. Lundin C, Nordstrom R, Wagner K, Windpassinger C, Andersson H, von Heijne G, et al. Membrane topology of the human seipin protein. FEBS Lett. 2006;580(9):2281-4.

9. Agarwal AK, Garg A. Seipin: a mysterious protein. Trends Mol Med. 2004;10(9):440-4.

10. Sánchez-Iglesias S, Fernández-Pombo A, Cobelo-Gómez S, Hermida-Ameijeiras Á, Alarcón-Martínez H, Domingo-Jiménez R, et al. Celia's Encephalopathy (BSCL2-Gene-Related): Current Understanding. 2021;10(7):1435.

11. Bohnert M. New friends for seipin - Implications of seipin partner proteins in the life cycle of lipid droplets. Semin Cell Dev Biol. 2020;108:24-32.

12. Klug YA, Deme JC, Corey RA, Renne MF, Stansfeld PJ, Lea SM, et al. Mechanism of lipid droplet formation by the yeast Sei1/Ldb16 Seipin complex. Nat Commun. 2021;12(1):5892.

13. Yan R, Qian H, Lukmantara I, Gao M, Du X, Yan N, et al. Human SEIPIN Binds Anionic Phospholipids. Dev Cell. 2018;47(2):248-56 e4.

14. Sui X, Arlt H, Brock KP, Lai ZW, DiMaio F, Marks DS, et al. Cryo-electron microscopy structure of the lipid droplet-formation protein seipin. J Cell Biol. 2018;217(12):4080-91.

15. Arlt H, Sui X, Folger B, Adams C, Chen X, Remme R, et al. Seipin forms a flexible cage at lipid droplet formation sites. Nat Struct Mol Biol. 2022;29(3):194-202.

16. Talukder MM, Sim MF, O'Rahilly S, Edwardson JM, Rochford JJ. Seipin oligomers can interact directly with AGPAT2 and lipin 1, physically scaffolding critical regulators of adipogenesis. Mol Metab. 2015;4(3):199-209.

17. Pagac M, Cooper DE, Qi Y, Lukmantara IE, Mak HY, Wu Z, et al. SEIPIN Regulates Lipid Droplet Expansion and Adipocyte Development by Modulating the Activity of Glycerol-3-phosphate Acyltransferase. Cell Rep. 2016;17(6):1546-59.

18. Salo VT, Hölttä-Vuori M, Ikonen E. Seipin-mediated contacts as gatekeepers of lipid flux at the endoplasmic reticulum–lipid droplet nexus. Contact. 2020;3:1-16.

19. Wei S, Soh SL, Qiu W, Yang W, Seah CJ, Guo J, et al. Seipin regulates excitatory synaptic transmission in cortical neurons. J Neurochem. 2013;124(4):478-89.

20. Yang W, Thein S, Guo X, Xu F, Venkatesh B, Sugii S, et al. Seipin differentially regulates lipogenesis and adipogenesis through a conserved core sequence and an evolutionarily acquired C-terminus. Biochem J. 2013;452(1):37-44.

21. Payne VA, Grimsey N, Tuthill A, Virtue S, Gray SL, Dalla Nora E, et al. The human lipodystrophy gene BSCL2/seipin may be essential for normal adipocyte differentiation. Diabetes. 2008;57(8):2055-60.

22. Zhang P, Takeuchi K, Csaki LS, Reue K. Lipin-1 phosphatidic phosphatase activity modulates phosphatidate levels to promote peroxisome proliferator-activated receptor gamma (PPARgamma) gene expression during adipogenesis. J Biol Chem. 2012;287(5):3485-94.

23. Subauste AR, Das AK, Li X, Elliott BG, Evans C, El Azzouny M, et al. Alterations in lipid signaling underlie lipodystrophy secondary to AGPAT2 mutations. Diabetes. 2012;61(11):2922-31.

24. Li Y, Yang X, Peng L, Xia Q, Zhang Y, Huang W, et al. Role of Seipin in Human Diseases and Experimental Animal Models. Biomolecules. 2022;12(6).

25. Craveiro Sarmento AS, de Azevedo Medeiros LB, Agnez-Lima LF, Lima JG, de Melo Campos JTA. Exploring Seipin: From Biochemistry to Bioinformatics Predictions. Int J Cell Biol. 2018;2018:5207608.

26. Yang W, Thein S, Wang X, Bi X, Ericksen RE, Xu F, et al. BSCL2/seipin regulates adipogenesis through actin cytoskeleton remodelling. Hum Mol Genet. 2014;23(2):502-13.

27. Combot Y, Salo VT, Chadeuf G, Holtta M, Ven K, Pulli I, et al. Seipin localizes at endoplasmic-reticulum-mitochondria contact sites to control mitochondrial calcium import and metabolism in adipocytes. Cell Rep. 2022;38(2):110213.

28. Bi J, Wang W, Liu Z, Huang X, Jiang Q, Liu G, et al. Seipin promotes adipose tissue fat storage through the ER Ca(2)(+)-ATPase SERCA. Cell Metab. 2014;19(5):861-71.

29. Olzmann JA, Carvalho P. Dynamics and functions of lipid droplets. Nat Rev Mol Cell Biol. 2019;20(3):137-55.

30. Choudhary V, Schneiter R. Lipid droplet biogenesis from specialized ER subdomains. Microb Cell. 2020;7(8):218-21.

31. Thiam AR, Ikonen E. Lipid Droplet Nucleation. Trends Cell Biol. 2021;31(2):108-18.

32. Henne M, Goodman JM, Hariri H. Spatial compartmentalization of lipid droplet biogenesis. Biochim Biophys Acta Mol Cell Biol Lipids. 2020;1865(1):158499.

33. Schneiter R, Choudhary V. Seipin collaborates with the ER membrane to control the sites of lipid droplet formation. Curr Opin Cell Biol. 2022;75:102070.

34. Wang H, Becuwe M, Housden BE, Chitraju C, Porras AJ, Graham MM, et al. Seipin is required for converting nascent to mature lipid droplets. Elife. 2016;5:e16582.

35. Schuldiner M, Bohnert M. A different kind of love - lipid droplet contact sites. Biochim Biophys Acta Mol Cell Biol Lipids. 2017;1862(10 Pt B):1188-96.

36. Salo VT, Belevich I, Li S, Karhinen L, Vihinen H, Vigouroux C, et al. Seipin regulates ER-lipid droplet contacts and cargo delivery. EMBO J. 2016;35(24):2699-716.

37. Geltinger F, Schartel L, Wiederstein M, Tevini J, Aigner E, Felder TK, et al. Friend or Foe: Lipid Droplets as Organelles for Protein and Lipid Storage in Cellular Stress Response, Aging and Disease. Molecules. 2020;25(21).

38. Thiam AR, Foret L. The physics of lipid droplet nucleation, growth and budding. Biochim Biophys Acta. 2016;1861(8 Pt A):715-22.

39. Adeyo O, Horn PJ, Lee S, Binns DD, Chandrahas A, Chapman KD, et al. The yeast lipin orthologue Pah1p is important for biogenesis of lipid droplets. J Cell Biol. 2011;192(6):1043-55.

40. Fei W, Shui G, Zhang Y, Krahmer N, Ferguson C, Kapterian TS, et al. A role for phosphatidic acid in the formation of "supersized" lipid droplets. PLoS Genet. 2011;7(7):e1002201.

41. Skinner JR, Shew TM, Schwartz DM, Tzekov A, Lepus CM, Abumrad NA, et al. Diacylglycerol enrichment of endoplasmic reticulum or lipid droplets recruits perilipin 3/TIP47 during lipid storage and mobilization. J Biol Chem. 2009;284(45):30941-8.

42. Ben M'barek K, Ajjaji D, Chorlay A, Vanni S, Foret L, Thiam AR. ER Membrane Phospholipids and Surface Tension Control Cellular Lipid Droplet Formation. Dev Cell. 2017;41(6):591-604 e7.

43. Choudhary V, Golani G, Joshi AS, Cottier S, Schneiter R, Prinz WA, et al. Architecture of Lipid Droplets in Endoplasmic Reticulum Is Determined by Phospholipid Intrinsic Curvature. Curr Biol. 2018;28(6):915-26 e9.

44. Chorlay A, Thiam AR. An Asymmetry in Monolayer Tension Regulates Lipid Droplet Budding Direction. Biophys J. 2018;114(3):631-40.

45. Wang S, Idrissi FZ, Hermansson M, Grippa A, Ejsing CS, Carvalho P. Seipin and the membrane-shaping protein Pex30 cooperate in organelle budding from the endoplasmic reticulum. Nat Commun. 2018;9(1):2939.

46. Joshi AS, Huang X, Choudhary V, Levine TP, Hu J, Prinz WA. A family of membrane-shaping proteins at ER subdomains regulates pre-peroxisomal vesicle biogenesis. J Cell Biol. 2016;215(4):515-29.

47. Joshi AS, Nebenfuehr B, Choudhary V, Satpute-Krishnan P, Levine TP, Golden A, et al. Lipid droplet and peroxisome biogenesis occur at the same ER subdomains. Nat Commun. 2018;9(1):2940.

48. Ferreira JV, Carvalho P. Pex30-like proteins function as adaptors at distinct ER membrane contact sites. J Cell Biol. 2021;220(10).

49. Eisenberg-Bord M, Mari M, Weill U, Rosenfeld-Gur E, Moldavski O, Castro IG, et al. Identification of seipin-linked factors that act as determinants of a lipid droplet subpopulation. J Cell Biol. 2018;217(1):269-82.

50. Castro IG, Eisenberg-Bord M, Persiani E, Rochford JJ, Schuldiner M, Bohnert M. Promethin Is a Conserved Seipin Partner Protein. Cells. 2019;8(3).

51. Chung J, Wu X, Lambert TJ, Lai ZW, Walther TC, Farese RV, Jr. LDAF1 and Seipin Form a Lipid Droplet Assembly Complex. Dev Cell. 2019;51(5):551-63 e7.

52. Prasanna X, Salo VT, Li S, Ven K, Vihinen H, Jokitalo E, et al. Seipin traps triacylglycerols to facilitate their nanoscale clustering in the endoplasmic reticulum membrane. PLoS Biol. 2021;19(1):e3000998.

53. Islinger M, Voelkl A, Fahimi HD, Schrader M. The peroxisome: an update on mysteries 2.0. Histochem Cell Biol. 2018;150(5):443-71.

54. Berger J, Dorninger F, Forss-Petter S, Kunze M. Peroxisomes in brain development and function. Biochim Biophys Acta. 2016;1863(5):934-55.

55. Jin Y, Tan Y, Zhao P, Ren Z. SEIPIN: A Key Factor for Nuclear Lipid Droplet Generation and Lipid Homeostasis. Int J Mol Sci. 2020;21(21).

56. Romanauska A, Kohler A. The Inner Nuclear Membrane Is a Metabolically Active Territory that Generates Nuclear Lipid Droplets. Cell. 2018;174(3):700-15 e18.

57. Soltysik K, Ohsaki Y, Tatematsu T, Cheng J, Maeda A, Morita SY, et al. Nuclear lipid droplets form in the inner nuclear membrane in a seipin-independent manner. J Cell Biol. 2021;220(1).

58. Du X, Yang H. Seipin regulates the formation of nuclear lipid droplets from a distance. J Cell Biol. 2021;220(1).

59. Cui X, Wang Y, Tang Y, Liu Y, Zhao L, Deng J, et al. Seipin ablation in mice results in severe generalized lipodystrophy. Hum Mol Genet. 2011;20(15):3022-30.

60. Zechner R, Strauss JG, Haemmerle G, Lass A, Zimmermann R. Lipolysis: pathway under construction. Curr Opin Lipidol. 2005;16(3):333-40.

61. Chen W, Chang B, Saha P, Hartig SM, Li L, Reddy VT, et al. Berardinelli-seip congenital lipodystrophy 2/seipin is a cell-autonomous regulator of lipolysis essential for adipocyte differentiation. Mol Cell Biol. 2012;32(6):1099-111.

62. Magre J, Prieur X. Seipin Deficiency as a Model of Severe Adipocyte Dysfunction: Lessons from Rodent Models and Teaching for Human Disease. Int J Mol Sci. 2022;23(2).

63. Zhou H, Lei X, Yan Y, Lydic T, Li J, Weintraub NL, et al. Targeting ATGL to rescue BSCL2 lipodystrophy and its associated cardiomyopathy. JCI Insight. 2019;5(14).

64. Zhou H, Lei X, Benson T, Mintz J, Xu X, Harris RB, et al. Berardinelli-Seip congenital lipodystrophy 2 regulates adipocyte lipolysis, browning, and energy balance in adult animals. J Lipid Res. 2015;56(10):1912-25.

65. Hamilton JA, Hillard CJ, Spector AA, Watkins PA. Brain uptake and utilization of fatty acids, lipids and lipoproteins: application to neurological disorders. J Mol Neurosci. 2007;33(1):2-11.

66. Zhang J, Liu Q. Cholesterol metabolism and homeostasis in the brain. Protein Cell. 2015;6(4):254-64.

67. Puchkov D, Haucke V. Greasing the synaptic vesicle cycle by membrane lipids. Trends Cell Biol. 2013;23(10):493-503.

68. Bruce KD, Zsombok A, Eckel RH. Lipid Processing in the Brain: A Key Regulator of Systemic Metabolism. Front Endocrinol (Lausanne). 2017;8:60.

69. Montesinos J, Guardia-Laguarta C, Area-Gomez E. The fat brain. Curr Opin Clin Nutr Metab Care. 2020;23(2):68-75.

70. Hamilton LK, Dufresne M, Joppe SE, Petryszyn S, Aumont A, Calon F, et al. Aberrant Lipid Metabolism in the Forebrain Niche Suppresses Adult Neural Stem Cell Proliferation in an Animal Model of Alzheimer's Disease. Cell Stem Cell. 2015;17(4):397-411.

71. Cole NB, Murphy DD, Grider T, Rueter S, Brasaemle D, Nussbaum RL. Lipid droplet binding and oligomerization properties of the Parkinson's disease protein alpha-synuclein. J Biol Chem. 2002;277(8):6344-52.

72. Farmer BC, Walsh AE, Kluemper JC, Johnson LA. Lipid Droplets in Neurodegenerative Disorders. Front Neurosci. 2020;14:742.

73. Marschallinger J, Iram T, Zardeneta M, Lee SE, Lehallier B, Haney MS, et al. Lipid-droplet-accumulating microglia represent a dysfunctional and proinflammatory state in the aging brain. Nat Neurosci. 2020;23(2):194-208.

74. Doetsch F, Garcia-Verdugo JM, Alvarez-Buylla A. Cellular composition and three-dimensional organization of the subventricular germinal zone in the adult mammalian brain. J Neurosci. 1997;17(13):5046-61.

75. Brawer JR, Walsh RJ. Response of tanycytes to aging in the median eminence of the rat. Am J Anat. 1982;163(3):247-56.

76. Liu L, MacKenzie KR, Putluri N, Maletic-Savatic M, Bellen HJ. The Glia-Neuron Lactate Shuttle and Elevated ROS Promote Lipid Synthesis in Neurons and Lipid Droplet Accumulation in Glia via APOE/D. Cell Metab. 2017;26(5):719-37 e6.

77. Ioannou MS, Jackson J, Sheu SH, Chang CL, Weigel AV, Liu H, et al. Neuron-Astrocyte Metabolic Coupling Protects against Activity-Induced Fatty Acid Toxicity. Cell. 2019;177(6):1522-35 e14.

78. Bozza PT, Viola JP. Lipid droplets in inflammation and cancer. Prostaglandins Leukot Essent Fatty Acids. 2010;82(4-6):243-50.

79. Bailey AP, Koster G, Guillermier C, Hirst EM, MacRae JI, Lechene CP, et al. Antioxidant Role for Lipid Droplets in a Stem Cell Niche of Drosophila. Cell. 2015;163(2):340-53.

80. Zhou L, Yin J, Wang C, Liao J, Liu G, Chen L. Lack of seipin in neurons results in anxiety- and depression-like behaviors via down regulation of PPARgamma. Hum Mol Genet. 2014;23(15):4094-102.

81. Zhou L, Chen T, Li G, Wu C, Wang C, Li L, et al. Activation of PPARgamma Ameliorates Spatial Cognitive Deficits through Restoring Expression of AMPA Receptors in Seipin Knock-Out Mice. J Neurosci. 2016;36(4):1242-53.

82. Wei S, Soh SL-Y, Xia J, Ong W-Y, Pang ZP, Han W. Motor neuropathy-associated mutation impairs Seipin functions in neurotransmission. Journal of Neurochemistry. 2014;129(2):328-38.

83. Li G, Zhou L, Zhu Y, Wang C, Sha S, Xian X, et al. Seipin knockout in mice impairs stem cell proliferation and progenitor cell differentiation in the adult hippocampal dentate gyrus via reduced levels of PPARgamma. Dis Model Mech. 2015;8(12):1615-24.

84. Chang H, Di T, Wang Y, Zeng X, Li G, Wan Q, et al. Seipin deletion in mice enhances phosphorylation and aggregation of tau protein through reduced neuronal PPARgamma and insulin resistance. Neurobiol Dis. 2019;127:350-61.

85. Qian Y, Yin J, Hong J, Li G, Zhang B, Liu G, et al. Neuronal seipin knockout facilitates Abeta-induced neuroinflammation and neurotoxicity via reduction of PPARgamma in hippocampus of mouse. J Neuroinflammation. 2016;13(1):145.

86. Wang L, Hong J, Wu Y, Liu G, Yu W, Chen L. Seipin deficiency in mice causes loss of dopaminergic neurons via aggregation and phosphorylation of alpha-synuclein and neuroinflammation. Cell Death Dis. 2018;9(5):440.

87. Cui W, Yang J, Tu C, Zhang Z, Zhao H, Qiao Y, et al. Seipin deficiency-induced lipid dysregulation leads to hypomyelination-associated cognitive deficits via compromising oligodendrocyte precursor cell differentiation. Cell Death Dis. 2024;15(5):350.

88. Jang M, Gould E, Xu J, Kim EJ, Kim JH. Oligodendrocytes regulate presynaptic properties and neurotransmission through BDNF signaling in the mouse brainstem. Elife. 2019;8.

89. Wang F, Yang YJ, Yang N, Chen XJ, Huang NX, Zhang J, et al. Enhancing Oligodendrocyte Myelination Rescues Synaptic Loss and Improves Functional Recovery after Chronic Hypoxia. Neuron. 2018;99(4):689-701 e5.

90. Trompier D, Vejux A, Zarrouk A, Gondcaille C, Geillon F, Nury T, et al. Brain peroxisomes. Biochimie. 2014;98:102-10.

91. Berardinelli W. An undiagnosed endocrinometabolic syndrome: report of 2 cases. J Clin Endocrinol Metab. 1954;14(2):193-204.

92. Seip M. Lipodystrophy and gigantism with associated endocrine manifestations. A new diencephalic syndrome? Acta Paediatr (Stockh). 1959;48:555-74.

93. Patni N, Garg A. Congenital generalized lipodystrophies--new insights into metabolic dysfunction. Nat Rev Endocrinol. 2015;11(9):522-34.

94. Craveiro Sarmento AS, Ferreira LC, Lima JG, de Azevedo Medeiros LB, Barbosa Cunha PT, Agnez-Lima LF, et al. The worldwide mutational landscape of Berardinelli-Seip congenital lipodystrophy. Mutat Res Rev Mutat Res. 2019;781:30-52.

95. Huang-Doran I, Sleigh A, Rochford JJ, O'Rahilly S, Savage DB. Lipodystrophy: metabolic insights from a rare disorder. J Endocrinol. 2010;207(3):245-55.

96. Raygada M, Rennert O. Congenital generalized lipodystrophy: profile of the disease and gender differences in two siblings. Clin Genet. 2005;67(1):98-101.

97. Simha V, Garg A. Phenotypic heterogeneity in body fat distribution in patients with congenital generalized lipodystrophy caused by mutations in the AGPAT2 or seipin genes. J Clin Endocrinol Metab. 2003;88(11):5433-7.

98. Altay C, Secil M, Demir T, Atik T, Akinci G, Ozdemir Kutbay N, et al. Determining residual adipose tissue characteristics with MRI in patients with various subtypes of lipodystrophy. Diagn Interv Radiol. 2017;23(6):428-34.

99. Araujo-Vilar D, Santini F. Diagnosis and treatment of lipodystrophy: a step-by-step approach. J Endocrinol Invest. 2018.

100. Araújo-Vilar D, Iglesias SS, Guillín-Amarelle C, Fernández-Pombo A, de Tudela Cánovas NEP, Tudela JC. Guía práctica para el diagnóstico y tratamiento de las lipodistrofias infrecuentes: AELIP; 2018.

101. Lupsa BC, Sachdev V, Lungu AO, Rosing DR, Gorden P. Cardiomyopathy in congenital and acquired generalized lipodystrophy: a clinical assessment. Medicine (Baltimore). 2010;89(4):245-50.

102. Javor ED, Moran SA, Young JR, Cochran EK, DePaoli AM, Oral EA, et al. Proteinuric nephropathy in acquired and congenital generalized lipodystrophy: baseline characteristics and course during recombinant leptin therapy. J Clin Endocrinol Metab. 2004;89(7):3199-207.

103. McNally M, Mannon RB, Javor ED, Swanson SJ, Hale DA, Gorden P, et al. Successful renal transplantation in a patient with congenital generalized lipodystrophy: a case report. Am J Transplant. 2004;4(3):447-9.

104. Akinci B, Oral EA, Neidert A, Rus D, Cheng WY, Thompson-Leduc P, et al. Comorbidities and Survival in Patients With Lipodystrophy: An International Chart Review Study. J Clin Endocrinol Metab. 2019;104(11):5120-35.

105. Cook K, Ali O, Akinci B, Foss de Freitas MC, Montenegro RM, Fernandes VO, et al. Effect of Leptin Therapy on Survival in Generalized and Partial Lipodystrophy: A Matched Cohort Analysis. J Clin Endocrinol Metab. 2021;106(8):e2953-e67.

106. Yildirim Simsir I, Tuysuz B, Ozbek MN, Tanrikulu S, Celik Guler M, Karhan AN, et al. Clinical features of generalized lipodystrophy in Turkey: A cohort analysis. Diabetes Obes Metab. 2023;25(7):1950-63.

107. Chandalia M, Garg A, Vuitch F, Nizzi F. Postmortem findings in congenital generalized lipodystrophy. J Clin Endocrinol Metab. 1995;80(10):3077-81.

108. Haghighi A, Kavehmanesh Z, Haghighi A, Salehzadeh F, Santos-Simarro F, Van Maldergem L, et al. Congenital generalized lipodystrophy: identification of novel variants and expansion of clinical spectrum. Clin Genet. 2016;89(4):434-41.

109. Liu Y, Li D, Ding Y, Kang L, Jin Y, Song J, et al. Further delineation of AGPAT2 and BSCL2 related congenital generalized lipodystrophy in young infants. Eur J Med Genet. 2019;62(9):103542.

110. Jiang M, Gao M, Wu C, He H, Guo X, Zhou Z, et al. Lack of testicular seipin causes teratozoospermia syndrome in men. Proc Natl Acad Sci U S A. 2014;111(19):7054-9.

111. Agarwal AK, Simha V, Oral EA, Moran SA, Gorden P, O'Rahilly S, et al. Phenotypic and genetic heterogeneity in congenital generalized lipodystrophy. J Clin Endocrinol Metab. 2003;88(10):4840-7.

112. Lima JG, Nobrega LHC, Lima NN, Dos Santos MCF, Silva PHD, Baracho MFP, et al. Causes of death in patients with Berardinelli-Seip congenital generalized lipodystrophy. PLoS One. 2018;13(6):e0199052.

113. Sim MF, Talukder MM, Dennis RJ, O'Rahilly S, Edwardson JM, Rochford JJ. Analysis of naturally occurring mutations in the human lipodystrophy protein seipin reveals multiple potential pathogenic mechanisms. Diabetologia. 2013;56(11):2498-506.

114. Rochford JJ. When Adipose Tissue Lets You Down: Understanding the Functions of Genes Disrupted in Lipodystrophy. Diabetes. 2022;71(4):589-98.

115. Windpassinger C, Auer-Grumbach M, Irobi J, Patel H, Petek E, Horl G, et al. Heterozygous missense mutations in BSCL2 are associated with distal hereditary motor neuropathy and Silver syndrome. Nat Genet. 2004;36(3):271-6.

116. Irobi J, Van den Bergh P, Merlini L, Verellen C, Van Maldergem L, Dierick I, et al. The phenotype of motor neuropathies associated with BSCL2 mutations is broader than Silver syndrome and distal HMN type V. Brain. 2004;127(Pt 9):2124-30.

117. Choi BO, Park MH, Chung KW, Woo HM, Koo H, Chung HK, et al. Clinical and histopathological study of Charcot-Marie-Tooth neuropathy with a novel S90W mutation in BSCL2. Neurogenetics. 2013;14(1):35-42.

118. Hsiao CT, Tsai PC, Lin CC, Liu YT, Huang YH, Liao YC, et al. Clinical and Molecular Characterization of BSCL2 Mutations in a Taiwanese Cohort with Hereditary Neuropathy. PLoS One. 2016;11(1):e0147677.

119. Auer-Grumbach M, Loscher WN, Wagner K, Petek E, Korner E, Offenbacher H, et al. Phenotypic and genotypic heterogeneity in hereditary motor neuronopathy type V: a clinical, electrophysiological and genetic study. Brain. 2000;123 (Pt 8):1612-23.

120. Ito D, Suzuki N. Molecular pathogenesis of seipin/BSCL2-related motor neuron diseases. Ann Neurol. 2007;61(3):237-50.

121. Ito D, Fujisawa T, Iida H, Suzuki N. Characterization of seipin/BSCL2, a protein associated with spastic paraplegia 17. Neurobiol Dis. 2008;31(2):266-77.

122. Ishihara S, Okamoto Y, Tanabe H, Yoshimura A, Higuchi Y, Yuan JH, et al. Clinical features of inherited neuropathy with BSCL2 mutations in Japan. J Peripher Nerv Syst. 2020;25(2):125-31.

123. Ferranti S, Lo Rizzo C, Renieri A, Galluzzi P, Grosso S. Focus on progressive myoclonic epilepsy in Berardinelli-Seip syndrome. Neurol Sci. 2020;41(11):3345-8.

124. Serino D, Davico C, Specchio N, Marras CE, Fioretto F. Berardinelli-Seip syndrome and progressive myoclonus epilepsy. Epileptic Disord. 2019;21(1):117-21.

125. Fernandez-Marmiesse A, Sanchez-Iglesias S, Darling A, O'Callaghan MM, Tonda R, Jou C, et al. A de novo heterozygous missense BSCL2 variant in 2 siblings with intractable developmental and epileptic encephalopathy. Seizure. 2019;71:161-5.

126. Alaei MR, Talebi S, Ghofrani M, Taghizadeh M, Keramatipour M. Whole Exome Sequencing Reveals a BSCL2 Mutation Causing Progressive Encephalopathy with Lipodystrophy (PELD) in an Iranian Pediatric Patient. Iran Biomed J. 2016;20(5):295-301.

127. Poisson A, Chatron N, Labalme A, Till M, Broussolle E, Sanlaville D, et al. Regressive Autism Spectrum Disorder Expands the Phenotype of BSCL2/Seipin-Associated Neurodegeneration. Biol Psychiatry. 2018;S0006-3223(18):31524-5.

128. Sanchez-Iglesias S, Crocker M, O'Callaghan M, Darling A, García-Cazorla A, Domingo-Jiménez R, et al. Celia's encephalopathy and c.974dupG in BSCL2 gene: a hidden change in a known variant. Neurogenetics. 2019;in press.

129. Opri R, Fabrizi GM, Cantalupo G, Ferrarini M, Simonati A, Dalla Bernardina B, et al. Progressive Myoclonus Epilepsy in Congenital Generalized Lipodystrophy type 2: Report of 3 cases and literature review. Seizure. 2016;42:1-6.

130. Zhang Y, Chen X, Luo F, Jiang L, Xu J, Chen S. Medical management of a child with congenital generalized lipodystrophy accompanied with progressive myoclonic epilepsy: A case report. Medicine (Baltimore). 2019;98(48):e18121.

131. Wu YR, Hung SI, Chang YC, Chen ST, Lin YL, Chung WH. Complementary mutations in seipin gene in a patient with Berardinelli-Seip congenital lipodystrophy and dystonia: phenotype variability suggests multiple roles of seipin gene. J Neurol Neurosurg Psychiatry. 2009;80(10):1180-1.

132. Huang HH, Chen TH, Hsiao HP, Huang CT, Wang CC, Shiau YH, et al. A Taiwanese boy with congenital generalized lipodystrophy caused by homozygous Ile262fs mutation in the BSCL2 gene. Kaohsiung J Med Sci. 2010;26(11):615-20.

133. Araujo-Vilar D, Domingo-Jimenez R, Ruibal A, Aguiar P, Ibanez-Mico S, Garrido-Pumar M, et al. Association of metreleptin treatment and dietary intervention with neurological outcomes in Celia's encephalopathy. Eur J Hum Genet. 2018;26(3):396-406.

134. Poisson A, Chatron N, Labalme A, Till M, Broussolle E, Sanlaville D, et al. Regressive Autism Spectrum Disorder Expands the Phenotype of BSCL2/Seipin-Associated Neurodegeneration. Biol Psychiatry. 2019;85(4):e17-e9.

135. Stanley NE, Robinson LJ, Mao Q. A Novel, Heterozygous BSCL2 Variant in Association With Early-Onset Epileptic Encephalopathy. J Neuropathol Exp Neurol. 2022;81(5):377-80.

136. Ruiz-Riquelme A, Sánchez-Iglesias S, Rábano A, Guillén-Navarro E, Domingo-Jiménez R, Ramos A, et al. Larger aggregates of mutant seipin in Celia's Encephalopathy, a new protein misfolding neurodegenerative disease. Neurobiology of Disease. 2015;83:44-53.

137. Havel LS, Wang CE, Wade B, Huang B, Li S, Li XJ. Preferential accumulation of N-terminal mutant huntingtin in the nuclei of striatal neurons is regulated by phosphorylation. Hum Mol Genet. 2011;20(7):1424-37.

138. Aguzzi A, De Cecco E. Shifts and drifts in prion science. Science. 2020;370(6512):32-4.

139. Sanchez-Iglesias S, Fernandez-Pombo A, Araujo-Vilar D. Focus on progressive myoclonic epilepsy in Berardinelli-Seip syndrome. Neurol Sci. 2020.

140. Nagy E, Maquat LE. A rule for termination-codon position within intron-containing genes: when nonsense affects RNA abundance. Trends Biochem Sci. 1998;23(6):198-9.

141. Hug N, Longman D, Caceres JF. Mechanism and regulation of the nonsense-mediated decay pathway. Nucleic Acids Res. 2016;44(4):1483-95.

142. Nickless A, Bailis JM, You Z. Control of gene expression through the nonsense-mediated RNA decay pathway. Cell Biosci. 2017;7:26.

143. Kim HK, Della-Fera M, Lin J, Baile CA. Docosahexaenoic acid inhibits adipocyte differentiation and induces apoptosis in 3T3-L1 preadipocytes. J Nutr. 2006;136(12):2965-9.

144. Hofer DC, Pessentheiner AR, Pelzmann HJ, Schlager S, Madreiter-Sokolowski CT, Kolb D, et al. Critical role of the peroxisomal protein PEX16 in white adipocyte development and lipid homeostasis. Biochim Biophys Acta Mol Cell Biol Lipids. 2017;1862(3):358-68.

145. Ebihara C, Ebihara K, Aizawa-Abe M, Mashimo T, Tomita T, Zhao M, et al. Seipin is necessary for normal brain development and spermatogenesis in addition to adipogenesis. Hum Mol Genet. 2015;24(15):4238-49.

146. Prieur X, Dollet L, Takahashi M, Nemani M, Pillot B, Le May C, et al. Thiazolidinediones partially reverse the metabolic disturbances observed in Bscl2/seipin-deficient mice. Diabetologia. 2013;56(8):1813-25.

147. McIlroy GD, Suchacki K, Roelofs AJ, Yang W, Fu Y, Bai B, et al. Adipose specific disruption of seipin causes early-onset generalised lipodystrophy and altered fuel utilisation without severe metabolic disease. Mol Metab. 2018;10:55-65.

148. Liu L, Jiang Q, Wang X, Zhang Y, Lin RC, Lam SM, et al. Adipose-specific knockout of SEIPIN/BSCL2 results in progressive lipodystrophy. Diabetes. 2014;63(7):2320-31.

149. Chen W, Zhou H, Saha P, Li L, Chan L. Molecular mechanisms underlying fasting modulated liver insulin sensitivity and metabolism in male lipodystrophic Bscl2/Seipin-deficient mice. Endocrinology. 2014;155(11):4215-25.

150. McIlroy GD, Mitchell SE, Han W, Delibegovic M, Rochford JJ. Ablation of Bscl2/seipin in hepatocytes does not cause metabolic dysfunction in congenital generalised lipodystrophy. Dis Model Mech. 2020;13(1).

151. Joubert M, Jagu B, Montaigne D, Marechal X, Tesse A, Ayer A, et al. The Sodium-Glucose Cotransporter 2 Inhibitor Dapagliflozin Prevents Cardiomyopathy in a Diabetic Lipodystrophic Mouse Model. Diabetes. 2017;66(4):1030-40.

152. Bai B, Yang W, Fu Y, Foon HL, Tay WT, Yang K, et al. Seipin Knockout Mice Develop Heart Failure With Preserved Ejection Fraction. JACC Basic Transl Sci. 2019;4(8):924-37.

153. Wang M, Xing J, Liu M, Gao M, Liu Y, Li X, et al. Deletion of Seipin Attenuates Vascular Function and the Anticontractile Effect of Perivascular Adipose Tissue. Front Cardiovasc Med. 2021;8:706924.

154. Liu XJ, Wu XY, Wang H, Wang SX, Kong W, Zhang L, et al. Renal injury in Seipin-deficient lipodystrophic mice and its reversal by adipose tissue transplantation or leptin administration alone: adipose tissue-kidney crosstalk. FASEB J. 2018;32(10):5550-62.

155. El Zowalaty AE, Baumann C, Li R, Chen W, De La Fuente R, Ye X. Seipin deficiency increases chromocenter fragmentation and disrupts acrosome formation leading to male infertility. Cell Death Dis. 2015;6:e1817.

156. Li R, El Zowalaty AE, Chen W, Dudley EA, Ye X. Segregated responses of mammary gland development and vaginal opening to prepubertal genistein exposure in Bscl2(-/-) female mice with lipodystrophy. Reprod Toxicol. 2015;54:76-83.

157. El Zowalaty AE, Li R, Chen W, Ye X. Seipin deficiency leads to increased endoplasmic reticulum stress and apoptosis in mammary gland alveolar epithelial cells during lactation. Biol Reprod. 2018;98(4):570-8.

158. Zowalaty AEE, Ye X. Seipin deficiency leads to defective parturition in mice. Biol Reprod. 2017;97(3):378-86.

159. Ito D, Suzuki N. Seipinopathy: a novel endoplasmic reticulum stress-associated disease. Brain. 2009;132(Pt 1):8-15.

160. Yagi T, Ito D, Nihei Y, Ishihara T, Suzuki N. N88S seipin mutant transgenic mice develop features of seipinopathy/BSCL2-related motor neuron disease via endoplasmic reticulum stress. Hum Mol Genet. 2011;20(19):3831-40.

161. Holtta-Vuori M, Salo VT, Ohsaki Y, Suster ML, Ikonen E. Alleviation of seipinopathy-related ER stress by triglyceride storage. Hum Mol Genet. 2013;22(6):1157-66.

162. Guo J, Qiu W, Soh SL, Wei S, Radda GK, Ong WY, et al. Motor neuron degeneration in a mouse model of seipinopathy. Cell Death Dis. 2013;4:e535.

163. Fei W, Li H, Shui G, Kapterian TS, Bielby C, Du X, et al. Molecular characterization of seipin and its mutants: implications for seipin in triacylglycerol synthesis. J Lipid Res. 2011;52(12):2136-47.

164. Gimeno RE, Klaman LD. Adipose tissue as an active endocrine organ: recent advances. Curr Opin Pharmacol. 2005;5(2):122-8.

165. Wang H, Xu PF, Li JY, Liu XJ, Wu XY, Xu F, et al. Adipose tissue transplantation ameliorates lipodystrophy-associated metabolic disorders in seipin-deficient mice. Am J Physiol Endocrinol Metab. 2019;316(1):E54-E62.

166. Gao M, Wang M, Guo X, Qiu X, Liu L, Liao J, et al. Expression of seipin in adipose tissue rescues lipodystrophy, hepatic steatosis and insulin resistance in seipin null mice. Biochem Biophys Res Commun. 2015;460(2):143-50.

167. Xiong J, Sun P, Wang Y, Hua X, Song W, Wang Y, et al. Heterozygous deletion of Seipin in islet beta cells of male mice has an impact on insulin synthesis and secretion through reduced PPARgamma expression. Diabetologia. 2020;63(2):338-50.

168. Wang M, Gao M, Liao J, Qi Y, Du X, Wang Y, et al. Adipose tissue deficiency results in severe hyperlipidemia and atherosclerosis in the low-density lipoprotein receptor knockout mice. Biochim Biophys Acta. 2016;1861(5):410-8.

169. Ebihara C, Aizawa-Abe M, Zhao M, Gumbilai V, Ebihara K. Different sites of actions make different responses to thiazolidinediones between mouse and rat models of fatty liver. Sci Rep. 2022;12(1):449.

170. Bruder-Nascimento T, Kress TC, Pearson M, Chen W, Kennard S, Belin de Chantemele EJ. Reduced Endothelial Leptin Signaling Increases Vascular Adrenergic Reactivity in a Mouse Model of Congenital Generalized Lipodystrophy. Int J Mol Sci. 2021;22(19).

171. Bruder-Nascimento T, Faulkner JL, Haigh S, Kennard S, Antonova G, Patel VS, et al. Leptin Restores Endothelial Function via Endothelial PPARgamma-Nox1-Mediated Mechanisms in a Mouse Model of Congenital Generalized Lipodystrophy. Hypertension. 2019;74(6):1399-408.

172. Dollet L, Levrel C, Coskun T, Le Lay S, Le May C, Ayer A, et al. FGF21 Improves the Adipocyte Dysfunction Related to Seipin Deficiency. Diabetes. 2016;65(11):3410-7.

173. Gao M, Liu L, Wang X, Mak HY, Liu G, Yang H. GPAT3 deficiency alleviates insulin resistance and hepatic steatosis in a mouse model of severe congenital generalized lipodystrophy. Hum Mol Genet. 2020;29(3):432-43.

174. Sommer N, Roumane A, Han W, Delibegovic M, Rochford JJ, McIlroy GD. Gene therapy restores adipose tissue and metabolic health in a pre-clinical mouse model of lipodystrophy. Mol Ther Methods Clin Dev. 2022;27:206-16.

175. Sanchez-Iglesias S, Unruh-Pinheiro A, Guillin-Amarelle C, Gonzalez-Mendez B, Ruiz-Riquelme A, Rodriguez-Canete BL, et al. Skipped BSCL2 Transcript in Celia's Encephalopathy (PELD): New Insights on Fatty Acids Involvement, Senescence and Adipogenesis. PLoS One. 2016;11(7):e0158874.

176. Sanchez-Iglesias S, Fernandez-Liste A, Guillin-Amarelle C, Rabano A, Rodriguez-Canete L, Gonzalez-Mendez B, et al. Does Seipin Play a Role in Oxidative Stress Protection and Peroxisome Biogenesis? New Insights from Human Brain Autopsies. Neuroscience. 2019;396:119-37.

177. Cobelo-Gomez S, Sanchez-Iglesias S, Rabano A, Senra A, Aguiar P, Gomez-Lado N, et al. A murine model of BSCL2-associated Celia's encephalopathy. Neurobiol Dis. 2023;187:106300.

178. Schaar KL, Brenneman MM, Savitz SI. Functional assessments in the rodent stroke model. Exp Transl Stroke Med. 2010;2(1):13.

179. Febinger HY, Thomasy HE, Gemma C. A Controlled Cortical Impact Mouse Model for Mild Traumatic Brain Injury. Bio-protocol. 2016;6(16):e1901.

180. Fujimoto ST, Longhi L, Saatman KE, Conte V, Stocchetti N, McIntosh TK. Motor and cognitive function evaluation following experimental traumatic brain injury. Neurosci Biobehav Rev. 2004;28(4):365-78.

181. Encarnacion A, Horie N, Keren-Gill H, Bliss TM, Steinberg GK, Shamloo M. Long-term behavioral assessment of function in an experimental model for ischemic stroke. J Neurosci Methods. 2011;196(2):247-57.

182. Tatem KS, Quinn JL, Phadke A, Yu Q, Gordish-Dressman H, Nagaraju K. Behavioral and locomotor measurements using an open field activity monitoring system for skeletal muscle diseases. J Vis Exp. 2014(91):51785.

183. Seibenhener ML, Wooten MC. Use of the Open Field Maze to measure locomotor and anxiety-like behavior in mice. J Vis Exp. 2015(96):e52434.

184. Shepherd JK, Grewal SS, Fletcher A, Bill DJ, Dourish CT. Behavioural and pharmacological characterisation of the elevated "zero-maze" as an animal model of anxiety. Psychopharmacology (Berl). 1994;116(1):56-64.

185. O'Leary TP, Gunn RK, Brown RE. What are we measuring when we test strain differences in anxiety in mice? Behav Genet. 2013;43(1):34-50.

186. Deacon RM. Measuring motor coordination in mice. J Vis Exp. 2013(75):e2609.

187. Brooks SP, Dunnett SB. Tests to assess motor phenotype in mice: a user's guide. Nat Rev Neurosci. 2009;10(7):519-29.

188. Curzon P, Zhang M, Radek RJ, Fox GB. The Behavioral Assessment of Sensorimotor Processes in the Mouse: Acoustic Startle, Sensory Gating, Locomotor Activity, Rotarod, and Beam Walking. In: Buccafusco JJ, editor. Methods of Behavior Analysis in Neuroscience. Frontiers in Neuroscience. 2nd ed. Boca Raton (FL)2009.

189. Aartsma-Rus A, van Putten M. Assessing functional performance in the mdx mouse model. J Vis Exp. 2014(85).

190. Bromley-Brits K, Deng Y, Song W. Morris water maze test for learning and memory deficits in Alzheimer's disease model mice. J Vis Exp. 2011(53).

191. Deacon RM. Shallow water (paddling) variants of water maze tests in mice. J Vis Exp. 2013(76).

192. Nunez J. Morris Water Maze Experiment. J Vis Exp. 2008(19).

193. Benede-Ubieto R, Estevez-Vazquez O, Ramadori P, Cubero FJ, Nevzorova YA. Guidelines and Considerations for Metabolic Tolerance Tests in Mice. Diabetes Metab Syndr Obes. 2020;13:439-50.

194. Mirrione MM, Schiffer WK, Fowler JS, Alexoff DL, Dewey SL, Tsirka SE. A novel approach for imaging brain-behavior relationships in mice reveals unexpected metabolic patterns during seizures in the absence of tissue plasminogen activator. Neuroimage. 2007;38(1):34-42.

195. Ma Y, Hof PR, Grant SC, Blackband SJ, Bennett R, Slatest L, et al. A three-dimensional digital atlas database of the adult C57BL/6J mouse brain by magnetic resonance microscopy. Neuroscience. 2005;135(4):1203-15.

196. Greenfield EA. Sampling and Preparation of Mouse and Rat Serum. Cold Spring Harb Protoc. 2017;2017(11):pdb prot100271.

197. Parasuraman S, Raveendran R, Kesavan R. Blood sample collection in small laboratory animals. J Pharmacol Pharmacother. 2010;1(2):87-93.

198. Golde WT, Gollobin P, Rodriguez LL. A rapid, simple, and humane method for submandibular bleeding of mice using a lancet. Lab Anim (NY). 2005;34(9):39-43.

199. Folch J, Lees M, Sloane Stanley GH. A simple method for the isolation and purification of total lipides from animal tissues. J Biol Chem. 1957;226(1):497-509.

200. L. SC. A practical guide to the histology of the mouse. Chichester, West Sussex, UK: Wiley Blackwell; 2014.

201. Kleiner DE, Brunt EM, Van Natta M, Behling C, Contos MJ, Cummings OW, et al. Design and validation of a histological scoring system for nonalcoholic fatty liver disease. Hepatology. 2005;41(6):1313-21.

202. Rinella ME, Lazarus JV, Ratziu V, Francque SM, Sanyal AJ, Kanwal F, et al. A multisociety Delphi consensus statement on new fatty liver disease nomenclature. J Hepatol. 2023;79(6):1542-56.

203. Rabano A, Guerrero Marquez C, Juste RA, Geijo MV, Calero M. Medial Temporal Lobe Involvement in Human Prion Diseases: Implications for the Study of Focal Non Prion Neurodegenerative Pathology. Biomolecules. 2021;11(3).

204. Haas M, Seshan SV, Barisoni L, Amann K, Bajema IM, Becker JU, et al. Consensus definitions for glomerular lesions by light and electron microscopy: recommendations from a working group of the Renal Pathology Society. Kidney Int. 2020;98(5):1120-34.

205. de Boer RA, De Keulenaer G, Bauersachs J, Brutsaert D, Cleland JG, Diez J, et al. Towards better definition, quantification and treatment of fibrosis in heart failure. A scientific roadmap by the Committee of Translational Research of the Heart Failure Association (HFA) of the European Society of Cardiology. Eur J Heart Fail. 2019;21(3):272-85.

206. OCDE. Guidance Document on the Collection of Eyes Tissues for Histological Evaluation and Collection of Data - Second Edition2018.

207. Victoria B, Cabezas-Agricola JM, Gonzalez-Mendez B, Lattanzi G, Del Coco R, Loidi L, et al. Reduced adipogenic gene expression in fibroblasts from a patient with type 2 congenital generalized lipodystrophy. Diabet Med. 2010;27(10):1178-87.

208. Livak KJ, Schmittgen TD. Analysis of relative gene expression data using real-time quantitative PCR and the 2(-Delta Delta C(T)) Method. Methods. 2001;25(4):402-8.

209. Bradford MM. A rapid and sensitive method for the quantitation of microgram quantities of protein utilizing the principle of protein-dye binding. Anal Biochem. 1976;72:248-54.

210. Sanchez-Iglesias S, Fernandez-Pombo A, Cobelo-Gomez S, Hermida-Ameijeiras A, Alarcon-Martinez H, Domingo-Jimenez R, et al. Celia's Encephalopathy (BSCL2-Gene-Related): Current Understanding. J Clin Med. 2021;10(7).

211. Voogd J, Glickstein M. The anatomy of the cerebellum. Trends Neurosci. 1998;21(9):370-5.

212. Kovacevic N, Henderson JT, Chan E, Lifshitz N, Bishop J, Evans AC, et al. A three-dimensional MRI atlas of the mouse brain with estimates of the average and variability. Cereb Cortex. 2005;15(5):639-45.

213. Yu X, Qian C, Chen DY, Dodd SJ, Koretsky AP. Deciphering laminar-specific neural inputs with line-scanning fMRI. Nat Methods. 2014;11(1):55-8.

214. Ding L, Yang X, Tian H, Liang J, Zhang F, Wang G, et al. Seipin regulates lipid homeostasis by ensuring calcium-dependent mitochondrial metabolism. EMBO J. 2018;37(17).

215. Salo VT. Seipin-still a mysterious protein? Front Cell Dev Biol. 2023;11:1112954.

216. Butterfield DA, Perluigi M, Reed T, Muharib T, Hughes CP, Robinson RA, et al. Redox proteomics in selected neurodegenerative disorders: from its infancy to future applications. Antioxid Redox Signal. 2012;17(11):1610-55.

217. Cipolla CM, Lodhi IJ. Peroxisomal Dysfunction in Age-Related Diseases. Trends Endocrinol Metab. 2017;28(4):297-308.

218. Dumont M, Wille E, Stack C, Calingasan NY, Beal MF, Lin MT. Reduction of oxidative stress, amyloid deposition, and memory deficit by manganese superoxide dismutase overexpression in a transgenic mouse model of Alzheimer's disease. FASEB J. 2009;23(8):2459-66.

219. Santos MJ, Quintanilla RA, Toro A, Grandy R, Dinamarca MC, Godoy JA, et al. Peroxisomal proliferation protects from beta-amyloid neurodegeneration. J Biol Chem. 2005;280(49):41057-68.

220. Baier MP, Nagaraja RY, Yarbrough HP, Owen DB, Masingale AM, Ranjit R, et al. Selective Ablation of Sod2 in Astrocytes Induces Sex-Specific Effects on Cognitive Function, d-Serine Availability, and Astrogliosis. J Neurosci. 2022;42(31):5992-6006.

221. Bhaskaran S, Kumar G, Thadathil N, Piekarz KM, Mohammed S, Lopez SD, et al. Neuronal deletion of MnSOD in mice leads to demyelination, inflammation and progressive paralysis that mimics phenotypes associated with progressive multiple sclerosis. Redox Biol. 2023;59:102550.

222. Stasko MR, Costa AC. Experimental parameters affecting the Morris water maze performance of a mouse model of Down syndrome. Behav Brain Res. 2004;154(1):1-17.

223. Arque G, Fotaki V, Fernandez D, Martinez de Lagran M, Arbones ML, Dierssen M. Impaired spatial learning strategies and novel object recognition in mice haploinsufficient for the dual specificity tyrosine-regulated kinase-1A (Dyrk1A). PLoS One. 2008;3(7):e2575.

224. Ramakrishna S, Jhaveri V, Konings SC, Nawalpuri B, Chakraborty S, Holst B, et al. APOE4 Affects Basal and NMDAR-Mediated Protein Synthesis in Neurons by Perturbing Calcium Homeostasis. J Neurosci. 2021;41(42):8686-709.

225. Srinivasan AR, Tran TT, Bonini NM. Loss of miR-34 in Drosophila dysregulates protein translation and protein turnover in the aging brain. Aging Cell. 2022;21(3):e13559.

226. Davies SW, Turmaine M, Cozens BA, DiFiglia M, Sharp AH, Ross CA, et al. Formation of neuronal intranuclear inclusions underlies the neurological dysfunction in mice transgenic for the HD mutation. Cell. 1997;90(3):537-48.

227. Sieradzan KA, Mechan AO, Jones L, Wanker EE, Nukina N, Mann DM. Huntington's disease intranuclear inclusions contain truncated, ubiquitinated huntingtin protein. Exp Neurol. 1999;156(1):92-9.

228. Patni N, Garg A. Lipodystrophy for the Diabetologist-What to Look For. Curr Diab Rep. 2022;22(9):461-70.

229. Gonzalo MM, Estefania CV. Congenital Generalized Lipodystrophy Type 2 in a Patient From a High-Prevalence Area. J Endocr Soc. 2017;1(8):1012-4.

230. Ribeiro A, Brandao JR, Cleto E, Santos M, Borges T, Santos Silva E. Fatty Liver and Autoimmune Hepatitis: Two Forms of Liver Involvement in Lipodystrophies. GE Port J Gastroenterol. 2019;26(5):362-9.

231. Javor ED, Ghany MG, Cochran EK, Oral EA, DePaoli AM, Premkumar A, et al. Leptin reverses nonalcoholic steatohepatitis in patients with severe lipodystrophy. Hepatology. 2005;41(4):753-60.

232. Xu P, Wang H, Kayoumu A, Wang M, Huang W, Liu G. Diet rich in Docosahexaenoic Acid/Eicosapentaenoic Acid robustly ameliorates hepatic steatosis and insulin resistance in seipin deficient lipodystrophy mice. Nutr Metab (Lond). 2015;12:58.

233. Liao J, Liu X, Gao M, Wang M, Wang Y, Wang F, et al. Dyslipidemia, steatohepatitis and atherogenesis in lipodystrophic apoE deficient mice with Seipin deletion. Gene. 2018;648:82-8.

234. Tian Y, Bi J, Shui G, Liu Z, Xiang Y, Liu Y, et al. Tissue-autonomous function of Drosophila seipin in preventing ectopic lipid droplet formation. PLoS Genet. 2011;7(4):e1001364.

235. Su X, Kong Y, Peng D. Fibroblast growth factor 21 in lipid metabolism and non-alcoholic fatty liver disease. Clin Chim Acta. 2019;498:30-7.

236. Miehle K, Ebert T, Kralisch S, Hoffmann A, Kratzsch J, Schlogl H, et al. Serum concentrations of fibroblast growth factor 21 are elevated in patients with congenital or acquired lipodystrophy. Cytokine. 2016;83:239-44.

237. Softic S, Boucher J, Solheim MH, Fujisaka S, Haering MF, Homan EP, et al. Lipodystrophy Due to Adipose Tissue-Specific Insulin Receptor Knockout Results in Progressive NAFLD. Diabetes. 2016;65(8):2187-200.

238. Thomou T, Mori MA, Dreyfuss JM, Konishi M, Sakaguchi M, Wolfrum C, et al. Adipose-derived circulating miRNAs regulate gene expression in other tissues. Nature. 2017;542(7642):450-5.

239. Dollet L, Magre J, Cariou B, Prieur X. Function of seipin: new insights from Bscl2/seipin knockout mouse models. Biochimie. 2014;96:166-72.

240. Fang T, Wang H, Pan X, Little PJ, Xu S, Weng J. Mouse models of nonalcoholic fatty liver disease (NAFLD): pathomechanisms and pharmacotherapies. Int J Biol Sci. 2022;18(15):5681-97.

241. Van Herck MA, Vonghia L, Francque SM. Animal Models of Nonalcoholic Fatty Liver Disease-A Starter's Guide. Nutrients. 2017;9(10).

242. Kubota N, Kado S, Kano M, Masuoka N, Nagata Y, Kobayashi T, et al. A high-fat diet and multiple administration of carbon tetrachloride induces liver injury and pathological features associated with non-alcoholic steatohepatitis in mice. Clin Exp Pharmacol Physiol. 2013;40(7):422-30.

243. Oniciu DC, Hashiguchi T, Shibazaki Y, Bisgaier CL. Gemcabene downregulates inflammatory, lipid-altering and cell-signaling genes in the STAM model of NASH. PLoS One. 2018;13(5):e0194568.

244. Park DH, Shin JW, Park SK, Seo JN, Li L, Jang JJ, et al. Diethylnitrosamine (DEN) induces irreversible hepatocellular carcinogenesis through overexpression of G1/S-phase regulatory proteins in rat. Toxicol Lett. 2009;191(2-3):321-6.

245. Chong AY, Lupsa BC, Cochran EK, Gorden P. Efficacy of leptin therapy in the different forms of human lipodystrophy. Diabetologia. 2010;53(1):27-35.

246. Stern JH, Rutkowski JM, Scherer PE. Adiponectin, Leptin, and Fatty Acids in the Maintenance of Metabolic Homeostasis through Adipose Tissue Crosstalk. Cell Metab. 2016;23(5):770-84.

247. Nasrallah MP, Ziyadeh FN. Overview of the physiology and pathophysiology of leptin with special emphasis on its role in the kidney. Semin Nephrol. 2013;33(1):54-65.

248. Goto K, Kaneko Y, Sato Y, Otsuka T, Yamamoto S, Goto S, et al. Leptin deficiency down-regulates IL-23 production in glomerular podocytes resulting in an attenuated immune response in nephrotoxic serum nephritis. Int Immunol. 2016;28(4):197-208.

249. Park HK, Ahima RS. Physiology of leptin: energy homeostasis, neuroendocrine function and metabolism. Metabolism. 2015;64(1):24-34.

250. Tschop J, Nogueiras R, Haas-Lockie S, Kasten KR, Castaneda TR, Huber N, et al. CNS leptin action modulates immune response and survival in sepsis. J Neurosci. 2010;30(17):6036-47.

251. Garg A. Gender differences in the prevalence of metabolic complications in familial partial lipodystrophy (Dunnigan variety). J Clin Endocrinol Metab. 2000;85(5):1776-82.

252. McIlroy GD, Mitchell SE, Han W, Delibegovic M, Rochford JJ. Female adipose tissue-specific Bscl2 knockout mice develop only moderate metabolic dysfunction when housed at thermoneutrality and fed a high-fat diet. Sci Rep. 2018;8(1):17863.

ANNEXES

Annex 1. Sequence of the final targeting vector.

Homology arms are in green. KI region (Human *BSCL2* without exon 7) is in blue, being in **bigger** letter the 3 different nucleotides from the *BSCL2* wild type sequence. Frt sites are in violet, LoxP sites are in red and Lox2272 sites are in pink. Exons are underlined.

```
1     CGCTTACAAT TTCCATTCGC CATTCAGGCT GCGCAACTGT TGGGAAGGGC GATCGGTGCG GGCCTCTTCG CTATTACGCC AGCTGGCGAA AGGGGGATGT
101   GCTGCAAGGC GATTAAGTTG GGTAACGCCA GGGTTTTCCC AGTCACGACG TTGTAAAACG ACGGCCAGTG AATTGTAATA CGACTCACTA TAGGGCGAAT
201   TGGAGCTCCA CCGCCCGGGC TGGTTCTTTC CGCCTCAGAA GCCATAGAGC CCACCGCATC CCCAGCATGC CTGCTATTGT CTTCCCAATC CTCCCCCTTG
301   CTGTCCTGCC CCACCCCACC CCCCAGAATA GAATGACACC TACTCAGACA ATGCGATGCA ATTTCCTCAT TTTATTAGGA AAGGACAGTG GGAGTGGCAC
401   CTTCCAGGGT CAAGGAAGGC ACGGGGGAGG GGCAAACAAC AGATGGCTGG CAACTAGAAG GCACAGTCGA GGCTGATCAG CGAGCTCTAG GATCTGCATT
501   CCACCACTGC TCCCATTCAT CAGTTCCATA GGTTGGAATC TAAAATACAC AAACAATTAG AATCAGTAGT TTAACACATT ATACACTTAA AAATTTTATA
601   TTTACCTTAG AGCTTTAAAT CTCTGTAGGT AGTTTGTCCA ATTATGTCAC ACCACAGAAG TAAGGTTCCT TCACAAAGAG ATCGCCTGAC ACGATTTCCT
701   GCACAGGCTT GAGCCATATA CTCATACATC GCATCTTGGC CACGTTTTCC ACGGGTTTCA AAATTAATCT CAAGTTCTAC GCTTAACGCT TTCGCCTGTT
801   CCCAGTTATT AATATATTCA ACGCTAGAAC TCCCCTCAGC GAAGGGAAGG CTGAGCACTA CACGCGAAGC ACCATCACCG AACCTTTTGA TAAACTCTTC
901   CGTTCCGACT TGCTCCATCA ACGGTTCAGT GAGACTTAAA CCTAACTCTT TCTTAATAGT TTCGGCATTA TCCACTTTTA GTGCGAGAAC CTTCGTCAGT
1001  CCTGGATACG TCACTTTGAC CACGCCTCCA GCTTTTCCAG AGAGCGGGTT TTCATTATCT ACAGAGTATC CCGCAGCGTC GTATTTATTG TCGGTACTAT
1101  AAAACCCTTT CCAATCATCG TCATAATTTC CTTGTGTACC AGATTTTGGC TTTTGTATAC CTTTTTGAAT GGAATCTACA TAACCAGGTT TAGTCCCGTG
1201  GTACGAAGAA AAGTTTTCCA TCACAAAAGA TTTAGAAGAA TCAACAACAT CATCAGGATC CATGGCACGC GCTTCTACAA GGCGCTGGCC GAAGAGGTGC
1301  GGGAGTTTCA CGCCACCAAG ATCTGCGGCA CGCTGTTGAC GCTGTTAAGC GGGTCGCTGC AGGGTCGCTC GGTGTTCGAG GCCACACGCG TCACCTTAAT
1401  ATGCGAAGTG GACCTGGGAC CGCGCCGCCC CGACTGCATC TGCGTGTTCG AATTCGCCAA TGACAAGACG CTGGGCGGGG TTTGCTCGAC ATTGGGTGGA
1501  AACATTCCAG GCCTGGGTGG AGAGGCTTTT TGCTTCCTCT TGCAAAACCA CACTGCTCGA CATTGGGTGG AAACATTCCA GGCCTGGGTG GAGAGGCTTT
1601  TTGCTTCCTC TTGAAAACCA CACTGCTCGA TTTGTTAGCA GCCTCGAATC AACCCGGGCG ATCCTAGGCG ATGAGATCTA GCTGTCGCGA AGAGTGGCGC
1701  GCCATACTGA AGTCTGCGTG TGTGCGCATG CACGCGCTCT AGAGAGAGAG TGTGCAGGGT ACTCTTGTGG AGTCAGAAAA ACTCTTGAGT TCTCCCCCAC
1801  CACCTTGATG GTTGAAACTC ACTGGGCCTG CAGTCAAACA CCTGTACCTG TTCAGCCATT TGGTTATGAC ACCCAGGGAA TAGTTAGACC TTCCTACCCA
1901  GAACGATTTG TCACCTAAAA CTAGAACAGC CGGGCATGGT GGCGCACGCC TTTAATCCCA GCATTCAGGG AGGCAGAGGC AGGCGGATCT CTGAGTTTGA
2001  GGCCAGCCTG GTCTACAAAG TGAGTTCCAG GACAGCCAGG GCTATACAGA GAAACCCTGT CTCGAAAAAC CAAAAAGAAT AAAAACAAAA ACAAAACAAC
2101  TAGGACATTT AAATGTAGCC CAGGATCCAA AACATATATG TACGTTCACT CAGACCAAAA AGCTTCTAGG CGGTGGCCTG GATCCCCTAA CCCTTTGCCG
2201  GGATCTCACT CTAGGAGGCA TTCTTGAGAC ATGGTTTCCA GTCAGACGAC ATTCTGAACC CTTGTGATGT TTTCAGTTAC CTTGAGGAGA AAATAAAAAA
2301  GCCCCAATTC AACAAGAAAA CAAATTTATT ACTTATTTAG ATCCCACAGA GACCAAGGAA CAGGGTGCTC CAAGATGGCC TGTTTAACAC ATTTGTGTTA
2401  TTACATACAC CTCAAAGGGA ACCTCTACTC AGGCGAGATT CTTATGCAAA ACTCACTCTG GGCTTCTTGG GTCCCAGTCC TAGTGACTGG TTGTTTTAAG
2501  TCAGGATTTC ATTGTGTATT GTGTGTCGTC GTGGCTGGCT TGGAACTCAG AGATCCATCT GCCTCTGTGT GTGTCCAACA CCTCCGGAGT GTTGGTCACC
2601  ACACTGAACT TAAGAACCCA TGACTGCTTT AGGTGTCTCC CCATCCCCAC TCCCCGTGAT TGGTCTCCAA AGCATGTCTA GTTCCAGATT CTATGGGACA
2701  GAGAACCTGA CTCTGACTTT GAGAGGGCAG GGGCAGCCAT TTTAAGACCA GAGGATCGCA TAAGGGATCG TTCCCTATTG GGAACGCTGG GGACCGCCAT
2801  TTTAAGAGCA CCCTCGGCGC GTGCCTCCAT GCGGGTACGA ACAGGCAGCC GCCATCTTGG GCATTGGCTG CCGCGCCGAG TCGCCCTGTC CCGCCCCACG
2901  GCCTCTCGGG CCACCTCCCC CCGGGGCTGC TGTCCCTGGG CCTGCGGAAA CCCACCCTGC TCGCCCTTGT GTGGTTCTCG CCGCTTACGT TGCGCGCTCG Exon 3
3001  TGTGAATGCT CCGCGGCTTC TGAGCGCTCG TTTTAACAAC CCCCCACTGG GGGCGCTCGG GCACCTTATA CTTTGCGATC TCCAATCCTT ACAATGTCTA Gng3
3101  ACGGGCTCGA CTGGCCCTGT TCCCTGGATA TGGCAAGTGT ATCGATTAAG GATCCTCTTT CCCAAGAACG CTAACACAGA CGTTGTCCTC TGAGGCTCTG
3201  AATGACTTTA TTCTTCAAAT GCCTTTACCT TTCATAGCTC CAGGTGAGCA CCCGGGCATC CCCCTCTCCA TTGCCTGAAC GGATGGATCA CCGAGGGAAA
3301  CAGGCAGGAT TTTGGCAGTT TAGCGGGGTC CCTTTATAGA TAGAGTAGAA GGTGCTTGGA GTTAGCCTGA AAGGGTGAGG AGATGGGGTA GACATGGGTA
3401  AGGAGGGCCT TGTGCTTCAA ATAATCTCCG GGTAAATGCG GGTAGAAGTG ATCTACTACA ATTTCCAATC TAAGGGCGGG TCTGGGAGGG GGCGATGAGT
3501  TCAGAGGAGG TCCACCGCTC TTCAGAGGAG CGCACAGAAG AACTTCTTCT CCCGGAAGGG GTTCTCGGAA GTGGGCACAG GAGTGATGAG GGGGTCCTCA
3601  CAAGCGTGGG CATCACAGTA TGTCATCAGG TCTGCTGCTG CCTTGGACAC CTGGAACCCA GCCAGGAAGG GATACATTAA CCAGAATTCC TGAAAGGGAC
3701  TGCAGTTCTC TTCTCCAATA GACTATCTTT TTGTTTCTAG TGCCCTTTGA GACAGCCCTC TCCCCCAACG CCAGTCCTCG GGAACAACTT TGCTGACAAA
3801  GCCCAGTTTC TGCCACTGAC CTCAGGGTGT CAAGAAAAGA AGCATCTTTT CTTGGGGGGA GGGGGGAGGG GAGGGTATTG CAAACCCACA GCTGAGCCCT
3901  GAAGGGCTGA TGGGAGCCAG GGTCGCACCC ACCTTTATCC GGCACAAGCT GGCCTCAATC TTAAGCTGTT CCACCATCTT GCGTGCTTGA CCAATACTCA Exon 2
4001  TAGTGCTGTT AACGGGGGTC TCCCCTTTCA TCCTGGAGTA AAGACAGTCA GCTGAAACAC TCAGCTCTTC ACAACCACAC ACCTGGGATT GTGCCCCCAT Gng3
4101  TCTCCAGTGG CCATCCCAGG TTTTTTTTTC TTTCTTTTTT TTTTTTTTTT TTAAGTAGGG AGAATGGAGA AGATAAAATG AAATATTCTC CTAACCCCTG
4201  GGTCCTGGTC ATCAAATTAT ACAAACGATT TAAGGATTTT AAGTCTTTGA GCCAAATATG TTACCAGCAA TGAAAGCCTC AGTCAGAAAG AGCCCCACCC
4301  TGATGAAATC ACATCAGCCA CCTGTCCCCC CTCAAGCCCT GAAGAGAAAA AAAGCTGCTT TCTACTCACC TGAAGTAACA GCAGCGGCAG CCAGGGATGT
4401  AGGGTCAGTG GGGAGGGGGC ACCAAACCCT GCCTCAGATA GGTGCCCCAC CCTGCCAGGA CTTGGAGCTA AAAATATCCG TAGCACTGAC AGTTAATGCA Exon 1
4501  GAGAAGGTCA CTAGAGATGC TCAGACGAGA TCCTTGGAGG GGTGGTCTCA GTCTCCACAG CTTAAGTTCT GCCCAGATGG CTGGTACCTG AAGGATGAAG Gng3
4601  GATGCTAGAA GGAGCTGCTG ATTCTGGCGC ATACCAACTG CCTGGACAGT GGGGGAGTCA GTCTGCTGTT TGCATCCCCT GTGCACACCC TCACTGCTGC
4701  TCTCTCACTA CCTGCCCCTG CCATTGTACA AGTCCTTAGT CTAAACTAGA TAGCTCCCCA AAGGGCCTGA GGCAGAAGCA GGCTCCCCTC TCAAATGGGG
4801  TGGTCTGGGC CTGTGACAGC CCCTGCATTA GAGTCTGTCC CCACTGCGGA AGACCCTGCT CATTTGAAAG TCTGACATCA GCTGGGCTGC TGCTCCCCCA
4901  CCCCCACCCC CACCCTGACA CAGCACTTAG CACCTGAATC TTGGTTTCTT TCAGTGACCC ACCGTTCTTC AGAGCTAGGA AAATGTAACA CTCTACAGGT
5001  GATCAGCTTC TAGATCACCA CTTTCTACCA CGTGAGTGAC GCGAGCTGGG AGACCCAGAG GTAACCCATC AGGAAGATAG CTAAAGAAAT GATACATCAA
5101  AGAAGAGAAG CTGGGGCAAG AGAGACATGC AGAGACCAGA TCAAAGGATC AGACAAAGAC GAGGTAAGGC ACCTTGCCAC GAGAGTTAGT GTGAATGTTG
5201  TGAACACAGG TGGGCTTCTC GGAGTGGGGA GTAGGGTGGC AAGAGTTGGC ACTGGGGAAA TAGGGAATCG ATTGGAAATT TTTCATGTAA TTTGAGTGGA
5301  TTACTACTAT TCAAAAAGAT GTGCATTGGC CTTGCCTCCT GGAGGACGTT ATCCAGACGA TGCCACCATC AGAAATCTAG TCTCATGGTT TTTTGTAGGG
5401  ATTTTGAGGT TGGCTGCATC ACGTGGGTCA CAGAAGGTCA ATCACGCAGC ATAAAAACTG GAGACTGAAA GGGGTTGAAA TGCCGCCACG CTTGACTAGC
5501  GGACGGCACC ATCTGCGCAC ACAACACACA AGATTCAGAT TCTGGCAGGG TGCAAGGCTC TCTGAGCTCC AGTTGGACTC CTACAGGCCC AAGGAACTCT
5601  ACTGAATTTA CAAAAAACAA ACAAACAAAA CAAAACAAAA CAAAATCAGC ATTTATTTCA CACCTCCATT CAATCACACT GAAAAGACAG GTGGTAAAGG
5701  TATGGGCAGA GGGTTGTGGT TGAGGCCTGG AAAGGAGGAC CAAGGAGTCC CAGACTGCGT TGGAGATTAT AATGGGTCCT TTGGTCACTT AACTAAAGTG
5801  TAATGGGCAG AGACACTGGG GAGCAAAGCA TTTTACAGGC TCTGCCCTCT ATGCAAGGCT CAGCCCCTGT AGGCGATTGA CAGTTGGGCG GGGCTTCCTC Exon 1
5901  GGCAGCCGGA ACTGCCTTCT GTATATTGCC TGGGCAGCGA GAGGCCGGTG AGTCTGCCTC GCCGCGGTGG CGATCTGGTG TACACCGCAT TACCCCAGGG
6001  GTGGGCGCCG CAGCGTCGGC CACAGGGTGC TGTGCGGGGG TAGGGGTCAC TTCCTCCGTG AGCGAGCACA GGTCCAGGCA GAGGAAAGAA ACTCTTGGGA
6101  GGCAATTTTG ACTGCTCTAA GGCTGCTGGC TTTGAGCCAG ACTGGCCGGC TGTGCAACCT TAGGCAAGTC ACTCACCTCC TTGCAAACCT CTGGCATTTT
6201  GGATCCATGT CATCTGGGTT TCGAGAGAGA TTTAAAGGCC TCGTTCTCTG TACGTTATAC TTCTGTGAAT GTATCAAGGA GGTTTGTCCC AGGCTCCCGA
6301  AACTGGAGGA AGAGGCTGGA AGCACACTCA GTGGAGGGAG GTGAAGGAGT AATTGGAAGA GAAGCGCATG TGAAGCAATG ACTTTGCTTT GCCCTGCTAC
6401  CTCTAGTTTT CAAAGCCAGT TGAATAAGCT TTTTTGTCTC CAGCTACCCT GGAAAAGAAA CTGTCTTTTC CCTTCTCTTT CTCCAGGAAC CTTCAGCTGC Exon 2
6501  CCTATCCCAT GGCCAAGGGT ATCGTCCCTG TGGAAGACCA GCCAGGAACT CAAAGCCTGA GGCTGGGGCC AGACCCCCTG CTGTCCCCAT CGTTTAACAC
6601  AGATAACTTC GTATAGCATA CATTATACGA AGTTATGACC GACGTCATAG GCGATCGCAT AACTTCGTAT AAAGTATCCT ATACGAAGTT ATTCAGGAAC
6701  TAGAGCAGGT GGGGCGCTGT CGGAGAGCAC CCCCAGCAGG TTCAGAGCTG CCCAGAGTCT CTAGGACAGG GGCAGAAGCA GAAGCAGGAG CAGGAGCAGG
```

```
6801  CAGGTTGGCC TCCGTCAGCA AAGCTGCATC TTCCCAGGAG CCTGAACCAT CACTGGCCTC AGGCTCTAGC TCCTCTTCTC CGCTCAGGGG CTGCTGATCT
6901  GGTTTCTCCT CCTCGGACAG CTGACCCTCT GTCCCTGAGG GATCTTCAGG GCTCTCACCA TCCTCTGTAA CATCTGATTG CGGAGTTGAC TCCTCCTGGC
7001  CTTCAGGCCC TGGCTGATGA GCAGAGATCC TTCGTTGGAC TTCCTTCCGG GAATTGTCTC TTTTTCGGAT GTTAACCTGA GCCCAGTGAA GTGCGCGTGG
7101  ATGCGGAGGT AGGCTCCATA CAGCTGGATG CGCTTGCTGT GGATCTCAAT GATCGCTCCA GTGGTCGGCA CATACGAGTT CTCTCTATAG TCTGCGTAGA
7201  GTTCCACCTC CAGCAGCTGC TTCTGCTCTG CAAAGCCAAA TAGCAGGAGG CTAGAGAAGA CCAGTGTGTC CAGCATCTGG AGCAGGTCTG AGCGGTAATG
7301  CAGCATCACC GAACGCGAAG AAGTGGAGAT GATTCGGCCA CCTCTGGTGT AGCAGGAAAT GGTGACCAAG AACATGCCCA AATCTTGATT CACAGGGGAC
7401  TCTGGCAGCT CAAGCTCTAA GGTAACACGA TACGGCTGTC CATACATCAG CACCCGATCA CGTCCACCCT TAGTCAGCGA GACATTGGCA ACAGGGAAGG
7501  AGCAGAGTGA GGTGGTGGAG GAATCACAGT CGGTCCTGTA GTAGAAATGC ACAGGGCTGA GGTGGCTGAC TGTCGGCATA TAGGAATAGT AGAAGGAGCC
7601  ATAGAGGAAG ACAGACACCC AGAGCAAAAG GAGGATGGTG CAGAAGAGCA CCCCAAACTG CAGCAGCAGC CTGCGGGCAC GGCCTGCCAA GACTTGGCCC
7701  ACCTCCTGGG CCCACAATAA GGCAGGAACT GGAGGGTCGT TGACCATGGC CGGGAGAGCA GGGTGTCTGG CCCCAGGTTC AGGCCTTGCG TTCCTAGCTG
7801  CTCTGCCACC TGGACGCCAC CCCTGGCCAT GGGATCCAGC AGCTGGTGGT TCCTCCTCTT TGTCCGGTCC TTTGATCTGG TCTCCGCACA CCTCTTTTTC
7901  CCCAGCTTCC TCCTTTTGGT CTACCTTTTC TGTAGAGTGA TGGTGATGGT GATGCATATA ACTTCGTATA ATGTATGCTA TACGAAGTTA TCATATGAAG
8001  TCTCGAGGTT ATGTACCTGA CTGATGAAGT TCCTATACTT TCTAGAGAAT AGGAACTTCG AAGGGTTCCG CAAGCTCTAG TCGAGCCCCA GCTGGTTCTT
8101  TCCGCCTCAG AAGCCATAGA GCCCACCGCA TCCCCAGCAT GCCTGCTATT GTCTTCCCAA TCCTCCCCCT TGCTGTCCTG CCCCACCCCA CCCCCAGAAA
8201  TAGAATGACA CCTACTCAGA CAATGCGATG CAATTTCCTC ATTTTATTAG GAAAGGACAG TGGGAGTGGC ACCTTCCAGG GTCAAGGAAG GCACGGGGGA
8301  GGGGCAAACA ACAGATGGCT GGCAACTAGA AGGCACAGTC GAGGCTGATC AGCGAGCTCT AGAGAATTGA TCCCCTCAGA AGAACTCGTC AAGAAGGCGA
8401  TAGAAGGCGA TGCGCTGCGA ATCGGGAGCG GCGATACCGT AAAGCACGAG GAAGCGGTCA GCCCATTCGC CGCCAAGCTC TTCAGCAATA TCACGGGTAG
8501  CCAACGCTAT GTCCTGATAG CGGTCCGCCA CACCCAGCCG GCCACAGTCG ATGAATCCAG AAAAGCGGCC ATTTTCCACC ATGATATTCG GCAAGCAGGC
8601  ATCGCCATGG GTCACGACGA GATCATCGCC GTCGGGCATG CGCGCCTTGA GCCTGGCGAA CAGTTCGGCT GGCGCGAGCC CCTGATGCTC TTCGTCCAGA
8701  TCATCCTGAT CGACAAGACC GGCTTCCATC CGAGTACGTG CTCGCTCGAT GCGATGTTTC GCTTGGTGGT CGAATGGGCA GGTAGCCGGA TCAAGCGTAT
8801  GCAGCCGCCG CATTGCATCA GCCATGATGG ATACTTTCTC GGCAGGAGCA AGGTGAGATG ACAGGAGATC CTGCCCCGGC ACTTCGCCCA ATAGCAGCCA
8901  GTCCCTTCCC GCTTCAGTGA CAACGTCGAG CACAGCTGCG CAAGGAACGC CCGTCGTGGC CAGCCACGAT AGCCGCGCTG CCTCGTCCTG CAGTTCATTC
9001  AGGGCACCGG ACAGGTCGGT CTTGACAAAA AGAACCGGGC GCCCCTGCGC TGACAGCCGG AACACGGCGG CATCAGAGCA GCCGATTGTC TGTTGTGCCC
9101  AGTCATAGCC GAATAGCCTC TCCACCCAAG CGGCCGGAGA ACCTGCGTGC AATCCATCTT GTTCAATGGC CGATCCCATG GTTTAGTTCC TCACCTTGTC
9201  GTATTATACT ATGCCGATAT ACTATGCCGA TGATTAATTG TCAACAGGCT GCAGGTCGAA AGGCCCGGAG ATGAGGAAGA GGAGAACAGC GCGGCAGACG
9301  TGCGCTTTTG AAGCGTGCAG AATGCCGGGC CTCCGGAGGA CCTTCGGGCG CCCGCCCCGC CCCTGAGCCC GCCCCTGAGC CCGCCCCCGG ACCCACCCCT
9401  TCCCAGCCTC TGAGCCCAGA AAGCGAAGGA GCAAAGCTGC TATTGGCCGC TGCCCCAAAG GCCTACCCGC TTCCATTGCT CAGCGGTGCT GTCCATCTGC
9501  ACGAGACTAG TGAGACGTGC TACTTCCATT TGTCACGTCC TGCACGACGC GAGCTGCGGG GCGGGGGGGA ACTTCCTGAC TAGGGGAGGA GTAGAAGGTG
9601  GCGCGAAGGG GCCACCAAAG AACGGAGCCG GTTGGCGCCT ACCGGTGGAT GTGGAATGTG TGCGAGGCCA GAGGCCACTT GTGTAGCGCC AAGTGCCCAG
9701  CGGGGCTGCT AAAGCGCATG CTCCAGACTG CCTTGGGAAA AGCGCCTCCC CTACCCGGTA GAATTTCGAC GACCTGCAGC CAATCCGCCT CAGAAGCCAT
9801  AGAGCCCACC GCATCCCCAG CATGCCTGCT ATTGTCTTCC CAATCCTCCC CCTTGCTGTC CTGCCCCACC CCACCCCCCA GAATAGAATG ACACCTACTC
9901  AGACAATGCG ATGCAATTTC CTCATTTTAT TAGGAAAGGA CAGTGGGAGT GGCACCTTCC AGGGTCAAGG AAGGCACGGG GGAGGGGCAA ACAACAGATG
10001 GCTGGCAACT AGAAGGCACA GTCGAGGCTG ATCAGCGTCA GATCCGCCTG TTGATGTAGC TGCTCAGGTA GTCCAGCACC TCCTGGCTGA TGATGCCGTT
10101 CCAGGCGGGG TATCTGATGC TGCCCTCGGC GCTGCCCTTC AGCTGCTCGA TGTGCTGCCA CTCCTCGATG GGGTTGGTCT CGTCCTTCAG GGCGATCATC
10201 TCCTTGCTGA TGGGGTCGTA GGCGTAGTAC CTGGACACCA GGGCGAAGTA GTGGTCGGGG ATGGCGGTGA TCTGGTGGGT GTAGGTGGTC CTGGCCACGG
10301 CGGAGGCCCT CTTGTCGCTC CAGTTGCCCA CCACGTTTGT CAGCTCGGTC AGGCCCTTCA TGCTCAGAAA GCTGGTCATC AGGTGCCTGC CGATGTGGCT
10401 CTTAGGGCCG TTCTTGATAG CGAAGATGGG GTAGGGGGCG TTCTTCTTCA GGGCCTTGTT GTAGCTGCGC ACCAGGTTGT CCTTCAGCAG CTGGTACTCC
10501 TGCTTGTTGC TGCTGCTGTT GCCGGTCCTG TTCACTCTCT TCAGCACGGG CTCGCTGTTC CTCAGGAACT CGTCCAGGTA CACCAGGGGG TCGATCCTGC
10601 CTCTGGCGCT GAAAAAGTAG ATGTGCCTGG ACACGCTTGT CTTGGTCTCG GTCACCAGGC ACTGAATGAT CACGCCCAGG TACTTGTTCT GCACCAGCTT
10701 GAAGCTCTTG GGGTCCACGT TCTTGATGTC GCTGAACCTG CCGCAGTTGA TGAATGTGGC CAGGAACAGG AACTGGTACA GGGTCTTGGT CTTGGTGAAC
10801 CTGCTGGTGT ACTCGAAGCT GTTCAGGATC TTCTCGGTGA TCTCCCAGAT GCTCTCGCCC TCGGACAGCA GGGCCTTCAG CATCTTCTTG CTGTGGCTGT
10901 TGCCCTTGTC GGCCTCCTCG CTGCTCTCGA ACTGCAGCTG CAGGCTGGAC ACGATGTCGG TGATGTCGCT CTGGTGCTTC TGGCCGTTGT AAGGGATGAT
11001 GGTGAACTCC CAGGCGGGGA TCAGCTTCTT CAGGCTGGCC TCCAGGATGG TGGCCTTCTG GGTCTTGTAC TTGAACTGCA GGCTCTTGTT CACGATGTCG
11101 AAGCTCAGGC TGTTGCTGAT GATGGTGTTG TAGCTCATGA AGGTGGCCCT CTTGATGGCG GTGCCGTTGT GGGTGATCAT CCAGCACAGG TAGGTCAGCT
11201 CGGCGGCACA GCTGGCGATC TTCTCGCCGC TGGGCCTCTC GAATCTCTCC ACGAACTGCC GCACCAGCAC CTTGGGGGGG GTCTTGCACA GGATGTCGAA
11301 CTGGCTCATC ACCTTCCTCT TCTTCTTAGG AGCCATGGCC GCAGGAAAGC AGAGCCCTGA AGCTCCCATC ACCGGCCAAT AAGAGCCAAG CCTGCAGTGT
11401 GACCTCATAG AGCAATGTGC CAGCCAGCCT GACCCCAAGG GCCCTCAGGC TTGGGCACAC TGTCTCTAGG ACCCTGAGAG AAAGACATAC CCATTTCTGC
11501 TTAGGGCCCT GAGGATGAGC CCAGGGGTGG CTTGGCACTG AAGCAAAGGA CACTGGGGCT CAGCTGGCAG CAAAGTGACC AGGATGCTGA GGCTTTGACC
11601 CAGAAGCCAG AGGCCAGAGG CCAGGACTTC TCTTGGTCCC AGTCCACCCT CACTCAGAGC TTTACCAATG CCCTCTGGAT AGTTGTCGGG TAACGGTGGA
11701 CGCCACTGAT TCTCTGGCCA GCCTAGGACT TCGCCATTCC GCTGATTCTG CTCTTCCAGC CACTGGCTGA CCGGTTGGAA GTACTCCAGC AGTGCCTTGG
11801 CATCCAGGGC ATCTGAGCCT ACCAGGTCCT TCAGTACCTC CTGCCAGGGC CTGGAGCAGC CAGCCTGCAA CACCTGCCTG CCAAGCAGAG TGACCACTGT
11901 GGGCACAGGG GACACAGGGT GGGGCCCACA ACAGCACCAT TGTCCACTTG TCCCTCACTA GTAAAAGAAC TCTAGGGTTG CGGGGGGTGG GGGAGGTCTC
12001 TGTGAGGCTG GTAAGGGATA TTTGCCTGGC CCATGGAGCT AGCTTGGCTG GACGTAAACT CCTCTTCAGA CCTGAAGTTC CTATACTTTC TAGAGAATAG
12101 GAACTTCGGA ATTCGATATC ATAACTTCGT ATAGGATACT TTATACGAAG TTATGTCAAT GACCCACCAG TCCCCGCCTT ACTGTGGGCC CAGGAAGTGG  Part of
12201 GCCACGTCTT GGCAGGCCGT GCCCGCAGGC TGATGCTGCA GTTTGGGGTG CTCTTCTGCA CCATCCTTCT TTTGCTTTGG GTGTCTGTGT TCCTCTATGG  Exon 2
12301 CTCCTTCTAC TACTCCTACA TGCCGACGGT CAGCCACCTC AGCCCTGTGC ACTTCCACTA CAGGTGAGAA GGCTGCTCCA TTCAAGTAGA TGGATCTTAA
12401 CTTGAAAATT ACTTCAGGGA CTTGTGGAGT CTCTCCTCTG TTGAATCCCA GTATTGACCG AGGGTGAAAT CTTATTCTAG TGTGCTATCA GGACTTCTGC
12501 CCTCCTGAGC CAAGGCTTGA GCAGGTCTGG GCTGGTAGGG CTTTAGGGTT CTAGGTCTGC CTCTGCTGGA AATTGTGGTT AAGAACTGAG AAAAAGAGCC
12601 TGGTCACGTG TGTAATACCA GTCTGGGGAG GCTGAGTTGG GAGAATTAGC ATGAGTTCCA GGCCAGCCTG GAAGACAGGT TGAGAACTTG TCTCAAAGGG
12701 GTCTAAAAAA AAAAAAAAGA CTAGGAAAAG AAAGTCACTT TTAGCCGGGC AGTGGTGGTG CATGCCTGTA ATCCCAGCAC TTGGGAGGCA GAGGCAGGTG
12801 GATTTCTGAG TTCGAGGCCA GCCTGGTCTA CAGAGTGAGT TCCAGGACAG CCAGGACTGC ACAGAGAAAC CCTGTCTCGA AAAAAAAAAA AAATCACTTT
12901 TAGACCAAGT AGGGCTCAGC GTCTGTTCTG TTGAGGTTGC ATGAAACCTT TGAGCCAATT CAACTGCCAT GGCATCTAAG AATTACACTG GCTTTATTAA
13001 CACGTGAGCT ATTAGGAAAT ACCTCCTTTG CCTTTTAGTG TACTGCCACT CACCCCCAAT GGTACATTCA GTAACCCAAG GCAGTCCTAC TGCTAACCTA
13101 GCCTTCGAGT TCATATCCAT TTTACTCACA CTGCCAAAGT CTCTGTATGT CTCCCAGCAA TGGCTATGAG ACAAATTAAC ATATACAGAA AACGCTTTTA
13201 TGATCATTGG TTTAAAACCT TTTTTCCCC TGTCCCAAAT CCCTAATCTT GTGTTGTCAT TTCTAAGGTA GACCCATGTA AACACTTAGG GAACATGAAT
13301 CCTTTTTTAA TAATTATTTT TGTTTCATGT GCATTGGTGT TTTGCCTGCC CGTGTGGTTG TGTGAAGGTG TCAGATCCCC TGCAACTGGA GTTACAGGCG
13401 GTCGTGAGCT GCCACGTGGT TGCTGGGAAT TGAACTCAGG TCCTCTGCAA GAGTAACCAG TGCTCTTGAC CAATGGGCCA TCTCTCCAGC CCCAAGGGAG
13501 CACGAGTCTT ACATACATGG GGTATATGTA TGTATACTGA GGTAGGAGCT GTGTACCATA TACTATGTGC AGTTTTGCGT ATAATTTATC TTTAAAAGAC
13601 ATATCCATAG GTCCTTTAGG ATGAATTTCT TTTTCCAACC TAGTCCAGAA CTGCTGAATC AGACTCTTTA GGAGAGGGAC CCTAAAATCC ACATGCCCTG
13701 AGATCTTCAA GGGAGCCTAT AGAAACCCTG AGTGTCCTTC GGCTCCTCCC TATGGGTTCT GTTCTCATGA GGAAGAGAAT GAAAGTCTTA TTAGGATCTC
13801 CTGACTCTAG TGTCCACTTC TGTTCTCCAT TTCCTGTAAT GGGGAAAAGG GATGAGTGAG GGGAGGGGCC CTAGAGACTA GGTGTGTGAG CAGGTAGGCT
13901 GGGCAGGCTG GCACCTCACA AAGCATTGTT CATCCCTTCT CATTTAGGAC AGACTGTGAT TCCTCCACCG CCTCTCTCTG CTCTTTCCCT GTTGCCAATG  Exon 3
14001 TCTCACTGGC TAAGAGTGGA CGTGATCGGG TGAGTATGAG AACTAGACAG AGGCTTTGAT TGCTTGAGGA AGATGGGGAG AGCAGGGATT GAGCAACCGA
14101 GATTGAAGAG AAAGGCTCTG ACGCAAACGG GTGGAAAAGA AAATCTGGAA GTTGGTCCCA GTCACTGTGA TACATATCTG TAATGCCAGC ACTAGGAGGA
14201 AAAAGACACA GGGAGATTAT TCCAAATCTG ATATCAGCTT GGGCTTCATA GCCAGACCCT ATCTCTCTAG AGGCTCTGAT AAAAAATAGA ATTACAAGCT
14301 TAAAATGTCC CTTGATATCA AAAAATAAAA CAAAAAAGGA CTTTGAGAAT TAATGTCATT TTTTATTAAA TGAGGTTTTT CTAGTTGTCA GTCTTAACTT
14401 GAACATTTTT TTAAAGTGGT ATTTAAGAAG AAACTGACTT TATAGTAGAA TATCAGCTCT GGCACAGTGG CACACATCTA TAATCACAAT ACTTAACATA
14501 GAAGGATGCT GCCCAGGCTG GCCTCGCACG CTGAGATCCA CTTGCCTTTG CCTCCTAAGT GTGGCCATCA CCACGCAAGG GAGGATATCT TGAGTTTAGG
14601 AGTTAAGAGC ATCCTGAATA AGTTAGTTCA AGGCCTCTCA TTAAAAAAAA AACAAAGGAG CTTGGGAGGT AGAGGCAGAA AGGCTAGCCT GGACTATTTA
14701 AAAAATAAAA AGTAGTTTAC CTTAAAGTTA TGGTCACTAT GTCTCCGCCT CCTATGTGCT GGAGTTAAAG GTACGCCATG TACCAATCCA GACTGGAAGT
14801 GAGTAACCTC AGACGTGCTC GGCTTCCTAA GCGTTGGGAT TGTTAGGAAG TGGGCACCAC CGTGCCAGGC TTGGATTTCT TTTTTCTTTT TTTTTTTCTT
14901 ACACACCAGA AGAGGGCTTG GGATCCCATT ACAGATGGTT GTGAGTCACC ATGTGATTGC TGGGAATTGA ACTCAGGACC TCTGGAAGAG TAGTCAGTGC
15001 TCTTAACTGC TGAGCCATCT CTCCAGACCC TCTTAATAGG TTTATTAAGT TAAAATTTAT ATGAGATACA GTTTACCTCT TAAGGTATAC AGTCGTCGTC
15101 ATATCATTCG ATGCATGTAT TTGGGACAGA GTTTCACTAT GTAGCCTTGG CTGGCCTGGA ACTGGCCATT TCAACCAGGT TGGCCTTGAA TCCACAGCTC
15201 TCCTCCTCCC TTTGGCCTCT TGTGTCGTGG GATTAAAACC ATGCACTGCC GCCCCAGGCA GTTCTATTGT TTTTAATAAG TTCAGTGTTG CACGCATACT
15301 GATATAAATA GACAAACTTA ATCTTTTTTT TAAATTAATA AGCACTCTGC CTTTAAAAAT GAAGAAAGAC CAGGATAACA AGATGATCTG CCACTGCAGT
15401 GATTGTGCAA GAGCTGACTA GGGAGGCAGC GGCCGCGTAC CAGCTTTTGT TCCCTTTAGT GAGGGTTAAT TTCGAGCTTG GCGTAATCAT GGTCATAGCT
15501 GTTTCCTGTG TGAAATTGTT ATCCGCTCAC AATTCCACAC AACATACGAG CCGGAAGCAT AAAGTGTAAA GCCTGGGGTG CCTAATGAGT GAGCTAACTC
15601 ACATTAATTG CGTTGCGCTC ACTGCCCGCT TTCCAGTCGG GAAACCTGTC GTGCCAGCTG CATTAATGAA TCGGCCAACG CGCGGGGAGA GGCGGTTTGC
15701 GTATTGGGCG CTCTTCCGCT TCCTCGCTCA CTGACTCGCT GCGCTCGGTC GTTCGGCTGC GGCGAGCGGT ATCAGCTCAC TCAAAGGCGG TAATACGGTT
15801 ATCCACAGAA TCAGGGGATA ACGCAGGAAA GAACATGTGA GCAAAAGGCC AGCAAAAGGC CAGGAACCGT AAAAAGGCCG CGTTGCTGGC GTTTTTCCAT
15901 AGGCTCCGCC CCCCTGACGA GCATCACAAA AATCGACGCT CAAGTCAGAG GTGGCGAAAC CCGACAGGAC TATAAAGATA CCAGGCGTTT CCCCCTGGAA
16001 GCTCCCTCGT GCGCTCTCCT GTTCCGACCC TGCCGCTTAC CGGATACCTG TCCGCCTTTC TCCCTTCGGG AAGCGTGGCG CTTTCTCATA GCTCACGCTG
16101 TAGGTATCTC AGTTCGGTGT AGGTCGTTCG CTCCAAGCTG GGCTGTGTGC ACGAACCCCC CGTTCAGCCC GACCGCTGCG CCTTATCCGG TAACTATCGT
16201 CTTGAGTCCA ACCCGGTAAG ACACGACTTA TCGCCACTGG CAGCAGCCAC TGGTAACAGG ATTAGCAGAG CGAGGTATGT AGGCGGTGCT ACAGAGTTCT
16301 TGAAGTGGTG GCCTAACTAC GGCTACACTA GAAGAACAGT ATTTGGTATC TGCGCTCTGC TGAAGCCAGT TACCTTCGGA AAAAGAGTTG GTAGCTCTTG
16401 ATCCGGCAAA CAAACCACCG CTGGTAGCGG TGGTTTTTTT GTTTGCAAGC AGCAGATTAC GCGCAGAAAA AAAGGATCTC AAGAAGATCC TTTGATCTTT
16501 TCTACGGGGT CTGACGCTCA GTGGAACGAA AACTCACGTT AAGGGATTTT GGTCATGAGA TTATCAAAAA GGATCTTCAC CTAGATCCTT TTAAATTAAA
```

```
16601 AATGAAGTTT TAAATCAATC TAAAGTATAT ATGAGTAAAC TTGGTCTGAC AGTTACCAAT GCTTAATCAG TGAGGCACCT ATCTCAGCGA TCTGTCTATT
16701 TCGTTCATCC ATAGTTGCCT GACTCCCCGT CGTGTAGATA ACTACGATAC GGGAGGGCTT ACCATCTGGC CCCAGTGCTG CAATGATACC GCGAGACCCA
16801 CGCTCACCGG CTCCAGATTT ATCAGCAATA AACCAGCCAG CCGGAAGGGC CGAGCGCAGA AGTGGTCCTG CAACTTTATC CGCCTCCATC CAGTCTATTA
16901 ATTGTTGCCG GGAAGCTAGA GTAAGTAGTT CGCCAGTTAA TAGTTTGCGC AACGTTGTTG CCATTGCTAC AGGCATCGTG GTGTCACGCT CGTCGTTTGG
17001 TATGGCTTCA TTCAGCTCCG GTTCCCAACG ATCAAGGCGA GTTACATGAT CCCCCATGTT GTGCAAAAAA GCGGTTAGCT CCTTCGGTCC TCCGATCGTT
17101 GTCAGAAGTA AGTTGGCCGC AGTGTTATCA CTCATGGTTA TGGCAGCACT GCATAATTCT CTTACTGTCA TGCCATCCGT AAGATGCTTT TCTGTGACTG
17201 GTGAGTACTC AACCAAGTCA TTCTGAGAAT AGTGTATGCG GCGACCGAGT TGCTCTTGCC CGGCGTCAAT ACGGGATAAT ACCGCGCCAC ATAGCAGAAC
17301 TTTAAAAGTG CTCATCATTG GAAAACGTTC TTCGGGGCGA AAACTCTCAA GGATCTTACC GCTGTTGAGA TCCAGTTCGA TGTAACCCAC TCGTGCACCC
17401 AACTGATCTT CAGCATCTTT TACTTTCACC AGCGTTTCTG GGTGAGCAAA AACAGGAAGG CAAAATGCCG CAAAAAAGGG AATAAGGGCG ACACGGAAAT
17501 GTTGAATACT CATACTCTTC CTTTTTCAAT ATTATTGAAG CATTTATCAG GGTTATTGTC TCATGAGCGG ATACATATTT GAATGTATTT AGAAAAATAA
17601 ACAAATAGGG GTTCCGCGCA CATTTCCCCG AAAAGTGCCA CCTGACGCGC CCTGTAGCGG CGCATTAAGC GCGGCGGGTG TGGTGGTTAC GCGCAGCGTG
17701 ACCGCTACAC TTGCCAGCGC CCTAGCGCCC GCTCCTTTCG CTTTCTTCCC TTCCTTTCTC GCCACGTTCG CCGGCTTTCC CCGTCAAGCT CTAAATCGGG
17801 GGCTCCCTTT AGGGTTCCGA TTTAGTGCTT TACGGCACCT CGACCCCAAA AAACTTGATT AGGGTGATGG TTCACGTAGT GGGCCATCGC CCTGATAGAC
17901 GGTTTTTCGC CCTTTGACGT TGGAGTCCAC GTTCTTTAAT AGTGGACTCT TGTTCCAAAC TGGAACAACA CTCAACCCTA TCTCGGTCTA TTCTTTTGAT
18001 TTATAAGGGA TTTTGCCGAT TTCGGCCTAT TGGTTAAAAA ATGAGCTGAT TTAACAAAAA TTTAACGCGA ATTTTAACAA AATATTAA
```

Annex 2. Knock-out and knock-in mice sequences.

6x-His-tag is in blue. Seipin sequence is underlined. Frt sites are in violet, LoxP sites are in red and Lox2272 sites are in pink. In **uppercase** the 3 different nucleotides from the *BSCL2* wild type sequence. Primer's hybridization site is shown as follow: F1, R1, F1b, R1b, F2, F3, R3, F4, F5, R5.

Knock-out sequence:

tggctttttaccacatctgagctgatagagattagtctttttagtctcttgctactccctgtgtacagtttaagcatatacac
atagaaaaaaacattcattaggtattaggcacctattgcattctagacattgtaagcaggcagggattataacaaggatcctt
cctggggttttcacaagaaagaaggagcaaaggttataaaatactgaagtctgcgtgtgtgcgcatgcacgcgctctagagag
agagtgtgcagggtactcttgtggagtcagaaaaactcttgagttctccccccaccaccttgatggttgaaactcactgggcct
gcagtcaaacacctgtacctgttcagccatttggttatgacacccagggaatagttagaccttcctacccagaacgatttgtc
acctaaaactagaacagccgggcatggtggcgcacgcctttaatcccagcattcagggaggcagaggcaggcggatctctgag
tttgaggccagcctggtctacaaagtgagttccaggacagccagggctatacagagaaaccctgtctcgaaaaaccaaaaaga
ataaaaacaaaaacaaaacaactaggacatttaaatgtagcccaggatccaaaacatatatgtacgttcactcagaccaaaaa
gcttctaggcggtggcctggatcccctaaccctttgccgggatctcactctaggaggcattcttgagacatggtttccagtca
gacgacattctgaaccctgtgatgttttcagttaccttgaggagaaaataaaaaagccccaattcaacaagaaaacaaattt
attacttatttagatcccacagagaccaaggaacagggtgctccaagatggcctgtttaacacatttgtgttattacatacac
ctcaaagggaacctctactcaggcgagattcttatgcaaaactcactctgggcttcttgggtcccagtcctagtgactggttg
ttttaagtcaggatttcattgtgtattgtgtgtcgtcgtggctggcttggaactcagagatccatctgcctctgtgtgtgtcc
aacacctccggagtgttggtcaccacactgaacttaagaacccatgactgctttaggtgtctccccatccccactccccgtga
ttggtctccaaagcatgtctagttccagattctatgggacagagaacctgactctgactttgagagggcaggggcagccattt
taagaccagaggatcgcataagggatcgttccctattgggaacgctggggaccgccatttaagagcaccctcggcgcgtgcc
tccatgcgggtacgaacaggcagccgccatcttgggcattggctgccgcgccgagtcgccctgtcccgccccacggcctctcg
ggccacctccccccggggctgctgtccctgggcctgcggaaacccaccctgctcgcccttgtgtggttctcgccgcttacgtt
gcgcgctcgtgtgaatgctccgcggcttctgagcgctcgttttaacaaccccccactgggggcgctcgggcaccttatacttt
gcgatctccaatccttacaatgtctaacgggctcgactggccctgttccctggatatggcaagtgtatcgattaaggatcctc
tttcccaagaacgctaacacagacgttgtcctctgaggctctgaatgactttattcttcaaatgcctttacctttcatagctc
caggtgagcacccgggcatccccctctccattgcctgaacggatggatcaccgagggaaacaggcaggattttggcagtttag
cggggtccctttatagatagagtagaaggtgcttggagttagcctgaaagggtgaggagatggggtagacatgggtaaggagg
gccttgtgcttcaaataatctccgggtaaatgcgggtagaagtgatctactacaatttccaatctaagggcgggtctgggagg
gggcgatgagttcagaggaggtccaccgctcttcagaggagcgcacagaagaacttcttctcccggaaggggttctcggaagt
gggcacaggagtgatgaggggtcctcacaagcgtgggcatcacagtatgtcatcaggtctgctgctgccttggacacctgga
acccagccaggaagggatacattaaccagaattcctgaaagggactgcagttctcttctccaatagactatctttttgtttct
agtgcccttgagacagccctctcccccaacgccagtcctcgggaacaactttgctgacaaagcccagtttctgccactgacc
tcagggtgtcaagaaaagaagcatcttttcttgggggggaggggggaggggagggtattgcaaacccacagctgagccctgaag
ggctgatgggagccagggtcgcacccacctttatccggcacaagctggcctcaatcttaagctgttccaccatcttgcgtgct
tgaccaatactcatagtgctgttaacgggggtctcccctttcatcctggagtaaagacagtcagctgaaacactcagctcttc
acaaccacacacctgggattgtgcccccattctccagtggccatcccaggttttttttttctttctttttttttttttttttta
agtagggagaatggagaagataaaatgaaatattctcctaacccctgggtcctggtcatcaaattatacaaacgatttaagga
ttttaagtctttgagccaaatatgttaccagcaatgaaagcctcagtcagaaagagccccaccctgatgaaatcacatcagcc
acctgtccccccctcaagccctgaagagaaaaaaagctgctttctactcacctgaagtaacagcagcggcagccagggatgtag
ggtcagtggggaggggcaccaaaccctgcctcagataggtgccccaccctgccaggacttggagctaaaaatatccgtagca
ctgacagttaatgcagagaaggtcactagagatgctcagacgagatccttggaggggtggtctcagtctccacagcttaagtt
ctgcccagatggctggtacctgaaggatgaaggatgctagaaggagctgctgattctggcgcataccaactgcctggacagtg
ggggagtcagtctgctgtttgcatcccctgtgcacaccctcactgctgctctctcactacctgcccctgccattgtacaagtc
cttagtctaaactagatagctccccaaagggcctgaggcagaagcaggctcccctctcaaatggggtggtctgggcctgtgac
agcccctgcattagagtctgtccccactgcggaagaccctgctcatttgaaagtctgacatcagctgggctgctgctccccca
cccccacccccaccctgacacagcacttagcacctgaatcttggtttctttcagtgacccaccgttcttcagagctaggaaaa
tgtaacactctacaggtgatcagcttctagatcaccactttctaccacgtgagtgacgcgagctgggagacccagaggtaacc
catcaggaagatagctaaagaaatgatacatcaaagaagagaagctggggcaagagagacatgcagagaccagatcaaaggat
cagacaaagacgaggtaaggcaccttgccacgagagttagtgtgaatgttgtgaacacaggtgggcttctcggagtggggagt

agggtggcaagagttggcactggggaaatagggaatcgattggaaatttttcatgtaatttgagtggattactactattcaaa
aagatgtgcattggccttgcctcctggaggacgttatccagacgatgccaccatcagaaatctagtctcatggtttttgtag
ggattttgaggttggctgcatcacgtgggtcacagaaggtcaatcacgcagcataaaaactggagactgaaaggggttgaaat
gccgccacgcttgactagcggacggcaccatctgcgcacacaacacacaagattcagattctggcagggtgcaaggctctctg
agctccagttggactcctacaggcccaaggaactctactgaatttacaaaaaacaaacaaacaaaacaaaacaaaacaaaatc
agcatttatttcacacctccattcaatcacactgaaaagacaggtggtaaaggtatgggcagagggttgtggttgaggcctgg
aaaggaggaccaaggagtcccagactgcgttggagattataatgggtcctttggtcacttaactaaagtgtaatgggcagaga
cactggggagcaaagcattttacaggctctgccctctatgcaaggctcagcccctgtaggcgattgacagttgggcggggctt
cctcggcagccggaactgccttctgtatattgcctgggcagcgagaggccggtgagtctgcctcgccgcggtggcgatctggt
gtacaccgcattaccccaggggtgggcgccgcagcgtcggccacagggtgctgtgcgggggtaggggtcacttcctccgtgag
cgagcacaggtccaggcagaggaaagaaactcttgggaggcaattttgactgctctaaggctgctggctttgagccagactgg
ccggctgtgcaaccttaggcaagtcactcacctccttgcaaacctctggcattttggatccatgtcatctgggtttcgagaga
gatttaaaggcctcgttctctgtacgttatacttctgtgaatgtatcaaggaggtttgtcccaggctcccgaaactggaggaa
gaggctggaagcacactcagtggagggaggtgaaggagtaattggaagagaagcgcatgtgaagcaatgacttgctttgccc
tgctacctctagttttcaaagccagttgaataagctttttgtctccagctaccctggaaaagaaactgtctttttcccttctc
tttctccaggaaccttcagctgccctatcccatggccaagggtatcgtccctgtggaagaccagccaggaactcaaagcctga
ggctggggccagaccccctgctgtccccatcgtttaaacacagataacttcgtatagcatacattatacgaagttatgaccga
cgtcataggcgatcgcataacttcgtataaagtatcctatacgaagttattcaggaactagagcaggtggggcgctgtcggag
agcacccccagcaggttcagagctgcccagagtctctaggacaggggcagaagcagaagcaggagcaggagcaggcaggttgg
cctccgtcagcaaagctgcatcttcccaggagcctgaaccatcactggcctcaggctctagctcctcttctccgctcaggggc
tgctgatctggtttctcctcctcggacagctgaccctctgtccctgagggatcttcaggggctctcaccatcctctgtaacatc
tgattgcggagttgactcctcctggccttcaggccctggctgatgagcagagatccttcgttggacttccttccgggaattgt
ctctttttcggatgttaacctgagcccagtgaagtgcgcgtggatgcggaggtaggctccatacagctggatgcgcttgctgt
ggatctcaatgatcgctccagtggtcggcacAtacgagttctctctatagtctgcgtagagttccacctccagcagctgcttc
tgctctgcaaagccaaatagcaggaggctagagaagaccagtgtgtccagcatctggagcaggtctgagcggtaatgcagcat
caccgaacgcgaagaagtggagatgattcggccacctctggtgtagcaggaaatggtgaccaagaacatgcccaaatcttgat
tcacaggggactctggcagctcaagctctaaggtaacacgatacggctgtccatacatcagcacccgatcacgtccaccctta
gtcagcgagacattggcaacagggaaggagcagagtgaggtggtggaggaatcacagtcggtcctgtagtagaaatgcacagg
gctgaggtggctgactgtcggcatataggaatagtagaaggagccatagaggaagacagacacccagagcaaaaggaggatgg
tgcagaagagcaccccaaactgcagcagcagcctgcgggcacggcctgccaagacttggcccacctcctgggcccacaAtaag
gcaggAactggagggtcgttgaccatggccgggagagcagggtgtctggccccaggttcaggccttgcgttcctagctgctct
gccacctggacgccacccctggccatgggatgcagcagctggtggttcctcctctttgtccggtcctttgatctggtctccgc
acacctctttttccccagcttcctccttttggtctacctttttctgtagagtgatggtgatggtgatgcataataacttcgtata
atgtatgctatacgaagttatcatatgaagtctcgaggttatgtacctgactgatgaagttcctatactttctagagaataagg
aacttcggaattcgatatcataacttcgtataggatactttatacgaagttatgtcaatgacccaccagtccccgccttactg
tgggcccaggaagtgggccacgtcttggcaggccgtgcccgcaggctgatgctgcagtttggggtgctcttctgcaccatcct
tctttgctttgggtgtctgtgttcctctatggctccttctactactcctacatgccgacggtcagccacctcagccctgtgc
acttccactacaggtgagaaggctgctccattcaagtagatggatcttaacttgaaaattacttcagggacttgtggagtctc
tcctctgttgaatcccagtattgaccgagggtgaaatcttattctagtgtgctatcaggacttctgccctcctgagccaaggc
ttgagcaggtctgggctggtagggctttagggttctaggtctgcctctgctggaaattgtggttaagaactgagaaaaagagc
ctggtcacgtgtgtaataccagtctggggaggctgagttgggagaattagcatgagttccaggccagcctggaagacaggttg
agaacttgtctcaaaggggtctaaaaaaaaaaaaaaagactaggaaaagaaagtcacttttagccgggcagtggtggtgcatgc
ctgtaatcccagcacttgggaggcagaggcaggtggatttctgagttcgaggccagcctggtctacagagtgagttccaggac
agccaggactgcacagagaaaccctgtctcgaaaaaaaaaaaaaaatcacttttagaccaagtagggctcagcgtctgttctgt
tgaggttgcatgaaacctttgagccaattcaactgccatggcatctaagaattacactggctttattaacacgtgagctatta
ggaaatacctcctttgccttttagtgtactgccactcacccccaatggtacattcagtaacccaaggcagtcctactgctaac
ctagccttcgagttcatatccattttactcacactgccaaagtctctgtatgtctcccagcaatggctatgagacaaattaac
atatacagaaaacgcttttatgatcattggtttaaaaccttttttttcccctgtcccaaatccctaatcttgtgttgtcatttc
taaggtagacccatgtaaacacttagggaacatgaatccttttttaataattatttttgtttcatgtgcattggtgttttgcc
tgcccgtgtggttgtgtgaaggtgtcagatcccctgcaactggagttacaggcggtcgtgagctgccacgtggttgctgggaa
ttgaactcaggtcctctgcaagagtaaccagtgctcttgaccaatgggccatctctccagccccaagggagcacgagtcttac
atacatggggtatatgtatgtatactgaggtaggagctgtgtaccatatactatgtgcagttttgcgtataatttatctttaa
aagacatatccataggtcctttaggatgaatttcttttccaacctagtccagaactgctgaatcagactctttaggagaggg
accctaaaatccacatgccctgagatcttcaagggagcctatagaaaccctgagtgtccttcggctcctccctatgggttctg
ttctcatgaggaagagaatgaaagtcttattaggatctcctgactctagtgtccacttctgttctccatttcctgtaatgggg
aaaagggatgagtgaggggagggccctagagactaggtgtgtgagcaggtaggctgggcaggctggcacctcacaaagcatt

gttcatcccttctcatttaggacagactgtgattcctccaccgcctctctctgctctttccctgttgccaatgtctcactggc
taagagtggacgtgatcgggtgagtatgagaactagacagaggctttgattgcttgaggaagatggggagagcagggattgag
caaccgagattgaagagaaaggctctgacgcaaacgggtggaaaagaaaatctggaagttggtcccagtcactgtgatacata
tctgtaatgccagcactaggaggaaaaagacacagggagattattccaaatctgatatcagcttgggcttcatagccagaccc
tatctctctagaggctctgataaaaaatagaattacaagcttaaaatgtcccttgatatcaaaaaataaaacaaaaaaggact
ttgagaattaatgtcatttttttattaaatgaggtttttctagttgtcagtcttaacttgaacatttttttaaagtggtattta
agaagaaactgactttatagtagaatatcagctctggcacagtggcacacatctataatcacaatacttaacatagaaggatg
ctgcccaggctggcctcgcacgctgagatccacttgcctttgcctcctaagtgtggccatcaccacgcaagggaggatatctt
gagtttaggagttaagagcatcctgaataagttagttcaaggcctctcattaaaaaaaaaacaaaggagcttgggaggtagag
gcagaaaggctagcctggactatttaaaaaatataaaagtagtttaccttaaagttatggtcactatgtctccgcctcctatgt
gctggagttaaaggtacgccatgtaccaatccagactggaagtgagtaacctcagacgtgctcggcttcctaagcgttgggat
tgttaggaagtgggcaccaccgtgccaggcttggatttctttttctttttttttttcttacacaccagaagagggcttggga
tcccattacagatggttgtgagtcaccatgtgattgctgggaattgaactcaggacctctggaagagtagtcagtgctcttaa
ctgctgagccatctctccagaccctcttaataggtttattaagttaaaatttatatgagatacagtttacctcttaaggtata
cagtcgtcgtcatatcattcgatgcatgtatttgggacagagtttcactatgtagccttggctggcctggaactggccatttc
aaccaggttggccttgaatccacagctctcctcctccctttggcctcttgtgtgctgggattaaaaccatgcactgccgcccc
aggcagttctattgtttttaataagttcagtgttgcacgcatactgatataaatagacaaacttaatctttttttttaaattaa
taagcactctgcctttaaaaatgaagaaagaccaggataacaagatgatctgccactgcagtgattgtgcaagagctgactag
ggaggcagagcagcacttgcttaattagcaagtgagggcagactaggcccaggggacagctccggcggcacacaggcctgaa
tcacagatgccccagttggcaatgtgactgttcacttttggaaaagaaatgcaacagggcacttctcgtaaacatagtagtcc
aagacagacctaagagctcacagggtgaatgtggtggtgcaagccta

Knock-in sequence:

attagtctttttagtctcttgctactccctgtgtacagtttaagcatatacacatagaaaaaaacattcattaggtattaggc
acctattgcattctagacattgtaagcaggcagggattataacaaggatccttcctggggttttcacaagaaagaaggagcaa
aggttataaaatactgaagtctgcgtgtgtgcgcatgcacgcgctctagagagagagtgtgcagggtactcttgtggagtcag
aaaaactcttgagttctcccccaccaccttgatggttgaaactcactgggcctgcagtcaaacacctgtacctgttcagccat
ttggttatgacacccagggaatagttagaccttcctacccagaacgatttgtcacctaaaactagaacagccgggcatggtgg
cgcacgcctttaatcccagcattcagggaggcagaggcaggcggatctctgagtttgaggccagcctggtctacaaagtgagt
tccaggacagccagggctatacagagaaaccctgtctcgaaaaaccaaaaagaataaaaacaaaaacaaaacaactaggacat
ttaaatgtagcccaggatccaaaacatatatgtacgttcactcagaccaaaaagcttctaggcggtggcctggatcccctaac
cctttgccgggatctcactctaggaggcattcttgagacatggtttccagtcagacgacattctgaaccttgtgatgttttc
agttaccttgaggagaaaataaaaaagccccaattcaacaagaaaacaaatttattacttatttagatcccacagagaccaag
gaacagggtgctccaagatggcctgtttaacacatttgtgttattacatacacctcaaagggaacctctactcaggcgagatt
cttatgcaaaactcactctgggcttcttgggtcccagtcctagtgactggttgttttaagtcaggatttcattgtgtattgtg
tgtcgtcgtggctggcttggaactcagagatccatctgcctctgtgtgtgtccaacacctccggagtgttggtcaccacactg
aacttaagaacccatgactgctttaggtgtctccccatccccactccccgtgattggtctccaaagcatgtctagttccagat
tctatgggacagagaacctgactctgactttgagagggcaggggcagccattttaagaccagaggatcgcataagggatcgtt
ccctattgggaacgctggggaccgccattttaagagcaccctcggcgcgtgcctccatgcgggtacgaacaggcagccgccat
cttgggcattggctgccgcgccgagtcgccctgtcccgccccacggcctctcgggccacctccccccggggctgctgtccctg
ggcctgcggaaacccaccctgctcgcccttgtgtggttctcgccgcttacgttgcgcgctcgtgtgaatgctccgcggcttct
gagcgctcgttttaacaaccccccactgggggcgctcgggcaccttatactttgcgatctccaatccttacaatgtctaacgg
gctcgactggccctgttccctggatatggcaagtgtatcgattaaggatcctctttcccaagaacgctaacacagacgttgtc
ctctgaggctctgaatgactttattcttcaaatgcctttaccttttcatagctccaggtgagcacccgggcatccccctctcca
ttgcctgaacggatggatcaccgagggaaacaggcaggattttggcagtttagcggggtccctttatagatagagtagaaggt
gcttggagttagcctgaaagggtgaggagatggggtagacatgggtaaggagggccttgtgcttcaaataatctccgggtaaa
tgcgggtagaagtgatctactacaatttccaatctaagggcgggtctgggaggggggcgatgagttcagaggaggtccaccgct
cttcagaggagcgcacagaagaacttcttctcccggaaggggttctcggaagtgggcacaggagtgatgagggggtcctcaca
agcgtgggcatcacagtatgtcatcaggtctgctgctgccttggacacctggaacccagccaggaagggatacattaaccaga
attcctgaaagggactgcagttctcttctccaatagactatctttttgtttctagtgccctttgagacagccctctcccccaa
cgccagtcctcgggaacaactttgctgacaaagcccagtttctgccactgacctcagggtgtcaagaaaagaagcatcttttc
ttgggggggaggggggaggggagggtattgcaaacccacagctgagccctgaagggctgatgggagccagggtcgcacccacct
ttatccggcacaagctggcctcaatcttaagctgttccaccatcttgcgtgcttgaccaatactcatagtgctgttaacgggg
gtctcccctttcatcctggagtaaagacagtcagctgaaacactcagctcttcacaaccacacacctgggattgtgcccccat
tctccagtggccatcccaggttttttttttctttctttttttttttttttttaagtagggagaatggagaagataaaatgaaa
tattctcctaacccctgggtcctggtcatcaaattatacaaacgatttaaggattttaagtctttgagccaaatatgttacca
gcaatgaaagcctcagtcagaaagagccccaccctgatgaaatcacatcagccacctgtccccctcaagccctgaagagaaa
aaaagctgctttctactcacctgaagtaacagcagcggcagccagggatgtagggtcagtggggagggggcaccaaaccctgc

ctcagataggtgccccaccctgccaggacttggagctaaaaatatccgtagcactgacagttaatgcagagaaggtcactaga
gatgctcagacgagatccttggaggggtggtctcagtctccacagcttaagttctgcccagatggctggtacctgaaggatga
aggatgctagaaggagctgctgattctggcgcataccaactgcctggacagtgggggagtcagtctgctgtttgcatcccctg
tgcacaccctcactgctgctctctcactacctgcccctgccattgtacaagtccttagtctaaactagatagctccccaaagg
gcctgaggcagaagcaggctcccctctcaaatggggtggtctgggcctgtgacagcccctgcattagagtctgtccccactgc
ggaagaccctgctcatttgaaagtctgacatcagctgggctgctgctcccccacccccacccccaccctgacacagcacttag
cacctgaatcttggtttctttcagtgacccaccgttcttcagagctaggaaaatgtaacactctacaggtgatcagcttctag
atcaccactttctaccacgtgagtgacgcgagctgggagacccagaggtaacccatcaggaagatagctaaagaaatgataca
tcaaagaagagaagctggggcaagagagacatgcagagaccagatcaaaggatcagacaaagacgaggtaaggcaccttgcca
cgagagttagtgtgaatgttgtgaacacaggtgggcttctcggagtggggagtagggtggcaagagttggcactggggaaata
gggaatcgattggaaatttttcatgtaatttgagtggattactactattcaaaaagatgtgcattggccttgcctcctggagg
acgttatccagacgatgccaccatcagaaatctagtctcatggttttttgtagggattttgaggttggctgcatcacgtgggt
cacagaaggtcaatcacgcagcataaaaactggagactgaaaggggttgaaatgccgccacgcttgactagcggacggcacca
tctgcgcacacaacacacaagattcagattctggcagggtgcaaggctctctgagctccagttggactcctacaggcccaagg
aactctactgaatttacaaaaaacaaacaaacaaaacaaaacaaaacaaaatcagcatttatttcacacctccattcaatcac
actgaaaagacaggtggtaaaggtatgggcagagggttgtggttgaggcctggaaaggaggaccaaggagtcccagactgcgt
tggagattataatgggtcctttggtcacttaactaaagtgtaatgggcagagacactggggagcaaagcattttacaggctct
gccctctatgcaaggctcagcccctgtaggcgattgacagttgggcggggcttcctcggcagccggaactgccttctgtatat
tgcctgggcagcgagaggccggtgagtctgcctcgccgcggtggcgatctggtgtacaccgcattaccccaggggtgggcgcc
gcagcgtcggccacagggtgctgtgcgggggtaggggtcacttcctccgtgagcgagcacaggtccaggcagaggaaagaaac
tcttgggaggcaattttgactgctctaaggctgctggctttgagccagactggccggctgtgcaaccttaggcaagtcactca
cctccttgcaaacctctggcattttggatccatgtcatctgggtttcgagagagatttaaaggcctcgttctctgtacgttat
acttctgtgaatgtatcaaggaggtttgtcccaggctcccgaaactggaggaagaggctggaagcacactcagtggagggagg
tgaaggagtaattggaagagaagcgcatgtgaagcaatgacttgctttgccctgctacctctagttttcaaagccagttgaa
taagctttttgtctccagctaccctggaaaagaaactgtcttttcccttctctttctccaggaaccttcagctgccctatcc
catggccaagggtatcgtccctgtggaagaccagccaggaactcaaagcctgaggctggggccagacccctgctgtccccat
cgtttaaacacagataacttcgtatagcatacattatacgaagttatatgcatcaccatcaccatcactctacagaaaaggta
gaccaaaaggaggaagctggggaaaaagaggtgtgcggagaccagatcaaaggaccggacaaagaggaggaaccaccagctgc
tgcatcccatggccaggggtggcgtccaggtggcagagcagctaggaacgcaaggcctgaacctggggccagacaccctgctc
tcccggccatggtcaacgaccctccagtTcctgccttaTtgtgggcccaggaggtgggccaagtcttggcaggccgtgcccgc
aggctgctgctgcagtttggggtgctcttctgcaccatcctccttttgctctgggtgtctgtcttcctcTatggctccttcta
ctattcctatatgccgacagtcagccacctcagccctgtgcatttctactacaggaccgactgtgattcctccaccacctcac
tctgctccttccctgttgccaatgtctcgctgactaagggtggacgtgatcgggtgctgatgtatggacagccgtatcgtgtt
accttagagcttgagctgccagagtcccctgtgaatcaagatttgggcatgttcttggtcaccatttcctgctacaccagagg
tggccgaatcatctccacttcttcgcgttcggtgatgctgcattaccgctcagacctgctccagatgctggacacactggtct
tctctagcctcctgctatttggctttgcagagcagaagcagctgctggaggtggaactctacgcagactatagagagaactcg
taTgtgccgaccactggagcgatcattgagatccacagcaagcgcatccagctgtatggagcctacctccgcatccacgcgca
cttcactgggctcaggttaacatccgaaaaagagacaattccggaaggaagtccaacgaaggatctctgctcatcagccagg
gcctgaaggccaggaggagtcaactccgcaatcagatgttacagaggatggtgagagccctgaagatccctcagggacagagg
gtcagctgtccgaggaggagaaaccagatcagcagcccctgagcggagaagaggagctagagcctgaggccagtgatggttca
ggctcctgggaagatgcagctttgctgacggaggccaacctgcctgctcctgctcctgcttctgcttctgcccctgtcctaga
gactctgggcagctctgaacctgctgggggtgctctccgacagcgccccacctgctctagttcctgaataacttcgtatagga
tacttatacgaagttatgtcaatgacccaccagtccccgccttactgtgggcccaggaagtgggccacgtcttggcaggccg
tgcccgcaggctgatgctgcagtttggggtgctcttctgcaccatccttcttttgctttgggtgtctgtgttcctctatggct
ccttctactactcctacatgccgacggtcagccacctcagccctgtgcacttccactacaggtgagaaggctgctccattcaa
gtagatggatcttaacttgaaaattacttcagggacttgtggagtctctcctctgttgaatcccagtattgaccgagggtgaa
atcttattctagtgtgctatcaggacttctgccctcctgagccaaggcttgagcaggtctgggctggtagggctttagggttc
taggtctgcctctgctggaaattgtggttaagaactgagaaaaagagcctggtcacgtgtgtaataccagtctggggaggctg
agttgggagaattagcatgagttccaggccagcctggaagacaggttgagaacttgtctcaaaggggtctaaaaaaaaaaaaa
agactaggaaaagaaagtcacttttagccgggcagtggtggtgcatgcctgtaatcccagcacttgggaggcagaggcaggtg
gatttctgagttcgaggccagcctggtctacagagtgagttccaggacagccaggactgcacagagaaaccctgtctcgaaaa
aaaaaaaaaatcacttttagaccaagtagggctcagcgtctgttctgttgaggttgcatgaaacctttgagccaattcaactg
ccatggcatctaagaattacactggctttattaacacgtgagctattaggaaatacctcctttgccttttagtgtactgccac
tcacccccaatggtacattcagtaacccaaggcagtcctactgctaacctagccttcgagttcatatccattttactcacact
gccaaagtctctgtatgtctcccagcaatggctatgagacaaattaacatatacagaaaacgcttttatgatcattggtttaa
aacctttttttccccctgtcccaaatccctaatcttgtgttgtcatttctaaggtagacccatgtaaacacttagggaacatga
atccttttttaataattatttttgtttcatgtgcattggtgttttgcctgcccgtgtggttgtgtgaaggtgtcagatccccct
gcaactggagttacaggcggtcgtgagctgccacgtggttgctgggaattgaactcaggtcctctgcaagagtaaccagtgct
cttgaccaatgggccatctctccagccccaagggagcacgagtcttacatacatggggtatatgtatgtatactgaggtagga
gctgtgtaccatatactatgtgcagttttgcgtataatttatctttaaaagacatatccataggtcctttaggatgaatttct

ttttccaacctagtccagaactgctgaatcagactctttaggagagggaccctaaaatccacatgccctgagatcttcaaggg
agcctatagaaaccctgagtgtccttcggctcctccctatgggttctgttctcatgaggaagagaatgaaagtcttattagga
tctcctgactctagtgtccacttctgttctccatttcctgtaatggggaaaagggatgagtgaggggaggggccctagagact
aggtgtgtgagcaggtaggctgggcaggctggcacctcacaaagcattgttcatcccttctcatttaggacagactgtgattc
ctccaccgcctctctctgctctttccctgttgccaatgtctcactggctaagagtggacgtgatcgggtgagtatgagaacta
gacagaggctttgattgcttgaggaagatggggagagcagggattgagcaaccgagattgaagagaaaggctctgacgcaaac
gggtggaaaagaaaatctggaagttggtcccagtcactgtgatacatatctgtaatgccagcactaggaggaaaaagacacag
ggagattattccaaatctgatatcagcttgggcttcatagccagaccctatctctctagaggctctgataaaaaatagaatta
caagcttaaaatgtcccttgatatcaaaaaataaaacaaaaaaggactttgagaattaatgtcatttttttattaaatgaggtt
tttctagttgtcagtcttaacttgaacatttttttaaagtggtatttaagaagaaactgactttatagtagaatatcagctct
ggcacagtggcacacatctataatcacaatacttaacatagaaggatgctgcccaggctggcctcgcacgctgagatccactt
gcctttgcctcctaagtgtggccatcaccacgcaagggaggatatcttgagtttaggagttaagagcatcctgaataagttag
ttcaaggcctctcattaaaaaaaaaacaaaggagcttgggaggtagaggcagaaaggctagcctggactatttaaaaaataaa
aagtagtttaccttaaagttatggtcactatgtctccgcctcctatgtgctggagttaaaggtacgccatgtaccaatccaga
ctggaagtgagtaacctcagacgtgctcggcttcctaagcgttgggattgttaggaagtgggcaccaccgtgccaggcttgga
tttctttttttctttttttttttcttacacaccagaagagggcttgggatcccattacagatggttgtgagtcaccatgtgatt
gctgggaattgaactcaggacctctggaagagtagtcagtgctcttaactgctgagccatctctccagaccctcttaataggt
ttattaagttaaaatttatatgagatacagtttacctcttaaggtatacagtcgtcgtcatatcattcgatgcatgtatttgg
gacagagtttcactatgtagccttggctggcctggaactggccatttcaaccaggttggccttgaatccacagctctcctcct
ccctttggcctcttgtgtgctgggattaaaaccatgcactgccgccccaggcagttctattgtttttaataagttcagtgttg
cacgcatactgatataaatagacaaacttaatctttttttttaaattaataagcactctgcctttaaaaatgaagaaagaccag
gataacaagatgatctgccactgcagtgattgtgcaagagctgactagggaggcagagcagcacttgcttaattagcaagtga
gggcagactaggcccaggggggacagctccggcggcacacaggcctgaatcacagatgccccagttggcaatgtgact

Annex 3. Table S1 and S2. Neurological evaluation and gnawing test.

Table S1. Neurological evaluation for wild type, *Bscl2*$^{+/Celia}$, *Bscl2*$^{Celia/Celia}$, *Bscl2*$^{+/-}$, *Bscl2*$^{-/-}$ and severely affected (S.A.) mice. Data is presented as mean ± SD. Data is presented as mean ± SD. Data were analysed using a Kolmogorov-Smirnov test for normality, followed by a Kruskal-Wallis test with Mann-Whitney post hoc comparisons. [a] $p < 0.05$ vs wild type ♀/♂; [b] $p < 0.05$ vs wild type ♀; [c] $p < 0.05$ vs wild type ♂; [d] $p < 0.05$ vs *Bscl2*$^{+/-}$ ♀/♂; [e] $p < 0.05$ vs *Bscl2*$^{+/-}$ ♀; [g] $p < 0.05$ vs *Bscl2*$^{-/-}$ ♀/♂; [i] $p < 0.05$ vs *Bscl2*$^{-/-}$ ♂; [j] $p < 0.05$ vs *Bscl2*$^{+/Celia}$ ♀/♂; [k] $p < 0.05$ vs *Bscl2*$^{+/Celia}$ ♀; [m] $p < 0.05$ vs *Bscl2*$^{Celia/Celia}$ ♀/♂ and [o] $p < 0.05$ *Bscl2*$^{Celia/Celia}$ ♂.

		N	Age (months)	**NeuroScore**	**Wellness score**
Wild type	♀/♂	32	7.4	0.15 ± 0.29	0.09 ± 0.20
Bscl2$^{+/Celia}$	♀/♂	37	7.5	0.15 ± 0.25	0.10 ± 0.14
Bscl2$^{Celia/Celia}$	♀/♂	25	7.4	0.04 ± 0.05[g]	0.54 ± 0.61[a,d,j]
Bscl2$^{+/-}$	♀/♂	36	7.4	0.07 ± 0.14[g]	0.15 ± 0.29
Bscl2$^{-/-}$	♀/♂	25	7.6	0.29 ± 0.39	0.38 ± 0.43[a,d,j]
S.A. *Bscl2*$^{+/Celia}$	♀/♂	1	7.6	2.12	2.75
S.A. *Bscl2*$^{Celia/Celia}$	♀/♂	3	7.5	2.88 ± 0.50[a,d,g,j,m]	2.83 ± 0.29[a,d,g,j,m]
Wild type	♀	20	7.4	0.14 ± 0.34	0.06 ± 0.23
	♂	12	7.4	0.18 ± 0.18	0.13 ± 0.13[b]
Bscl2$^{+/Celia}$	♀	25	7.5	0.12 ± 0.21	0.06 ± 0.13[c]
	♂	12	7.5	0.21 ± 0.31	0.19 ± 0.11[b,e,k]
Bscl2$^{Celia/Celia}$	♀	14	7.5	0.04 ± 0.05[i]	0.38 ± 0.37[b,e,k]
	♂	11	7.4	0.05 ± 0.06[i]	0.75 ± 0.80[a,e,k]
Bscl2$^{+/-}$	♀	19	7.4	0.08 ± 0.18	0.08 ± 0.34[c]
	♂	17	7.5	0.05 ± 0.10[c]	0.23 ± 0.18[b,e,k]
Bscl2$^{-/-}$	♀	10	7.5	0.03 ± 0.04[i]	0.24 ± 0.42[b,e,o]
	♂	15	7.6	0.47 ± 0.43[b,d,k]	0.47 ± 0.43[a,e,k]

Table S2. Gnawing test for wild type, *Bscl2*$^{+/Celia}$, *Bscl2*$^{Celia/Celia}$, *Bscl2*$^{+/-}$and *Bscl2*$^{-/-}$ mice. Data is presented as mean ± SD. Data is presented as mean ± SD. Data were analysed using a Kolmogorov-Smirnov test for normality, followed by a Kruskal-Wallis test with Mann-Whitney post hoc comparisons. [a] $p < 0.05$ vs wild type ♀/♂; [c] $p < 0.05$ vs wild type ♂; [g] $p < 0.05$ vs *Bscl2*$^{-/-}$ ♀/♂; [j] $p < 0.05$ vs *Bscl2*$^{+/Celia}$ ♀/♂; [k] $p < 0.05$ vs *Bscl2*$^{+/Celia}$ ♀/; [n] $p < 0.05$ vs *Bscl2*$^{Celia/Celia}$ ♀.

	Wild type	*Bscl2*$^{+/Celia}$	*Bscl2*$^{+Cela/Celia}$	*Bscl2*$^{+/-}$	*Bscl2*$^{-/-}$	*Bscl2*$^{+/Celia}$		*Bscl2*$^{+Cela/Celia}$		*Bscl2*$^{-/-}$
Sex	♂	♀/♂	♀/♂	♀	♀/♂	♀	♂	♀	♂	♀
N	2	23	19	3	7	9	14	10	4	4
Mean age (months)	g gnawed/animal/day									
0.9	-	-	-	-	-	-	-	-	0.00	-
1.1	-	-	-	-	-	0.01	-	-	-	-
1.2	-	-	-	-	-	-	-	-	0.00	-
1.3	-	-	-	-	-	0.01	-	-	-	-
1.4	-	-	-	-	-	-	-	-	0.00	-
1.5	-	-	-	-	-	0.04	-	-	-	-
1.6	-	-	-	-	-	-	-	-	0.00	-
1.8	-	-	-	-	-	0.05	-	-	-	-
1.9	-	-	-	-	-	-	-	-	0.01	-
2.0	-	-	-	-	-	0.01	-	-	-	-
2.1	-	-	-	-	-	-	-	-	0.01	-
2.2	-	-	-	-	-	0.08	-	-	-	-
2.3	-	-	-	-	-	-	-	-	0.01	-
2.5	-	-	-	-	-	0.06	-	-	-	-
2.6	-	-	-	-	-	0.21	-	-	0.01	-
2.7	-	-	-	-	-	0.03	-	-	-	-
2.8	-	-	-	-	-	0.24	-	-	0.00	-
2.9	-	-	0.08 ± 0.06	-	0.06 ± 0.06	0.11	-	-	-	0.14
2.9	-	-	-	-	0.14	-	-	-	-	-
3.0	-	-	-	-	-	-	-	0.01 ± 0.00	0.02	-
3.1	-	-	0.16 ± 0.26	-	0.04 ± 0.01	0.21	-	-	-	0.09
3.1	-	0.13 ± 0.07	0.05 ± 0.01	-	0.09	-	-	-	-	-
3.2	-	-	-	-	-	0.13	-	-	-	-
3.3	-	0.11 ± 0.11	0.06 ± 0.07	-	-	0.24	-	0.03 ± 0.04	0.01	-
3.4	-	-	0.16 ± 0.12	-	0.04 ± 0.01	0.02	0.10 ± 0.04	-	-	0.08
3.4	-	-	-	-	0.08	-	-	-	-	-
3.5	-	0.13 ± 0.07	0.07 ± 0.04	-	-	0.16	-	0.07 ± 0.05	0.04	-
3.5	-	-	0.11	-	-	-	-	0.11	-	-
3.6	-	-	0.10 ± 0.06	-	0.02 ± 0.01	0.11	0.05 ± 0.00	-	-	0.10
3.6	-	-	-	-	0.10	-	-	-	-	-
3.7	-	-	0.09 ± 0.10	-	-	0.22	-	0.12	0.08	-
3.8	-	0.14 ± 0.09	-	-	0.03 ± 0.01	0.07	0.09 ± 0.01	0.04 ± 0.01	-	0.04
3.8	-	-	-	-	0.04	-	-	-	-	-
3.9	-	-	0.08 ± 0.06	-	-	-	-	0.05 ± 0.03	0.01	-
4.0	0.26	0.09 ± 0.06	-	-	0.01 ± 0.00	0.13	0.10 ± 0.02	0.04	-	0.06
4.0	-	-	-	-	0.06	-	-	-	-	-
4.1	-	-	0.05 ± 0.05	-	-	0.12	-	0.02 ± 0.00	-	-
4.2	0.12	0.11 ±	-	-	-	-	-	0.07	0.01	-

		0.09								
4.3	-	-	-	0.08	0.01 ± 0.01	0.07	0.06 ± 0.02	-	-	0.02
4.3	-	-	-	-	0.02	0.06	-	-	-	-
4.4	-	-	0.10 ± 0.13	-	-	-	-	0.03 ± 0.00	0.02	-
4.4	-	-	-	-	-	-	-	0.06	-	-
4.5	0.10	0.08 ± 0.04	-	0.22	0.06 ± 0.07	0.17	0.06 ± 0.00	-	-	-
4.5	-	-	-	-	-	0.07	-	-	-	-
4.6	-	-	0.07 ± 0.09	-	-	-	-	0.02 ± 0.01	0.02	0.10
4.7	0.04	0.07 ± 0.02	-	0.16	-	0.17	-	-	-	-
4.8	-	-	-	-	-	0.12	0.06 ± 0.00	-	-	0.03
4.9	0.09	-	0.04 ± 0.04	0.01	-	0.12	-	0.06 ± 0.05	0.05	-
5.0	-	0.10 ± 0.06	-	-	-	0.09	0.08 ± 0.02	-	-	0.05
5.1	-	-	0.11 ± 0.08	-	-	-	-	0.07 ± 0.01	0.02	-
5.2	0.00	0.11 ± 0.07	-	0.00	-	0.19	0.07 ± 0.00	-	-	0.03
5.2	-	-	-	-	-	0.05	-	-	-	-
5.3	-	-	-	-	-	-	-	-	0.03	-
5.4	0.00	0.06 ± 0.06	0.07 ± 0.04	-	-	0.14	-	0.05 ± 0.03	-	0.04
5.5	-	-	-	-	-	-	0.08 ± 0.06	-	-	-
5.6	-	0.07 ± 0.11	0.10 ± 010	-	-	-	-	0.05 ± 0.02	0.04	-
5.7	0.02	0.02 ± 0.01	-	-	-	0.09	0.03 ± 0.04	-	-	0.01
5.8	-	-	0.12 ± 0.11	-	-	-	-	0.06 ± 0.02	0.02	-
5.9	0.38	-	-	-	0.00	0.10	0.01 ± 0.01	-	-	0.00
6.0	-	0.02 ± 0.01	0.08 ± 0.05	-	-	-	-	0.06 ± 0.02	0.03	0.00
6.1	0.04	0.01 ± 0.01	-	-	0.01	0.07	0.01 ± 0.01	-	-	0.01
6.2	-	0.03 ± 0.02	-	-	-	-	-	-	-	0.11
6.3	0.03	-	0.07 ± 0.03	-	0.00	-	-	0.06 ± 0.04	0.02	0.00
6.4	-	0.02 ± 0.01	-	-	-	0.13	0.02 ± 0.01	-	-	-
6.4	-	0.05 ± 0.01	-	-	-	-	-	-	-	-
6.5	-	-	0.03 ± 0.02	-	0.02	-	-	0.03 ± 0.02	0.01	0.02
6.6	0.23	0.13 ± 0.06	-	-	-	0.20	0.13 ± 0.06	-	-	-
6.7	-	0.02 ± 0.01	-	-	-	-	-	-	0.03	-
6.8	0.09	-	0.12 ± 0.09	-	0.00	0.23	-	0.07 ± 0.01	-	0.00
6.9	-	0.12 ± 0.04	0.11 ± 0.10	-	-	-	0.12 ± 0.04	0.050	-	-
6.9	-	0.09 ± 0.06	-	-	-	-	-	-	-	-

7.0	-	-	-	-	0.00	-	-	-	0.02	0.00
7.1	0.09	0.06 ± 0.00	0.10 ± 0.13	-	-	0.08	0.06 ± 0.00	0.03 ± 0.02	-	-
7.1	-	0.04 ± 0.02	-	-	-	-	-	-	-	-
7.2	-	-	-	-	-	-	-	-	0.01	-
7.3	0.27	0.06 ± 0.02	-	-	0.01	0.18	0.06 ± 0.02	-	-	0.01
7.4	-	0.03 ± 0.03	0.09 ± 0.08	-	-	-	-	0.05 ± 0.04	0.01	-
7.5	0.09	-	-	-	0.03	0.13	-	-	-	0.03
7.6	-	0.10 ± 0.03	0.06 ± 0.05	-	-	-	0.10 ± 0.03	0.04 ± 0.03	-	-
7.6	-	0.06 ± 0.05	-	-	-	-	-	-	-	-
7.7	-	-	-	-	0.02	-	-	-	0.00	0.02
7.8	-	0.11 ± 0.03	-	-	-	0.07	0.11 ± 0.03	0.05 ± 0.07	-	-
7.8	-	0.06 ± 0.06	-	-	-	-	-	-	-	-
7.9	-	-	0.11 ± 0.11	-	-	-	-	-	0.00	-
8.0	0.19	-	-	-	0.01	0.11	-	-	-	0.01
8.1	-	0.04 ± 0.01	0.13 ± 0.14	-	-	-	0.04 ± 0.01	0.05 ± 0.02	0.00	-
8.1	-	0.02 ± 0.01	-	-	-	-	0.03 ± 0.01	-	-	-
8.2	0.06	-	-	-	0.00	0.10	-	-	-	0.00
8.3	-	0.07 ± 0.01	0.10 ± 0.10		-	-	0.07 ± 0.01	0.04 ± 0.03	-	-
8.3	-	0.07 ± 0.05	-	-	-	-	-	-	-	-
8.4	0.09	-	-	-	0.00	-	0.02 ± 0.01	-	0.01	0.00
8.5	-	0.07 ± 0.04	-	-	-	0.05	0.07 ± 0.04	-	-	-
8.5	-	0.08 ± 0.01	-	-	-	-	-	-	-	-
8.6	-	-	-	-	0.01	-	0.02 ± 0.01	-	-	0.01
8.7	0.14	0.08 ± 0.04	-	-	0.01	-	0.08 ± 0.04	-	-	0.01
8.8	-	0.07 ± 0.05	0.02 ± 0.01	-	-	-	0.06 ± 0.01	0.03 ± 0.03	-	-
8.8	-	-	0.09 ± 0.11	-	-	-	-	-	-	-
8.9	0.01	-		-	-	-	-	-	-	-
9.0	-	0.28 ± 0.29	0.00 ± 0.01	-	-	-	0.28 ± 0.29	0.04 ± 0.02	-	-
9.0	-	0.05 ± 0.02	0.10 ± 0.11	-	-	-	-	-	-	-
9.1	-	-	-	-	0.03	-	0.02 ± 0.00	-	-	0.03
9.2	-	0.19 ± 0.19	0.07 ± 0.06	-	-	-	0.19 ± 0.19	0.04 ± 0.01	-	-
9.2	-	0.04 ± 0.03	-	-	-	-	-	-	-	-
9.3	-	-	0.01 ± 0.00	-	-	-	0.09 ± 0.08	-	-	-
9.4	-	-	-	-	0.00	-	-	-	-	0.00
9.5	-	0.14 ± 0.17	0.01 ± 0.01	-	-	-	0.14 ± 0.17	0.03 ± 0.01	-	-
9.5	-	0.06 ± 0.06	0.13 ± 0.18	-	-	-	0.04 ± 0.02	-	-	-

9.6	-	-	-	-	0.02	-	-	-	-	0.02
9.7	-	0.18 ± 0.22	0.08 ± 0.11	-	-	-	0.18 ± 0.22	0.02 ± 0.00	-	-
9.7	-	0.06 ± 0.04	0.02 ± 0.01	-	-	-	-	-	-	-
9.8	-	-	-	-	0.01	-	0.03 ± 0.04	-	-	0.01
9.9	-	0.05 ± 0.02	-	-	-	-	-	0.03 ± 0.01	-	-
10.0	-	-	0.02 ± 0.01	-	0.00	-	0.04 ± 0.04	-	-	0.00
10.0	-	-	0.07 ± 0.08	-	-	-	-	-	-	-
10.1	-	0.07 ± 0.06	0.03 ± 0.02	-	-	-	-	-	-	-
10.2	-	-	-	-	-	-	0.02 ± 0.01	-	-	-
10.3	-	-	0.01 ± 0.00	-	-	-	-	0.04 ± 0.04	-	-
10.3	-	-	0.01 ± 0.01	-	-	-	-	-	-	-
10.4	-	0.06 ± 0.05	0.10 ± 0.12	-	0.01	-	-	0.03 ± 0.02	-	0.01
10.5	-	-	0.08 ± 0.09	-	-	-	0.02 ± 0.01	-	-	-
10.6	-	0.05 ± 0.05	0.02 ± 0.02	-	-	-	0.03	-	-	-
10.6	-	0.03	0.01 ± 0.01	-	-	-	-	-	-	-
10.7	-	-	-	-	-	-	0.05 ± 0.05	-	-	-
10.8	-	0.08 ± 0.02	0.03 ± 0.02	-	0.00	-	-	-	-	0.00
10.8	-	-	0.02 ± 0.01	-	-	-	-	-	-	-
10.9	-	-	0.07 ± 0.08	-	0.00	-	0.08 ± 0.01	0.02 ± 0.00	-	0.00
11.0	-	-	0.01 ± 0.01	-	0.00	-	-	-	-	0.00
11.1	-	0.07 ± 0.06	0.01 ± 0.00	-	-	-	0.02	0.02 ± 0.01	-	-
11.1	-	0.02	0.07 ± 0.10	-	-	-	0.05 ± 0.03	-	-	-
11.3	-	0.08 ± 0.10	0.02 ± 0.02	-	-	-	0.05	0.05 ± 0.01	-	0.00
11.3	-	0.05	0.02 ± 0.02	-	0.00	-	-	-	-	-
11.4	-	-	0.16 ± 0.19	-	-	-	0.05 ± 0.02	0.05 ± 0.01	-	-
11.4	-	-	0.05 ± 0.01	-	-	-	-	0.04 ± 0.02	-	-
11.4	-	-	0.04 ± 0.02	-	-	-	-	-	-	-
11.5	-	0.10 ± 0.12	0.01 ± 0.01	-	-	-	0.04	-	-	-
11.5	-	0.04	0.05 ± 0.03	-	-	-	-	-	-	-
11.6	-	-	0.06 ± 0.07	-	-	-	0.03 ± 0.03	0.06 ± 0.07	-	-
11.7	-	-	0.01 ± 0.01	-	-	-	-	-	-	-
11.8	-	0.05 ± 0.03	0.01 ± 0.00	-	-	-	0.02	-	-	-
11.8	-	0.02	-	-	-	-	0.04 ± 0.04	-	-	-
11.9	-	-	0.02 ± 0.00	-	-	-	-	0.02 ± 0.00	-	-
12.0	-	0.08 ± 0.09	0.02 ± 0.02	-	-	-	0.02	0.02 ± 0.01	-	-
12.0	-	0.02	0.01 ± 0.01	-	-	-	-	-	-	-
12.0	-	-	0.02 ± 0.01	-	-	-	-	-	-	-

12.1	-	-	-	-	-	-	0.05 ± 0.05	-	-	-
12.2	-	0.06 ± 0.06	0.01 ± 0.01	-	-	-	-	-	-	-
12.2	-	-	0.01 ± 0.01	-	-	-	-	-	-	-
12.3	-	-	0.03 ± 0.02	-	-	-	0.05 ± 0.03	0.03 ± 0.02	-	-
12.4	-	0.05	0.01 ± 0.00	-	-	-	0.05	-	-	-
12.5	-	0.05 ± 0.03	0.01 ± 0.01	-	-	-	0.04 ± 0.01	0.02 ± 0.00	-	-
12.5	-	-	0.02 ± 0.00	-	-	-	-	-	-	-
12.7	-	0.06 ± 0.04	0.01 ± 0.00	-	0.00	-	0.07	0.03 ± 0.01	-	0.00
12.7	-	0.07	0.02 ± 0.03	-	-	-	-	-	-	
12.8	-	-	-	-	0.00	-	0.05 ± 0.06	-	-	0.00
12.9	-	0.02	0.00 ± 0.00	-	0.00	-	0.02	-	-	0.00
12.9	-	0.07 ± 0.03	-	-	-	-	-	-	-	-
13.0	-	-	-	-	-	-	0.02 ± 0.01	0.01 ± 0.01	-	-
13.1	-	-	0.00 ± 0.00	-		-	-	-	-	-
13.2	-	0.03 ± 0.02	-	-	0.01	-	0.08 ± 0.03	0.01 ± 0.00	-	0.01
13.3	-	0.01	-	-	0.00	-	0.01	-	-	0.00
13.4	-	-	0.00 ± 0.00	-	0.00	-	-	0.02 ± 0.01	-	0.00
13.5	-	-	-	-	-	-	0.04 ± 0.03	-	-	-
13.5	-	0.00	-	-	-	-	0.00	-	-	-
13.6	-	-	0.00 ± 0.00	-	0.00	-	-	-	-	0.00
13.7	-	-	-	-	-	-	0.02 ± 0.01	0.03 ± 0.01	-	-
13.8	-	0.00	-	-	-	-	0.00	-	-	-
13.9	-	0.04	-	-	0.01	-	0.04	0.02 ± 0.01	-	0.01
13.9	-	-	-	-	-	-	0.04 ± 0.06	0.04 ± 0.01	-	-
14.0	-	0.03	-	-	-	-	0.03	-	-	-
14.1	-	-	-	-	0.01	-	-	-	-	0.01
14.2	-	0.02	-	-	-	-	0.03 ± 0.00	0.01	-	-
14.2	-	-	-	-	-	-	0.02	-	-	-
14.3	-	0.05	-	-	0.00	-	0.05	-	-	0.00
14.4	-	-	-	-	-	-	0.04 ± 0.02	-	-	-
14.5	-	0.02	-	-	-	-	0.02	0.01 ± 0.01	-	-
14.6	-	-	-	-	0.01	-	0.03 ± 0.01	-	-	0.01
14.7	-	0.04	-	-	-	-	0.04	-	-	-
14.8	-	-	-	-	0.00	-	-	0.02 ± 0.01	-	0.00
14.9	-	0.03	-	-	-	-	0.04 ± 0.03	-	-	-
14.9	-	-	-	-	-	-	0.03	-	-	-
15.0	-	-	-	-	0.00	-	-	0.01 ± 0.00	-	0.00
15.1	-	-	-	-	-	-	0.04 ± 0.00	-	-	-
15.2	-	-	-	-	-	-	-	0.02 ± 0.01	-	-

15.3	-	-	-	-	0.01	-	0.06 ± 0.01	-	-	0.01
15.5	-	-	-	-	0.01	-	-	0.03 ± 0.00	-	0.01
15.5	-	-	-	-	-	-	-	0.01 ± 0.00	-	-
15.6	-	-	-	-	-	-	0.02 ± 0.02	-	-	-
15.7	-	-	-	-	0.01	-	-	0.01 ± 0.00	-	0.01
15.8	-	-	-	-	-	-	-	0.00	-	-
15.9	-	-	-	-	-	-	-	0.02 ± 0.01	-	-
16.0	-	-	-	-	0.01	-	-	0.01	-	0.01
16.2	-	-	-	-	0.01	-	-	0.01 ± 0.00	-	0.01
16.2	-	-	-	-	-	-	-	0.01	-	-
16.4	-	-	-	-	0.01	-	-	0.00 ± 0.00	-	0.01
16.5	-	-	-	-	-	-	-	0.01	-	-
16.6	-	-	-	-	-	-	-	0.01 ± 0.00	-	-
16.7	-	-	-	-	0.02	-	-	0.00	-	0.02
16.9	-	-	-	-	0.02	-	-	0.00	-	0.02
17.1	-	-	-	-	0.06	-	-	-	-	0.06
17.2	-	-	-	-	-	-	-	0.00	-	-
17.4	-	-	-	-	0.02	-	-	0.00	-	0.02
17.6	-	-	-	-	0.01	-	-	0.00	-	0.01
17.8	-	-	-	-	0.02	-	-	-	-	0.02
17.9	-	-	-	-	-	-	-	0.00	-	-
18.1	-	-	-	-	0.00	-	-	0.00	-	0.00
18.3	-	-	-	-	0.02	-	-	0.00	-	0.02
18.5	-	-	-	-	0.02	-	-	-	-	0.02
18.6	-	-	-	-	-	-	-	0.00	-	-
18.8	-	-	-	-	0.02	-	-	0.00	-	0.02
19.0	-	-	-	-	0.01	-	-	-	-	0.01
19.2	-	-	-	-	0.02	-	-	-	-	0.02
19.5	-	-	-	-	0.01	-	-	-	-	0.01
19.7	-	-	-	-	0.02	-	-	-	-	0.02
19.9	-	-	-	-	0.02	-	-	-	-	0.02
20.2	-	-	-	-	0.00	-	-	-	-	0.00
Mean (g gnawed/ animal/day)	0.11 ± 0.10	0.07 ± 0.05	0.03 ± 0.02^{a,g,j}	0.09 ± 0.10	0.02 ± 0.03^{a,j}	0.11 ± 0.07	0.05 ± 0.04^{c,j}	0.03 ± 0.02^{c,k}	0.02 ± 0.02^{c,k,n}	0.02 ± 0.03^{c,k,n}

Annex 4. Table S3, S4, S5 and S6. Behavioural test and covariance analysis considering the covariates liver and body weight.

Table S3. Behavioural test for wild type, *Bscl2*$^{+/Celia}$, *Bscl2*$^{Celia/Celia}$, *Bscl2*$^{+/-}$, *Bscl2*$^{-/-}$ and severely affected (S.A.) mice. Data is presented as mean ± SD. Data is presented as mean ± SD. Data were analysed using a Kolmogorov-Smirnov test for normality, followed by a Kruskal-Wallis test with Mann-Whitney post hoc comparisons. [a] $p < 0.05$ vs wild type ♀/♂; [b] $p < 0.05$ vs wild type ♀; [c] $p < 0.05$ vs wild type ♂; [d] $p < 0.05$ vs *Bscl2*$^{+/-}$ ♀/♂; [e] $p < 0.05$ vs *Bscl2*$^{+/-}$ ♀; [f] $p < 0.05$ vs *Bscl2*$^{+/-}$ ♂; [g] $p < 0.05$ vs *Bscl2*$^{-/-}$ ♀/♂; [h] $p < 0.05$ vs *Bscl2*$^{-/-}$ ♀; [i] $p < 0.05$ vs *Bscl2*$^{-/-}$ ♂; [j] $p < 0.05$ vs *Bscl2*$^{+/Celia}$ ♀/♂; [k] $p < 0.05$ vs *Bscl2*$^{+/Celia}$ ♀; [l] $p < 0.05$ vs *Bscl2*$^{+/Celia}$ ♂; [m] $p < 0.05$ vs *Bscl2*$^{Celia/Celia}$ ♀/♂; [n] $p < 0.05$ vs *Bscl2*$^{Celia/Celia}$ ♀; [o] $p < 0.05$ vs *Bscl2*$^{Celia/Celia}$ ♂; [p] $p < 0.05$ vs S.A. *Bscl2*$^{+/Celia}$ ♀/♂ and [q] $p < 0.05$ vs S.A. *Bscl2*$^{Celia/Celia}$ ♀/♂.

		Rotarod test			Beam walking test								Wire hang test		
		N	Age (months)	Distance (cm)	N	Age (months)	Time (s)	Slips (nº)	Falls (%)	Immobility (%)	Backward motion (%)	Drag walk (%)	N	Age (months)	Time (s)
Wild type	♀/♂	29	7.1	180.50 ± 68.06	17	8.9	11.96 ± 4.16	0.95 ± 1.28	0.00 ± 0.00	11.76 ± 0.53	11.76 ± 0.33	29.41 ± 0.80	24	9.0	63.12 ± 60.97
Bscl2$^{+/Celia}$	♀/♂	28	7.2	195.09 ± 95.28	26	8.9	14.38 ± 9.41	0.90 ± 0.73	7.69 ± 0.27	3.85 ± 0.20	3.85 ± 0.20	7.69 ± 0.27	33	8.9	56.68 ± 133.87
Bscl2$^{Celia/Celia}$	♀/♂	25	7.1	149.21 ± 70.69[j]	18	9.0	28.52 ± 14.23[a,d,j]	2.64 ± 1.85[a,d,j]	50.00 ± 0.51[a,d,j]	0.00 ± 0.00	0.00 ± 0.00	11.11 ± 0.32	23	9.0	34.30 ± 23.20
Bscl2$^{+/-}$	♀/♂	30	7.0	192.05 ± 94.65	24	9.0	13.7 ± 15.7	1.01 ± 1.09	50.00 ± 0.51	0.00 ± 0.00	0.00 ± 0.00	11.11 ± 0.32	28	9.0	69.50 ± 72.28
Bscl2$^{-/-}$	♀/♂	23	7.2	141.78 ± 61.25[a,d,j]	10	9.0	37.3 ± 21.7[a,d,j]	2.82 ± 2.35[a,d,j]	8.33 ± 0.45	8.33 ± 0.28	8.33 ± 0.28	12.50 ± 0.66	12	9.0	27.00 ± 13.44
Wild type	♀	19	7.1	204.35 ± 69.96	13	9.0	10.54 ± 3.44	1.01 ± 1.41	0.00 ± 0.00	0.00 ± 0.00	7.69 ± 0.28	23.08 ± 0.87	15	9.0	58.49 ± 48.22
	♂	10	7.1	135.18 ± 33.78[b]	4	8.8	16.58 ± 2.79[b]	0.75 ± 0.88	0.00 ± 0.00	50.00 ± 0.96	25.00 ± 0.50	50.00 ± 0.58	9	9.0	70.85 ± 80.68
Bscl2$^{+/Celia}$	♀	17	7.2	200.44 ± 115.96	15	8.8	11.82 ± 5.72	0.64 ± 0.36	6.67 ± 0.26	6.67 ± 0.26	6.67 ± 0.26	6.67 ± 0.26	21	8.9	89.06 ± 133.87
	♂	11	7.2	186.82 ± 53.58[c,e]	11	9.0	17.88 ± 12.35	1.26 ± 0.95[k]	9.09 ± 0.30	0.00 ± 0.00	0.00 ± 0.00	9.09 ± 0.30	12	9.0	40.97 ± 27.30
Bscl2$^{Celia/Celia}$	♀	15	7.2	168.30 ± 68.99	10	9.1	22.55 ± 14.16[b,d,k]	2.77 ± 1.93[a,e,j]	60.00 ± 0.53[b]	0.00 ± 0.00	0.00 ± 0.00	0.00 ± 0.00	13	9.0	39.13 ± 28.09
	♂	10	7.0	120.58 ± 66.36[b,h,l,n]	8	8.9	35.98 ± 10.94[a,d,j,n]	2.48 ± 1.88[b,e,k]	37.50 ± 0.52	0.00 ± 0.00	0.00 ± 0.00	25.00 ± 0.46	10	8.9	28.03 ± 13.63
Bscl2$^{+/-}$	♀	16	7.0	230.16 ± 96.95[c]	13	9.1	9.45 ± 4.41[c,l]	0.64 ± 0.54	7.69 ± 0.28	7.69 ± 0.28	0.00 ± 0.00	0.00 ± 0.00	14	9.1	69.48 ± 94.17
	♂	14	7.0	148.50 ± 72.86[e]	11	9.0	18.68 ± 22.14[e]	1.45 ± 1.41	9.09 ± 0.60	9.09 ± 0.30	18.18 ± 0.40	27.27 ± 0.93	14	9.0	69.52 ± 53.88
Bscl2$^{-/-}$	♀	10	7.2	164.76 ± 48.04	3	8.9	36.22 ± 22.70[a,e]	2.28 ± 0.86[e,k]	66.67 ± 1.00	0.00 ± 0.00	0.00 ± 0.00	0.00 ± 0.00	3	8.9	21.89 ± 15.99
	♂	13	7.2	124.10 ± 66.09[b,e,h,j,n]	7	9.1	37.71 ± 23.10[a,d,j]	3.05 ± 2.80[e,k]	14.29 ± 0.76	42.86 ± 0.53	28.57 ± 0.49	71.43 ± 1.72[e,j,n]	9	9.0	28.70 ± 13.09

		Open field test								Elevated zero maze								
		N	Age (months)	Distance (m)	Mean speed (m/s)	Time mobile (s)	Time in centre (s)	Crossing top-bottom (nº)	Crossing left-right (nº)	N	Age (months)	Distance (m)	Mean speed (m/s)	Time mobile (s)	Time immobile (s)	Rotations (nº)	Time in open zones (s)	Time in hidden zones (s)
Wild type	♀/♂	29	6.5	12.83 ± 7.70	0.04 ± 0.02	199.14 ± 79.67	8.47 ± 12.36	1.24 ± 1.50	0.98 ± 1.39^{q}	78	7.3	8.99 ± 5.07	0.03 ± 0.02	157.15 ± 55.08	132.85 ± 55.08	7.21 ± 4.46	18.01 ± 16.11^{p}	271.30 ± 16.39
Bscl2$^{+/Celia}$	♀/♂	27	6.6	12.77 ± 6.22^{d}	0.04 ± 0.02^{d}	204.22 ± 74.83^{d}	8.33 ± 9.08	1.23 ± 1.39^{d}	0.80 ± 1.09^{q}	84	7.4	8.06 ± 5.31^{d}	0.03 ± 0.02^{d}	151.18 ± 67.16	138.74 ± 67.07	6.10 ± 4.68	20.66 ± 21.95^{p}	268.78 ± 22.18
Bscl2$^{Celia/Celia}$	♀/♂	25	6.5	5.78 ± 4.38^{a,d,j}	0.02 ± 0.01^{a,d,j}	99.96 ± 73.88^{a,d,j}	3.76 ± 9.25^{a,d,j}	0.54 ± 1.26^{a,d,j}	0.36 ± 0.88^{a,d,j}	76	7.3	3.78 ± 2.20^{a,d,g,j}	0.01 ± 0.01^{a,d,j}	81.15 ± 51.75^{a,d,j}	208.81 ± 51.84^{a,d,j}	2.37 ± 3.03^{a,d,j}	7.75 ± 12.61^{a,d,j,p}	281.81 ± 12.69^{a,d,j}
Bscl2$^{+/-}$	♀/♂	30	6.5	10.46 ± 5.40^{a}	0.03 ± 0.02^{a}	172.72 ± 77.02^{a}	13.22 ± 28.91	0.94 ± 1.35	0.56 ± 0.88^{a,q}	99	7.4	9.1 ± 4.47	0.03 ± 0.02	164.31 ± 60.65	125.62 ± 60.64	7.30 ± 4.90	24.18 ± 24.61^{p}	264.79 ± 25.19
Bscl2$^{-/-}$	♀/♂	23	6.5	5.90 ± 4.28^{a,d,j}	0.02 ± 0.01^{a,d,j}	107.35 ± 69.98^{a,d,j}	6.47 ± 19.50^{a,d,j}	0.52 ± 0.91^{a,d,j}	0.35 ± 0.82^{a,d,j}	40	7.4	2.9 ± 1.41^{a,d,j}	0.01 ± 0.00^{a,d,j}	66.43 ± 42.55^{a,d,j}	223.58 ± 42.55^{a,d,j}	1.10 ± 1.37^{a,d,j}	4.81 ± 13.20^{a,d,j,p}	285.09 ± 13.21^{a,d,j}
S.A. *Bscl2*$^{+/Celia}$	♀/♂	8	6.6	5.81 ± 1.98^{a,d,j}	0.02 ± 0.01^{a,d,j}	149.25 ± 46.64^{a,g,j,m}	11.38 ± 13.03^{m}	0.38 ± 0.74^{j}	0.75 ± 1.04	4	7.4	1.93 ± 0.79^{a,d,j,m}	0.01 ± 0.00^{a,d,j,m}	87.70 ± 51.04^{a,d,j}	202.30 ± 51.04^{a,d,j}	2.75 ± 1.71^{a,d,g}	0.00 ± 0.00	289.35 ± 1.30^{a,d,j}
S.A. *Bscl2*$^{Celia/Celia}$	♀/♂	12	6.7	1.29 ± 0.29^{a,d,g,j,m}	0.00 ± 0.00^{a,d,g,j,m}	57.03 ± 45.38^{a,d,g,j,m}	8.01 ± 8.44^{g,m}	0.17 ± 0.39^{a,d,j}	0.00 ± 0.00	10	7.3	1.19 ± 0.72^{a,d,g,j,m}	0.00 ± 0.00^{a,d,g,j,m}	37.64 ± 19.17^{a,d,g,j,m}	252.36 ± 19.17^{a,d,g,j,m}	0.40 ± 0.70^{a,d,j,m,p}	7.24 ± 17.97^{a,d,j}	282.43 ± 17.85^{a,d,j}
Wild type	♀	20	6.5	13.53 ± 8.66	0.04 ± 0.02	202.25 ± 85.68	9.28 ± 13.96	1.33 ± 1.60	0.96 ± 1.48	60	7.3	9.62 ± 5.53	0.03 ± 0.02	158.75 ± 52.93	131.25 ± 52.93	7.92 ± 4.35	19.86 ± 17.11	269.43 ± 17.30
	♂	9	6.4	11.27 ± 4.66	0.03 ± 0.01	192.23 ± 64.92	6.66 ± 7.58	1.06 ± 1.24	1.03 ± 1.18	18	7.2	6.91 ± 2.08	0.02 ± 0.01	151.82 ± 63.07	138.18 ± 63.07	4.83 ± 4.05^{b}	11.84 ± 10.36	277.55 ± 11.18
Bscl2$^{+/Celia}$	♀	17	6.5	13.68 ± 6.75^{d}	0.04 ± 0.02^{d}	211.58 ± 77.30^{d}	9.85 ± 10.00	1.45 ± 1.56^{d}	0.97 ± 1.18	40	7.4	9.07 ± 6.82	0.03 ± 0.02	154.10 ± 77.53	135.72 ± 77.36	7.50 ± 5.44^{l}	20.53 ± 22.37^{f}	268.45 ± 22.82^{f}
	♂	10	6.7	11.24 ± 4.94	0.03 ± 0.01^{d}	191.88 ± 69.71	5.77 ± 6.64^{k}	0.88 ± 0.97	0.53 ± 0.85^{c,k}	44	7.4	7.15 ± 3.22^{b,f}	0.02 ± 0.01^{b,f}	148.52 ± 56.92^{f}	141.48 ± 56.92^{f}	4.82 ± 3.46^{b}	20.77 ± 21.82^{f}	269.08 ± 21.83^{f}
Bscl2$^{Celia/Celia}$	♀	14	6.6	7.04 ± 4.56^{a,d,i,j,o}	0.02 ± 0.01^{a,d,i,j,o}	117.08 ± 72.18^{a,d,i,j,o}	5.73 ± 11.62^{a,d,j,o}	0.75 ± 1.47^{a,k,o}	0.41 ± 0.76^{a,k,o}	44	7.4	3.76 ± 2.04^{a,d,j}	0.01 ± 0.01^{a,d,j}	88.14 ± 60.13^{a,d,j}	201.78 ± 60.25^{a,d,j}	2.89 ± 3.49^{a,d,i,j}	7.03 ± 10.60^{a,d,j}	282.21 ± 10.81^{a,d,j}
	♂	11	6.3	4.19 ± 3.59^{a,d,j}	0.01 ± 0.01^{a,d,j}	78.18 ± 70.96^{a,d,j}	1.26 ± 3.57^{a,d,j}	0.27 ± 0.87^{a,d,j}	0.30 ± 1.02^{a,d,j}	32	7.3	3.80 ± 2.43^{a,d,j}	0.01 ± 0.01^{a,d,j}	71.53 ± 36.05^{a,d,j}	218.47 ± 36.05^{a,d,j}	1.66 ± 2.10^{a,d,j}	8.74 ± 15.06^{a,d,j}	281.26 ± 15.06^{a,d,j}
Bscl2$^{+/-}$	♀	16	6.5	11.11 ± 5.32	0.03 ± 0.01	174.32 ± 74.22^{b}	9.93 ± 16.34	0.83 ± 1.07	0.62 ± 0.91^{c}	55	7.4	7.8 ± 4.43^{f}	0.03 ± 0.02^{f}	147.13 ± 66.92^{f}	142.84 ± 66.91^{f}	6.40 ± 4.02	14.16 ± 15.72^{f}	275.05 ± 15.93^{f}
	♂	14	6.5	9.69 ± 5.43^{a,j}	0.03 ± 0.02^{a}	170.86 ± 80.79^{b}	17.04 ± 38.53	1.07 ± 1.62	0.50 ± 0.85^{c,k}	44	7.3	10.6 ± 4.06^{a}	0.04 ± 0.01^{a}	185.79 ± 43.70^{a}	104.09 ± 43.65^{a}	8.43 ± 5.66^{c,l}	36.71 ± 27.94^{a}	251.97 ± 28.71^{a}
Bscl2$^{-/-}$	♀	10	6.5	8.28 ± 4.53^{a,e,i,j,o}	0.02 ± 0.01^{a,e,i,j,o}	138.97 ± 72.48^{a,e,i,j,o}	4.55 ± 7.80^{a,e,j,o}	0.77 ± 1.13^{k,o}	0.56 ± 1.10^{c,k,o}	12	7.3	3.3 ± 1.57^{a,d,j}	0.01 ± 0.01^{a,d,j}	84.38 ± 59.12^{a,d}	205.62 ± 59.12^{a,d}	1.92 ± 1.73^{a,d,i,j}	3.29 ± 3.35^{a,d,j}	286.57 ± 3.50^{a,d,j}
	♂	13	6.5	4.11 ± 3.07^{a,d,j}	0.01 ± 0.01^{a,d,j}	83.63 ± 58.21^{a,d,j}	7.90 ± 24.92^{a,d,h,j,o}	0.33 ± 0.65^{a,d,h,j}	0.19 ± 0.49^{a,d,j}	28	7.4	2.6 ± 1.31^{a,d,j,n}	0.01 ± 0.00^{a,d,j,n}	58.73 ± 31.40^{a,d,j}	231.27 ± 31.40^{a,d,j}	0.75 ± 1.04^{a,d,j}	5.45 ± 15.67^{a,d,j}	284.45 ± 15.68^{a,d,j,n}

				Morris water maze														
				Day 1	Day 2	Day 3	Day 4	Day 8										
		N	Age (months)	Time to reach platform (s)				Distance (m)	Mean speed (m/s)	Maximum speed (m/s)	Time mobile (s)	Time immobile (s)	Floating time (s)	Floating number (nº)	Platform zone			
															Entries (nº)	Time (s)	Distance (m)	Time immobile (s)	Time mobile (s)
Wild type	♀/♂	27	8.5	27.57 ± 8.24	18.69 ± 9.89	10.21 ± 5.69	6.57 ± 4.30	8.44 ± 0.63	0.14 ± 0.05	0.31 ± 0.04	58.07 ± 3.53	1.35 ± 3.11	9.22 ± 12.76	1.02 ± 1.39	4.51 ± 2.26	16.05 ± 10.50	2.10 ± 1.10	0.60 ± 2.45[g]	15.45 ± 9.32
Bscl2$^{+/Celia}$	♀/♂	29	8.0	29.09 ± 11.41	13.00 ± 7.45[a]	11.68 ± 9.60	10.13 ± 6.43	7.95 ± 0.77[a]	0.12 ± 0.05[a]	0.30 ± 0.05	56.82 ± 5.97	3.17 ± 5.97[a]	10.88 ± 13.99	1.43 ± 1.80	3.77 ± 2.04[a]	16.42 ± 11.16	1.92 ± 1.13	0.46 ± 2.32	15.96 ± 10.45
Bscl2$^{Celia/Celia}$	♀/♂	23	7.9	26.33 ± 12.42	14.25 ± 7.62	10.80 ± 5.88	7.93 ± 4.39	7.90 ± 0.58[d,j]	0.14 ± 0.04[d,j]	0.26 ± 0.02[a,d,j]	58.40 ± 5.24[a,d,j]	1.60 ± 5.24[j]	3.68 ± 9.71[a,d,j]	0.39 ± 0.93[a,d,j]	4.64 ± 1.96[j]	14.38 ± 7.04	2.12 ± 0.99	0.22 ± 1.69[a]	14.16 ± 6.79
Bscl2$^{+/-}$	♀/♂	27	8.5	35.95 ± 10.83	16.34 ± 10.16	15.30 ± 10.20	11.95 ± 7.76[a]	8.48 ± 0.38[a,j]	0.16 ± 0.04[a,j]	0.32 ± 0.04[a,]	57.69 ± 3.67	1.21 ± 3.08[j]	4.65 ± 6.36[j]	0.86 ± 1.08	4.79 ± 1.77[j]	14.08 ± 7.57	2.21 ± 1.05	0.54 ± 2.14[g]	13.54 ± 6.80
Bscl2$^{-/-}$	♀/♂	15	8.7	32.00 ± 10.56	4.81 ± 14.23[j,m]	14.23 ± 6.38	11.04 ± 4.59[a]	8.65 ± 0.53[j,m]	0.16 ± 0.03[j,m]	0.26 ± 0.03[a,d,j]	58.86 ± 2.76[d,m]	0.54 ± 2.32[a,j]	1.74 ± 4.34[a,d,j]	0.23 ± 0.46[a,d,j]	5.10 ± 1.53[a,j]	14.43 ± 5.66	2.40 ± 0.90[a,j]	0.00 ± 0.00	14.43 ± 5.66
Wild type	♀	19	8.4	26.48 ± 7.34	19.29 ± 10.25	10.13 ± 5.69	6.58 ± 4.39	8.83 ± 3.33	0.15 ± 0.06	0.31 ± 0.04	58.44 ± 2.92	1.07 ± 2.56	8.17 ± 12.58	1.00 ± 1.51	4.70 ± 2.37	15.74 ± 9.73	2.17 ± 1.10	0.46 ± 2.02	15.29 ± 8.99
	♂	8	8.5	31.13 ± 11.15	16.75 ± 9.70	10.44 ± 6.57	6.56 ± 4.65	7.62 ± 3.13	0.13 ± 0.05	0.31 ± 0.04	57.23 ± 4.59	1.99 ± 4.08	11.64 ± 13.04	1.06 ± 1.08	4.06 ± 1.95	16.78 ± 12.21	1.94 ± 1.09	0.95 ± 3.25	15.83 ± 10.16
Bscl2$^{+/Celia}$	♀	20	8.1	28.50 ± 11.43	12.54 ± 7.39	11.46 ± 9.59	10.91 ± 6.89	7.32 ± 3.25[b]	0.12 ± 0.05[b]	0.30 ± 0.05[e]	57.35 ± 5.72	2.64 ± 5.72	10.73 ± 14.39	1.51 ± 2.04	3.81 ± 2.08[b]	16.72 ± 11.43	1.93 ± 1.15	0.63 ± 2.78	16.09 ± 10.44
	♂	9	7.6	30.13 ± 12.09	13.81 ± 8.00	12.06 ± 10.25	8.75 ± 5.69	6.64 ± 3.18[b]	0.11 ± 0.05[b]	0.31 ± 0.06	55.69 ± 6.40[b,k]	4.31 ± 6.40[b,k]	11.18 ± 13.29[b,d]	1.27 ± 1.17[b]	3.68 ± 1.99[b]	15.78 ± 10.69	1.91 ± 1.11	0.10 ± 0.59	15.68 ± 10.61
Bscl2$^{Celia/Celia}$	♀	14	7.8	27.48 ± 14.04	13.10 ± 6.30	7.50 ± 3.48	6.96 ± 3.93	8.38 ± 2.44[d,j]	0.14 ± 0.04[b,d,j]	0.26 ± 0.02[a,d,j]	57.93 ± 6.18[a,d,j]	2.07 ± 6.18[l]	4.66 ± 11.59[a,f,j]	0.46 ± 1.09[a,d,j]	4.66 ± 2.01[j]	14.69 ± 6.61	2.16 ± 0.95	0.00 ± 0.00	14.69 ± 6.61
	♂	9	8.1	24.47 ± 9.81	16.13 ± 9.56	16.16 ± 5.01	9.50 ± 4.90	9.11 ± 1.96[c,j]	0.15 ± 0.06[c,j]	0.26 ± 0.02[a,d,j]	59.12 ± 3.23[a,d,j]	0.88 ± 3.23[j]	2.14 ± 5.46[a,d,j]	0.28 ± 0.57[a,d,j]	4.61 ± 1.90[j]	13.89 ± 7.73	2.06 ± 1.06	0.57 ± 2.69	13.32 ± 7.08
Bscl2$^{+/-}$	♀	14	8.5	37.43 ± 12.36	16.45 ± 11.80	16.83 ± 11.87	10.43 ± 6.70	9.69 ± 2.37[c,j]	0.17 ± 0.04[c,j]	0.33 ± 0.04[a]	57.12 ± 3.90[b,k]	1.44 ± 3.32[l]	4.61 ± 6.67[c]	0.76 ± 0.98[l]	4.78 ± 1.64[j]	14.75 ± 7.69	2.33 ± 1.00	0.60 ± 2.28	14.15 ± 6.60
	♂	13	8.5	33.50 ± 8.09	16.17 ± 7.68	12.75 ± 6.78	14.50 ± 9.35	9.50 ± 2.31[c,j]	0.16 ± 0.04[c,j]	0.31 ± 0.04[e]	58.30 ± 3.35[e]	0.96 ± 2.82[j]	4.68 ± 6.09[c]	0.96 ± 1.17	4.79 ± 1.91[j]	13.37 ± 7.44	2.09 ± 1.10	0.47 ± 2.01	12.90 ± 7.01
Bscl2$^{-/-}$	♀	7	8.9	25.61 ± 8.60	21.61 ± 3.67	12.39 ± 5.94	9.54 ± 3.67	9.21 ± 1.63[c,j]	0.15 ± 0.03[c,j]	0.24 ± 0.03[a,d,j]	59.00 ± 2.02[e,l,m]	0.55 ± 1.95[j]	1.56 ± 4.72[a,d,j]	0.18 ± 0.48[a,d,j]	5.29 ± 1.63[c,j]	15.39 ± 5.51	2.46 ± 0.91	0.00 ± 0.00	15.39 ± 5.51
	♂	8	8.5	38.39 ± 8.50	16.36 ± 4.54	16.07 ± 6.70	6.70 ± 12.54	9.82 ± 2.07[c,j,n]	0.17 ± 0.03[c,j,n]	0.27 ± 0.03[a,d,h,j]	58.73 ± 3.30[e,m]	0.53 ± 2.63[a,k]	1.88 ± 4.06[c,f,j]	0.28 ± 0.46[c,d,j]	4.94 ± 1.44[j]	13.60 ± 5.73	2.35 ± 0.91	0.00 ± 0.00	13.60 ± 5.73

Table S4. Covariance analysis for behavioural studies with significant differences considering the covariates liver and body weight between wild type and *Bscl2*$^{Celia/Celia}$ mice separated by sex. Data is presented as mean ± SEM and significance (p). Data were analysed using Analysis of Covariance (ANCOVA) to control for liver weight and overall body weight.

		Wild type ♂			*Bscl2*$^{Celia/Celia}$ ♂			Wild type ♂ vs *Bscl2*$^{Celia/Celia}$ ♂			Wild type ♀			*Bscl2*$^{Celia/Celia}$ ♀			Wild type ♀ vs *Bscl2*$^{Celia/Celia}$ ♀		
		Values			Values			Significance (p)			Values			Values			Significance (p)		
	Covariate	-	Liver weight	Body weight	-	Liver weight	Body weight	-	Liver weight	Body weight	-	Liver weight	Body weight	-	Liver weight	Body weight	-	Liver weight	Body weight
Open field test	N	9	9	9	11	10	11				20	19	20	14	12	14			
	Distance (m)	11.27 ± 0.69	12.19 ± 1.12	11.35 ± 0.70	4.42 ± 0.66	3.60 ± 1.03	4.35 ± 0.67	0.000	0.000	0.000	13.39 ± 0.86	11.56 ± 1.70	12.76 ± 0.87	7.03 ± 1.09	9.91 ± 2.57	8.02 ± 1.12	0.000	0.685	0.002
	Mean speed (m/s)	0.03 ± 0.00	0.03 ± 0.00	0.03 ± 0.00	0.01 ± 0.00	0.01 ± 0.00	0.01 ± 0.00	0.000	0.000	0.000	0.04 ± 0.00	0.03 ± 0.01	0.04 ± 0.00	0.02 ± 0.00	0.03 ± 0.01	0.02 ± 0.00	0.000	0.696	0.002
	Time mobile (s)	192.23 ± 11.51	206.83 ± 18.56	193.82 ± 11.64	81.60 ± 10.92	68.46 ± 17.06	80.17 ± 11.04	0.000	0.000	0.000	197.59 ± 9.25	172.70 ± 18.21	194.24 ± 9.57	117.37 ± 11.64	156.76 ± 27.45	122.66 ± 12.29	0.000	0.713	0.000
	Time in centre (s)	6.66 ± 0.98	7.37 ± 1.59	6.80 ± 0.99	1.36 ± 0.93	0.72 ± 1.46	1.23 ± 0.94	0.000	0.017	0.000	8.91 ± 1.54	2.81 ± 3.00	8.51 ± 1.60	6.09 ± 1.94	15.76 ± 4.53	6.74 ± 2.06	0.257	0.072	0.516
	Crossing top-bottom (nº)	1.06 ± 0.18	1.20 ± 0.29	1.10 ± 0.18	0.30 ± 0.17	0.17 ± 0.27	0.26 ± 0.17	0.003	0.045	0.001	1.32 ± 0.18	0.85 ± 0.36	1.23 ± 0.19	0.73 ± 0.23	1.46 ± 0.55	0.86 ± 0.24	0.049	0.478	0.251
	Crossing left-right (nº)	1.03 ± 0.19	1.34 ± 0.30	1.04 ± 0.19	0.33 ± 0.18	0.04 ± 0.28	0.31 ± 0.18	0.008	0.014	0.008	0.90 ± 0.14	0.61 ± 0.28	0.89 ± 0.15	0.42 ± 0.18	0.87 ± 0.42	0.42 ± 0.19	0.037	0.687	0.064
Elevated zero maze	N	5	5	5	8	8	8				15	14	14	11	10	11			
	Distance (m)	6.91 ± 0.54	7.32 ± 1.02	6.83 ± 0.58	3.80 ± 0.41	3.57 ± 0.63	3.84 ± 0.42	0.000	0.016	0.000	9.66 ± 0.61	9.66 ± 0.61	9.66 ± 0.61	3.78 ± 0.72	3.78 ± 0.72	3.78 ± 0.72	0.000	0.000	0.000
	Mean speed (m/s)	0.02 ± 0.00	0.03 ± 0.00	0.02 ± 0.00	0.01 ± 0.00	0.01 ± 0.00	0.01 ± 0.00	0.000	0.018	0.000	0.03 ± 0.00	0.03 ± 0.00	0.03 ± 0.00	0.01 ± 0.00	0.01 ± 0.00	0.02 ± 0.00	0.000	0.013	0.001
	Maximum speed (m/s)	0.24 ± 0.01	0.21 ± 0.03	0.24 ± 0.02	0.20 ± 0.01	0.21 ± 0.02	0.19 ± 0.01	0.014	0.875	0.017	0.27 ± 0.02	0.24 ± 0.04	0.26 ± 0.03	0.23 ± 0.03	0.27 ± 0.05	0.24 ± 0.03	0.288	0.684	0.658
	Time mobile (s)	151.82 ± 11.18	168.31 ± 20.73	153.20 ± 11.83	71.53 ± 8.38	62.25 ± 12.91	70.75 ± 8.69	0.000	0.001	0.000	158.01 ± 7.55	154.56 ± 13.88	157.39 ± 9.04	86.99 ± 8.94	91.82 ± 18.58	87.86 ± 11.31	0.000	0.041	0.000
	Time immobile (s)	138.18 ± 11.18	121.69 ± 20.73	136.80 ± 11.83	218.47 ± 8.38	227.75 ± 12.91	219.25 ± 8.69	0.000	0.001	0.000	131.99 ± 7.56	135.48 ± 13.89	132.61 ± 9.05	202.93 ± 8.95	198.04 ± 18.60	202.05 ± 11.32	0.000	0.042	0.000
	Rotations (nº)	4.83 ± 0.69	5.39 ± 1.30	4.97 ± 0.73	1.66 ± 0.52	1.35 ± 0.81	1.58 ± 0.54	0.001	0.040	0.001	7.93 ± 0.54	8.16 ± 0.99	8.02 ± 0.64	2.78 ± 0.64	2.46 ± 1.32	2.65 ± 0.81	0.000	0.010	0.000
	Time in open zones (s)	11.84 ± 3.20	15.33 ± 5.96	10.64 ± 3.34	8.74 ± 2.40	6.78 ± 3.72	9.42 ± 2.46	0.442	0.337	0.776	18.82 ± 1.98	18.44 ± 3.63	21.11 ± 2.33	7.52 ± 2.34	8.05 ± 4.86	4.31 ± 2.91	0.000	0.193	0.000
	Time in hidden zones (s)	277.55 ± 3.26	273.90 ± 6.06	278.75 ± 3.40	281.26 ± 2.44	283.31 ± 3.78	280.58 ± 2.50	0.367	0.299	0.676	270.62 ± 1.98	271.02 ± 3.64	268.04 ± 2.32	281.71 ± 2.34	281.15 ± 4.87	285.31 ± 2.90	0.000	0.205	0.000

Rotarod test	N	10	10	10	10	9	10				19	18	19	15	13	15			
	Distance (m)	135.17 ± 17.13	176.07 ± 25.00	134.36 ± 16.90	121.24 ± 18.05	75.80 ± 27.22	122.14 ± 17.81	0.583	0.049	0.626	204.40 ± 16.45	220.93 ± 32.90	200.99 ± 16.95	175.72 ± 19.36	152.83 ± 43.91	180.43 ± 20.13	0.268	0.355	0.454
Morris water maze	N	8	8	8	9	9	9				19	19	19	14	12	14			
	Distance (m)	7.62 ± 0.46	7.35 ± 0.70	7.76 ± 0.48	9.08 ± 0.44	9.33 ± 0.65	8.96 ± 0.45	0.024	0.104	0.083	8.83 ± 0.34	8.61 ± 0.65	8.97 ± 0.35	8.41 ± 0.43	8.76 ± 0.97	8.20 ± 0.44	0.447	0.920	0.182
	Mean speed (m/s)	0.13 ± 0.01	0.12 ± 0.01	0.13 ± 0.01	0.15 ± 0.01	0.16 ± 0.01	0.15 ± 0.01	0.035	0.122	0.115	0.15 ± 0.01	0.14 ± 0.01	0.15 ± 0.01	0.14 ± 0.00	0.15 ± 0.02	0.14 ± 0.01	0.388	0.952	0.151
	Maximum speed (m/s)	0.31 ± 0.01	0.30 ± 0.01	0.31 ± 0.01	0.26 ± 0.01	0.27 ± 0.01	0.25 ± 0.01	0.000	0.019	0.000	0.31 ± 0.00	0.30 ± 0.01	0.31 ± 0.00	0.26 ± 0.01	0.27 ± 0.01	0.25 ± 0.01	0.000	0.088	0.000
	Time mobile (s)	57.23 ± 0.70	57.07 ± 1.07	57.40 ± 0.73	59.09 ± 0.67	59.24 ± 1.00	58.94 ± 0.70	0.058	0.238	0.145	58.44 ± 0.50	56.73 ± 0.92	58.56 ± 0.51	58.43 ± 0.62	61.13 ± 1.38	58.25 ± 0.64	0.996	0.045	0.716
	Time immobile (s)	1.99 ± 0.65	2.18 ± 1.00	1.73 ± 0.67	0.91 ± 0.62	0.73 ± 0.93	1.15 ± 0.64	0.232	0.397	0.551	1.07 ± 0.48	2.80 ± 0.89	0.95 ± 0.49	1.57 ± 0.60	-1.15 ± 1.33	1.76 ± 0.62	0.524	0.062	0.320
	Floating time (s)	11.64 ± 1.74	12.54 ± 2.66	10.94 ± 1.80	2.20 ± 1.67	1.38 ± 2.48	2.84 ± 1.71	0.000	0.017	0.003	8.17 ± 1.29	6.67 ± 2.44	7.60 ± 1.30	3.47 ± 1.61	5.83 ± 3.64	4.37 ± 1.65	0.024	0.884	0.136
	Floating number (nº)	1.06 ± 0.15	1.18 ± 0.23	1.00 ± 0.16	0.29 ± 0.14	0.18 ± 0.21	0.35 ± 0.15	0.000	0.013	0.005	1.00 ± 0.16	0.69 ± 0.30	0.92 ± 0.16	0.45 ± 0.20	0.94 ± 0.44	0.58 ± 0.20	0.030	0.714	0.191
	Platform zone: Entries (nº)	2.75 ± 0.46	1.19 ± 0.66	3.35 ± 0.40	3.80 ± 0.44	5.23 ± 0.62	3.25 ± 0.38	0.107	0.001	0.857	3.35 ± 0.31	2.00 ± 0.58	3.12 ± 0.31	4.34 ± 0.39	6.47 ± 0.87	4.70 ± 0.39	0.052	0.001	0.002
	Platform zone: Time (s)	11.66 ± 1.88	6.78 ± 2.77	13.74 ± 1.74	10.68 ± 1.80	15.15 ± 2.58	8.78 ± 1.66	0.708	0.081	0.050	12.59 ± 1.17	8.76 ± 2.19	11.42 ± 1.09	13.93 ± 1.47	19.96 ± 3.27	15.77 ± 1.38	0.476	0.031	0.018
	Platform zone: Distance (m)	1.45 ± 0.24	0.76 ± 0.35	1.72 ± 0.22	1.69 ± 0.23	2.32 ± 0.33	1.44 ± 0.21	0.475	0.012	0.376	1.59 ± 0.15	0.99 ± 0.27	1.47 ± 0.14	2.00 ± 0.18	2.95 ± 0.40	2.19 ± 0.18	0.082	0.002	0.002
	Platform zone: Time immobile (s)	0.31 ± 0.16	0.19 ± 0.24	0.36 ± 0.17	0.14 ± 0.15	0.25 ± 0.23	0.09 ± 0.16	0.455	0.883	0.255	0.46 ± 0.18	0.34 ± 0.35	0.38 ± 0.19	-5.55E-17 ± 0.23	0.18 ± 0.52	0.12 ± 0.24	0.126	0.840	0.407
	Platform zone: Time mobile (s)	11.36 ± 1.81	6.59 ± 2.65	13.38 ± 1.66	10.55 ± 1.73	14.90 ± 2.47	8.70 ± 1.58	0.746	0.071	0.053	12.13 ± 1.11	8.42 ± 2.08	11.04 ± 1.04	13.93 ± 1.40	19.78 ± 3.10	15.65 ± 1.32	0.315	0.021	0.008

Table S5. Covariance analysis for behavioural studies with significant differences considering the covariates liver and body weight between wild type and *Bscl2*$^{-/-}$ mice separated by sex. Data is presented as mean ± SEM and significance (p). Data were analysed using Analysis of Covariance (ANCOVA) to control for liver weight and overall body weight.

		Wild type ♂			*Bscl2*$^{-/-}$ ♂			Wild type ♂ vs *Bscl2*$^{-/-}$ ♂			Wild type ♀			*Bscl2*$^{-/-}$ ♀			Wild type ♀ vs *Bscl2*$^{-/-}$ ♀		
		Values			Values			Significance (p)			Values			Values			Significance (p)		
	Covariate	-	Liver weight	Body weight	-	Liver weight	Body weight	-	Liver weight	Body weight	-	Liver weight	Body weight	-	Liver weight	Body weight	-	Liver weight	Body weight
Open field test	N	9	9	9	13	11	13				20	19	20	10	10	10			
	Distance (m)	11.27 ± 0.61	11.22 ± 1.20	11.29 ± 0.61	3.75 ± 0.56	3.79 ± 1.01	3.73 ± 0.55	0.000	0.000	0.000	13.39 ± 0.88	14.74 ± 1.28	13.26 ± 0.89	8.59 ± 1.22	6.03 ± 2.14	8.84 ± 1.24	0.002	0.006	0.005
	Mean speed (m/s)	0.03 ± 0.00	0.03 ± 0.00	0.03 ± 0.00	0.01 ± 0.00	0.01 ± 0.00	0.01 ± 0.00	0.000	0.000	0.000	0.04 ± 0.00	0.04 ± 0.00	0.04 ± 0.00	0.02 ± 0.00	0.02 ± 0.01	0.03 ± 0.00	0.002	0.007	0.006
	Time mobile (s)	192.23 ± 9.60	204.06 ± 18.62	192.65 ± 9.41	78.21 ± 8.69	68.53 ± 15.68	77.87 ± 8.51	0.000	0.000	0.000	197.59 ± 9.39	217.19 ± 13.48	199.32 ± 9.44	142.97 ± 12.94	105.72 ± 22.56	139.67 ± 13.13	0.001	0.001	0.000
	Time in centre (s)	6.66 ± 3.33	15.43 ± 6.38	6.69 ± 3.35	7.79 ± 3.01	0.62 ± 5.37	7.77 ± 3.03	0.801	0.177	0.811	8.91 ± 1.42	9.67 ± 2.07	8.97 ± 1.44	4.89 ± 1.95	3.46 ± 3.46	4.78 ± 2.00	0.098	0.215	0.095
	Crossing top-bottom (nº)	1.06 ± 0.16	0.97 ± 0.31	1.07 ± 0.14	0.30 ± 0.14	0.37 ± 0.26	0.29 ± 0.13	0.001	0.254	0.000	1.32 ± 0.18	1.65 ± 0.25	1.33 ± 0.18	0.88 ± 0.24	0.24 ± 0.42	0.86 ± 0.25	0.141	0.022	0.130
	Crossing left-right (nº)	1.03 ± 0.14	0.76 ± 0.27	1.03 ± 0.14	0.14 ± 0.13	0.36 ± 0.23	0.13 ± 0.12	0.000	0.388	0.000	0.90 ± 0.15	1.04 ± 0.22	0.93 ± 0.15	0.55 ± 0.21	0.27 ± 0.37	0.49 ± 0.21	0.189	0.150	0.108
Elevated zero maze	N	5	5	5	3	2	2				15	14	14	7	7	7			
	Distance (m)	6.91 ± 0.40	3.48 ± 1.49	6.91 ± 0.39	2.66 ± 0.34	5.23 ± 1.13	2.66 ± 0.34	0.000	0.500	0.000	9.66 ± 0.70	9.94 ± 1.33	9.29 ± 0.73	3.33 ± 1.52	2.02 ± 5.47	5.04 ± 1.80	0.000	0.234	0.042
	Mean speed (m/s)	0.02 ± 0.00	0.01 ± 0.01	0.02 ± 0.00	0.01 ± 0.00	0.02 ± 0.00	0.01 ± 0.00	0.000	0.536	0.000	0.03 ± 0.00	0.03 ± 0.01	0.03 ± 0.00	0.01 ± 0.00	0.01 ± 0.02	0.02 ± 0.01	0.000	0.242	0.046
	Maximum speed (m/s)	0.24 ± 0.01	0.19 ± 0.04	0.24 ± 0.01	0.16 ± 0.01	0.20 ± 0.03	0.16 ± 0.01	0.000	0.815	0.000	0.27 ± 0.01	0.27 ± 0.02	0.26 ± 0.01	0.21 ± 0.02	0.19 ± 0.07	0.23 ± 0.02	0.007	0.360	0.190
	Time mobile (s)	151.82 ± 11.22	107.79 ± 44.48	151.82 ± 11.08	59.95 ± 9.71	92.98 ± 33.71	59.95 ± 9.60	0.000	0.848	0.000	158.01 ± 7.38	150.37 ± 13.93	156.60 ± 7.77	84.38 ± 15.95	120.04 ± 57.31	90.97 ± 19.31	0.000	0.662	0.004
	Time immobile (s)	138.18 ± 11.22	182.21 ± 44.48	138.18 ± 11.08	230.05 ± 9.71	197.03 ± 33.71	230.05 ± 9.60	0.000	0.848	0.000	131.99 ± 7.38	139.63 ± 13.93	133.40 ± 7.77	205.62 ± 15.95	169.96 ± 57.31	199.03 ± 19.31	0.000	0.662	0.004
	Rotations (nº)	4.83 ± 0.65	5.47 ± 2.61	4.83 ± 0.65	0.75 ± 0.56	0.27 ± 1.98	0.75 ± 0.56	0.000	0.256	0.000	7.93 ± 0.56	8.45 ± 1.05	7.92 ± 0.59	1.92 ± 1.20	-0.52 ± 4.32	1.95 ± 1.46	0.000	0.090	0.001
	Time in open zones (s)	11.84 ± 3.38	30.25 ± 13.24	11.84 ± 3.42	5.58 ± 2.93	-8.23 ± 10.03	5.58 ± 2.96	0.169	0.100	0.174	18.82 ± 2.08	20.70 ± 3.92	19.81 ± 2.16	3.29 ± 4.49	-5.46 ± 16.15	-1.31 ± 5.36	0.003	0.184	0.001
	Time in hidden zones (s)	277.55 ± 3.44	257.60 ± 13.44	277.55 ± 3.48	284.31 ± 2.98	299.27 ± 10.18	284.31 ± 3.02	0.145	0.080	0.150	270.62 ± 2.07	268.79 ± 3.91	269.50 ± 2.14	286.57 ± 4.48	295.08 ± 16.10	291.77 ± 5.31	0.002	0.180	0.000

Rotarod test	N	10	10	10	13	11	13				19	18	19	10	10	10			
	Distance (m)	135.17 ± 17.98	82.17 ± 24.84	134.50 ± 18.40	121.53 ± 17.14	169.71 ± 23.02	122.14 ± 17.54	0.589	0.056	0.633	204.39 ± 15.25	209.60 ± 22.43	203.58 ± 15.63	164.76 ± 20.47	155.38 ± 35.83	166.22 ± 21.10	0.133	0.309	0.171
Morris water maze	N	8	8	8	8	7	8				19	19	19	7	7	7			
	Distance (m)	7.62 ± 0.48	7.62 ± 1.14	7.87 ± 0.50	9.81 ± 0.51	9.81 ± 1.28	9.52 ± 0.54	0.003	0.347	0.041	8.83 ± 0.35	8.40 ± 0.58	9.00 ± 0.35	9.21 ± 0.56	10.35 ± 1.36	8.77 ± 0.60	0.566	0.289	0.746
	Mean speed (m/s)	0.13 ± 0.01	0.13 ± 0.02	0.13 ± 0.01	0.17 ± 0.01	0.16 ± 0.02	0.16 ± 0.01	0.003	0.392	0.046	0.15 ± 0.01	0.14 ± 0.01	0.15 ± 0.01	0.16 ± 0.00	0.17 ± 0.02	0.15 ± 0.01	0.547	0.320	0.763
	Maximum speed (m/s)	0.31 ± 0.01	0.31 ± 0.01	0.31 ± 0.01	0.26 ± 0.01	0.26 ± 0.02	0.26 ± 0.01	0.000	0.092	0.000	0.31 ± 0.01	0.30 ± 0.01	0.31 ± 0.01	0.24 ± 0.01	0.27 ± 0.02	0.24 ± 0.01	0.000	0.156	0.000
	Time mobile (s)	57.23 ± 0.62	56.58 ± 1.48	57.55 ± 0.66	59.27 ± 0.67	60.01 ± 1.68	58.90 ± 0.71	0.029	0.261	0.194	58.44 ± 0.51	57.99 ± 0.53	58.58 ± 0.32	59.00 ± 0.51	60.19 ± 1.24	58.62 ± 0.54	0.352	0.189	0.950
	Time immobile (s)	1.99 ± 0.53	2.19 ± 1.26	1.45 ± 0.53	0.08 ± 0.57	-0.15 ± 1.43	0.70 ± 0.57	0.017	0.367	0.366	1.07 ± 0.28	1.32 ± 0.47	0.92 ± 0.28	0.55 ± 0.46	-0.10 ± 1.11	0.96 ± 0.48	0.333	0.341	0.956
	Floating time (s)	11.64 ± 1.73	11.20 ± 4.12	10.66 ± 1.82	1.38 ± 1.85	1.88 ± 4.65	2.49 ± 1.96	0.000	0.271	0.006	8.17 ± 1.28	8.69 ± 2.17	7.47 ± 1.29	1.56 ± 2.08	0.20 ± 5.07	3.42 ± 2.20	0.008	0.217	0.130
	Floating number (nº)	1.06 ± 0.15	1.12 ± 0.35	0.97 ± 0.16	0.25 ± 0.16	0.18 ± 0.40	0.36 ± 0.16	0.000	0.200	0.015	1.00 ± 0.15	0.99 ± 0.26	0.90 ± 0.15	0.18 ± 0.25	0.21 ± 0.60	0.43 ± 0.26	0.006	0.340	0.135
	Platform zone: Entries (nº)	2.75 ± 0.45	6.11 ± 0.88	3.39 ± 0.39	4.00 ± 0.42	0.16 ± 1.00	3.27 ± 0.42	0.049	0.002	0.855	3.35 ± 0.33	3.44 ± 0.57	3.14 ± 0.33	2.11 ± 0.54	1.88 ± 1.32	2.66 ± 0.57	0.053	0.382	0.486
	Platform zone: Time (s)	11.66 ± 1.82	19.16 ± 4.19	13.89 ± 1.76	11.19 ± 1.94	2.62 ± 4.74	8.64 ± 1.90	0.860	0.058	0.062	12.59 ± 1.24	12.66 ± 2.10	11.38 ± 1.18	5.80 ± 2.01	5.60 ± 4.90	8.99 ± 2.00	0.005	0.287	0.325
	Platform zone: Distance (m)	1.45 ± 0.23	3.03 ± 0.49	1.74 ± 0.22	1.85 ± 0.24	0.05 ± 0.56	1.52 ± 0.24	0.299	0.004	0.534	1.59 ± 0.16	1.71 ± 0.26	1.47 ± 0.15	0.97 ± 0.25	0.65 ± 0.62	1.28 ± 0.26	0.039	0.200	0.528
	Platform zone: Time immobile (s)	0.31 ± 0.13	0.25 ± 0.30	0.40 ± 0.13	0.00 ± 0.14	0.06 ± 0.34	-0.11 ± 0.14	0.105	0.763	0.017	0.46 ± 0.20	0.35 ± 0.34	0.36 ± 0.20	-5.55E-17 ± 0.33	0.28 ± 0.80	0.25 ± 0.35	0.238	0.947	0.781
	Platform zone: Time mobile (s)	11.36 ± 1.75	18.91 ± 4.02	13.49 ± 1.70	11.19 ± 1.87	2.56 ± 4.54	8.75 ± 1.83	0.947	0.051	0.079	12.13 ± 1.17	12.31 ± 1.98	11.02 ± 1.12	5.80 ± 1.90	5.32 ± 4.63	8.75 ± 1.90	0.005	0.264	0.323

Table S6. Covariance analysis for behavioural studies with significant differences considering the covariates liver and body weight between *Bscl2*$^{Celia/Celia}$ and *Bscl2*$^{-/-}$ mice separated by sex. Data is presented as mean ± SEM and significance (p). Data were analysed using Analysis of Covariance (ANCOVA) to control for liver weight and overall body weight.

		Bsc2$^{Celia/Celia}$ ♂			*Bscl2*$^{-/-}$ ♂			*Bscl2*$^{Celia/Celia}$ ♂ vs *Bscl2*$^{-/-}$ ♂			*Bsc2*$^{Celia/Celia}$ ♀			*Bscl2*$^{-/-}$ ♀			*Bscl2*$^{Celia/Celia}$ ♀ vs *Bscl2*$^{-/-}$ ♀		
		Values			Values			Significance (p)			Values			Values			Significance (p)		
	Covariate	-	Liver weight	Body weight	-	Liver weight	Body weight	-	Liver weight	Body weight	-	Liver weight	Body weight	-	Liver weight	Body weight	-	Liver weight	Body weight
Open field test	N	11	10	11	13	11	13				14	12	14	10	10	10			
	Distance (m)	4.42 ± 0.50	4.44 ± 0.50	4.42 ± 0.51	3.75 ± 0.48	3.73 ± 0.48	3.75 ± 0.49	0.332	0.310	0.346	7.03 ± 0.69	6.93 ± 0.69	7.08 ± 0.69	8.59 ± 0.76	8.70 ± 0.76	8.53 ± 0.75	0.130	0.089	0.159
	Mean speed (m/s)	0.01 ± 0.00	0.01 ± 0.00	0.01 ± 0.00	0.01 ± 0.00	0.01 ± 0.00	0.01 ± 0.00	0.322	0.301	0.339	0.02 ± 0.00	0.02 ± 0.00	0.02 ± 0.00	0.02 ± 0.00	0.02 ± 0.00	0.02 ± 0.00	0.116	0.082	0.141
	Time mobile (s)	81.60 ± 9.82	82.01 ± 9.79	81.73 ± 10.02	78.21 ± 9.36	77.84 ± 9.33	78.09 ± 9.55	0.803	0.758	0.796	117.37 ± 10.77	116.27 ± 10.80	118.33 ± 10.65	142.97 ± 11.80	144.28 ± 11.84	141.81 ± 11.67	0.113	0.086	0.142
	Time in centre (s)	1.36 ± 3.01	1.46 ± 3.01	1.08 ± 3.06	7.79 ± 2.87	7.70 ± 2.87	8.05 ± 2.92	0.126	0.137	0.108	6.09 ± 1.53	6.26 ± 1.54	6.05 ± 1.54	4.89 ± 1.68	4.69 ± 1.68	4.94 ± 1.69	0.600	0.494	0.631
	Crossing top-bottom (nº)	0.30 ± 0.12	0.30 ± 0.12	0.30 ± 0.13	0.30 ± 0.12	0.29 ± 0.12	0.30 ± 0.12	0.979	0.956	0.984	0.73 ± 0.21	0.72 ± 0.21	0.74 ± 0.21	0.88 ± 0.23	0.89 ± 0.23	0.87 ± 0.23	0.639	0.602	0.678
	Crossing left-right (nº)	0.33 ± 0.12	0.33 ± 0.12	0.35 ± 0.13	0.14 ± 0.12	0.13 ± 0.12	0.11 ± 0.12	0.272	0.249	0.172	0.42 ± 0.13	0.42 ± 0.14	0.42 ± 0.13	0.55 ± 0.15	0.55 ± 0.15	0.55 ± 0.15	0.503	0.524	0.528
Elevated zero maze	N	8	8	8	3	2	2				11	10	11	7	7	7			
	Distance (m)	3.80 ± 0.36	3.76 ± 0.38	3.83 ± 0.37	2.66 ± 0.41	2.71 ± 0.45	2.62 ± 0.43	0.043	0.097	0.046	3.78 ± 0.32	3.77 ± 0.32	3.79 ± 0.32	3.33 ± 0.58	3.39 ± 0.58	3.33 ± 0.59	0.500	0.576	0.495
	Mean speed (m/s)	0.01 ± 0.00	0.01 ± 0.00	0.01 ± 0.00	0.01 ± 0.00	0.01 ± 0.00	0.01 ± 0.00	0.047	0.105	0.051	0.01 ± 0.00	0.01 ± 0.00	0.01 ± 0.00	0.01 ± 0.00	0.01 ± 0.00	0.01 ± 0.00	0.515	0.592	0.509
	Maximum speed (m/s)	0.20 ± 0.01	0.19 ± 0.01	0.19 ± 0.01	0.16 ± 0.01	0.17 ± 0.01	0.17 ± 0.01	0.033	0.303	0.065	0.23 ± 0.03	0.23 ± 0.03	0.23 ± 0.03	0.20 ± 0.06	0.21 ± 0.06	0.20 ± 0.06	0.708	0.795	0.718
	Time mobile (s)	71.53 ± 6.05	72.26 ± 6.45	72.03 ± 6.28	59.95 ± 6.99	58.98 ± 7.58	59.29 ± 7.32	0.216	0.212	0.205	86.99 ± 9.37	86.50 ± 9.41	87.12 ± 9.41	84.38 ± 17.11	86.02 ± 17.26	83.94 ± 17.19	0.894	0.981	0.872
	Time immobile (s)	218.47 ± 6.05	217.74 ± 6.45	217.97 ± 6.28	231.02 ± 7.58	227.75 ± 12.91	230.71 ± 8.69	0.216	0.212	0.205	202.93 ± 9.39	203.42 ± 9.43	202.79 ± 9.43	205.62 ± 17.14	203.98 ± 17.29	206.06 ± 17.22	0.891	0.978	0.869
	Rotations (nº)	1.66 ± 0.31	1.72 ± 0.33	1.71 ± 0.32	0.75 ± 0.36	0.67 ± 0.39	0.68 ± 0.37	0.059	0.056	0.047	2.77 ± 0.47	2.77 ± 0.48	8.02 ± 0.64	1.92 ± 0.86	1.94 ± 0.87	2.65 ± 0.81	0.386	0.413	0.375
	Time in open zones (s)	8.74 ± 2.79	9.81 ± 2.94	9.92 ± 2.81	5.58 ± 3.22	4.16 ± 3.46	4.02 ± 3.28	0.461	0.244	0.191	7.52 ± 1.55	7.44 ± 1.56	7.53 ± 1.57	3.29 ± 2.84	3.57 ± 2.86	3.27 ± 2.86	0.197	0.242	0.198
	Time in hidden zones (s)	281.26 ± 2.79	280.17 ± 2.94	280.07 ± 2.81	284.31 ± 3.22	285.76 ± 3.46	285.89 ± 3.28	0.476	0.250	0.197	281.71 ± 1.58	281.79 ± 1.59	281.70 ± 1.60	286.57 ± 2.89	286.29 ± 2.92	286.60 ± 2.92	0.147	0.183	0.147

Rotarod test	N	10	9	10	13	11	13				15	13	15	10	10	10			
	Distance (m)	121.24 ± 23.66	122.05 ± 24.43	119.67 ± 21.22	121.53 ± 21.40	120.87 ± 22.07	122.81 ± 19.20	0.993	0.972	0.914	175.72 ± 16.46	174.74 ± 16.88	174.63 ± 16.78	164.76 ± 18.77	166.04 ± 19.28	166.18 ± 19.16	0.665	0.740	0.745
Morris water maze	N	9	9	9	8	7	8				14	12	14	7	7	7			
	Distance (m)	9.08 ± 0.34	9.10 ± 0.35	9.07 ± 0.35	9.81 ± 0.38	9.79 ± 0.39	9.82 ± 0.39	0.163	0.184	0.155	8.41 ± 0.29	8.36 ± 0.28	8.30 ± 0.29	9.21 ± 0.38	9.29 ± 0.37	9.40 ± 0.38	0.099	0.049	0.027
	Mean speed (m/s)	0.15 ± 0.01	0.15 ± 0.01	0.15 ± 0.01	0.17 ± 0.01	0.17 ± 0.01	0.17 ± 0.01	0.111	0.126	0.105	0.14 ± 0.01	0.14 ± 0.01	0.14 ± 0.01	0.16 ± 0.01	0.16 ± 0.01	0.16 ± 0.01	0.073	0.036	0.019
	Maximum speed (m/s)	0.26 ± 0.00	0.26 ± 0.00	0.26 ± 0.00	0.26 ± 0.00	0.26 ± 0.00	0.26 ± 0.00	0.291	0.322	0.242	0.26 ± 0.00	0.25 ± 0.00	0.25 ± 0.00	0.24 ± 0.01	0.25 ± 0.01	0.25 ± 0.01	0.097	0.159	0.529
	Time mobile (s)	59.09 ± 0.45	59.11 ± 0.45	59.09 ± 0.45	59.27 ± 0.50	59.26 ± 0.51	59.27 ± 0.51	0.798	0.826	0.792	58.43 ± 0.69	58.33 ± 0.68	58.33 ± 0.71	59.00 ± 0.90	59.18 ± 0.88	59.17 ± 0.93	0.620	0.449	0.496
	Time immobile (s)	0.91 ± 0.42	0.90 ± 0.42	0.91 ± 0.42	0.08 ± 0.46	0.09 ± 0.47	0.8 ± 0.47	0.191	0.202	0.191	1.57 ± 0.69	1.66 ± 0.68	1.67 ± 0.71	0.55 ± 0.90	0.39 ± 0.88	0.39 ± 0.93	0.374	0.259	0.286
	Floating time (s)	2.20 ± 0.78	2.16 ± 0.78	2.25 ± 0.77	1.38 ± 0.88	1.44 ± 0.87	1.32 ± 0.87	0.486	0.541	0.423	3.47 ± 1.02	3.50 ± 1.03	3.73 ± 1.03	1.56 ± 1.32	1.51 ± 1.34	1.12 ± 1.36	0.259	0.244	0.139
	Floating number (nº)	0.29 ± 0.09	0.28 ± 0.09	0.29 ± 0.09	0.25 ± 0.10	0.26 ± 0.10	0.25 ± 0.10	0.787	0.862	0.733	0.45 ± 0.13	0.45 ± 0.13	0.46 ± 0.13	0.18 ± 0.17	0.18 ± 0.17	0.17 ± 0.17	0.210	0.212	0.199
	Platform zone: Entries (nº)	3.80 ± 0.40	3.83 ± 0.40	3.74 ± 0.36	4.00 ± 0.45	3.97 ± 0.45	4.07 ± 0.40	0.741	0.820	0.547	4.34 ± 0.35	4.30 ± 0.35	4.04 ± 0.31	2.11 ± 0.46	2.18 ± 0.45	2.61 ± 0.41	0.000	0.000	0.008
	Platform zone: Time (s)	10.68 ± 1.38	10.77 ± 1.37	10.54 ± 1.31	11.19 ± 1.55	11.08 ± 1.53	11.37 ± 1.46	0.808	0.884	0.676	13.93 ± 1.04	13.87 ± 1.05	13.11 ± 0.94	5.80 ± 1.35	5.90 ± 1.36	7.17 ± 1.23	0.000	0.000	0.000
	Platform zone: Distance (m)	1.69 ± 0.21	1.70 ± 0.21	1.67 ± 0.20	1.85 ± 0.23	1.84 ± 0.23	1.88 ± 0.22	0.601	0.657	0.468	2.00 ± 0.16	1.99 ± 0.16	1.87 ± 0.14	0.97 ± 0.21	0.99 ± 0.21	1.18 ± 0.19	0.000	0.000	0.006
	Platform zone: Time immobile (s)	0.14 ± 0.11	0.14 ± 0.11	0.14 ± 0.11	-1.39E-17 ± 0.12	-0.01 ± 0.12	0.00 ± 0.12	0.375	0.351	0.393	0.00	0.00	0.00	0.00	0.00	0.00	-	-	-
	Platform zone: Time mobile (s)	10.55 ± 1.36	10.63 ± 1.35	10.41 ± 1.29	11.19 ± 1.52	11.08 ± 1.51	11.37 ± 1.44	0.753	0.826	0.621	13.93 ± 1.04	13.87 ± 1.05	13.11 ± 0.94	5.80 ± 1.35	5.90 ± 1.36	7.17 ± 1.23	0.000	0.000	0.000

Annex 5. Table S7 and S8. Brain [^{18}F]-2-fluoro-2-deoxy-D-glucose by positron emission tomography with computed tomography.

Table S7. Brain [^{18}F]-2-fluoro-2-deoxy-D-glucose by positron emission tomography with computed tomography comparing severely affected (S.A.), *Bscl2*$^{Celia/Celia}$ and wild type animals. Mean standardized uptake value (SUV_{mean}) and mean % of change related to wild type animals. Data is presented as mean ± SD or mean %. Data were analysed using a Shapiro-Wilk test for normality, followed by an ANOVA test.

	SUV_{mean}				% Change			SUV_{mean}				% Change	
	Wild type	*Bscl2*$^{Celia/Celia}$	S.A. *Bscl2*$^{+/Celia}$	S.A. *Bscl2*$^{Celia/Celia}$	*Bscl2*$^{Celia/Celia}$ vs wild type	S.A. *Bscl2*$^{+/Celia}$ vs wild type	S.A. *Bscl2*$^{Celia/Celia}$ vs wild type	Wild type		*Bscl2*$^{Celia/Celia}$		*Bscl2*$^{Celia/Celia}$ vs wild type	
Sex	♀/♂	♀/♂	♂	♀				♀	♂	♀	♂	♀	♂
N	6	6	1	1				3	3	3	3		
Mean age (months)	7.4	7.3	7.9	4.6				7.0	8.0	7.3	7.3		
Amygdala left	1.67 ± 0.29	1.30 ± 0.29	1.17	1.38	-23.42	-28.69	-15.90	1.79 ± 0.34	1.57 ± 0.13	1.31 ± 0.36	1.30 ± 0.28	-28.58	-19.40
Amygdala right	1.58 ± 0.27	1.51 ± 0.36	1.21	1.29	-7.42	-21.73	-16.36	1.72 ± 0.22	1.44 ± 0.21	1.53 ± 0.39	1.48 ± 0.42	-13.19	-1.92
Basal forebrain and septum	1.99 ± 0.31	1.58 ± 0.24	1.61	1.70	-20.93	-17.52	-12.97	2.14 ± 0.27	1.95 ± 0.37	1.59 ± 0.22	1.56 ± 0.31	-25.72	-20.10
Brain stem	1.94 ± 0.29	1.78 ± 0.38	1.74	1.86	-10.12	-8.53	-2.37	2.07 ± 0.31	1.83 ± 0.17	1.67 ± 0.28	1.89 ± 0.50	-19.38	-1.49
Central gray matter	2.27 ± 0.23	1.72 ± 0.19	1.99	2.17	-24.36	-11.56	-3.61	2.29 ± 0.07	2.47 ± 0.51	1.67 ± 0.27	1.76 ± 0.10	-28.10	-26.45
Cerebellum	1.97 ± 0.33	1.47 ± 0.32	1.55	1.87	-26.81	-19.21	-2.66	2.04 ± 0.32	1.96 ± 0.35	1.47 ± 0.30	1.47 ± 0.40	-28.98	-27.43
Cortex	1.79 ± 0.33	1.37 ± 0.24	1.20	1.54	-23.07	-30.54	-11.25	1.86 ± 0.31	1.89 ± 0.48	1.35 ± 0.27	1.39 ± 0.27	-27.89	-24.45
Hippocampus left	1.77 ± 0.17	1.37 ± 0.19	1.30	1.74	-23.62	-26.01	-1.07	1.74 ± 0.08	2.00 ± 0.39	1.33 ± 0.26	1.41 ± 0.12	-26.07	-27.81
Hippocampus right	1.76 ± 0.16	1.52 ± 0.18	1.51	1.82	-14.23	-13.70	4.00	1.81 ± 0.05	1.85 ± 0.34	1.49 ± 0.25	1.55 ± 0.14	-19.21	-14.79
Hypothalamus	1.76 ± 0.22	1.54 ± 0.27	1.54	1.53	-13.65	-11.39	-11.83	1.86 ± 0.20	1.73 ± 0.23	1.53 ± 0.26	1.56 ± 0.33	-18.74	-11.54
Inferior colliculus left	2.13 ± 0.26	1.60 ± 0.18	1.72	2.04	-25.01	-18.44	-3.10	2.17 ± 0.11	2.29 ± 0.51	1.62 ± 0.24	1.58 ± 0.16	-26.62	-29.16
Inferior colliculus right	2.09 ± 0.35	1.32 ± 0.20	1.58	1.99	-36.80	-22.52	-2.62	2.09 ± 0.17	2.26 ± 0.55	1.36 ± 0.26	1.27 ± 0.17	-36.06	-41.85

Midbrain left	2.01 ± 0.11	1.72 ± 0.21	1.76	1.86	-15.46	-12.00	-6.89	2.03 ± 0.05	2.19 ± 0.40	1.65 ± 0.27	1.79 ± 0.16	-20.46	-16.98
Midbrain right	1.95 ± 0.13	1.79 ± 0.23	1.77	1.88	-9.20	-8.93	-3.44	2.01 ± 0.06	2.02 ± 0.31	1.75 ± 0.28	1.83 ± 0.21	-14.67	-8.77
Olfactory bulb	2.10 ± 0.39	1.79 ± 0.31	1.47	1.28	-14.42	-28.09	-37.35	2.18 ± 0.32	2.29 ± 0.68	1.65 ± 0.28	1.94 ± 0.31	-24.93	-11.25
Striatum left	1.98 ± 0.23	1.62 ± 0.20	1.50	1.85	-18.36	-23.74	-5.71	2.08 ± 0.21	2.04 ± 0.39	1.58 ± 0.16	1.67 ± 0.26	-24.20	-17.88
Striatum right	2.01 ± 0.21	1.62 ± 0.18	1.65	1.82	-19.41	-17.08	-8.42	2.08 ± 0.11	2.10 ± 0.43	1.62 ± 0.23	1.62 ± 0.17	-23.07	-21.30
Superior colliculi	2.10 ± 0.27	1.48 ± 0.18	1.73	2.08	-29.82	-16.39	0.52	2.10 ± 0.09	2.31 ± 0.53	1.49 ± 0.28	1.47 ± 0.06	-31.16	-34.17
Thalamus	1.93 ± 0.13	1.63 ± 0.20	1.71	1.94	-16.26	-11.24	1.13	1.93 ± 0.01	2.12 ± 0.38	1.56 ± 0.26	1.70 ± 0.14	-20.78	-18.05
Whole-brain	1.89 ± 0.27	1.53 ± 0.24	1.46	1.70	-19.73	-21.26	-8.43	1.96 ± 0.24	1.95 ± 0.39	1.49 ± 0.25	1.57 ± 0.29	-25.00	-19.39

Table S8. Brain [^{18}F]-2-fluoro-2-deoxy-D-glucose by positron emission tomography with computed tomography comparing severely affected (S.A.), *Bscl2*$^{Celia/Celia}$ and wild type animals separated by age. Mean standardized uptake value (SUV_{mean}) and mean % of change related to wild type animals. Data is presented as mean ± SD or mean %. Data were analysed using a Shapiro-Wilk test for normality, followed by an ANOVA test.

	4.3 months					8.4 months				
	SUV_{mean}			% Change		SUV_{mean}			% Change	
	Wild type	*Bscl2*$^{Celia/Celia}$	S.A. *Bscl2*$^{Celia/Celia}$	*Bscl2*$^{Celia/Celia}$ vs wild type	S.A. *Bscl2*$^{Celia/Celia}$ vs wild type	Wild type	*Bscl2*$^{Celia/Celia}$	S.A. *Bscl2*$^{+/Celia}$	*Bscl2*$^{Celia/Celia}$ vs wild type	S.A. *Bscl2*$^{+/Celia}$ vs wild type
Sex	♀	♀/♂	♀			♀/♂	♀/♂	♂		
N	1	2	1			5	4	1		
Mean age (months)	4.6	3.7	4.6			8.1	9.2	7.9		
Amygdala left	1.42	1.07 ± 0.09	1.38	-25.30	-3.29	1.73 ± 0.25	1.42 ± 0.29	1.17	-19.20	-31.49
Amygdala right	1.48	1.20 ± 0.28	1.29	-21.36	-12.83	1.60 ± 0.27	1.66 ± 0.31	1.21	3.58	-22.36
Basal forebrain and septum	1.85	1.41 ± 0.27	1.70	-24.73	-7.92	2.08 ± 0.32	1.66 ± 0.22	1.61	-19.69	-20.90
Brain stem	1.76	1.52 ± 0.29	1.86	-14.70	5.98	1.99 ± 0.27	1.91 ± 0.38	1.74	-5.72	-10.95
Central gray matter	2.28	1.77 ± 0.16	2.17	-22.86	-5.00	2.40 ± 0.38	1.69 ± 0.22	1.99	-28.87	-15.43
Cerebellum	1.71	1.20 ± 0.24	1.87	-31.35	9.22	2.06 ± 0.30	1.60 ± 0.28	1.55	-22.67	-23.03
Cortex	1.51	1.25 ± 0.19	1.54	-18.10	2.13	1.94 ± 0.35	1.43 ± 0.26	1.20	-26.15	-36.03
Hippocampus left	1.66	1.39 ± 0.15	1.74	-16.85	5.11	1.92 ± 0.30	1.36 ± 0.23	1.30	-29.36	-30.75
Hippocampus right	1.75	1.53 ± 0.20	1.82	-12.99	4.00	1.85 ± 0.24	1.51 ± 0.21	1.51	-18.21	-17.12
Hypothalamus	1.64	1.37 ± 0.25	1.53	-17.50	-6.43	1.82 ± 0.22	1.63 ± 0.26	1.54	-11.61	-14.34
Inferior colliculus left	2.06	1.57 ± 0.23	2.04	-24.81	-0.98	2.27 ± 0.37	1.61 ± 0.19	1.72	-28.12	-22.57
Inferior colliculus right	1.89	1.23 ± 0.15	1.99	-35.40	5.14	2.23 ± 0.39	1.36 ± 0.23	1.58	-38.77	-27.05
Midbrain left	2.00	1.73 ± 0.19	1.86	-13.66	-6.65	2.13 ± 0.30	1.71 ± 0.25	1.76	-20.24	-16.23

Midbrain right	1.95	1.79 ± 0.29	1.88	-9.36	-3.66	2.03 ± 0.22	1.79 ± 024	1.77	-12.30	-12.02
Olfactory bulb	1.82	1.75 ± 0.22	1.28	-4.39	-29.64	2.32 ± 0.48	1.81 ± 0.38	1.47	-21.40	-34.13
Striatum left	1.85	1.54 ± 0.24	1.85	-17.62	-0.14	2.10 ± 0.29	1.66 ± 0.20	1.50	-20.65	-27.72
Striatum right	1.96	1.61 ± 0.26	1.82	-18.99	-7.23	2.12 ± 0.30	1.62 ± 0.17	1.65	-22.65	-20.72
Superior colliculi	2.02	1.54 ± 0.18	2.08	-24.45	2.94	2.24 ± 0.39	1.44 ± 0.20	1.73	-35.14	-20.85
Thalamus	1.92	1.68 ± 0.19	1.94	-12.75	1.30	2.05 ± 0.29	1.60 ± 0.23	1.71	-21.68	-15.38
Whole-brain	1.69	1.40 ± 0.22	1.70	-18.52	0.42	2.01 ± 0.29	1.59 ± 0.26	1.46	-21.15	-25.76

Annex 6. Table S9, S10, S11 and S12. Relative gene expression in brain or liver tissues.

Table S9. Relative expression of *Ffg21* gene in liver tissue and *Gng3* gene in brain regions for wild type, *Bscl2*$^{+/Celia}$, *Bscl2*$^{Celia/Celia}$, *Bscl2*$^{+/-}$, *Bscl2*$^{-/-}$ and severely affected (S.A.) mice. Data is presented as mean ± SD. Results were normalized for the *Rn18S* gene and referred to liver of wild type in *Fgf21* and to Cerebellum of wild type in *Gng3* gene. [a] $p < 0.05$ vs wild type ♀/♂; [d] $p < 0.05$ vs *Bscl2*$^{+/-}$ ♀/♂; [g] $p < 0.05$ vs *Bscl2*$^{-/-}$ ♀/♂; [j] $p < 0.05$ vs *Bscl2*$^{+/Celia}$ ♀/♂; [m] $p < 0.05$ vs *Bscl2*$^{Celia/Celia}$ ♀/♂; [p] $p < 0.05$ vs S.A *Bscl2*$^{+/Celia}$. Data were analysed using a Kolmogorov-Smirnov test for normality, followed by a Kruskal-Wallis test with Mann-Whitney post hoc comparisons.

		Wild type	*Bscl2*$^{+/Celia}$	*Bscl2*$^{Celia/Celia}$	*Bscl2*$^{+/-}$	*Bscl2*$^{-/-}$	S.A. *Bscl2*$^{+/Celia}$	S.A. *Bscl2*$^{Celia/Celia}$
Fgf21	Sex	♀/♂	♀/♂	♀/♂	♀/♂	♀/♂	♀/♂	♀/♂
	N	28	42	18	29	15	4	10
	Age (months)	3.6	9.7	9.4	7.7	6.8	6.3	11.5
	Liver	1.49 ± 1.27	2.40 ± 2.04[a]	22.03 ± 24.84[a,d,j]	4.29 ± 4.98[a]	30.64 ± 25.36[a,d,j]	0.71 ± 0.39[d,g,j,m]	23.15 ± 28.09[a,j,p]
		Wild type	*Bscl2*$^{+/Celia}$	*Bscl2*$^{Celia/Celia}$	*Bscl2*$^{+/-}$	*Bscl2*$^{-/-}$	S.A. *Bscl2*$^{+/Celia}$	S.A. *Bscl2*$^{Celia/Celia}$
Gng3	Sex	♀/♂	♀/♂	♀/♂				
	N	2	2	3				
	Age (months)	6	7.5	6.3				
	Cerebellum	1.08 ± 0.56	0.47 ± 0.26	0.83 ± 0.51				
	Midbrain	1.05 ± 0.63	0.75 ± 0.39	1.56 ± 1.53				
	Hypothalamus	1.16 ± 0.67	0.88 ± 0.64	2.33 ± 3.12				
	Cortex	1.04 ± 0.21	1.06 ± 0.70	1.56 ± 1.45				
	Hippocampus	1.05 ± 0.32	0.80 ± 0.43	1.54 ± 1.89				
	Striatum	1.23 ± 0.34	0.97 ± 0.72	3.42 ± 5.10				

Table S10. Relative expression of *Ffg21* gene in liver tissue and *Gng3* gene in brain regions for wild type, *Bscl2*$^{+/Celia}$, *Bscl2*$^{Celia/Celia}$, *Bscl2*$^{+/-}$ and *Bscl2*$^{-/-}$ mice separated by sex. Data is presented as mean ± SD. Results were normalized for the *Rn18S* gene and referred to liver of wild type in *Fgf21* and to Cerebellum of wild type in *Gng3* gene. [a] $p < 0.05$ vs wild type ♀/♂; [b] $p < 0.05$ vs wild type ♀; [d] $p < 0.05$ vs *Bscl2*$^{+/-}$ ♀/♂; [i] $p < 0.05$ vs *Bscl2*$^{-/-}$ ♂; [j] $p < 0.05$ vs *Bscl2*$^{+/Celia}$ ♀/♂. Data were analysed using a Kolmogorov-Smirnov test for normality, followed by a Kruskal-Wallis test with Mann-Whitney post hoc comparisons.

		Wild type		*Bscl2*$^{+/Celia}$		*Bscl2*$^{Celia/Celia}$		*Bscl2*$^{+/-}$		*Bscl2*$^{-/-}$	
Fgf21	Sex	♀	♂	♀	♂	♀	♂	♀	♂	♀	♂
	N	15	13	18	24	8	10	12	17	6	9
	Age (months)	3.1	4.1	9.4	9.9	14.7	5.2	6.4	8.7	10.2	4.6
	Liver	1.33 ± 1.51	1.68 ± 0.93	2.07 ± 1.41[b]	2.64 ± 2.41[b]	34.78 ± 32.71[a,d,j]	11.82 ± 8.54[a,d,i,j]	3.51 ± 3.81[b]	4.84 ± 5.71[b]	32.09 ± 28.73[a,d,j]	29.67 ± 24.64[a,d,j]

		Wild type		*Bscl2*$^{+/Celia}$		*Bscl2*$^{Celia/Celia}$		*Bscl2*$^{+/-}$	*Bscl2*$^{-/-}$
Gng3	Sex	♀	♂	♀	♂	♀	♂		
	N	1	1	-	2	1	2		
	Age (months)	6.0	6.0	-	7.5	9.0	5.0		
	Cerebellum	0.68	1.47	-	0.47 ± 0.26	1.27	0.61 ± 0.47		
	Midbrain	0.60	1.49	-	0.75 ± 0.39	3.20	0.73 ± 0.77		
	Hypothalamus	0.69	1.64	-	0.88 ± 0.64	5.90	0.54 ± 0.64		
	Cortex	0.89	1.19	-	1.06 ± 0.70	3.17	0.75 ± 0.56		
	Hippocampus	0.82	1.27	-	0.80 ± 0.43	3.71	0.45 ± 0.32		
	Striatum	0.99	1.47	-	0.97 ± 0.72	9.29	0.48 ± 0.56		

Table S11. Relative expression of *Bscl2*; Celia *BSCL2*-TG; *Ppary*; *Pex16*; *Sod1*; *Sod2*; *Cat*; *Pex11g* and *Gpx1* genes in brain regions for wild type, *Bscl2*$^{+/Celia}$, *Bscl2*$^{Celia/Celia}$, *Bscl2*$^{+/-}$, *Bscl2*$^{-/-}$ and severely affected (S.A.) mice. Data is presented as mean ± SD. Data were analysed using a Kolmogorov-Smirnov test for normality, followed by a Kruskal-Wallis test with Mann-Whitney post hoc comparisons. Results were normalized for the *Rn18S* gene and referred to Cerebellum of *Bscl2*$^{+/Celia}$ in Celia *BSCL2*-TG gene. ^{a} $p < 0.05$ vs wild type ♀/♂; ^{d} $p < 0.05$ vs *Bscl2*$^{+/-}$ ♀/♂; ^{g} $p < 0.05$ vs *Bscl2*$^{-/-}$ ♀/♂; ^{j} $p < 0.05$ vs *Bscl2*$^{+/Celia}$ ♀/♂; ^{m} $p < 0.05$ vs *Bscl2*$^{Celia/Celia}$ ♀/♂; ^{p} p < 0.05 vs S.A *Bscl2*$^{+/Celia}$ and ^{q} $p < 0.05$ vs S.A *Bscl2*$^{Celia/Celia}$. ^{A} $p < 0.05$ vs cerebellum ^{D} $p < 0.05$ vs midbrain ♀/♂; ^{G} $p < 0.05$ vs hypothalamus ♀/♂; ^{J} $p < 0.05$ vs cortex ♀/♂; ^{M} $p < 0.05$ vs hippocampus ♀/♂; ^{P} $p < 0.05$ vs striatum ♀/♂.

		Wild type	*Bscl2*$^{+/Celia}$	*Bscl2*$^{Celia/Celia}$	*Bscl2*$^{+/-}$	*Bscl2*$^{-/-}$	S.A. *Bscl2*$^{+/Celia}$	S.A. *Bscl2*$^{Celia/Celia}$
	Sex	♀/♂	♀/♂	♀/♂	♀/♂	♀/♂	♀/♂	♀/♂
	N	14	14	14	14	14	6	5
	Age (months)	9.5	9.6	9.4	9.5	9.5	6.6	6.2
Bscl2	Cerebellum	5.17 ± 3.19^{g,m,q}	3.70 ± 1.56^{g,m,q}	0.00 ± 0.00	2.30 ± 1.92^{a,g,j,m,q}	0.00 ± 0.00	1.41 ± 1.41^{a,g,j,m,q}	0.00 ± 0.00
	Midbrain	4.41 ± 3.83^{g,m,q,P}	2.26 ± 1.86^{g,m,q,A}	0.00 ± 0.00	2.40 ± 2.74^{a,g,m,q}	0.00 ± 0.00	2.70 ± 1.96^{g,m,q}	0.00 ± 0.00
	Hypothalamus	3.69 ± 2.90^{g,m,q,P}	3.05 ± 2.67^{g,m,q,J}	0.00 ± 0.00	2.61 ± 2.15^{g,m,q}	0.00 ± 0.00	2.16 ± 0.96^{g,m,q}	0.00 ± 0.00
	Cortex	2.56 ± 1.63^{g,m,q,A,P}	1.46 ± 1.50^{g,m,q,A}	0.00 ± 0.00	1.82 ± 2.21^{g,m,q}	0.00 ± 0.00	1.11 ± 0.87^{a,g,m,q}	0.00 ± 0.00
	Hippocampus	4.77 ± 3.21^{g,m,q}	2.34 ± 2.34^{a,g,m,q,A}	0.00 ± 0.00	1.99 ± 1.78^{a,g,m,q}	0.00 ± 0.00	2.97 ± 3.73^{g,m,q}	0.00 ± 0.00
	Striatum	7.33 ± 3.18^{g,m,q}	2.95 ± 1.80^{a,g,m,q,J}	0.00 ± 0.00	1.89 ± 0.89^{a,g,m,q}	0.00 ± 0.00	2.07 ± 0.92^{a,g,m,q}	0.00 ± 0.00
Celia *BSCL2*-TG	Cerebellum	0.00 ± 0.00	1.18 ± 0.74^{a,d,g,J}	2.73 ± 1.18^{a,d,g,j,J}	0.00 ± 0.00	0.00 ± 0.00	0.74 ± 0.76^{a,d,g,m}	1.92 ± 1.08^{a,d,g}
	Midbrain	0.00 ± 0.00	0.80 ± 0.80^{a,d,g,J}	1.28 ± 1.58^{a,d,g,A}	0.00 ± 0.00	0.00 ± 0.00	0.54 ± 0.13^{a,d,g}	2.06 ± 1.39^{a,d,g,j,p}
	Hypothalamus	0.00 ± 0.00	0.68 ± 0.50^{a,d,g,J}	2.31 ± 1.44^{a,d,g,j,J,M}	0.00 ± 0.00	0.00 ± 0.00	0.67 ± 0.52^{d,g,m}	1.97 ± 2.02^{a,d,g}
	Cortex	0.00 ± 0.00	0.20 ± 0.11^{a,d,g}	0.35 ± 0.21^{a,d,g,j}	0.00 ± 0.00	0.00 ± 0.00	0.27 ± 0.18^{a,d,g}	0.69 ± 0.27^{a,d,g,j,m,p}
	Hippocampus	0.00 ± 0.00	0.49 ± 0.36^{a,d,g,A,J}	0.99 ± 0.84^{a,d,g,A,J}	0.00 ± 0.00	0.00 ± 0.00	0.40 ± 0.45^{a,d,g,m}	1.88 ± 1.75^{a,d,g,j,p}
	Striatum	0.00 ± 0.00	0.58 ± 0.38^{a,d,g,A,J}	1.72 ± 1.06^{a,d,g,j,A,J,M}	0.00 ± 0.00	0.00 ± 0.00	0.41 ± 0.21^{a,d,g,m}	1.63 ± 1.60^{a,d,g,p}
Ppary	Cerebellum	0.29 ± 0.22	0.26 ± 0.10	0.45 ± 0.70	0.25 ± 0.20	0.36 ± 0.38	0.29 ± 0.35	0.19 ± 0.14
	Midbrain	0.13 ± 0.16^{A}	0.08 ± 0.05^{A,G,J}	0.09 ± 0.12^{A}	0.11 ± 0.09^{A,G,J}	0.09 ± 0.08^{A,G}	0.16 ± 0.11	0.15 ± 0.13
	Hypothalamus	0.02 ± 0.02^{A,D}	0.04 ± 0.03^{A}	0.03 ± 0.03^{A,D}	0.03 ± 0.02^{A}	0.05 ± 0.07^{A}	0.20 ± 0.34	0.05 ± 0.02
	Cortex	0.25 ± 0.17^{G}	0.40 ± 0.36^{G}	0.31 ± 0.50^{D,G}	0.17 ± 0.08^{G}	0.22 ± 0.21^{G}	0.21 ± 0.09	0.27 ± 0.13
	Hippocampus	0.14 ± 0.15^{A,D,G,J}	0.14 ± 0.14^{A,G,J}	0.20 ± 0.20^{D,G}	0.20 ± 0.25^{G}	0.11 ± 0.16^{A,G}	0.13 ± 0.15	0.22 ± 0.20
	Striatum	0.11 ± 0.08^{A,G}	0.13 ± 0.08^{A,G,J}	0.14 ± 0.12^{A,G}	0.10 ± 0.06^{A,G,J}	0.32 ± 0.62^{G}	0.10 ± 0.06	0.11 ± 0.06
Pex16	Cerebellum	1.81 ± 0.93	2.31 ± 1.50	1.61 ± 0.74^{P,M}	2.10 ± 2.14	3.28 ± 2.44	2.13 ± 2.21	1.39 ± 0.76
	Midbrain	1.40 ± 1.02^{P}	2.16 ± 1.58^{P}	2.32 ± 2.22	2.27 ± 1.52^{G}	1.25 ± 0.69^{A,M,P}	1.62 ± 0.69	2.39 ± 2.77
	Hypothalamus	0.97 ± 0.94^{A,P}	1.54 ± 1.02^{P}	1.63 ± 1.12^{P}	1.08 ± 0.71	1.44 ± 0.69^{A,M,P}	1.12 ± 0.48	0.95 ± 0.51
	Cortex	1.10 ± 0.50^{A}	1.92 ± 1.91	1.15 ± 0.45^{P,M}	1.48 ± 1.08	1.15 ± 1.05^{A,M,P}	0.78 ± 0.59	1.05 ± 0.65
	Hippocampus	2.19 ± 1.73^{A,G,P}	3.13 ± 2.88^{J}	3.06 ± 2.22	2.66 ± 2.26^{G}	3.08 ± 2.54	1.50 ± 1.00	1.62 ± 0.47
	Striatum	2.65 ± 1.33	3.34 ± 1.60	2.81 ± 1.24	3.17 ± 1.76^{G,J}	3.62 ± 3.32	1.64 ± 1.44	2.12 ± 2.21

Sod1	Cerebellum	18.31 ± 11.40^{J}	18.26 ± 8.98	17.90 ± 10.00	12.72 ± 7.07	18.62 ± 14.63	26.91 ± 31.96	31.49 ± 21.15
	Midbrain	13.58 ± 7.12	19.40 ± 10.86	19.38 ± 13.95^{G,J}	24.46 ± 12.29^{a,A,J}	22.20 ± 13.89^{G}	52.69 ± 27.67^{a,d,g,j,m}	22.87 ± 13.08
	Hypothalamus	25.90 ± 12.17^{D}	61.73 ± 26.34^{a,A,D,M}	46.86 ± 27.83^{a,g,A}	34.00 ± 19.43^{g,j,A}	79.61 ± 57.56^{a,A}	48.80 ± 20.79^{a}	25.77 ± 10.98^{g,j}
	Cortex	42.39 ± 31.67^{D}	54.98 ± 40.88^{A,D,M}	58.26 ± 43.66^{A}	63.95 ± 42.55^{A}	37.20 ± 33.78^{A,G,M}	29.83 ± 26.87	22.95 ± 11.70
	Hippocampus	20.16 ± 15.03^{J}	18.05 ± 11.65	26.40 ± 28.22^{G,J}	19.71 ± 14.43^{G,J}	18.49 ± 13.30^{G}	16.10 ± 9.56	21.07 ± 6.35
	Striatum	27.44 ± 13.64^{D}	43.02 ± 21.36^{A,D,M}	27.99 ± 13.10^{A,G,J}	31.60 ± 18.90^{A,J}	52.27 ± 54.93^{A}	30.77 ± 15.90	27.13 ± 7.98
Sod2	Cerebellum	42.02 ± 34.28^{G,J}	51.73 ± 24.25^{G}	65.19 ± 51.96	40.19 ± 21.68^{G}	67.52 ± 39.92	58.83 ± 50.11	48.78 ± 63.40
	Midbrain	30.00 ± 16.61^{G,J}	57.44 ± 42.99^{G}	23.44 ± 14.94^{A,P}	49.60 ± 31.52	38.96 ± 29.58^{A,G,J}	51.48 ± 22.32	41.59 ± 38.85
	Hypothalamus	12.47 ± 9.95	19.16 ± 12.45	13.04 ± 6.85^{A,P}	13.64 ± 9.47^{D}	16.89 ± 7.76^{A}	26.09 ± 12.14	19.47 ± 13.82
	Cortex	16.63 ± 8.83	32.69 ± 22.51^{A}	25.92 ± 16.97^{A,G,P}	25.49 ± 19.60^{D}	14.11 ± 8.78^{A}	22.85 ± 6.77	13.15 ± 1.000
	Hippocampus	30.25 ± 22.31^{G,J}	35.56 ± 24.26	31.34 ± 17.93^{G,P}	27.79 ± 29.79^{D}	33.62 ± 27.18^{A,J}	16.00 ± 8.27	20.00 ± 6.87
	Striatum	41.96 ± 28.32^{G,J}	51.03 ± 36.94^{G}	50.34 ± 22.81	28.75 ± 12.89^{m,G}	47.95 ± 47.49^{G,J}	16.04 ± 6.12^{a,d,j,m}	22.00 ± 9.81^{m}
Cat	Cerebellum	4.51 ± 2.49^{J}	4.02 ± 2.52^{J}	8.32 ± 10.94^{G,J}	3.87 ± 3.07^{J}	4.68 ± 3.07^{J}	4.51 ± 4.36	2.93 ± 2.48
	Midbrain	4.48 ± 3.39^{J}	6.03 ± 3.36^{G,J,M}	3.74 ± 2.42^{J}	7.45 ± 5.57	3.15 ± 2.27^{J}	5.02 ± 1.67	9.07 ± 9.58
	Hypothalamus	3.20 ± 3.50	2.84 ± 2.50	2.09 ± 1.28	3.00 ± 2.81^{D}	2.58 ± 1.83^{J}	2.75 ± 1.39	2.50 ± 1.38
	Cortex	1.85 ± 1.20	1.66 ± 0.92^{M}	1.78 ± 1.41	1.85 ± 1.67^{D}	0.96 ± 0.65	1.25 ± 0.61	1.66 ± 1.45
	Hippocampus	5.54 ± 4.14^{J}	3.09 ± 1.87	4.90 ± 5.31^{J}	3.74 ± 3.88^{D}	3.47 ± 4.92^{A}	4.14 ± 4.60	2.42 ± 0.49
	Striatum	4.91 ± 1.91^{G,J}	7.18 ± 5.14^{G,J,M}	7.45 ± 5.93^{G,J}	4.75 ± 3.15^{J}	3.67 ± 2.52^{J}	2.57 ± 1.49	3.50 ± 3.91
Pex11g	Cerebellum	0.06 ± 0.04^{J}	0.08 ± 0.05^{J,M}	0.07 ± 0.06^{J,M}	0.06 ± 0.05	0.08 ± 0.09^{J,M}	0.05 ± 0.06	0.04 ± 0.02
	Midbrain	0.05 ± 0.04^{J}	0.09 ± 0.11^{J,M}	0.05 ± 0.05^{J}	0.07 ± 0.05	0.08 ± 0.10^{J,M}	0.06 ± 0.04^{J}	0.07 ± 0.06
	Hypothalamus	0.04 ± 0.03^{P}	0.09 ± 0.06^{a,J,M}	0.06 ± 0.05^{a,J,M}	0.06 ± 0.05	0.07 ± 0.07^{J,M}	0.12 ± 0.11^{a,J}	0.08 ± 0.04
	Cortex	0.03 ± 0.03	0.04 ± 0.05	0.02 ± 0.02	0.02 ± 0.02^{A,D}	0.01 ± 0.01^{M}	0.02 ± 0.01	0.03 ± 0.02
	Hippocampus	0.04 ± 0.03^{P}	0.02 ± 0.01	0.03 ± 0.04	0.02 ± 0.01^{A,D}	0.03 ± 0.04	0.05 ± 0.04	0.03 ± 0.02
	Striatum	0.07 ± 0.05^{J}	0.08 ± 0.07^{J,M}	0.06 ± 0.03^{J,M}	0.04 ± 0.03	0.08 ± 0.09^{J}	0.05 ± 0.04	0.04 ± 0.03
Gpx1	Cerebellum	17.15 ± 11.02^{P}	19.11 ± 9.92^{G,P}	16.18 ± 9.05^{G,P}	13.75 ± 12.74	14.47 ± 8.83^{G,P}	14.04 ± 16.40	16.32 ± 15.42
	Midbrain	17.68 ± 12.18^{P}	19.63 ± 12.89^{G,P}	21.58 ± 14.81^{P}	32.65 ± 16.58^{A,J,M}	18.35 ± 8.63^{G,P}	19.83 ± 7.00	19.50 ± 15.29
	Hypothalamus	20.61 ± 13.87^{P}	41.65 ± 20.22	27.71 ± 14.02	26.93 ± 13.79^{A,J,M}	32.19 ± 15.66	26.79 ± 27.54	20.13 ± 12.89
	Cortex	12.44 ± 5.34^{P}	17.38 ± 12.24^{G,P}	12.58 ± 4.67^{G,P}	13.87 ± 8.26	10.54 ± 6.04^{D,G,P}	11.00 ± 10.44	11.08 ± 4.66
	Hippocampus	13.32 ± 8.51^{P}	17.13 ± 14.80^{G,P}	13.46 ± 8.84^{G,P}	12.82 ± 8.69	15.68 ± 11.92^{G,P}	15.05 ± 16.20	12.74 ± 9.19
	Striatum	60.08 ± 28.19	73.59 ± 45.16	64.97 ± 39.67^{G}	56.55 ± 40.50^{A,J,M}	55.18 ± 40.26	26.03 ± 32.41	27.81 ± 16.20

Table S12. Relative expression of *Bscl2*; Celia *BSCL2*-TG; *Ppary*; *Pex16*; *Sod1*; *Sod2*; *Cat*; *Pex11g* and *Gpx1* genes in brain regions for wild type, *Bscl2*$^{+/Celia}$, *Bscl2*$^{Celia/Celia}$, *Bscl2*$^{+/-}$ and *Bscl2*$^{-/-}$ mice separated by sex. Data is presented as mean ± SD. Data were analysed using a Kolmogorov-Smirnov test for normality, followed by a Kruskal-Wallis test with Mann-Whitney post hoc comparisons. Results were normalized for the *Rn18S* gene and referred to Cerebellum of *Bscl2*$^{+/Celia}$ in Celia *BSCL2*-TG gene. [a] $p < 0.05$ vs wild type ♀/♂; [b] $p < 0.05$ vs wild type ♀; [c] $p < 0.05$ vs wild type ♂; [d] $p < 0.05$ vs *Bscl2*$^{+/-}$ ♀/♂; [g] $p < 0.05$ vs *Bscl2*$^{-/-}$ ♀/♂; [i] $p < 0.05$ vs *Bscl2*$^{-/-}$ ♂; [j] $p < 0.05$ vs *Bscl2*$^{+/Celia}$ ♀/♂; [k] $p < 0.05$ vs *Bscl2*$^{+/Celia}$ ♀; [m] $p < 0.05$ vs *Bscl2*$^{Celia/Celia}$ ♀/♂; [l] $p < 0.05$ vs *Bscl2*$^{+/Celia}$ ♂. [A] $p < 0.05$ vs cerebellum ♀/♂; [B] $p < 0.05$ vs cerebellum ♀; [C] $p < 0.05$ vs cerebellum ♂; [D] $p < 0.05$ vs midbrain ♀/♂; [E] $p < 0.05$ vs midbrain ♀; [F] $p < 0.05$ vs midbrain ♂; [G] $p < 0.05$ vs hypothalamus ♀/♂; [H] $p < 0.05$ vs hypothalamus ♀; [I] $p < 0.05$ vs hypothalamus ♂; [J] $p < 0.05$ vs cortex ♀/♂; [K] $p < 0.05$ vs cortex ♀; [L] $p < 0.05$ vs cortex ♂; [M] $p < 0.05$ vs hippocampus ♀/♂; [N] $p < 0.05$ vs hippocampus ♀; [O] $p < 0.05$ vs hippocampus ♂; [P] $p < 0.05$ vs striatum ♀/♂; [Q] $p < 0.05$ vs striatum ♀; [R] $p < 0.05$ vs striatum ♂.

		Wild type		*Bscl2*$^{+/Celia}$		*Bscl2*$^{Celia/Celia}$		*Bscl2*$^{+/-}$		*Bscl2*$^{-/-}$	
	Sex	♀	♂	♀	♂	♀	♂	♀	♂	♀	♂
	N	7	7	7	7	7	7	7	7	7	7
	Age (months)	9.4	9.5	9.6	9.6	9.4	9.4	9.5	9.5	9.5	9.5
Bscl2	Cerebellum	6.20 ± 3.17^{g,m}	4.15 ± 3.09^{g,m,J}	3.63 ± 1.73^{a,g,j,m}	3.78 ± 1.50^{g,m}	0.00 ± 0.00	0.00 ± 0.00	1.37 ± 0.91^{g,m}	3.23 ± 2.27^{g,m}	0.00 ± 0.00	0.00 ± 0.00
	Midbrain	4.16 ± 2.90^{g,m}	4.63 ± 4.72^{g,m}	1.63 ± 1.32^{g,m}	2.88 ± 2.21^{g,m}	0.00 ± 0.00	0.00 ± 0.00	2.64 ± 3.69^{g,m}	2.15 ± 1.59^{g,m}	0.00 ± 0.00	0.00 ± 0.00
	Hypothalamus	4.37 ±2.94^{g,m}	3.01 ± 2.90^{g,m}	3.91 ± 3.19^{g,m}	2.19 ± 1.88^{g,m}	0.00 ± 0.00	0.00 ± 0.00	2.71 ± 2.80^{g,m}	2.48 ± 1.29^{g,m}	0.00 ± 0.00	0.00 ± 0.00
	Cortex	2.69 ± 1.25^{g,m}	2.44 ± 1.85^{g,m}	1.78 ± 1.91^{g,m}	1.15 ± 1.02^{g,m}	0.00 ± 0.00	0.00 ± 0.00	1.55 ± 0.74^{g,m}	2.09 ± 3.15^{g,m}	0.00 ± 0.00	0.00 ± 0.00
	Hippocampus	3.66 ± 2.33^{g,m}	5.87 ± 3.74^{g,m}	2.44 ± 2.98^{g,m}	2.24 ± 1.71^{g,m}	0.00 ± 0.00	0.00 ± 0.00	1.61 ± 1.38^{g,m}	2.37 ± 2.15^{g,m}	0.00 ± 0.00	0.00 ± 0.00
	Striatum	7.21 ± 3.99^{g,m,I,J}	7.46 ± 2.43^{g,m,I,J,N}	2.76 ± 1.71^{a,g,m}	3.14 ± 1.99^{a,g,m}	0.00 ± 0.00	0.00 ± 0.00	1.95 ± 0.94^{a,g,m}	1.83 ± 0.91^{a,g,m}	0.00 ± 0.00	0.00 ± 0.00
Celia *BSCL2*-TG	Cerebellum	0.00 ± 0.00	0.00 ± 0.00	1.33 ± 0.59^{a,d,g,J}	1.04 ± 0.88^{a,d,g,J}	2.89 ± 1.41^{a,d,g,I,J}	2.60 ± 1.05^{a,d,g,j,J,Q}	0.00 ± 0.00	0.00 ± 0.00	0.00 ± 0.00	0.00 ± 0.00
	Midbrain	0.00 ± 0.00	0.00 ± 0.00	1.00 ± 1.01^{a,d,g,K}	0.60 ± 0.51^{a,d,g,A}	0.62 ± 0.65^{a,d,g,A,I,Q}	1.95 ± 1.99^{a,d,g}	0.00 ± 0.00	0.00 ± 0.00	0.00 ± 0.00	0.00 ± 0.00
	Hypothalamus	0.00 ± 0.00	0.00 ± 0.00	0.67 ± 0.64^{a,d,g}	0.68 ± 0.37^{a,d,g,J}	2.03 ± 1.48^{a,d,g,J}	2.63 ± 1.45^{a,d,g,j,J}	0.00 ± 0.00	0.00 ± 0.00	0.00 ± 0.00	0.00 ± 0.00
	Cortex	0.00 ± 0.00	0.00 ± 0.00	0.17 ± 0.08^{a,d,g}	0.24 ± 0.14^{a,d,g}	0.40 ± 0.16^{a,d,g,k}	0.31 ± 0.24^{a,d,g}	0.00 ± 0.00	0.00 ± 0.00	0.00 ± 0.00	0.00 ± 0.00
	Hippocampus	0.00 ± 0.00	0.00 ± 0.00	0.51 ± 0.30^{a,d,g,A}	0.47 ± 0.43^{a,d,g,A,K}	1.17 ± 1.12^{a,d,g,A}	0.80 ± 0.44^{a,d,g,A,J,I}	0.00 ± 0.00	0.00 ± 0.00	0.00 ± 0.00	0.00 ± 0.00
	Striatum	0.00 ± 0.00	0.00 ± 0.00	0.66 ± 0.53^{a,d,g,K}	0.49 ± 0.14^{a,d,g,A,J}	1.45 ± 0.79^{a,d,g,j,J}	1.99 ± 1.29^{a,d,g,j,J}	0.00 ± 0.00	0.00 ± 0.00	0.00 ± 0.00	0.00 ± 0.00
Ppary	Cerebellum	0.34 ± 0.26^{G}	0.24 ± 0.17^{G}	0.27 ± 0.12	0.26 ± 0.09	0.62 ± 0.98^{E,G}	0.28 ± 0.21^{E,G}	0.21 ± 0.23^{G}	0.29 ± 0.18^{G}	0.50 ± 0.49	0.23 ± 0.16
	Midbrain	0.15 ± 0.16^{G}	0.12 ± 0.17^{A,G,L}	0.08 ± 0.06^{A,I,K}	0.08 ± 0.05^{A,K}	0.05 ± 0.03	0.14 ± 0.16	0.08 ± 0.06^{C,K}	0.14 ± 0.10^{G}	0.10 ± 0.09^{B,H}	0.09 ± 0.07^{B}
	Hypothalamus	0.02 ± 0.02	0.02 ± 0.01	0.04 ± 0.03^{A}	0.03 ± 0.02^{A}	0.04 ± 0.03	0.03 ± 0.02^{F}	0.03 ± 0.02	0.03 ± 0.02	0.03 ± 0.02^{A}	0.06 ± 0.09^{A,K}

	Cortex	0.25 ± 0.23^{G}	0.25 ± 0.11^{G}	0.50 ± 0.41^{G}	0.30 ± 0.31^{G}	0.20 ± 0.12^{E,G}	0.43 ± 0.71^{E,G}	0.20 ± 0.05^{G}	0.14 ± 0.09^{G}	0.33 ± 0.25^{H}	0.10 ± 0.09^{B,H}
	Hippocampus	0.13 ± 0.18^{B,G,L}	0.15 ± 0.11^{G}	0.09 ± 0.06^{A,I,K}	0.19 ± 0.19^{G}	0.17 ± 0.18^{E,G}	0.23 ± 0.23^{G}	0.08 ± 0.08^{K}	0.31 ± 0.31^{C,G}	0.06 ± 0.06^{A,K}	0.16 ± 0.21^{H}
	Striatum	0.14 ± 0.09^{G,L}	0.08 ± 0.05^{A,G,J}	0.10 ± 0.08^{A,I,K}	0.15 ± 0.08^{G,K}	0.13 ± 0.09^{G}	0.16 ± 0.15^{E,G}	0.11 ± 0.05^{C,G,K}	0.08 ± 0.07^{C,K}	0.18 ± 0.27^{H}	0.46 ± 0.85
Pex16	Cerebellum	2.37 ± 0.58	1.25 ± 0.89^{Q}	2.98 ± 1.74	1.65 ± 0.91	1.59 ± 0.55^{Q}	1.62 ± 0.92	1.57 ± 1.56	2.64 ± 2.61	3.81 ± 2.87	2.75 ± 2.01
	Midbrain	1.23 ± 0.99^{B}	1.57 ± 1.09^{I,Q}	1.92 ± 0.92	2.39 ± 2.10	2.19 ± 2.74^{Q}	2.45 ± 1.76	1.91 ± 1.86	2.63 ± 1.13	1.27 ± 0.75^{B,O,R}	1.23 ± 0.68^{B,O,R}
	Hypothalamus	1.37 ± 1.19^{B,Q}	0.57 ± 0.33^{B,P}	1.66 ± 1.44	1.41 ± 0.41	1.07 ± 0.72^{M,P}	2.28 ± 1.20	0.84 ± 0.43	1.31 ± 0.89	1.52 ± 0.83	1.34 ± 0.53^{B,O}
	Cortex	1.22 ± 0.48^{B,I,P}	0.98 ± 0.52^{B,P}	1.98 ± 2.61	1.86 ± 1.03	1.09 ± 0.32^{M,P}	1.20 ± 0.57^{P}	1.60 ± 1.26	1.35 ± 0.95	0.95 ± 0.87^{B,O,R}	1.34 ± 1.24
	Hippocampus	2.16 ± 2.17^{E}	2.22 ± 1.35^{I}	3.18 ± 3.08	3.08 ± 2.91	2.98 ± 1.88	3.15 ± 2.67	1.91 ± 1.31	3.42 ± 2.84	1.83 ± 1.08^{B,O,R}	4.34 ± 3.02
	Striatum	2.84 ± 1.24	2.45 ± 1.49	2.77 ± 1.36	3.91 ± 1.71	3.10 ± 1.42	2.46 ± 1.01	3.24 ± 1.51	3.10 ± 2.11	3.49 ± 3.88	3.76 ± 2.90
Sod1	Cerebellum	22.10 ± 12.43	15.07 ± 10.23^{H,L,Q}	16.25 ± 4.68^{G,L}	20.27 ± 12.08^{G,L}	13.87 ± 4.47^{H,L}	21.35 ± 12.38^{H,L}	8.31 ± 3.64	15.93 ± 8.13	14.62 ± 7.00^{G}	22.04 ± 18.90^{G}
	Midbrain	14.97 ± 9.70^{H,L}	12.19 ± 3.56^{H,L,Q}	18.89 ± 8.28^{G,L}	19.84 ± 13.36^{G,L,Q}	15.29 ± 11.93^{L}	23.48 ± 15.49^{L}	20.24 ± 15.61^{K}	28.08 ± 8.12^{A,K,N}	20.67 ± 12.59^{G}	23.99 ± 16.31^{G}
	Hypothalamus	35.45 ± 7.17	17.72 ± 9.17^{b,H,L,Q}	62.56 ± 27.35^{c}	60.90 ± 27.45^{a}	44.60 ± 19.36^{c,E,N}	49.12 ± 36.29^{c,N,E,N}	39.04 ± 25.81^{i,B}	29.68 ± 12.35^{i,j,A,K,N}	70.70 ± 47.76^{c}	100.21 ± 63.89^{a}
	Cortex	21.20 ± 5.95^{F,H,L}	60.55 ± 33.80	56.25 ± 46.69^{B}	62.14 ± 39.25	66.02 ± 57.99^{B,E,N}	49.21 ± 18.89^{N}	77.34 ± 47.63^{A}	48.32 ± 32.85^{B}	45.68 ± 44.83	34.71 ± 19.40^{I}
	Hippocampus	18.61 ± 14.38^{H,L}	21.71 ± 16.64^{H,L}	17.36 ± 9.24^{G,L,Q}	18.63 ± 14.12^{G,L}	14.68 ± 6.97	36.44 ± 36.02	12.90 ± 9.09^{K}	25.55 ± 16.16^{B,K}	15.44 ± 14.15^{G}	22.06 ± 12.49^{G}
	Striatum	33.52 ± 14.74	20.35 ± 8.57^{H,L}	42.67 ± 23.56^{B}	43.43 ± 20.69^{B,O}	28.57 ± 13.08^{B,E,N}	27.30 ± 14.34^{B,H,N}	25.75 ± 11.22^{B,K}	38.42 ± 24.55^{B}	34.47 ± 19.42^{I}	73.04 ± 76.33^{N}
Sod2	Cerebellum	57.14 ± 34.34^{I}	24.38 ± 26.69^{B,I,Q}	58.66 ± 28.71^{B,G}	43.64 ± 16.64^{G}	45.14 ± 33.79	85.24 ± 61.92	37.14 ± 26.51^{H}	43.23 ± 17.58^{G}	80.13 ± 48.64^{G,J}	52.81 ± 22.46^{G,J}
	Midbrain	27.98 ± 21.44^{I}	31.74 ± 12.69^{I}	32.18 ± 14.44^{F}	82.70 ± 48.23	24.24 ± 16.35^{C}	22.50 ± 14.59^{C,Q}	38.92 ± 22.66^{G}	62.07 ± 37.70	38.79 ± 34.96^{B}	39.16 ± 25.16
	Hypothalamus	18.35 ± 11.13^{B,I,Q}	6.59 ± 3.16	17.60 ± 12.95^{F}	20.72 ± 12.75^{F}	14.07 ± 8.46^{C}	11.83 ± 4.85^{C}	11.82 ± 6.84^{F}	15.46 ± 11.81^{F}	14.85 ± 6.15^{F}	18.94 ± 9.11
	Cortex	15.27 ± 8.99^{B,F,I}	18.21 ± 9.20^{B,F,I,Q}	26.24 ± 27.93^{F}	38.22 ± 16.91^{G}	21.13 ± 8.89^{C,P}	30.03 ± 21.62	25.95 ± 19.30^{F}	24.95 ± 21.77	15.63 ± 9.51	12.59 ± 8.43^{F}
	Hippocampus	32.86 ± 30.72^{I}	27.64 ± 10.88^{I,K}	30.28 ± 19.23^{F}	40.09 ± 28.58	34.99 ± 22.49^{G}	28.20 ± 14.04^{C,G,Q}	18.03 ± 14.71^{C,F}	36.15 ± 37.65	24.09 ± 21.13^{B}	44.75 ± 31.01^{H,J}
	Striatum	55.28 ± 32.71^{I,K}	26.42 ± 10.13^{I,Q}	53.79 ± 42.01^{G,I}	48.67 ± 35.27	53.37 ± 26.64^{G}	47.31 ± 19.89^{D,G}	33.05 ± 14.18^{H}	24.46 ± 10.97^{F,H}	40.08 ± 12.58^{G,J}	55.81 ± 68.23
Cat	Cerebellum	4.57 ± 2.78	4.44 ± 2.38	4.20 ± 3.23	3.86 ± 2.00^{J}	7.78 ±9.74	6.65 ± 5.41	2.04 ± 1.12^{F}	5.71 ± 3.37	5.64 ± 3.79^{J}	3.86 ± 2.27^{J}
	Midbrain	4.19 ± 2.52	4.81 ± 4.45	5.91 ± 3.38^{H,J}	6.16 ± 3.60^{H,J}	2.28 ± 1.14^{C,F,P}	5.19 ± 2.55	5.92 ± 5.98	8.99 ± 5.08	3.13 ± 2.30^{J}	3.18 ± 2.45

	Hypothalamus	3.13 ± 3.90	3.27 ± 3.36	2.12 ± 1.22	3.45 ± 3.21	1.63 ± 0.83^{A,F,P}	2.62 ±1.57	3.22 ± 3.69^{F}	2.77 ± 1.82^{F}	1.73 ± 1.17^{B}	3.44 ± 2.04
	Cortex	1.79 ± 0.91	1.90 ± 1.52	1.65 ± 1.24	1.66 ± 0.64^{N}	1.48 ± 1.46^{A,F,P}	2.07 ± 1.39^{C,F,P}	1.74 ± 1.82^{C,F}	1.95 ± 1.65^{C,F}	0.92 ± 0.46	0.99 ± 0.83^{I}
	Hippocampus	4.39 ± 3.56	6.70 ± 4.62	3.16 ± 1.38	3.02 ± 2.38	5.34 ± 6.44^{K}	4.38 ± 4.14^{K}	3.34 ± 3.64^{F}	4.15 ± 4.36^{F}	1.96 ± 1.08^{B,K}	4.98 ± 6.78
	Striatum	5.39 ± 2.40	4.50 ± 1.45	5.15 ± 2.87^{H,J}	8.92 ± 6.19^{G,J,N}	7.07 ± 4.96	7.83 ± 7.16	4.61 ± 3.48	4.90 ± 3.07^{L}	3.11 ± 1.84^{J}	4.32 ± 3.20
Pex11g	Cerebellum	0.09 ± 0.03	0.03 ± 0.02^{B,Q}	0.09 ± 0.06^{L,M}	0.07 ± 0.03^{L,M}	0.07 ± 0.06^{K}	0.07 ± 0.05^{J}	0.04 ± 0.03	0.08 ± 0.06	0.10 ± 0.12^{J,N}	0.06 ± 0.04^{L}
	Midbrain	0.06 ± 0.05^{K}	0.04 ± 0.03^{B,K}	0.09 ± 0.14^{L,M}	0.08 ± 0.09	0.03 ± 0.02	0.07 ± 0.06	0.07 ± 0.06^{N}	0.07 ± 0.05	0.09 ± 0.14^{L}	0.08 ± 0.04^{J,N}
	Hypothalamus	0.05 ± 0.03^{B}	0.02 ± 0.01^{B,P}	0.08 ± 0.07^{L}	0.10 ± 0.07^{J,L}	0.04 ± 0.01^{K}	0.08 ± 0.07^{J}	0.06 ± 0.07	0.05 ± 0.04^{C,N}	0.05 ± 0.03^{J}	0.08 ± 0.09^{J,N}
	Cortex	0.02 ± 0.01^{B,P}	0.03 ± 0.05^{B,Q}	0.05 ± 0.07	0.02 ± 0.01	0.02 ± 0.01^{J}	0.02 ± 0.02^{J}	0.02 ± 0.02^{F}	0.02 ± 0.02^{F}	0.02 ± 0.02	0.01 ± 0.01
	Hippocampus	0.03 ± 0.04^{B}	0.04 ± 0.03^{B}	0.03 ± 0.02	0.02 ± 0.01^{H}	0.03 ± 0.04	0.03 ± 0.05	0.02 ± 0.01^{C,F}	0.02 ± 0.02^{C,F}	0.02 ± 0.02	0.05 ± 0.05^{L}
	Striatum	0.08 ± 0.07	0.06 ± 0.04	0.07 ± 0.05^{L,M}	0.09 ± 0.10^{L,M}	0.05 ± 0.02	0.07 ± 0.04	0.05 ± 0.04^{N}	0.03 ± 0.03	0.06 ± 0.05^{L}	0.10 ± 0.13^{L}
Gpx1	Cerebellum	22.26 ± 12.67^{P}	12.05 ± 6.46^{P}	18.49 ± 8.82^{G,P}	19.74 ± 11.59^{I,R}	14.02 ± 8.97^{P}	18.04 ± 9.38^{P}	7.98 ± 5.97^{F,I,P}	19.52 ± 15.44^{F}	15.67 ± 7.23	13.45 ± 10.47
	Midbrain	19.15 ± 15.60^{P}	15.97 ± 7.58^{P}	20.66 ± 15.68^{P}	18.75 ± 11.20^{I,P}	16.38 ± 11.28^{P}	26.78 ± 16.88^{R}	27.50 ± 21.18	37.79 ± 9.24	19.65 ± 10.34	16.85 ± 6.74
	Hypothalamus	26.98 ± 15.91^{R}	14.24 ± 8.32^{P}	39.78 ± 22.40	43.53 ± 19.40	22.26 ± 11.13^{R}	33.15 ± 15.41^{R}	23.17 ± 14.17	30.68 ± 13.56	36.82 ± 19.41^{C,J,M}	26.79 ± 8.44^{A,J}
	Cortex	11.68 ± 5.65^{P}	13.20 ± 5.33^{P}	17.31 ± 14.56^{I,P}	17.45 ± 10.60^{I,P}	11.98 ± 4.52^{I,P}	13.17 ± 5.10^{I,P}	14.38 ± 8.97^{F,P}	13.36 ± 8.17^{F,I,P}	9.37 ± 5.30	11.71 ± 6.91
	Hippocampus	13.95 ± 11.36^{P}	12.70 ± 5.18^{P}	19.93 ± 18.64^{I,R}	14.32 ± 10.43^{G,P}	11.69 ± 6.48^{I,P}	14.98 ± 10.74^{P}	11.64 ± 9.37^{F,I,P}	14.00 ± 8.51^{F,I,P}	14.24 ± 10.82	17.13 ± 13.63
	Striatum	42.81 ± 14.31^{R}	77.35 ± 28.77	66.50 ± 49.70	80.69 ± 43.53	41.49 ± 26.87	88.46 ± 37.64	66.04 ± 50.98^{C}	47.05 ± 27.28	49.18 ± 25.81^{C,J}	62.39 ± 55.68^{C,J,M}

Annex 7. Table S13 and Figures S1, S2 and S3. Image J quantification and full-length blots and Ponceau S staining.

Table S13. Relative intensity of 6x His-tagged Celia seipin normalized to GAPDH in *Bscl2*$^{+/Celia}$ and *Bscl2*$^{Celia/Celia}$ animals. Area and percentage of GADPH as loading control and 6x His-tagged Celia seipin protein in six brain tissues (cerebellum, midbrain, hypothalamus, cortex, hippocampus, striatum) and the hypothalamus of a human without the disease as a negative control.

	Bscl2$^{+/Celia}$					*Bscl2*$^{Celia/Celia}$				
	GAPDH		Celia seipin + 6x His Tag		**6x His-tagged Celia seipin relative intensity / GAPDH**	GAPDH		Celia seipin + 6x His Tag		**6x His-tagged Celia seipin relative intensity / GAPDH**
	Area	Percent	Area	Percent		Area	Percent	Area	Percent	
Cerebellum	11020.48	19.76	169.61	0.30	0.02	8100.75	9.34	687.09	0.79	0.08
Midbrain	8330.75	14.94	303.51	0.54	0.04	9451.41	10.90	1062.75	1.23	0.11
Hypothalamus	5258.39	9.43	6450.97	11.57	1.23	14936.38	17.22	8394.05	9.68	0.56
Cortex	7214.89	12.94	957.72	1.72	0.13	13312.89	15.35	5160.85	5.95	0.39
Hippocampus	6420.05	11.51	1175.48	2.06	0.18	11242.95	12.96	1707.06	1.97	0.15
Striatum	6075.49	10.89	372.85	0.67	0.06	10154.63	11.71	176.02	0.20	0.02
Negative control	2064.13	3.63	24.12	0.04	0.01	2323.96	2.68	12.12	0.01	0.01

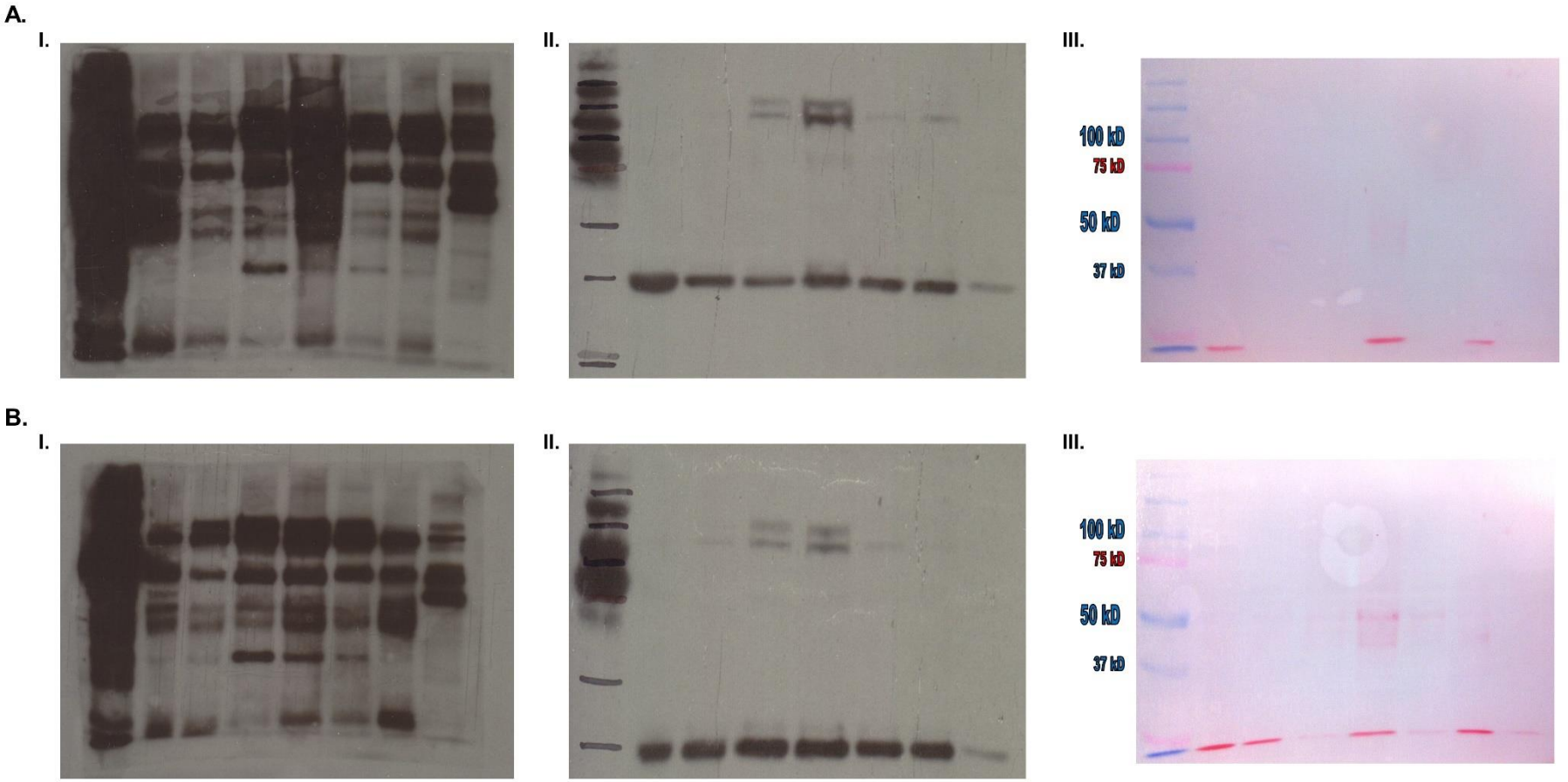

Figure S1. Full-length blot and Ponceau S staining. A. Full-length blot for anti 6x His tagged seipin antibody (**I**) and anti-GAPDH antibody (**II**) and Ponceau S staining (**II**) in ***Bscl2***$^{+/Celia}$ mouse. **B.** Full-length blot for anti 6x His tagged seipin antibody (**I**) and anti-GAPDH antibody (**II**) and Ponceau S staining (**II**) in ***Bscl2***$^{Celia/Celia}$ mouse.

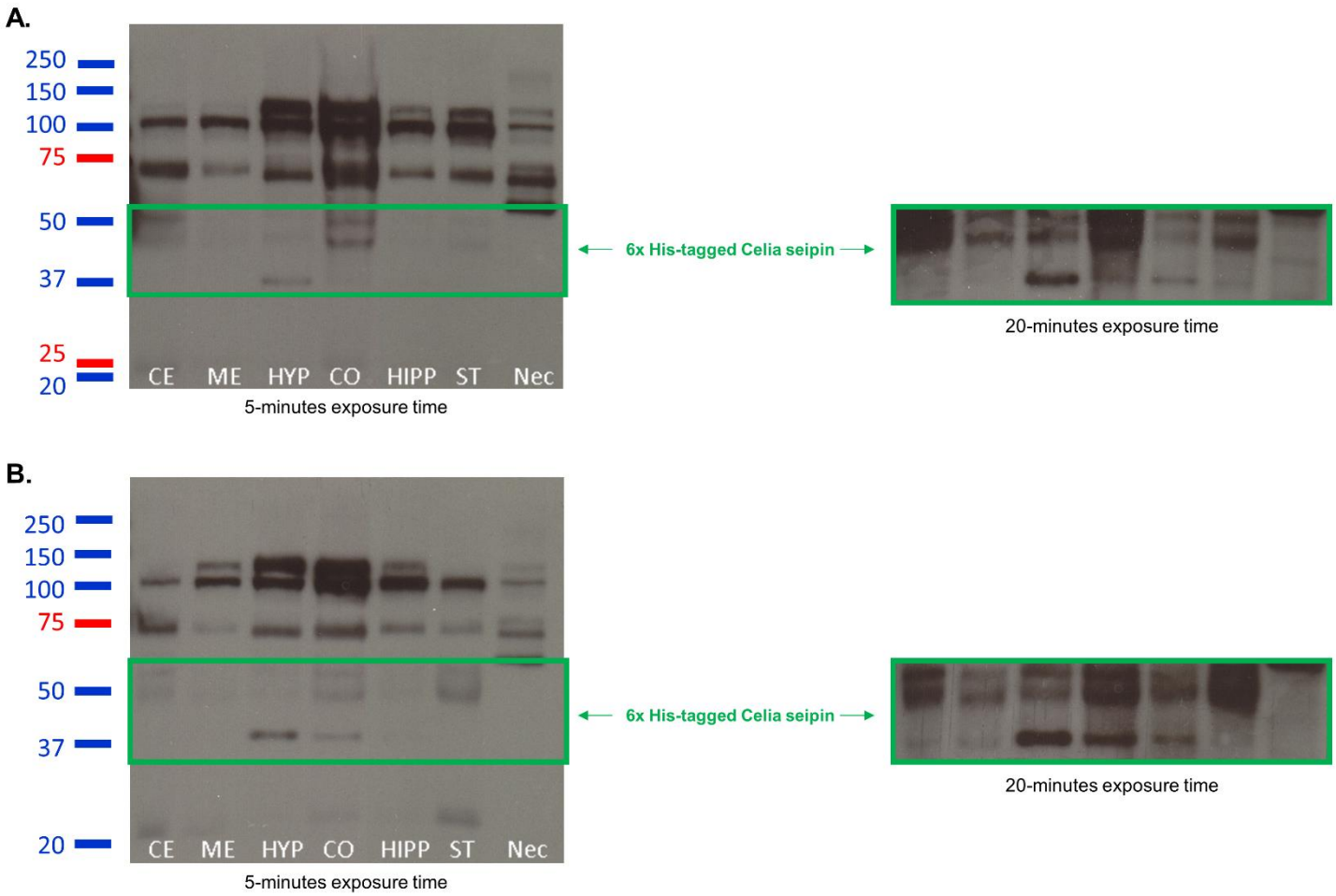

Figure S2. Selected anti 6x His tagged seipin antibody in *Bscl2*$^{+/Celia}$ (A) and *Bscl2*$^{Celia/Celia}$ mouse (B) with different exposure times. CE: cerebellum; ME: midbrain; HYP: hypothalamus; CO: cortex; HIPP: hippocampus; ST: striatum and Nec: Negative control.

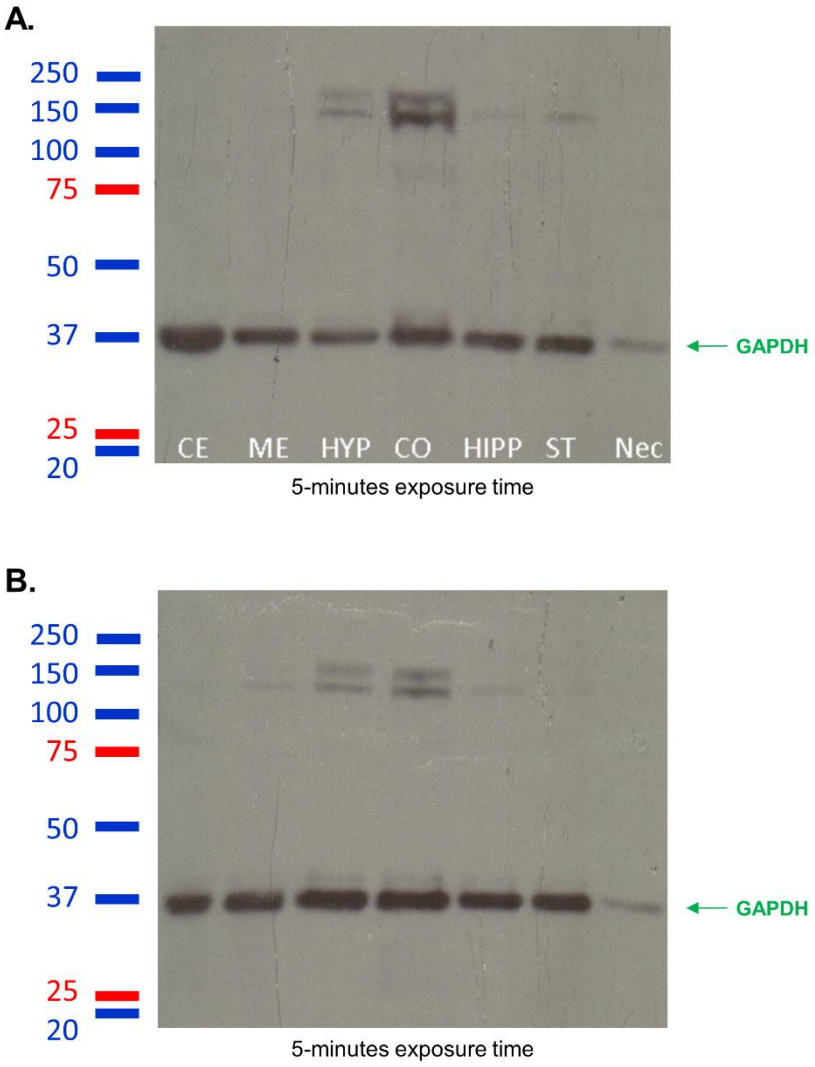

Figure S3. Full-length blot for anti-GAPDH antibody. A. Full-length blot in ***Bscl2***$^{+/Celia}$ mouse. **B.** Full-length blot in ***Bscl2***$^{Celia/Celia}$ mouse. CE: cerebellum; ME: midbrain; HYP: hypothalamus; CO: cortex; HIPP: hippocampus; ST: striatum and Nec: Negative control.

Annex 8. Table S14 and S15. Evolution of weight and basal glucose.

Table S14. Evolution of weight and basal glucose for wild type, *Bscl2*$^{+/Celia}$, *Bscl2*$^{Celia/Celia}$, *Bscl2*$^{+/-}$, *Bscl2*$^{-/-}$ and severe affected (S.A.) *Bscl2*$^{+/Celia}$ and *Bscl2*$^{Celia/Celia}$ mice. Follow-up of the animals from 0.5 M (months) to the end point (9.5 M). Data is presented as mean ± SD or n (%) ± SD. Data were analysed using a Kolmogorov-Smirnov test for normality, followed by a Kruskal-Wallis test with Mann-Whitney post hoc comparisons. [a] $p < 0.05$ vs wild type ♀/♂; [d] $p < 0.05$ vs *Bscl2*$^{+/-}$ ♀/♂; [g] $p < 0.05$ vs *Bscl2*$^{-/-}$ ♀/♂; [j] $p < 0.05$ vs *Bscl2*$^{+/Celia}$ ♀/♂; [m] $p < 0.05$ vs *Bscl2*$^{Celia/Celia}$ ♀/♂.

	0.5 M		1 M		1.5 M		2 M		3 M		4 M		5 M		6 M		7 M		8 M		9 M		9.5 M
	General weight																						
	N	Weight (g)	N	Weight (g)	N	Weight (g)	N	Weight (g)	N	Weight (g)	N	Weight (g)	N	Weight (g)	N	Weight (g)	N	Weight (g)	N	Weight (g)	N	Weight (g)	N	Weight (g)
Wild type ♀/♂	85	7.75 ± 1.27	73	15.14 ± 2.59	45	19.03 ± 2.12	46	21.80 ± 2.01	45	25.55 ± 2.89	37	27.56 ± 3.24	38	28.75 ± 2.69	42	31.38 ± 3.94	32	33.33 ± 3.53	29	34.45 ± 3.47	30	35.11 ± 3.77	35	35.72 ± 4.54
Bscl2$^{+/Celia}$ ♀/♂	106	7.63 ± 1.24	106	14.87 ± 2.54	72	18.20 ± 2.00	73	21.25 ± 2.14	62	25.23 ± 2.51	61	27.81 ± 3.20	63	29.02 ± 3.68	59	31.53 ± 5.35	60	32.75 ± 5.59	58	33.43 ± 4.60	57	34.03 ± 5.00	62	34.22 ± 4.90
Bscl2$^{Celia/Celia}$ ♀/♂	53	5.88 ± 1.11	48	12.66 ± 2.36^{a,d,g,j}	44	17.54 ± 1.57	38	20.97 ± 1.44	38	25.82 ± 1.98	36	28.60 ± 2.48^{j}	30	30.21 ± 2.16	29	32.51 ± 2.36	29	33.73 ± 2.65	27	34.87 ± 2.69	27	35.64 ± 3.10	27	35.98 ± 3.27
Bscl2$^{+/-}$ ♀/♂	65	7.72 ± 1.25	52	15.53 ± 2.07	45	19.69 ± 1.55	54	22.65 ± 2.04	65	25.94 ± 3.21	33	27.59 ± 3.87	46	28.89 ± 3.52	43	30.58 ± 4.11	42	31.96 ± 4.03	33	32.95 ± 4.15	27	34.10 ± 3.36	33	34.59 ± 4.45
Bscl2$^{-/-}$ ♀/♂	42	6.13 ± 1.03	29	14.82 ± 4.21^{d}	33	18.74 ± 2.52	24	23.08 ± 1.46	40	27.18 ± 2.82	24	28.43 ± 3.78	25	30.01 ± 3.32	28	32.12 ± 3.66	25	33.18 ± 3.71	18	33.65 ± 3.63	21	34.57 ± 4.18	27	35.01 ± 4.46
S.A. *Bscl2*$^{+/Celia}$ ♀/♂	-	-	5	11.34 ± 2.14^{a,d,g,j}	5	16.38 ± 1.77	4	18.95 ± 1.84	4	21.63 ± 0.83	6	21.15 ± 2.26^{a,d,g,j,m}	4	20.28 ± 2.13	4	19.70 ± 2.40^{a,d,g,j,m}	1	17.40	1	17.10	-	-		-
S.A. *Bscl2*$^{Celia/Celia}$ ♀/♂	-	-	3	9.20 ± 2.79^{a,d,g,j}	1	16.00	2	17.95 ± 1.20	3	21.90 ± 1.93	3	20.95 ± 0.79^{a,d,g,j,m}	3	20.27 ± 0.47	3	18.27 ± 1.29^{a,d,g,j,m}	3	18.67 ± 0.84	2	20.70 ± 0.42^{a,d,g,j,m}	2	20.15 ± 0.07		-

							Basal glucose															
							N	Glucose (mg/dL)	N	Glucose (mg/dL)	N	Glucose (mg/dL)	N	Glucose (mg/dL)	N	Glucose (mg/dL)	N	Glucose (mg/dL)	N	Glucose (mg/dL)	N	Glucose (mg/dL)
Wild type ♀/♂	-	-	-	-	-	-	33	95.26 ± 24.73	28	100.04 ± 19.22	27	98.15 ± 26.75	26	93.88 ± 22.89	35	90.59 ± 20.26	30	95.62 ± 18.26	24	92.31 ± 18.88	24	92.48 ± 21.93	30	101.27 ± 21.13
Bscl2$^{+/Celia}$ ♀/♂	-	-	-	-	-	-	46	95.62 ± 17.84	33	94.55 ± 18.72	33	94.20 ± 38.04	25	104.66 ± 26.17	44	88.31 ± 16.48	39	94.59 ± 21.64	44	88.14 ± 16.15	45	86.79 ± 12.46	46	98.32 ± 16.83
Bscl2$^{Celia/Celia}$ ♀/♂	-	-	-	-	-	-	31	130.16 ± 35.24^{a,d,j}	29	120.26 ± 30.20	32	147.02 ± 52.41	28	136.52 ± 42.87^{a,d,j}	22	101.09 ± 23.16	20	98.03 ± 25.80	22	104.41 ± 17.01^{j}	23	114.28 ± 51.93	22	115.11 ± 33.77
Bscl2$^{+/-}$ ♀/♂	-	-	-	-	-	-	35	106.93 ± 21.15^{a,j}	26	109.94 ± 18.57	31	106.26 ± 25.29	27	108.78 ± 32.15	32	98.41 ± 16.68	25	103.20 ± 19.48	24	100.04 ± 20.27	22	104.20 ± 16.12	29	105.78 ± 16.19
Bscl2$^{-/-}$ ♀/♂	-	-	-	-	-	-	27	137.39 ± 41.54^{a,d,j}	24	128.10 ± 26.03	26	155.31 ± 46.05	23	144.33 ± 42.23^{a,d,j}	23	120.76 ± 40.09	19	117.24 ± 31.46	22	109.93 ± 24.03^{a,j}	17	104.85 ± 24.21	24	102.60 ± 23.47
							Fasting weight loss															
							N	%	N	%	N	%	N	%	N	%	N	%	N	%	N	%	N	%
Wild type ♀/♂	-	-	-	-	-	-	27	14.52 ± 1.97	26	11.61 ± 2.53	20	11.30 ± 1.72	29	10.55 ± 1.75	36	9.64 ± 1.91	30	9.45 ± 1.96	26	9.10 ± 2.04	24	8.47 ± 1.61	39	8.74 ± 1.55
Bscl2$^{+/Celia}$ ♀/♂	-	-	-	-	-	-	41	15.02 ± 2.15	28	12.91 ± 2.27	21	11.17 ± 2.36	25	10.59 ± 2.45	45	10.28 ± 2.20	42	10.04 ± 2.72	44	9.64 ± 2.41	49	8.97 ± 2.34	64	9.26 ± 2.15
Bscl2$^{Celia/Celia}$ ♀/♂	-	-	-	-	-	-	30	17.89 ± 2.19^{a,d,g,j}	31	17.38 ± 1.66	26	16.14 ± 2.02	28	14.27 ± 1.62^{a,d,j}	25	13.01 ± 1.68	20	12.35 ± 4.35	22	13.08 ± 3.11^{a,d,j}	24	12.80 ± 2.38	33	13.08 ± 2.47
Bscl2$^{+/-}$ ♀/♂	-	-	-	-	-	-	19	14.63 ± 2.49	39	11.44 ± 2.22	19	10.65 ± 2.64	36	9.01 ± 2.09^{j}	32	9.81 ± 1.76	26	9.08 ± 2.00	24	8.68 ± 2.06	23	9.58 ± 1.71	42	8.66 ± 1.95
Bscl2$^{-/-}$ ♀/♂	-	-	-	-	-	-	20	21.09 ± 2.17^{a,d,j}	32	17.75 ± 3.06	20	15.54 ± 2.01	25	14.66 ± 1.74^{a,d,j}	23	13.70 ± 2.24	19	13.05 ± 3.10	22	12.90 ± 3.04^{a,d,j}	17	12.88 ± 2.33	26	12.78 ± 2.98

Table S15. Evolution of weight and basal glucose for wild type, *Bscl2*$^{+/Celia}$, *Bscl2*$^{Celia/Celia}$, *Bscl2*$^{+/-}$and *Bscl2*$^{-/-}$ separated by sex. Follow-up of the animals from 0.5 M (months) to the end point (9.5 M). Data is presented as mean ± SD or n (%) ± SD. Data were analysed using a Kolmogorov-Smirnov test for normality, followed by a Kruskal-Wallis test with Mann-Whitney post hoc comparisons. [a] $p < 0.05$ vs wild type ♀/♂; [b] $p < 0.05$ vs wild type ♀; [c] $p < 0.05$ vs wild type ♂; [d] $p < 0.05$ vs *Bscl2*$^{+/-}$ ♀/♂; [e] $p < 0.05$ vs *Bscl2*$^{+/-}$ ♀; [f] $p < 0.05$ vs *Bscl2*$^{+/-}$ ♂; [g] $p < 0.05$ vs *Bscl2*$^{-/-}$ ♀/♂; [j] $p < 0.05$ vs *Bscl2*$^{+/Celia}$ ♀/♂; [k] $p < 0.05$ vs *Bscl2*$^{+/Celia}$ ♀; [l] $p < 0.05$ vs *Bscl2*$^{+/Celia}$ ♂.

	0.5 M		1 M		1.5 M		2 M		3 M		4 M		5 M		6 M		7 M		8 M		9 M		9.5 M	
	General weight																							
	N	Weight (g)	N	Weight (g)	N	Weight (g)	N	Weight (g)	N	Weight (g)	N	Weight (g)	N	Weight (g)	N	Weight (g)	N	Weight (g)	N	Weight (g)	N	Weight (g)	N	Weight (g)
Wild type ♀	40	7.84 ± 1.18	37	13.63 ± 2.31	18	16.64 ± 1.53	18	18.96 ± 1.68	18	22.20 ± 2.97	16	23.74 ± 3.08	20	24.45 ± 2.25	20	26.68 ± 3.61	14	28.51 ± 2.51	17	29.90 ± 3.44	17	30.69 ± 3.78	21	31.58 ± 5.23
Wild type ♂	45	7.65 ± 1.36	36	16.65 ± 2.87	27	21.41 ± 2.71	28	24.64 ± 2.33	27	28.90 ± 2.82	21	31.39 ± 3.39	18	33.04 ± 3.14	22	36.08 ± 4.28	18	38.14 ± 4.56	12	39.00 ± 3.50	13	39.54 ± 3.76	14	39.87 ± 3.86
Bscl2$^{+/Celia}$ ♀	48	7.48 ± 1.11	48	13.75 ± 2.23	36	16.29 ± 1.52	40	18.73 ± 1.62	33	22.20 ± 2.28	37	24.15 ± 3.11	37	25.77 ± 3.75	34	28.20 ± 4.80	33	29.73 ± 5.07	38	30.84 ± 4.79	39	31.47 ± 4.80	39	31.81 ± 4.66
Bscl2$^{+/Celia}$ ♂	58	7.78 ± 1.37	58	16.00 ± 2.85	36	20.12 ± 2.48	33	23.76 ± 2.66	29	28.25 ± 2.73	24	31.48 ± 3.29	26	32.27 ± 3.62	25	34.86 ± 5.91	27	35.77 ± 6.11	20	36.02 ± 4.41	18	36.60 ± 5.20	23	36.63 ± 5.14
Bscl2$^{Celia/Celia}$ ♀	32	5.98 ± 1.06	32	12.06 ± 2.54[b,e,k]	25	16.17 ± 1.79	26	19.07 ± 2.00	23	23.86 ± 1.66	22	26.08 ± 2.59	20	28.08 ± 2.21[b,k]	17	30.45 ± 1.89	19	31.93 ± 1.84	17	33.48 ± 2.64	17	34.28 ± 2.62	17	34.86 ± 3.30
Bscl2$^{Celia/Celia}$ ♂	21	5.78 ± 1.16 ±	16	13.27 ± 2.18[c,f,l]	19	18.91 ± 1.36	12	22.88 ± 0.88	15	27.78 ± 2.30	14	31.11 ± 2.37	10	32.34 ± 2.11	12	34.58 ± 2.84	10	35.52 ± 3.46	10	36.26 ± 2.75	10	37.00 ± 3.58	10	37.11 ± 3.25
Bscl2$^{+/-}$ ♀	32	7.89 ± 1.45	25	14.63 ± 2.26	25	17.75 ± 1.51	31	20.19 ± 2.32	31	23.15 ± 3.06	18	25.09 ± 3.50	25	25.63 ± 2.63	23	27.23 ± 3.69	24	28.99 ± 3.37	17	30.35 ± 3.45	14	31.82 ± 3.12	13	32.52 ± 3.57
Bscl2$^{+/-}$ ♂	33	7.55 ± 1.06	27	16.44 ± 1.87	20	21.63 ± 1.59	23	25.11 ± 1.76	34	28.74 ± 3.36	15	30.09 ± 4.24	21	32.14 ± 4.40	20	33.92 ± 4.52	18	34.93 ± 4.69	16	35.56 ± 4.84	13	36.38 ± 3.60	20	36.66 ± 5.34
Bscl2$^{-/-}$ ♀	17	6.35 ± 0.93	12	13.51 ± 1.95	14	17.37 ± 1.74	10	20.99 ± 1.67	15	25.10 ± 3.07	9	26.66 ± 2.94	8	28.14 ± 2.21[b,k]	11	30.62 ± 3.09	8	31.71 ± 2.80	4	32.28 ± 2.28	5	33.22 ± 3.04	10	34.01 ± 3.18
Bscl2$^{-/-}$ ♂	25	5.92 ± 1.12	17	16.14 ± 6.46	19	20.10 ± 3.30	14	25.18 ± 1.26	25	29.26 ± 2.57	15	30.21 ± 4.62	17	31.89 ± 4.42	17	33.62 ± 4.22	17	34.65 ± 4.62	14	35.03 ± 4.97	16	35.92 ± 5.32	17	36.00 ± 5.75
	Basal glucose																							
							N	Glucose (mg/dL)	N	Glucose (mg/dL)	N	Glucose (mg/dL)	N	Glucose (mg/dL)	N	Glucose (mg/dL)	N	Glucose (mg/dL)	N	Glucose (mg/dL)	N	Glucose (mg/dL)	N	Glucose (mg/dL)
Wild type ♀	-	-	-	-	-	-	21	91.19 ± 24.12	17	98.24 ± 23.85	15	87.63 ± 19.45	15	87.40 ± 24.50	18	81.75 ± 15.22	15	89.60 ± 19.35	13	83.62 ± 11.99	13	80.92 ± 14.36	17	97.18 ± 19.69
Wild type ♂	-	-	-	-	-	-	12	102.38 ± 25.18	11	102.82 ± 8.56	12	111.29 ± 29.50	11	102.73 ± 17.90	17	99.94 ± 21.09	15	101.63 ± 15.45	11	102.59 ± 20.80	11	106.14 ± 21.90	13	106.62 ± 22.52
Bscl2$^{+/Celia}$ ♀	-	-	-	-	-	-	22	92.82 ± 19.11	18	85.94 ± 18.65	19	73.87 ± 18.83	16	93.06 ± 22.07	23	82.50 ± 16.54	22	87.25 ± 12.19	29	84.07 ± 16.14	35	83.97 ± 10.20	32	95.06 ± 18.65

Bscl2$^{+/Celia}$ ♂	-	-	-	-	-	-	24	98.19 ± 16.58	15	104.87 ± 13.02	14	121.79 ± 40.60	9	125.28 ± 19.86^{a,e,k}	21	94.67 ± 20.83	17	104.09 ± 27.34	15	96.00 ± 13.40	10	96.65 ± 15.06	14	105.75 ± 8.13
Bscl2$^{Celia/Celia}$ ♀	-	-	-	-	-	-	15	127.13 ± 38.03^{b,e,j}	15	137.27 ± 32.44	17	150.65 ± 49.87	15	130.40 ± 33.40^{a,e,k}	13	104.62 ± 22.62	10	95.35 ± 22.63	10	109.15 ± 15.97^{b,k}	10	123.30 ± 70.99	11	103.36 ± 28.12
Bscl2$^{Celia/Celia}$ ♂	-	-	-	-	-	-	16	133.00 ± 33.42^{a,e,j}	14	102.04 ± 11.84	15	142.90 ± 56.61	13	143.58 ± 52.28^{a,e,k}	9	96.00 ± 24.31	10	100.70 ± 29.61	12	100.46 ± 17.50	13	107.35 ± 32.32	11	126.86 ± 36.06
Bscl2$^{+/-}$ ♀	-	-	-	-	-	-	20	98.25 ± 21.16	13	104.81 ± 16.34	19	95.34 ± 20.92	13	92.19 ± 18.40	17	85.79 ± 9.18	14	95.36 ± 14.28	10	84.75 ± 15.16	8	97.38 ± 15.13	15	97.13 ± 9.89
Bscl2$^{+/-}$ ♂	-	-	-	-	-	-	15	118.50 ± 15.08^{b,e,j}	13	115.08 ± 19.86	12	123.54 ± 22.28	14	124.18 ± 34.99^{b,e,k}	15	112.70 ± 18.70	11	113.18 ± 21.22	14	110.96 ± 16.11^{b,e,k}	14	108.11 ± 15.86	14	115.04 ± 16.75
Bscl2$^{-/-}$ ♀	-	-	-	-	-	-	11	134.95 ± 50.03^{b,e,j}	10	133.65 ± 31.95	10	135.75 ± 49.03	10	132.70 ± 33.77^{a,e,k}	12	114.08 ± 36.06	11	124.45 ± 31.42	11	109.77 ± 22.69^{b,e,k}	6	124.83 ± 24.13	10	102.35 ± 24.16
Bscl2$^{-/-}$ ♂	-	-	-	-	-	-	16	139.06 ± 36.26^{a,e,j}	14	124.14 ± 21.24	16	167.53 ± 40.96	13	153.27 ± 47.06^{a,e,k}	11	128.05 ± 44.64	8	107.31 ± 30.67	11	110.09 ± 26.42^{b,e,k}	11	93.95 ± 16.62	14	102.79 ± 23.88

Fasting weight loss

							N	%	N	%	N	%	N	%	N	%	N	%	N	%	N	%	N	%
Wild type ♀	-	-	-	-	-	-	15	14.77 ± 2.26	11	11.55 ± 2.60	8	11.62 ± 1.74	15	11.19 ± 2.01	18	10.80 ± 1.71	15	10.12 ± 2.27	13	9.72 ± 2.16	13	8.45 ± 1.69	23	8.83 ± 1.57
Wild type ♂	-	-	-	-	-	-	12	14.20 ± 1.57	15	11.66 ± 2.56	12	11.08 ± 1.74	14	9.86 ± 1.13	18	8.47 ± 1.33	15	8.78 ± 1.35	13	8.47 ± 1.78	11	8.49 ± 1.59	16	8.62 ± 1.57
Bscl2$^{+/Celia}$ ♀	-	-	-	-	-	-	20	15.46 ± 2.24	17	12.96 ± 1.97	13	11.22 ± 1.67	16	10.96 ± 2.90	23	10.35 ± 2.57	23	9.94 ± 2.94	29	9.53 ± 2.38	36	8.47 ± 2.07	40	8.87 ± 1.89
Bscl2$^{+/Celia}$ ♂	-	-	-	-	-	-	21	14.60 ± 2.02	11	12.85 ± 2.77	8	11.10 ± 3.34	9	9.94 ± 1.23	22	10.20 ± 1.80	19	10.17 ± 2.49	15	9.85 ± 2.54	13	10.34 ± 2.58	24	9.92 ± 2.42
Bscl2$^{Celia/Celia}$ ♀	-	-	-	-	-	-	12	18.60 ± 1.37^{a,d,g,j}	17	17.38 ± 1.82	12	15.90 ± 2.57	15	13.86 ± 1.26^{a,d,j}	16	13.10 ± 2.01	10	11.97 ± 4.10	10	12.70 ± 1.81^{a,d,j}	11	12.73 ± 2.75	20	13.07 ± 2.66
Bscl2$^{Celia/Celia}$ ♂	-	-	-	-	-	-	18	19.44 ± 2.49^{a,d,j}	14	17.38 ± 1.52	14	16.35 ± 1.47	13	14.74 ± 1.90^{a,d,j}	9	12.87 ± 0.92	10	12.72 ± 4.78	12	13.40 ± 3.94^{a,d,j}	13	12.86 ± 2.13	13	13.11 ± 2.25
Bscl2$^{+/-}$ ♀	-	-	-	-	-	-	10	14.71 ± 2.07	17	12.27 ± 1.93	11	11.53 ± 1.28	18	9.58 ± 1.52	17	10.17 ± 1.81	14	9.36 ± 2.14	10	8.43 ± 1.83	8	9.73 ± 2.08	21	8.75 ± 2.05
Bscl2$^{+/-}$ ♂	-	-	-	-	-	-	9	14.54 ± 3.02	22	10.80 ± 2.25	8	9.44 ± 3.56	18	8.44 ± 2.44^{b,k}	15	9.40 ± 1.67	12	8.75 ± 1.85	14	8.86 ± 2.25^{c}	15	9.50 ± 1.56	21	8.58 ± 1.88
Bscl2$^{-/-}$ ♀	-	-	-	-	-	-	9	21.14 ± 1.62^{a,d,j}	13	16.98 ± 3.17	9	15.14 ± 2.47	11	14.72 ± 1.73^{a,d,j}	12	13.70 ± 2.17	11	13.90 ± 2.57	11	13.14 ± 3.21^{a,d,j}	6	12.62 ± 2.67	11	11.82 ± 2.86
Bscl2$^{-/-}$ ♂	-	-	-	-	-	-	11	21.04 ± 2.62^{a,d,j}	19	18.27 ± 3.06	11	15.86 ± 1.59	14	14.62 ± 1.81^{a,d,j}	11	13.71 ± 2.42	8	11.88 ± 3.55	11	12.66 ± 3.00^{a,d,j}	11	13.02 ± 2.26	15	13.49 ± 2.96

Annex 9. Table S16 and S17. Organ's weight and NAS score evaluations.

Table S16. Weight for liver, heart, spleen and kidneys for wild type, *Bscl2*$^{+/Celia}$, *Bscl2*$^{Celia/Celia}$, *Bscl2*$^{+/-}$, *Bscl2*$^{-/-}$ and severely affected (S.A) animals. Data is presented as n (%) ± SD. Data for liver and spleen were analysed using a Kolmogorov-Smirnov test for normality, followed by a Kruskal-Wallis test with Mann-Whitney post hoc comparisons. Data for heart and kidneys were analysed using a Kolmogorov-Smirnov test for normality, followed by an ANOVA test with T3 Dunnett or Bonferroni post hoc comparisons. [a] $p < 0.05$ vs wild type ♀/♂; [b] $p < 0.05$ vs wild type ♀; [c] $p < 0.05$ vs wild type ♂; [d] $p < 0.05$ vs *Bscl2*$^{+/-}$ ♀/♂; [e] $p < 0.05$ vs *Bscl2*$^{+/-}$ ♀; [f] $p < 0.05$ vs *Bscl2*$^{+/-}$ ♂; [g] $p < 0.05$ vs *Bscl2*$^{-/-}$ ♀/♂; [h] $p < 0.05$ vs *Bscl2*$^{-/-}$ ♀; [i] $p < 0.05$ vs *Bscl2*$^{-/-}$ ♂; [j] $p < 0.05$ vs *Bscl2*$^{+/Celia}$ ♀/♂; [k] $p < 0.05$ vs *Bscl2*$^{+/Celia}$ ♀; [l] $p < 0.05$ vs *Bscl2*$^{+/Celia}$ ♂; [m] $p < 0.05$ vs *Bscl2*$^{Celia/Celia}$ ♀/♂.

		N	Age (months)	Liver (%)	Heart (%)	Spleen (%)	Kidneys (%)
Wild type	♀/♂	33	9.5	3.58 ± 0.64	0.40 ± 0.08	0.26 ± 0.11	1.13 ± 0.20
Bscl2$^{+/Celia}$	♀/♂	43	9.5	3.97 ± 0.53	0.42 ± 0.11	0.30 ± 0.10	1.19 ± 0.18
Bscl2$^{Celia/Celia}$	♀/♂	23	9.3	16.71 ± 3.32[a,d,j]	0.58 ± 0.05[a,d,j]	0.56 ± 0.14[a,d,g,j]	1.52 ± 0.22[a,d,j]
Bscl2$^{+/-}$	♀/♂	46	9.7	3.90 ± 1.43	0.37 ± 0.10	0.29 ± 0.15	1.14 ± 0.25
Bscl2$^{-/-}$	♀/♂	24	9.5	15.15 ± 4.09[a,d,j]	0.59 ± 0.11[a,d,j]	0.48 ± 0.15[a,d,j]	1.50 ± 0.20[a,d,j]
S.A. *Bscl2*$^{+/Celia}$	♀/♂	2	6.1	4.65 ± 0.10[a,d,g,j,m]	0.64 ± 0.20	0.26 ± 0.02[g,m]	1.78 ± 0.19[a,d,j]
S.A. *Bscl2*$^{Celia/Celia}$	♀/♂	2	9.3	7.07 ± 0.76[a,d,g,j,m]	0.62 ± 0.19	0.22	1.76
Wild type	♀	21	9.6	3.59 ± 0.76	0.41 ± 0.08	0.31 ± 0.11	1.09 ± 0.20
	♂	12	9.4	3.57 ± 0.38	0.39 ± 0.07	0.18 ± 0.04[b]	1.18 ± 0.20
Bscl2$^{+/Celia}$	♀	26	9.5	3.95 ± 0.63[c]	0.41 ± 0.11	0.30 ± 0.07[c,f]	1.10 ± 0.14
	♂	17	9.6	4.01 ± 0.35	0.42 ± 0.11	0.29 ± 0.13[c]	1.32 ± 0.16[b,e,k]
Bscl2$^{Celia/Celia}$	♀	13	9.4	16.53 ± 2.89[a,d,j]	0.57 ±0.06[a,d,j]	0.55 ± 0.08[a,d,l,j]	1.41 ± 0.18[b,e,k]
	♂	10	9.1	16.93 ± 3.93[a,d,j]	0.58 ± 0.04[a,d,j]	0.56 ± 0.18[a,d,l,j]	1.66 ± 0.19[a,d,h,j]
Bscl2$^{+/-}$	♀	23	9.8	4.02 ± 2.01[l]	0.35 ± 0.09	0.33 ± 0.16[c,f]	1.00 ± 0.20
	♂	23	9.6	3.78 ± 0.37	0.38 ± 0.10	0.25 ± 0.14[b]	1.27 ± 0.23[e]
Bscl2$^{-/-}$	♀	10	9.5	14.62 ± 4.11[a,d,j]	0.54 ± 0.09[a,d,k]	0.51 ± 0.09[a,d,l,j]	1.38 ± 0.14[b,e,k]
	♂	14	9.5	15.57 ± 4.20[a,d,l]	0.62 ± 0.11[a,d,j]	0.46 ± 0.18[a,d,j]	1.59 ± 0.20[a,d,j]

Table S17. NAS score, fibrosis stage and MASLD evaluation for wild type, *Bscl2*$^{+/Celia}$, *Bscl2*$^{Celia/Celia}$, *Bscl2*$^{+/-}$, *Bscl2*$^{-/-}$ and severely affected (S.A) animals. Data is presented as mean ± SD for NAS score and as percentage (%) of animals with 1a fibrosis stage, MASL (metabolic-dysfunction associated steatotic liver) and MASH (metabolic dysfunction-associated steatohepatitis). Statistical significance for categorical data was assessed using Fisher's exact test. [a] $p < 0.05$ vs wild type ♀/♂; [b] $p < 0.05$ vs wild type ♀; [d] $p < 0.05$ vs *Bscl2*$^{+/-}$ ♀/♂; [e] $p < 0.05$ vs *Bscl2*$^{+/-}$ ♀; [f] $p < 0.05$ vs *Bscl2*$^{+/-}$ ♂; [j] $p < 0.05$ vs *Bscl2*$^{+/Celia}$ ♀/♂; [p] $p < 0.05$ vs S.A. *Bscl2*$^{+/Celia}$ ♀/♂.

		N	Age (months)	NAS score [0-8]	Fibrosis stage (1a)	MASL	MASH
Wild type	♀/♂	29	3.3	0.07 ± 0.26	0%	7%	0%
Bscl2$^{+/Celia}$	♀/♂	27	11.4	0.37 ± 0.88	0%	22%	4%
Bscl2$^{Celia/Celia}$	♀/♂	21	9.1	3.57 ± 2.34[a,d,j,p]	38%[a,d,j]	76%[a,d,j,p]	57%[a,d,j,p]
Bscl2$^{+/-}$	♀/♂	25	6.4	0.24 ± 0.88	0%	8%	4%
Bscl2$^{-/-}$	♀/♂	15	7.0	2.67 ± 2.41[a,d,j]	27%[a,d,j]	67%[a,d,j]	47%[a,d,j]
S.A. *Bscl2*$^{+/Celia}$	♀/♂	5	5.8	0.20 ± 0.45	0%	20%	0%
S.A. *Bscl2*$^{Celia/Celia}$	♀/♂	8	11.1	2.63 ± 1.85[a,d,j,p]	50%[a,d,j]	88%[a,d,j]	25%[a]
Wild type	♀	16	2.7	0.06 ± 0.25	0%	6%	0%
	♂	13	4.1	0.08 ± 0.28	0%	8%	0%
Bscl2$^{+/Celia}$	♀	11	11.3	0.18 ± 0.40	0%	18%	0%
	♂	16	11.5	0.50 ± 1.10	0%	25%	6%
Bscl2$^{Celia/Celia}$	♀	12	11.4	4.00 ± 2.26[a,d,j]	58%[a,d,j]	83%[a,d,j]	67%[a,d,j]
	♂	9	6.0	3.00 ± 2.45[a,d,j]	11%	67%[a,f]	44%[a,f,j]
Bscl2$^{+/-}$	♀	10	5.9	0.60 ± 1.35	0%	20%	10%
	♂	15	6.8	0.00 ± 0.00	0%	0%	0%
Bscl2$^{-/-}$	♀	6	11.7	3.67 ± 2.50[a,d,j]	33%	83%[a,d,j]	67%[a,d,j]
	♂	9	3.9	2.00 ± 2.24[e]	22%	56%[a,f]	33%[b,f]

Annex 10. Table S18 and S19. Renal histopathological analysis.

Table S18. Renal histopathological analysis for wild type, *Bscl2*$^{+/Celia}$, *Bscl2*$^{Celia/Celia}$, *Bscl2*$^{+/-}$, *Bscl2*$^{-/-}$ and severely affected (S.A.) animals. Data is presented as number (N) and percentage (Pct.) (%) of animals with each pattern. Statistical significance for categorical data was assessed using Fisher's exact test. [a] $p < 0.05$ vs wild type ♀/♂; [d] $p < 0.05$ vs *Bscl2*$^{+/-}$ ♀/♂; [g] $p < 0.05$ vs *Bscl2*$^{-/-}$ ♀/♂; [j] $p < 0.05$ vs *Bscl2*$^{+/Celia}$ ♀/♂; [m] $p < 0.05$ vs *Bscl2*$^{Celia/Celia}$ ♀/♂; [p] $p < 0.05$ vs S.A. *Bscl2*$^{+/Celia}$ ♀/♂; [q] $p < 0.05$ vs S.A. *Bscl2*$^{Celia/Celia}$ ♀/♂.

		Wild type		*Bscl2*$^{+/Celia}$		*Bscl2*$^{Celia/Celia}$		*Bscl2*$^{+/-}$		*Bscl2*$^{-/-}$		S.A. *Bscl2*$^{+/Celia}$		S.A. *Bscl2*$^{Celia/Celia}$	
Sex		♀/♂		♀/♂		♀/♂		♀/♂		♀/♂		♀/♂		♀/♂	
N		11		12		12		11		12		6		5	
Age (months)		9.5		9.6		9.4		9.5		9.5		6.6		6.2	
		N	Pct. (%)	N	Pct. (%)	N	Pct. (%)	N	Pct. (%)	N	Pct. (%)	N	Pct. (%)	N	Pct. (%)
Kidney glomerulus	**Focal lesions**	**7**	**64%**	**6**	**50%**	**10**	**83%**	**5**	**45%**	**7**	**58%**	**4**	**67%**	**3**	**60%**
	Mesangial proliferation	2	18%	4	33%	2	17%	2	18%	2	17%	1	17%	2	40%
	Endocapillary proliferation	1	9%	0	0%	2	17%	1	9%	4	33%	1	17%	0	0%
	Focal segmental glomerulosclerosis	1	9%	1	8%	4	33%	0	0%	1	8%	1	17%	0	0%
	Nodular sclerosing lesion	1	9%	0	0%	1	8%	0	0%	0	0%	0	0%	0	0%
	Glomerulomegaly	2	18%	2	17%	1	8%	0	0%	0	0%	1	17%	1	20%
	Inflammatory exudate	0	0%	0	0%	0	0%	2	18%	0	0%	0	0%	0	0%
	Diffuse lesions	**1**	**9%**	**5**	**42%**	**8**	**67%**[a,d]	**1**	**9%**	**11**	**92%**[a,d,j]	**3**	**50%**	**3**	**60%**
	Mesangial proliferation	1	9%	3	25%	8	67%[a,d]	1	9%	10	83%[a,d,j]	3	50%	3	60%
	Endocapillary proliferation	0	0%	2	17%	2	17%	0	0%	0	0%	0	0%	0	0%
	Focal segmental glomerulosclerosis	0	0%	0	0%	0	0%	0	0%	0	0%	0	0%	1	20%
	Nodular sclerosing lesions	0	0%	0	0%	0	0%	0	0%	0	0%	0	0%	0	0%
	Glomerulomegaly	0	0%	0	0%	0	0%	0	0%	0	0%	0	0%	0	0%
	Inflammatory exudate	0	0%	0	0%	0	0%	0	0%	1	8%	0	0%	0	0%
Renal interstitium	**Tubules**	**2**	**18%**	**2**	**17%**	**3**	**25%**	**1**	**9%**	**2**	**17%**	**0**	**0%**	**1**	**20%**
	Normal	9	82%	10	83%	9	75%	10	91%	10	83%	6	100%	4	80%
	Vacuolization	2	18%	2	17%	0	0%	1	9%	0	0%	0	0%	0	0%
	Tubular atrophy	0	0%	0	0%	2	17%	0	0%	2	17%	0	0%	0	0%
	Focal tubulitis	0	0%	0	0%	1	8%	0	0%	0	0%	0	0%	0	0%
	Acute tubular necrosis	0	0%	0	0%	0	0%	0	0%	0	0%	0	0%	1	20%
	Inflammation	**2**	**18%**	**0**	**0%**	**6**	**50%**[j]	**2**	**18%**	**2**	**17%**	**1**	**17%**	**0**	**0%**
	Normal	9	82%	12	100%	6	50%[j]	9	82%	10	83%	5	83%	4	80%
	Mild	2	18%	0	0%	4	33%	2	18%	1	8%	1	17%	0	0%

	Severe	0	0%	0	0%	2	17%	0	0%	1	8%	0	0%	0	0%
Blood vessels	**Pattern**	**3**	**27%**	**2**	**17%**	**8**	**67%**[j]	**4**	**36%**	**10**	**83%**[a,d,j,q]	**2**	**33%**	**1**	**20%**
	Normal	8	73%	10	83%	4	33%[j]	7	64%	2	17%[a,d,j,q]	4	67%	4	80%
	Arteriolar hyalinosis	3	27%	2	17%	8	67%[j]	3	27%	9	75%[a,d,j,p]	1	17%	1	20%
	Arteriolar hypertrophy	0	0%	0	0%	0	0%	1	9%	2	17%	1	17%	0	0%
	Arteriolar lipidization	0	0%	0	0%	1	8%	0	0%	0	0%	0	0%	0	0%
	Non-hyaline thickening	0	0%	0	0%	0	0%	0	0%	0	0%	0	0%	0	0%
Glomerulonephritic patterns	**Pattern**	**7**	**64%**	**9**	**75%**	**12**	**100%**[a]	**5**	**45%**	**12**	**100%**[a]	**5**	**83%**[a]	**5**	**100%**[a]
	Minimal changes diseases	3	27%	3	25%	0	0%	2	18%	1	8%	1	17%	1	20%
	Mild mesangial pattern	2	18%	2	17%	1	8%	2	18%	1	8%	0	0%	0	0%
	Mesangial pattern	0	0%	2	17%	5	42%[a]	1	9%	7	58%[a,d]	3	50%[a]	3	60%[a]
	Focal segmental sclerosis	1	9%	1	8%	2	17%	0	0%	0	0%	0	0%	0	0%
	Endocapillary pattern	1	9%	0	0%	1	8%	0	0%	0	0%	1	17%	0	0%
	Mesangial and endocapillary pattern	0	0%	0	0%	1	8%	0	0%	3	25%	0	0%	0	0%
	Hyperfiltration	0	0%	1	8%	0	0%	0	0%	0	0%	0	0%	1	20%
	Type diabetes	0	0%	0	0%	1	8%	0	0%	0	0%	0	0%	0	0%
	Diffuse sclerosis	0	0%	0	0%	1	8%	0	0%	0	0%	0	0%	0	0%
	Hydronephrosis	0	0%	0	0%	0	0%	0	0%	1	8%	0	0%	0	0%
	No significant changes	4	36%[g,m]	3	25%	0	0%	6	55%[g,m,p]	0	0%	0	0%	0	0%

Table S19. Renal histopathological analysis for wild type, *Bscl2*$^{+/Celia}$, *Bscl2*$^{Celia/Celia}$, *Bscl2*$^{+/-}$ and *Bscl2*$^{-/-}$ animals separated by sex. Data is presented as number (N) and percentage (Pct.) (%) of animals with each pattern. Statistical significance for categorical data was assessed using Fisher's exact test. [b] $p < 0.05$ vs wild type ♀; [c] $p < 0.05$ vs wild type ♂; [e] $p < 0.05$ vs *Bscl2*$^{+/-}$ ♀; [f] $p < 0.05$ vs *Bscl2*$^{+/-}$ ♂; [h] $p < 0.05$ vs *Bscl2*$^{-/-}$ ♀; [j] $p < 0.05$ vs *Bscl2*$^{+/Celia}$ ♀/♂.

		Wild type				*Bscl2*$^{+/Celia}$				*Bscl2*$^{Celia/Celia}$				*Bscl2*$^{+/-}$				*Bscl2*$^{-/-}$			
Sex		♀		♂		♀		♂		♀		♂		♀		♂		♀		♂	
N		5		6		6		6		6		6		6		5		6		6	
Age (months)		9.4		9.5		9.6		9.6		9.4		9.4		9.5		9.5		9.5		9.5	
		N	Pct. (%)	N	Pct. (%)	N	Pct. (%)	N	Pct. (%)	N	Pct. (%)	N	Pct. (%)	N	Pct. (%)	N	Pct. (%)	N	Pct. (%)	N	Pct. (%)
Kidney glomerulus	**Focal lesions**	**2**	**40%**	**5**	**83%**	**2**	**33%**	**4**	**67%**	**6**	**100%**[e]	**4**	**67%**	**1**	**17%**	**4**	**80%**	**4**	**67%**[b,f]	**3**	**50%**[b,f]
	Mesangial proliferation	1	20%	1	17%	0	0%	4	67%	1	17%	1	17%	0	0%	2	40%	1	17%[b,f]	1	17%[b,f]
	Endocapillary proliferation	0	0%	1	17%	0	0%	0	0%	2	33%	0	0%	0	0%	1	20%	3	50%	1	17%
	Focal segmental glomerulosclerosis	0	0%	1	17%	1	17%	0	0%	1	17%	3	50%	0	0%	0	0%	0	0%	1	17%
	Nodular sclerosing lesion	0	0%	1	17%	0	0%	0	0%	1	17%	0	0%	0	0%	0	0%	0	0%	0	0%
	Glomerulomegaly	1	20%	1	17%	1	17%	1	17%	1	17%	0	0%	0	0%	0	0%	0	0%	0	0%
	Inflammatory exudate	0	0%	0	0%	0	0%	0	0%	0	0%	0	0%	1	17%	1	20%	0	0%	0	0%
	Diffuse lesions	**0**	**0%**	**1**	**17%**	**3**	**50%**	**2**	**33%**	**4**	**67%**	**4**	**67%**	**1**	**17%**	**0**	**0%**	**6**	**100%**[c]	**5**	**83%**
	Mesangial proliferation	0	0%	1	17%	2	33%	1	17%	4	67%	4	67%	1	17%	0	0%	5	83%	5	83%
	Endocapillary proliferation	0	0%	0	0%	1	17%	1	17%	0	0%	2	33%	0	0%	0	0%	0	0%	0	0%
	Focal segmental glomerulosclerosis	0	0%	0	0%	0	0%	0	0%	0	0%	0	0%	0	0%	0	0%	0	0%	0	0%
	Nodular sclerosing lesions	0	0%	0	0%	0	0%	0	0%	0	0%	0	0%	0	0%	0	0%	0	0%	0	0%
	Glomerulomegaly	0	0%	0	0%	0	0%	0	0%	0	0%	0	0%	0	0%	0	0%	0	0%	0	0%
	Inflammatory exudate	0	0%	0	0%	0	0%	0	0%	0	0%	0	0%	0	0%	0	0%	1	17%	0	0%
Renal interstitium	**Tubules**	**0**	**0%**	**2**	**33%**	**0**	**0%**	**2**	**33%**	**0**	**0%**	**3**	**50%**	**1**	**17%**	**0**	**0%**	**1**	**17%**	**1**	**17%**
	Normal	5	100%	4	67%	6	100%	4	67%	6	100%	3	50%	5	83%	5	100%	5	83%	5	83%
	Vacuolization	0	0%	2	33%	0	0%	2	33%	0	0%	0	0%	1	17%	0	0%	0	0%	0	0%
	Tubular atrophy	0	0%	0	0%	0	0%	0	0%	0	0%	2	33%	0	0%	0	0%	1	17%	1	17%
	Focal tubulitis	0	0%	0	0%	0	0%	0	0%	0	0%	1	17%	0	0%	0	0%	0	0%	0	0%
	Acute tubular necrosis	0	0%	0	0%	0	0%	0	0%	0	0%	0	0%	0	0%	0	0%	0	0%	0	0%
	Inflammation	**0**	**0%**	**2**	**33%**	**0**	**0%**	**0**	**0%**	**1**	**17%**	**5**	**83%**[b,f,j]	**2**	**33%**	**0**	**0%**	**1**	**17%**	**1**	**17%**
	Normal	5	100%	4	67%	6	100%	6	100%	5	83%	1	17%[b,f,j]	4	67%	5	100%	5	83%	5	83%
	Mild	0	0%	2	33%	0	0%	0	0%	1	17%	3	50%	2	33%	0	0%	1	17%	0	0%
	Severe	0	0%	0	0%	0	0%	0	0%	0	0%	2	33%	0	0%	0	0%	0	0%	1	17%
Blood vessels	**Pattern**	**1**	**20%**	**2**	**33%**	**1**	**17%**	**1**	**17%**	**4**	**67%**	**4**	**67%**	**1**	**17%**	**3**	**60%**	**6**	**100%**[b,e,j]	**4**	**67%**
	Normal	4	80%[h]	4	67%	5	83%[h]	5	83%[h]	2	33%	2	33%	5	83%[h]	2	40%	0	0%	2	33%
	Arteriolar hyalinosis	1	20%	2	33%	1	17%	1	17%	4	67%	4	67%	0	0%	3	60%	6	100%[b,e,j]	3	50%

	Arteriolar hypertrophy	0	0%	0	0%	0	0%	0	0%	0	0%	0	0%	1	17%	0	0%	0	0%	2	33%
	Arteriolar lipidization	0	0%	0	0%	0	0%	0	0%	0	0%	1	17%	0	0%	0	0%	0	0%	0	0%
	Non-hyaline thickening	0	0%	0	0%	0	0%	0	0%	0	0%	0	0%	0	0%	0	0%	0	0%	0	0%
Glomerulonephritic patterns	**Pattern**	**3**	**60%**	**4**	**67%**	**3**	**50%**	**6**	**100%**	**6**	**100%**	**6**	**100%**	**2**	**33%**	**3**	**60%**	**6**	**100%**[b]	**6**	**100%**[c,f]
	Minimal changes diseases	2	40%	1	17%	1	17%	2	33%	0	0%	0	0%	1	17%	1	20%	0	0%	1	17%
	Mild mesangial pattern	1	20%	1	17%	0	0%	2	33%	1	17%	0	0%	0	0%	2	40%	1	17%	0	0%
	Mesangial pattern	0	0%	0	0%	1	17%	1	17%	3	50%	2	33%	1	17%	0	0%	2	33%[b]	5	83%[c,f]
	Focal segmental sclerosis	0	0%	1	17%	1	17%	0	0%	0	0%	2	33%	0	0%	0	0%	0	0%	0	0%
	Endocapillary pattern	0	0%	1	17%	0	0%	0	0%	0	0%	1	17%	0	0%	0	0%	0	0%	0	0%
	Mesangial and endocapillary pattern	0	0%	0	0%	0	0%	0	0%	1	17%	0	0%	0	0%	0	0%	3	50%	0	0%
	Hyperfiltration	0	0%	0	0%	0	0%	1	17%	0	0%	0	0%	0	0%	0	0%	0	0%	0	0%
	Type diabetes	0	0%	0	0%	0	0%	0	0%	0	0%	1	17%	0	0%	0	0%	0	0%	0	0%
	Diffuse sclerosis	0	0%	0	0%	0	0%	0	0%	1	17%	0	0%	0	0%	0	0%	0	0%	0	0%
	Hydronephrosis	0	0%	0	0%	0	0%	0	0%	0	0%	0	0%	0	0%	0	0%	0	0%	1	17%
	No significant changes	2	40%	2	33%	3	50%	0	0%	0	0%	0	0%	4	67%	2	40%	0	0%	0	0%

Annex 11. Table S20. Glucose tolerance test and Insulin tolerance test.

Table S20. Glucose tolerance test (GTT) and Insulin tolerance test (ITT) for wild type, *Bscl2*$^{+/Celia}$, *Bscl2*$^{Celia/Celia}$, *Bscl2*$^{+/-}$ and *Bscl2*$^{-/-}$ animals. Both tests were measure as evolution of glucose concentration over time (minutes) and area under the curve (AUC). Data is presented as mean ± SD. Data were analysed using a Kolmogorov-Smirnov test for normality, followed by a Kruskal-Wallis test with Mann-Whitney post hoc comparisons. [a] $p < 0.05$ vs wild type ♀/♂; [b] $p < 0.05$ vs wild type ♀; [c] $p < 0.05$ vs wild type ♂; [d] $p < 0.05$ vs *Bscl2*$^{+/-}$ ♀/♂; [e] $p < 0.05$ vs *Bscl2*$^{+/-}$ ♀; [i] $p < 0.05$ vs *Bscl2*$^{-/-}$ ♂; [j] $p < 0.05$ vs *Bscl2*$^{+/Celia}$ ♀/♂; [k] $p < 0.05$ vs *Bscl2*$^{+/Celia}$ ♀.

		N	Age (months)	0 min Glucose (mg/dL)	15 min Glucose (mg/dL)	30 min Glucose (mg/dL)	60 min Glucose (mg/dL)	90 min Glucose (mg/dL)	120 min Glucose (mg/dL)	AUC (mg/dLxmin)
						GTT				
Wild type	♀/♂	23	3.0	103.24 ± 10.05	306.02 ± 41.21	278.54 ± 55.98	195.50 ± 44.70	147.48 ± 27.68	128.09 ± 23.44	23842.50 ± 3767.38
Bscl2$^{+/Celia}$	♀/♂	20	3.1	105.40 ± 11.77	339.80 ± 44.23	302.00 ± 58.29	196.58 ± 68.36	148.83 ± 37.66	121.53 ± 25.82	24867.38 ± 4948.69
Bscl2$^{Celia/Celia}$	♀/♂	29	3.1	120.26 ± 30.20	289.07 ± 60.63	294.53 ± 71.29	203.14 ± 75.77	158.10 ± 56.38	140.05 ± 47.35	24803.02 ± 5910.37
Bscl2$^{+/-}$	♀/♂	24	3.1	111.50 ± 17.74	311.98 ± 32.78	272.31 ± 64.66	187.75 ± 49.66	153.56 ± 38.12	127.96 ± 29.84	23801.72 ± 4277.86
Bscl2$^{-/-}$	♀/♂	24	3.1	128.10 ± 26.03	286.58 ± 58.50	306.29 ± 76.20	212.40 ± 87.96	174.44 ± 64.30	148.73 ± 52.23	25987.03 ± 7032.75
Wild type	♀	12	3.0	103.63 ± 11.62	299.13 ± 44.42	247.71 ± 38.29	167.21 ± 30.46	129.79 ± 18.83	111.79 ± 15.98	21424.38 ± 2210.13[c]
	♂	11	3.1	102.82 ± 8.56	313.55 ± 38.02	312.18 ± 53.82	226.36 ± 36.98	166.77 ± 22.59	145.86 ± 16.18	26480.45 ± 3343.70
Bscl2$^{+/Celia}$	♀	10	3.0	100.40 ± 10.63	341.95 ± 29.60	269.45 ± 39.11	152.70 ± 24.92	121.25 ± 18.45	104.50 ± 12.74	21730.88 ± 2214.56[c]
	♂	10	3.1	110.40 ± 11.12	337.65 ± 56.95	334.55 ± 57.35	240.45 ± 70.47	176.40 ± 31.05	138.55 ± 24.51	28003.88 ± 4993.44[b,e,k]
Bscl2$^{Celia/Celia}$	♀	16	3.1	134.06 ± 33.86	307.22 ± 44.10	313.00 ± 73.64	209.31 ± 72.31	157.59 ± 50.90	138.53 ± 28.94	25741.41 ± 5695.55[b,e,k]
	♂	13	3.1	103.27 ± 11.35	266.73 ± 71.89	271.81 ± 63.75	195.54 ± 82.15	158.73 ± 64.64	141.92 ± 64.63	23648.08 ± 6192.00
Bscl2$^{+/-}$	♀	12	3.1	107.42 ± 13.96	320.88 ± 36.10	224.71 ± 33.46	150.63 ± 21.53	124.83 ± 16.96	108.21 ± 9.99	20561.56 ± 1888.14[c]
	♂	12	3.1	115.58 ± 20.65	303.08 ± 27.76	319.92 ± 51.76	224.88 ± 41.07	182.29 ± 30.82	147.71 ± 30.18	27041.88 ± 3434.04[b,e,k]
Bscl2$^{-/-}$	♀	10	3.0	133.65 ± 31.95	307.05 ± 42.54	335.90 ± 78.86	221.95 ± 112.58	183.60 ± 87.63	144.85 ± 53.90	27505.13 ± 8592.11[b,e]
	♂	14	3.2	124.14 ± 21.24	271.96 ± 65.19	285.14 ± 69.36	205.57 ± 69.23	167.89 ± 43.45	151.50 ± 54.61	24902.68 ± 5775.57[b,e,k]

				ITT						
Wild type	♀/♂	23	3.4	161.00 ± 24.24	100.87 ± 20.86	87.28 ± 17.03	78.39 ± 20.67	80.50 ± 25.14	93.41 ± 25.48	10852.34 ± 2348.67
Bscl2$^{+/Celia}$	♀/♂	20	3.5	152.83 ± 12.27	101.18 ± 20.68	86.65 ± 16.02	73.83 ± 23.22	80.83 ± 28.74	94.60 ± 31.37	10671.94 ± 2487.96
Bscl2$^{Celia/Celia}$	♀/♂	29	3.4	159.48 ± 49.94	180.45 ± 47.42	154.14 ± 46.83	132.07 ± 40.49	135.81 ± 34.24	137.12 ± 45.07	17464.14 ± 4539.48[a,d,j]
Bscl2$^{+/-}$	♀/♂	24	3.4	173.65 ± 19.90	122.10 ± 35.12	98.00 ± 19.92	89.29 ± 24.70	95.40 ± 32.23	107.46 ± 35.95	12491.41 ± 3038.38[a]
Bscl2$^{-/-}$	♀/♂	24	3.4	178.21 ± 49.97	210.40 ± 69.23	183.52 ± 80.16	163.17 ± 63.38	161.15 ± 51.24	155.63 ± 52.36	20685.47 ± 7116.31[a,d,j]
Wild type	♀	12	3.4	151.04 ± 17.58	88.42 ± 9.21	74.58 ± 8.44	63.58 ± 9.10	62.33 ± 8.91	74.67 ± 10.64	9034.69 ± 748.96
	♂	11	3.3	171.86 ± 26.53	114.45 ± 21.80	101.14 ± 12.44	94.55 ± 17.27	100.32 ± 21.79	113.86 ± 20.55	12835.23 ± 1796.95[b]
Bscl2$^{+/Celia}$	♀	10	3.4	146.75 ± 6.82	89.90 ± 12.59	77.60 ± 15.56	55.70 ± 12.98	58.55 ± 9.90	72.60 ± 9.73	8711.63 ± 1183.22
	♂	10	3.5	158.90 ± 13.77	112.45 ± 21.49	95.70 ± 10.84	91.95 ± 15.47	103.10 ± 23.32	116.60 ± 30.11	12632.25 ± 1768.64[b,k]
Bscl2$^{Celia/Celia}$	♀	16	3.4	171.41 ± 56.04	200.63 ± 38.24	153.94 ± 30.68	131.16 ± 18.61	138.59 ± 21.44	140.13 ± 32.71	17952.89 ± 2668.49[a,d,i,j]
	♂	13	3.4	144.81 ± 38.34	155.62 ± 47.00	154.38 ± 62.77	133.19 ± 58.22	132.38 ± 46.25	133.42 ± 58.10	16862.60 ± 6202.51[a,e,i,j]
Bscl2$^{+/-}$	♀	12	3.5	160.29 ± 16.15	97.33 ± 8.41	82.33 ± 8.86	70.75 ± 16.50	69.58 ± 15.47	79.54 ± 22.75	9917.81 ± 1316.96[c,j]
	♂	12	3.4	187.00 ± 13.34	146.88 ± 34.20	113.67 ± 14.69	107.83 ± 15.90	121.21 ± 21.88	135.38 ± 22.02	15065.00 ± 1765.58[a,e,i,j]
Bscl2$^{-/-}$	♀	10	3.3	151.80 ± 26.05	176.50 ± 68.48	138.25 ± 43.82	132.55 ± 35.04	133.95 ± 30.03	132.55 ± 44.10	16879.88 ± 4580.44[a,e,i,j]
	♂	14	3.5	197.07 ± 55.02	234.61 ± 60.99	215.86 ± 85.66	185.04 ± 70.86	180.57 ± 55.18	172.11 ± 52.93	23403.75 ± 7481.60[a,e,j]

Annex 12. Table S21 and S22. Metabolic measurements.

Measurements for triglycerides, insulin, leptin and VetScan VS2 profile: alanine aminotransferase (ALT), albumin (ALB), alkaline phosphatase (ALP), amylase (AMY) total calcium (CA^{++}), creatinine (CRE), globulin (GLOB), phosphorus (PHOS), potassium (K^{+}), sodium (NA^{+}), total bilirubin (TBIL), total protein (TP), and urea nitrogen (BUN).

Table S21. Metabolic measurements for wild type, *Bscl2*$^{+/Celia}$, *Bscl2*$^{Celia/Celia}$, *Bscl2*$^{+/-}$, *Bscl2*$^{-/-}$ and severely affected (S.A.) animals. Data is presented as mean ± SD. Data were analysed using a Kolmogorov-Smirnov test for normality, followed by a Kruskal-Wallis test with Mann-Whitney post hoc comparisons. [a] $p < 0.05$ vs wild type ♀/♂; [d] $p < 0.05$ vs *Bscl2*$^{+/-}$ ♀/♂; [g] $p < 0.05$ vs *Bscl2*$^{-/-}$ ♀/♂; [j] $p < 0.05$ vs *Bscl2*$^{+/Celia}$ ♀/♂; [m] $p < 0.05$ vs *Bscl2*$^{Celia/Celia}$ ♀/♂; [q] $p < 0.05$ vs S.A. *Bscl2*$^{Celia/Celia}$ ♀/♂.

			Wild type	*Bscl2*$^{+/Celia}$	*Bscl2*$^{Celia/Celia}$	*Bscl2*$^{+/-}$	*Bscl2*$^{-/-}$	S.A. *Bscl2*$^{+/Celia}$	S.A. *Bscl2*$^{Celia/Celia}$
		Sex	♀/♂	♀/♂	♀/♂	♀/♂	♀/♂	♀/♂	♀/♂
Triglycerides	Serum	N	21	21	25	24	24	4	3
		Age (months)	4.1	4.0	4.1	4.1	4.1	4.3	4.1
		[mg/dL]	76.81 ± 15.03	83.15 ± 15.92	38.49 ± 19.70[a,d,j]	72.37 ± 16.95[j]	39.84 ± 21.58[a,d,j]	63.81 ± 17.44[g]	51.52 ± 24.51
		N	29	36	23	36	22	2	2
		Age (months)	9.5	9.5	9.4	9.6	9.5	9.3	6.1
		[mg/dL]	82.45 ± 14.96	89.76 ± 21.09	125.81 ± 71.87	86.90 ± 24.51	104.15 ± 42.21	53.77 ± 52.87	52.56 ± 7.28[a,m]
	Liver	N	20	20	20	19	20	1	2
		Age (months)	9.5	9.6	9.3	9.5	9.5	6.8	9.3
		[mg/g liver]	7.52 ± 2.70	8.48 ± 2.34	18.06 ± 5.86[a,d,j]	9.55 ± 4.04	21.06 ± 5.65[a,d,j]	8.33	4.84 ± 3.93[g,m]
Insulin		N	18	18	18	17	18	-	2
		Age (months)	9.5	9.5	9.4	9.5	9.5	-	9.3
		[ng/mL]	0.83 ± 0.65	1.19 ± 0.72	14.21 ± 10.49[a,d,j]	0.92 ± 0.54	12.23 ± 7.91[a,d,j]	-	2.53 ± 1.86[g]
Leptin		N	16	16	16	16	16	1	2
		Age (months)	9.5	9.5	9.2	9.7	9.5	6.8	9.3
		[ng/mL]	19.30 ± 8.80[q]	9.68 ± 9.44[a,q]	0.01 ± 0.05[a,d,j]	14.18 ± 11.18[q]	0.26 ± 0.49[a,d,j]	0.00	0.00 ± 0.00

VetScan VS2 Profile	N	12	12	12	12	12	-	1
	Age (months)	9.5	9.6	9.4	9.5	9.5	-	9.3
	ALB (g/dL)	4.88 ± 0.27	4.84 ± 0.13	6.14 ± 0.12[a,d,j]	4.92 ± 0.16	6.13 ± 0.38[a,d,j]	-	5.10
	ALP (U/L)	68.33 ± 19.44	68.75 ± 19.23	215.17 ± 21.53[a,d,j]	68.75 ± 19.42	185.50 ± 50.36[a,d,j]	-	98.00
	ALT (U/L)	27.75 ± 7.53	48.17 ± 60.18	487.17 ± 144.63[a,d,j]	30.42 ± 5.53	463.83 ± 213.92[a,d,j]	-	78.00
	AMY (U/L)	1222.00 ± 250.74	1299.50 ± 327.27	1765.42 ± 257.79[a,d,j]	1101.58 ± 114.49	1895.00 ± 373.62[a,d,j]	-	1379.00
	TBIL (mg/dL)	0.29 ± 0.03	0.28 ± 0.06	0.28 ± 0.04	0.28 ± 0.06	0.25 ± 0.07	-	0.30
	BUN (mg/dL)	26.92 ± 5.57	25.00 ± 4.45	37.00 ± 5.19[a,d,j]	22.17 ± 2.59	35.17 ± 5.20[a,d,j]	-	37.00
	CA^{++} (mg/dL)	11.29 ± 0.38	11.66 ± 0.33[a]	13.79 ± 0.51[a,d,j]	11.63 ± 0.29[a]	13.39 ± 0.92[a,d,j]	-	12.10
	PHOS (mg/dL)	10.83 ± 0.89	11.08 ± 0.73	11.33 ± 1.84	11.49 ± 0.68	12.66 ± 1.63[a]	-	14.10
	CRE (mg/dL)	0.27 ± 0.12	0.28 ± 0.12	0.24 ± 0.08	0.23 ± 0.08	0.30 ± 0.13	-	0.20
	GLU (mg/dL)	191.25 ± 55.91	194.83 ± 48.88	318.92 ± 53.14[a,d,j]	229.42 ± 61.64	265.17 ± 56.11[a,j]	-	209.00
	Na^{+} (mmol/L)	159.75 ± 1.48	159.42 ± 1.56	161.92 ± 2.50	159.83 ± 1.90	161.67 ± 3.06	-	164.00
	K^{+} (mmol/L)	8.46 ± 0.10	8.48 ± 0.04	8.50 ± 0.00	8.50 ± 0.00	8.50 ± 0.00	-	8.50
	TP (g/dL)	6.32 ± 0.30	6.47 ± 0.21	8.72 ± 0.39[a,d,j]	6.40 ± 0.16	8.64 ± 0.67[a,d,j]	-	6.30
	GLOB (g/dL)	1.43 ± 0.14	1.62 ± 0.25[a]	2.59 ± 0.33[a,d,j]	1.48 ± 0.18	2.53 ± 0.43[a,d,j]	-	1.20

Table S22. Metabolic measurements for wild type, *Bscl2*$^{+/Celia}$, *Bscl2*$^{Celia/Celia}$, *Bscl2*$^{+/-}$ and *Bscl2*$^{-/-}$ mice separated by sex. Data is presented as mean ± SD. Data were analysed using a Kolmogorov-Smirnov test for normality, followed by a Kruskal-Wallis test with Mann-Whitney post hoc comparisons. [a] $p < 0.05$ vs wild type ♀/♂; [b] $p < 0.05$ vs wild type ♀; [c] $p < 0.05$ vs wild type ♂; [d] $p < 0.05$ vs *Bscl2*$^{+/-}$ ♀/♂; [e] $p < 0.05$ vs *Bscl2*$^{+/-}$ ♀; [f] $p < 0.05$ vs *Bscl2*$^{+/-}$ ♂; [g] $p < 0.05$ vs *Bscl2*$^{-/-}$ ♀/♂; [h] $p < 0.05$ vs *Bscl2*$^{-/-}$ ♀; [i] $p < 0.05$ vs *Bscl2*$^{-/-}$ ♂; [j] $p < 0.05$ vs *Bscl2*$^{+/Celia}$ ♀/♂; [k] $p < 0.05$ vs *Bscl2*$^{+/Celia}$ ♀; [l] $p < 0.05$ vs *Bscl2*$^{+/Celia}$ ♂; [m] $p < 0.05$ vs *Bscl2*$^{Celia/Celia}$ ♀/♂; [n] $p < 0.05$ vs *Bscl2*$^{Celia/Celia}$ ♀ and [o] $p < 0.05$ vs *Bscl2*$^{Celia/Celia}$ ♂.

			Wild type		*Bscl2*$^{+/Celia}$		*Bscl2*$^{Celia/Celia}$		*Bscl2*$^{+/-}$		*Bscl2*$^{-/-}$	
		Sex	♀	♂	♀	♂	♀	♂	♀	♂	♀	♂
Tryglicerides	Serum	N	11	10	12	9	15	10	12	12	10	14
		Age (months)	4.0	4.2	3.9	4.0	4.0	4.1	4.0	4.1	4.1	4.2
		[mg/dL]	74.50 ± 12.34	79.36 ± 17.86	88.54 ± 17.05[b]	75.97 ± 11.50	38.91 ± 19.42[a,d,j]	37.87 ± 21.15[a,d,j]	70.22 ± 20.51[k]	74.53 ± 13.03	27.62 ± 13.25[a,d,j]	48.56 ± 22.48[a,d,h,j]
		N	19	10	23	13	13	10	18	18	10	12
		Age (months)	9.6	9.5	9.5	9.6	9.4	9.4	9.7	9.6	9.5	9.5
		[mg/dL]	80.00 ± 13.91	87.10 ± 16.52	89.89 ± 20.32	89.54 ± 23.24	130.28 ± 77.18	120.0 ± 68.00	90.44 ± 20.22	83.35 ± 28.31	84.64 ± 36.19	120.41 ± 41.18
	Liver	N	10	10	10	10	10	10	9	10	10	10
		Age (months)	9.5	9.5	9.6	9.6	9.4	9.1	9.6	9.4	9.5	9.5
		[mg/g liver]	8.91 ± 2.83[c]	6.12 ± 1.74	9.77 ± 2.30[c]	7.20 ± 1.62[k]	17.65 ± 7.56[a,d,j]	18.46 ± 3.89[a,d,i,j]	9.01 ± 3.65	10.04 ± 4.50[c]	18.25 ± 4.37[a,d,i,j]	23.88 ± 5.53[a,d,j]
Insulin		N	9	9	9	9	9	9	8	9	9	9
		Age (months)	9.5	9.5	9.5	9.6	9.4	9.4	9.6	9.4	9.5	9.5
		[ng/mL]	0.64 ± 0.42	1.02 ± 0.80	0.87 ± 0.48	1.51 ± 0.80[c,e]	19.17 ± 11.73[a,d,i,j]	9.26 ± 6.40[a,d,j]	0.64 ± 0.31	1.16 ± 0.60[c,e]	16.50 ± 9.11[a,d,i,j]	7.95 ± 2.96[a,d]
Leptin		N	8	8	8	8	8	8	8	8	8	8
		Age (months)	9.6	9.4	9.5	9.5	9.5	9.0	9.8	9.7	9.5	9.5
		[ng/mL]	20.11 ± 12.03	18.49 ± 4.45	13.79 ± 10.86	5.57 ± 5.87[a,e]	0.02 ± 0.07[a,d,j]	0.00 ± 0.00[a,d,j]	20.07 ± 11.69	8.29 ± 7.19[c]	0.15 ± 0.29[a,d,j]	0.37 ± 0.63[a,d,j]

VetScan VS2 Profile	N	6	6	6	6	6	6	6	6	6	6
	Age (months)	9.4	9.5	9.5	9.6	9.4	9.5	9.5	9.5	9.5	9.5
	ALB (g/dL)	4.95 ± 0.33	4.82 ± 0.19	4.88 ± 0.13	4.80 ± 0.13	6.20 ± 0.13[a,d,j]	6.08 ± 0.10[a,d,j]	4.87 ± 0.08	4.97 ± 0.21	6.25 ± 0.19[a,d,j]	6.02 ± 0.51[a,d,j]
	ALP (U/L)	85.17 ± 10.30	51.50 ± 6.72[b]	83.00 ± 16.65[c]	54.50 ± 7.01[b,e,k]	220.17 ± 21.99[a,d,j]	210.17 ± 21.82[a,d,j]	82.33 ± 17.82[c]	55.17 ± 8.33[b,e,k]	164.83 ± 63.42[a,d]	206.17 ± 23.04[a,d]
	ALT (U/L)	25.67 ± 5.32	29.83 ± 9.28	63.33 ± 85.61	33.00 ± 9.27	549.50 ± 150.69[a,d,j]	424.83 ± 118.27[a,d,j]	29.50 ± 3.83	31.33 ± 7.12	358.83 ± 186.19[a,d,j]	568.83 ± 198.86[a,d,j]
	AMY (U/L)	1067.67 ± 222.03	1376.33 ± 178.47	1317.67 ± 477.92	1281.33 ± 80.24	1672.00 ± 121.92[a,d,l]	1858.83 ± 332.26[a,d,l,n]	1024.50 ± 76.23	1178.67 ± 93.64	1712.00 ± 127.78	2078.00 ± 458.70
	TBIL (mg/dL)	0.30 ± 0.00	0.28 ± 0.04	0.27 ± 0.08	0.30 ± 0.00	0.28 ± 0.04	0.28 ± 0.04	0.30 ± 0.00	0.27 ± 0.08	0.22 ± 0.08	0.28 ± 0.04
	BUN (mg/dL)	26.00 ± 4.73	27.83 ± 6.62	22.33 ± 4.18	27.67 ± 3.01	38.17 ± 5.53[a,d,j]	35.83 ± 5.04[b,d,k]	22.00 ± 2.90	22.33 ± 2.50	35.33 ± 4.32[d,k]	35.00 ± 6.39[d,k]
	CA^{++} (mg/dL)	11.43 ± 0.29	11.15 ± 0.44	11.57 ± 0.39	11.75 ± 0.27[c]	14.00 ± 0.52[b,d,j]	13.58 ± 0.44[b,d,j]	11.47 ± 0.20	11.80 ± 0.28[c,e]	13.47 ± 1.14[b,d,j]	13.32 ± 0.75[b,d,j]
	PHOS (mg/dL)	11.13 ± 0.64	10.52 ± 1.05	10.87 ± 0.82	11.28 ± 0.63	12.02 ± 2.09	10.65 ± 1.40	11.17 ± 0.47	11.82 ± 0.75	13.53 ± 1.72[a,e,k,o]	11.78 ± 1.03
	CRE (mg/dL)	0.25 ± 0.12	0.28 ± 0.12	0.27 ± 0.08	0.30 ± 0.15	0.22 ± 0.04	0.27 ± 0.10	0.23 ± 0.08	0.23 ± 0.08	0.28 ± 0.13	0.32 ± 0.15
	GLU (mg/dL)	165.83 ± 53.65	216.67 ± 49.48	172.33 ± 39.14	217.33 ± 50.09	348.50 ± 51.13[a,e,j]	289.33 ± 38.69[b]	192.17 ± 49.97	266.67 ± 50.32[b]	260.83 ± 65.58	269.50 ± 50.80[b]
	Na^{+} (mmol/L)	160.00 ± 1.10	159.50 ± 1.87	159.17 ± 1.60	159.67± 1.63	161.67 ± 1.37[b,e,k]	162.17 ± 3.43[e]	158.33 ± 1.03[b]	161.33 ± 1.21[e,k]	161.67 ± 3.33	161.67 ± 3.08[e]
	K^{+} (mmol/L)	8.50 ± 0.00	8.42 ± 0.13	8.48 ± 0.04	8.48 ± 0.04	8.50 ± 0.00	8.50 ± 0.00	8.50 ± 0.00	8.50 ± 0.00	8.50 ± 0.00	8.50 ± 0.00
	TP (g/dL)	6.33 ± 0.29	6.30 ± 0.34	6.37 ± 0.19	6.57 ± 0.19[e]	8.98 ± 0.27[a,d,j]	8.45 ± 0.31[a,d,j,n]	6.30 ± 0.06	6.50 ± 0.17	8.65 ± 0.64[a,d,j]	8.63 ± 0.76[a,d,j]
	GLOB (g/dL)	1.40 ± 0.09	1.47 ± 0.18	1.48 ± 0.24	1.75 ± 0.20[e]	2.83 ± 0.19[a,d,j]	2.35 ± 0.24[a,d,j]	1.42 ± 0.08	1.55 ± 0.23	2.40 ± 0.51[a,d,j,n]	2.65 ± 0.33[a,d,j]

Annex 13. Table S23 and S24. Hematological measurements.

Parameters from BC5000-Vet analyser: White Blood Cells (WBC), Lymphocytes (Lym %; Lym 10^9/L), Monocyte (Mon %, Mon 10^9/L), Neutrophils (Neu %, Neu 10^9/L), Basophils (Bas %, Bas 10^9/L), Eosinophils (Eos %, Eos 10^9/L), Red Blood Cells (RBC), Hemoglobin (HGB), Hematocrit (HCT), Mean corpuscular volume (MCV), Mean corpuscular hemoglobin (MCH), Mean corpuscular hemoglobin concentration (MCHC), Red cell distribution width: coefficient of variation (RDW-CV), Red cell distribution width: standard deviation (RDW-SD), Platelet (PLT), Mean platelet volume (MPV), Platelet distribution width (PDW), Plateletcrit (PCT).

Table S23. Hematological measurements for wild type, *Bscl2*$^{+/Celia}$, *Bscl2*$^{Celia/Celia}$, *Bscl2*$^{+/-}$, *Bscl2*$^{-/-}$ and severely affected (S.A.) animals. Data is presented as mean ± SD or n (%) ± SD. Data were analysed using a Kolmogorov-Smirnov test for normality, followed by a Kruskal-Wallis test with Mann-Whitney post hoc comparisons. $^{a}p < 0.05$ vs wild type ♀/♂; $^{d}p < 0.05$ vs *Bscl2*$^{+/-}$ ♀/♂; $^{g}p < 0.05$ vs *Bscl2*$^{-/-}$ ♀/♂; $^{j}p < 0.05$ vs *Bscl2*$^{+/Celia}$ ♀/♂; $^{m}p < 0.05$ vs *Bscl2*$^{Celia/Celia}$ ♀/♂.

	Wild type	*Bscl2*$^{+/Celia}$	*Bscl2*$^{Celia/Celia}$	*Bscl2*$^{+/-}$	*Bscl2*$^{-/-}$	S.A. *Bscl2*$^{+/Celia}$	S.A. *Bscl2*$^{Celia/Celia}$
Sex	♀/♂	♀/♂	♀/♂	♀/♂	♀/♂	♀/♂	♀/♂
N	21	23	25	26	23	2	3
Age (months)	5.1	5	5.1	5.1	5.4	4.9	5.1
WBC (10^9/L)	6.19 ± 1.84	6.10 ± 2,37	8.73 ± 2.71^{a,d,j}	6.90 ± 3.41	8.28 ± 3.09^{a,d,j}	7.81 ± 4.35	9.02 ± 3.58
Neu (10^9/L)	1.13 ± 0.40	0.85 ± 0.42^{a}	1.07 ± 0.77	1.21 ± 0.82	1.28 ± 0.60^{d,j}	1.29 ± 0.27	1.64 ± 1.51
Lym (10^9/L)	4.73 ± 1.58	4.99 ± 1.85	7.54 ± 2.60^{a,d,j}	5.34 ± 2.40	6.76 ± 2.56^{a,d,j}	6.34 ± 4.06	7.27 ± 2.01a
Mon (10^9/L)	0.12 ± 0.05	0.19 ± 0.29	0.08 ± 0.05	0.14 ± 0.13	0.13 ± 0.17	0.08 ± 0.03	0.09 ± 0.06
Eos (10^9/L)	0.18 ± 0.17	0.06 ± 0.08^{a,d}	0.04 ± 0.04^{a,d,g}	0.18 ± 0.25	0.09 ± 0.08	0.09 ± 0.01	0.02 ± 0.01^{a,d}
Bas (10^9/L)	0.03 ± 0.05	0.01 ± 0.01	0.00 ± 0.01^{a}	0.04 ± 0.07^{j,m}	0.02 ± 0.02^{j,m}	0.00 ± 0.00	0.00 ± 0.00
Neu (%)	18.65 ± 6.27	14.26 ± 4.29^{a}	12.67 ± 7.42^{a,d,g}	17.05 ± 6.05	15.79 ± 5.55	18.48 ± 6.82	15.80 ± 8.86
Lym (%)	76.07 ± 7.85	82.05 ± 5.67^{a}	85.86 ± 7.60^{a,d,g,j}	78.22 ± 7.32	81.45 ± 6.53^{a}	79.00 ± 8.06	83.00 ± 9.08
Mon (%)	1.95 ± 0.80	2.57 ± 2.67	0.91 ± 0.53^{a,d,j}	2.06 ± 1.78	1.31 ± 1.29^{a,d,j}	1.08 ± 0.18	0.97 ± 0.37^{a,j}
Eos (%)	2.85 ± 2.26	1.02 ± 0.74^{a}	0.52 ± 0.48^{a,d,g,j}	2.23 ± 1.67^{a,j}	1.19 ± 0.97^{d}	1.33 ± 0.88	0.20 ± 0.05^{a,d,j}
Bas (%)	0.48 ± 0.60	0.11 ± 0.17^{a}	0.04 ± 0.07^{a,d,g}	0.43 ± 0.51^{j}	0.27 ± 0.29^{j}	0.13 ± 0.18	0.03 ± 0.03
RBC (10^{12}/L)	11.34 ± 0.50	10.90 ± 0.86	11.44 ± 0.69	10.99 ± 0.81	11.36 ± 0.53	11.58 ± 0.15	11.96 ± 0.28^{a,d,g,j}
HGB (g/L)	128.41 ± 21.20	121.68 ± 21.71	139.97 ± 26.97^{d,j}	123.08 ± 20.71	147.33 ± 22.81^{a,d,j}	118.25 ± 28.50	38.88 ± 29.63
HCT (%)	47.04 ± 1.74	46.12 ± 3.45	50.65 ± 2.63^{a,d,j}	45.63 ± 3.01^{a}	49.76 ± 1.93^{a,d,j}	48.35 ± 0.64	51.30 ± 1.97^{a,d,j}
MCV (fL)	41.52 ± 1.15	42.35 ± 1.03	44.32 ± 1.37^{a,d,j}	41.56 ± 0.92	43.83 ± 0.89^{a,d,j}	41.78 ± 1.10	42.92 ± 1.20
MCH (pg)	13.13 ± 0.26	13.14 ± 0.25	14.05 ± 0.37^{a,d,j}	13.21 ± 0.29	14.02 ± 0.25^{a,d,j}	13.35 ± 0.14^{g,m}	13.58 ± 0.38^{g}

MCHC (g/L)	316.57 ± 5.03	310.52 ± 8.73	317.20 ± 7.08	317.81 ± 4.37[j]	320.00 ± 5.12[j]	319.75 ± 5.30	316.50 ± 9.99
RDW-CV (%)	14.04 ± 0.72	13.97 ± 0.66	14.11 ± 0.60	13.78 ± 0.53	14.08 ± 0.49	13.33 ± 0.11[g,j,m]	12.98 ± 0.70[a,g,j,m]
RDW-SD (fL)	28.05 ± 1.90	28.26 ± 1.45	30.14 ± 1.37[a,d,j]	27.31 ± 1.15	29.80 ± 1.13[a,d,j]	27.13 ± 0.11	26.53 ± 1.66[g,m]
PLT (10^9/L)	1491.64 ± 252.58	1454.04 ± 246.39	1368.90 ± 268.86	1496.33 ± 360.70	1622.50 ± 234.70[m]	1795.75 ± 169.35	1556.83 ± 233.74
MPV (fL)	5.63 ± 0.16	5.53 ± 0.25	6.13 ± 0.44[a,d,j]	5.62 ± 0.16	6.15 ± 0.28[a,d,j]	5.13 ± 0.39[a,d,g,m]	5.33 ± 0.31[g,m]
PDW (fL)	15.35 ± 0.11	15.42 ± 0.15	15.49 ± 0.17[a,d]	15.37 ± 0.20	15.53 ± 0.25[a,d]	15.43 ± 0.18	15.57 ± 0.16[a,d]
PCT (%)	0.82 ± 0.13	0.80 ± 0.12	0.82 ± 0.12	0.83 ± 0.18	0.95 ± 0.08[a,d,j,m]	0.83 ± 0.03	0.82 ± 0.08[g]

Table S24. Hematological measurements for wild type, *Bscl2*$^{+/Celia}$, *Bscl2*$^{Celia/Celia}$, *Bscl2*$^{+/-}$and *Bscl2*$^{-/-}$ mice separated by sex. Data is presented as mean ± SD or n (%) ± SD. Data were analysed using a Kolmogorov-Smirnov test for normality, followed by a Kruskal-Wallis test with Mann-Whitney post hoc comparisons. [a] $p < 0.05$ vs wild type ♀/♂; [b] $p < 0.05$ vs wild type ♀; [c] $p < 0.05$ vs wild type ♂; [d] $p < 0.05$ vs *Bscl2*$^{+/-}$ ♀/♂; [e] $p < 0.05$ vs *Bscl2*$^{+/-}$ ♀; [f] $p < 0.05$ vs *Bscl2*$^{+/-}$ ♂; [g] $p < 0.05$ vs *Bscl2*$^{-/-}$ ♀/♂; [h] $p < 0.05$ vs *Bscl2*$^{-/-}$ ♀; [i] $p < 0.05$ vs *Bscl2*$^{-/-}$ ♂; [j] $p < 0.05$ vs *Bscl2*$^{+/Celia}$ ♀/♂; [k] $p < 0.05$ vs *Bscl2*$^{+/Celia}$ ♀; [l] $p < 0.05$ vs *Bscl2*$^{+/Celia}$ ♂; [m] $p < 0.05$ vs *Bscl2*$^{Celia/Celia}$ ♀/♂; [n] $p < 0.05$ vs *Bscl2*$^{Celia/Celia}$ ♀ and [o] $p < 0.05$ vs *Bscl2*$^{Celia/Celia}$ ♂.

	Wild type		*Bscl2*$^{+/Celia}$		*Bscl2*$^{Celia/Celia}$		*Bscl2*$^{+/-}$		*Bscl2*$^{-/-}$	
Sex	♀	♂	♀	♂	♀	♂	♀	♂	♀	♂
N	11	10	14	9	14	11	12	14	10	13
Age (months)	5	5.2	5	4.9	5	5.2	5.0	5.2	5.3	5.4
WBC (10^9/L)	5.60 ± 1.52	6.83 ± 2.03	5.99 ± 2.55	6.27 ± 2.19	8.48 ± 2.20[b,e,j]	9.04 ± 3.34[a,e,j]	5.51 ± 1.84	8.10 ± 4.02	7.93 ± 3.15[e]	8.54 ± 3.15[b,e,k]
Neu (10^9/L)	1.18 ± 0.52	1.08 ± 0.23	0.83 ± 0.51[b]	0.88 ± 0.25	1.26 ± 0.98[k]	0.82 ± 0.20[b]	1.00 ± 0.50	1.39 ± 1.00[k]	1.43 ± 0.67[j,o]	1.16 ± 0.54[k,o]
Lym (10^9/L)	4.09 ± 1.20	5.43 ± 1.70	4.86 ± 1.88	5.20 ± 1.88	7.08 ± 2.01[a,e,k]	8.12 ± 3.22[a,e,j]	4.21 ± 1.51	6.30 ± 2.64[b,e]	6.18 ± 2.49[b,e]	7.21 ± 2.63[b,e,k]
Mon (10^9/L)	0.09 ± 0.04	0.15 ± 0.04[b]	0.22 ± 0.37[c]	0.14 ± 0.11	0.09 ± 0.06[c,f]	0.07 ± 0.05[c,f]	0.11 ± 0.15[c,f]	0.17 ± 0.10[b]	0.17 ± 0.22	0.09 ± 0.11[c,f]
Eos (10^9/L)	0.21 ± 0.17	0.15 ± 0.17	0.08 ± 0.09[b,e]	0.04 ± 0.04[b,d]	0.05 ± 0.04[b,e]	0.03 ± 0.02[a,d,k,n]	0.16 ± 0.09	0.19 ± 0.34	0.12 ± 0.09[i,l,n]	0.07 ± 0.07[e]
Bas (10^9/L)	0.04 ± 0.05	0.03 ± 0.04	0.01 ± 0.01[e]	0.00 ± 0.01[e]	0.00 ± 0.00[e,h]	0.00 ± 0.01[e,h]	0.03 ± 0.03	0.05 ± 0.09	0.02 ± 0.02[j]	0.02 ± 0.02
Neu (%)	20.89 ± 7.61	16.19 ± 3.20	14.04 ± 5.05[b]	14.61 ± 2.97[b]	14.63 ± 8.66[b,k]	10.17 ± 4.72[a,d,g]	17.99 ± 7.97	16.24 ± 3.90	18.37 ± 6.31	13.80 ± 4.10[b,h]
Lym (%)	73.20 ± 9.29	79.23 ± 4.48	81.65 ± 7.13[b]	82.66 ± 2.22[b,c]	83.67 ± 8.70[a,d,h,o]	88.66 ± 4.98[a,d,h,j]	76.53 ± 8.85	79.67 ± 5.65	77.83 ± 7.14	84.23 ± 4.54[a,d,h,o]
Mon (%)	1.75 ± 0.88	2.17 ± 0.67	2.87 ± 3.34	2.09 ± 1.04	1.02 ± 0.62[a,f,j]	0.76 ± 0.36[a,d,j]	2.04 ± 2.53	2.08 ± 0.83	1.82 ± 1.68	0.92 ± 0.72[a,d,j]
Eos (%)	3.53 ± 2.48	2.11 ± 1.84	1.29 ± 0.80[b]	0.59 ± 0.40[b,k]	0.64 ± 0.54[b,d,h,k]	0.36 ± 0.35[a,d,h,k]	2.95 ± 1.40[j]	1.62 ± 1.69[b,e]	1.66 ± 1.04[e,l]	0.83 ± 0.77[b,e]
Bas (%)	0.64 ± 0.74	0.31 ± 0.37	0.15 ± 0.19[e]	0.04 ± 0.10[a,e]	0.04 ± 0.06[a,e,h]	0.04 ± 0.08[a,e,h]	0.49 ± 0.38	0.39 ± 0.61	0.34 ± 0.30[j]	0.22 ± 0.29[e,l]
RBC (10^{12}/L)	11.28 ± 0.56	11.41 ± 0.44	10.92 ± 0.64	10.87 ± 1.17	11.09 ± 0.53[o]	11.88 ± 0.62[b,d,j]	11.18 ± 0.62	10.83 ± 0.94	11.29 ± 0.34[o]	11.41 ± 0.65[f,k]
HGB (g/L)	119.24 ±	138.50 ±	127.70 ±	112.31 ±	127.58 ±	155.74	117.93 ±	127.49 ±	149.49 ±	145.67 ±

	17.97	20.60	22.36	17.94[c]	24.71	21.51[a,d,j,n]	14.13	24.71	20.31[a,d,j,n]	25.25[b,d,j]
HCT (%)	47.20 ± 1.83	46.87 ± 1.72	45.73 ± 2.31[b]	46.74 ± 4.84[k]	49.74 ± 2.05[a,d,j]	51.81 ± 2.91[a,d,j]	46.60 ± 2.24	44.80 ± 3.40[b,d]	49.33 ± 1.15[a,j,o]	50.08 ± 2.36[a,d,j]
MCV (fL)	41.90 ± 0.99	41.10 ± 1.22	41.90 ± 0.79	43.04 ± 1.01[c]	44.88 ± 1.21[a,d,j]	43.60 ± 1.27[a,d,k]	41.71 ± 0.66	41.43 ± 1.11[l]	43.72 ± 0.80[a,d,k]	43.91 ± 0.98[a,d,k]
MCH (pg)	13.15 ± 0.22	13.11 ± 0.31	13.18 ± 0.28	13.09 ± 0.19	14.23 ± 0.32[a,j]	13.83 ± 0.32[a,d,j,n]	13.34 ± 0.22[a,d,j]	13.10 ± 0.29	14.04 ± 0.26[a,d,j]	14.01 ± 0.26[a,d,j]
MCHC (g/L)	314.23 ± 4.13	319.15 ± 4.81	314.68 ± 7.66	304.06 ± 6.08[a,d,g,k,m]	317.00 ± 7.47	317.45 ± 6.90	319.54 ± 4.01	316.32 ± 4.23	321.30 ± 5.60	319.00 ± 4.69
RDW-CV (%)	14.05 ± 0.83	14.03 ± 0.61	14.04 ± 0.45	13.87 ± 0.92	14.05 ± 0.48	14.20 ± 0.75	13.93 ± 0.26	13.66 ± 0.67	14.19 ± 0.59	14.00 ± 0.41
RDW-SD (fL)	28.07 ± 2.25	28.03 ± 1.54	28.36 ± 1.35	28.11 ± 1.67	30.09 ± 1.18[a,d]	30.21 ± 1.64[a,d]	27.55 ± 0.71	27.11 ± 1.42	29.98 ± 1.17[d]	29.66 ± 1.13[d]
PLT (10^9/L)	1377.73 ± 215.34	1616.95 ± 238.62	1368.71 ± 89.44	1586.78 ± 348.40	1414.25 ± 294.30	1311.18 ± 233.13	1356.54 ± 338.47	1616.14 ± 346.08	1692.60 ± 255.44	1568.58 ± 211.67
MPV (fL)	5.69 ± 0.15	5.57 ± 0.15	5.61 ± 0.25	5.40 ± 0.21[b,e]	6.20 ± 0.54[a,d,j]	6.04 ± 0.27[a,d,j]	5.72 ± 0.12[a]	5.54 ± 0.14[d]	6.27 ± 0.24[a,d,j]	6.06 ± 0.28[a,d,j]
PDW	15.35 ± 0.09	15.36 ± 0.13	15.44 ± 0.14	15.39 ± 0.16	15.54 ± 0.18[a,d]	15.42 ± 0.13	15.38 ± 0.17	15.36 ± 0.22	15.61 ± 0.32[a,d]	15.47 ± 0.18
PCT (%)	0.78 ± 0.13	0.87 ± 0.11	0.77 ± 0.05[c]	0.85 ± 0.18[k]	0.84 ± 0.12	0.78 ± 0.11[f,l]	0.77 ± 0.19	0.87 ± 0.16[k]	0.97 ± 0.05[c,e,j,m]	0.93 ± 0.09[b,e,k,o]

Annex 14. ARRIVE guidelines (Animal Research: Reporting of In Vivo Experiments)

Sí/no/NA		Página
	Título	
Sí	Proporcionar una descripción tan exacta y concisa como sea posible sobre el contenido del trabajo.	Portada
	Resumen	
Sí	Proporcionar un resumen preciso de los antecedentes, los objetivos de la investigación, incluyendo detalles de la especie y cepa de los animales utilizados, métodos relevantes, hallazgos principales y conclusiones del estudio.	7-27
	Antecedentes	
Sí	Incluir suficientes antecedentes científicos (incluyendo las referencias pertinentes al trabajo anterior) a fin de comprender la motivación y el contexto para el estudio, y explicar las bases y el enfoque experimental.	49-82
Sí	Explicar cómo y por qué la especie y el modelo animal utilizados permiten abordar los objetivos científicos y, cuando sea apropiado, la relevancia del estudio para la biología humana.	49-82
	Objetivos	
Sí	Describir claramente los objetivos primarios y secundarios del estudio, o las hipótesis específicas que se van a probar.	83
	Declaración Ética	
Sí	Indicar el permiso del comité ético, y las leyes o decretos pertinentes para el cuidado y uso de animales, bajo las que se realiza la investigación.	85 y 295-298
	Diseño del estudio	
Sí	Número de grupos experimentales y control.	111-198 y 241-291
Sí	Cualquier medida adoptada para minimizar los efectos de sesgo subjetivo al asignar los animales a los grupos de tratamiento (por ej., procedimiento aleatorio) y al evaluar los resultados (por ej., si se hace, describir quiénes eran ciegos y cuándo).	85-110
Sí	La unidad experimental (por ej., un solo animal, grupos o jaulas de animales). Un diagrama cronológico o de flujo pueden ser útiles para ilustrar cómo se realizaron los diseños de estudio complejos.	111-198 y 241-291
	Procedimientos experimentales	
Sí	Cómo (por ej., formulación y dosis del tratamiento, el sitio y la vía de administración, anestesia y analgesia utilizadas [incluyendo la monitorización], procedimiento quirúrgico, el método de eutanasia). Proporcionar detalles de cualquier equipo especializado utilizado, incluyendo proveedor(es).	85-110
Sí	Cuándo (por ej., la hora del día).	85-110
Sí	Dónde (por ej., jaula de alojamiento, laboratorio, prueba del laberinto acuático).	85-110
Sí	Por qué (por ej., fundamentos para la elección del anestésico específico, la vía de administración, dosis del fármaco utilizado).	85-110
	Animales de experimentación	
Sí	Proporcionar detalles de los animales utilizados, incluyendo especie, cepa, sexo, etapa de desarrollo (por ej., edad media o mediana de	111-198 y

	edad y rango) y peso (por ej., media o mediana más rango de peso).	241-291
Sí	Proporcionar otra información pertinente, como la procedencia de los animales, nomenclatura internacional de la cepa, modificación genética (por ej., animal deficiente o transgénico), genotipo, estado de salud/inmune, si los animales han sido incluidos en estudios o recibido tratamientos anteriormente, procedimientos previos, etc.	85-90 y 111-119
	Animales	
Sí	Alojamiento (tipo de instalación por ej., libre de patógenos específicos [SPF], tipo de jaula o habitáculo, material del lecho, número de animales por jaula, forma y material del tanque, etc. para peces).	93
Sí	Condiciones de cría (por ej., programa de reproducción, ciclo de luz/oscuridad, temperatura, calidad de agua, etc. para peces, el tipo de alimentación, el acceso a los alimentos y al agua, enriquecimiento ambiental).	93
Sí	Evaluaciones e intervenciones relacionadas con el bienestar que se llevaron a cabo antes, durante o después del experimento	85-110
	Tamaño de la muestra	
Sí	Especificar el número total de animales utilizados en cada experimento, y el número de animales en cada grupo experimental.	111-198 y 241-291
Sí	Explicar cómo se determinó el número de animales. Proporcionar detalles del cálculo del tamaño muestral utilizado.	85-210 y 241-291
Sí	Indicar el número de repeticiones independientes de cada experimento, si es pertinente.	85-110
	Asignación de animales a grupos experimentales	
Sí	Proporcionar detalles completos de la forma en que los animales fueron asignados a grupos experimentales, incluyendo distribución aleatoria o asignación específica, si así se hizo.	85-110
NA	Describir el orden en el que los animales en los diferentes grupos experimentales fueron tratados y evaluados.	111-198
	Resultados experimentales	
Sí	Definir claramente los resultados primarios y secundarios evaluados (por ej., muerte celular, marcadores moleculares, cambios de comportamiento).	111-198
	Métodos estadísticos	
Sí	Proporcionar detalles sobre los métodos estadísticos utilizados para cada análisis.	110
Sí	Especificar la unidad de análisis para cada grupo de datos (por ej., un solo animal, grupo de animales, neurona individual).	110
Sí	Describir los métodos utilizados para evaluar si los datos corroboran las suposiciones del método estadístico.	110
	Datos basales	
Sí	Para cada grupo experimental, indicar las características relevantes y estado de salud de los animales (por ej., peso, estado microbiológico, si los animales han sido incluidos en estudios o recibido drogas anteriormente) antes de iniciar el tratamiento o prueba. (Esta información puede ser a menudo tabulada).	111-198
	Cantidades analizadas	
Sí	Indicar el número de animales en cada grupo incluido en cada análisis. Presentar números absolutos (por ej., 10/20, no 50 %2).	111-198 y 241-291
Sí	Si alguno de los animales o datos no fue incluido en el análisis, explicar por qué.	111-198

	Resultados y Discusión	
Sí	Indicar los resultados de cada análisis llevado a cabo, con una medida de precisión (por ej., error estándar o intervalo de confianza).	111-198 y 241-291
	Eventos adversos	
Sí	Dar detalles de todos los eventos adversos importantes en cada grupo experimental.	111-212
Sí	Describir las modificaciones a los protocolos experimentales realizadas para reducir los eventos adversos.	85-110
	Interpretación /implicaciones científicas	
Sí	Interpretar los resultados, teniendo en cuenta los objetivos y las hipótesis del estudio, la teoría actual y otros estudios pertinentes en la literatura.	199-210
Sí	Comentar las limitaciones del estudio incluyendo cualquier fuente potencial de sesgo, cualquier limitación del modelo animal y la imprecisión asociada con los resultados	199-210
Sí	Describir cualquier implicación de los métodos experimentales o hallazgos para el reemplazo, refinamiento o reducción (las 3 R) del uso de los animales en investigación.	199-210
	Capacidad de generalización/aplicabilidad	
Sí	Comentar si, y de qué forma, los hallazgos de este estudio son aplicables a otras especies o sistemas, incluyendo cualquier relevancia para la biología humana.	199-210
	Financiación	
Sí	Listar todas las fuentes de financiación (incluyendo el número del proyecto) y el papel de la fuente(s) de financiación en el estudio.	1

Basado en The ARRIVE guidelines: Animal Research: Reporting of In Vivo Experiments.

Annex 15. Authorization for animal experimentation project

XUNTA DE GALICIA
CONSELLERÍA DO MEDIO RURAL

Departamento Territorial
Edificio Administrativo de Servizos Múltiples
Vicente Ferrer, 2
15071 – A Coruña

REXISTRO XERAL DA XUNTA DE GALICIA
REXISTRO DO EDIFICIO ADMINISTRATIVO DE A CORUÑA
A CORUÑA
Data 21/02/2018 10:09:53
SAÍDA 18169 / RX 264121

José Manuel Cifuentes
Departamento de Anatomía
Facultade de Veterinaria
Campus Universitario
27002 Lugo

RESOLUCIÓN DE AUTORIZACIÓN DE PROXECTOS DE EXPERIMENTACIÓN ANIMAL

Expediente núm.: 15010/17/004
Persoa interesada: Jesús Rodríguez Requena
Procedemento: resolución de autorización
Data de inicio: 19.02.2018
Forma de inicio: solicitude do interesado

ANTECEDENTES

A persoa interesada, como representante do centro CIMUS (Universidade de Santiago de Compostela), presentou con data 15.09.2017 e rexistro de entrada 95988/RX 2267695, unha solicitude para a realización do proxecto de experimentación animal, cuxos datos se detallan a continuación:

Denominación do proxecto: Modelos animais na encefalopatía de Celia
Nome do centro usuario: Animalario do CIMUS
Persoa responsable do proxecto: Jesús Rodríguez Requena
Establecemento onde se realizarán os procedementos do proxecto (ou lugar xeográfico no caso de traballos de campo): Facultade de Medicina do CIMUS
Clasificación do proxecto : Tipo I ☐ Tipo II ☐ Tipo III ☒

CONSIDERACIÓNS LEGAIS E TÉCNICAS

1. O Real decreto 53/2013, de 1 de febreiro (BOE 34, do 8 de febreiro), polo que se establecen as normas básicas aplicables para a protección dos animais utilizados en experimentación e outros fins científicos, incluíndo a docencia, establece no seu artigo 33 as condicións de autorizacións dos proxectos con animais de experimentación.

2. O artigo 88 da Lei 39/2015, de 1 de outubro, do procedemento administrativo común das administracións públicas (BOE 236, do 2 de outubro de 2015) establece que a resolución que poña fin o procedemento decidirá todas as cuestións expostas polos interesados e aquelas outras derivadas deste.

XUNTA DE GALICIA
CONSELLERÍA DO MEDIO RURAL

Departamento Territorial
Edificio Administrativo de Servizos Múltiples
Vicente Ferrer, 2
15071 – A Coruña

3. O Servizo de Gandaría da Coruña revisou a documentación achegada na solicitude e o resultado favorable da avaliación do proxecto, realizada polo órgano habilitado da Sección de Experimentación Animal do Comité de Bioética da Universidade de Santiago de Compostela.

Esta xefatura territorial é competente para ditar unha resolución, de conformidade co artigo 11 do Decreto 245/2009 de 30 de abril, polo que se regulan as delegacións territoriais da Xunta de Galicia (DOG 84, do 1 de maio de 2009) e o Decreto 166/2015, de 13 de novembro, polo que se aproba a estrutura orgánica da Consellería do Medio Rural (DOG 220, do 18 de novembro de 2015).

De acordo con todo o indicado, RESOLVO:

1 Autorizar o proxecto solicitado.
2 O mencionado proxecto precisa someterse a unha avaliación retrospectiva aos dous anos.
3 A autorización deste proxecto terá unha duración de tres anos, transcorrido este tempo, deberá ser renovada esta autorización.

A citada autorización é unicamente válida nas condicións que figuran no expediente. Ante calquera cambio significativo no proxecto que poida ter efectos negativos sobre o benestar dos animais, deberá solicitar a confirmación da autorización ao Servizo Provincial de Gandaría.

Esta autorización poderá ser suspendida, no caso de que o proxecto non se leve a cabo de acordo coas condicións de autorización e retirala, previo expediente tramitado ao que se lle dará audiencia.

Contra a presente resolución, que non lle pon fin á vía administrativa, poderá interpoñer un recurso de alzada ante a conselleira de Medio Rural. O prazo comezará a contar dende o día seguinte ao da recepción desta resolución. Todo isto, segundo o disposto nos artigos 121 e 122 da citada Lei 39/2015.

Mediante este escrito notificaselle ao CIMUS da USC esta resolución segundo o esixido no artigo 40.1 da antedita Lei 39/2015.

A Coruña, 19 de febreiro de 2018
O xefe territorial

Manuel Rodríguez Vázquez

XUNTA DE GALICIA
CONSELLERÍA DO MEDIO RURAL

Xefatura Territorial
6ª da Ganadaría
Edificio administrativo Monelos, 4º andar
Rúa Vicente Ferrer, Nº 2
15008 A Coruña
Tfno.: 981 184 585
Correo electrónico: servizo.ganderia.a.coruna@xunta.gal

galicia

RESOLUCIÓN DE AUTORIZACIÓN DE PROXECTO DE EXPERIMENTACIÓN ANIMAL

Expediente núm.: 15012/2021/014
Persoa solicitante: Anxo Vidal Figueroa
Forma de inicio: solicitude da persoa interesada

Data de inicio do expediente: 16.4.2021
Procedemento: resolución de autorización

ANTECEDENTES

A persoa solicitante presentou con data 16.4.2021 unha solicitude para a realización do proxecto de experimentación animal (entrada no Rexistro electrónico da Xunta de Galicia 2021/882143). Posteriormente, presentou documentación complementaria o 5.5.2021 (entrada no Rexistro electrónico da Xunta de Galicia 2021/1055687) , cuxos datos se detallan a continuación:

Denominación do proxecto: Modelos animais na encefalopatía de Celia

Nome do centro usuario: Centro de Biomedicina Experimental (CEBEGA) da Universidade de Santiago de Compostela
Persoa responsable do proxecto: Jesús Rodríguez Requena

Establecemento onde se realizarán os procedementos do proxecto (ou lugar xeográfico no caso de traballos de campo): Centro de Biomedicina Experimental (CEBEGA)

Clasificación do proxecto : Tipo I ☐ Tipo II ☐ Tipo III ☒

CONSIDERACIÓNS LEGAIS E TÉCNICAS

1 O Real decreto 53/2013, de 1 de febreiro (BOE 34, do 8 de febreiro), polo que se establecen as normas básicas aplicables para a protección dos animais utilizados en experimentación e outros fins científicos, incluíndo a docencia, establece no seu artigo 33 as condicións de autorizacións dos proxectos con animais de experimentación.

2 O artigo 88 da Lei 39/2015, de 1 de outubro, do procedemento administrativo común das administracións públicas (BOE 236, do 2 de outubro de 2015) establece que a resolución que poña fin o procedemento decidirá todas as cuestións expostas polos interesados e aquelas outras derivadas deste.

Xacobeo 21·22

XUNTA DE GALICIA
CONSELLERÍA DO MEDIO RURAL

Xefatura Territorial
Dª de Gandaría
Edificio administrativo Monelos, 4º andar
Rúa Vicente Ferrer, Nº 2
15008 A Coruña
Tfno.: 981 184 585
Correo electrónico: servizo.gandaria.a.coruna@xunta.gal

galicia

3 O Servizo de Gandaría da Coruña revisou a documentación achegada na solicitude e o resultado favorable da avaliación do proxecto realizada polo órgano habilitado, a Sección de Experimentación Animal do Comité de Bioética da Universidade de Santiago de Compostela.

Esta xefatura territorial é competente para ditar unha resolución, de conformidade co Decreto 149/2018, do 5 de decembro, polo que se establece a estrutura orgánica da Consellería do Medio Rural e se modifica parcialmente o Decreto 177/2016, do 15 de decembro, polo que se fixa a estrutura orgánica da Vicepresidencia e das consellerías da Xunta de Galicia (DOG 235, do 11 de novembro).

De acordo con todo o indicado, RESOLVO:

1 Autorizar o proxecto solicitado.

2 O proxecto precisa someterse a unha avaliación retrospectiva aos tres anos de concederlle esta autorización.

3 A autorización deste proxecto terá unha duración de tres anos e unha vez transcorrido este tempo, deberá ser renovada.

A citada autorización é unicamente válida nas condicións que figuran no expediente. Ante calquera cambio significativo no proxecto que poida ter efectos negativos sobre o benestar dos animais, deberá solicitar a confirmación da autorización ao Servizo Provincial de Gandaría.

Esta autorización poderá ser suspendida no caso de que o proxecto non se leve a cabo de acordo coas condicións de autorización e retirala, previo expediente tramitado ao que se lle dará audiencia.

Contra a presente resolución, que non pon fin á vía administrativa, poderá interpoñer un recurso de alzada ante o conselleiro de Medio Rural. O prazo comezará a contar dende o día seguinte ao da recepción desta resolución. Todo isto, segundo o disposto nos artigos 121 e 122 da citada Lei 39/2015.

Mediante este escrito notifícaselle a Anxo Vidal Figueroa esta resolución segundo o esixido no artigo 40.1 da antedita Lei 39/2015.

Xacobeo 21·22

Annex 16. Animal handling training

AXENCIA GALEGA DA CALIDADE ALIMENTARIA

Xacobeo 21·22

REF: MJIA

Dna. Silvia Cobelo Gómez
Rúa Xosé Rubia Barcia 3, 4ºIZQ
15404 Ferrol
A Coruña

Asunto: **Remisión certificado**

Achégase certificados de experimentación animal das funcións:

"b" en roedores

"c" en roedores

Santiago de Compostela,

A xefa de sección

Asinado dixitalmente

Axencia Galega da Calidade Alimentaria
Avda. do Camiño Francés nº 10 - Baixo
15781 Santiago de Compostela
agacal@xunta.gal

Axencia Galega da Calidade Alimentaria
Avda. do Camiño Francés nº 10 - Baixo
15781 Santiago de Compostela
agacal@xunta.gal

AXENCIA GALEGA DA CALIDADE ALIMENTARIA
Avda. Do Camiño Francés, 10, Baixo
15703 Santiago de Compostela
A Coruña

Xacobeo 21·22

MÓDULOS FUNDAMENTAIS OU TRONCAIS E ESPECÍFICOS CORRESPONDENTES Á FUNCIÓN "b" EUTANASIA DOS ANIMAIS – ORDE ECC/566/2015, DE 20 DE MARZO

MÓDULOS FUNDAMENTAIS OU TRONCAIS

1.- Lexislación nacional (1 hora).

2.- Ética, benestar animal e as "tres erres", nivel 1 (2 horas).

3.- Bioloxía básica e adecuada, nivel 1 (3 horas).

4.- Coidado, saúde e manexo dos animais, nivel 1 (5 horas).

5.- Recoñecemento da dor, o sufrimento e a angustia (3 horas).

6.- Métodos incruentos de sacrificio, nivel 1 (2 horas)

MÓDULOS ESPECÍFICOS DA FUNCIÓN "b"

1.- Bioloxía básica e adecuada, nivel 2 (3 horas)

2.- Métodos incruentos de sacrificio, nivel 2 (3 horas)

.....

MÓDULOS FUNDAMENTALES O TRONCALES Y ESPECÍFICOS CORRESPONDIENTES A LA FUNCIÓN "b" EUTANASIA DE LOS ANIMALES – ORDEN ECC/566/2015, DE 20 DE MARZO

MÓDULOS FUNDAMENTALES O TRONCALES

1.- Legislación nacional (1 hora).

2.- Ética, bienestar animal y las "tres erres", nivel 1 (2 horas).

3.- Biología básica y adecuada, nivel 1 (3 horas).

4.- Cuidado, salud y manejo de los animales, nivel 1 (5 horas).

5.- Reconocimiento del dolor, el sufrimiento y la angustia (3 horas).

6.- Métodos incruentos de sacrificio, nivel 1 (2 horas)

MÓDULOS ESPECÍFICOS DE LA FUNCIÓN "b"

1.- Biología básica y adecuada, nivel 2 (3 horas)

2.- Métodos incruentos de sacrificio, nivel 2 (3 horas)

AXENCIA GALEGA DA CALIDADE ALIMENTARIA
Avda. Do Camiño Francés, 10, Baixo
15703 Santiago de Compostela
A Coruña

Xacobeo 21·22

Certificado de capacitación en materia de protección de animais utilizados, criados ou subministrados con fins de experimentación e outros fins científicos, incluíndo a docencia conforme coa Orde ECC/566/2015 de 20 de marzo.

Certificado de capacitación en materia de protección de animales utilizados, criados o suministrados con fines de experimentación y otros fines científicos, incluyendo la docencia conforme con la Orden ECC/566/2015 de 20 de marzo.

1. IDENTIFICACIÓN / *IDENTIFICACIÓN*		
1.1. Apelidos / *Apellidos* **Cobelo Gómez**		
1.2. Nome / *Nombre* **Silvia**		DNI / *DNI* **32714960J**
1.3. Función / *Función* **"b"**	1.4. Grupo ou grupos de especies* / *Grupo o grupos de especies** **ro**	1.5. Data inicial de vixencia** / *Fecha inicial de vigencia*** **10/12/2021**
2. Nº DO CERTIFICADO / *Nº DEL CERTIFICADO*		
b626		
3.ORGANISMO QUE EXPIDE O CERTIFICADO / *ORGANISMO QUE EXPIDE EL CERTIFICADO*		
3.1. Nome e enderezo do organismo que expide o certificado / *Nombre y dirección del organismo que expide el certificado* **AXENCIA GALEGA DA CALIDADE ALIMENTARIA** **CONSELLERÍA DO MEDIO RURAL – XUNTA DE GALICIA** Rúa do Camiño Francés, 10 baixo 15781 Santiago de Compostela A Coruña (España)		
3.2. Teléfono / *Teléfono* 981 546 657	3.3. Fax / *Fax* 981 546 651	3.4. Correo electrónico / *Correo electrónico* formacion.cmrm@xunta.es
3.5. Data / *Fecha*	3.6. Lugar / *Lugar* **Santiago de Compostela**	
3.7. Nome e sinatura / *Nombre y firma* **Santiago de Compostela,** **O director da Axencia Galega da Calidade Alimentaria** **Por delegación de sinatura (Resolución do 15/02/2022)** **O xefe da Área de Formación, Innovación e Investigación Agraria** **Manuel López Luaces**		

* ro (roedores), la (lagomorfos), ca (carnívoros), ga (équidos, ruminantes e porcino), re (réptiles), pa (peixes e anfibios), ce (cefalópodos), as (animais silvestres), oe (outras especies), te (tódalas especies) / * ro (roedores), la (lagomorfos), ca (carnívoros), ga (équidos, rumiantes y porcino), re (reptiles), pa (peces y anfibios), ce (cefalópodos), as (animales silvestres), oe (otras especies), te (todas las especies)

** A validez deste certificado será de oito anos contados a partir da data inicial de vixencia. O mantemento da capacitación deberá solicitarse durante os 6 meses anteriores á finalización do prazo de vixencia /***La validez de este certificado será de ocho años contados a partir de la fecha inicial de vigencia. El mantenimiento de la capacitación deberá solicitarse durante los 6 meses anteriores a la finalización del plazo de vigencia.*

AXENCIA GALEGA DA CALIDADE ALIMENTARIA
Avda. Do Camiño Francés, 10, Baixo
15703 Santiago de Compostela
A Coruña

MÓDULOS FUNDAMENTAIS OU TRONCAIS E ESPECÍFICOS CORRESPONDENTES Á FUNCIÓN "c" REALIZACIÓN DOS PROCEDEMENTOS – ORDE ECC/566/2015, DE 20 DE MARZO

MÓDULOS FUNDAMENTAIS OU TRONCAIS

1.- Lexislación nacional (1 hora).

2.- Ética, benestar animal e as "tres erres", nivel 1 (2 horas).

3.- Bioloxía básica e adecuada, nivel 1 (3 horas).

4.- Coidado, saúde e manexo dos animais, nivel 1 (5 horas).

5.- Recoñecemento da dor, o sufrimento e a angustia (3 horas).

6.- Métodos incruentos de sacrificio, nivel 1 (2 horas)

MÓDULOS ESPECÍFICOS DA FUNCIÓN "c"

1.- Bioloxía básica e adecuada, nivel 2 (3 horas)

2.- Procedementos minimamente invasores sen anestesia, nivel 1 (5 horas)

3.- Procedementos minimamente invasores sen anestesia, nivel 2 (10 horas)

4.- Anestesia para procedementos menores (5 horas)

5.- Anestesia avanzada para intervencións cirúrxicas ou procedementos prolongados (8 horas)

6.- Principios de cirurxía (5 horas)

.....

MÓDULOS FUNDAMENTALES O TRONCALES Y ESPECÍFICOS CORRESPONDIENTES A LA FUNCIÓN "c" REALIZACIÓN DE LOS PROCEDIMIENTOS – ORDEN ECC/566/2015, DE 20 DE MARZO

MÓDULOS FUNDAMENTALES O TRONCALES

1.- Legislación nacional (1 hora).

2.- Ética, bienestar animal y las "tres erres", nivel 1 (2 horas).

3.- Biología básica y adecuada, nivel 1 (3 horas).

4.- Cuidado, salud y manejo de los animales, nivel 1 (5 horas).

5.- Reconocimiento del dolor, el sufrimiento y la angustia (3 horas).

6.- Métodos incruentos de sacrificio, nivel 1 (2 horas)

MÓDULOS ESPECÍFICOS DE LA FUNCIÓN "c"

1.- Biología básica y adecuada, nivel 2 (3 horas)

2.- Procedimientos mínimamente invasivos sin anestesia, nivel 1 (5 horas)

3.- Procedimientos mínimamente invasivos sin anestesia, nivel 2 (10 horas)

4.- Anestesia para procedimientos menores (5 horas)

5.- Anestesia avanzada para intervenciones quirúrgicas o procedimientos prolongados (8 horas)

6.- Principios de cirugía (5 horas)

AXENCIA GALEGA DA CALIDADE ALIMENTARIA

Avda. Do Camiño Francés, 10, Baixo
15703 Santiago de Compostela
A Coruña

Xacobeo 21·22

Certificado de capacitación en materia de protección de animais utilizados, criados ou subministrados con fins de experimentación e outros fins científicos, incluíndo a docencia conforme coa Orde ECC/566/2015 de 20 de marzo.

Certificado de capacitación en materia de protección de animales utilizados, criados o suministrados con fines de experimentación y otros fines científicos, incluyendo la docencia conforme con la Orden ECC/566/2015 de 20 de marzo.

1. IDENTIFICACIÓN / *IDENTIFICACIÓN*

1.1. Apelidos / *Apellidos*

Cobelo Gómez

1.2. Nome / *Nombre*	DNI / *DNI*
Silvia	**32714960J**

1.3. Función / *Función*	1.4. Grupo ou grupos de especies* / *Grupo o grupos de especies**	1.5. Data inicial de vixencia** / *Fecha inicial de vigencia***
"c"	**ro**	**10/12/2021**

2. Nº DO CERTIFICADO / *Nº DEL CERTIFICADO*

c670

3.ORGANISMO QUE EXPIDE O CERTIFICADO / *ORGANISMO QUE EXPIDE EL CERTIFICADO*

3.1. Nome e enderezo do organismo que expide o certificado / *Nombre y dirección del organismo que expide el certificado*

AXENCIA GALEGA DA CALIDADE ALIMENTARIA
CONSELLERÍA DO MEDIO RURAL – XUNTA DE GALICIA
Rúa do Camiño Francés, 10 baixo
15781 Santiago de Compostela
A Coruña (España)

3.2. Teléfono / *Teléfono*	3.3. Fax / *Fax*	3.4. Correo electrónico / *Correo electrónico*
981 546 657	981 546 651	formacion.cmrm@xunta.es

3.5. Data / *Fecha*	3.6. Lugar / *Lugar*
	Santiago de Compostela

3.7. Nome e sinatura / *Nombre y firma*

Santiago de Compostela,

O director da Axencia Galega da Calidade Alimentaria

Por delegación de sinatura (Resolución do 15/02/2022)

O xefe da Área de Formación, Innovación e Investigación Agraria

Manuel López Luaces

* ro (roedores), la (lagomorfos), ca (carnívoros), ga (équidos, ruminantes e porcino), re (réptiles), pa (peixes e anfibios), ce (cefalópodos), as (animais silvestres), oe (outras especies), te (tódalas especies) / * ro (roedores), la (lagomorfos), ca (carnívoros), ga (équidos, rumiantes y porcino), re (reptiles), pa (peces y anfibios), ce (cefalópodos), as (animales silvestres), oe (otras especies), te (todas las especies)

** A validez deste certificado será de oito anos contados a partir da data inicial de vixencia. O mantemento da capacitación deberá solicitarse durante os 6 meses anteriores á finalización do prazo de vixencia /***La validez de este certificado será de ocho años contados a partir de la fecha inicial de vigencia. El mantenimiento de la capacitación deberá solicitarse durante los 6 meses anteriores a la finalización del plazo de vigencia.*

Annex 17. Copyright permissions

- **Copyright permission for Figure 2:**

ELSEVIER LICENSE
TERMS AND CONDITIONS
Oct 05, 2024

This Agreement between Silvia Cobelo Gómez ("You") and Elsevier ("Elsevier") consists of your license details and the terms and conditions provided by Elsevier and Copyright Clearance Center.

License Number	5882450793284
License date	Oct 05, 2024
Licensed Content Publisher	Elsevier
Licensed Content Publication	Developmental Cell
Licensed Content Title	Human SEIPIN Binds Anionic Phospholipids
Licensed Content Author	Renhong Yan,Hongwu Qian,Ivan Lukmantara,Mingming Gao,Ximing Du,Nieng Yan,Hongyuan Yang
Licensed Content Date	Oct 22, 2018
Licensed Content Volume	47
Licensed Content Issue	2
Licensed Content Pages	13
Start Page	248
End Page	256.e4
Type of Use	reuse in a thesis/dissertation
Portion	figures/tables/illustrations
Number of figures/tables/illustrations	1
Format	both print and electronic
Are you the author of this Elsevier article?	No
Will you be translating?	No
Title of new work	Unravelling the Pathogenesis of Celia's Encephalopathy (PELD): The Role of Seipin in Neurodegeneration, Lipodystrophy, and other Tissue Damage in a Humanized Murine Model
Institution name	Universidade de Santiago de Compostela
Expected presentation date	Dec 2024
Portions	Figure 2 on page 54
The Requesting Person / Organization to Appear on the License	Silvia Cobelo Gómez
Requestor Location	University of Santiago de Compostela Campus Vida Avenida Barcelona, s/n

	Santiago de Compostela, A Coruña 15782 Spain Attn: University of Santiago de Compostela
Publisher Tax ID	GB 494 6272 12
Total	0.00 EUR
Terms and Conditions	

INTRODUCTION

1. The publisher for this copyrighted material is Elsevier. By clicking "accept" in connection with completing this licensing transaction, you agree that the following terms and conditions apply to this transaction (along with the Billing and Payment terms and conditions established by Copyright Clearance Center, Inc. ("CCC"), at the time that you opened your RightsLink account and that are available at any time at https://myaccount.copyright.com).

GENERAL TERMS

2. Elsevier hereby grants you permission to reproduce the aforementioned material subject to the terms and conditions indicated.

3. Acknowledgement: If any part of the material to be used (for example, figures) has appeared in our publication with credit or acknowledgement to another source, permission must also be sought from that source. If such permission is not obtained then that material may not be included in your publication/copies. Suitable acknowledgement to the source must be made, either as a footnote or in a reference list at the end of your publication, as follows:

"Reprinted from Publication title, Vol /edition number, Author(s), Title of article / title of chapter, Pages No., Copyright (Year), with permission from Elsevier [OR APPLICABLE SOCIETY COPYRIGHT OWNER]." Also Lancet special credit - "Reprinted from The Lancet, Vol. number, Author(s), Title of article, Pages No., Copyright (Year), with permission from Elsevier."

4. Reproduction of this material is confined to the purpose and/or media for which permission is hereby given. The material may not be reproduced or used in any other way, including use in combination with an artificial intelligence tool (including to train an algorithm, test, process, analyse, generate output and/or develop any form of artificial intelligence tool), or to create any derivative work and/or service (including resulting from the use of artificial intelligence tools).

5. Altering/Modifying Material: Not Permitted. However figures and illustrations may be altered/adapted minimally to serve your work. Any other abbreviations, additions, deletions and/or any other alterations shall be made only with prior written authorization of Elsevier Ltd. (Please contact Elsevier's permissions helpdesk here). No modifications can be made to any Lancet figures/tables and they must be reproduced in full.

6. If the permission fee for the requested use of our material is waived in this instance, please be advised that your future requests for Elsevier materials may attract a fee.

7. Reservation of Rights: Publisher reserves all rights not specifically granted in the combination of (i) the license details provided by you and accepted in the course of this licensing transaction,

(ii) these terms and conditions and (iii) CCC's Billing and Payment terms and conditions.

8. License Contingent Upon Payment: While you may exercise the rights licensed immediately upon issuance of the license at the end of the licensing process for the transaction, provided that you have disclosed complete and accurate details of your proposed use, no license is finally effective unless and until full payment is received from you (either by publisher or by CCC) as provided in CCC's Billing and Payment terms and conditions. If full payment is not received on a timely basis, then any license preliminarily granted shall be deemed automatically revoked and shall be void as if never granted. Further, in the event that you breach any of these terms and conditions or any of CCC's Billing and Payment terms and conditions, the license is automatically revoked and shall be void as if never granted. Use of materials as described in a revoked license, as well as any use of the materials beyond the scope of an unrevoked license, may constitute copyright infringement and publisher reserves the right to take any and all action to protect its copyright in the materials.

9. Warranties: Publisher makes no representations or warranties with respect to the licensed material.

10. Indemnity: You hereby indemnify and agree to hold harmless publisher and CCC, and their respective officers, directors, employees and agents, from and against any and all claims arising out of your use of the licensed material other than as specifically authorized pursuant to this license.

11. No Transfer of License: This license is personal to you and may not be sublicensed, assigned, or transferred by you to any other person without publisher's written permission.

12. No Amendment Except in Writing: This license may not be amended except in a writing signed by both parties (or, in the case of publisher, by CCC on publisher's behalf).

13. Objection to Contrary Terms: Publisher hereby objects to any terms contained in any purchase order, acknowledgment, check endorsement or other writing prepared by you, which terms are inconsistent with these terms and conditions or CCC's Billing and Payment terms and conditions. These terms and conditions, together with CCC's Billing and Payment terms and conditions (which are incorporated herein), comprise the entire agreement between you and publisher (and CCC) concerning this licensing transaction. In the event of any conflict between your obligations established by these terms and conditions and those established by CCC's Billing and Payment terms and conditions, these terms and conditions shall control.

14. Revocation: Elsevier or Copyright Clearance Center may deny the permissions described in this License at their sole discretion, for any reason or no reason, with a full refund payable to you. Notice of such denial will be made using the contact information provided by you. Failure to receive such notice will not alter or invalidate the denial. In no event will Elsevier or Copyright Clearance Center be responsible or liable for any costs, expenses or damage incurred by you as a result of a denial of your permission request, other than a refund of the amount(s) paid by you to Elsevier and/or Copyright Clearance Center for denied permissions.

LIMITED LICENSE

The following terms and conditions apply only to specific license types:

15. **Translation**: This permission is granted for non-exclusive world **English** rights only unless your license was granted for translation rights. If you licensed translation rights you may only translate this content into the languages you requested. A professional translator must perform all translations and reproduce the content word for word preserving the integrity of the article.

16. **Posting licensed content on any Website**: The following terms and conditions apply as follows: Licensing material from an Elsevier journal: All content posted to the web site must maintain the copyright information line on the bottom of each image; A hyper-text must be included to the Homepage of the journal from which you are licensing at http://www.sciencedirect.com/science/journal/xxxxx or the Elsevier homepage for books at http://www.elsevier.com; Central Storage: This license does not include permission for a scanned version of the material to be stored in a central repository such as that provided by Heron/XanEdu.

Licensing material from an Elsevier book: A hyper-text link must be included to the Elsevier homepage at http://www.elsevier.com . All content posted to the web site must maintain the copyright information line on the bottom of each image.

Posting licensed content on Electronic reserve: In addition to the above the following clauses are applicable: The web site must be password-protected and made available only to bona fide students registered on a relevant course. This permission is granted for 1 year only. You may obtain a new license for future website posting.

17. **For journal authors:** the following clauses are applicable in addition to the above:

Preprints:

A preprint is an author's own write-up of research results and analysis, it has not been peer-reviewed, nor has it had any other value added to it by a publisher (such as formatting, copyright, technical enhancement etc.).

Authors can share their preprints anywhere at any time. Preprints should not be added to or enhanced in any way in order to appear more like, or to substitute for, the final versions of articles however authors can update their preprints on arXiv or RePEc with their Accepted Author Manuscript (see below).

If accepted for publication, we encourage authors to link from the preprint to their formal publication via its DOI. Millions of researchers have access to the formal publications on ScienceDirect, and so links will help users to find, access, cite and use the best available version. Please note that Cell Press, The Lancet and some society-owned have different preprint policies. Information on these policies is available on the journal homepage.

Accepted Author Manuscripts: An accepted author manuscript is the manuscript of an article that has been accepted for publication and which typically includes author-incorporated changes suggested during submission, peer review and editor-author communications.

Authors can share their accepted author manuscript:

- immediately
  - via their non-commercial person homepage or blog
  - by updating a preprint in arXiv or RePEc with the accepted manuscript
  - via their research institute or institutional repository for internal institutional uses or as part of an invitation-only research collaboration work-group
  - directly by providing copies to their students or to research collaborators for their personal use
  - for private scholarly sharing as part of an invitation-only work group on commercial sites with which Elsevier has an agreement
- After the embargo period
  - via non-commercial hosting platforms such as their institutional repository
  - via commercial sites with which Elsevier has an agreement

In all cases accepted manuscripts should:

- link to the formal publication via its DOI
- bear a CC-BY-NC-ND license - this is easy to do
- if aggregated with other manuscripts, for example in a repository or other site, be shared in alignment with our hosting policy not be added to or enhanced in any way to appear more like, or to substitute for, the published journal article.

Published journal article (JPA): A published journal article (PJA) is the definitive final record of published research that appears or will appear in the journal and embodies all value-adding publishing activities including peer review co-ordination, copy-editing, formatting, (if relevant) pagination and online enrichment.

Policies for sharing publishing journal articles differ for subscription and gold open access articles:

Subscription Articles: If you are an author, please share a link to your article rather than the full-text. Millions of researchers have access to the formal publications on ScienceDirect, and so links will help your users to find, access, cite, and use the best available version.

Theses and dissertations which contain embedded PJAs as part of the formal submission can be posted publicly by the awarding institution with DOI links back to the formal publications on ScienceDirect.

If you are affiliated with a library that subscribes to ScienceDirect you have additional private sharing rights for others' research accessed under that agreement. This includes use for classroom teaching and internal training at the institution (including use in course packs and courseware programs), and inclusion of the article for grant funding purposes.

Gold Open Access Articles: May be shared according to the author-selected end-user license and should contain a CrossMark logo, the end user license, and a DOI link to the formal publication on ScienceDirect.

Please refer to Elsevier's posting policy for further information.

18. **For book authors** the following clauses are applicable in addition to the above: Authors are permitted to place a brief summary of their work online only. You are not allowed to download and post the published electronic version of your chapter, nor may you scan the printed edition to create an electronic version. **Posting to a repository:** Authors are permitted to post a summary of their chapter only in their institution's repository.

19. **Thesis/Dissertation**: If your license is for use in a thesis/dissertation your thesis may be submitted to your institution in either print or electronic form. Should your thesis be published commercially, please reapply for permission. These requirements include permission for the Library and Archives of Canada to supply single copies, on demand, of the complete thesis and include permission for Proquest/UMI to supply single copies, on demand, of the complete thesis. Should your thesis be published commercially, please reapply for permission. Theses and dissertations which contain embedded PJAs as part of the formal submission can be posted publicly by the awarding institution with DOI links back to the formal publications on ScienceDirect.

Elsevier Open Access Terms and Conditions

You can publish open access with Elsevier in hundreds of open access journals or in nearly 2000 established subscription journals that support open access publishing. Permitted third party re-use of these open access articles is defined by the author's choice of Creative Commons user license. See our open access license policy for more information.

Terms & Conditions applicable to all Open Access articles published with Elsevier:

Any reuse of the article must not represent the author as endorsing the adaptation of the article nor should the article be modified in such a way as to damage the author's honour or reputation. If any changes have been made, such changes must be clearly indicated.

The author(s) must be appropriately credited and we ask that you include the end user license and a DOI link to the formal publication on ScienceDirect.

If any part of the material to be used (for example, figures) has appeared in our publication with credit or acknowledgement to another source it is the responsibility of the user to ensure their reuse complies with the terms and conditions determined by the rights holder.

Additional Terms & Conditions applicable to each Creative Commons user license:

CC BY: The CC-BY license allows users to copy, to create extracts, abstracts and new works from the Article, to alter and revise the Article and to make commercial use of the Article (including reuse and/or resale of the Article by commercial entities), provided the user gives appropriate credit (with a link to the formal publication through the relevant DOI), provides a link to the license, indicates if changes were made and the licensor is not represented as endorsing the use made of the work. The full details of the license are available at http://creativecommons.org/licenses/by/4.0.

- **Copyright permission for Figure 4:**

SPRINGER NATURE LICENSE
TERMS AND CONDITIONS
Oct 05, 2024

This Agreement between Silvia Cobelo Gómez ("You") and Springer Nature ("Springer Nature") consists of your license details and the terms and conditions provided by Springer Nature and Copyright Clearance Center.

License Number	5882451459764
License date	Oct 05, 2024
Licensed Content Publisher	Springer Nature
Licensed Content Publication	Nature Reviews Molecular Cell Biology
Licensed Content Title	Dynamics and functions of lipid droplets
Licensed Content Author	James A. Olzmann et al
Licensed Content Date	Dec 6, 2018
Type of Use	Thesis/Dissertation
Requestor type	academic/university or research institute
Format	print and electronic
Portion	figures/tables/illustrations
Number of figures/tables/illustrations	1
Would you like a high resolution image with your order?	No
Will you be translating?	No
Circulation/distribution	100 – 199
Author of this Springer Nature content	No
Title of new work	Unravelling the Pathogenesis of Celia's Encephalopathy (PELD): The Role of Seipin in Neurodegeneration, Lipodystrophy, and other Tissue Damage in a Humanized Murine Model
Institution name	Universidade de Santiago de Compostela
Expected presentation date	Dec 2024
Portions	Figure 4 on page 58
The Requesting Person / Organization to Appear on the License	Silvia Cobelo Gómez University of Santiago de Compostela Campus Vida Avenida Barcelona, s/n
Requestor Location	Santiago de Compostela, A Coruña 15782 Spain Attn: University of Santiago de Compostela

Billing Type	Invoice
Billing Address	University of Santiago de Compostela Campus Vida Avenida Barcelona, s/n Santiago de Compostela, Spain 15782 Attn: University of Santiago de Compostela
Total	0.00 EUR

Terms and Conditions

Springer Nature Customer Service Centre GmbH Terms and Conditions

The following terms and conditions ("Terms and Conditions") together with the terms specified in your [RightsLink] constitute the License ("License") between you as Licensee and Springer Nature Customer Service Centre GmbH as Licensor. By clicking 'accept' and completing the transaction for your use of the material ("Licensed Material"), you confirm your acceptance of and obligation to be bound by these Terms and Conditions.

1. **Grant and Scope of License**

1.1. The Licensor grants you a personal, non-exclusive, non-transferable, non-sublicensable, revocable, world-wide License to reproduce, distribute, communicate to the public, make available, broadcast, electronically transmit or create derivative works using the Licensed Material for the purpose(s) specified in your RightsLink Licence Details only. Licenses are granted for the specific use requested in the order and for no other use, subject to these Terms and Conditions. You acknowledge and agree that the rights granted to you under this License do not include the right to modify, edit, translate, include in collective works, or create derivative works of the Licensed Material in whole or in part unless expressly stated in your RightsLink Licence Details. You may use the Licensed Material only as permitted under this Agreement and will not reproduce, distribute, display, perform, or otherwise use or exploit any Licensed Material in any way, in whole or in part, except as expressly permitted by this License.

1.2. You may only use the Licensed Content in the manner and to the extent permitted by these Terms and Conditions, by your RightsLink Licence Details and by any applicable laws.

1.3. A separate license may be required for any additional use of the Licensed Material, e.g. where a license has been purchased for print use only, separate permission must be obtained for electronic re-use. Similarly, a License is only valid in the language selected and does not apply for editions in other languages unless additional translation rights have been granted separately in the License.

1.4. Any content within the Licensed Material that is owned by third parties is expressly excluded from the License.

1.5. Rights for additional reuses such as custom editions, computer/mobile applications, film or TV reuses and/or any other derivative rights requests require additional permission and may be subject to an additional fee. Please apply to journalpermissions@springernature.com or bookpermissions@springernature.com for these rights.

2. **Reservation of Rights**

Licensor reserves all rights not expressly granted to you under this License. You acknowledge and agree that nothing in this License limits or restricts Licensor's rights in or use of the Licensed Material in any way. Neither this License, nor any act, omission, or statement by Licensor or you, conveys any ownership right to you in any Licensed Material, or to any element or portion thereof. As between Licensor and you, Licensor owns and retains all right, title, and interest in and to the Licensed Material subject to the license granted in Section 1.1. Your permission to use the Licensed Material is expressly conditioned on you not impairing Licensor's or the applicable copyright owner's rights in the Licensed Material in any way.

3. **Restrictions on use**

3.1. Minor editing privileges are allowed for adaptations for stylistic purposes or formatting purposes provided such alterations do not alter the original meaning or intention of the Licensed Material and the new figure(s) are still accurate and representative of the Licensed Material. Any other changes including but not limited to, cropping, adapting, and/or omitting material that affect the meaning, intention or moral rights of the author(s) are strictly prohibited.

3.2. You must not use any Licensed Material as part of any design or trademark.

3.3. Licensed Material may be used in Open Access Publications (OAP), but any such reuse must include a clear acknowledgment of this permission visible at the same time as the figures/tables/illustration or abstract and which must indicate that the Licensed Material is not part of the governing OA license but has been reproduced with permission. This may be indicated according to any standard referencing system but must include at a minimum 'Book/Journal title, Author, Journal Name (if applicable), Volume (if applicable), Publisher, Year, reproduced with permission from SNCSC'.

4. **STM Permission Guidelines**

4.1. An alternative scope of license may apply to signatories of the STM Permissions Guidelines ("STM PG") as amended from time to time and made available at https://www.stm-assoc.org/intellectual-property/permissions/permissions-guidelines/.

4.2. For content reuse requests that qualify for permission under the STM PG, and which may be updated from time to time, the STM PG supersede the terms and conditions contained in this License.

4.3. If a License has been granted under the STM PG, but the STM PG no longer apply at the time of publication, further permission must be sought from the Rightsholder. Contact journalpermissions@springernature.com or bookpermissions@springernature.com for these rights.

5. **Duration of License**

5.1. Unless otherwise indicated on your License, a License is valid from the date of purchase ("License Date") until the end of the relevant period in the below table:

Reuse in a medical	Reuse up to distribution or time period

communications project	indicated in License
Reuse in a dissertation/thesis	Lifetime of thesis
Reuse in a journal/magazine	Lifetime of journal/magazine
Reuse in a book/textbook	Lifetime of edition
Reuse on a website	1 year unless otherwise specified in the License
Reuse in a presentation/slide kit/poster	Lifetime of presentation/slide kit/poster. Note: publication whether electronic or in print of presentation/slide kit/poster may require further permission.
Reuse in conference proceedings	Lifetime of conference proceedings
Reuse in an annual report	Lifetime of annual report
Reuse in training/CME materials	Reuse up to distribution or time period indicated in License
Reuse in newsmedia	Lifetime of newsmedia
Reuse in coursepack/classroom materials	Reuse up to distribution and/or time period indicated in license

6. **Acknowledgement**

6.1. The Licensor's permission must be acknowledged next to the Licensed Material in print. In electronic form, this acknowledgement must be visible at the same time as the figures/tables/illustrations or abstract and must be hyperlinked to the journal/book's homepage.

6.2. Acknowledgement may be provided according to any standard referencing system and at a minimum should include "Author, Article/Book Title, Journal name/Book imprint, volume, page number, year, Springer Nature".

7. **Reuse in a dissertation or thesis**

7.1. Where 'reuse in a dissertation/thesis' has been selected, the following terms apply: Print rights of the Version of Record are provided for; electronic rights for use only on institutional repository as defined by the Sherpa guideline (www.sherpa.ac.uk/romeo/) and only up to what is required by the awarding institution.

7.2. For theses published under an ISBN or ISSN, separate permission is required. Please contact journalpermissions@springernature.com or bookpermissions@springernature.com f

or these rights.

7.3. Authors must properly cite the published manuscript in their thesis according to current citation standards and include the following acknowledgement: '*Reproduced with permission from Springer Nature*'.

8. **License Fee**

You must pay the fee set forth in the License Agreement (the "License Fees"). All amounts payable by you under this License are exclusive of any sales, use, withholding, value added or similar taxes, government fees or levies or other assessments. Collection and/or remittance of such taxes to the relevant tax authority shall be the responsibility of the party who has the legal obligation to do so.

9. **Warranty**

9.1. The Licensor warrants that it has, to the best of its knowledge, the rights to license reuse of the Licensed Material. **You are solely responsible for ensuring that the material you wish to license is original to the Licensor and does not carry the copyright of another entity or third party (as credited in the published version).** If the credit line on any part of the Licensed Material indicates that it was reprinted or adapted with permission from another source, then you should seek additional permission from that source to reuse the material.

9.2. EXCEPT FOR THE EXPRESS WARRANTY STATED HEREIN AND TO THE EXTENT PERMITTED BY APPLICABLE LAW, LICENSOR PROVIDES THE LICENSED MATERIAL "AS IS" AND MAKES NO OTHER REPRESENTATION OR WARRANTY. LICENSOR EXPRESSLY DISCLAIMS ANY LIABILITY FOR ANY CLAIM ARISING FROM OR OUT OF THE CONTENT, INCLUDING BUT NOT LIMITED TO ANY ERRORS, INACCURACIES, OMISSIONS, OR DEFECTS CONTAINED THEREIN, AND ANY IMPLIED OR EXPRESS WARRANTY AS TO MERCHANTABILITY OR FITNESS FOR A PARTICULAR PURPOSE. IN NO EVENT SHALL LICENSOR BE LIABLE TO YOU OR ANY OTHER PARTY OR ANY OTHER PERSON OR FOR ANY SPECIAL, CONSEQUENTIAL, INCIDENTAL, INDIRECT, PUNITIVE, OR EXEMPLARY DAMAGES, HOWEVER CAUSED, ARISING OUT OF OR IN CONNECTION WITH THE DOWNLOADING, VIEWING OR USE OF THE LICENSED MATERIAL REGARDLESS OF THE FORM OF ACTION, WHETHER FOR BREACH OF CONTRACT, BREACH OF WARRANTY, TORT, NEGLIGENCE, INFRINGEMENT OR OTHERWISE (INCLUDING, WITHOUT LIMITATION, DAMAGES BASED ON LOSS OF PROFITS, DATA, FILES, USE, BUSINESS OPPORTUNITY OR CLAIMS OF THIRD PARTIES), AND WHETHER OR NOT THE PARTY HAS BEEN ADVISED OF THE POSSIBILITY OF SUCH DAMAGES. THIS LIMITATION APPLIES NOTWITHSTANDING ANY FAILURE OF ESSENTIAL PURPOSE OF ANY LIMITED REMEDY PROVIDED HEREIN.

10. **Termination and Cancellation**

10.1 The License and all rights granted hereunder will continue until the end of the applicable period shown in Clause 5.1 above. Thereafter, this license will be terminated and

all rights granted hereunder will cease.

10.2 Licensor reserves the right to terminate the License in the event that payment is not received in full or if you breach the terms of this License.

11. **General**

11.1. The License and the rights and obligations of the parties hereto shall be construed, interpreted and determined in accordance with the laws of the Federal Republic of Germany without reference to the stipulations of the CISG (United Nations Convention on Contracts for the International Sale of Goods) or to Germany´s choice-of-law principle.

11.2. The parties acknowledge and agree that any controversies and disputes arising out of this License shall be decided exclusively by the courts of or having jurisdiction for Heidelberg, Germany, as far as legally permissible.

11.3. This License is solely for Licensor's and Licensee's benefit. It is not for the benefit of any other person or entity.

Questions? For questions on Copyright Clearance Center accounts or website issues please contact springernaturesupport@copyright.com or +1-855-239-3415 (toll free in the US) or +1-978-646-2777. For questions on Springer Nature licensing please visit https://www.springernature.com/gp/partners/rights-permissions-third-party-distribution

Other Conditions:

Version 1.4 - Dec 2022

Questions? customercare@copyright.com.

- **Copyright permissions for Figure 8:**

SPRINGER NATURE LICENSE
TERMS AND CONDITIONS
Oct 05, 2024

This Agreement between Silvia Cobelo Gómez ("You") and Springer Nature ("Springer Nature") consists of your license details and the terms and conditions provided by Springer Nature and Copyright Clearance Center.

License Number	5882460338945
License date	Oct 05, 2024
Licensed Content Publisher	Springer Nature
Licensed Content Publication	European Journal of Human Genetics
Licensed Content Title	Association of metreleptin treatment and dietary intervention with neurological outcomes in Celia's encephalopathy
Licensed Content Author	David Araújo-Vilar et al
Licensed Content Date	Jan 24, 2018
Type of Use	Thesis/Dissertation
Requestor type	academic/university or research institute
Format	print and electronic
Portion	figures/tables/illustrations
Number of figures/tables/illustrations	1
Would you like a high resolution image with your order?	No
Will you be translating?	No
Circulation/distribution	100 – 199
Author of this Springer Nature content	No
Title of new work	Unravelling the Pathogenesis of Celia's Encephalopathy (PELD): The Role of Seipin in Neurodegeneration, Lipodystrophy, and other Tissue Damage in a Humanized Murine Model
Institution name	Universidade de Santiago de Compostela
Expected presentation date	Dec 2024
Portions	Figure 8 on page 71
The Requesting Person / Organization to Appear on the License	Silvia Cobelo Gómez
Requestor Location	University of Santiago de Compostela Campus Vida Avenida Barcelona, s/n Santiago de Compostela, A Coruña 15782

	Spain Attn: University of Santiago de Compostela
Billing Type	Invoice
Billing Address	University of Santiago de Compostela Campus Vida Avenida Barcelona, s/n Santiago de Compostela, Spain 15782 Attn: University of Santiago de Compostela
Total	0.00 EUR

Terms and Conditions

Springer Nature Customer Service Centre GmbH Terms and Conditions

The following terms and conditions ("Terms and Conditions") together with the terms specified in your [RightsLink] constitute the License ("License") between you as Licensee and Springer Nature Customer Service Centre GmbH as Licensor. By clicking 'accept' and completing the transaction for your use of the material ("Licensed Material"), you confirm your acceptance of and obligation to be bound by these Terms and Conditions.

1. **Grant and Scope of License**

1.1. The Licensor grants you a personal, non-exclusive, non-transferable, non-sublicensable, revocable, world-wide License to reproduce, distribute, communicate to the public, make available, broadcast, electronically transmit or create derivative works using the Licensed Material for the purpose(s) specified in your RightsLink Licence Details only. Licenses are granted for the specific use requested in the order and for no other use, subject to these Terms and Conditions. You acknowledge and agree that the rights granted to you under this License do not include the right to modify, edit, translate, include in collective works, or create derivative works of the Licensed Material in whole or in part unless expressly stated in your RightsLink Licence Details. You may use the Licensed Material only as permitted under this Agreement and will not reproduce, distribute, display, perform, or otherwise use or exploit any Licensed Material in any way, in whole or in part, except as expressly permitted by this License.

1.2. You may only use the Licensed Content in the manner and to the extent permitted by these Terms and Conditions, by your RightsLink Licence Details and by any applicable laws.

1.3. A separate license may be required for any additional use of the Licensed Material, e.g. where a license has been purchased for print use only, separate permission must be obtained for electronic re-use. Similarly, a License is only valid in the language selected and does not apply for editions in other languages unless additional translation rights have been granted separately in the License.

1.4. Any content within the Licensed Material that is owned by third parties is expressly excluded from the License.

1.5. Rights for additional reuses such as custom editions, computer/mobile applications, film or TV reuses and/or any other derivative rights requests require additional permission and may be subject to an additional fee. Please apply to journalpermissions@springernature.com or bookpermissions@springernature.com for

these rights.

2. **Reservation of Rights**

Licensor reserves all rights not expressly granted to you under this License. You acknowledge and agree that nothing in this License limits or restricts Licensor's rights in or use of the Licensed Material in any way. Neither this License, nor any act, omission, or statement by Licensor or you, conveys any ownership right to you in any Licensed Material, or to any element or portion thereof. As between Licensor and you, Licensor owns and retains all right, title, and interest in and to the Licensed Material subject to the license granted in Section 1.1. Your permission to use the Licensed Material is expressly conditioned on you not impairing Licensor's or the applicable copyright owner's rights in the Licensed Material in any way.

3. **Restrictions on use**

3.1. Minor editing privileges are allowed for adaptations for stylistic purposes or formatting purposes provided such alterations do not alter the original meaning or intention of the Licensed Material and the new figure(s) are still accurate and representative of the Licensed Material. Any other changes including but not limited to, cropping, adapting, and/or omitting material that affect the meaning, intention or moral rights of the author(s) are strictly prohibited.

3.2. You must not use any Licensed Material as part of any design or trademark.

3.3. Licensed Material may be used in Open Access Publications (OAP), but any such reuse must include a clear acknowledgment of this permission visible at the same time as the figures/tables/illustration or abstract and which must indicate that the Licensed Material is not part of the governing OA license but has been reproduced with permission. This may be indicated according to any standard referencing system but must include at a minimum 'Book/Journal title, Author, Journal Name (if applicable), Volume (if applicable), Publisher, Year, reproduced with permission from SNCSC'.

4. **STM Permission Guidelines**

4.1. An alternative scope of license may apply to signatories of the STM Permissions Guidelines ("STM PG") as amended from time to time and made available at https://www.stm-assoc.org/intellectual-property/permissions/permissions-guidelines/.

4.2. For content reuse requests that qualify for permission under the STM PG, and which may be updated from time to time, the STM PG supersede the terms and conditions contained in this License.

4.3. If a License has been granted under the STM PG, but the STM PG no longer apply at the time of publication, further permission must be sought from the Rightsholder. Contact journalpermissions@springernature.com or bookpermissions@springernature.co

m for these rights.

5. **Duration of License**

5.1. Unless otherwise indicated on your License, a License is valid from the date of purchase ("License Date") until the end of the relevant period in the below table:

Reuse in a medical communications project	Reuse up to distribution or time period indicated in License
Reuse in a dissertation/thesis	Lifetime of thesis
Reuse in a journal/magazine	Lifetime of journal/magazine
Reuse in a book/textbook	Lifetime of edition
Reuse on a website	1 year unless otherwise specified in the License
Reuse in a presentation/slide kit/poster	Lifetime of presentation/slide kit/poster. Note: publication whether electronic or in print of presentation/slide kit/poster may require further permission.
Reuse in conference proceedings	Lifetime of conference proceedings
Reuse in an annual report	Lifetime of annual report
Reuse in training/CME materials	Reuse up to distribution or time period indicated in License
Reuse in newsmedia	Lifetime of newsmedia
Reuse in coursepack/classroom materials	Reuse up to distribution and/or time period indicated in license

6. **Acknowledgement**

6.1. The Licensor's permission must be acknowledged next to the Licensed Material in print. In electronic form, this acknowledgement must be visible at the same time as the figures/tables/illustrations or abstract and must be hyperlinked to the journal/book's homepage.

6.2. Acknowledgement may be provided according to any standard referencing system and at a minimum should include "Author, Article/Book Title, Journal name/Book imprint, volume, page number, year, Springer Nature".

7. **Reuse in a dissertation or thesis**

7.1. Where 'reuse in a dissertation/thesis' has been selected, the following terms apply: Print rights of the Version of Record are provided for; electronic rights for use only on institutional repository as defined by the Sherpa guideline (www.sherpa.ac.uk/romeo/) and only up to what is required by the awarding institution.

7.2. For theses published under an ISBN or ISSN, separate permission is required. Please contact journalpermissions@springernature.com or bookpermissions@springernature.com for these rights.

7.3. Authors must properly cite the published manuscript in their thesis according to current citation standards and include the following acknowledgement: '*Reproduced with permission from Springer Nature*'.

8. **License Fee**

You must pay the fee set forth in the License Agreement (the "License Fees"). All amounts payable by you under this License are exclusive of any sales, use, withholding, value added or similar taxes, government fees or levies or other assessments. Collection and/or remittance of such taxes to the relevant tax authority shall be the responsibility of the party who has the legal obligation to do so.

9. **Warranty**

9.1. The Licensor warrants that it has, to the best of its knowledge, the rights to license reuse of the Licensed Material. **You are solely responsible for ensuring that the material you wish to license is original to the Licensor and does not carry the copyright of another entity or third party (as credited in the published version).** If the credit line on any part of the Licensed Material indicates that it was reprinted or adapted with permission from another source, then you should seek additional permission from that source to reuse the material.

9.2. EXCEPT FOR THE EXPRESS WARRANTY STATED HEREIN AND TO THE EXTENT PERMITTED BY APPLICABLE LAW, LICENSOR PROVIDES THE LICENSED MATERIAL "AS IS" AND MAKES NO OTHER REPRESENTATION OR WARRANTY. LICENSOR EXPRESSLY DISCLAIMS ANY LIABILITY FOR ANY CLAIM ARISING FROM OR OUT OF THE CONTENT, INCLUDING BUT NOT LIMITED TO ANY ERRORS, INACCURACIES, OMISSIONS, OR DEFECTS CONTAINED THEREIN, AND ANY IMPLIED OR EXPRESS WARRANTY AS TO MERCHANTABILITY OR FITNESS FOR A PARTICULAR PURPOSE. IN NO EVENT SHALL LICENSOR BE LIABLE TO YOU OR ANY OTHER PARTY OR ANY OTHER PERSON OR FOR ANY SPECIAL, CONSEQUENTIAL, INCIDENTAL, INDIRECT, PUNITIVE, OR EXEMPLARY DAMAGES, HOWEVER CAUSED, ARISING OUT OF OR IN CONNECTION WITH THE DOWNLOADING, VIEWING OR USE OF THE LICENSED MATERIAL REGARDLESS OF THE FORM OF ACTION, WHETHER FOR BREACH OF CONTRACT, BREACH OF WARRANTY, TORT, NEGLIGENCE, INFRINGEMENT OR OTHERWISE (INCLUDING, WITHOUT LIMITATION, DAMAGES BASED ON LOSS OF PROFITS, DATA, FILES, USE, BUSINESS OPPORTUNITY OR CLAIMS OF THIRD PARTIES), AND WHETHER OR NOT THE PARTY HAS BEEN ADVISED OF THE POSSIBILITY OF SUCH DAMAGES. THIS LIMITATION APPLIES NOTWITHSTANDING ANY FAILURE OF ESSENTIAL PURPOSE OF ANY LIMITED REMEDY PROVIDED

HEREIN.

10. **Termination and Cancellation**

10.1. The License and all rights granted hereunder will continue until the end of the applicable period shown in Clause 5.1 above. Thereafter, this license will be terminated and all rights granted hereunder will cease.
10.2. Licensor reserves the right to terminate the License in the event that payment is not received in full or if you breach the terms of this License.

11. **General**

11.1. The License and the rights and obligations of the parties hereto shall be construed, interpreted and determined in accordance with the laws of the Federal Republic of Germany without reference to the stipulations of the CISG (United Nations Convention on Contracts for the International Sale of Goods) or to Germany´s choice-of-law principle.
11.2. The parties acknowledge and agree that any controversies and disputes arising out of this License shall be decided exclusively by the courts of or having jurisdiction for Heidelberg, Germany, as far as legally permissible.
11.3. This License is solely for Licensor's and Licensee's benefit. It is not for the benefit of any other person or entity.

Questions? For questions on Copyright Clearance Center accounts or website issues please contact springernaturesupport@copyright.com or +1-855-239-3415 (toll free in the US) or +1-978-646-2777. For questions on Springer Nature licensing please visit https://www.springernature.com/gp/partners/rights-permissions-third-party-distribution

Other Conditions:
Version 1.4 - Dec 2022

Questions? customercare@copyright.com.

BMJ PUBLISHING GROUP LTD. LICENSE
TERMS AND CONDITIONS
Oct 05, 2024

This Agreement between Silvia Cobelo Gómez ("You") and BMJ Publishing Group Ltd. ("BMJ Publishing Group Ltd.") consists of your license details and the terms and conditions provided by BMJ Publishing Group Ltd. and Copyright Clearance Center.

License Number	5882460612347
License date	Oct 05, 2024
Licensed Content Publisher	BMJ Publishing Group Ltd.
Licensed Content Publication	Journal of Medical Genetics
Licensed Content Title	A new seipin-associated neurodegenerative syndrome
Licensed Content Author	Encarna Guillén-Navarro,Sofía Sánchez-Iglesias,Rosario Domingo-Jiménez,Berta Victoria,Alejandro Ruiz-Riquelme,Alberto Rábano,Lourdes Loidi,Andrés Beiras,Blanca González-Méndez,Adriana Ramos,Vanesa López-González,María Juliana Ballesta-Martínez,Miguel Garrido-Pumar,Pablo Aguiar,Alvaro Ruibal,Jesús R Requena,David Araújo-Vilar
Licensed Content Date	Jun 1, 2013
Licensed Content Volume	50
Licensed Content Issue	6
Type of Use	Dissertation/Thesis
Requestor type	Individual
Format	Print and electronic
Portion	Figure/table/extract
Number of figure/table/extracts	1
Descriptionof figure/table/extracts	Figure 8 on page 71
Will you be translating?	No
Circulation/distribution	200
Title of new work	Unravelling the Pathogenesis of Celia’s Encephalopathy (PELD): The Role of Seipin in Neurodegeneration, Lipodystrophy, and other Tissue Damage in a Humanized Murine Model
Institution name	Universidade de Santiago de Compostela
Expected presentation date	Dec 2024
Portions	Figure 8 on page 71
The Requesting Person / Organization to Appear on the	Silvia Cobelo Gómez

License	
	University of Santiago de Compostela Campus Vida Avenida Barcelona, s/n
Requestor Location	
	Santiago de Compostela, A Coruña 15782 Spain Attn: University of Santiago de Compostela
Publisher Tax ID	GB674738491
Billing Type	Invoice
	University of Santiago de Compostela Campus Vida Avenida Barcelona, s/n
Billing Address	
	Santiago de Compostela, Spain 15782 Attn: University of Santiago de Compostela
Total	0.00 EUR

Terms and Conditions

BMJ Terms and Conditions for Permissions

When you submit your order you are subject to the terms and conditions set out below. You will also have agreed to the Copyright Clearance Center's ("CCC") terms and conditions regarding billing and payment https://s100.copyright.com/App/PaymentTermsAndConditions.jsp. CCC are acting as BMJ Publishing Group Limited's ("BMJs") agent.

Subject to the terms set out herein, BMJ hereby grants to you (the Licensee) a non-exclusive, non-transferable licence to re-use material as detailed in your request for this/those purpose(s) only and in accordance with the following conditions:

1) **Scope of Licence:** Use of the Licensed Material(s) is restricted to the ways specified by you during the order process and any additional use(s) outside of those specified in that request, require a further grant of permission.

2) **Acknowledgement:** In all cases, due acknowledgement to the original publication with permission from BMJ should be stated adjacent to the reproduced Licensed Material. The format of such acknowledgement should read as follows:
"Reproduced from [publication title, author(s), volume number, page numbers, copyright notice year] with permission from BMJ Publishing Group Ltd."

3) **Third Party Material**: BMJ acknowledges to the best of its knowledge, it has the rights to licence your reuse of the Licensed Material, subject always to the caveat that images/diagrams, tables and other illustrative material included within, which have a separate copyright notice, are presumed as excluded from the licence. Therefore, you should ensure that the Licensed Material you are requesting is original to BMJ and does not carry the copyright of another entity (as credited in the published version). If the credit line on any part of the material you have requested in any way indicates that it was reprinted or adapted by BMJ with permission from another source, then you should seek permission from that source directly to re-use the Licensed Material, as this is outside of the licence granted herein.

4) **Altering/Modifying Material:** The text of any material for which a licence is granted may not be altered in any way without the prior express permission of BMJ. If adaptation of the material has been approved via bmj.permissions@bmj.com you must include the disclaimer: "Adapted by

permission from BMJ Publishing Group Limited. [publication title, author, volume number, page numbers, copyright notice year]

5) **Reservation of Rights:** BMJ reserves all rights not specifically granted in the combination of (i) the licence details provided by you and accepted in the course of this licensing transaction, (ii) these terms and conditions and (iii) CCC's Billing and Payment Terms and Conditions.

6) **Timing of Use:** First use of the Licensed Material must take place within 12 months of the grant of permission.

7) **Creation of Contract and Termination:** Once you have submitted an order via RightsLink and this is received by CCC, and subject to you completing accurate details of your proposed use, this is when a binding contract is in effect and our acceptance occurs. As you are ordering rights from a periodical, to the fullest extent permitted by law, you will have no right to cancel the contract from this point other than for BMJ's material breach or fraudulent misrepresentation or as otherwise permitted under a statutory right. Payment must be made in accordance with CCC's Billing and Payment Terms and conditions. In the event that you breach any material condition of these terms and condition or any of CCC's Billing and Payment Terms and Conditions, the license is automatically terminated upon written notice from BMJ or CCC or as otherwise provided for in CCC's Billing and Payment Terms and Conditions, where these apply. Continued use of materials where a licence has been terminated, as well as any use of the Licensed Materials beyond the scope of an unrevoked licence, may constitute intellectual property rights infringement and BMJ reserves the right to take any and all action to protect its intellectual property rights in the Licensed Materials.

8) **Warranties:** BMJ makes no express or implied representations or warranties with respect to the Licensed Material and to the fullest extent permitted by law this is provided on an "as is" basis. For the avoidance of doubt BMJ does not warrant that the Licensed Material is accurate or fit for any particular purpose.

9) **Limitation of Liability:** To the fullest extent permitted by law, BMJ disclaims all liability for any indirect, consequential or incidental damages (including without limitation, damages for loss of profits, information or interruption) arising out of the use or inability to use the Licensed Material or the inability to obtain additional rights to use the Licensed Material. To the fullest extent permitted by law, the maximum aggregate liability of BMJ for any claims, costs, proceedings and demands for direct losses caused by BMJ's breaches of its obligations herein shall be limited to twice the amount paid by you to CCC for the licence granted herein.

10) **Indemnity:** You hereby indemnify and hold harmless BMJ and their respective officers, directors, employees and agents, from and against any and all claims, costs, proceeding or demands arising out of your unauthorised use of the Licensed Material.

11) **No Transfer of License:** This licence is personal to you, and may not be assigned or transferred by you without prior written consent from BMJ or its authorised agent(s). BMJ may assign or transfer any of its rights and obligations under this Agreement, upon written notice to you.

12) **No Amendment Except in Writing:** This licence may not be amended except in a writing signed by both parties (or, in the case of BMJ, by CCC on BMJ's behalf).

13) **Objection to Contrary terms:** BMJ hereby objects to any terms contained in any purchase order, acknowledgment, check endorsement or other writing prepared by you, which terms are inconsistent with these terms and conditions or CCC's Billing and Payment Terms and Conditions. These terms and conditions, together with CCC's Billing and Payment Terms and Conditions

(which to the extent they are consistent are incorporated herein), comprise the entire agreement between you and BMJ (and CCC) and the Licensee concerning this licensing transaction. In the event of any conflict between your obligations established by these terms and conditions and those established by CCC's Billing and Payment Terms and Conditions, these terms and conditions shall control.

14) **Revocation:** BMJ or CCC may, within 30 days of issuance of this licence, deny the permissions described in this licence at their sole discretion, for any reason or no reason, with a full refund payable to you should you have not been able to exercise your rights in full. Notice of such denial will be made using the contact information provided by you. Failure to receive such notice from BMJ or CCC will not, to the fullest extent permitted by law alter or invalidate the denial. For the fullest extent permitted by law in no event will BMJ or CCC be responsible or liable for any costs, expenses or damage incurred by you as a result of a denial of your permission request, other than a refund of the amount(s) paid by you to BMJ and/or CCC for denied permissions.

15) **Restrictions to the license**:

15.1) **Promotion:** BMJ will not give permission to reproduce in full or in part any Licensed Material for use in the promotion of the following:

a) non-medical products that are harmful or potentially harmful to health

b) medical products that do not have a product license granted by the Medicines and Healthcare products Regulatory Agency (MHRA) or its international equivalents. Marketing of the product may start only after data sheets have been released to members of the medical profession and must conform to the marketing authorization contained in the product license.

16) **Translation**: This permission is granted for non-exclusive world English language rights only unless explicitly stated in your licence. If translation rights are granted, a professional translator should be employed and it must be a true reproduction, accurately conveying the original meaning and of the same quality.

17) **STM Permissions Guidelines**: For content reuse in journals that qualify for permission under the STM Permissions Guidelines (which may be updated from time to time) the terms and conditions of the Guidelines supersede those in this licence. https://www.stm-assoc.org/intellectual-property/permissions/permissions-guidelines/

18) **General:** Neither party shall be liable for failure, default or delay in performing its obligations under this Licence, caused by a Force Majeure event which shall include any act of God, war, or threatened war, act or threatened act of terrorism, riot, strike, lockout, individual action, fire, flood, drought, tempest or other event beyond the reasonable control of either party.

18.1) In the event that any provision of this Agreement is held to be invalid, the remainder of the provisions shall continue in full force and effect.

18.2) There shall be no right whatsoever for any third party to enforce the terms and conditions of this Agreement. The Parties hereby expressly wish to exclude the operation of the Contracts (Rights of Third Parties) Act 1999 and any other legislation which has this effect and is binding on this agreement.

18.3) To the fullest extent permitted by law, this Licence will be governed by the laws of England and shall be governed and construed in accordance with the laws of England. Any action arising out of or relating to this agreement shall be brought in courts situated in England

save where it is necessary for BMJ for enforcement to bring proceedings to bring an action in an alternative jurisdiction.

V1.1

Questions? customercare@copyright.com.

- **Copyright permission for Figure 10:**

ELSEVIER LICENSE
TERMS AND CONDITIONS
Oct 05, 2024

This Agreement between Silvia Cobelo Gómez ("You") and Elsevier ("Elsevier") consists of your license details and the terms and conditions provided by Elsevier and Copyright Clearance Center.

License Number	5882460838570
License date	Oct 05, 2024
Licensed Content Publisher	Elsevier
Licensed Content Publication	Neurobiology of Disease
Licensed Content Title	Larger aggregates of mutant seipin in Celia's Encephalopathy, a new protein misfolding neurodegenerative disease
Licensed Content Author	Alejandro Ruiz-Riquelme,Sofía Sánchez-Iglesias,Alberto Rábano,Encarna Guillén-Navarro,Rosario Domingo-Jiménez,Adriana Ramos,Isaac Rosa,Ana Senra,Peter Nilsson,Ángel García,David Araújo-Vilar,Jesús R. Requena
Licensed Content Date	Nov 1, 2015
Licensed Content Volume	83
Licensed Content Issue	n/a
Licensed Content Pages	10
Start Page	44
End Page	53
Type of Use	reuse in a thesis/dissertation
Portion	figures/tables/illustrations
Number of figures/tables/illustrations	1
Format	both print and electronic
Are you the author of this Elsevier article?	No
Will you be translating?	No
Title of new work	Unravelling the Pathogenesis of Celia’s Encephalopathy (PELD): The Role of Seipin in Neurodegeneration, Lipodystrophy, and other Tissue Damage in a Humanized Murine Model
Institution name	Universidade de Santiago de Compostela
Expected presentation date	Dec 2024
Portions	Figure 10 on page 77
The Requesting Person / Organization to Appear on the License	Silvia Cobelo Gómez

	University of Santiago de Compostela Campus Vida Avenida Barcelona, s/n
Requestor Location	Santiago de Compostela, A Coruña 15782 Spain Attn: University of Santiago de Compostela
Publisher Tax ID	GB 494 6272 12
Total	0.00 EUR

Terms and Conditions

INTRODUCTION

1. The publisher for this copyrighted material is Elsevier. By clicking "accept" in connection with completing this licensing transaction, you agree that the following terms and conditions apply to this transaction (along with the Billing and Payment terms and conditions established by Copyright Clearance Center, Inc. ("CCC"), at the time that you opened your RightsLink account and that are available at any time at https://myaccount.copyright.com).

GENERAL TERMS

2. Elsevier hereby grants you permission to reproduce the aforementioned material subject to the terms and conditions indicated.

3. Acknowledgement: If any part of the material to be used (for example, figures) has appeared in our publication with credit or acknowledgement to another source, permission must also be sought from that source. If such permission is not obtained then that material may not be included in your publication/copies. Suitable acknowledgement to the source must be made, either as a footnote or in a reference list at the end of your publication, as follows:

"Reprinted from Publication title, Vol /edition number, Author(s), Title of article / title of chapter, Pages No., Copyright (Year), with permission from Elsevier [OR APPLICABLE SOCIETY COPYRIGHT OWNER]." Also Lancet special credit - "Reprinted from The Lancet, Vol. number, Author(s), Title of article, Pages No., Copyright (Year), with permission from Elsevier."

4. Reproduction of this material is confined to the purpose and/or media for which permission is hereby given. The material may not be reproduced or used in any other way, including use in combination with an artificial intelligence tool (including to train an algorithm, test, process, analyse, generate output and/or develop any form of artificial intelligence tool), or to create any derivative work and/or service (including resulting from the use of artificial intelligence tools).

5. Altering/Modifying Material: Not Permitted. However figures and illustrations may be altered/adapted minimally to serve your work. Any other abbreviations, additions, deletions and/or any other alterations shall be made only with prior written authorization of Elsevier Ltd. (Please contact Elsevier's permissions helpdesk here). No modifications can be made to any Lancet figures/tables and they must be reproduced in full.

6. If the permission fee for the requested use of our material is waived in this instance, please be advised that your future requests for Elsevier materials may attract a fee.

7. Reservation of Rights: Publisher reserves all rights not specifically granted in the combination

of (i) the license details provided by you and accepted in the course of this licensing transaction, (ii) these terms and conditions and (iii) CCC's Billing and Payment terms and conditions.

8. License Contingent Upon Payment: While you may exercise the rights licensed immediately upon issuance of the license at the end of the licensing process for the transaction, provided that you have disclosed complete and accurate details of your proposed use, no license is finally effective unless and until full payment is received from you (either by publisher or by CCC) as provided in CCC's Billing and Payment terms and conditions. If full payment is not received on a timely basis, then any license preliminarily granted shall be deemed automatically revoked and shall be void as if never granted. Further, in the event that you breach any of these terms and conditions or any of CCC's Billing and Payment terms and conditions, the license is automatically revoked and shall be void as if never granted. Use of materials as described in a revoked license, as well as any use of the materials beyond the scope of an unrevoked license, may constitute copyright infringement and publisher reserves the right to take any and all action to protect its copyright in the materials.

9. Warranties: Publisher makes no representations or warranties with respect to the licensed material.

10. Indemnity: You hereby indemnify and agree to hold harmless publisher and CCC, and their respective officers, directors, employees and agents, from and against any and all claims arising out of your use of the licensed material other than as specifically authorized pursuant to this license.

11. No Transfer of License: This license is personal to you and may not be sublicensed, assigned, or transferred by you to any other person without publisher's written permission.

12. No Amendment Except in Writing: This license may not be amended except in a writing signed by both parties (or, in the case of publisher, by CCC on publisher's behalf).

13. Objection to Contrary Terms: Publisher hereby objects to any terms contained in any purchase order, acknowledgment, check endorsement or other writing prepared by you, which terms are inconsistent with these terms and conditions or CCC's Billing and Payment terms and conditions. These terms and conditions, together with CCC's Billing and Payment terms and conditions (which are incorporated herein), comprise the entire agreement between you and publisher (and CCC) concerning this licensing transaction. In the event of any conflict between your obligations established by these terms and conditions and those established by CCC's Billing and Payment terms and conditions, these terms and conditions shall control.

14. Revocation: Elsevier or Copyright Clearance Center may deny the permissions described in this License at their sole discretion, for any reason or no reason, with a full refund payable to you. Notice of such denial will be made using the contact information provided by you. Failure to receive such notice will not alter or invalidate the denial. In no event will Elsevier or Copyright Clearance Center be responsible or liable for any costs, expenses or damage incurred by you as a result of a denial of your permission request, other than a refund of the amount(s) paid by you to Elsevier and/or Copyright Clearance Center for denied permissions.

LIMITED LICENSE

The following terms and conditions apply only to specific license types:

15. **Translation**: This permission is granted for non-exclusive world **English** rights only unless your license was granted for translation rights. If you licensed translation rights you may only translate this content into the languages you requested. A professional translator must perform all translations and reproduce the content word for word preserving the integrity of the article.

16. **Posting licensed content on any Website**: The following terms and conditions apply as follows: Licensing material from an Elsevier journal: All content posted to the web site must maintain the copyright information line on the bottom of each image; A hyper-text must be included to the Homepage of the journal from which you are licensing at http://www.sciencedirect.com/science/journal/xxxxx or the Elsevier homepage for books at http://www.elsevier.com; Central Storage: This license does not include permission for a scanned version of the material to be stored in a central repository such as that provided by Heron/XanEdu.

Licensing material from an Elsevier book: A hyper-text link must be included to the Elsevier homepage at http://www.elsevier.com . All content posted to the web site must maintain the copyright information line on the bottom of each image.

Posting licensed content on Electronic reserve: In addition to the above the following clauses are applicable: The web site must be password-protected and made available only to bona fide students registered on a relevant course. This permission is granted for 1 year only. You may obtain a new license for future website posting.

17. **For journal authors:** the following clauses are applicable in addition to the above:

Preprints:

A preprint is an author's own write-up of research results and analysis, it has not been peer-reviewed, nor has it had any other value added to it by a publisher (such as formatting, copyright, technical enhancement etc.).

Authors can share their preprints anywhere at any time. Preprints should not be added to or enhanced in any way in order to appear more like, or to substitute for, the final versions of articles however authors can update their preprints on arXiv or RePEc with their Accepted Author Manuscript (see below).

If accepted for publication, we encourage authors to link from the preprint to their formal publication via its DOI. Millions of researchers have access to the formal publications on ScienceDirect, and so links will help users to find, access, cite and use the best available version. Please note that Cell Press, The Lancet and some society-owned have different preprint policies. Information on these policies is available on the journal homepage.

Accepted Author Manuscripts: An accepted author manuscript is the manuscript of an article that has been accepted for publication and which typically includes author-incorporated changes suggested during submission, peer review and editor-author communications.

Authors can share their accepted author manuscript:

- immediately
  - via their non-commercial person homepage or blog

    - by updating a preprint in arXiv or RePEc with the accepted manuscript
    - via their research institute or institutional repository for internal institutional uses or as part of an invitation-only research collaboration work-group
    - directly by providing copies to their students or to research collaborators for their personal use
    - for private scholarly sharing as part of an invitation-only work group on commercial sites with which Elsevier has an agreement
- After the embargo period
    - via non-commercial hosting platforms such as their institutional repository
    - via commercial sites with which Elsevier has an agreement

In all cases accepted manuscripts should:

- link to the formal publication via its DOI
- bear a CC-BY-NC-ND license - this is easy to do
- if aggregated with other manuscripts, for example in a repository or other site, be shared in alignment with our hosting policy not be added to or enhanced in any way to appear more like, or to substitute for, the published journal article.

Published journal article (JPA): A published journal article (PJA) is the definitive final record of published research that appears or will appear in the journal and embodies all value-adding publishing activities including peer review co-ordination, copy-editing, formatting, (if relevant) pagination and online enrichment.

Policies for sharing publishing journal articles differ for subscription and gold open access articles:

Subscription Articles: If you are an author, please share a link to your article rather than the full-text. Millions of researchers have access to the formal publications on ScienceDirect, and so links will help your users to find, access, cite, and use the best available version.

Theses and dissertations which contain embedded PJAs as part of the formal submission can be posted publicly by the awarding institution with DOI links back to the formal publications on ScienceDirect.

If you are affiliated with a library that subscribes to ScienceDirect you have additional private sharing rights for others' research accessed under that agreement. This includes use for classroom teaching and internal training at the institution (including use in course packs and courseware programs), and inclusion of the article for grant funding purposes.

Gold Open Access Articles: May be shared according to the author-selected end-user license and should contain a CrossMark logo, the end user license, and a DOI link to the formal publication on ScienceDirect.

Please refer to Elsevier's posting policy for further information.

18. **For book authors** the following clauses are applicable in addition to the above: Authors are permitted to place a brief summary of their work online only. You are not allowed to download and post the published electronic version of your chapter, nor may you scan the printed edition to create an electronic version. **Posting to a repository:** Authors are permitted to post a summary of

their chapter only in their institution's repository.

19. **Thesis/Dissertation**: If your license is for use in a thesis/dissertation your thesis may be submitted to your institution in either print or electronic form. Should your thesis be published commercially, please reapply for permission. These requirements include permission for the Library and Archives of Canada to supply single copies, on demand, of the complete thesis and include permission for Proquest/UMI to supply single copies, on demand, of the complete thesis. Should your thesis be published commercially, please reapply for permission. Theses and dissertations which contain embedded PJAs as part of the formal submission can be posted publicly by the awarding institution with DOI links back to the formal publications on ScienceDirect.

Elsevier Open Access Terms and Conditions

You can publish open access with Elsevier in hundreds of open access journals or in nearly 2000 established subscription journals that support open access publishing. Permitted third party re-use of these open access articles is defined by the author's choice of Creative Commons user license. See our open access license policy for more information.

Terms & Conditions applicable to all Open Access articles published with Elsevier:

Any reuse of the article must not represent the author as endorsing the adaptation of the article nor should the article be modified in such a way as to damage the author's honour or reputation. If any changes have been made, such changes must be clearly indicated.

The author(s) must be appropriately credited and we ask that you include the end user license and a DOI link to the formal publication on ScienceDirect.

If any part of the material to be used (for example, figures) has appeared in our publication with credit or acknowledgement to another source it is the responsibility of the user to ensure their reuse complies with the terms and conditions determined by the rights holder.

Additional Terms & Conditions applicable to each Creative Commons user license:

CC BY: The CC-BY license allows users to copy, to create extracts, abstracts and new works from the Article, to alter and revise the Article and to make commercial use of the Article (including reuse and/or resale of the Article by commercial entities), provided the user gives appropriate credit (with a link to the formal publication through the relevant DOI), provides a link to the license, indicates if changes were made and the licensor is not represented as endorsing the use made of the work. The full details of the license are available at http://creativecommons.org/licenses/by/4.0.

CC BY NC SA: The CC BY-NC-SA license allows users to copy, to create extracts, abstracts and new works from the Article, to alter and revise the Article, provided this is not done for commercial purposes, and that the user gives appropriate credit (with a link to the formal publication through the relevant DOI), provides a link to the license, indicates if changes were made and the licensor is not represented as endorsing the use made of the work. Further, any new works must be made available on the same conditions. The full details of the license are available at http://creativecommons.org/licenses/by-nc-sa/4.0.

CC BY NC ND: The CC BY-NC-ND license allows users to copy and distribute the Article,

Lipodystrophies are rare disorders, with Celia's encephalopathy, identified by our research group in 2013, being exceptionally rare with only 33 cases to date. Over the years, our research group has unravelled key pathogenic mechanisms of this disease. However, its rarity, severity, and predominant brain involvement pose significant challenges for human studies. Therefore, in this study, we developed a knock-in mouse model expressing the aberrant human *BSCL2* transcript, alongside a *Bscl2* knock-out model, to compare the effects of *BSCL2* deficiency and overexpression. These models replicate aspects of Celia's encephalopathy and congenital generalized lipodystrophy, offering valuable preclinical tools for studying these conditions and exploring potential therapies.